Convection and Substorms

Paradigms of Magnetospheric Phenomenology

Charles F. Kennel

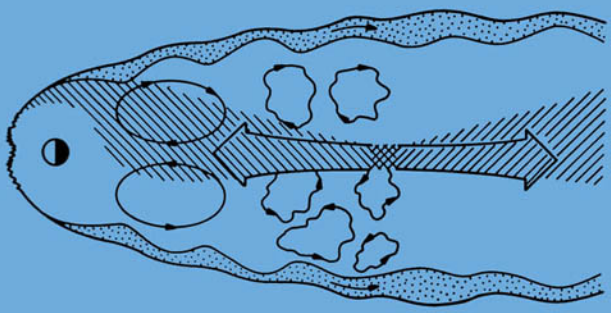

INTERNATIONAL SERIES ON ASTRONOMY AND ASTROPHYSICS

CONVECTION AND SUBSTORMS

INTERNATIONAL SERIES ON ASTRONOMY AND ASTROPHYSICS

1. E. N. Parker, *Spontaneous Current Sheets in Magnetic Fields with Applications to Stellar X-rays*
2. C. F. Kennel, *Convection and Substorms: Paradigms of Magnetosperic Phenomenology*
3. L. F. Burlaga, *Interplanetary Magnetohydrodynamics*

Convection and Substorms

Paradigms of Magnetospheric Phenomenology

Charles F. Kennel

Geophysical Institute
University of Alaska, Fairbanks

Institute of Geophysics and Planetary Physics
University of California, Los Angeles

New York Oxford
Oxford University Press
1995

Oxford University Press

Oxford New York
Athens Auckland Bangkok Bombay
Calcutta Cape Town Dar es Salaam Delhi
Florence Hong Kong Istanbul Karachi
Kuala Lumpur Madras Madrid Melbourne
Mexico City Nairobi Paris Singapore
Taipei Tokyo Toronto

and associated companies in
Berlin Ibadan

Published by Oxford University Press, Inc.
198 Madison Avenue, New York, New York 10016

Oxford is a registered trademark of Oxford University Press

Library of Congress Cataloging-in-Publication Data
Kennel, Charles F., 1939-
Convection and substorms : paradigms of magnetospheric
phenomenology / Charles F. Kennel
p. cm. —(International series on astronomy and astrophysics; 1)
Includes bibliographical references and index.
ISBN 0-19-508529-9
1. Magnetosphere. 2. Magnetospheric substorms.
3. Convection (Meteorology)
I. Title. II. Series.
QC809.M35K46 1994 538'.766—dc20

Printing (last digit): 9 8 7 6 5 4 3 2 1

Printed in the United States of America
on acid-free paper

Dedicated

to

Ellen

This page intentionally left blank

PREFACE

Convection and substorms are *the* paradigms of magnetospheric phenomenology. As paradigms, they take precedence over theory or experiment: they are the mental pictures that we carry around in our heads to give context to equations and meaning to data. They are almost as old as the concept of the magnetosphere itself. They have been quietly present in our thinking for virtually the entire space age. Even if we wished to deny their pertinence, and some do, we cannot avoid them, for they are expressed in the technical infrastructure of magnetospheric physics. They have guided 30 years of advance in the diversity, integration, and quality of the observations, not to mention impressive growth in the size and capability of the magnetospheric research community. The past decade has seen a striking rise in the professionalism and quality of the phenomenological research on the earth's magnetosphere. Much larger and more diverse data sets are being analyzed and compared with unprecedented articulation, completeness, sophistication, and open-mindedness. The essay to follow is an attempt to set forth the present content of the convection and substorm paradigms by seeing how effectively they organize recent as well as older observations.

This is a research essay, not a monograph. It is a personal essay, with all the advantages and disadvantages that entails. The reader may find it useful to have a large observational phenomenology patterned by one mind, despite our unconscious lapses of perspective and failures of conscious understanding. We will employ a conversational style unusual in contemporary scientific discourse, because we hope to convey a picture, not only of magnetospheric physics, but also of magnetospheric research. Yet the picture we draw will be cruelly incomplete, because we will discuss results, and not the effort and organization and creativity that went into obtaining them. Our picture will be of experimental results, yet the palette and brushes used to paint it come from theory, modeling, and numerical simulation. Just as the viewer sees only the painting, and not the tools used to paint it, so the reader of this essay will not see anything substantial about theory, modeling, and simulation. Even so, we will gloss over what is essential to all experimentalists: We will neither explain how nor criticize how measurements are made. Our basic instinct has been to trust the observers, to believe that "they really did see what they said they saw." If they disagree amongst themselves, our response has been to seek a conceptual framework, however loose, that encompasses all their experience.

We cite no literature appearing after the end of 1992. Only the literature published in the author's native language, English, has been cited, and primarily that after 1961, when he began his research in space physics. The author grew up with the American space program, and so he comprehends its *ethos* better than any other. He became acquainted with European space scientists early in his career, and Japanese somewhat later; so West European research is covered in some detail, Japanese, somewhat less so. But experimental work by former Eastern-bloc scientists has been slighted, not from malice but from insufficient grasp of the inner logic of their nations' methods of experimental space research. Our presentation is saturated in the history of our subject, yet we will not always present an orderly historical development, and we will cite older observations unsystematically, doing so primarily when they contribute to our current understanding of convection and substorms. Although we try to be sensitive to the issue of research priority, we will make no explicit attempt to adjudicate priority, and we sacrifice a discussion of it altogether when it impedes the conceptual flow of our exposition. We undoubtedly have been unfair to individuals and groups. We have also been unfair to topics. In failing to include topics such as the dynamics of the ring current, radiation belts, and plasmapause, or the interaction of convection with thermospheric winds, we reveal, not their unimportance, but our lack of diligence.

We looked to theory only for general ideas. We neither explain nor assess the theoretical foundations of the ideas we employ to interpret observations. We freely use basic concepts of magnetohydrodynamics (MHD) even when the quantitative justification in the underlying plasma physics may be in question, if it seems to us to be a constructive provisional step. At least, we may spotlight where it is critical to question the MHD approximation. Nowhere is this truer than with the two motivating conceptions of the entire field, reconnection and anomalous viscosity. Our use of MHD thus conforms to its original, paradigmatic, function: to be a skeleton of thought that articulates a diverse phenomenology.

We were wary of showing data. Displays of data, particularly if they are two-dimensional and color-coded, are preoccupyingly evocative, yet they are no more objective than the instruments that collected the data, the algorithms used to reduce the data, and the conventions chosen to display the data. In the original papers, these displays are embedded in the context of the instruments, algorithms, and conventions, and it is ultimately better for the reader's own understanding to view them there; this essay can be a guide to the primary literature, but it cannot replace that literature. In short, we tried to present issues commensurately; words and pictures being incommensurate, we chose to rely on words. Yet we were naive to expect that we could communicate our ideas without sketches. Where the literature seemed to speak with one voice, we included a few sketches. It was our explicit intention not to show quantitative experimental information in them. The dangers are obvious. A line carelessly drawn in an odd corner of an explanatory diagram can suggest completely unintended things; a sketch interpreting measurements at two different places in space can imply things about the intervening regions that are untested or unsupported by observation. The figures and the captions accompanying them are the most speculative part of our essay.

It was vain to hope that we could present experimental results in a strictly commensurate fashion. In some cases, it wasn't even desirable. We will sometimes adopt the descriptive language used by the original observers to communicate the immediacy and individuality of their research; when we do that, we cannot always find a common terminology that links their results to others'. In some cases, we will reinterpret or rephrase original observations, in an attempt to find just such a common terminology. From time to time, we will purposely array individually persuasive results that, when taken together, do *not* lead to a consistent view, in order to convey that point by indirection.

This essay will challenge students who have not already been introduced to the magnetospheric and auroral literature. We refer to spacecraft and ground-based facilities without specifically identifying them; we introduce sophisticated terminology and conceptions in early sections and reserve amplification and detail for later. The observational literature is multiply connected, and we simply could not make our presentation of it linear. Like that literature, this essay cannot be read in one sitting, and it needs to be read more than once. Teachers may find the essay a useful adjunct to courses having to do with magnetospheric physics, though they will soon realize that our approach requires them to exercise their own pedagogical creativity in the exposition of basic conceptual material. We hope that it also allows them the freedom to do so. To both student and teacher, we can only plead that if we had stopped to explain, we would have obscured the threads of an already complex argument.

To appeal to experts, we tried to keep our discussion of the literature up-to-date, yet those experts who read this essay only a few years hence will be the first to wish it were up-to-date at that time. Some experts will differ with our selection of observational material; some would organize what we have selected in a different way. Our treatments of individual topics have to be less expert than any expert's, and each will wish for the deeper exposition of his own field that he is capable of. We could not regularize the inconsistencies in the literature, but we also will not always point them out, nor will we draw attention to the many areas where more research would be useful. These, we hope, will be obvious from our exposition. Where we succeed in being coherent, it is because expert research has reached clear conclusions. On the other hand, a lack of clarity on our part may only mean that we misunderstand what is clear to our more expert readers. (Those who wish to point our needed changes may wish to write to the author.) Despite our misgivings, the need for concise summaries compelled us to indicate where the preponderance of evidence has directed our own belief. It is in the nature of science that such summaries are provisional, and the experts will know precisely where and in what ways.

If there is a redeeming incentive to read on, it is that the observations juxtaposed here, in their variety, intricacy, and contradiction, express the fascination of contemporary research on the earth's magnetosphere, the scientific arena in which upper atmospheric science, geomagnetism, cosmic-ray physics, fluid mechanics, and plasma physics interact to form a subject entirely its own, with its own mythology and its own hundred-year history. The magnetosphere, the outer sphere of the earth's environment, is the astrophysical plasma about which we will always know the most.

Acknowledgments

I got an idea that an essay like this might be an interesting thing to do from my participation in the Crafoord Symposium honoring James A. Van Allen held in Stockholm in September, 1989. The essay began to take shape while I was a summer visitor at the Geophysical Institute of the University of Alaska in 1990, and inspired by its mission. The writing and discussions continued at Alaska in the summers of 1991 and 1992. I wish to thank the Geophysical Institute for its generous support, and its director, Syun-Ichi Akasofu, for his friendship, hospitality, and, most of all, his scientific counsel. Each year, I returned to UCLA fired with ambition to improve on what had been started in Alaska, and ultimately two-thirds of the thinking and writing took place in Los Angeles. In December, 1992, I was privileged to outline some of the fruits of my labors in the James A. Van Allen Lecture of the American Geophysical Union. Clearly, Van Allen's life and work have been an inspiration to me.

The whole field owes a debt to Syun-Ichi Akasofu, W. Ian Axford, and James W. Dungey, and no one more so than I. Magnetospheric research would not be what it is today without them. My personal debts to others are great. I was taught magnetospheric convection by Harry Petschek, to whom I owe a lifetime debt that can never be repaid. I benefitted from deep and constructive criticism in many searching discussions with Ferd Coroniti and Joe Kan. Coroniti's consistent interest in the substorm problem over 20 years has prompted and preserved my own, and Kan's careful exploration of his magnetosphere–ionosphere coupling model of substorms awakened my appreciation of many modern issues. I must also acknowledge NSF ATM-90-24363 not only for my personal support but also that of my colleagues Vassilis Angelopoulos and Rene Pellat; what is here about time-dependent flows in the plasma sheet was inspired by my work with them. Tony Lui read an early draft of this article, and pointed out numerous interesting research papers to me; Yuri Gal'perin read a more mature version, made many valuable comments, and again indicated ideas and references I had missed. Pu Song graciously provided me with a draft of his excellent review article on magnetosheath flow structures in advance of publication. Rob Elphinstone, Bill Feldman, Jack Gosling, Ed Hones, Matthew Kennel, Margaret Kivelson, Lou Lee, Bob McPherron, John Olson, Chris Russell, George Siscoe, David Southwood, and Chin-Chin Wu shared with me their considerable wisdom. By their questions, the students in seminar courses at the UCLA Institute of Geophysics and Planetary Physics and at Alaska's Geophysical Institute told me where the essay needed improvement, awakened me to fundamental issues, and reminded me of my responsibility to explain my subject. Finally, the participants in the Alaska Workshop on Substorms, September 18–21, 1991, and in the First International Conference on Substorms, Kiruna, March 23–28, 1992, conveyed to me their enthusiasm, their knowledge, and especially, their insights about substorms. Beyond what I owe to individuals and groups of individuals, my greatest debt of all is to the many hundreds of creative scientists who created the literature on convection and substorms. I freely used their best insights and ideas. Of course, the responsibility for the errors of fairness, citation, fact, interpretation, perspective, and understanding contained herein is entirely mine.

I would neither have started nor finished this book without the encouragement and advice of Melvin L. Schwartz. Many thanks also go to the staff of Oxford University Press, particularly to Laura Calderone and Jeff Robbins. The office staff of the UCLA plasma physics group, and particularly Melissa Licker and James Rose, were invariably helpful. Jackie Payne and James Rose helped me with the figures.

My wife, Ellen Lehman, was extraordinarily supportive throughout all my many months of professorial absentmindedness. She knows the ways in which this is her book.

Los Angeles C. F. Kennel
October 1993

This page intentionally left blank

CONTENTS

This page intentionally left blank

CONVECTION AND SUBSTORMS

This page intentionally left blank

1

INTRODUCTION

1.1 Geomagnetism

In the year 1600, the the man about to become physician to Queen Elizabeth I of England published a long treatise summarizing his two decades of experimentation on magnetism. After disposing of such issues as whether garlic causes magnets to "lose their virtue" William Gilbert recounted his observations upon moving a compass over the surface of a permanent magnet that had been specially fashioned in the form of a sphere (Gilbert, 1893, 1958). The similarity between the compass readings on the surface of his magnet and those recorded in mariners' charts led Gilbert to conclude that his magnet was a *terrella,* a little earth, and that our big earth is (among other things) a giant magnet. Gilbert's little earth organized the pattern of compass readings not only on its surface but also in the space surrounding it. From this, he boldly asserted that the big earth's magnetic influence continues far into empty space, where no mariner of his day could ever go. The profundity of this remark was not lost on Gilbert's younger contemporary, Johannes Kepler, who found in it an explanation of the earth's annual motion around the sun. Kepler reasoned more or less as follows (in modern language): Since the earth and the sun are both celestial bodies, they both should rotate, and they both should have magnetic fields surrounding them in space. Their two rotating fields interact somehow, somewhere, in the space between them, communicating the sun's rotational motion to the earth and pushing the earth around its orbit. In this curious way, Kepler might have been the first to perceive that the sun acts upon terrestrial magnetism. He was not the last.

In 1580, Kepler's teacher, Michael Maestlin, had recorded an observation of a distinct region of oscillating luminosity in the northern sky, an aurora. The aurora had been a topic of scientific interest since Graeco-Roman antiquity [of particular importance was Aristotle's (384-322 B.C.) discussion of it in his *Meteorology*], but it had become an object of superstition in the European Middle Ages, and scientific interest in it only began to re-emerge in the second half of the 16th century (Link, 1957). In 1621, the mathematician and astronomer Pierre Gassendi reported on a great display observed all over France (Gassendi, 1658). It was Gassendi who gave it the name *Aurora Borealis.* An 80-year period of unusually low geomagnetic activity (Maunder, 1890) had to pass before a new display stimulated the next scientific discussion of the aurora, Edmond Halley's report on the great aurora seen in London on March 16, 1716 (Halley, 1716).

Halley had the remarkable insight to see that its pattern of illumination had been organized by the earth's magnetic field. In 1733, the first treatise wholly devoted to the aurora was published by the French Academy of Sciences (de Mairan, 1733). In this book, J. J. de Mairan mentions the work of George Graham (1724), the first to document the short-term variability of the geomagnetic field from the relentless motion of the compass; Graham's discovery was later confirmed by Andreas Celsius (1740). From a study of more than 20,000 observations (on the average 20 per day), Celsius' colleague, Olav Hiorter, concluded that geomagnetic variability was caused by the aurora (Hiorter, 1747). ("Who could have thought that the *northern lights* would have a connection and a sympathy with the magnet?"[1]). Hiorter pointed out that Graham, in London, had detected magnetic variations at the same time as he had recorded variations and an aurora in Uppsala, the large spatial scale conveying the high altitude of the aurora. In his second edition, de Mairan (1754) referred to an auroral theory by Benjamin Franklin, who pictured hot tropical air rising and traveling at high altitudes to the polar regions where it created auroral lightning (Franklin, 1779; Chapman, 1967). Thus the analogy between electrical discharges and the aurora was established. Better understanding of auroral physics waited throughout the nineteenth century for better understanding of discharges. By the 1890s, with the analogy between discharges in a Crookes tube and auroral phenomena firmly in their minds, Scandinavian scientists concluded that the aurora was a form of cathode ray, that is, caused by electron bombardment of the earth's upper atmosphere (Hultquist, 1992). Kristian Birkeland (1896) noted that the cathode rays in his terrella experiments were absorbed mainly in the polar regions of the dipole field, explaining why auroras were so frequently observed at the high Norwegian latitudes rather than at lower latitudes where most European scientists lived. Beginning in 1907, C. Stormer (1907) studied the phenomena mathematically by considering the motion of single charged particles in the earth's dipole field and so laid the foundations of the field of cosmic-ray trajectories.

A fairly complete chronology of sunspots and of auroral displays in Europe existed from the time geomagnetic activity resumed in 1710 (Link, 1957). A century later, Alexander von Humboldt advocated that geomagnetic observations be made simultaneously over the globe, and in 1836, C. F. Gauss and W. Weber organized a group of European observatories to take readings every 5 minutes during four prearranged 24-hour intervals each year. The results for 1836–1841 were published (Chapman and Bartels, 1940). From 1846 on, essentially continuous observations of the earth's magnetic field were made (e.g., Moos, 1910). It was then that relationships between solar phenomena, magnetic storms, and other geomagnetic disturbances began to be noted. J. A. Broun (1858) found a 27-day recurrence period in geomagnetic disturbances, the same as the sun's rotation period. Magnetic storms were catalogued, 276 between 1882 and 1903 alone (Chapman and Bartels, 1940). The sunspot cycle was discovered by Schwabe about 1844, and by 1851, its association with magnetic disturbances and storms was discussed (Chapman, 1967). However, precisely how the sun interacts with the earth's magnetic field was still not much clearer than it had been to Kepler.

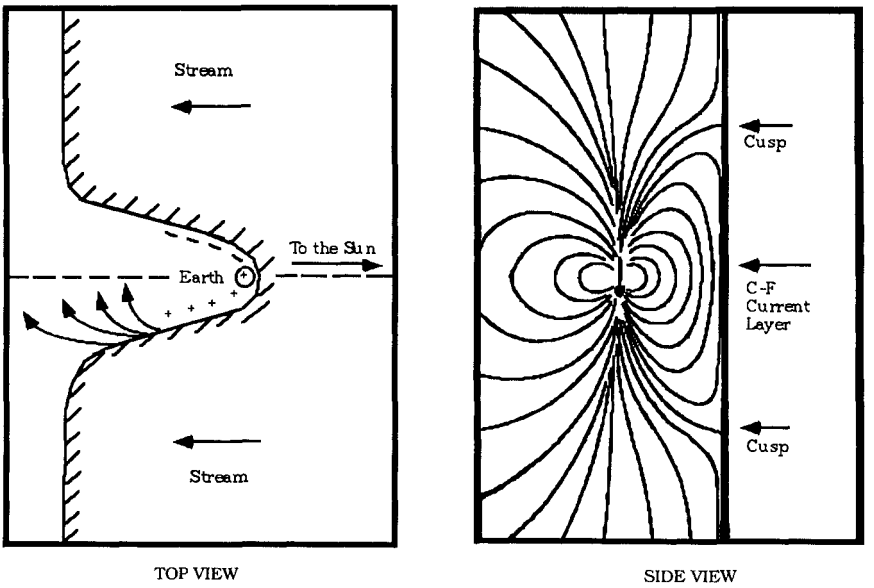

Figure 1.1. A New Theory of Magnetic Storms: Chapman and Ferraro (1930-1933). Shown here are two sketches adapted from Chapman and Ferraro's original papers (1931a,b). The right-hand panel shows the magnetic field in the the noon-midnight meridian plane viewed from the dawn-side. An unmagnetized, electrically neutral stream of charged particles has swept up all the magnetic flux of the earth's dipole and confined it behind a current layer [later named the Chapman-Ferraro (or C-F) layer]. There is no magnetic field upstream of the layer, and the field strength on the earthward side of the current sheet is twice its dipole value. The geomagnetic field has neutral points on the surface of the current layer labeled "cusp." Somewhat later, the stream has passed beyond the earth, and the C-F layer has bent around the earth (left panel), still confining the earth's magnetic field inside it. Some charged particles ought to get inside the current layer on the night-side, where they will move earthward under the influence of a dawn-dusk polarization electric field. Ultimately, they will form a ring current that depresses the strength of magnetic field measured on the ground.

The connection was so utterly mysterious that it attracted a prominent skeptic. In an important address to the Royal Society, Lord Kelvin (1892) asserted that the correlation between solar and terrestrial phenomena was a "mere coincidence," that the "supposed connection between magnetic storms and sunspots is unreal" (cf. Meadows, 1966).

On September 1, 1859, R. C. Carrington (1860) made the first sighting of a solar flare, one so intense that it could be seen against the total white light of the sun. One or two days later, Carrington learned from Balfour Stewart that there had been a brief magnetic disturbance at the time of the flare, and that a violent magnetic disturbance had begun about 18 hours later (Stewart, 1861). A great auroral display was seen in Europe, North and South America, Hawaii, the West

Indies, and Australia on that day (Loomis, 1860). Probably the greatest display on record occurred on February 4, 1872, when aurorae were seen in Bombay, Egypt, Santo Domingo, Guatemala, the West Indies, and the islands of Reunion and Mauritius (Chapman, 1967; Siscoe, 1976). The peak of the storm came during night-time in Europe, and the sky became bright with activity from Sicily to Scandinavia and from Ireland to the Ukraine. Disruption of telegraphic communication was extensive and nearly total. The third great storm of this period, on November 17–21, 1882, coincided with the passage across the solar disc of the largest sunspot group of its cycle (Chapman and Bartels, 1940).

George F. Fitzgerald (1892) and Sir Oliver Lodge (1900) argued that "a torrent or flying cloud of charged atoms or ions" emitted from sunspots caused the magnetic storm. The storm begins with a worldwide "sudden commencement," in which the geomagnetic field abruptly increases by 10–30 nT over its quiet day value. The enhanced magnetic field endures for anywhere from 1 to 10 hours, albeit with variations. In the main phase, the field magnitude drops below the quiet day value by 200 to 2000 nT in the great storms. A recovery phase follows, in which the field recovers on a few-hour time scale and then with a time scale of a day, the last vestiges of the storm disappearing after about a week. The speed of the "torrent or flying cloud" can be judged from the delay between the solar flare and the sudden commencement, or by how much the spot group has rotated from the central meridian of the sun at the time of the sudden commencement (Fitzgerald estimated an average speed of 300 miles/s using this method). Fitzgerald and Lodge's suggestion led directly to the notion that the main phase was due to the development of electrical currents flowing near the earth that were fed by the charged particle streams coming from the sun (Schmidt, 1917; Chapman, 1918, 1919, 1923). The name of Sydney Chapman, which made its first appearance at this time, would be prominent in the field for half a century.

At first, it was thought that the "torrent or flying cloud" contained flowing charges of only one sign, as in electrical discharges, but Schuster (1912) pointed out that electrostatic repulsion would disperse the streams as they traversed the huge distance from the earth to the sun. Consequently, F. A. Lindemann (1919) proposed that the intermittent solar streams consisted of equal densities of charges of both signs and were electrically neutral. This suggestion has to rank as one of the starting points of the modern science of space plasma physics. A decade later, S. Chapman and V. C. A. Ferraro (1930, 1931a,b,c, 1933) realized that the neutralized solar streams would not reach the upper atmosphere directly, but would be deflected around the earth by a strong current that develops at a thin interface separating the solar particles from the geomagnetic field. The geomagnetic field would carve out a temporary "hollow" in the solar stream, shielding the earth from direct bombardment by most of the solar particles. Chapman and Ferraro did not know whether the magnetic hollow would be open or closed on the side of the earth away from the sun, but they reasoned that the solar particles would approach the earth from the nightside and current would eventually envelop the earth to create the storm main phase.

1.2 The Discovery of the Solar Wind and the Magnetosphere

The era of geomagnetism ended and the era of space research began in 1957, the International Geophysical Year. One can feel the pace of discovery quickening even as the pioneering decade opened. In 1950, Hannes Alfven (1950) published his *Cosmical Electrodynamics*, which summarized major conceptual advances in magnetohydrodynamic and particle orbit theory that guide the field to this day. In 1951, D. F. Martyn (1951) estimated the size of the "geomagnetic hollow." He located the Chapman–Ferraro boundary at the distance where the pressure of the geomagnetic field balances the solar stream's dynamic pressure. The "hollow" soon seemed not to be so hollow: L. R. O. Storey (1953) adduced evidence that Very Low Frequency lightning whistlers propagated along geomagnetic field lines between hemispheres, something not possible unless ionospheric plasma expanded to fill the magnetic tubes of force to distances of several earth radii. In other words, the space surrounding the earth had to be permanently filled with plasma. James W. Dungey (1954, 1955) proposed that the sheared flow at Chapman and Ferraro's boundary would lead to a collisionless version of the fluid-mechanical Kelvin–Helmholtz instability, possibly generating the so-called "micropulsations" of the geomagnetic field that accompany magnetic storms. By the end of the decade, the very first American and Soviet spacecraft had found belts of highly energetic particles trapped deep within the expected position of the Chapman–Ferraro boundary (Vernov et al., 1958; Van Allen, 1959), prompting Thomas Gold (1959a,b) to coin the picturesque and apt name *magnetosphere* for what seemed no longer an empty, passive hollow.

By that time, it was clear that the solar stream was there all the time. The change in perception came about because of comet tails. In the seventeenth century, Isaac Newton pointed out that the alignment of comet tails in the antisolar direction might be evidence that comets move through a resisting ether that fills the solar system. In the nineteenth century, after Maxwell's electromagnetic theory, it was argued that the alignment was due to the action of solar radiation pressure. Fitzgerald (1900) concluded from the simple observation that stars were visible through the comet tails that the tails could not absorb enough solar light to align them; Wurm (1943) later came to the same conclusion. Just before the space age opened, Ludwig Biermann (1951, 1953, 1957) proposed that momentum transfer from a continuous flow of solar corpuscular radiation was responsible for the alignment.[2] If so, the intermittent solar corpuscular stream responsible for magnetic storms was not so intermittent after all. Gold (1955) argued that the suddenness of storm sudden commencements was not because the solar stream turned on and off but because it developed shock waves. This had the important implication that even though the plasma streams were collisionless, they somehow had enough dissipation to make shock waves and that one could treat them as fluids. Using a fluid theory, Eugene Parker (1957) showed that Biermann's continuous flow was due to a steady expansion of the solar corona into space. Only 3 years passed before the first confirming observations of what Parker called the

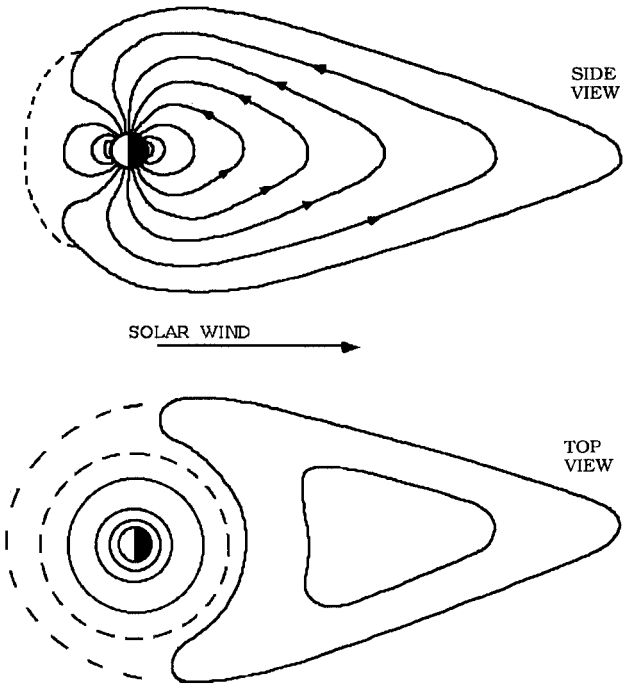

Figure 1.2. The Teardrop Magnetosphere. This sketch is adapted from Francis Johnson's original paper (1960). In the top panel we view the magnetic field in the noon-midnight meridian plane from the evening side. In the bottom, we see the teardrop from above the north geomagnetic pole. All the flux of the geomagnetic dipole field is confined within a teardrop-shaped cavity whose dimensions on the dayside are set by the balance of magnetic field and solar wind pressure, and whose night-side closure distance is set by the reexpansion of the heated solar wind. The closure distance is of the order of the sonic Mach number of the solar wind times the distance to the dayside magnetopause. Note that Chapman and Ferraro's cusp region has opened up and now extends all the way to the high-latitude ionosphere on the dayside. F.S. Johnson, *J. Geophys. Res. 65*, 3050 (1960), copyright by the American Geophysical Union.

"solar wind" were reported. In 1960, sensors on Luniks 2 and 3 and Explorer 10 collected tentative evidence of a continuous supersonic solar wind, and decisive Mariner 2 results were reported 2 years later (Neugebauer and Snyder, 1962).

All this had important implications for the magnetosphere. Ferraro (1960) proposed that the Chapman–Ferraro geomagnetic cavity might extend to infinity on the nightside (since the solar wind went on forever), but Francis Johnson (1960) pointed out that gas-dynamic re-expansion of the compressed solar wind would close the magnetospheric cavity at a finite distance downstream. Johnson's magnetosphere had a teardrop shape. Shortly thereafter, W. Ian Axford (1962) and Paul Kellogg (1962) argued that a collisionless bow shock wave would stand upstream of what by then was clearly a permanent magnetosphere. In only 5 years,

the term *solar wind* had completely supplanted *solar corpuscular stream* and its variants.

The actual discovery of the Chapman–Ferraro layer did not seem anticlimactic when it finally occurred, certainly not to Chapman, who lived to see it (Chapman, 1966). Ness (1967) has recounted the sequence of events. The first measurements of the outer region of the magnetosphere were made in 1958 on the Pioneer I spacecraft (Sonett et al., 1960). The data transmission was discontinuous and covered only the geocentric distance ranges 3.7–7 and 12.3–14.8 R_E (earth radii) on the sunward side of the earth. The data obtained closest to earth indicated that the geomagnetic field was approximately dipolar. The second transmission indicated an abrupt decrease of field magnitude and a substantial increase of rapid fluctuations. The boundary of the magnetosphere evidently fell into the data gap, about 10 R_E upstream. Moreover, the plasma beyond the boundary was both magnetized and turbulent. The same behavior was observed on Pioneer 5 in 1960; the first detection of the boundary itself was made in March 1961 by Explorer 10. The boundary was observed to move back and forth many times across the orbit of the spacecraft over an interval of 48 hours. When the magnetic field was strong, plasma was absent; when the plasma was present, the field was weaker and much more variable. The magnetic field on the magnetospheric side of the boundary was larger than predicted by the extrapolation of the dipole field to the spacecraft distance. The first measurements of trapped particles, fields, and plasmas at the boundary of the geomagnetic field were carried out late in 1961 by Explorer 12 (Cahill and Amazeen, 1963). The termination of the geomagnetic field was coincident with the termination of the trapping of energetic particles and the appearance of low-energy plasma of solar wind origin that had been thermalized upon crossing the bow shock.

The long-awaited discovery of the boundary of the geomagnetic field had been the work of many hands, and Chapman and Ferraro's layer needed a new, more modern, more objective name. A very good one was already waiting in the wings: the *magnetopause* (Hines, 1963).

1.3 Viscous Convection

We have now arrived at the starting point of our story. Gold (1959a) had already pointed out that, while magnetic lines of force may be frozen in the interior of the earth, and while they may be frozen into the plasma in the ionosphere, they are not frozen into the neutral atmosphere, and as a result two lines of force can be interchanged in a continuous manner. Thus plasma motions inside the magnetosphere would not be stifled by the high conductivity of the earth. Following this up, Axford and Colin Hines (1961) then proposed that a collisionless interaction that mimics viscosity in the sheared flow near the magnetopause drives a general circulation of plasma throughout the magnetospheric cavity. They called this *internal magnetospheric convection*. In Axford and Hines' picture, plasma and field lines were dragged by the solar wind from the dayside to the nightside along

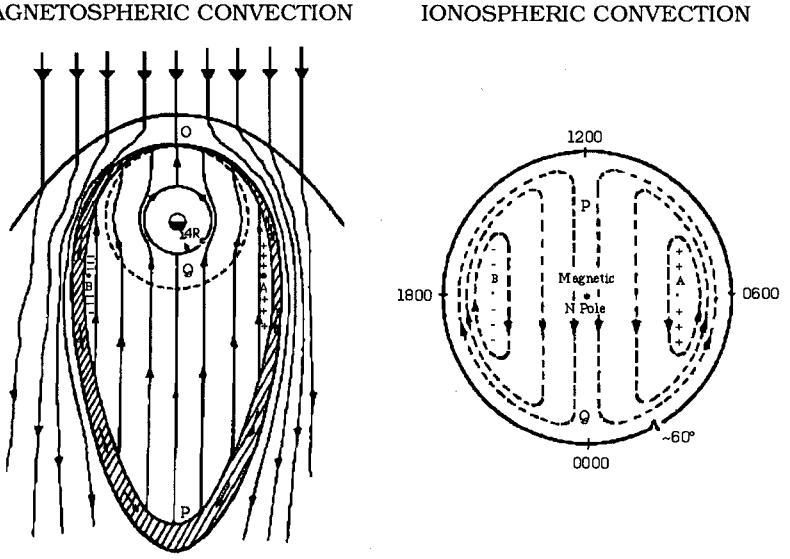

Figure 1.3. Viscous Convection. These two sketches are based upon Axford and Hines's original paper (1961). The left-hand panel shows a cut through the equatorial plane of the magnetosphere viewed from above the north pole, and the right-hand panel shows the northern high-latitude ionosphere. On the left, we see a teardrop magnetosphere standing in the solar wind with a collisionless bow shock upstream of it. Viscosity exerts a tangential stress at the magnetopause, which drags the plasma tailward in a thin boundary layer (shaded). Eventually, the tension in the stretched magnetic field lines overcomes the tangential stress due to viscosity and the field lines and the plasma contained in them flow back towards the earth in the center of the tail. This flow corresponds to a dawn-dusk electric field. The flow avoids the region closest to earth, where, it will soon be realized, the plasmapause forms. Because the magnetosphere is symmetric about the noon–midnight meridian, there will be two convection cells. These map down into the ionosphere as two convection cells (right-hand panel) with anti-sunward flow at high latitudes and sunward flow in the auroral zone at low latitudes. Field-aligned currents will flow into the region marked "A" and out of the region marked "B," and the convection electric field is directed from "A" to "B." Reproduced by permission of the National Research Council of Canada from the *Canadian J. of Phys. 39,* 1441 and 1446 (1961).

what are today called the *low-latitude boundary layers*. Because the earth–solar wind interaction is symmetric about the noon–midnight meridian plane, there would be two boundary layers and two convection cells. In each cell, plasma that reached the nightside returned back to the dayside in the interior of the magnetosphere. So, solar wind energy first approached the earth not from the direction of the sun but from the nightside.

The aurora is most intense and active at night even though the sun is the ultimate source of the energy for geomagnetic activity. Why this is so had been a long-standing puzzle. Axford and Hines' (1961) model linked nightside auroral activity to magnetospheric convection, and convection to the solar wind, which in

its turn extended all the way back to the sun. The model also retained the connection between magnetic storms and solar activity that had been the principal attraction of the Chapman–Ferraro model. The Axford and Hines picture made it explicit that particles convect toward the earth from the nightside and, in doing so, gain energy from the convection electric field; some of these eventually end up on closed orbits and drift completely around the earth, thereby populating the so-called "ring current." The ring current in turn is responsible for the strong depression of the geomagnetic field that had been the defining signature of the magnetic storm for 2 centuries. In short, the once utterly mysterious relationships between geomagnetic, auroral, and solar activity were one step further along the way to being understood.

All in all, three important ideas stemming directly from Axford and Hines' (1961) paper have stood the test of time. The first was simply the perception that the solar wind drives magnetospheric convection, with all the implications outlined already (and to follow). The second idea was that magnetospheric convection maps into the high-latitude ionosphere, and is responsible for the auroral electrojets and the motions of ionospheric irregularities. Axford and Hines (1961) described convection in terms of "E x B" particle motions in crossed electric and magnetic fields. If the convection is steady, the electric field will be uniform and directed from dawn to dusk. If the plasma is cold, the flow streamlines in the magnetic equatorial plane are equipotentials of this field. Even a small plasma density is sufficient to ensure that each magnetic field line is an equipotential. The convection electric field then maps along field lines into a dawn–dusk electric field in the ionosphere. The mapped E x B flow in the ionosphere will also comprise two symmetric cells, with antisunward flow over the polar caps and sunward flow at auroral latitudes. The flow should divide in the night–side auroral oval, turning westward before local midnight, and eastward after local midnight. This agreed with what Axford and Hines (1961) already knew: that co-moving density irregularities generally drift westward before midnight and eastward afterwards. A Hall current directed opposite to E x B should flow between 100 and 130 km altitude because collisional drag with neutrals reduces the ions' drift speeds essentially to zero, while electrons continue to drift at the E x B speed. The general behavior of the auroral electrojet currents, eastward before midnight, westward after midnight, was consistent with the motions of the density irregularities on the nightside. It took only a decade for the entire two-cell convection to emerge from averages of global measurements of the electric field made by OGO 6 and Cosmos 184 polar orbiting spacecraft (Heppner, 1972b,c, 1977; Galperin et al., 1974).

In retrospect, magnetospheric convection and its mapping to the ionosphere are fairly straightforward applications of magnetohydrodynamic reasoning. However, Axford and Hines' (1961) third idea, that a collisionless process with properties reminiscent of fluid viscosity operates at the magnetopause, invoked a statement of faith about a physical effect that still does not have a generally accepted explanation today. Another point is important in retrospect. Even though viscous convection was a concept born in musings about the effects of magnetopause instability and turbulent transport, the first sketch of the viscous

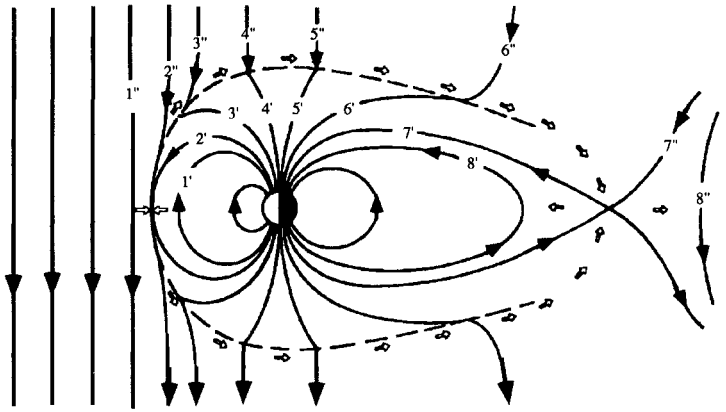

Figure 1.4. The Reconnection Model of the Magnetosphere. This is Dungey's (1961a) original sketch showing the effects of reconnection on a teardrop magnetosphere. Here we view the magnetic field in the noon–midnight meridian plane from the evening side, with the solar wind flowing towards the earth from the left. The bow shock is not shown and is not necessary to the argument. The magnetic field in the solar wind is due south. Eight field lines, marked 1", 2", . . ., if they connect to the sun, and 1', 2', . . ., if they connect to the earth, have been singled out to illustrate the circulation of the flow at key moments in time. At time 1, the closed field line 1' is convecting towards the subsolar magnetopause, while its eventual partner 1" is flowing with the solar wind to the earth. They meet at the subsolar magnetopause where they reconnect (2" to 2'). The tension in the newly reconnected field lines accelerates the plasma over the polar cap (3'–3", 4'–4", 5'–5"). The solar wind (arrows) continues to drag the flux tubes, extending the geomagnetic field into a long tail on the night side (6'–6"). The stretched field lines, now oppositely directed in the northern and southern tail lobes, reconnect a second time in the tail (7'–7"). The reconnection heats the plasma, creating a hot plasma sheet, and sends flow (arrows) towards the earth (8') and tailward (8") back into the solar wind. In the fullness of time, line 8' will convect to where 1' is and the convection cycle will start again. J.W. Dungey, *Phys. Rev. Lett. 6*, 47 (1961) copyright by the American Physical Society.

convection pattern showed a laminar flow. This paradoxical drawing has influenced our thinking to the present day.

1.4 Reconnection-Driven Convection

In 1961, Dungey (1961a) set forth his own convection model, in which the dissipative interaction with the solar wind was not due to viscosity, but to resistive reconnection of the interplanetary and geomagnetic fields at the dayside magnetopause. Dungey, stimulated by Giovanelli's (1947) and Hoyle's (1949) observation that solar flares frequently occur near magnetic neutral regions, had earlier proposed an x-type neutral line mechanism for particle acceleration, the

development of sheet currents, and energy release in solar flares (Dungey, 1953, 1958). So, once he learned that the solar wind was magnetized, he realized that an x-type neutral point would form on the dayside magnetopause on those occasions when the interplanetary field was southward, the direction opposite to the earth's field at the magnetopause. Reconnection at this neutral point could then set the plasma inside the magnetosphere in motion.

In Dungey's model of convection, solar wind plasma and energy enters the nightside of the magnetosphere flowing antisunward over the geomagnetic poles in what are today called the *plasma mantles* (Levy et al., 1964). In either the reconnection or the viscous convection model, the convecting plasma should return to the dayside on closed field lines, and there is a basic two-cell pattern of convection in the high-latitude ionosphere. Despite this similarity, the models could be easily distinguished. Dungey's reconnecting magnetosphere had to have a specific structure. Open field lines had to connect the earth's magnetic polar caps directly to the interplanetary magnetic field. There had to be a long, low-density magnetic tail, with a current layer separating its northern and southern lobes. Surrounding the current layer there would be a sheet of heated plasma convecting earthward on closed field lines. There would be a magnetic neutral line that terminates that plasma sheet, and tailward flow on open field lines downstream of that neutral line. Another telltale sign would be for strong convection to correlate with southward interplanetary magnetic field.

The key question for the credibility of Dungey's model concerned the rate of reconnection, the subject of the next section.

1.5 Petschek Reconnection

Sweet (1958) was the first to propose two oppositely directed magnetic fields pressed together in a plane sheet as a reconnection configuration. When the plasma pressure separating two regions of oppositely directed field is insufficient to keep the fields apart, the fluid is squeezed from in between, and the two fields approach one another. The magnetic field gradient steepens and eventually the current density becomes so large that there will be strong resistive dissipation no matter how small the electrical resistivity. The topology of the magnetic lines of force, which is fixed in the highly conducting fluid elsewhere, is broken by the dissipation in the thin layer between the oppositely directed fields. The magnetic field lines diffuse across the resistive layer and reconnect. The Maxwell stresses in the new field configuration accelerate the fluid parallel to the plane of the resistive layer, thereby evacuating the resistive layer and permitting new plasma and new magnetic flux to be brought forward to be reconnected. Unfortunately, Parker (1957a, 1963) and Sweet (1958) concluded using dimensional arguments that the reconnection rate would scale as the square root of the resistivity, which would make it much too small to be significant if the resistivity were based upon Coulomb collisions.

It was natural to ask whether other configurations might produce faster reconnection. Chapman and Kendall (1963) solved the nonlinear equations of ideal

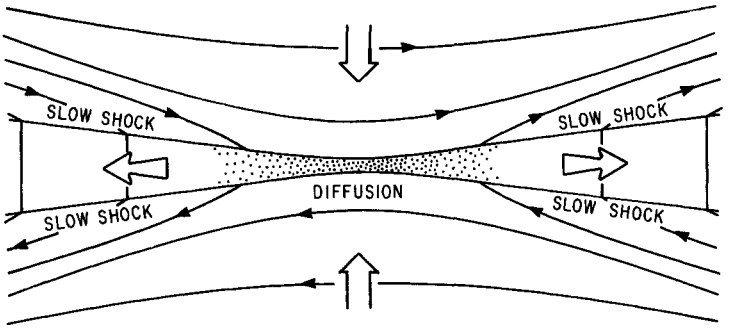

Figure 1.5. Petschek Reconnection. This sketch is adapted from Petschek (1964). Shown is the simplest MHD reconnection configuration, in which the plasmas have identical properties on either side of the reconnection layer, except that the magnetic fields are antiparallel. The two plasmas flow towards one another at a rate that is limited by the rate of resistive diffusion in the small region at the center and the rate of escape of plasma downstream of the pairs of switch-off slow shocks that attach to the resistive region. The component of magnetic field tangential to the shock plane is zero downstream of a switch-off shock. The magnetic tension across the slow shocks accelerates the escaping plasma to approximately the Alfven speed upstream. Plasma and magnetic flux flow into the diffusive reconnection region at a speed that depends upon the logarithm of the resistivity, and is about 10% of the Alfven speed upstream.

The important point is that reconnection in a small region organizes the larger surrounding flow field via MHD waves. A generalized Petschek solution using more standing waves can be constructed when the plasma properties on either side of the reconnection region differ and the magnetic fields are not strictly antiparallel. In general, one expects to find intermediate and slow shocks of differing strengths on either side of the reconnection region, and a slow rarefaction on the low density side. National Aeronautics and Space Administration.

magnetohydrodynamics and found that an x-type neutral line is unstable on the time scale for an Alfven wave to traverse the system. Petschek (1964, 1966) realized that waves propagating along MHD characteristics will preadjust the overall flow configuration to the change in magnetic topology taking place in a small reconnection region. He constructed a fully nonlinear model of steady reconnection in which a diffusive magnetic neutral region that looked planar in the small would generate an x-like configuration of standing shock waves in the large. Petschek showed that magnetic flux and plasma could flow into this reconnecting structure at about 20% of the Alfven speed, a rate fast enough to be interesting.

Let us recapitulate Petschek's arguments. An active reconnection region will notify its surroundings of the change in magnetic topology and stress configuration taking place by stimulating magnetohydrodynamic waves to propagate along the characteristics of the exterior flow. Which waves are radiated depend upon the boundary conditions on either side of the reconnection region, but in all cases, resistive diffusion creates the actual region of reconnection. At the reconnection point, the normal component of the magnetic field is zero by the symmetry of the problem, and it will be small in the neighborhood of the origin.

Since the propagation speeds of the intermediate and slow MHD waves are proportional to the normal magnetic field component, the wave speeds will be small in this neighborhood. Locally, therefore, the flow will be controlled by diffusion. However, the normal component will increase with distance from the diffusion region until it is large enough that wave propagation becomes faster than diffusion. Beyond that point, waves predominate; viewed in the large, standing waves form an x-type configuration about the diffusion region. If the waves steepen into shocks, dissipation takes place over a region much larger than where diffusion dominates, and overall will exceed that in a plane sheet of the same dimension. The reconnection rate scales as the logarithm of the resistivity, not the square root..

If Dungey (1961a) had pointed out that reconnection between the interplanetary magnetic field and the geomagnetic field would occur in the first place, it was Petschek and his co-workers who first elucidated the structure of a reconnecting magnetosphere in terms of the basic principles of magnetohydrodynamics (Levy et al., 1964; Axford et al., 1965, Kennel and Petschek, 1969). Their strategy was to extend to the whole magnetosphere the system of wave structures generated by reconnection at the nose and in the tail of the magnetosphere. The program they started has not been fully completed: We still have not articulated fully how changes in magnetospheric state are transmitted along MHD characteristics in different circumstances. Part of the difficulty has been visualizing the three-dimensional behavior of the magnetosphere, part in computing it numerically with sufficient resolution to trace out characteristic families. Certainly, the MHD approximation is not always valid, nor will it always produce quantitatively accurate predictions, but it is the one conceptual tool we have to connect observations made at distant points in space with one another, our only guide to understanding the causal order of magnetospheric events. We continue to use it for guidance.

1.6 Substorms

It was apparent at once that the steady version of Dungey's convection model could not be realistic. The solar wind is variable, and it is difficult to find periods of calm. If anything, the direction of the interplanetary magnetic field is more variable than anything else in the solar wind; so Dungey's magnetospheric convection should be rarely if ever in a steady state. The question was, would the magnetosphere simply follow with some delay the changes of the interplanetary field, or would an additional pattern of time dependence be interposed between the variability of the solar wind and the magnetosphere's direct response to it? This question was already influencing the climate of thought at the time that Syun-Ichi Akasofu (1964) arranged all-sky camera observations of the complex time dependence of the aurora into the auroral substorm.

Kristian Birkeland (1908) had tried to classify magnetic storms into five types, one of which was the "polar elementary storm." Sydney Chapman preferred a slightly different name, "polar magnetic substorm," because it communicated the

idea that magnetic storms often develop in a sequence of smaller intensifications. Chapman had also understood that the polar magnetic substorm had an auroral counterpart, the "auroral substorm." Inspired by Chapman, Akasofu (1964) outlined a characteristic sequence of auroral events that accompanies polar magnetic substorms. When there has been magnetic quiet for about 3 hours, the evening aurorae settle down into several quiet and homogeneous arcs that drift slowly equatorward. Discrete and diffuse auroral forms in the polar cap gradually disappear. The substorm onset is defined by a rapid brightening of the most equatorward auroral arc typically just before local midnight. Within a minute or so, the westward electrojet current intensifies, a very bright aurora develops at its westward extremity, and both aurora and electrojet would surge poleward and westward. This phenomenon, one of the most repeatable features of the premidnight sector substorm, is called the *westward traveling surge*. The surge marks the westward end of an expanding "bulge" of bright aurora. The onset of Akasofu's substorm was thus followed by an "expansion phase," which could last 10–30 minutes and terminated when the auroral bulge achieved its maximum poleward extent. The expansion phase was followed by a typically longer recovery phase, during which time quiet auroral arcs reform and start to migrate equatorward again. The recovery phase could last a variable length of time, that is to say, until the next substorm. Ultimately, the fact that isolated auroral substorms also occur in otherwise quiet geomagnetic periods made it clear that substorms were independent of the magnetic storm. Today, Birkeland's original name seems more appropriate, but we continue to use the term *substorm.*

In 1966, Fairfield and Cahill (1966) established that substorm occurrence is statistically correlated with southward interplanetary field, and therefore that substorms have something to do with the stimulation of convection. Since that moment, convection and substorms have been locked in mutual embrace, yet we still have no clear idea how they are related. The two have different heritages; we might even go so far as to say they are genetically different. Convection, which is based on magnetohydrodynamics, promises to lead to quantitative content, while the substorm is a purely phenomenological construct. Convection deals with the large-scale structure of the magnetosphere and the circulation of plasma and energy in it. To those who first thought about convection, the ionosphere was a tiny passive screen on which magnetospheric motions were imprinted. In contrast, the violent and spectacular phenomena that first defined the term *substorm* all took place in the auroral ionosphere, and no knowledge of their magnetospheric counterparts was needed to perceive the pattern of auroral events that is the substorm. The challenge has been to tie together the profoundly different scales and physics of the magnetosphere and ionosphere so as to understand the relation between magnetospheric convection and auroral substorms.

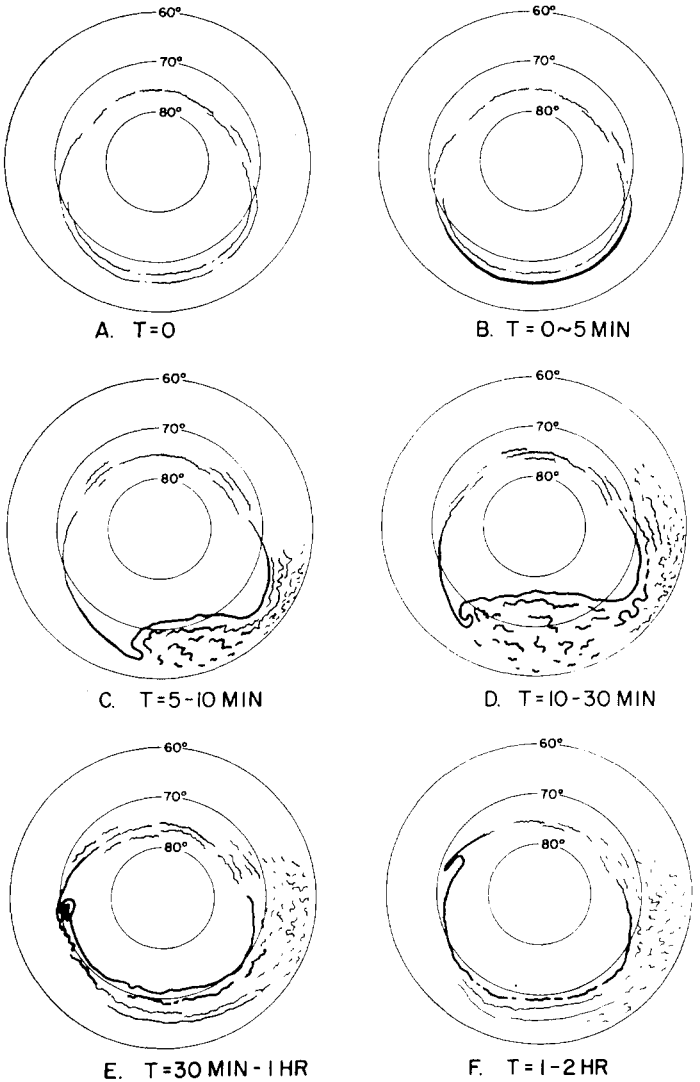

Figure 1.6. The Auroral Substorm. The sketch of the auroral substorm that was first drawn by Akasofu (1964) is still shown at professional meetings today and not only for its historical interest. Before the substorm starts (T = 0), the polar cap darkens, and quiet auroral arcs migrate equatorward. The substorm onset is defined by the brightening of the most equatorward arc on the night side (T = 0–5 min). A region of bright aurora then expands poleward of the site of the most equatorward arc; the westward extremity of this "auroral bulge" is the so-called *westward surge* (T = 5–10 min). The auroral expansion is said to end when the auroral bulge has reached its maximum poleward extent (T = 10–30 min); north–south aligned auroral fragments are visible equatorward of the poleward border of the auroral bulge, and activity has spread to the morning sector. The poleward border of the auroral retreats equatorward during the recovery phase of the substorm as the auroral activity equatorward of it subsides (T = 30 min–1 hr, T = 1–2 hr). Copyright by D. Reidel Publishing Company, reprinted by permission of Kluwer Academic Publishers.

1.7 Overview

This essay is divided into four parts. Chapters 2 and 3 describe how the magnetosphere might appear and behave if there were no convection and no substorms. Chapters 4 through 10 are devoted to magnetospheric convection. A simple model of substorms suggested by convection theory is evaluated observationally in Chapter 7, but we reserve a detailed discussion of substorm observations to Chapters 11–15. We discuss the relationship between convection and substorms in Chapter 16.

We will present our observational material in layers. In Chapters 2 and 3, we discuss the equilibrium structure of the magnetosphere and how the magnetosphere would respond to the variability of the solar wind in the absence of viscosity and reconnection. The usefulness of the viscous and reconnection models of convection depends on the extent to which between them they organize the observations of magnetospheric structure. To illuminate their powers as co-paradigms, in Chapters 4 and 5 we describe the dynamics of the magnetosphere that would occur if only one of the two mechanisms acted at a time. In Chapter 4, we discuss the kinds of observations that tell us most about the viscous interaction with the solar wind and its consequences. Although reconnection phenomena are undoubtedly mixed into many of the observations we discuss, we hope that Chapter 4 will convey an overall impression of how the magnetosphere would behave if there were only anomalous viscosity. In Chapter 5, we present observational tests of the reconnection model's most important predictions about the structure of the magnetosphere. Most of the material discussed in Chapter 5 is very familiar, but it still conveys why the reconnection model was so compelling when it was first proposed.

The steady reconnection model inspired a variety of approaches to the study of how the magnetosphere responds to the short-term variations of the interplanetary field. The simplest approach for the experimentalist was to ask if the state of the magnetosphere correlates statistically with the direction of the interplanetary field (Chapter 6). The simplest for the theoretician was to ask how the magnetosphere reacts to an isolated, sudden southward turning of the interplanetary field. The attempts to answer this question led to the reconnection model of magnetospheric substorms discussed in Chapter 7. In Chapter 8, we move on to discuss the time-dependent, "bursty," convection that is actually generated at the dayside magnetopause by reconnection, without referring to the deeply patterned modes of thought that have characterized substorm research. There is no mention of viscous phenomena in Chapters 7 and 8. Finally, in Chapter 9, we arrive at a perception of bimodal plasma sheet convection, wherein a highly intermittent, high-speed reconnection flow is interspersed with an ever-present irregular low-speed flow, presumably connected with viscosity. Chapter 10 takes up observations of convection during intervals of northward interplanetary field, when the effects of reconnection are minimized and the more subtle effects field, when the effects of reconnection are minimized and the more subtle effects of viscosity may eventually emerge without competition.

Even in Chapter 7, there will have been no mention of detailed substorm observations. These are reserved for Chapters 11–15. Chapter 11 introduces the concept of the auroral oval, the geographical arena in which the drama of the substorm is played out (Chapter 12). The substorm events in the auroral oval ionosphere have close counterparts in phenomena that take place in the region first explored by spacecraft in geosynchronous orbit (Chapters 13 and 14). The substorm does not unfold completely without reference to contemporaneous conditions in the solar wind (Chapter 15), but overall, the whole tone and texture of our discourse changes so much between Parts 1 and 2 that we are led to conclude that the substorm onset and expansion are more likely to be coupled to the dayside magnetopause than they are to most convection events occurring in the tail (Chapter 16).

1.8 The Equilbrium Magnetosphere

Having outlined how we will approach our subjects overall, we can describe the individual chapters in more detail.

Our conceptual starting point is also where the field started, with the *teardrop magnetosphere* (Section 2.2). This picturesque term describes the form the magnetopause would acquire in an unmagnetized solar wind of finite temperature when neither viscosity nor reconnection are active at the magnetopause. By far, the most consequential observational property of the magnetopause is its position. Once the position and shape of the magnetopause are given, for example, standard hypersonic flow theory slightly modified for MHD effects successfully predicts the position and shape of the bow shock (Section 2.5), and full MHD theory predicts that standing intermediate and/or slow shocks and a slow rarefaction wave also stand in the magnetosheath upstream of the magnetopause (Sections 2.6 and 2.7).

Concerning the physics of the magnetopause, the first thing people asked was whether its position and shape were in accord with the Chapman–Ferraro model. The location of the magnetopause is set by the balance of pressure between the variable solar wind and the earth's dipole field; so this question can only be answered statistically (Section 2.3). In the absence of viscosity and reconnection, the magnetopause would be a tangential discontinuity, a simple current layer separating the magnetosheath flow from the interior geomagnetic field. Because the magnetopause never stands still, its thickness could be estimated only after we knew its speed (Section 2.4). The thickness turned out to be several ion Larmor radii, which, since it was much larger than the collisionless skin depth, indicated that the magnetopause was not free of dissipation. Indeed, the ceaseless motion of the magnetopause told us at once that its physics was far more complex than we had originally envisioned. It is also far richer in implication. As our story unfolds, we will see ever more clearly that the causes of geomagnetic activity are revealed in the motion of the magnetopause, what causes it, and how it is communicated to the interior of the magnetosphere and to the surface of the earth.

In Chapter 3, we consider a form of geomagnetic activity that is always present, even in the absence of viscosity and reconnection. The magnetosphere has to adjust its internal pressure to the ceaseless variability of the solar wind dynamic pressure. The teardrop and the true magnetosphere alike adjust to changes in their confining pressures by propagating fast magnetohydrodynamic waves throughout their interiors. The magnetosphere responds by ringing magnetically. In Section 3.2, we introduce the topic of geomagnetic micropulsations, and in Sections 3.3–3.7, we describe the local toroidal Alfven resonances that are stimulated inside the magnetosphere by magnetopause motions. Having discussed the eigenmodes of the magnetospheric bell, we turn to some of the structures in the solar wind that make it ring. Solar wind structures may be classified into discontinuities, pulses, and extended structures, according to their time scales relative to the magnetosphere's own pressure response time (Section 3.8). When the fast-mode perturbations from interplanetary shock waves (Section 3.9) and solar wind tangential discontinuities (Section 3.10) reach the surface of the earth, they create sudden increases in surface field strength that are called *storm sudden commencements* and *sudden impulses*, respectively. The polarizations of the fast-mode perturbations are modified by currents induced in the ionosphere before they are registered on ground magnetometers (Section 3.11). In Section 3.12, we will next describe the magnetosphere's quasiresonant response to solar wind pressure "pulses," whose durations are comparable with the magnetosphere's intrinsic pressure equilibration time.

1.9 The Convecting Magnetosphere

Chapter 4 describes a purely viscous magnetosphere. The so-called low-latitude boundary layers just inside the magnetopause on the dayside and flanks of the magnetosphere are probably as good a place as any in plasma physics to study anomalous viscosity. The basic observational properties of the low-latitude boundary layer (LLBL) next to the magnetopause are introduced in Section 4.2. Field-aligned currents generated in the LLBL (Section 4.3) connect to a corresponding layer in the high-latitude ionosphere (Section 4.4). Kelvin-Helmholtz instability generated by the shear flow in the LLBL may be responsible for some of the geomagnetic micropulsations in the so-called Pc 4–5 band (Section 4.5). The vertical flow generated by the Kelvin–Helmholtz instability may also generate a line of auroral spots in the afternoonside auroral oval, which we call *vortex aurora* (Section 4.6). The next two sections point to the unifying discussion of bimodal plasma sheet flow to come later. A hierarchy of vortices is occasionally observed even in the center of the plasma sheet (Section 4.7), and a thick boundary layer has been encountered on closed field lines next to the magnetopause in the deep tail (Section 4.8). These observations suggest that the viscous transport of solar wind momentum extends well inside the low-latitude boundary layer, sometimes to the very center of the tail. It is noteworthy that the effects of viscosity continue to be prominent more than 200 earth radii downtail. This

increases significantly the net particle and energy injection into the magnetosphere by the viscous interaction (Section 4.9).

Chapter 5 describes phenomena that would be found in a purely reconnecting magnetosphere. These include the direct entry of solar and solar wind energetic particles into the tail lobes and polar caps (Section 5.2), the supersonic flow of ionospheric plasma into the tail lobes (Section 5.3), the open field line region inside the auroral oval (Section 5.4), the removal by convection of cold plasma of ionospheric origin beyond the plasmapause (Section 5.5), the flow of high-speed plasma from the dayside reconnection region (Section 5.6), the entry of magnetosheath plasma into the polar cusp ionosphere (Section 5.7) and magnetotail (Section 5.8), the convection of plasma across the tail lobes (Section 5.9), the reconnection region in the tail (Section 5.10), the layered structure of the plasma sheet boundary layer (Section 5.11), and the very long length of the tail (Section 5.12). Field-aligned currents clearly respond to changes in the reconnection rate on the dayside, but the independent evidence for viscously driven convection and field-aligned currents prompts us to ask how the two convection systems manage to coexist, since they must come to terms with each other in the ionosphere where they drive the same cross-field current system (Section 5.13). We cannot avoid dealing with both systems of convection since they inject energy and particles into the magnetosphere at competitive rates (Section 5.14).

The effects of reconnection are certainly more showy than those of viscosity. Nothing makes this point more eloquently than the fact that major features and subtle details of geomagnetic activity correlate with the direction of the interplanetary magnetic field. In Chapter 6, we discuss statistical studies aimed at elucidating the causes of geomagnetic activity. As the steady reconnection model clearly suggests, geomagnetic activity (Section 6.2), the size and direction of the convection electric field (Sections 6.3 and 6.4), along with the intensity and location of the system of field-aligned currents (Section 6.5) all correlate with the direction of the interplanetary magnetic field. The reconnection component of geomagnetic activity responds to changes in the direction of the interplanetary field on at least two characteristic time scales (Section 6.6). The first, 10–20 minutes, is the time to establish convection in the polar cap ionosphere, and the second, about an hour, reflects the delayed response of the geomagnetic tail to changes in the dayside reconnection rate. It is less obvious, but no less important, that there is a component of geomagnetic activity that does not depend upon the direction of the interplanetary field but does depend upon the solar wind momentum flux density. This component of convection corresponds to a small residual potential across the polar cap that never disappears and is in all likelihood associated with viscosity (Section 6.7).

Fairfield and Cahill (1966) were the first of many to show that auroral substorms are statistically associated with an enhanced southward component of the interplanetary magnetic field. Shortly afterwards, Rostoker and Falthammar (1967) found a positive correlation between the interplanetary electric field and the level of geomagnetic activity. Various structural features of the magnetosphere also proved to correlate with the direction of the interplanetary field, from which it was inferred

that the structure of the magnetosphere depends on the rate of reconnection. Statistical studies of this kind motivated the idea that the substorm has a growth phase that follows a southward shift of the interplanetary magnetic field and precedes the expansion phase of the substorm. They also prompted a number of questions that are still asked today. Could a quasistationary version of Dungey's (1961a) reconnection model explain the changes in magnetospheric structure? Would the evolution in magnetospheric structure lead directly to substorm onset? Would the quasistationary model also describe separate expansion and recovery phases, as in the auroral substorm?

The first attempts to answer these questions took the simplest possible approach to the problem of time dependence. They formed what Coroniti (1985b) was to call later a "conceptual" substorm model, one that explains what happens to the magnetosphere after an initially quiet solar wind field suddenly turns southward and remains southward (chapter 7). No real substorm was expected to be like the conceptual one, whose function was only to outline how the reconnection paradigm might be extended to substorms. The substorm growth phase is the chain of events that takes place after the dayside reconnection rate has increased and before tail reconnection is stimulated. The quasistatic equilibrium structure of the magnetosphere evolves (Sections 7.2 and 7.3) in concert with an increase in the rate of convection in the ionosphere (Section 7.4) and dayside magnetosphere (Section 7.5). According to the theory of MHD characteristics, the start of dayside reconnection sends a number of different waves into the tail lobes, whose functions include increasing the rate of convection in the lobes, adjusting the flaring angle of the tail magnetopause, and ultimately stimulating tail reconnection (Section 7.6). The tail reconnection often occurs at a new "nearer-earth" neutral line (Section 7.7). In Section 7.8, we sample the kinds of evidence that indicate that tail reconnection occurs during the substorm sequence, that it acts to reduce the flux in the tail lobes, and occasionally can be closely associated with the substorm onset itself. Two neutral lines will form between them a region of closed field—a "plasmoid." When reconnection at the nearer-earth neutral line reaches tail lobe field lines, the plasmoid will be accelerated tailward. The evidence for tailward-moving plasmoids is reviewed in Section 7.9. The passage of a plasmoid in the plasma sheet induces a so-called "traveling compression region" (TCR) in the tail lobes (Section 7.10). The statistical attempts to pin down when plasmoids and TCRs are made relative to the onset of the auroral substorm are inconclusive, and there may not be a one-to-one relationship between the occurrence of plasmoids and substorms (Section 7.11).

The reconnection model of substorms is a "phenomenological Green's function" for the quasisteady reconnection model. Like the mathematical Green's function, the model uses the simplest possible stimulus to illuminate the time-variable response of the magnetosphere to changes in the interplanetary field. The solar wind stimulus is, however, bound to be complex, and the issue is whether the phenomenological Green's function can be "conceptually convolved" with that more complex stimulus to account for the unsteady convection that is observed. At stake is the validity of the assumption of quasisteady convection on which this

whole approach is based. All this is entirely independent of whether the reconnection model of substorms can also be related to the auroral observations defining the substorm.

The next two chapters describe the unsteady and structured convection that emerges when we resolve its behavior on an a time scale better than the 10–20 minute time scale for fast-mode pressure equilibration and ionospheric coupling. Chapter 8 is devoted to the response of the dayside magnetosphere and ionosphere to changes in the interplanetary field on time scales ranging from 1–2 minutes to tens of minutes. The energetic particles escaping into the solar wind from the magnetopause favor the existence of bursty magnetopause reconnection (Section 8.2). We then argue (summarized in Section 8.6) that so-called flux transfer events near the dayside magnetopause (Sections 8.3–8.5), transient micropulsations near the polar cusp (Section 8.7), Alfven waves at the equatorward border of the cusp (Section 8.8), dispersed ions precipitating into the cusp (Section 8.9), bursty ionospheric flows (Section 8.10), transient aurora (Section 8.11), and F-region density patches in the high-latitude ionosphere (Section 8.12) can be tied together by the notion that a repeating quasiperiodic sequence of bursts of magnetopause reconnection organizes the global pattern of convective flow.

The flow in the plasma sheet has to respond to the complex input coming to it over the poles from dayside reconnection and from viscous coupling in the low-latitude boundary layer. In Chapter 9, we build an argument that it does so bimodally. We start by reviewing the famous plasma sheet pressure paradox: Steady earthward convection in the average plasma sheet magnetic field profile cannot reproduce the average plasma sheet pressure profile (Section 9.2). It is natural to ask whether averaging the plasma sheet flow reproduces the steady convection model. Statistical studies that started out by searching for steady convection ended up focusing on the breadth of the distribution of flow states and the remarkable contrast between its extremes (Section 9.3). The low-velocity flow does not have a strongly preferred direction, whereas the high-velocity flow is directed almost precisely earthward near the earth, and tailward further downstream. The persistent low-speed flow is irregular in direction and magnitude. The high-speed flow is organized into infrequent bursts of 5–10 minutes' duration (Section 9.5). The plasma sheet flow is bursty even in carefully chosen time intervals in which the interplanetary and geomagnetic variability is unusually small (Section 9.4).

Taken together, the opposite directions of the bursty flows in the near and distant tail, the bursts of high-energy particles that come from the events that create the high-speed flows, and the one-to-one relationship between very high-speed flows and plasmoids in the deep tail suggest that nightside reconnection is localized and intermittent. There is evidence for bursty convection in the night-side ionosphere; localized bursts of flow are responsible for a dominant fraction of the Joule heating in the nightside auroral ionosphere, and small, brief, few-minute, auroral activations at high latitudes occur during bursty plasma sheet flow events. A spacecraft in the plasma sheet encounters bursts of fast flow like those envisioned in the reconnection model a few percent of the time, and the rest of the

time, it is immersed in a low-velocity chaotic flow, which it is natural to connect with Axford and Hines' original ideas about collisionless viscosity (Sections 9.6–9.17). One wonders if steady uniform convection has ever been found.

Can one find the state of pure viscosity-driven convection by examining northward interplanetary field conditions? Chapter 10 is devoted to outlining the sequence of events that occurs after the interplanetary field swings northward and stays northward long enough to approach the viscous convection state. Our discussion is very much in the spirit of our earlier discussion of the substorm growth phase; again we try to order a complex phenomenology using an idealized conceptual framework. Clearly, any real observational sequence may differ from our synthetic description. The pattern of polar cap convection typical for southward field conditions disappears within 10–15 minutes of a northward turning (Section 10.2), but an intermediate convection state driven by tail-lobe reconnection is interposed between the southward field state and the viscous state we are seeking (Sections 10.3 and 10.4). This convection is sunward in the center of the polar cap (Section 10.5) and corresponds to a system of field-aligned currents that is poleward of the currents that prevail during southward field conditions (Section 10.6). Clearly defined patterns of reverse convection can ordinarily be found in the summer polar cap, whereas the flow is nearly always irregular on small scales in the winter polar cap (Section 10.7). Sun-aligned auroral arcs extend across the polar cap in northward field conditions (Section 10.8), many on closed field lines (Section 10.9). The larger pattern of convection can be inferred from the pattern of sun-aligned arcs (Section 10.10). The open region of the polar cap shrinks in northward field conditions, indicating that the tail lobes are losing flux (Section 10.11). What happens as the magnetosphere approaches the more nearly teardrop configuration? The evolution of the polar cap aurora during an extended interval of northward interplanetary field is taken up in Section 10.12. During intervals of the most extreme geomagnetic quiet, irregular convection and field-aligned currents on small spatial scales can always be found in the winter polar cap (Section 10.13). Study of such periods may eventually allow a detailed characterization of the ionospheric counterpart of purely viscous convection and/or the underlying state of chaotic plasma sheet flow.

1.10 Auroral and Magnetospheric Substorms

Since the discovery of the relationship between auroral and solar activity 2 centuries ago, people have understood that auroral events are related to others in the vastness of space. The steady reconnection model accounted in a quite natural way for the most basic fact of geomagnetic and auroral morphology deducible from ground-based measurements, the partition of the polar ionosphere into a relatively quiet polar cap surrounded by an active auroral "oval" (Chapter 11). Just as the substorm concept had first been synthesized from ground-based observations of the aurora, so also had been its static cousin, the auroral oval concept (Feldstein, 1963a,b; 1973). The issue most critical to the interpretation of auroral observations

has been how the auroral oval maps into the magnetosphere. The most direct yet not manifestly the most illuminating approach to this problem is simply to "map" field lines from the auroral oval to the magnetosphere using empirical models of the magnetic field near the earth and in space (Section 11.2). Modern empirical models reveal how the shape of the auroral oval changes with the level of geomagnetic activity, but since they represent better the more prevalent viscous convection state, and geomagnetic activity is closely tied to reconnection, their significance is unclear (Section 11.3). Moreover, magnetic field maps are singular and inherently inaccurate near the poleward border of the auroral oval (Section 11.4). Identification of similar physical structures in the auroral oval and in space also implies a mapping, a physical mapping, which often can be successful where the mathematical magnetic field maps are misleading. So we need to know what structures are inside the oval. To this end, we characterize some of the oval's more obvious features, such as the diffuse aurora (Section 11.5), inverted-V precipitation structures (Section 11.6), and auroral arcs. We discuss their relationship to the pattern of convection and field-aligned currents in the nightside oval in Sections 11.7–11.11. The relationship between the thin arcs observed at low altitudes and the inverted Vs observed in polar orbit is taken up in Section 11.12.

One thing is certain: High-latitude closed field lines map closer to the magnetopause on the dayside and flanks, and deeper into the magnetic tail on the nightside than their cousins at lower latitudes. They connect to the places where convection is driven. At the time the concepts of substorm and oval were formulated, the oval's poleward boundary had been difficult to identify and certainly could not be systematically monitored. This *lacuna* in our understanding has now been filled in by spacecraft imaging of the whole oval and by ground-based studies of employing coordinated multispectral all-sky imaging and radar scatter measurements. Section 11.13 is devoted to the appearance of the most poleward arc system to the ground observer. Where do the nightside poleward arcs map? In one case the poleward border of the auroral emission observed by DE 1 mapped magnetically into the plasma sheet boundary layer encountered by ISEE 1 within the accuracy of the measurements (Section 11.14). The so-called "auroral kilometric radiation" (AKR) is generated at the poleward boundary of the oval, so that AKR bursts monitor the activity of the poleward arc system (Section 11.15). In Section 11.16 we relate the ordering in magnetic latitude of the structures in the auroral oval to the layering of the plasma sheet, and in Section 11.17 we turn to the issue of the conjugacy of the aurora between hemispheres.

In Chapter 12 we embellish the suite of observations that originally defined the auroral substorm with new ones that enlarge Akasofu's (1964) picture. We would not be talking about substorms today unless the modern observations of auroral oval phenomenology could be fit into the framework provided by Akasofu's original conception. On the other hand, what was not contained in the original picture of substorms has subtly circumscribed our perceptions to the present time. The exceptions have to do with the limitations of ground-based observations of the aurora in 1964. In particular, there was less-than-ideal coverage at high magnetic latitudes, and it was difficult to follow the development of the substorm around the

whole auroral oval from the dayside to the nightside. We can now complete the time-dependent pattern of auroral luminosity that originally defined the substorm and supplement it with a wide range of other measurements. Although it is of commanding interest to know what is happening above the aurora and in the magnetosphere before, during, and after a substorm, it is an act of essential rigor to be clear about Akasofu's original definition of a substorm; so we restrict ourselves to the events occurring in the ionosphere in this chapter. We discuss their magnetospheric counterparts in Chapter 13.

Global auroral imaging has made it possible to follow the development of the substorm growth phase in the polar cap (Section 12.2) and around the whole oval, from the first stimulation of convection in the dayside polar cusp to the onset near local midnight (Section 12.3). The classical definition of the preonset sequence of events was derived largely from auroral observations in the local evening sector; an ordered network of auroral activity is observed to slowly drift equatorward (Section 12.4). Premonitory pseudoexpansions (Section 12.5) and precursory auroral activations and fadings (Section 12.6) often occur, particularly as onset approaches. The initiation of the substorm expansion takes place in two steps. The onset itself is a localized brightening of the pre-existing most equatorward auroral arc (Section 12.7) occurring deep within the closed-field-line region (Section 12.8). The launching of the westward-traveling surge, the second stage in the initiation of the auroral expansion, occurs several minutes after onset (Section 12.9). The surge marks the westward end of an expanding "bulge" of bright, active aurora and terminates the westward electrojet with a strong upward field-aligned current (Section 12.10). The westward surge and auroral bulge often develop as a quasiperiodic series of discrete activations (Section 12.11). The substorm was originally defined by observations of the aurora, which is created by the acceleration of few-keV electrons into the atmosphere. The corresponding proton aurora substorm is discussed in Section 12.12. The waxing and waning of the auroral bulge has provided the traditional definition of the expansion and recovery phases of the auroral substorm (Section 12.13). The bulge at maximum expansion approaches but usually does not reach the most poleward arc system (Section 12.14). Structured activations of the most poleward arc systems are a characteristic feature of the substorm recovery phase (Section 12.15), and when this occurs the oval has two bright regions. The equatorward region contains the classical phenomena associated with recovery phase, such as the so-called "omega bands" and pulsating aurora (Section 12.16). There is no unique sequence of events that characterizes the end of the recovery phase when one looks at the poleward and equatorward aurora simultaneously (Section 12.17).

In Chapter 13, we discuss the geosynchronous substorm, the counterpart near the geostationary orbit of the dramatic auroral events that first defined the term *substorm*. This research area, pioneered 2 decades ago, has seen a rapid improvement of understanding in the past decade. The development of a tail-like magnetic field during growth phase (Section 13.1), corresponding to the evolution of an extremely thin current layer near the earth (Section 13.2), and the subsequent relaxation to a more dipolar state during expansion phase (Section 13.3) are the

most salient characteristics of the geosynchronous substorm. The depolarization of the magnetic field is always accompanied by so-called "dispersionless injections" of energetic particles (Section 13.4), and generates the "substorm current wedge" (Section 13.5). The fine structure of the depolarization generates bursts of Pi 1 and Pi 2 magnetic field micropulsations, which may be used to determine both the universal time and local time of substorm onset (Section 13.6). The oscillating currents of the depolarization couple to a compressional modes that stimulate toroidal resonances in the inner magnetosphere, enabling Pi 2 bursts to be observed worldwide at midlatitudes (Section 13.7). The depolarization starts in a very small region (Section 13.9) and propagates both eastward and westward to form an expanding wedge of field-aligned current (Section 13.8).

The last part of Chapter 13 deals with the relationship between events in the geosynchronous region and those slightly farther downstream in the plasma sheet. Whether depolarization propagates radially to stimulate other substorm effects, such as reconnection, further downtail is a matter of active investigation. Unfortunately, the attempts to determine whether and how depolarization propagates radially, when they are taken together, appear to be inconclusive (Section 13.10). This only emphasizes the interest in what happens just tailward of the geosynchronous region. If reconnection occurs in the geosynchronous region, one ought to detect plasmoids escaping downstream, and occasionally one does; however, indisputable observations of plasmoids escaping the geostationary region are relatively rare (Section 13.11). What is more likely to be observed just downstream of the geosynchronous region is a "dropout" due to thinning of the plasma sheet (Section 13.12). The dropout is followed by plasma sheet recovery, which appears to be a consequence of reconnection occurring tailward of the observing spacecraft.

In Chapter 14, we discuss the relationship between the geosynchronous and auroral substorms. The geosynchronous depolarization occurs at about the same time as the auroral expansion is observed at conjugate ground stations, and the accompanying dispersionless injection of energetic particles is related to the brightening of the auroral X-ray arc (Section 14.2). Dipolarizations propagate azimuthally over the spacecraft in close association with westward surges in the conjugate ionosphere (Section 14.3), and in one particularly clearcut case, multiple surges could be associated with an oscillatory depolarization event at geosynchronous orbit (Section 14.4). In contrast, the response at geosynchronous orbit to the brightening of the poleward arc system is remote, and there is no evidence of nearby field-aligned currents (Section 14.5).

The second part of Chapter 14 takes up the issue of plasma composition. Because field-aligned streams of oxygen ions stream upward out of the auroral acceleration region, their detection in deep space would be a signature of magnetic connection to an inverted-V or to the westward surge. Because we have not discussed composition previously, we give a brief overview of some salient general results and then return to our theme. The rate of injection of singly ionized oxygen into the magnetosphere depends on a complex interplay of geomagnetic and solar activity, the rate depending on the solar cycle through the flux of solar EUV

(Section 14.6). The plasma sheet contains a mixture of ions of solar wind and ionospheric origin, whose relative proportions depend upon the auroral electrojet index, and thus are linked to the strength of the auroral current system (Section 14.7). The O^+ density increases dramatically during the substorm expansion phase both in the geosynchronous region (Section 14.8) and in the plasma sheet just downstream (Section 14.9), presumably in part because of connection to the westward surge.

When Arnoldy (1971) showed that substorms were more likely to occur approximately 1 hour after a southward turning of the interplanetary field, four types of questions arose. First, what is happening during that precursory period? The attempts to answer this question led to the concept of the substorm growth phase (Pudovkin et al., 1968; McPherron, 1970) taken up in Chapter 7. Next, are precursors to substorm onset driven by variations in the solar wind? Third, can the onset, a discrete, localized event, be triggered by something in the solar wind, does it happen on its own, or both? Finally, can the subsequent intensifications of the substorm expansion be influenced by events occurring in the solar wind? Chapter 15 is devoted to these last three questions. The term *pseudoexpansion* refers to an auroral activation that resembles a small westward surge but does not lead to an auroral bulge that expands over a large distance. Auroral pseudoexpansions are accompanied by "pseudodipolarizations" and "pseudoinjections" at geostationary orbit (Section 15.2). The events leading up to expansions and pseudoexpansions appear to be similar, and it may be that pseudoexpansions are caused by transient increases in the dayside reconnection rate that occur as the magnetosphere is approaching the threshold condition for the full substorm. We present clear evidence that the passage of an interplanetary shock or a compressive sudden impulse over earth can "trigger" an auroral onset, providing there has been a preceding period of southward interplanetary magnetic field (Section 15.3). The issue of a possible relationship between northward turnings of the interplanetary field and substorm onsets/intensifications at high latitudes is discussed in Section 15.4. One can also ask what happens when there is very little possibility of a solar wind trigger. During extended periods of southward interplanetary field, it appears that either structureless but intense "convection bays" or quasiperiodically recurring substorms can occur (Section 15.5).

Convection and substorms continue to be *the* paradigms of magnetospheric phenomenology. Between them, they have articulated a rich and diverse experimental literature, they show no signs of weakening, and there are no credible replacements on the horizon. One day we will create a more capacious new paradigm that articulates the relationship between them and replaces our present phenomenological reasoning by more quantitative understanding. We have not yet found that capacious new paradigm, but the most recent research in the past few years seems to be pointing a clear path to it (Chapter 16).

NOTES

1. We are indebted to Chapman and Bartels (1940) for much of this historical account.
2. We are indebted to Dessler (1968) for this account.

2

THE TEARDROP MAGNETOSPHERE

2.1 Introductory Remarks

In this chapter, we try to infer from magnetohydrodynamic reasoning and observation how the magnetosphere might look and behave if the magnetopause were inactive. Since there probably never has been an occasion when both viscosity and reconnection were absent, all we can do is array observations of phenomena that do not depend on either mechanism for their existence. As a result, we end up focusing on how the magnetosphere arrives at a balance of pressure with the solar wind. How it responds to changes in its confining pressure will be the topic of the next chapter.

All discussions of the magnetosphere start with the magnetopause, and, indeed, the first models of the magnetosphere were calculations of the shape of the magnetopause. Without reconnection and without viscosity, the magnetopause would be given by the Chapman–Ferraro model on the dayside and close due to the reexpansion of the finite-temperature solar wind on the nightside (Section 2.2). This magnetosphere has a teardrop shape. After the dependence upon the interplanetary field via the reconnection process is taken into account, the average position and shape of the dayside magnetopause is in general accord with the Chapman–Ferraro model (Section 2.3). Because the magnetopause is always in motion, the early estimates of its thickness were uncertain until the first two-spacecraft observations were made (Section 2.4). The magnetopause current layer proved to be several ion Larmor radii thick, significantly thicker than the electron inertial length. Once the average position of the magnetopause is specified, the position of the bow shock can be calculated using methods first employed for hypersonic flow around blunt bodies, which are easily extended to a weak-field MHD regime. The measured average positions of the bow shock and magnetopause agree once variations in solar wind dynamic pressure are taken into account (Section 2.5). While weak-field MHD does a good job with the bow shock, it fails in the subsolar magnetosheath, where a plasma depletion layer forms just upstream of the magnetopause (Section 2.6). Full MHD theory suggests that as many as three shocks could be standing in the flow enclosing the magnetosphere, a fast bow shock, an intermediate shock, and a slow shock. The depletion layer is then a slow- mode rarefaction separating the slow shock and the magnetopause.

2.2 The Teardrop Model

The first models of the magnetosphere were calculations of the position of the dayside magnetopause in a steady unmagnetized solar wind. Ferraro (1952) had pointed out that the size and shape of the geomagnetic "hollow" could be obtained from integrating the relation equating the pressure of the vacuum dipole field to the component of the solar wind stress tensor normal to the magnetopause surface. This simple calculational algorithm, which is based upon the Newtonian approximation for the hypersonic solar wind flow, produced a reasonable picture of the dayside magnetopause in two (Zhigulev and Romishevskii, 1960; Dungey, 1961b; Hurley; 1961a,b) and three dimensions (Beard, 1960, 1962; Spreiter and Briggs, 1962; Midgley and Davis, 1963; Mead, 1964; Mead and Beard, 1964). Full hydrodynamic calculations for an unmagnetized solar wind soon substantiated the reliability of the Newtonian method (Spreiter and Jones, 1963).

Chapman and Ferraro's picture of the magnetopause layer thus led straightforwardly to a model for the size and shape of the dayside magnetopause in an unmagnetized solar wind. However, it was not clear what happened downstream of earth. Ferraro (1960) had the geomagnetic cavity extending to infinity on the nightside, but Johnson (1960) pointed out that the gas-dynamic reexpansion of the compressed solar wind would force closure of the magnetospheric cavity. Spreiter and Hyett (1963) and Slutz and Winkelman (1964) also emphasized the importance of the thermal pressure of the solar wind. Johnson's magnetosphere had the shape of a teardrop. The distance to the subsolar point on the blunt dayside magnetopause was determined by the usual balance of dynamic and magnetic pressure, while the distance to the reclosure point of the solar wind scaled as the sonic Mach number of the flow times the subsolar magnetopause distance. Ferraro's magnetosphere turned out to be the infinite Mach number limit of Johnsons. Later, Wu et al. (1981) numerically simulated the teardrop magnetosphere produced by the flow of an unmagnetized solar wind over a three-dimensional magnetic dipole. They found that the internal magnetospheric field in the simulation agreed, to a quite remarkable degree, with the quiet-time geomagnetic field.

2.3 The Position and Shape of the Magnetopause

One of the more urgent tasks facing the first spacecraft experimentalists was to ascertain the average shape and position of the magnetopause. The results of the earliest studies were in general accord with Chapman and Ferraro's model (Ness et al., 1964; Bridge et al., 1965; Gosling et al., 1967; Heppner et al., 1967; Behannon, 1968, 1970; Egidi et al., 1970; Fairfield, 1971), but important quantitative deviations were manifest. For example, Chapman and Ferraro assumed that the highly conducting solar stream sweeps up the magnetic flux of the geomagnetic field, compresses it, and confines it all within a closed boundary so that none escapes; the compression of the geomagnetic field into a smaller volume increases

its energy, which is gained at the expense of the kinetic energy of the solar wind. If no flux escapes, the magnetic field strength just within the boundary would be twice the dipole value at the same radial distance. People looked for and did not always find the doubling of the magnetic field. An approximately doubled field was found near the subsolar magnetopause (Cahill and Patel, 1967), but, while the magnetopause field generally exceeded the vacuum dipole value, strict doubling was usually not observed. This was a relatively small matter compared to the fact that the magnetopause was nearly always in motion (Kauffmann and Konradi, 1969), indicating that Chapman–Ferraro theory applies, at best, in an average statistical sense.

One source of the variability in magnetopause position is the variability of the solar wind dynamical pressure. For example, the yearly average pressure varied between about 1.5 and 4 nPa between 1963 and 1989 (Fairfield, 1991). The minimum average pressures occurred near solar maximum, and the maximum pressures occurred during the declining phase of the solar cycle when high-speed streams are the most prevalent. The Chapman–Ferraro magnetopause distance scales self-similarly as the one-sixth root of the pressure, implying that the average position of the subsolar magnetopause should have moved between about 9. 5 and 11 R_E with the solar cycle. The distributions of hourly averaged solar wind pressure within given years had a dispersion of more than a factor two about the annual averages, and the dispersion depended upon the phase of the solar cycle. These shorter-term variations account for much but not all of the variability in magnetopause position found on individual spacecraft experiments.

Chapman–Ferraro scaling has been used to normalize the data in almost all studies of magnetopause position. Consider, as an example, the first empirical determination of the three-dimensional shape of the magnetosphere (Formisano et al., 1979), which employed more 1000 magnetopause crossings from the HEOS 1, OGO 5, and 5 different IMP spacecraft at low latitudes, and HEOS 2 at high latitudes. No other spacecraft has explored the high-latitude region where HEOS 2 went, and subsequent studies of magnetopause position still rely on this particular data set. All magnetopause distances were normalized to the average 1972–1973 solar wind (density, 9.4 cm^{-3}; speed, 450 km/s). Since the average density in 1972–1973 was about twice "typical," the distance to the best-fit subsolar magnetopause, 8.8 R_E, was about 15% smaller than the 10 R_E that best characterizes the longer interval 1963-1989 (Fairfield, 1991). The distances to the dusk and dawn terminators were 14.7 and 13.4 R_E, respectively, so that the magnetosphere axis was rotated away from the earth–sun line by 6.6 degrees. The distance to the magnetopause in the direction normal to the ecliptic plane, 13.7 R_E, was smaller than the average of the dawn–dusk positions, indicating that the terminator plane magnetopause crosssection was slightly flattened.

A dawn–dusk asymmetry in magnetopause position is expected because of the earth's motion in the solar wind. The symmetry of the magnetosphere is organized around three vectors—the direction of the dipole axis of the geomagnetic field, the direction of the interplanetary magnetic field, and the velocity of the solar

wind in the frame of reference of the moving earth. The first produces seasonal and diurnal "tilts" of the magnetosphere, which have to be taken into account to clarify the comparison between magnetospheric models and observation (Olson, 1969; Choe et al., 1973). The second is important in the context of reconnection and will be discussed later, and the third is responsible for the dawn–dusk magnetopause asymmetry described. The term *subsolar magnetopause*, which strictly speaking means the point where the earth–sun line intersects the magnetopause, is not always distinguished in casual discourse from the point where the aberrated solar wind velocity vector intersects the magnetopause (at, say, the geomagnetic equator) since the projection of the aberrated velocity onto the ecliptic plane typically makes a small angle of order 5 degrees with the earth–sun line. It is the aberrated point of symmetry that has the dynamical significance, but we will continue with the simpler usage "subsolar magnetopause" when it is harmless to do so. However, we must keep in mind that the aberration angle varies inversely with the speed of the solar wind.

Now we come to an important point. Despite the use of Chapman–Ferraro normalization, there was at least a ± 1 R_E scatter in the Formisano et al. (1979) magnetopause position. This is true for other statistical analyses as well; taking into account the variability of solar wind pressure reduces the scatter in magnetopause position but only partially. By implication, processes other than the simple establishment of pressure balance affect the position of the magnetopause significantly, and only a multivariate statistical analysis can be a fair test of the Chapman–Ferraro model.

Reconnection proved to the most important process affecting magnetopause position after solar wind pressure variations. After taking the dependence upon the direction of the interplanetary field into account, Holzer and Slavin (1978) found that the magnetopause's location was consistent with Chapman–Ferraro theory, assuming that its shape was self-similar to variations in dynamic pressure. The assumption of self-similarity was subsequently removed by Sibeck et al. (1991), who analyzed a set of 1821 magnetopause crossings recorded on 18 spacecraft over 2 decades. Separate fits to subsets of this data set determined the dependences of magnetopause location upon dynamic pressure and upon the orientation of the interplanetary field. When the effects of the interplanetary field were removed, the best-fit magnetopause was almost but not quite a figure of revolution about the aberrated solar wind velocity direction; its equatorial dimension near dawn and dusk exceeded its polar dimension by about 8% on average. The fact that the ratio of the distance to the subsolar point to that of the dawn–dusk terminator was independent of dynamic pressure was one indication of self-similarity. Dynamic pressure variations on time scales longer than 1 hour produced self-similar magnetopause motions. Finally, the distance to the subsolar magnetopause was one- or two-tenths of an earth radius larger than the theoretically expected value over the entire range of dynamic pressure. This discrepancy should not blind us to the essential point: When currently known effects are accounted for, the Chapman–Ferraro model predicts the position of the dayside magnetopause with 2% accuracy.

2.4 The Thickness of the Magnetopause Current Layer

In the absence of reconnection, we expect the magnetopause to be an MHD tangential discontinuity that separates the magnetosheath magnetic field, which has a variable direction, from the magnetospheric field, which has a predictable direction. If the magnetopause were stationary, it would take a spacecraft many minutes to traverse this boundary, but traversals are an order of magnitude shorter because the magnetopause is always moving. Because it is moving with an unknown speed, definitive measurement of one of its most important properties, its thickness, had to wait until the two-spacecraft ISEE 1 and 2 project (Ogilvie et al., 1977), Indeed, this measurement was one of the prime objectives of the project. Before that time, the techniques that had been used to estimate the speed of the boundary motion and thence the magnetopause thickness had all been model dependent in one way or another. Recounting some of these attempts is an interesting object lesson: In retrospect, many of the estimates of thickness were reasonable, but it was impossible to say so with any assurance at the time.

Most early estimates of magnetopause thickness employed data from multiple magnetopause encounters, assuming that the boundary oscillated sinusoidally. Speeds of about 10 km/s emerged from this method, leading to 10–1000 km boundary thicknesses (Cahill and Amazeen, 1963; Holzer et al., 1966; Ogilvie et al., 1971). By comparing the rate of change of the magnetic field with the prediction of an image dipole model, Cummings and Coleman (1968) estimated the magnetopause speed and thickness to be 60 km/s and 300–600 km, respectively, for a set of unusual magnetopause encounters at geosynchronous orbit. Kauffmann and Konradi (1973) used the variations of the energetic protons to find that the magnetopause usually moved at a speed less than 20 km/s; later, Williams (1980), using three-dimensional measurements of energetic particles, observed large-scale radial motions with speeds somewhat less than 25 km/s. Assuming the magnetopause thickness was one gyro-radius led Neugebauer et al. (1974) to an estimate of 200 km; using the plasma flow velocity to determine the boundary thickness led to 1730 km. Sonnerup and Ledley (1979) calculated a thickness of 470 km from the magnetosheath flow speed and crossing durations. By using ISEE 1 electric and magnetic field data, Mozer et al. (1978) estimated the average speed and thickness to be 30 km/s and 270 km, respectively, for a sequence of eleven multiple crossings observed on a single inbound pass near 1030 UT.

The first ISEE 1 and 2 results produced much greater confidence.[1] Even with two spacecraft, the analysis is not assumption-free: One has to assume the magnetopause is locally planar and moves with a constant speed. Measurements obtained just after the launch of the ISEEs indicated that the magnetopause speed was highly variable, ranging from 4 to 40 km/s (Russell and Elphic, 1978; Elphic and Russell, 1979); on one occasion, an interplanetary shock caused the magnetopause to race over ISEE 1 and 2 at a speed of 195 km/s (Winterhalter et al., 1981). All these results necessitated a more complete study. Berchem and Russell (1982) selected 30 magnetopause crossings in which the separation between the two ISEEs was comparable with the expected boundary thickness (<1000 km), so

that the effects of variable and/or wavy boundary motion could be minimized. These events were distributed between 0800 and 1700 MLT and magnetic latitudes below 35 degrees. The magnetopause speeds in this data ensemble varied from 10 to 80 km/s. The current sheet was in all cases thicker than the electron or ion inertial lengths, and it was even thicker than a thermal ion gyro-radius, about 100 km. The measured thicknesses ranged from 400 to 1000 km, and averaged 923 km, consistent with the thicknesses of 860 km at ISEE 1 and 780 km at ISEE 2 found in the high-speed event studied by Winterhalter et al. (1981). The current sheet thickness did not depend upon the orientation of the magnetosheath magnetic field but was generally ordered by dipole magnetic latitude in such a way that the current sheet was thinnest nearest the geomagnetic equator.

2.5 The Position and Shape of the Bow Shock

The discovery of the earth's bow shock (Ness et al., 1964) confirmed the idea that the solar wind and its interaction with the magnetosphere could be described in fluid rather than single-particle terms. If so, a technique could be borrowed from the theory of hypersonic aerodynamic flow around blunt bodies to calculate the position of the bowshock. Spreiter and Stahara (1985) have reviewed the various approaches to the precise computation of the bow shock position and shape, given the location and form of the magnetopause. The earliest calculations (Axford, 1962; Kellogg, 1962; Spreiter and Jones, 1963) were purely gas dynamical, and neglected the magnetic field in the solar wind altogether. The standoff distance of a gas-dynamic shock upstream of the obstacle is set by the requirement that all the fluid crossing the shock can flow downstream between the obstacle and the shock. Experience with such shocks suggested a general rule of thumb: The distance between the subsolar bow shock and subsolar magnetopause in units of the magnetopause nose radius would be given by $1.1r$, where r is the ratio of the densities upstream and downstream of the shock (Spreiter et al., 1966). In the high-Mach-number limit, the density compression ratio, and therefore shock position, depend primarily on the adiabatic index of the fluid, and weakly upon Mach number. Since the effective adiabatic index of a collisionless plasma is not known a priori, and may depend on plasma parameters, it was not obvious that the position of the bow shock would always be in accord with a fluid theory. Moreover, it was not clear how significant the dependence would be upon the solar wind magnetic field introduced by magnetohydrodynamic corrections to the hydrodynamic limit.

An approximate theory based on magnetohydrodynamics was subsequently developed to justify and extend the gas-dynamic calculations (Dryer and Faye-Peterson, 1966; Spreiter et al., 1966, 1968; Dryer and Heckman, 1967; Alksne, 1967; Spreiter and Summers, 1967; Spreiter and Alksne, 1969b, 1970; Alksne and Webster, 1970). In this approach, the magnetopause was taken to be a nondissipative tangential discontinuity, and the shock satisfied the Rankine–Hugoniot conditions for an MHD fast shock. The key point was to notice that the Alfven Mach number of the solar wind is ordinarily very large, which suggested

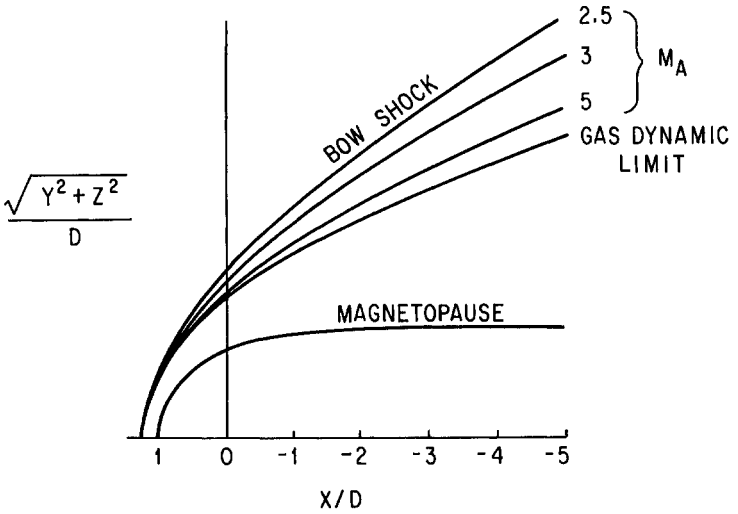

Figure 2.1. Approach to the Gas-Dynamic Limit. One can calculate the shape and size of the bow shock given the shape and size of the Chapman-Ferraro magnetopause. The case of field-aligned MHD flow is especially easy to solve. The position of the bow shock approaches the one calculated in the gas dynamic limit in which the solar wind is unmagnetized as the Alfven Mach number of the solar wind increases (Spreiter and Rizzi, 1974). Since the Alfven Mach number of the solar wind is typically around ten, one would expect that the gas dynamic limit to yield reasonable results, and so it does for many purposes (Spreiter and Stahara, 1985). However, a reconnecting magnetopause consists of intermediate and slow waves (Petschek, 1964), and observations of slow and intermediate wave structures standing in the subsolar magnetosheath flow for northward interplanetary field (Song et al., 1992a) indicate that they are present in the absence of reconnection. Thus, the gas dynamic approximation fails to describe the flow near the magnetopause in the subsolar magnetosheath. Reprinted from John R. Spreiter and Arthur W. Rizzi, ACTA ASTRONAUTICA, Copyright 1974, page 22, with kind permission from Elsevier Science Ltd, The boulevard, Langford Lane, Kidlington 0X5 1GB, UK.

that the magnetic terms be dropped in the energy and momentum conservation laws, in which case the equations for the magnetosheath flow are identical to those of gas dynamics. All that remained of MHD was the familiar provision that the magnetic flux carried by an element of flow be conserved. This approximation, which should work wherever the magnetic field does not build up to too large a strength, was amenable to computation with the limited resources available in the early days of space science. We will see that its success blinded us to its omissions.

A full MHD solution can easily be obtained for the case of field-aligned flow. The electric field is zero, and the exact MHD equations can be transformed

into those of pure gas dynamics with a modified equation of state, and purely gas-dynamical solutions for the earth's magnetosphere can be used to calculate the dependences on solar wind Alfven Mach number of the shock shape and standoff distance and magnetosheath profile. Spreiter and Rizzi (1974) surveyed the solutions for highly supersonic flows with Alfven Mach numbers exceeding 2.5. This procedure only found the fast shock, and the possibility of other discontinuities was not investigated.

The first years of space research saw many experimental studies of the average shape and position of the bow shock, either close to the ecliptic plane (Ness et al., 1964; Bridge et al., 1965; Wolfe et al., 1966; Fairfield and Ness, 1967; Heppner et al., 1967; Gosling 1967c; Russell et al., 1968; Behannon et al., 1968; Egidi et al., 1970), or rotated into the ecliptic plane (Fairfield, 1971). The first study of bow shock location in three dimensions was carried out by Formisano in 1979 (but see Slavin and Holzer, 1981). Fairfield (1971) found good agreement between his observational model of the shock and gas-dynamic calculations of shock position by Spreiter and Jones (1963), who assumed a ratio of specific heats of two and a sonic Mach number of 8.7. After scaling for the effects of differing solar wind dynamic pressure upon magnetopause location, Slavin and Holzer (1981) found only minor variations in bow shock shape and position with solar cycle during 1965–1972. The variations that remained depended on the sonic Mach number of the solar wind, and not upon any properties of the magnetic field, in support of the gas-dynamic approximation. The bow shock location was symmetric between dawn and dusk to within 1 R_E. Later, it was explicitly shown that a gas-dynamic theory with a ratio of specific heats of 2 (Spreiter and Stahara, 1980) could predict the average dayside shock position with an accuracy of about 2% (Slavin et al., 1983), about the same accuracy with which the magnetopause position itself can be predicted.

2.6 The Failure of Weak-Field MHD and the "Plasma Depletion Layer"

The weak-field MHD approximation used in the by-and-large successful bowshock computations breaks down near the stagnation point of the magnetosheath flow. That it must do so is obvious from its requirement that the magnetic flux be carried passively with the gas-dynamic flow. On those streamlines that pass near the stagnation point, the flow speed approaches zero, the plasma density increases, and, to preserve flux conservation, the magnetic field strength builds up to the point that the magnetic pressure and plasma pressure become comparable and the weak-field approximation fails. This defect was recognized at once and a remedy was proposed (Midgley and Davis, 1963; Lees, 1964; Sonnerup and Priest, 1975; Zwan and Wolf, 1976). The plasma density also becomes singular at the stagnation point of the gas-dynamic model, which is unphysical, and it was argued that the compressed plasma would escape along draped field lines to form a plasma depletion layer, rather than a compression layer, near the stagnation point. The depletion process preserves the balance of perpendicular plasma pressure and

magnetic pressure, while the escape of plasma along field lines reduces the parallel pressure, creating a thermal anisotropy conducive to instabilities such as the mirror instability (Crooker and Siscoe, 1977).

Crooker et al. (1975, 1979, 1982) made several systematic studies of the magnetosheath density, pressure, magnetic field, and thermal anisotropy near the dayside magnetopause. Of 17 midlatitude IMP 6 crossings of the dayside magnetopause, 11 showed density depletions just outside the magnetopause (Crooker et al., 1979). The proton density typically decreased by about 40% in the 10–15 minutes adjacent to the magnetopause, but did not go to zero. All the depletions were smaller than had been theoretically anticipated, but the magnetopause crossings studied were more than 35 degrees from the subsolar point, where depletion should be the most pronounced. Thermal anisotropy was relatively common in both Explorer 33 (Crooker et al., 1976) and IMP 6 (Crooker et al., 1979) dayside magnetosheath measurements, and there was some evidence of low-frequency magnetic field oscillations attributable to the mirror mode. Crooker et al. (1982) determined the compression of the solar wind magnetic field after it has convected to the subsolar magnetopause, using ISEE 3 solar wind data and ISEE 1 magnetosheath data. The stagnation field was roughly the geometric mean of the field strength whose pressure equals the solar wind dynamic pressure and the field just downstream of the subsolar shock. For the usual spiral pattern of the solar wind field, the magnetosheath field was about 20% stronger on the morning side than on the evening side, and there was no apparent dependence on the north–south component of the interplanetary field.

2.7 Standing Slow and Intermediate Waves in the Magnetosheath

The structure of the subsolar magnetosheath can also be described in MHD terms (Southwood and Kivelson, 1992). The magnetopause radiates waves upstream along various MHD characteristics in order to divert the solar wind flow around it, and to orient the magnetic field upstream of it. The specific type and pattern of waves radiated depend upon the boundary conditions imposed by the magnetopause, whether it is reconnecting, whether it is an absorbing boundary, and so on. In all cases, a fast wave is required to adjust the total pressure. The fast waves go the farthest and eventually steepen to form the bow shock. The various weak-field magnetohydrodynamic theories employ only the fast characteristic field, and they retrieve only the bow shock. Because of their success in predicting the location of the bow shock and the general configuration of the magnetosheath, not much attention was paid to activity on the intermediate and slow characteristic fields. However, while the flow downstream of the bow shock is subsonic to the fast mode, it can still be supersonic to the intermediate and slow waves. These, too, can steepen to form standing shocks. Because the phase speeds of the small-amplitude intermediate and slow waves depend sensitively upon their angles of propagation to the magnetic field, it is difficult to guess where the shocks might

stand in the absence of detailed computation. However, since their speeds are small, we expect to find them near the stagnation region.

Several rigorous calculations find that slow and intermediate waves stand in the flow around obstacles. Wolfson (1987) pointed out that when the Alfven speed exceeds the sound speed, parallel propagating fast waves have no perturbed density to first order in the amplitude, and so might not be able to deflect the flow in the neighborhood of the stagnation line. In the case of field-aligned or near-field-aligned, sub-fast upstream flow, a slow shock is needed. In contrast to the fast and gas-dynamic shocks, the slow shock is concave facing upstream. For a low Alfven Mach number (< 2) field-aligned, ß = 0.5 flow, Steinolfson and Hundhausen (1990a) found that concave intermediate and slow shocks stood upstream of the stagnation region; the intermediate shock converted into an ordinary fast shock about one body diameter away from the stagnation line. Intermediate and slow shocks are expected when the upstream Alfven Mach number is above the fast speed but below the critical value above which switchoff and intermediate shocks cease to exist. In another case, a fast simple wave preceded a standing intermediate wave and a slow shock (Steinolfson and Hundhausen, 1990b), indicating that all three modes could be found simultaneously.

The question for the magnetosphere is to define the circumstances in which slow and intermediate waves form downstream of the super-Alfvenic bow shock. An early analytical calculation found that both a fast shock and slow shock stand upstream of a two-dimensional non-conducting wedge when the upstream flow speed greatly exceeds the fast MHD speed, provided the flow and magnetic field are nonaligned (Chu and Lynn, 1962). Beginning in the 1980s, fully self-consistent MHD computations of bow shock and magnetopause became feasible in two (Leboeuf et al., 1978; Lyon et al., 1981) and three dimensions (Leboeuf et al., 1981; Wu et al., 1981; Wu, 1983, 1984, 1985; Ogino and Walker, 1984). However, extensive data analyses had already proved semiquantitative agreement between the measured shock position and weak-field magnetohydrodynamics, and modern numerical computations only recently have returned to the MHD structure of the magnetosheath (Lee et al., 1991; Wu, 1992). Lee et al. (1991) found evidence for slow-mode structures in the subsolar magnetosheath when there was a component of magnetic field normal to the magnetopause.

Let us turn to the experimental evidence for slow or intermediate wave structures standing in the magnetosheath. Compressive density structures have been found in the magnetosheath upstream of the subsolar magnetopause. An enhancement in density occurred in 17 of 26 ISEE 1 and 2 passes near the stagnation streamline (Song et al., 1990). In most of the passes, the density remained relatively constant across the magnetosheath, except ahead of the magnetopause. In only one case did the density increase monotonically all the way from the shock to the magnetopause, and this was the pass with the highest plasma pressure when the gas-dynamic picture should be most nearly correct. In two other cases, the density decreased, but had small maxima upstream of the magnetopause. The fractional density increase was of order unity at small plasma beta, averaged 44%, and decreased with increasing beta. The magnetosheath density enhancement

regions were 0.4 R_E thick on average and were clearly separated from the magnetopause by a rarefaction region of roughly 0.2 R_E thickness (Song et al., 1990). It took about 12 minutes to cross a typical rarefaction region, in rough agreement with the durations of the IMP 6 plasma depletions studied by Crooker et al. (1979). There was no clear relationship between the occurrence of the density maxima and the shear between the magnetosheath and magnetopause fields among the 17 examples studied, and they were found for both northward and southward magnetosheath field.

The density and magnetic field profiles in the compression regions appeared to be composed of nearly standing waves. Song et al. (1992b) showed that there was a difference between the low-frequency waves upstream of and within the standing density enhancements in the magnetosheath. Those upstream had wave vectors nearly perpendicular to the background magnetic field, a small, nearly zero, propagation speed, and appeared to be convected with the magnetosheath flow, consistent with mirror modes (Tsurutani et al., 1982). While the waves within the density enhancements had power in the 0.1–0.4 Hz frequency range similar to that in the upstream magnetosheath, there was an additional component centered at 0.008 Hz in the enhancement region. The phase difference between the magnetic and thermal pressures was 180 degrees for those frequencies with significant coherence. The time delay between ISEE 1 and ISEE 2 exceeded 88 s, more than 5 times the delay for the upstream component. The waves comprising the low-frequency component were quasistanding in the spacecraft frame, or moving slowly upstream from the magnetopause.

Three magnetosheath structures were subjected to detailed study using ISEEs 1, 2, and 3 (Song et al., 1992a). Examination of ISEE 3 data upstream in the solar wind indicated that the structures had not been convected into the magnetosheath from the solar wind, and were not triggered by any changes in the direction of the interplanetary field. In one case when ISEE 1 and 2 were particularly well separated, cross-correlation showed that the density structure was quasistationary in the magnetosheath, possibly moving only with the magnetopause. Given the speed of this structure, its relatively sharp leading edge could be subjected to a shock normal analysis reminiscent of those commonly used in studies of the bow shock. The derived flow velocity normal to the discontinuity was 42 km/s upstream and 28 km/s downstream; the upstream flow was definitely super-slow and possibly super-Alfvenic, and the downstream flow was close to the intermediate and slow speeds. The tangential component of the magnetic field rotated by 30 degrees; so the structure cannot have been purely slow mode. It resembled a rotational discontinuity followed by a slow shock, and may have been a 2–4 time-dependent intermediate shock (P. Song, private communication, 1993). Standing downstream of this structure was a slow-mode rarefaction that continued until the magnetopause.

2.8 Summary

The static equilibrium model of the magnetosphere is essentially a model of the magnetopause. Chapman and Ferraro's gas-dynamic calculation of the shape and size of the magnetopause specifies a model of the interior field that is a reasonable description of the dayside magnetosphere. In the absence of viscosity and reconnection, their calculation leads to a reasonable description of the nightside as well. Such a magnetosphere has the shape of a teardrop, blunt at its leading edge and faring smoothly into an elongated tail-like structure on the nightside. The distance to its subsolar magnetopause is determined by the balance of the dynamic pressure of the solar wind and the vacuum pressure of the geomagnetic dipole, and scales as the one-sixth root of the dynamic pressure; under normal circumstances, this so-called "nose radius" is about 10 R_E. The teardrop closes 50–100 earth radii downstream, depending upon the sonic Mach number of the solar wind.

When the solar wind is magnetized, the gas-dynamic teardrop and its interaction with the solar wind is modified in several ways. The gas-dynamic rarefaction that closed the original teardrop is replaced by a combination of a fast and a slow rarefaction. The slow expansion is the one that lies next to the magnetopause everywhere until the magnetopause closes downstream. Second, in addition to a fast bow shock, an intermediate and/or a slow shock may also stand upstream of earth. Little is known as yet about how their configuration depends upon the state of the solar wind. For this reason, even tentative experimental evidence for slow and intermediate waves upstream of the subsolar magnetopause is important. Extended and irregular density maxima in the magnetosheath flow have been observed to stand upstream of the near-subsolar magnetopause for all orientations of the magnetosheath magnetic field. It is not clear whether the structures were intrinsically thick or broadened by magnetopause motion. One particularly well-diagnosed example proved to be a combination of a standing intermediate wave and a slow shock.

When the magnetopause is no longer dissipation free, the positions, orientations, and strengths of the intermediate and slow wave structures will be modified. Indeed, in Petschek's (1964, 1966) model of reconnection, the outward-facing intermediate and slow waves are pulled into the dayside magnetopause at the reconnection layer (Levy et al., 1964).

NOTES

1. Some of these results are summarized in the April 1982 issue of the *Journal of Geophysical Research* (Vol. *87*).

3

THE BELL-LIKE MAGNETOSPHERE

3.1 Introductory Remarks

The fact that the geomagnetic field "pulsates" was known a century before the space age opened. The century of ground-based observations did lead to an effective empirical classification of the pulsations based on period, wave form, and geographical distribution (Section 3.1), but why the magnetic field of an astronomical body should oscillate on short time scales was a first-class scientific puzzle that could only by solved in the space age. Low-frequency hydromagnetic waves were first observed in the distant magnetosphere on Explorer 6 (Judge and Coleman, 1962). The task for space research was to relate the oscillations of plasma and fields in deep space to the ground observations using the refined theoretical languages of magnetohydrodynamics and plasma physics. There have been two critical issues. The first was to understand how plasma instabilities generate some of the observed pulsations. The second, the subject of this chapter, has been to understand how motions of the magnetopause induced by the variability of the solar wind are communicated to the interior of the magnetosphere. The breakthrough came when it was understood that the MHD fast mode can cross field lines and couple resonantly to localized standing Alfven waves. What is seen on the ground is due primarily to the resonant Alfven waves (Section 3.3). In Section 3.4, we provide basic theoretical information about the eigenmodes of the "MHD box" as a conceptual framework for the observations of oscillating fields and particles in the magnetospheric cavity. Space observations provided convincing evidence for the existence of standing Alfven waves shortly after the fast-wave coupling theory was proposed (Section 3.5). The next issue was which standing wave harmonics are excited (Section 3.6). Multiharmonic excitations now seem to be a semipermanent feature of the dayside magnetosphere, attesting to the constant activity at the magnetopause. There have been a few observations of the "global mode," the low-frequency, radially standing compressional wave that may be responsible for discrete frequency resonant oscillations (Section 3.7).

Having learned something about the modes of the magnetospheric bell, we are in a better position to understand how the magnetosphere responds to the solar wind structures that pass by it. We will be concerned here with those structures that affect the magnetosphere primarily by altering its balance of pressure. Clearly, how the magnetosphere responds will depend upon the relative time scales of the

solar wind driver and the magnetosphere's natural response, reflected in the periods of its eigenmodes (Section 3.8). Interplanetary shocks provide an opportunity to study the propagation of fast compressional waves across the magnetosphere to the earth's surface and geomagnetic tail (Section 3.9). Solar wind tangential discontinuities enable one to study rarefactions as well as compressions of the magnetosphere in a controlled manner (Section 3.10). The ground response to interplanetary shocks and tangential discontinuities is mediated by the ionosphere in an important way (Section 3.11). The effects of short-term solar wind pressure variations have now been studied on a global scale using data from many satellites and/or ground stations (Baumjohann et al., 1983, 1984; Wilken et al., 1986). Section 3.12 reviews three case studies of the response to quasiperiodic variations of solar wind dynamic pressure with time scales comparable with that of the magnetosphere's global mode, the basic mode regulating its pressure equilibrium.

3.2 Geomagnetic Pulsations

Stewart (1861) reported the first measurements of "pulsations" in the geomagnetic field, made at Kew Observatory during the great magnetic storm of September 1, 1859. Later, Birkeland (1901) described what were later called "giant" pulsations of geomagnetic field at auroral latitudes. The most pressing issues were to classify the various types of geomagnetic field pulsations and to understand how those in midlatitudes are related to those in auroral and to to other forms of geomagnetic activity. During the first half of the twentieth century, geomagnetic pulsations were observed on the ground with rapid-run magnetometers and measuring the electric potential difference between electrodes induced by the pulsating magnetic field. The modern era of pulsation research began in the 1960s, when arrays of ground-based magnetometers became standard and spacecraft magnetometers became sensitive enough for ultra-low-frequency (ULF) waves to be observed in space. The advance into the modern era was also hastened by the formal classification of a complex micropulsation phenomenology whose outline came into view after the International Geophysical Year (1957). In 1964, the thirteenth General Assembly of the International Union of Geodesy and Geophysics approved the classification of geomagnetic pulsations into ones of regular and continuous appearance called Pc, and pulsations with an irregular form called Pi (Jacobs et al., 1964). The pulsations were also classified by period into Pc 1 (0.2–5 s), Pc 2 (5–10 s), Pc 3 (10–45 s), Pc 4 (45–150 s), and Pc 5 (150–600 s), and irregular pulsations in the Pi 1 (5–40 s) and Pi 2 (40–250 s) bands. The first statistical study of the geographical distribution of geomagnetic pulsations (Saito, 1962) had pointed to the classification scheme. The data showed separate spectral peaks in Pc 3, Pc 4, and Pc 5, bands, and that the different bands had different geographical distributions. For example, the Pc 3–4 pulsations were most frequently observed near local noon, whereas Pc 5 pulsations were distributed over a much wider region.

Low-frequency micropulsations have proved to have such a variety of energy sources that extensive diagnosis is now required to sort them out. Studies of

storm sudden commencements and sudden impulses indicated that sudden solar wind pressure variations stimulated hydromagnetic oscillations that could be registered on the ground (Voelker, 1966; Saito and Matsushita, 1967; Fukunishi, 1979) or, sometimes, only in space (Kauffmann and Walker, 1974). Dungey (1954, 1955) suggested that the Kelvin–Helmholtz instability at the magnetopause would cause the geomagnetic field to pulsate; morningside Pc 4–5 pulsations now appear to be due to this mechanism. Very early on, Tamao (1961, 1969) deduced from ground observations (Kato and Saito, 1962) that some Pc 3, Pc 4, and Pc 5 pulsations were likely to be driven from outside the magnetosphere and had proposed that magnetosheath disturbances were transmitted into the magnetosphere where they stimulated Alfven waves. This mechanism may be responsible for the harmonically structured Pc 3, occasionally Pc 4, waves that occur on the dayside when the interplanetary field is radial (Engebretsen et al., 1987; Anderson et al., 1991). The radial interplanetary field orientation puts the subsolar bow shock into the quasiparallel configuration known to produce Pc 3–4 band waves upstream of the shock and strong, more broadband fluctuations downstream (Engebretsen et al., 1991; Lin et al., 1991). Some of the magnetosheath wave energy may be transmitted across the magnetopause to stimulate the structured modes observed on the ground. Not all micropulsations are driven externally. "Storm-time Pc 5 pulsations," which are observed mostly in the dusk and afternoon sectors, have been linked to the injection of ring current plasma during geomagnetic storms (Barfield and McPherron, 1972, 1978; Kokobun, 1985; Pangia et al., 1990).

3.3 Coupling of Magnetopause Motions to Resonant Alfven Waves

Dungey (1954, 1955) was the first to suggest that low-frequency geomagnetic micropulsations might be due to surface waves on the magnetopause. However, ground observation later showed that the amplitude of Pc 4–5 pulsations did not peak near the ionospheric footprint of the magnetopause but at lower latitudes in the auroral oval (Samson et al., 1971). How could wave energy generated at the magnetopause cross field lines to the observing stations without being detected in between? To add to the puzzle, studies near the plasmapause (Fukunishi and Lanzerotti, 1974; Lanzerotti et al., 1974) revealed a consistent but complicated geographical pattern of pulsation amplitude and polarization. For each event, the wave amplitude maximized at a particular latitude, which was frequency dependent in a statistical sense. The sense of wave polarization switched from north to south across the amplitude maximum and the entire pattern reversed sense near local noon. On the theoretical side, Sugiura and Wilson (1964) and Tamao (1965) had suggested that individual flux tubes or shells could oscillate in a manner reminiscent of the resonant waves on a vibrating string. The eigenmodes of such oscillations were then calculated by Radoski (1966) and Cummings et al. (1969). The theoretical question was the same as the experimental one: The eigenmodes were localized to a particular L shell, and it was not clear how energy would reach them from the magnetopause. The conondrum was resolved in 1974, when

Southwood (1974) and Chen and Hasegawa (1974 a,b) showed that magnetopause motions would couple to an evanescent compressional mode that extends across field lines and stimulates a localized resonance where its frequency matches that of a standing Alfven wave (see also Hughes et al., 1977).

3.4 The Eigenmodes of the Magnetospheric Cavity

Study of the modes of the "MHD box" (Radoski, 1971) clarifies our intuition about the eigenmodes of the magnetospheric cavity. Consider a cold plasma contained in a box of finite extent in the x, y, and z directions with a uniform magnetic field in the z direction and plasma density that varies in the x direction and is uniform in y and z. Boundaries at $z = \pm L$ correspond to the northern and southern ionospheres; the x direction corresponds to the radial direction in the magnetosphere; and the y direction, to azimuth in dipole geometry. We first describe monochromatic excitations of this MHD box. If the density were uniform, the box would contain two uncoupled MHD waves, in the fast and intermediate modes. The fast mode is variously called the *compressional mode*, or in dipole geometry, the *poloidal mode*. The fast mode resembles the sound wave in an organ pipe. The MHD box supports a discrete spectrum of eigenoscillations whose frequencies are set by the dimensions of the box. The intermediate mode propagates its energy precisely along the magnetic field direction, and a standing oscillation can be set up along a single field line when both its ends are "tied" by the conductivity of the ionosphere. It is sometimes called the *Alfven wave*, or *shear Alfven wave*, or just simply the *shear wave*; sometimes it is called the *transverse mode* because it has no compressional component; in dipole geometry, it is called the *toroidal mode* because the perturbed magnetic field and field line displacement are in the toroidal direction.

So much for terminology. When the density is nonuniform, the fast and intermediate modes couple to one another. The differential equation describing the spatial dependence of the fast mode has a turning point, where the mode switches from propagating to evanescent, and a singular point where the wave frequency equals that of a standing intermediate wave. If the Alfven speed decreases monotonically outward with radial distance (x), a fast wave propagating inward from the magnetopause will be reflected at the turning point. The turning point is always beyond the resonance point; so the fast mode is evanescent when it couples energy from the magnetopause to the Alfven resonance. Because the resonance is a singular point of the differential equation, the coupling is strong despite the fact that the fast wave is evanescent. In the absence of dissipation, the Alfven eigenmode would be singular, but in the presence of any dissipation whatsoever, the singularity is removed, and a detailed balance is reached between the flow of wave energy from the magnetopause and its dissipation at the resonance point. The fact is that a balance is reached is independent of the details of the dissipation because wave energy will build up at the turning point, and therefore also in the evanescent region, until balance is achieved. At the same time, the dissipation

matters. For a given resonant L shell, the damping rate of the toroidal mode peaks at values of the height-integrated Pedersen conductivity that are comparable to those typical of the nightside midlatitude ionosphere. For this reason, the damping rate on the nightside is an order of magnitude larger on the nightside than on the dayside (Newton et al., 1978). All things being equal, this leads one to expect a significant day–night asymmetry in the occurrence and amplitude of micropulsations.

At this point, we have learned our first lesson. If an excited Alfven resonance is found, it is being driven. The second lesson is that the driver will be difficult to observe either in space or on the ground. If its azimuthal wave number is large enough, the fast wave is evanescent everywhere inside the magnetospheric cavity. Even if the fast mode does propagate in space, it carries no field-aligned current and is almost completely reflected by the ionosphere (Kivelson and Southwood, 1988); so it will be hard to detect on the ground. What is observed on the ground is due primarily to the Alfven resonance. The Alfven wave, which carries field-aligned current, is partially reflected and partially absorbed by the ionosphere. The reflection coefficient depends only on the height-integrated Pedersen conductivity (Hughes, 1974; Hughes and Southwood, 1976; Ellis and Southwood, 1983). The ground magnetic signature is due to the ionospheric current driven by the Alfven wave, primarily a Hall current that oscillates at right angles to the Pedersen currents that close the field-aligned currents carried by the resonant mode. The ground polarization is thus rotated by as much as 90 degrees relative to that in space (Hughes and Southwood, 1974; Hughes, 1974). Finally, small-scale structures are not easy to observe: Waves with horizontal wavelengths less than 120 km are typically absorbed before they reach the ground (Hughes, 1974; Hughes and Southwood, 1976).

The first papers on the coupling between compressional modes and resonant Alfven waves treated the case where the fast mode is evanescent everywhere inside the magnetopause (Chen and Hasegawa, 1974a; Southwood, 1974). The assumption of monochromatic excitation in these papers was adapted, at least qualitatively, to the the suggestion that the Kelvin–Helmholtz instability at the magnetopause would produce waves in a restricted frequency range (Chen and Hasegawa, 1974a). This theory indicated that a circularly polarized monochromatic perturbation generated by the K–H instability at the magnetopause stimulates an elliptical polarization of the opposite sense in a thin region just beyond the resonant field line, a peak in amplitude at the resonance, and an elliptically polarized wave of the reversed sense within the resonant field line. The overall radial–latitudinal sequence reverses sense at local noon. These features had clear counterparts in micropulsation observations. However, the magnetopause is also subject to buffeting, an erratic series of short impulses that creates a broadband response. To model this process, Chen and Hasegawa (1974b) studied the long-time asymptotic response of the coupled wave system to a delta-function impulse, still in the limit of large azimuthal wave number, where the compressional mode is evanescent. In this case, a continuum of transverse Alfven eigenmodes persists well after all compressional magnetic field perturbations have died away. Each

field line rings at its own resonant frequency. Of course, the stimulus need not be a sharp impulse: a sufficiently broadband source would excite the continuum almost as well (Hasegawa et al., 1983). Chen and Hasegawa (1974b) showed the plasmapause can support a discrete-frequency surface mode whose persistence increases as the plasmapause density gradient scale length diminishes.

The so-called global mode is a propagating fast wave whose azimuthal wavelength is the order of the size of the magnetospheric cavity. Reports of discrete frequency ULF oscillations on the ground (Kokobun and Nagata, 1965; Stuart et al., 1971; Samson et al., 1971; Rostoker and Samson, 1972) has stimulated considerable interest in the idea that standing poloidal eigenmodes might stimulate discrete toroidal resonances (Allan et al., 1986a,b; Inhester, 1987; Krauss-Verban and Patel, 1988; Zhu and Kivelson, 1988, 1989; Lee and Lysak, 1989, 1991). For monochromatic excitation, MHD box theory indicates that a discrete standing fast mode can be radially confined between a turning point and the magnetopause (Kivelson and Southwood, 1985, 1986). This standing mode will "tunnel" energy via an evanescent field structure to the Alfven resonance inside the turning point. The damping at the resonance will drain energy from the global mode, which thus must be continually fed by an external source. Numerical computations have strengthened the belief in the possiblity of global modes (Allan et al., 1986a,b). Broadband excitation should excite a discrete spectrum of global modes, each of whose eigenfrequencies matches a field line resonance frequency somewhere in the system (Kivelson and Southwood, 1986). Thus, for impulsive excitation, both global modes and the Alfven continuum ought to be excited. Zhu and Kivelson (1988) found that the global modes of the MHD box emerged immediately following the disappearance of the initial transients stimulated by impulsive excitation. During this phase, discrete components with the same frequencies were found over the entire spatial region. The discrete modes were damped exponentially, and the Alfven continuum was all that remained in the long-time limit.

Global modes can also exist inside the plasmasphere. Krauss-Verban and Patel (1988) numerically solved the MHD box equations for both discrete and continuum modes in conditions approximating the interior of the plasmasphere. The eigenperiods of the interior global modes were in the Pc 3 range, 20–30 s, for a plasmapause located at L = 5–6, and did not match those of standing Alfven resonances, except for a few locations in the sharp density gradient of the plasmapause. These global modes therefore were weakly damped and lost their energy directly through ionospheric Joule dissipation, since they could not do so via mode conversion to Alfven resonances.

Once it became clear that a continuum would be excited, the question arose as to how many continuum modes would be excited at a given point in space. The first theories had treated only one standing resonant mode per field line, presumably the fundamental, and of course there can be higher harmonics. The structures of the harmonics in turn depend upon the distribution of density along field lines. When the density depends upon both x and z in the MHD box model, a fourth-order differential equation describes the coupling between fast and

intermediate modes (Southwood and Kivelson, 1986). If the density were constant along x but varied with z, the fast and intermediate box modes would again be uncoupled. The structures of the z eigenmodes obtained assuming there is no coupling between the poloidal and toroidal modes give a useful indication of the general situation in dipole geometry (Radoski and Carovillano, 1966; Radoski, 1967). The standing eigenmodes may either be symmetric or antisymmetric about the "equator" ($z = 0$). For the fundamental, the plasma displacement in the fundamental mode is symmetric, and the perturbed magnetic field is antisymmetric about the equator; harmonics with successively higher frequencies alternate symmetry. When the density distribution is concentrated toward the equator, so also are the gradients of the eigenmodes. The higher-harmonic Alfven resonances may be excited by either the fully evanescent fast mode, by the discrete global modes, or both. In the case of discrete mode excitation, a fast wave propagating in from the magnetopause can drive harmonic field line resonances in the region exterior to its turning point, where its amplitude has not yet decayed, whereas it drives the fundamental in its evanescent region (Southwood and Kivelson, 1986). The z structure of the discrete global modes can again be understood qualitatively by assuming the density is independent of x. In this case, there can be turning points located between the "equatorial plane" and the "ionospheres," in which case the discrete mode is confined between them and is evanescent beyond them. The compressional eigenmodes can be either symmetric or antisymmetric, as before. The coupling between fast and intermediate modes at the resonance points will be the most efficient when their z eigenmodes have the same parity, that is, symmetric to symmetric, antisymmetric to antisymmetric. For these reasons, the fundamental Alfven resonance will not necessarily be the most strongly excited or the most frequently observed.

By and large, the studies of the eigenmodes of the MHD box have successfully created a conceptual underpinning for the interpretation of observations. However, the many issues of detail and quantity that immediately spring to mind on reflecting upon this theoretical literature are best addressed by resorting to the observations themselves.

3.5 Observations of Standing Alfven Waves

Strong evidence for standing waves had been provided by early observations of pulsations at magnetically conjugate ground stations. Not only were similar wave forms observed at opposite foot points of a magnetic field line, the phase relations between the same field components at both northern and southern stations also were consistent with the elastic string analogy of standing Alfven waves (Sugiura and Wilson, 1964). Multispacecraft observations gave unambiguous evidence for the position dependence of the wave frequency (Takahashi et al., 1984). Geosynchronous spacecraft stay on approximately the same L shell throughout the day. However, the plasma density distribution is not axisymmetric around the dipole axis, and the magnetic field is not strictly dipolar, so that there will be a slow

diurnal variation in the fundamental frequency of standing waves. Slightly different frequencies were observed at three geosynchronous spacecraft, ATS 6, SMS 1, and SMS 2, which were separated by 20 degrees in longitude. These could be explained by assuming that each spacecraft was observing the third-harmonic frequency of the local field line.

Because the earth's dipole and spin axes are inclined by 11 degrees, geosynchronous spacecraft can be stationed anywhere between plus and minus 11 degrees geomagnetic latitude. Because the different harmonics have different latitude variations, the harmonics may appear different at different geostationary spacecraft. The latitude-dependent occurrence of the waves was consistent with the latitude dependence of the standing-wave eigenmodes (Singer and Kivelson, 1979; Baker et al., 1980; Takahashi and McPherron, 1982). Proof that the waves were standing modes came when it was found that the wave electric and magnetic fields phases were in quadrature (Kokobun et al., 1977; Hughes et al., 1978a; Cummings et al., 1978; Singer et al., 1982); originally, the wave electric field had been inferred from particle drifts, but later it was measured directly (Singer et al., 1982; Junginger et al., 1983).

Hughes et al. (1978b) investigated the localization of the resonance region using observations made on ATS 6 and SMS 2, which were separated by 0.1 R_E. By considering the 180 degree phase reversal of the azimuthal field perturbation across the resonant structure, they inferred an L-shell thickness of 0.25 R_E in the Pc 3 band and 0.6 R_E in the Pc 4 band for one event. The widths of the resonant regions in three Pc 4–5 events estimated from ISEE 1 and 2 observations ranged between 0.2 and 1.6 L shells (Singer et al., 1982). Thus, the Alfven wave structures were radially localized. Further confirmation came from observing the ionospheric footprints of the resonant field line; STARE radar observations verified that individual geomagnetic field shells oscillated in the toroidal mode simultaneously at their separate eigenperiods (Poulter and Nielsen, 1982; Allan et al., 1985). Greenwald and Walker (1980) estimated that about 6 GW of power was delivered to the ionosphere by resonant toroidal oscillations and dissipated by Joule heating.

3.6 Occurrence and Distribution of Standing-Wave Harmonics

In principle, there are an infinite number of standing-wave harmonics; since not all occur, the harmonic numbers of the ones that are observed contain important clues to possible driving mechanisms. Although the existence of harmonics had been recognized in early ground (Duncan, 1961; Hirasawa and Nagata, 1966; Annexstad and Wilson, 1968) and space observations (Barfield et al., 1972; Cummings et al., 1975; Patel et al., 1979; Singer et al., 1979), the first extensive survey of harmonic content was carried out using observations made onboard ATS 6 in geosynchronous orbit (Takahashi and McPherron, 1982, 1984; Takahashi et al., 1984). The power spectrum of the toroidal magnetic field component at ATS 6 often showed multiple peaks with nearly constant frequency separation. Up to six harmonics could be observed. Such quasicontinuous multiple-harmonic events were seen throughout

the dayside of the magnetosphere, some lasting as long as 10 hours. The spectral peaks were regularly spaced with the typical separation of 14 mHz near noon gradually decreasing to 10 mHz in the afternoon as would be expected if they were locally resonant. These waves, which were in the Pc 3–4 band, corresponded to the second and higher Alfven wave harmonics, and the fundamental mode seemed to be absent at geosynchronous orbit. The quasigeosynchronous spacecraft AMPTE/CCE surveyed the occurrence of ULF waves over a wider distance range, 5–8.8 R_E, and to slightly higher magnetic latitudes (±16 degrees) than are available to geosynchronous spacecraft. Harmonically structured, toroidal magnetic field oscillations were encountered on approximately half of the 120 dayside passes and on none of the nightside passes examined by Engebretsen et al. (1986b). The dependences of frequency upon radial distance and amplitude upon geomagnetic latitude were consistent with localized Alfven resonance models. The toroidal modes were truly localized: No instances of of toroidal oscillations whose frequency was constant over more than 1/2 R_E were found in the AMPTE/CCE data set (B. J. Anderson et al., 1989).

Further statistical analysis of the AMPTE/CCE data set was carried out by B.J. Anderson et al. (1990, 1991). Fundamental toroidal resonances, missing at geosynchronous orbit, occurred about 40–50% of the time in the dawnside region beyond $L = 8$. Their periods were in the Pc 5 band. Their latitudinal occurrence distribution was consistent with the magnetic field node at the equator and increase in field strength with latitude expected for the fundamental. Taking into account the fact that the fundamental was more likely to be detected away from the equator, the authors concluded that the true occurrence rate exceeded 80%, which means that fundamental resonances are really excited almost all the time outside geosynchronous orbit on the dawnside. In sharp contrast, fundamental resonances were present less than 10% of the time beyond $L = 8$ near dusk. A similar dawn–dusk asymmetry in satellite observations of azimuthal Pc 5 pulsations was reported on several earlier occasions (Takahashi and McPherron, 1984; Kokobun, 1985; Kokobun et al., 1989).

Harmonic toroidal resonances in the Pc 3 frequency band were the dominant form of ULF wave activity detectable at low latitudes, being present 60% of the time in the prenoon hours (B. J. Anderson et al., 1990). These harmonic resonances were remarkably uniformly distributed in radial distance between $L = 5$ and the spacecraft apogee, $L = 8.8$. The local time distribution of intense events was essentially uniform on the dayside and cut off sharply at 0600 and 1600 MLT. Between 0600 and 0400 MLT on the dawnside, and between 1600 and 1800 MLT on the eveningside, the occurrence rate dropped to near zero; since lower frequency fundamental modes could be found in these local time sectors, it appeared that the cutoff of the harmonic mode distribution was not due to the change in ionospheric conductivity near the terminator. The local time distribution was essentially the same as for dayside Pc 3 pulsations measured on the ground, indicating that dayside Pc 3 pulsations at high latitudes are signatures of harmonic resonances.

Two other classes of ULF micropulsations appeared to be generated by energetic particles (B. J. Anderson et al., 1990). Radially polarized monochromatic

waves in the Pc 4 band, which were probably second-harmonic poloidal mode resonances, occurred predominantly on the nightside and were absent on the morningside. The eveningside Pc 5 wave population contains waves with significantly more compressional power than on the dawnside. So-called "storm-time Pc 5" waves occurred primarily beyond geosynchronous orbit at dusk and predawn and were localized within 15 degrees of the equator. Their spatial distribution suggested that they were associated with drifting energetic protons in both the dusk and predawn regions. Allan et al. (1983) showed that such compressional Pc 5 pulsations would not be easily detectable on the ground. Finally, another unidentified, amorphous class of broadband waves without discernible frequency structure constituted about 30–40% of the events on the dayside.

3.7 Observations of the Global Mode

Despite the intense theoretical interest in the discrete global modes, there have been relatively few direct observations of them. Kivelson et al. (1984) reported ISEE 1 observations of compressional oscillations with an 8-minute period that remained roughly constant for almost 3 hours as the spacecraft moved between $L = 5$ and 10 near local noon. The density and magnetic field compressions were in phase; so the oscillations were in the fast MHD mode. The authors suggested that this had been the quarter-wave fundamental of the global mode. A similar event was observed on ISEE 1 and 2 between $L = 5.6$ and 7.3 at about 1000 MLT during the recovery phase of a magnetic storm (Takahashi et al., 1985). The wave propagated westward with a large azimuthal wave number, about 30, and exhibit in-phase ocillations of density and magnetic field magnitude. Crowley et al. (1987) presented ground magnetometer and EISCAT observations of two large-amplitude Pc 5 pulsations excited by a sudden impulse. The ionospheric electron density inferred for the northern hemisphere from EISCAT measurements and modeled for the southern hemisphere, predicted a higher rate of dampling than was observed. The authors suggested that the ionospheric damping was competing with excitation by the global mode, which, once it is excited, feeds energy into field line resonances at a known rate.

3.8 Response of the Magnetosphere to Passing Solar Wind Structures

We will classify solar wind structures according to time scale as extended structures, pulses, and discontinuities. Extended structures are of long duration, produce a slow evolution of the configuration of the magnetosphere, and can be understood using the equilibrium picture developed earlier. In this chapter, we focus on the magnetosphere's response to discontinuities and pulses. The discontinuities are those of magnetohydrodynamics, the forward and reverse fast, intermediate, and slow shocks, and the tangential discontinuity. These sudden

changes induce a broadband response inside the magnetosphere, which can ring as a whole in a global fast mode and/or couple to field-line resonances. The pulses comprise a variety of perturbations that stimulate the magnetosphere in a more nearly monochromatic way because their temporal scales are comparable with the periods of the basic magnetospheric eigenmodes.

While each of the MHD discontinuities produces pressure variations, the fast shock and the tangential discontinuity are the most frequently encountered discontinuities in the solar wind context. The pressure pulse we might imagine to be like a simple density wave, a smoothly varying nonlinear wave of a few minutes duration. The solar wind is not the only source of small-scale pressure variations that interact with the magnetopause. The turbulence associated with the bow shock will produce small-scale pressure variations in the magnetosheath even when the solar wind is quiet. And so, the magnetosphere is constantly buffeted by both sudden and smooth magnetosheath pressure changes on time and space scales comparable with that required to establish basic pressure equilibrium between the magnetosphere and the solar wind. These would be responsible for some geomagnetic activity even in the absence of viscosity and reconnection, and on occasion it is difficult to distinguish the activity due to pressure variability from that due to viscosity and reconnection.

3.9 The Response of the Magnetosphere to Interplanetary Shocks

Of all the various types of solar wind structures that pass by the magnetosphere, the interplanetary shock associated with magnetic storms is the simplest. It is essentially a step increase in pressure that propagates more or less radially outward from the sun. As it approaches the earth, it hits the bow shock first, launching several additional magnetohydrodynamic waves into the magnetosheath in the process, and creating more as they interact with any intermediate/slow structures standing upstream of the magnetopause. The major step-like increase of pressure is carried by the transmitted interplanetary shock and begins to compress the magnetosphere the moment it hits the dayside magnetopause. By Huygen's principle, the progressive compression of the magnetopause as the shock propagates around it launches a series of fast magnetohydrodynamic waves into the interior of the magnetosphere. Some of these are reflected at the plasmapause, and some are transmitted into the plasmasphere. When the transmitted wave front hits the ionosphere, it stimulates the flow of ionospheric currents that rotate the direction of the perturbation field. When the magnetic field perturbation reaches the ground after having been modified in these ways, it is registered as a so-called "storm sudden commencement," (SSC), for short.

The tailward-traveling compression of the magnetopause due to interplanetary shocks was first reported by Kauffmann and Konradi (1969). The fast waves launched into the magnetosphere by sudden compressions of the magnetopause can propagate faster than the solar wind, or the discontinuities that launched them. For example, Sugiura et al. (1968) reported a fast compression

associated with an SSC that traveled down the geomagnetic tail at a speed well in excess of the solar wind speed. The interaction between shocks and the magnetosphere has been investigated in detail in several case studies. The shock event of August 27, 1978 is a good example. The shock was first observed in the solar wind by ISEE 3 far upstream (163 R_E) of earth (Winterhalter et al., 1981). It hit the earth's bow shock somewhat more than 40 minutes later (Zhuang et al., 1981). At the time, ISEEs 1 and 2 were just inside the subsolar magnetopause about 9 R_E upstream of earth. These spacecraft encountered the following sequence of events. The transmitted interplanetary shock launched a compressional wave into the magnetosphere when it hit the magnetopause. The magnetic field and density were observed to increase in phase at both spacecraft indicating that the compression was in the fast mode; its speed based on the observed delay, 1410–1560 km/s, was slightly larger than the small-amplitude fast speed based on locally measured plasma parameters, 1340 km/s. After the fast compression had passed, the magnetopause current layer was then observed to move inward over the two spacecraft at the unusually high speed of 195 km/s. This was followed by a contact discontinuity, and finally the reflected shock front (the new bow shock front). Ground stations began to observe a sudden commencement about 3 minutes after the compression wave passed over the ISEEs.

3.10 Magnetospheric Response to Solar Wind Tangential Discontinuities

The tangential discontinuity is a sudden change in plasma pressure (or other plasma property) that takes place at constant total pressure and comoves with the fluid. In the solar wind, tangential discontinuities are likely to be large-scale corotating structures aligned typically with the spiral interplanetary field. Three waves are created when a tangential discontinuity collides with the bow shock (Wu et al., 1992), in order, a forward fast shock, the transmitted tangential discontinuity, and a reverse fast shock (the perturbed bow shock). The forward shock carries a total pressure increase and hits the magnetopause first, followed by the tangential discontinuity, which does not change the total pressure. Apart from possible differences in orientation, the sequence of events that follows inside the magnetosphere is similar to that already described for interplanetary shocks. The ground signatures produced by the small pressure variations associated with tangential discontinuities are called *sudden impulses* (SIs); sudden impulses as a class can be compressional or rarefactive, whereas SSC are always compressional. Patel (1968), by comparing data from ground magnetic observatories with IMP 1 magnetic field data, found that SI signatures traveled from the earth to the geomagnetic tail at average speeds in the range 870–1300 km/s, well above the speeds of most high-speed solar wind streams.

The second Coordinated Data Analysis Workshop (CDAW-2) provided an excellent opportunity to study the effects of a tangential discontinuity on the magnetosphere (Nopper et al., 1982). The effects could be followed from the solar wind into the magnetosphere and to the ground. On July 29, 1977, IMP-H was

about 30 R_E upstream of earth in the solar wind, while IMP-J was in the magnetosheath near the dusk meridian. At 1420 UT on that day, IMP-H observed an increase in density without an accompanying change in flow speed; this tangential discontinuity produced a sharp spike in dynamic pressure. This pressure pulse should have reached the dayside magnetopause about 5 minutes later at the measured solar wind speed of 420 km/s. By using data from over 50 ground observatories, the development of the sudden impulse over the earth's surface could be followed with about half-minute timing accuracy. Ground SI signals were registered beginning 5 minutes after the pressure pulse presumably hit the magnetopause; they appeared first near the noon meridian and progressively later away from noon. The SIs arrived at the dawn and dusk meridians at 1432 UT, 2 minutes after they were registered at noon. The ground response also had interesting spatial structure. A maximum in ground amplitude was found near the $L = 5$ magnetic shell, suggesting that a resonant oscillation had been excited there. The magnitude of the SI was also amplified by at least a factor of five near the geomagnetic equator relative to other ground stations.

The CDAW-2 pressure pulse was monitored by the GEOS 1, GOES 1, GOES 2, and ATS 6 geostationary spacecraft (Nopper et al., 1982). GOES 1 and 2, near one another in the prenoon sector, saw similar signals: an essentially simultaneous compression, which gave way to four cycles of oscillations in the so-called D component of the magnetic field with about a 4 minute period. GEOS 1 was in the postnoon sector, about the same distance back from the subsolar magnetopause as GOES 1 and 2, and saw essentially the same signature as they did at the same time, within measurement accuracy. The sudden compression was seen 30 s later at ATS 6, where a similar oscillation in the D component was also excited. ATS 6 was further tailward than the other geostationary spacecraft, and the delay between GOES 1-2 and ATS 6 yielded a local propagation speed of 1500 km/s tailward.

3.11 Ionospheric Response to Sudden Pressure Variations in the Solar Wind

Wilson and Sugiura (1961) first established the pattern of the direction of the perturbation field on the ground associated with a sudden impulse. They also noted that geomagnetic pulsations often accompanied SIs. The counterparts in deep space of SSCs and SIs were first studied by Nishida and Cahill (1964) on Explorer 12, who showed that they were either sudden compressions or relaxations of the magnetosphere due to abrupt changes in magnetopause position. Gosling et al. (1967a,b), Ogilvie et al. (1968), and Burlaga and Ogilvie (1969) related interplanetary shocks and tangential discontinuities directly to SSCs and SIs, respectively, and Siscoe (1966), Siscoe et al. (1968), and, later, Smith et al. (1986), extracted the magnitudes of the sudden solar wind pressure changes just from ground magnetograms (see also Nishida, 1978). The successful interpretation of these observations rested on understanding how the new perturbations in space were related to those that had been recorded for decades on the ground. Nishida

(1964), and later, Inoue (1973) and Hughes and Southwood (1976), showed that ionospheric currents rotate the SSC perturbation field to be at right angles to that in space.[1] Kitamura (1963), Sarma et al. (1974), and Jain and Srinivasacharya (1975) noted that especially large enhancements in the H-component oscillations from sudden impulses are found near the geomagnetic equator, an effect that is undoubtedly due to an especially strong coupling of the SSC with the equatorial electrojet (Nopper et al., 1982).

3.12 Quasiresonant Response to Solar Wind Pressure Pulses

Imagine a pressure pulse convected with the solar wind toward earth; if the perturbed pressure is small relative to the overall pressure, the pulse will essentially be carried along the streamlines of the steady-state magnetosheath flow. Since the stagnation streamline forms the magnetopause, the pressure pulse will first compress or rarefy the subsolar magnetopause, and then propagate around it to the nightside. Thus, the pulse ought to stimulate a tailward-propagating magnetopause deformation. This deformation will couple to both fast and Alfven waves inside the magnetosphere. The field-aligned current response inside the magnetosphere, and in turn the ionospheric current response, will contain longer-lived oscillations when the dominant frequencies of the source spectrum match local field line resonances. In addition to any resonant response, there will be a nonresonant internal response whose time profile will reflect that of the solar wind perturbation.

Three modern case studies have investigated the magnetosphere's "resonant" response to variations in solar wind dynamic pressure on the roughly 10-minute time scale that it takes for the dayside magnetosphere to adjust to a change in its confining pressure. All three concluded that the pattern of standing oscillations induced inside the magnetosphere was consistent with excitation by tailward-propagating magnetopause compressions and rarefactions. We mention two of the case studies only briefly. Allan et al. (1985) and Poulter and Allan (1986) devoted the full resources of the 25-station Scandinavian Magnetometer Array (Kuppers et al., 1979), the Scandinavian Twin Auroral Radar Experiment (STARE), and the GEOS 2 geostationary spacecraft to elucidating the pattern of 6-minute period pulsations induced by a tailward-propagating perturbation. Sibeck et al. (1989b) showed that the time-dependent pattern of toroidal resonances created by a series of large-amplitude 8–10 minute oscillations in solar wind dynamic pressure was consistent with excitation by a series of tailward-propagating waves on the magnetopause. We now describe the third case study in more detail.

Potemra et al. (1989) contrasted the magnetosphere's responses to an 8 min step increase in solar wind density and to a two-cycle (8 and 11 min) quasiperiodic density variation identified by IMP 8 in the solar wind. *Viking*, AMPTE/CCE, and the EISCAT magnetometer array happened to be lined up in the 0600–0800 MLT sector at the times of these events. Oscillations in all magnetic field components began at AMPTE/CCE when the factor 2 density increase ought to have reached the subsolar magnetopause traveling at the solar wind speed. The

compressional component of the magnetic field varied with a 2–5 min period for 20 min, while a similarly unstructured variation in the poloidal component decayed after 2 cycles. In contrast, the toroidal component had a harmonically pure oscillation that lasted for three cycles. Its 3.5 min period was the same as that of the small-amplitude resonant mode that had been observed prior to the event. In the case of the second, quasiperiodic driver, the wave form of the compressional component was nearly identical to its solar wind driver, yet the transverse oscillations stimulated by this compression had roughly twice its frequency; this frequency was close to the local toroidal resonance frequency. *Viking,* in polar orbit essentially on AMPTE/CCE's field line, observed only the transverse oscillation in both the electric and magnetic fields, as did the ground array. It did not observe the compressional mode. In summary, the step input caused the magnetosphere to "ring" in various modes, while the quasiperiodic driver stimulated primarily a single resonant mode at the second harmonic. In both cases, the time delays between the two spacecraft, between ground and space, and the roughly 10 km/s propagation speed measured on the ground were consistent with a global perturbation propagating tailward on the magnetopause.

Data acquired using the Scandinavian and Greenland arrays of magnetometers have provided detailed information about the class of ground variations that probably corresponds to events like those described. The ground signals correspond to antisunward-convecting twin-vortex magnetic field perturbations of 10–15 min duration, 20 nT amplitude, and several thousand kilometer spatial scale (Friis-Christensen et al., 1988; Glassmeier et al., 1989; Glassmeier and Heppner, 1992). A survey of 82 events indicated that twin-vortex structures are detected most frequently during periods of low geomagnetic disturbance, $Kp < 2$, and have a pronounced peak of occurrence near 0800 MLT (Glassmeier et al., 1989). One event, which occurred during a period of steady northward interplanetary field, began 10 min after the solar wind density dropped by a factor two at IMP 8 (Friis-Christensen et al., 1988). This rarefaction created an isolated magnetic field oscillation, about one and a half cycles of a 7 min period wave. The ground equivalent currents had a twin-vortex pattern, corresponding to a pair of antiparallel field-aligned currents separated by about 700 km in the east–west direction. The twin vortex propagated tailward at a speed consistent with excitation by the rarefaction as it propagated over the magnetopause.

The twin vortices stimulated by solar wind rarefactions and compressions may have opposite polarities. Two events studied using the Scandinavian Magnetometer Array exhibited ground equivalent currents with a clockwise vortex to the west and counterclockwise to the east (Glassmeier et al., 1989), corresponding to downward field-aligned current in the west and upward in the east. The east–west scale lengths of the vortex pairs were about 2000 km^2, and both structures moved tailward with a speed of about 2.5 km/s (Glassmeier et al., 1989). During one of the events, GEOS 2, which was stationed about 500 km west of Kiruna, detected a compression of about 12 nT in the H component of the local magnetic field, suggesting that the magnetosphere was responding globally to an increase in solar wind dynamic pressure. On the other hand, another case study

found a twin-vortex system with the *opposite* polarity that propagated tailward at a comparable speed, 5.5 km/s (Glassmeier and Heppner, 1992).

3.13 Summary

Given the variability of the solar wind, even the teardrop magnetosphere would provide observers with a satisfying degree of variability. One form of geomagnetic activity would be present even in the absence of viscosity and reconnection, for the magnetosphere constantly responds to the variability of the solar wind and magnetosheath by ringing magnetically. In effect, the magnetospheric cavity is an MHD bell.

Occasionally, an interplanetary shock, or other pressure discontinuity, passes over the magnetosphere, providing the experimentalist with an opportunity to study how it responds to a sudden change in the pressure that confines it. About 2 min after such a shock arrives at the subsolar magnetopause, a fast MHD wave launched by the sudden compression of the magnetopause reaches the subsolar ionosphere, where it induces a shielding current that rotates the direction of the magnetic field perturbation registered on the ground. Two or so minutes after that, the fast compression reaches the inner edge of the plasma sheet on the nightside, and adjusts the strength of the cross-tail current dividing the two lobes of the tail. The compressional fast wave then races down the tail faster than the shock that set it up. The effects of tangential discontinuities are similar. In both the case of the interplanetary shock and of the tangential discontinuity, the effects of a sudden pressure variation in the solar wind begin to be felt on the ground some 2–3 min after they hit the dayside magnetopause. They are felt over the entire near-earth magnetosphere within, say, 10 R_E radial distance, in some 5 min. By doubling this time scale to allow the magnetosphere to react, we arrive at a time scale of order 10 min for the equilibration of the pressure in the near-earth magnetosphere. This is, not by accident, roughly the period of the MHD global mode.

No other solar wind perturbation is as simple as the interplanetary shock. The magnetosphere must also cope with a broad spectrum of smaller, less spactacular boundary perturbations. Some are smaller or less sudden pressure variations that are intrinsic to the solar wind. Even if the solar wind pressure were constant, the magnetopause would be buffeted by pressure variations induced by the bow shock's attempt to bring the plasma in the magnetosheath to thermal equlilibrium. The activity at the magnetopause is communicated to the interior of the magnetosphere by various MHD waves; of these, the fast waves are the most responsive to simple pressure variations. Because fast waves are efficiently reflected from the ionosphere and plasmasphere, all this would leave little impression on the ground, but for the fact that they couple to resonant toroidal Alfven modes on a field line by field line basis. The toroidal modes carry field-aligned current perturbations to the ionosphere, where they induce Pedersen and, especially, Hall currents, which rotate the direction of the incoming perturbation field vector. The variable magnetic fields created by these ionospheric currents are

detected on the ground as "pulsations" of the geomagnetic field. With present spacecraft magnetometer sensitivities, toroidal modes are found to be present in the dayside magnetosphere in some form more than half the time, attesting to the ceaseless activity at the magnetopause.

The compressional drivers of the toroidal modes are usually not identifiable, except in one very clearcut situation. The near-earth magnetosphere adjusts to a change in its pressure boundary conditions in about the time it takes a fast wave to propagate from the nose of the magnetosphere to the inner edge of the plasma sheet, perhaps 4–5 min, and the magnetosphere can react back in another 4–5 min. Solar wind pressure variations on the 5–15 min time scale thus ought to drive the magnetosphere in a quasiresonant way. For this reason, we have given them the special name *pulses*. Such pulses are observed to stimulate a time-dependent pattern of toroidal modes from which the spacecraft observer can qualitatively reconstruct the tailward propagation of the original solar wind perturbation.

The fact that wave energy from the magnetopause can stimulate a large resonant response at a distance implies that local toroidal Alfven modes of about the same frequency respond in about the same way to different external perturbations; so it is difficult to sort out the sources of geomagnetic variations in the Pc 3–5 frequency band. Great care has been needed to distinguish modes stimulated by various solar wind structures, magnetosheath noise, the Kelvin–Helmholtz instability, bursty dayside reconnection, local velocity–space instabilities, and probably other sources. The present rich and only partially differentiated picture will probably not become clearer until enough ground data are collected to reconstruct the distribution of resonant modes in space and time on a global basis, that is to say, until geomagnetic tomography becomes routine.

NOTES

1. Later, Shutz et al. (1974) used magnetometer and rocket electric field data to show that the low-latitude magnetic field signature could be explained by ionospheric currents.

2. This fact that this is getting to be larger than the scale sizes associated with the polar cusp also argues against a reconnection source. See the discussion in Chapter 8 about cusp hydromagnetic variations.

4

THE VISCOUS MAGNETOSPHERE

4.1 Introductory Remarks

This chapter describes how the magnetosphere is shaped by the tangential shear stress exerted at the magnetopause by collisionless viscosity. In Section 4.2, we discuss the low-latitude boundary layer (LLBL), which contains plasma of solar wind origin that has been transported across the magnetopause current layer. The velocity shear in the LLBL drives field-aligned currents into the ionosphere on the morning side and out of the ionosphere on the evening side (Section 4.3). These currents are of the appropriate sense to drive two-cell convection in the high-latitude ionosphere. The footprint of the LLBL in the ionosphere to which the field aligned currents connect is clearly identifiable by its characteristic particle precipitation (Section 4.4). The shear in the LLBL also generates 1–20 mHz Pc 4–5 micropulsations whose polarizations, tailward propagation, and phase speeds are consistent with the Kelvin–Helmholtz (K–H) instability (Section 4.5). The K–H vortices may couple to "vortex auroras" in the local afternoon sector of the auroral oval (Section 4.6). Vortex auroral dissipation may be responsible for a morning–evening asymmetry in the viscous interaction and its manifestations. Organized vortical flows have been observed not only next to the magnetopause, but also near the center of the plasma sheet, accompanied by local quasiperiodic magnetic field oscillations and Pc 5 micropulsations on the ground (Section 4.7). In Section 4.8, we discuss observations of a thick boundary layer flow on closed field lines next to the magnetopause 220 R_E downstream. This puts us in a position to estimate the rates of particle and energy injection into the magnetosphere due to the viscous interaction (Section 4.9).

4.2 The Low-Latitude Boundary Layer

Spacecraft crossings of the magnetopause last from a few seconds to a few minutes and are characterized by a rapid, distinct rotation of the magnetic field and striking changes in plasma density, pressure, flow velocity, composition, and energetic particle distribution (Williams, 1979a; 1980; Williams et al., 1979). A broader boundary layer lies just inside the magnetopause. The so-called low-latitude boundary layer was first identified at 18 R_E radial distance in the magnetotail using

Vela 4B (Hones et al., 1972) and *Vela 5 and 6* (Akasofu et al., 1973b) low-energy plasma measurements. The density and flow speed in the LLBL ranged from magnetosheath values next to the magnetopause down to 0.5/cm^3 and 100 km/s, respectively, at the inner edge of the LLBL. The fact that the flow speed was lower than in the adjoining magnetosheath was consistent with viscositylike transport, and excluded large-scale reconnection (Haerendel et al., 1978). The flow velocity was often but not always directed in the same sense as in the adjoining magnetosheath (Haerendel et al., 1978), and was nearly perpendicular to the local magnetic field (Eastman, 1979; Sckopke et al., 1981). The LLBL was soon found over much or all of the dayside and near-tail magnetopause (Rosenbauer et al., 1975; Eastman et al., 1976; Paschmann et al., 1976b, 1978; Crooker, 1977; Haerendel et al., 1978), and by 1979 it was possible to arrive at a clear definition of its essential properties (Eastman and Hones, 1979).

The outermost plasma region of the low-latitude magnetosphere containing (usually) tangentially flowing magnetosheathlike plasma of progressively decreasing density and flow velocity and increasing thermal energy (for an inbound crossing) with enhanced variability in flow direction relative to the adjacent magnetosheath. Magnetosheath level fluctuations continue through the LLBL and usually cease near its inner surface. The LLBL is bounded along its inner surface by the low-density, higher thermal energy magnetospheric plasma.[1]

Energetic electron measurements showed that the LLBL was "normally" on closed field lines (Eastman and Hones, 1979). The dusk-to-dawn electric field corresponding to tailward flow on closed field lines was found in a layer 1–2 earth radii thick just inside the magnetopause. Almost all the 28 ISEE 1 magnetopause encounters within 2 hours of local dusk studied by Mozer (1984) had a dusk–dawn electric field. The total electromotive force (emf) across the antisunward flow layer averaged about 2.5 kV, so that, given a similar boundary layer at the dawn magnetopause, the average emf attributable to the viscous interaction was 5 kV, a factor of four smaller than Axford's (1964) original estimate. The emf across the LLBL had no discernible relationship to the north–south component of the magnetosheath magnetic field, indicating it was not influenced by reconnection. Further downstream, at the orbit of the moon, the emf across each boundary layer was estimated to be 4.2 kV, based on a tailward flow speed of 200 km/s, a northward magnetic field of 5 nT, and a thickness of 4200 km deduced from the orbital speed of the moon (Sanders et al., 1980).

It is very difficult to measure the thickness of the LLBL because the magnetopause is constantly in motion. Eastman and Hones (1979) could find the ratio of the LLBL and magnetopause thicknesses from the ratio of their crossing times, but not the absolute value of either one. For a set of 90 well-defined nonmultiple boundary-layer crossings, the average LLBL thickness scaled to 0.4 R_E assuming the magnetopause field rotation was one Larmor radius, or about 100 km, thick. More recent two-spacecraft measurements indicate the magnetopause thickness is really 700 km (Winterhalter et al., 1981; Berchem and Russell, 1982), which increases this estimate by a factor of 7. Eastman and Hones (1979) found the the boundary layer thickness, whatever it is, increased from the subsolar point

to the flanks. Overall, the quoted thicknesses range from very small values to perhaps 2 R_E (Wei et al., 1990; Newell et al., 1991b). Because the ionospheric footprint of the LLBL remains connected to the moving magnetopause, the problem of multiple magnetopause crossings is eliminated, and low-altitude measurements may prove better at determining LLBL thicknesses and potentials than measurements next to the magnetopause (Newell et al., 1991b).

Later research (Sckopke et al., 1981; Mozer, 1984; Eastman et al., 1985a; Williams et al., 1985; Lundin et al., 1987; Mitchell et al., 1987; Bryant and Riggs, 1989; Phan et al., 1989) showed that the LLBL contains a highly structured mixture of low-energy magnetosheath and higher-energy magnetospheric particle populations. The temperature of the magnetosheath component is higher than in the adjoining magnetosheath, which is consistent with the idea that a dissipative process forms the LLBL. Williams et al. (1985) found that the LLBL near dawn and evening could be separated into two regions according to energetic particle diagnostics, a magnetosheathlike "outer LLBL" and an inner stagnation region that may contain the convection reversal boundary. Traver et al. (1991) examined the particle energy spectra and angular anisotropies measured during ISEE 1 traversals of the dawn (December 19, 1977) and dusk flanks (July 7, 1977) during periods of predominantly northward magnetosheath field when the boundary layer was presumably as free of reconnection as it is likely to get. No ion heating was observed, but there may have been some thermalization of electrons. Both ions and electrons exhibited bidirectional anisotropies; quantitative flux balance between oppositely streaming field-aligned electrons indicated that both the dawn and dusk LLBLs were on closed field lines. Flux balance was preserved in both the outer LLBL and stagnation region. There was an abrupt change in energy spectra, and ion bulk flow speed and direction upon entry into the stagnation region. The change may have reflected the fact that the plasma in the two regions had very different convection histories, that in the stagnation region having been generated near the spacecraft, while that next to the magnetopause had traveled a long way with the flow.

Song et al. (1990) contrasted subsolar magnetopause crossings in northward and southward interplanetary field conditions. In both cases, the magnetopause was a current-carrying layer across which the plasma density decreased and the magnetic field strength increased to nearly its magnetospheric value at its inner edge. The plasma itself was of magnetosheath origin, so that the entire magnetic field transition took place in magnetosheath plasma. No significant heating or cooling was observed. In the northward field case, the LLBL was divided into outer and inner regions. The plasma in both regions was a simple mixture of magnetosheath and magnetosphere plasma. In the outer LLBL, the ion density dropped with little increase in temperature, while the density decrease was accompanied by a large temperature increase in the inner LLBL. The ratio of electron to ion temperature was constant in the magnetopause, increased in the outer LLBL, and increased dramatically in the inner LLBL. The magnetopause and outer and inner LLBL thicknesses were 500–1300, 380–1000, and 170–430 km, respectively. The boundary layer had no substructure in the southward field

crossing. No fast flow was observed, suggesting that no reconnection was active at the time. The magnetic field rotated by 180 degrees during the crossing, and ions and electrons appeared to be heated.

Since reconnection does occur at the magnetopause, it has proved difficult to isolate the "pure" LLBL. Gosling et al. (1986) reported that an LLBL was typically not observed when the magnetopause contained accelerated ions, a signature of reconnection. On the other hand, Mitchell et al. (1987) found that the LLBL did exist but was was partly on open and partly on closed field lines for southward interplanetary field; it was entirely on closed field lines for northward field. The thickness of the LLBL has been positively correlated with northward interplanetary magnetic field (Haerendel et al., 1978; Mitchell et al., 1987), suggesting that the effects of viscosity not only are relatively more pronounced when there is no magnetopause reconnection but they may also be stronger in absolute terms.

4.3 Field-Aligned Currents

The link between convection in the ionosphere and in space is forged by field-aligned currents, sometimes called *Birkeland currents* after their discoverer. Field-aligned currents communicate stress between the neutral atmosphere, the ionosphere, the magnetosphere, and the solar wind, by connecting regions where there is a divergence of perpendicular, stress-bearing currents (Kern, 1966; Vasyliunas, 1970; Harel et al., 1981). They emerged as a quasipermanent feature of the magnetosphere–ionosphere system during the 1970s and early 1980s, having been detected onboard rockets (Casserly and Cloutier, 1975), low-altitude polar orbiting satellites (Zmuda et al., 1966, 1970; Zmuda and Armstrong, 1974; Iijima and Potemra, 1976, 1978; Potemra, 1979) and on higher altitude magnetospheric spacecraft such as OGO 5, IMP 4, and ISEE 1 & 2 (Aubry et al., 1972; Fairfield, 1973; Iijima, 1974; McPherron et al., 1975; Mozer et al., 1979; McPherron and Barfield, 1980; Frank et al., 1981).

The large-scale field-aligned currents above the ionosphere were first mapped using magnetic field data acquired on the *Triad* polar orbiting spacecraft (Zmuda and Armstrong, 1974; Iijima and Potemra, 1976, 1978). Field-aligned currents flow in or out of a 6-degree swath in magnetic latitude that more or less coincides with the auroral oval. This swath is divided into a poleward "region 1" zone and an equatorward "region 2" zone. Region 1 currents flow into the ionosphere in the morning sector and out of the ionosphere in the evening. Region 2 currents have the opposite sense at any local time. The two systems overlap near local midnight. Most low-altitude magnetic observations have been and are interpreted as being due to current sheets whose dimension in longitude is very much larger than it is in latitude. Typical current density, surface current density, and total field-aligned currents are about 1 mA/m^2, 0.1 A/m, and a million amperes, respectively; the total region 1 current usually exceeds that of region 2 by 20–25%.

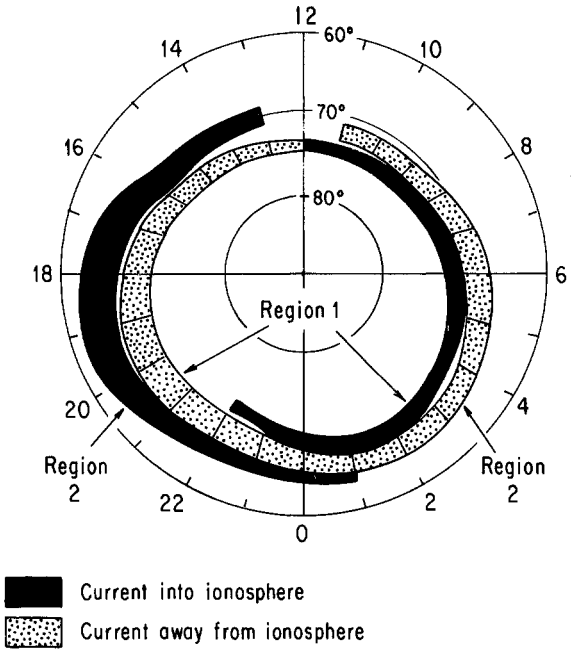

Figure 4.1. High Latitude Field-Aligned Current Systems. This figure, which has been adapted from Iijima and Potemra (1978), maps the average large-scale configuration of field-aligned currents threading the high latitude ionosphere as a function of magnetic local time and latitude. It is useful to divide the currents into two systems, called region 1 and region 2. The region 1 system is poleward of the region 2 system, and is downward on the morning side and upward on the evening side; the region 2 system has the opposite sense. The region 1 system connects to the drivers of ionospheric convection, whereas the region 2 currents connect the internal convective flow to its ionospheric load. While there will be a region 1/region 2 pattern in a purely viscous magnetosphere (Sonnerup, 1980), the intensity of the currents and the size of the pattern wax and wane with the north-south component of the interplanetary field, more or less in consonance with the behavior of the auroral oval. The field-aligned currents are weaker and more disorderly during prolonged intervals of northward interplanetary field. Note the more complex pattern of currents in the local midnight sector that is related to the convection reversal region and the so-called "Harang Discontinuity." T. Iijima and T. A. Potemra, *J. Geophys. Res., 83*, 612 (1978) copyright by the American Geophysical Union.

The separation in that first and all subsequent maps of the field-aligned currents into two regions, 1 and 2, has acquired a separate status as a subparadigm of magnetospheric physics. Region 1 currents communicate stresses whose ultimate origin is the solar wind, and so drive ionospheric convection, while Region 2 currents communicate stresses whose ultimate origin is the neutral atmosphere

and generally resist enhancement of convection. The regions of field-aligned current are regions of energy exchange between the magnetosphere and ionosphere, and we expect there to be a correlation between the electric field and the perturbed magnetic field from considerations of current continuity and energy flow (Bostrom, 1974). In other words, we expect to find a Poynting flux. Qualitative comparisons between simultaneous electric and magnetic field observations were made with data from the polar-orbiting spacecraft AE-C (Bythrow et al., 1980) and S3-3 (Smiddy et al., 1980; Rich et al., 1981). Quantitative comparisons made using DE-2 data established that the perturbation magnetic field and the electric field were generally orthogonal and highly correlated, implying a nonzero Poynting flux (Sugiura et al., 1982, 1983). Assuming current continuity, the downward Poynting flux was responsible for the energy dissipation by Pedersen closure currents in the ionosphere (Sugiura, 1984).

While the region1/region 2 pattern of field-aligned broadens and shifts equatorward with increasing geomagnetic activity, and therefore with the reconnection rate, the basic system would exist even if there were only viscously driven convection. The shear stresses in the low-latitude boundary layer drive region 1 field-aligned current into the ionosphere on the morning side and out on the evening side, and the overall dynamics of the low-latitude boundary layer is tightly regulated by its interaction with the ionosphere (Sonnerup, 1980). Indeed, the low-latitude boundary layer generates the most intense field-aligned currents to flow in and out of the auroral oval ionosphere. Iijima and Potemra (1978) found that the most intense upward region 1 field-aligned currents were located in the 1400–1600 MLT sector of the high-latitude ionosphere, while the most intense downward currrents were located in the symmetrically placed 0800–1000 MLT sector. Bythrow et al. (1981) showed that these currents connect to the ionospheric LLBL, whose properties we discuss next.

4.4 The Ionospheric Footprint of the Low-Latitude Boundary Layer

The ionospheric footprint of the low-latitude boundary layer has been identified in a number of diagnostics. Antisunward convection on closed field lines has been observed by low-altitude spacecraft (Coley et al., 1987; Newell et al., 1991b) and by ground-based radar (Lockwood et al., 1988). The ionospheric convection reversal boundary identified by radar lies equatorward of the boundary between open and closed field lines, consistent with the position of the LLBL in space (Lockwood et al., 1988), and the measured speeds and layer thicknesses imply a 1-10 kV emf between the last-closed field line and the convection reversal boundary. Newell et al. (1991b) compared nine prenoon LLBL precipitation regions in data acquired by the DMSP polar-orbiting spacecraft with the locations of the convection reversal boundaries determined either by the Sondrestromfjiord radar or by the drift meter on board DMSP F9. In eight of the nine cases, the convection reversal boundary was slightly poleward of the equatorward edge of the the LLBL precipitation region. The equatorward edge often had weak or erratic convection,

and may have mapped to the stagnation region near the magnetopause. The average width of the nine low-altitude LLBLs, 1.85 degrees MLAT, maps to roughly 1.85 R_E at the magnetopause, larger than is usually estimated, but the study sample may have been biased towards thicker, more easily recognizable LLBLs. The measured east–west ion drift, the magnetic field strength at the DMSP altitude (835 km), and the typical width led to a 5 kV potential across a single LLBL layer. Thus, the estimates of the viscous interaction potential using ionospheric radar measurements, drift meter measurements in low-altitude polar orbit, and electric field measurements near the magnetopause are all consistent.

The footprint of the LLBL in the high-latitude morning side ionosphere is the site of a complex interplay of aurora, field-aligned currents, and electric fields. From simultaneous Chatanika radar and *Triad* spacecraft data, Senior et al. (1982) concluded that sunward convection and the westward electrojet extended across the boundary between the region 1 and region 2 current systems (Iijima and Potemra, 1976) in the morning sector. Somewhat later, the Chatanika radar facility was moved to Sondrestromfjiord, Greenland, where among other things it was employed to study the same boundary from a much higher magnetic latitude. In one experiment, the radar followed a system of east–west-aligned structured aurora for several hours while DMSP F6 spacecraft made three consecutive passes over the radar (Robinson et al. 1988). The aurora were in the local dawn sector near 75 degrees invariant latitude. To the south of Sondrestrom, there were localized auroral intensity enhancements embedded within a broad diffuse aurora. To the north, a system of arc fragments extended 5 degrees poleward of the diffuse aurora. Measurements made as the spacecraft passed overhead showed that the diffuse aurora was due to the precipitation of 5 keV electrons, while 0.1–1 keV electrons precipitated into poleward auroral region in a spatially structured, unsteady fashion. Correspondingly, the radar measured ionospheric plasma density enhancements near 115 km altitude in the equatorward diffuse aurora and above 180 km in the poleward arc fragments. The ionospheric plasma drifted sunward in the diffuse auroral region; the corresponding southward electric field peaked precisely in the region separating the two types of aurora. The peak remained there for over an hour, during which time the intensities and spatial profiles of the aurora changed. The region 1/region 2 reversal measured by the spacecraft mapped just poleward of the boundary separating the two types of auroral precipitation near 75 degrees invariant latitude. Thus, the peak sunward convection rate, the region 1/region 2 reversal, and the change in character of the electron precipitation and aurora went together.

The convection reversal boundary was apparently too far poleward to be in the field of view of the radar, either when it had been in Chatanika or after it had been moved to Sondrestrom. In both cases, it appeared that the weak, structured arcs poleward of the morningside diffuse aurora were due to the precipitation of low-energy electrons from closed field lines that connected to the low-latitude boundary layer on the flanks of the magnetosphere. The complexity of the system of fragmentary arcs certainly conveys a sense of the disorder that must rule the low-latitude boundary layer, and suggests that continuous high-resolution ground

observations might shed considerable light on the hierarchy of time-dependent structures that is present next to the magnetopause.

4.5 Micropulsations Associated with the Kelvin–Helmholtz Instability

Sckopke et al. (1981) suggested that the complex arrays of high-contrast density structures in the LLBL were signatures of Lagrangian mixing in vortex structures generated by an unstable shear flow. In some particularly clear-cut cases, the ion bulk velocity and the density increased together, suggesting that the density had been carried along flow streamlines, consistent with this interpretation. We discuss here some of the observations that have been organized by the idea that the low-latitude boundary layer is unstable to a fluid shear-flow instability. The idea is not new. After Dungey's (1954, 1955) original suggestion that the magnetopause might be Kelvin–Helmholtz unstable, Atkinson and Watanabe (1966) proposed that the K–H instability would specifically generate Pc 4–5 micropulsations (see also Southwood, 1968). They argued furthermore that the propagation of the waves away from the noon meridian would produce elliptically polarized magnetic field perturbations that reversed sense near noon. The expected reversal near noon is present (Nagata et al., 1963; Kato and Utsumi, 1964; Troitskaya, 1967; Rankin and Kurtz, 1970; Samson et al., 1971), still the strongest reason to associate the pulsations with the Kelvin–Helmholtz instability.

Olson and Rostoker (1978) established the phase velocities and directions of propagation of LLBL-associated Pc 4–5 micropulsations from a set of 61 events detected on an east–west line of magnetometers operated by the University of Alberta. They found a linear relationship between phase shift and frequency that corresponded to a frequency-independent phase velocity of about 14 km/s. Projecting this to the 10–15 R_E magnetopause distance gave a speed of 140–210 km/s, consistent with the flow speed in the LLBL. This speed is 3–6 times that of the twin-vortex systems associated with solar wind pressure variations. The direction of the phase velocity changed abruptly 1–2 hours before local noon, and the signals propagated away from the reversal region towards the local morning and evening terminators. Aside from this basic regularity, the local time dependence of the signals presented a complex pattern. As one proceeded from the dawn meridian toward noon, the pulsations were nearly sinusoidal, with large-amplitude smoothly varying envelopes. Approaching noon, the pulsations began to decrease in amplitude and develop more irregular wave forms and envelopes. It was rare to find large-amplitude sinusoidal micropulsations in the afternoon sector; the oscillations were irregular, though quasiperiodic, with an evidently complex spectral content. We will see that a morning–afternoon asymmetry is common in the phenomenology related to the K–H instability.

Where is the velocity shear that generates the observed K–H waves, near the magnetopause or near the convection reversal boundary? Both cases seem to have been observed. On one hand, an unusually clear example of quasiperiodic magnetopause surface waves traveling tailward was found late on March 24, 1991

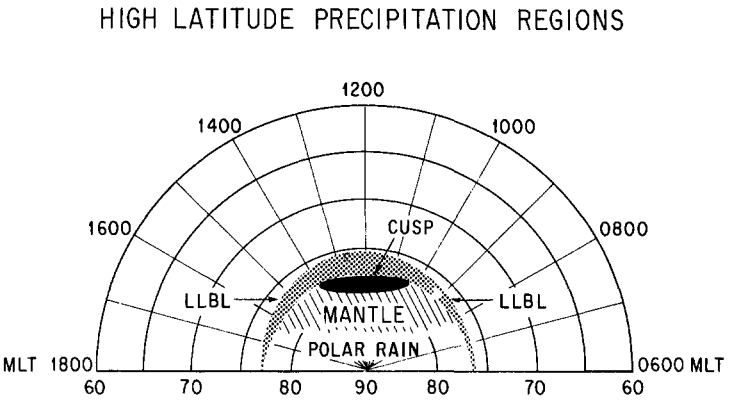

Figure 4.2. High Latitude Precipitation Regions on the Dayside. This figure, which has been simplified and adapted from Newell and Meng (1992), summarizes the relationships between the regions of particle precipitation into the high latitude dayside ionosphere. Each region has a characteristic signature in the ion and electron distributions. The ionospheric footprint of the low-latitude boundary layer (LLBL) may be found at all local times on the dayside, and is the most equatorward of the regions. It is characterized by structured bursts of particles that have been energized in the viscous boundary layer. Just poleward of the LLBL in the local noon sector is the polar cusp, containing plasma directly precipitated from the magnetosheath. Poleward of that is the mantle precipitation region, created by electrons and superthermal ions backstreaming along field lines from the mantle flow over the polar caps. The cusp ion distributions blend smoothly into the mantle ions. Finally, the electrons responsible for most of the solar wind heat flux precipitate directly into the ionosphere on open field lines in the form of polar rain. The last three precipitation regions are due to reconnection and are activated during southward interplanetary field conditions, while the LLBL precipitation is present during northward field conditions as well. P.T. Newell and C.I. Meng, Geophys. Res. Lett., **19**, 611 (1992), copyright by the American Geophysical Union.

after the magnetopause had moved into geosynchronous orbit (Cahill and Winckler, 1992). The magnetopause moved inward and outward six times over GOES 6, which was near 1030 LT. The regular appearance of the boundary oscillations was striking, and Fourier analysis led to an extremely well-defined frequency, 3 ± 1 mHz. Somewhat later, the magnetopause moved over GOES 7, which was closer to the subsolar magnetopause near 1245 LT. GOES 7 saw no oscillations; so the periodic waves at GOES 6 had been generated between the two spacecraft and were propagating with the magnetosheath flow towards the dawn meridian. On the other hand, observations made by the Greenland magnetometer chain suggested that K–H vortices are generated at the convection reversal boundary (McHenry et al. 1990).

A several-hour continuous series of vortices moving generally antisunward could occasionally be found on the dayside at quiet times. The vortices traveled between magnetometer arrays on the west and east coasts of Greenland at speeds of order 5 km/s. Multiple vortices of alternating sense traveled tailward on a line; their latitudinal dimensions were about 500 km and were the same from event to event. Polar orbit DMSP observations indicated that the vortices were on field lines that mapped to the equatorward edge of the low-latitude boundary layer, and Sondrestrom radar observations showed they were precisely on the convection reversal boundary. The fact that they mapped to the inner edge of the LLBL and not the magnetopause indicated that they were not stimulated by solar wind pressure pulses.

A dawn–dusk asymmetry in the occurrence of Pc 4–5 toroidal modes inside the magnetosphere has been noted many times (Kokobun and Nagata, 1965; Kokobun et al., 1976; Kokobun, 1980; Walker and Greenwald, 1981; Takahashi and McPherron, 1984; Kokobun, 1985). Fundamental toroidal modes are present between $L = 8$ and 9 about 40–50% of the time near dawn and less than 10% of the time near dusk flank (Anderson et al. 1990). Their occurrence is statistically correlated with solar wind speed (Kokobun et al. 1989), and they are almost always observed near the dawn flank when the solar wind speed exceeds 600 km/s. The correlation with solar wind speed suggests that they are stimulated by the Kelvin–Helmholtz instability. The K–H instability creates vorticity and small-scale field-aligned currents with a single predominant sign in the morning and afternoon sectors. The small-scale currents would have the same sense as the large-scale current system associated with the LLBL: downward in the morning and upward in the afternoon. The Kelvin–Helmholtz instability may be an unlikely source for the traveling twin-vortex systems, which involve field-aligned currents of both signs, but it does make it a plausible explanation for the vortex aurora we discuss next.

4.6 Vortex Auroras

Observations from polar-orbiting spacecraft have found spatially quasiperiodic bright auroral spots in the afternoon sector between 1400 and 1600 MLT whose luminosity is comparable with that of discrete nightside auroras during substorms. On May 3, 1986, *Viking* imaged four spots that were quasiperiodically spaced at 0.7–1.1 hour intervals of magnetic local time (Potemra et al. 1990). The spots ranged from 50 to 200 km in size, the separations between spots were 100-500 km, and the string of spots covered 1000 km. A similar series of bright spots was found embedded in a continuous band of ultraviolet emission that extended between 1300 and 1800 MLT at latitudes between 74 and 77 degrees (Potemra et al. 1990). Magnetic field and hot plasma measurements confirmed that these spots were colocated with the projections of upward field-aligned currents and with the precipitation of the roughly 200 eV electrons that characterizes the LLBL. Optical and ion drift measurements showed that another set of spots near 1400 MLT moved tailward (eastward) with a velocity of 1.5 km/s along the poleward boundary of the

persistent background aurora (Sandholt et al. 1990b). Occasional flow reversals were observed, but this does not necessarily subvert the identification with the LLBL, since flow reversals have also been observed in the LLBL in space (Gosling et al. 1990).

In one case, the appearance of such periodically spaced bright forms coincided with the onset of Pc 5 magnetic pulsations detected at an observatory directly under the drifting forms (Rostoker et al., 1992). The forms drifted eastward (tailwards) with a speed of about 1.8 km/s. Lui et al. (1987, 1989) suggested that auroral bright spots are due to small-scale intensifications in the upward field-aligned currents caused by the Kelvin–Helmholtz instability. The shear vorticity induces downward currents on the morning side and upward currents on the evening side; since structured aurora are associated with upward current, auroral spots should be found in the afternoon sector, and not in the morning, as is observed. Wei and Lee (private communication, 1992) pointed out that the dissipation of the instability by the production of auroral light in the afternoon might be responsible for the general asymmetry between the morning and afternoon high-latitude region 1 field-aligned current systems found by Iijima and Potemra (1978), a persistent enhancement in auroral intensity between 1400 and 1600 MLT (Cogger et al., 1977) and a local postnoon statistical maximum in the precipitating particle energy flux (Evans, 1985). The extra dissipation due to the coupling to the aurora on the afternoon side might also account for the dawn–dusk asymmetry in the occurrence of Pc 5 fundamental toroidal modes beyond $L = 8$.

4.7 Vortex Structures in the Plasma Sheet

The plasma sheet ion flow at ISEE 1 and 2 occasionally exhibited a distinct vortical structure, whose signature was a recurrent or continuing rotation of the bulk velocity vector essentially in the ecliptic plane (Hones et al., 1978). On one occasion, March 2, 1978, vortical activity continued without essential interruption for 9 hours, but most of the other vortex events were much more short-lived. The speeds of the vortical flows ranged from 30 to 200 km/s, and the periods for a 360 degree rotation ranged from 5 to 20 min. Typically, several complete cycles could be followed. Phase lags were determined from the plasma and magnetic field variations recorded during four vortex events by the two ISEEs, which were separated by several hundreds to several thousands of kilometers. These phase lags implied vortex scale sizes in the range 1–16 R_E, the larger size being comparable with the magnetotail's radius (Hones et al., 1983). The vortices were accompanied by magnetic field oscillations at the ISEEs and by Pc 5 pulsations in ground magnetometer records (Hones et al., 1981). In one case, Saunders et al. (1981) found that large-amplitude sinusoidal oscillations in all components of the magnetic field accompanied the plasma flow rotations. The plasma and magnetic pressure oscillations were in strict antiphase, but did not balance precisely, at least if one assumed isotropic ion pressure. Rostoker and Eastman (1987) suggested that such plasma sheet vortices might produce auroral bright spots in the evening sector.

Hones et al. (1981) searched for vortices during all the times when ISEE 2 was in the plasma sheet or boundary layer from the time of the ISEE launches in October 1977 through May 1979. They noted all clear instances of vortical motion, clockwise or counterclockwise, that lasted for at least one complete rotation. Clear-cut vortices could be discerned at intervals of several days. Vortices, even though they were infrequent, were found more or less equally regularly throughout the nightside plasma sheet out to the 23 R_E apogee of the ISEE orbit. The sense of vortex rotation was clockwise in the morning half and counterclockwise in the evening half of the plasma sheet, with a sharp line of demarcation on the midnight meridian. This suggested that the vortices were driven by the Kelvin–Helmholtz instability even though they were well inside the low-latitude boundary layer (Hones et al., 1981, 1983).

4.8 The Boundary Layer in the Magnetospheric Tail

The low-latitude boundary layer was found far downtail in the same year that it was discovered at *Vela* distance. Intriligator and Wolfe (1972) reported a single Pioneer 8 observation of a 2 R_E thick region of magnetosheathlike plasma just within the low-latitude magnetotail at 40 R_E downstream. Spacecraft orbiting the moon also found the LLBL at 60 R_E downstream. There was a sharp dropoff in density when the moon entered the tail at high latitudes, whereas when the moon entered the tail near the neutral plane, the magnetosheath flow underwent progressive changes similar to those in the LLBL nearer the earth before the plasma sheet proper was encountered. Howe and Siscoe (1972) estimated the thickness of the LLBL at lunar distance to be about 2 R_E from Explorer 35 observations. Sanders et al. (1980) estimated a typical thickness by multiplying the moon's speed by the duration of the LLBL encounters measured on Apollos 14 and 15 to obtain a thickness of about 0.7 R_E, slightly less than twice that found at the flanks of the magnetosphere by Eastman and Hones (1979); this estimate was a lower limit because it neglected the motions of the magnetopause.

Finally, a very thick boundary layer has been found on closed field lines at ISEE 3 distances. It has a typical electron temperature of 80 eV (Bame et al., 1983) and a density of 1 cm^{-3} at 200 R_E downstream (Zwickl et al., 1984; Sibeck et al., 1985). Richardson et al. (1989) examined three periods of low and intermittent geomagnetic activity in which the plasma bulk velocity was low, 100–200 km/s, and directed tailward, just as in the low-latitude boundary layer near the earth. However, the density and temperature in this deep-tail boundary layer were typical of the plasma sheet and were not magnetosheathlike. Two of the three periods in which the boundary layer was observed contained direct transitions to the magnetosheath. Judging from how long they were observed, the boundary layers were about 10 R_E thick in both dimensions transverse to the tail axis. The presence of isotropic electron fluxes indicated the boundary layers were on closed field lines. For a northward field component of 1 nT and a tailward flow speed of 100 km/s, the potential drop across each 10 R_E boundary layer was about 6 kV.

The thick boundary layer in the distant tail may actually be present all the time. Slavin et al. (1985) found that the plasma sheet magnetic field generally had a northward component, implying closed field lines, in the region next to the magnetopause. Somewhat later, Slavin et al. (1987) concluded that the boundary layer actually extended all the way across the tail at low levels of magnetic activity (AL < 100 nT). In a different approach to the issue, Heikkila (1988) found the ISEE 3 magnetic field to be more often northward than southward, and northward on average, at the moment of neutral sheet crossing when the flow speed was less than 400 km/s, whereas southward fields were more frequent when the flow speed exceeded 400 km/s. He suggested that the southward field events were associated with the occasional passage of a plasmoid past the spacecraft. Analysis of Pioneer 7 neutral sheet crossings yielded a similar result at 1000 R_E downtail: The magnetic field was generally northward, with only occasional southward turnings (Villante, 1976).

4.9 Boundary Layer Transport

The issue of overall LLBL transport splits into two parts: the transport across the magnetopause into the low-latitude boundary layer, and the transport within the LLBL. Candidates for anomalous transport mechanisms have included the Kelvin–Helmholtz instability in the region of shear flow (Southwood, 1968; Sckopke et al., 1981; Lee et al., 1981; Pu and Kivelson, 1983; Miura, 1984; Wu, 1986; La Belle-Hamer et al., 1988), and wave–particle interactions, perhaps with lower hybrid waves (Huba et al., 1977; Gary and Eastman, 1979; Lee 1982; Tsurutani and Thorne, 1982). The Kelvin–Helmholtz instability can transport momentum, but not mass (Miura, 1984), so that it cannot play a role in the transport of magnetosheath plasma across the magnetopause into the LLBL; the entry of plasma into the magnetosphere has usually been ascribed to reconnection or to diffusion across the magnetopause driven by local plasma turbulence. Prompted by observations of alternating regions of very high density contrast in the LLBL, other authors have suggested that plasma penetrates directly through the magnetopause and into the LLBL without benefit of reconnection (Lemaire, 1977; Lemaire and Roth, 1978; Heikkila, 1982; Lundin and Dubinin, 1984, 1985). (The large density contrast could also be due to Lagrangian mixing.)

Eastman (1979) estimated that the particle diffusion flux across the magnetopause that accounts for the thickness of the low-latitude boundary layer is responsible for the injection of 7 x 10^{26} particles per second into the dayside and near-tail magnetosphere. A diffusion velocity of 6 km/s follows from simple conservation arguments and Eastman's (1979) 0.5 R_E LLBL thickness. The ion diffusion coefficient associated with the plasma waves observed in the magnetopause (Tsurutani and Thorne, 1982; Gary and Sgro, 1990) can account for this diffusion velocity (Wei et al., 1990). To estimate the total particle injection rate into the low-latitude boundary layer, it is helpful to use a unit of number flux that is scaled to the magnetosphere. Approximately 10^{26} solar wind particles per

second cross an area of one square earth radius for typical solar wind conditions. Let us call this unit the *Dungey (D).* Lee and Akasofu (1989) compared the rates of particle injection into the low-latitude boundary layer by viscosity with that by reconnection. (We will take up their estimate of the input due to reconnection in the next chapter.) If particle injection and a viscous boundary layer extend to the distance of ISEE 3, viscous transport of solar wind particles and momentum will be an important factor in the dynamics of the plasma sheet all along its length. Eastman (1979) estimated that the dayside LLBL diffuses 7D magnetosheath particles into the LLBL within 20 R_E downstream of earth. However, this rate should be scaled to the entire length of the boundary layer. Use of the lower-limit estimate for the length of the boundary layer, 200 R_E, increases the input to 70D.

Pu and Kivelson (1983) estimated the power delivered to the interior of the magnetosphere by the Kelvin–Helmholtz instability at the magnetopause. The simple theory of the K–H instability in a cold plasma does not make clear how energy is transported from the magnetopause to the resonance regions, because the unstable waves are evanescent and have no Poynting flux. However, in a warm compressible plasma, the K–H instability destabilizes both the fast mode and the slow mode, and both modes carry Poynting flux into the magnetosphere. Using linear theory, Pu and Kivelson (1983) calculated the wave phase velocities, energy transport velocities, and energy fluxes in two representative geometries. In the frames of reference with respect to the plasma on each side, the energy fluxes and energy transport velocities were directed toward the bulk plasma. They estimated the energy flux carried across field lines by the fast mode from the power levels in waves with 150–200 s periods detected by OGO-5 in the magnetosheath and inside the magnetopause (Saito et al., 1979). The power flux density for typical conditions on the dayside magnetopause proved to be 0.04–0.2 GW/R_E^2 (1 GW $=10^{16}$ ergs cm^{-2} s). If the unstable regions on the magnetopause extend from 1030 MLT to the dawn terminator and from 1330 MLT to the dusk terminator, the total power input would be about 100 GW at disturbed times. During quieter intervals, the unstable region is smaller, and the power input diminishes to about 10 GW. Using STARE radar data, Greenwald and Walker (1980) estimated the Joule heating of the ionosphere by resonant toroidal oscillations to be 6 GW, so that the lower estimate of the K–H energy flux would be sufficent to maintain the observed pulsation levels. The total K–H power delivered to the magnetosphere would increase by up to a factor of ten if any contribution from the downtail magnetopause were included.

4.10 Summary

The idea that the magnetopause might be Kelvin–Helmholtz unstable suggested a way for the solar wind to exert a shear stress on the magnetosphere. It was a small step from there to expect that the magnetopause would be dissipative and that there would be a viscous boundary layer just inside the magnetopause. Indeed, observed low-latitude boundary layer fulfills many of the expectations for a viscous

boundary later. It contains a mixture of magnetospheric and heated magnetosheath plasma, which share a sheared tangential velocity profile. A reversal from tailward to earthward flow has been found within it. The density and temperature profiles in the boundary layer are highly structured and "contrasty" as though the flow streamlines had been rendered complex by Lagrangian mixing due to the development of an instability. There is abundant evidence for a viscous stress exerted across the low-latitude boundary layer. The strongest field-aligned currents observed anywhere are in the morning and afternoon sectors on field lines that map to LLBL in space. These regions may also be identified with the LLBL through the existence of few hundred eV electron streams and other particle signatures. A variety of techniques all indicate that a 1–10 kV emf develops across each two low-latitude boundary layers at dawn and dusk. The estimated emf, which depends upon poorly measured thickness of the LLBL, is about a factor two smaller than the emf found across the polar caps found during times of extreme geomagnetic quiet.

One type of geomagnetic pulsation has been identified with oscillations induced by the Kelvin–Helmholtz shear-flow instability. These have opposite senses of elliptical polarization in the morning and afternoon sectors, in accordance with the reversal in direction of the vorticity between the dawn and dusk magnetopauses, and propagate tailward at speeds, projected to the ionosphere, that are somewhat less than the magnetosheath speed. Moreover, the occurrence of fundamental toroidal modes on the dawn side is statistically correlated with the solar wind speed, consistent with an origin in boundary oscillations driven by the Kelvin–Helmholtz instability; the relative absence of these modes on the afternoon side may be due to auroral dissipation.

Two lines of evidence indicate that the low-latitude boundary layer, if it is restrictively defined as the closed-field line region containing tailward flow of magnetosheath origin, cannot account for all the viscous transport in the magnetosphere. First, the ISEE 1 and 2 observations of vortices in the plasma sheet proper suggest the existence of efficient viscous transport of momentum. Most of the vortices were larger than the thickness of the LLBL, and they were not restricted to the low-latitude boundary layers, but could be found clear across the plasma sheet on both sides of the midnight meridian. The sign of the vorticity reversed on the midnight meridian, suggesting that they were ultimately driven by the velocity shears at the morning and evening magnetopauses. Given poetic license, we might say that the vortex found by Hones et al. (1983) that was 16 earth radii in scale could have been one of the two convection cells of the original Axford and Hines (1961) picture. If so, the existence of smaller-scale vortices only tells us that Axford and Hines's convection can develop a turbulent hierarchy of cells at other times. The truly interesting question is why plasma sheet vortices were observed so infrequently. Is it reasonable for viscous transport to the center of the plasma sheet to be intermittent, when it is more or less steady in the low-latitude boundary layer? Is it conceivable that the viscous transport is present all the time but an organized pattern of convection cells is not?

A second observation suggests efficient viscous transport. Although the LLBL defined by magnetosheath plasma does not become significantly thicker at

large distances downtail than it is near the flanks of the magnetosphere, there is a thick layer of low-speed tailward-streaming plasma on closed field lines next to the magnetopause at ISEE 3 distances in the deep tail. The ion distribution function in this layer resembles that of the plasma sheet and not of the magnetosheath, again suggesting that magnetosheath momentum diffuses much farther across the plasma sheet than does the magnetosheath plasma. Most important, this implies that viscosity is still spinning a long tail-like field even at 200 earth radii distance downstream.

All this raises some interesting questions. Where *is* the viscous convection in the center of the plasma sheet when we do not see it? Perhaps, like other turbulent convection systems, the plasma sheet has transitions to chaotic flow, and that a relatively featureless chaotic flow state is the one we are most likely to encounter. Where does it all end? In other words, how does a viscous magnetosphere terminate downstream? How is the magnetic flux spun out by turbulent convection ultimately returned to the dayside of the magnetosphere? As our discussion evolves, it will become apparent that these questions are no longer academic. In some sense, despite the incontrovertible evidence for reconnection discussed next, we also have many aspects of a fully developed viscous magnetosphere.

NOTES

1. T.E. Eastman and E.W. Hones Jr., J. Geophys. Res., *84*, 2020 (1979), copyright by the American Geophysical Union.

5

THE RECONNECTING MAGNETOSPHERE

5.1 Introductory Remarks

Dungey's (1961a) pattern of internal magnetospheric convection was similar to that of Axford and Hines (1961). However, his model made testable statements about the structure of the magnetosphere that were not contained in the viscous convection model. It predicted that solar wind plasma enters the magnetosphere over the polar caps, that open field lines connect the polar caps directly to the interplanetary magnetic field, and that these field lines are stretched into a long, low-density magnetic tail. There would be a current layer separating the two lobes of the tail, and surrounding it, a sheet of relatively dense, hot, earthward-convecting plasma confined by closed field lines. A second magnetic neutral line would terminate the earthward flow region (Levy et al., 1964; Axford et al., 1965; Petschek, 1966; Axford, 1969). To preserve the steady state, reconnection at the tail neutral line had to have the same rate as at the dayside magnetopause. Clearly, the two reconnection regions ought to be major drivers of magnetospheric activity. Yet unambiguous proof of the existence of magnetopause reconnection was not found until 1979, 18 years after the reconnection model was proposed, and no one knew where to look for tail reconnection, because Dungey's model did not say how far away the tail neutral line was. However, the closure of the slow expansion fans carrying solar wind plasma into the tail lobes was a natural way to force tail reconnection (Coroniti and Kennel, 1979). This closure point is fifty to one hundred earth radii downstream of earth. Twenty-four years were to pass before the average location of the tail neutral line could be established, because no spacecraft until ISEE-3 spent enough time that far downtail. In retrospect, it is a testament to the power of the paradigm that so many would search for so long for direct evidence of dayside and nightside reconnection without jettisoning Dungey's model altogether.

Faith in Dungey's model was sustained by its collateral predictions. The access of energetic particles of solar origin to the polar cap ionosphere confirmed that reconnection occurs. The most persuasive case is made by observations of the precipitation of the solar coronal electron heat flux onto the polar cap that is magnetically connected to the sun (Section 5.2). The reverse process occurs: Ionospheric plasma escapes supersonically from the polar caps into the low-pressure tail lobes (Section 5.3). The configuration of the auroral oval (Section 5.4)

and the plasmasphere (Section 5.5) are natural byproducts of the reconnection model.

In the following sections, we present direct evidence that reconnection occurs on the dayside magnetopause (Section 5.6), for the injection of magnetosheath plasma into the polar cusp ionosphere (Section 5.7), for a flow of magnetosheath plasma over the poles and into the tail lobes (Section 5.8), for the convection of that plasma across the lobes of a long magnetic tail (Section 5.9), and, finally, for a magnetic neutral line in the tail and for a sheet of hot flowing plasma contained on the closed field lines within that neutral line (Section 5.10). The layered structure of the plasma sheet boundary layer is consistent with steady-state convection into the tail reconnection region (Section 5.11). In 1965, Dungey (1965) argued that the tail of an open magnetosphere would extend much further downstream than the teardrop closure point, and shortly thereafter, attenuated but definite tail lobes, and a plasma sheet, were found a thousand earth radii downstream of earth (Section 5.12).

We cannot avoid discussing the interrelationship of viscosity- and reconnection-driven convection. Field-aligned currents communicate the stresses between both components of convection, and the ionosphere and the two systems have to satisfy a common set of electrical boundary conditions there (Section 5.13). The two components of convection are competitive in terms of particle and energy transport, though not magnetic flux transport (Section 5.14), and influence one another by their joint interaction with the ionosphere.

5.2 The Polar Rain

If the magnetosphere is open, solar wind energetic particles should have direct access to the polar cap via the tail lobes. Confirmation of this prediction was the first "proof" that reconnection occurs, and is still the most direct demonstration that the polar cap magnetic field connects to the interplanetary magnetic field. Lin and Anderson (1966) were the first to find solar flare energetic electrons in the magnetotail, and shortly thereafter, West and Vampola (1971) observed that they can have equal intensities over the polar caps and in interplanetary space. Somewhat later, similar results were obtained for solar energetic protons (Fennell, 1973). Already by the time of Paulikas' (1974) review, the evidence that energetic particles access the polar caps was persuasive.

Perhaps the clearest demonstration of all comes from observations of the entry of the solar coronal electron heat flux into the tail lobes and its subsequent precipitation into one polar cap ionosphere as "polar rain" (Winningham and Heikkila, 1974). The solar wind electron heat flux is carried by a highly anisotropic and strongly field-aligned distribution of 10–1000 eV electrons. These electrons have smaller Larmor radii than more energetic and massive solar protons, and all things being equal, they are less likely to enter the magnetosphere by diffusing across field lines. No diffusion is needed to explain the trajectories of the coronal heat flux electrons from the solar corona to the earth, and it seems likely

that they will not diffuse much after they enter the magnetosphere either. A further bonus is the fact that the electron distribution is highly field aligned. All in all, the coronal electron heat flux, and especially its energetic and most field-aligned component, the so-called "strahl," should be wonderful tracers of where the field lines go.

It has been known for some time that electrons with energies similar to those in the solar wind precipitate rather uniformly into the polar cap that is connected magnetically to the sun (Fennell et al., 1975, Meng and Kroehl, 1977; Mizera and Fennell, 1978). More recently, the path the electrons take was clarified by measurements made in the near tail by ISEE 1 (Fairfield and Scudder, 1985) and in the distant tail by ISEE 3 (Baker et al., 1986b, 1987b,c, 1988). Both spacecraft found strongly anisotropic, field-aligned 50–500 eV electrons in the magnetosheath and tail lobes. The energy fluxes, 0.001–0.1 ergs/cm^2 s sr, were consistent with both the polar rain and the solar wind heat flux. The electron anisotropy near the magnetopause at ISEE 3 often changed smoothly from unidirectional away from the sun in the magnetosheath to bidirectional inside the tail. The bidirectionality developed from electrons that mirrored near the ionosphere after entering the tail and returned back to the tail lobes. Because the distant tail is constantly in motion, the ISEE 3 spacecraft was on occasion able to sample the northern and southern tail lobes in rapid succession. In these cases the bidirectional electrons electrons were found only in that lobe whose field lines lead back to the sun, that is, the southern tail lobe in an "away" sector of the solar wind, and the northern tail lobe in a "toward" sector. The field lines in the opposite lobe had virtually no heat flux of solar origin, and it was clear that dayside reconnection had disconnected these field lines from the sun.

5.3 The Polar Wind

Dungey (1961a) himself noted that the ionospheric plasma on open field lines would have difficulty achieving the sort of equilibrium it does on closed field lines. Subsequently, Dessler and Michel (1966) and Nishida (1966) pointed out that given sufficiently high temperature, hydrogen ions would evaporate from the polar cap ionosphere and escape into the tail lobes. At this point, it became clear that there would be three very different regions containing plasma of ionospheric origin in the space surrounding the earth. Inside the plasmasphere, the plasma would approach diffusive equilibrium with the ionosphere; then there would be an enclosing region on closed field lines in which the ionospheric plasma is pumped out by convection; finally, ionospheric plasma would escape freely into the tail lobes from the polar caps. Subsequently, Banks and Holzer (1968, 1969a,b) argued that an ambipolar electric field that develops in the presence of a dominant oxygen ion component will preferentially accelerate the lighter hydrogen and helium ions upward to supersonic speeds, and Axford (1968) used this "polar wind" concept to account for the anomalously rapid escape of helium from the atmosphere. As time passed, more detailed multifluid and kinetic models were developed to account for the

escape into space of singly ionized hydrogen, helium, and oxygen (for a review, see Raitt and Schunk, 1983).

The first observations of the expected nondiffusive equilibrium density profiles and upward hydrogen ion outflow were made onboard Explorer 31 (Hoffman, 1970); soon after, the outflow of helium ions was also detected on ISIS 2 (Hoffman et al., 1974). Full analysis of the ISIS 2 data set established that the upward flux of hydrogen ions at 1000 km altitude is typically about $10^8/cm^2$ s, with the helium ion flux a factor of ten smaller (Hoffman and Dodson, 1980); a systematic study of polar wind data acquired on the Dynamics Explorer (DE 2) spacecraft confirmed this result (Chandler et al., 1991). DE 2 data also provided the proof that polar wind was supersonic at high altitudes (Nagai et al., 1984). Finally, while the classical picture of a steady outflow of light ions through a heavier ion plasma did emerge when the DE 2 data were averaged, it did so only after averaging over a period of months: The short-term data were dominated by variability on a time scale of hours or less associated with substorms and other forms of geomagnetic variability (Chandler et al., 1991).

5.4 The Auroral Oval

Auroral observers have known for more than a century that discrete aurora in the late morning and early afternoon sectors are found at higher latitudes than they are in the evening sector, so that the maximum auroral occurrence region encloses the geomagnetic pole but is not centered on it (Tromholt, 1880). The concept of the auroral oval was proposed by Feldstein (1960, 1963a,b), Feldstein and Solomatina (1961) and Khorosheva (1961a,b, 1962, 1963) to account for the statistical regularities in all-sky camera observations of discrete auroras at the observer's zenith, together with the orientations of extended auroral forms. The oval concept has been widely used ever since to organize observations both of the optical aurora and of the energetic particles associated with the production of the auroral light. As soon as it could be confirmed by a single glance at a satellite photograph, the auroral oval achieved its own status as a paradigm of magnetospheric phenomenology.

It was quickly recognized that the basic geometry of the oval was implied by the reconnection model of the magnetosphere–its dayside position at high latitudes with the compression of the magnetopause, the dark polar cap with the open tail lobes, and nightside auroral activity with the precipitation of energetic electrons from the plasma sheet (Feldstein, 1966; Akasofu and Chapman, 1972). The oval therefore ought to depend upon the level of geomagnetic activity. Feldstein and Starkov (1970, 1971) approximated the equatorward and poleward boundaries of the statistical oval with circles; during magnetic quiescence, when the oval is the smallest, the centers of the circles were shifted antisunward by 3 and 4 degrees from the geomagnetic pole along the midnight meridian, and their radii were 17 and 15 degrees. As magnetic activity increased, the radii of the bounding circles increased.

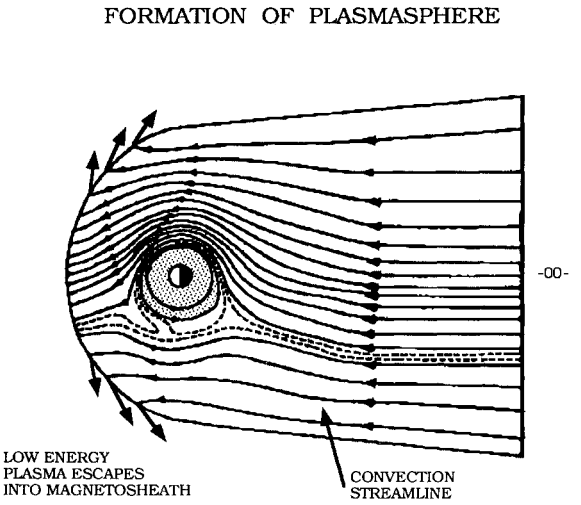

Figure 5.1. The Formation of the Plasmapause by Steady Convection. The magnetic equatorial plane of the magnetosphere is shown from above the north pole (Brice, 1967). Convection streamlines are drawn with arrows denoting the direction of the flow. Co-rotation dominates in the shaded region, leading to closed convection streamlines encircling the earth. Ionospheric plasma expanding into the low pressure magnetosphere will have time to reach diffusive equilibrium in this region (the plasmasphere.) Beyond the separatrix indicated by the dotted lines, the flow streamlines are open and the flow proceeds from the deep tail to the dayside magnetopause. In steady state, this separatrix marks the plasmapause. If the plasma of ionospheric origin escapes to the magnetosheath, convection acts to empty the field lines beyond the separatrix of their ionospheric plasma. The continuous existence of a plasmapause indicates that convection and magnetopause loss processes are not absent for long periods of time. The loss of ionospheric plasma to the magnetosheath should be particularly efficient if the magnetopause is frequently opened magnetically by reconnection. N.M. Brice, *J. Geophys. Res., 72,* 5206 (1967), copyright by the American Geophysical Union.

The attempts over the years to flesh out preceding statements with richer physical content led to the realization that there are several auroral ovals, one for the geographical distribution of each physical phenomenon related to the aurora, and that the precise definition of each specific type of oval depends upon the thresholds, resolutions, and sensitivities of the pertinent measuring instruments, as well as their particular vantage points (Feldstein and Galperin, 1985; Galperin and Feldstein, 1991). Thus, one cannot discuss auroral oval without introducing some basic information about how auroral measurements have been made. This will be deferred to the second half of our essay, where, as a prelude to the discussion of auroral substorms, we spotlight the nightside of the auroral oval. In the meantime, we will refer to this most basic of magnetospheric concepts frequently.

5.5 The Plasmasphere

The plasmasphere had been anticipated by Axford and Hines (1961), who understood that there would be a region close to the earth where corotation would dominate convection. The reconnection model made the plasmapause's origin in convection all the more persuasive, as we now recount.

The plasmasphere is a region of high-density, cold plasma of ionospheric origin that encloses the earth (Gringauz et al., 1960) and often has a sharp outer boundary, the plasmapause (Carpenter, 1966). The first hints of its existence came from studies of the propagation of lightning whistlers along field lines between hemispheres (Storey, 1953). Nishida (1966) and Brice (1967) explained its behavior as follows. The electric field generated by the rotation of the earth's conducting ionosphere maps along the geomagnetic field into space and adds to the convection electric field. The radial electric field due to rotation causes magnetic flux tubes near the earth to corotate, while the dawn–dusk convection electric field causes flux tubes beyond the region of corotation to convect toward the dayside magnetopause. Cold plasma expanding from the ionosphere into corotating flux tubes has time to arrive at a relatively dense diffusive equilibrium, since convection cannot carry this plasma to the magnetopause where it would be lost. On the other hand, the ionospheric plasma expanding into convecting flux tubes will not reach diffusive equilibrium before escapes into the magnetosheath. In a steady state, a sharp gradient in the cold plasma density would mark the separatrix between open and closed corotating flow streamlines. The separatrix is nearest the earth at local dawn, and furthest at local sunset; it moves in and out for larger and smaller convection rates. The real plasmapause is not always sharp, and its location is not always the instantaneous separatrix; nonetheless, the relatively continuous presence of a plasmapause suggests that convection is nearly always active enough to scour the outer magnetosphere of much of its cold plasma of ionospheric origin.

5.6 Direct Evidence for Dayside Magnetopause Reconnection

The first MHD model of fast reconnection (Petschek, 1964, 1966) indicated that the actual magnetic neutral region is so small that a spacecraft would hardly ever encounter it. Thus, virtually from the time the magnetopause was discovered (Cahill and Amazeen, 1963), people understood that they would have to identify and find remote signatures of reconnection taking place at a small neutral region of unknown position and size on a magnetopause that responds to a naturally turbulent magnetosheath environment as well as to a variable solar wind. Soon it became evident that reconnection itself affects the position of the magnetopause, and that the orientation and possibly the position of the reconnection region on the magnetopause surface respond to changes in the y and x components of the magnetosheath field. The magnetopause on occasion is displaced and distorted by surface waves whose presence is unrelated to reconnection. For probably all these reasons, the dayside magnetopause is almost always in motion, with a typical speed

of 40 km/s (Song et al., 1988). The few hundred kilometer thickness of the magnetopause (Berchem and Russell, 1982) together with this speed defines a short observational scale time of tens of seconds.

Sorting out unambiguous signatures of dayside reconnection proved to be a difficult observational issue. An early search of Explorer 12 measurements by Sonnerup and Cahill (1967) turned up only a few cases where the magnetic field component normal to the magnetopause surface could reliably be considered nonzero. Ironically, the normal component, the clearest difference between a reconnecting and a nonreconnecting magnetopause to the theoretician, may be the most difficult thing of all for the experimentalist to measure. Clear evidence of dayside reconnection was finally found by Paschmann et al. (1979) half a generation after the discovery of the magnetopause. An accelerated flow was detected just inside the magnetopause field rotation on eleven ISEE 1 and 2 passes. The fast flows were encountered between 0900–1700 MLT and 2–43 degrees GSM latitude. The change in velocity ranged between 0.6 and 1.2 and averaged 0.8 of the MHD prediction based upon the change in magnetic field. The density, temperature, and composition of the high-speed flows inside the magnetopause were consistent with a magnetosheath source. In several cases, the anisotropy of > 5 keV magnetospheric particles outside but adjacent to the magnetopause indicated they were streaming parallel to the magnetic field across a magnetically open boundary. The leaking energetic particles often terminated abruptly at a well-defined separatrix.

The average electric field components tangential to the magnetopause were 0.4–2.8 mV/m, or 2.6–18 kV/RE in magnetospheric units, about 20–150% of the solar wind electric field (Sonnerup et al., 1981). In all cases, net power was dissipated in the magnetopause. The electric field measured on ISEE 1 near the magnetopause fluctuated with typical amplitudes of 1–2 mV/m and time constants of 5–30 s so that the variation in the magnetopause field was comparable with the solar wind electric field (Pedersen et al., 1984). Despite the variability from one crossing to the next, the magnetopause electric fields were definitely larger for southward magnetosheath magnetic field. Aggson et al. (1983) studied five ISEE 1 magnetopause crossings in which the plasma density was high enough, > 10 cm^{-3}, to permit direct measurements of the x and y components of the electric field. Very large electric fields, 65–145 kV/R_E, were directed normal to the plane of the magnetic field rotations. For several of the cases, transformation to the de Hoffman–Teller (1950) reference frame, in which the electric field is zero, ordered the data, but the data were more disordered than expected for standing rotational discontinuities in the remaining cases. The role of steady rotational discontinuities in MHD models of reconnection may be taken by time-dependent intermediate shocks, in which case we do not expect exact agreement anyway (Wu and Kennel, 1992a,b; Lin et al., 1992).

The ISEE 1 and 2 fast plasma experiment detected fast flows in the near-tail dusk magnetopause that separates the plasma sheet from the magnetosheath when the local magnetosheath and plasma sheet magnetic fields were nearly antiparallel (Gosling et al., 1991). Some could be observed for hours. Fast flows

were found only in the layer containing the magnetic field rotation. The plasma number densities were slightly lower in the field rotation than in the adjoining magnetosheath, and the ion and electron temperatures were between those in the magnetosheath and plasma sheet, suggesting that some plasma heating occurred in the field rotation. Thus, these rotations differed from ideal MHD rotational discontinuities.

Most ISEE 1 and 2 crossings of the dayside magnetopause did not reveal the high-speed flow signature of reconnection. Part of the difficulty was the relatively low time resolution of the ISEE plasma measurements, as results from the faster three-dimensional AMPTE/IRM plasma instrument subsequently showed (Paschmann et al., 1986). Of 40 passes of this spacecraft through the 0800–1600 MLT magnetopause region, 22 had substantial magnetic field rotations, and of these, 11 had flows whose speeds exceeded those in the adjacent magnetosheath by at least a factor of 2. The durations of the high-speed flows were occasionally as short as 10 s and rarely exceeded 30 s, indicating either that the magnetopause was in motion when it was actively reconnecting, that the reconnection process was transient, or both. Nine of the 11 events could be subjected to a detailed test of momentum and energy balance; the agreement was generally good. In particular, the signs of the magnetic field component normal to the magnetopause deduced from the directions of the plasma velocity increase agreed with the signs inferred from the proton heat flux. Of course, not all AMPTE/IRM dayside magnetopause crossings showed signs of reconnection, nor would we expect them to. Twelve of the 21 passes through the multiple magnetopause crossing region, or 57%, did have at least one event in which the flow change that was half or more of the theoretically expected change; 31 of 70, or 45%, of the individual magnetopause crossings had significant flow changes. In five cases, essentially no change was found even though the magnetic field rotation was pronounced. Three of these lasted long enough that no high-speed flow could have been missed; these were certainly tangential discontinuities. Magnetopause reconnection could evidently be highly time dependent: Some individual magnetopause crossings with high-speed flows occurred only minutes from crossings without high-speed flows.

5.7 Precipitation of Magnetosheath Plasma into the Dayside Ionosphere

The northern and southern nulls in the dayside magnetopause field are prominent features of the Chapman–Ferraro model. In a closed magnetosphere, the null points are where all the magnetic field lines that compose the magnetopause surface in that hemisphere meet; each is connected to the dayside ionosphere below it by a single field line, a bundle of magnetic flux of measure zero (Spreiter and Summers, 1967). The low-altitude regions near the singular field lines have been given the name *polar cusps*. Null points did not appear in the first empirical magnetic field map of the high-latitude magnetopause (Formisano et al., 1979), but electrons of magnetosheath origin were found to trace out the bundle of field lines connecting the cusps to the magnetopause (Formisano, 1980). This was no surprise, since

plasma with magnetosheath density, temperature, and composition was known to precipitate directly into the ionosphere from cusp field lines (Frank, 1971; Heikkila and Winningham, 1971; Russell et al., 1971b; Shelley et al., 1976; Reiff et al., 1977; Crooker and Burke, 1991). The precipitation region is typically centered on local magnetic noon at 75 degrees MLAT, is about 1 degree MLAT x 2–4 hours MLT in area, and so corresponds to a magnetic flux of 5–10 x 10^6 webers (Stasiewicz, 1991).

The polar cusp is populated by particles of magnetosheath origin because of dayside reconnection. In a self-consistent MHD model with zero or northward interplanetary field, direct particle entry into the cusp region does not occur because dayside field line draping leads to a smooth, cusp-free magnetopause (Wu, 1983). When reconnection creates a component of field normal to the magnetopause, magnetic cusps are no longer single field lines but become funnels of magnetic flux that map to the ionosphere. The longitudinal width of the funnel depends on the rate of reconnection as well as the length of the reconnection region on the magnetopause (Crooker et al., 1991). The injection of measurable fluxes of plasma of solar wind origin is then *prima facie* evidence that dayside reconnection broadens the open field line region from a set of measure zero to one of finite measure. Furthermore, the cusp precipitation is accompanied by a separate field-aligned current system (Iijima and Potemra, 1976), indicating that stresses that drive antisunward ionospheric convection are being exerted on the open field lines poleward of the cusp.

The noon sector auroral oval contains four distinct regions (Newell et al., 1991b): the polar cusp, the ionospheric footprint of the plasma mantle (see the following), the footprint of low-latitude boundary layer (discussed in the previous chapter), and the dayside projection of the "boundary plasma sheet" (BPS). For a variant of this classification, see Kremser and Lundin (1990). These regions may be distinguished on the basis of electron and ion distribution functions and spatio-temporal morphology. Newell and Meng (1988, 1989) and Newell et al. (1989, 1991a,b) classified them using particle distribution function data acquired onboard various polar orbiting DMSP spacecraft; the DMSP classifications were related to *Viking* uv observations by Elphinstone et al. (1992b).

According to this scheme, the cusp (or "true cusp," or "proper cusp") is that low-altitude region near magnetic local noon where plasma precipitating directly from the magnetosheath is observed. Its activity is therefore is ascribable directly to reconnection. The cusp is characterized by precipitating ion fluxes larger than anywhere else around the auroral oval; owing to its source in accelerated magnetosheath plasma, most of the ion energy is invested in flow and not thermal energy. The electrons have an isotropic pitch angle distribution (Lundin, 1988), suggesting they approach the strong pitch angle diffusion limit (Kennel and Rees, 1972). There is often a mid-day gap in green auroral light emission where no stable discrete aurora are found, but where persistent red 630 nm emission is nearly always present. This red aurora may be generated by the precipitation of soft magnetosheath electrons.

The mantle is the region poleward of the cusp containing the lowest average ion energy of any particle precipitation observed at high latitude. The average energies are usually no more than a few hundred eV; the densities are low, and the flow velocities and temperatures generally fall off moving poleward. Poleward convection gives rise to a velocity-filter effect in which ions are dispersed in latitude according to energy; the ion energy usually falls smoothly with increasing latitude across the cusp–mantle boundary, suggesting that cusp and mantle ions undergo the same injection and transport process (Smith et al., 1992). However, not all cusp–mantle traversals for southward IMF show smooth energy-latitude dispersion; Newell and Meng (1991) identified 13 passes of the DMSP F7 spacecraft (out of about 100 examined) where a sharp boundary separated the main cusp from an equatorward patch of faster ion flow. At these times, the precipitating ions in the main cusp had 200–300 km/s flow velocities, while those in the discrete patches had 460–640 km/s flow speeds. The ion acceleration could not be attributed to electrostatic potentials because electrons were also observed to be accelerated. The patches of accelerated ions were found only for southward interplanetary field and seemed to be a low-altitude signature of bursty magnetopause reconnection. We will return to this topic frequently.

The region of precipitation from the low-latitude boundary layer, sometimes called the *cleft*, is found equatorward and never poleward of the cusp (Newell et al., 1991b). It forms a band 2-3 degrees MLAT thick centered on local noon and extending from 0800–0900 to 1500–1600 MLT (Newell and Meng, 1992). The cleft maps magnetically into the LLBL in the flanks of the magnetosphere between the dawn and evening flanks and about 20 R_E downtail (Vasyliunas, 1979; Oguti, 1989a,b; Stasiewicz, 1991). The LLBL precipitation is similar to the cusp's, but the ions are hotter, have smaller bulk velocities, a density a factor of five smaller, and a precipitation flux a factor of ten smaller than in the cusp. The electrons are typically a factor of two hotter (Formisano, 1980), and almost always have a 50–200 eV beamlike component similar to that observed in the LLBL in space (Ogilvie et al., 1984; Traver et al., 1991).

What Newell et al. (1991b) called the *dayside BPS* is any region of soft electron precipitation that does not fall into the three categories listed; its particle characteristics resemble those of the nightside BPS (Winningham et al., 1975). The dayside BPS lies equatorward of the LLBL, therefore maps earthward of the LLBL in space (Hansen et al., 1992), and extends around into the nightside (Newell and Meng, 1992).

5.8 Direct Entry of Solar Wind Plasma into the Magnetotail

In Petschek's (1964, 1966) model of symmetric steady-state reconnection, the reconnection region is bounded by a pair of slow shocks. However, this model is not adapted to the dayside magnetopause, which is asymmetric. To first approximation, the plasma pressure inside the magnetopause may be taken to be zero. In this case, Levy et al. (1964) showed that Petschek's small diffusive

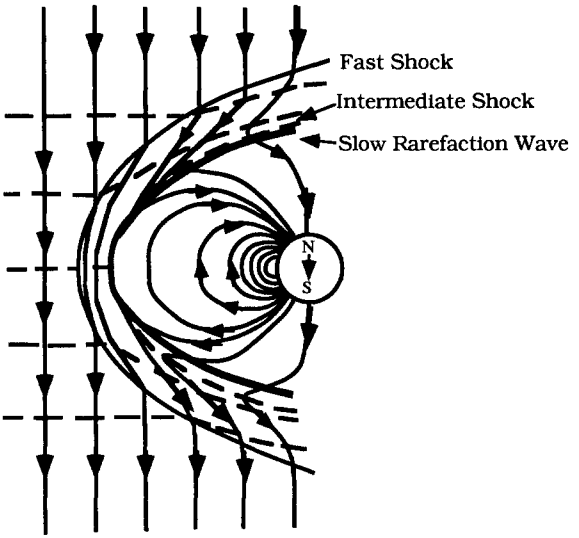

Figure 5.2. Entry of Solar Wind Plasma into an Empty Magnetosphere. Levy, et al. (1964) adapted Petschek's (1964) model of symmetric reconnection to the Chapman-Ferraro magnetopause in which the plasma density and pressure are zero in the interior of the magnetosphere. This figure shows a view of the noon–midnight meridian plane from the evening side for equinoctial conditions, when the earth's dipole axis is perpendicular to the ecliptic plane. A fast shock stands upstream of the magnetosphere. Reconnection in a small region on the subsolar magnetopause launches a rotational discontinuity that faces upstream into the magnetosheath flow. (Today, we would call it an intermediate shock, provided the flow is dissipative.) Reconnection allows solar wind plasma into the empty magnetosphere via a slow expansion wave. The intermediate shock and the slow rarefaction curve back over the poles to form the tail-lobe magnetopause and the so-called *mantle* or solar wind plasma entry layer. The slow rarefaction wave solution indicates how typical thermal particles enter the tail lobes; selected single particles can free-stream along open field lines and reach the polar cap ionosphere.

The night-side magnetosphere is not shown in this sketch. The northern and southern slow rarefaction fans ultimately close across the tail lobes, at which point tail reconnection takes place. The tail reconnection region connects magnetically to the poleward borders of the northern and southern auroral oval ionospheres. In the precisely symmetric case shown here, tail reconnection will create the Petschek (1964) configuration–symmetric north- and south-facing slow shocks. The real picture is more elaborate than this. The magnetosphere will generally not be north-south symmetric. The pressure of the plasma in the dayside magnetosphere is not negligible, and as a result an inward-facing slow shock will also be radiated by the dayside reconnection region. Finally, when the magnetosheath field has an east-west component, intermediate waves or shocks will generally emanate from the dayside reconnection region. When the density in the tail lobes is nonzero, the inward–facing slow and intermediate waves can curve over the poles and close on the plasma sheet.

reconnection region connects to an outward-facing rotational discontinuity followed by a slow rarefaction. The rotational discontinuity curves around the magnetosphere while the trailing slow mode rarefaction injects plasma into the vacuum lobes of the tail. The magnetic field rotation stands upstream to orient the field so that it can pass smoothly through the slow rarefaction. In ideal MHD, this will be a rotational discontinuity, but in the more general dissipative MHD case, it can attach to the slow wave to form an intermediate shock. Either way, a magnetically open magnetopause will in general have a field rotation followed by a slow expansion fan.

How in principle should solar wind plasma that enters the magnetosphere via dayside reconnection eventually fill the tail lobes? Let us neglect the polar wind for a moment and assume the solar wind plasma expands into vacuum lobes. The theory of MHD characteristics tells us that a slow rarefaction is the only wave that allows expansion into the vacuum (Kantrowitz and Petschek, 1966). Thus, the solar wind should enter the northern and southern tail lobes in slow expansion fans that converge towards the center of the tail (Levy et al., 1964; Yang and Sonnerup, 1976; Coroniti and Kennel, 1979). The profiles of decreasing field magnitude and increasing mass density, temperature, and flow speed measured as IMP 8 passed between the magnetosheath and tail lobes were quantitatively consistent with a slow expansion fan (Siscoe and Sanchez, 1987). Now, let us put back the polar wind. If a plasma of finite but small density populates the otherwise empty tail lobes, a contact discontinuity will precede the slow expansion into the tail lobes. The discontinuity separates the plasmas of solar wind origin in the rarefaction from polar wind that has expanded into the tail lobes. These are the waves expected for the purest version of Dungey's paradigm: steady-state convection driven by reconnection with a purely southward interplanetary field.

The observers' name for the slow rarefaction wave is the plasma *mantle* (Rosenbauer et al., 1975). The flow of magnetosheathlike mantle plasma over the poles carries about 2 Dungeys of plasma tailward (Sckopke and Paschmann, 1978). The plasma speed and density decrease inward from the magnetopause, the density ranging from about $5/cm^3$ at the magnetopause to $0.1/cm^3$ at its inner edge in the tail lobe proper. The thickness measured over the poles by HEOS 2 ranged between 0.5 and 4 R_E. The mantle was larger and denser for southward interplanetary field (Paschmann et al., 1976a,b), and it decreased dramatically in size when the interplanetary field turned northward, possibly to disappear altogether (Sckopcke et al., 1976). Observations such as these communicate the mantle's origin in dayside reconnection.

Sanchez et al. (1990) found many examples of field-rotation–slow-expansion pairs among the high-latitude nightside IMP 8 traversals of the high-latitude tail magnetopause near 25 R_E geocentric distance. Other magnetopause traversals were consistent with a simple tangential discontinuity with no entry layer, which suggested that the tail magnetopause was locally closed on those occasions. Of course, dayside reconnection does not always occur, and the relative proportion of open and closed tail magnetopause crossings is an unavoidable issue. The important point for us is that the open magnetopauses had the structure

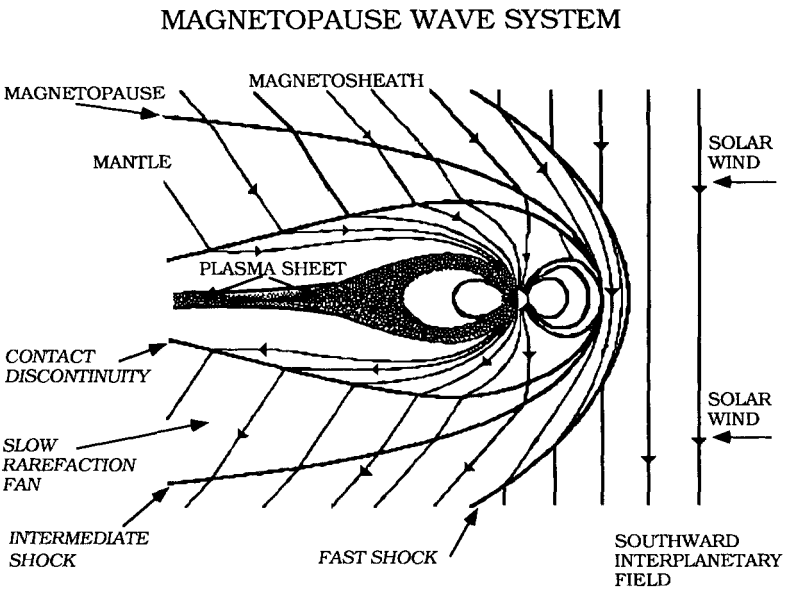

Figure 5.3. Magnetopause Wave System. This figure sketches the situation visualized by Siscoe and Sanchez (1987). Though the interplanetary field is drawn predominantly in the north-south direction, in general it has an east-west component as well. In this case, the magnetopause consists of a rotational discontinuity or intermediate shock, across which the magnetic field rotates sharply, followed by a slow mode rarefaction fan in which solar wind plasma enters the tail lobes (the mantle). We have added to the picture a contact discontinuity, which in MHD separates plasma of solar wind and magnetospheric-ionospheric origin. (Kinetic processes will tend to blur the sharp boundary between the two plasmas.) We have not drawn the slow and intermediate waves that can propagate towards the plasma sheet ahead of the contact discontinuity when the plasma density is non-zero in the tail lobes. We purposely have not shown where the waves close upon the plasma sheet, a topic that can be discussed more meaningfully after the material in Chapters 7, 8, and 9 has been digested. Original drawing.

predicted by the theory of MHD characteristics. This encourages our continued use of MHD characteristic theory as the conceptual framework that defines the causal relationships between magnetospheric structures.

Clearly where the northern and southern mantles converge onto the plasma sheet is of great interest. Already at lunar distance, 60 R_E, all but the inner 15% by radius of the tail lobes appear to be filled with mantlelike plasma (Hardy et al., 1975), suggesting that the slow expansion fan typically closes only a little further downstream than that. Although the actual point of first closure of the mantle, and any wake shock that might be radiated from it into the tail lobe, has never been identified in data, it is clear that the mantle nearly always closes within 200 R_E. Analysis of many hundreds of ISEE 3 magnetotail crossings indicated that a

mantlelike plasma frequently fills the tail lobes near 220 R_E distance (Gosling et al., 1984). The electron density averaged across the lobes increased with increasing distance downtail, and reached 0.1/ cm^3 at 220 R_E, suggesting that the mantle typically converges to the center of the tail before that distance. The mantle plasma appeared to blend smoothly into the solar wind at 220 RE. Very occasionally, the transition between magnetosheath and lobe was abrupt, indicating that the magnetopause was locally magnetically closed, but more often there was a smooth decrease of varying thickness of electron density and flow speed, and a smooth increase of electron temperature, in passing from the magnetosheath to the lobe. A major change in magnetic field orientation occurred in a thin current layer at the magnetopause, and the field orientation did not change much within this boundary layer, consistent with the intermediate shock-expansion fan picture. Unless plasma entry is distributed along the length of the tail, the cross-tail drift would deplete the plasma next to the magnetopause. The smoothness of the mantle boundary layer suggested that much of the area of the tail magnetopause had been effectively open during the time it takes the magnetosheath flow to traverse the distance from the nose of the magnetosphere to ISEE 3, about 1 hour at a speed of 400 km/s (Gosling et al., 1984).

5.9 Convection across the Tail Lobes

Analysis of the energetic particle "shadows" produced by the moon provided the first clear evidence that open field lines convect across the tail lobes (Anderson and Lin, 1969). Four types of field lines can be observed from lunar orbit: interplanetary field lines that do not connect to earth, closed plasma sheet field lines that connect to earth at both ends, open plasma sheet field lines that connect to the solar wind at both ends, and open lobe field lines that connect the earth to interplanetary space. The interplanetary and lobe field lines are frequently populated by solar coronal heat flux electrons, and occasionally by larger fluxes of solar flare electrons (Lin et al., 1972). Magnetic field lines pass through the moon with little distortion, so that electrons spiraling along them with gyroradii small compared to the radius of the moon will be absorbed by the moon (Lin, 1968). The resulting shadow pattern can be used to deduce the topology and speed of the magnetotail field lines (Anderson, 1970).

Interplanetary field lines were observed at lunar orbit very infrequently (Lin et al., 1977). Tail lobe field lines were found to be continually moving toward the center of the tail from both the north and south lobes (McCoy et al., 1975). The inferred electric fields persisted for periods of several hours. A dawn–dusk component was required in almost every instance to fit the data; only once was a dusk-to-dawn field needed. The dawn–dusk electric fields ranged up to 2 mV/m, with the median being 0.15 mV/m, or equivalently 0.9 kV/R_E. In a 10 nT magnetic field, the measured electric fields implied an $\mathbf{E} \times \mathbf{B}$ speed from < 5 to 190 km/s, with a median of 15 km/s. If the median electric field extended uniformly across a 40 R_E tail lobe, the net emf would be 36 kV. For comparison, the emf across the

polar cap ionosphere varies between roughly 20 kV in northward field conditions to about 150 kV for southward interplanetary field conditions. For a cross-tail flow speed of 15 km/s and a 40 R_E tail lobe, it takes 4 hours for a field line to travel from the magnetopause to the center of the tail. Thus, the cross-tail drift time is compatible with the time required for the foot of that field line to cross the polar cap at typical ionospheric convection speeds.

The distance where the mantle closes can be estimated from the cross-tail drift velocity (Pilipp and Morfill, 1978). The plasma in the expansion fan should **E x B** drift toward the center of the tail as it convects tailward at some fraction of the solar wind speed. If the average tailward flow component in the mantle is the order of the sound speed, say 40–80 km/s, the mantle would close about 100–200 R_E downtail. These figures establish illustrative time and distance scales for the slow rarefaction wave to respond to a change in the dayside reconnection rate.

5.10 Average Tail Reconnection Region

Steady-state models give some insight into what determines the length of the closed field line region in the tail. The magnetosphere would approach the teardrop configuration (Johnson, 1960) if there were no open flux and no reconnection anywhere. Quasiteardrops might develop during prolonged periods of northward interplanetary field. However, there is evidence that residual open flux remains for many hours after the interplanetary field turns northward, so that there can be times in which the flux in the tail lobes changes very slowly. Let us suppose the flux in the tail lobes does not change at all. In the static model of the tail lobes (Coroniti and Kennel, 1972a), an inactive, asymmetric Y-type neutral line is located where the flaring of the tail magnetopause ceases (Birn et al., 1992). For typical values of the tail lobe flux and solar wind parameters, this neutral region begins 100–200 R_E downstream. The static model probably defines an upper limit distance to the neutral line, but it does not allow the neutral line to respond in a structurally stable way to changes in the dayside reconnection rate. Thus another mechanism must come into play. The closure of the slow rarefaction fan is one place where changes in dayside boundary conditions can be communicated to the nightside plasma sheet to force tail reconnection (Pilipp and Morfill, 1978; Coroniti and Kennel, 1979).

So much for theory. Let us turn to the observational record. Lunar shadowing measurements indicated that there is a clear separatrix across which open field lines reconnect to form a closed plasma sheet. The plasma sheet field lines were often closed at 60 R_E (Lin et al., 1977), implying that the reconnection region was usually tailward of the moon. However, the neutral line could be found both tailward and earthward of the moon (McCoy et al., 1975; Lin et al., 1977). On one occasion, the Apollo 16 subsatellite found itself earthward of the reconnection region for about 6 hours, and then tailward for the next 4 hours. Energized particles were observed to travel first earthward and then tailward in a separatrix layer between the plasma sheet and tail lobe. When the spacecraft was earthward of the neutral region, the earthward flux of energetic particles in the boundary layer was

suffucient to populate the plasma sheet. The length and thickness of the reconnection region were about 10 R_E and 4000 km, respectively. On another occasion, just before Apollo 16 crossed the separatrix between open and closed field lines, it detected a 30–60 km/s convection velocity toward the reconnection region in the tail lobe; with this convection speed, the thickness of the separatrix layer came out to be 2000 km (Lin et al., 1977).

Analysis of the ensemble of ISEE 3 magnetic field and electron flow measurements in the deep tail indicated that the tail neutral line typically lies beyond 100 earth radii distance (Slavin et al., 1985). Earthward of 100 R_E, the normal component of the magnetic field was generally northward, implying that the neutral line was more often than not farther than 100 R_E downtail. Unfortunately, this could not be confirmed with flow measurements, because the velocity was typically less than 200 km/s and therefore difficult to infer using electron measurements, the only ones available on ISEE 3 (Zwickl et. al., 1984; Slavin et al., 1985). Between 100 and 180 R_E, the average flow velocity increased until it was measurable. At this point, it proved on average to be tailward and super-Alfvenic across the width of the plasma sheet. However, the magnetic field was predominantly southward only in a 10 R_E-wide region near the (aberrated) noon–midnight meridian. The field lines nearer the magnetopauses on either side of midnight appeared always to be closed. Richardson et al. (1989) later studied several of the closed boundary layer regions in detail. Between 180 and 225 R_E, the width of the negative B_Z region increased to 30 R_E, but still no "intersection" of the neutral line with the magnetopause was found within the orbit of ISEE 3. Boundary layers of closed field lines next to the dawnside and duskside magnetopauses evidently continue to exist beyond 220 R_E downtail.

The above data are consistent with the idea that the average position of the neutral line is closest to the earth near the tail axis and is swept back from the center of the tail with increasing distance downstream (Russell, 1977). However, it is critical to keep in mind that "the average neutral line" emerged only after very extensive averaging. The ISEE 3 data were not sorted with respect to the interplanetary field, or any geomagnetic activity index, and so certainly contained very different convection states and magnetic field topologies. Counterexamples to the average picture were common within the ISEE 3 data set itself, and they abound in other studies. For example, there was the 4-hour period reported in which the neutral line was earthward of the moon, transient fast tailward flows have been found on the ISEE 1 and 2 spacecraft within 23 R_E distance downtail, and, at the other extreme, Schindler et al. (1989) found an earthward flow near the center of the tail at 217 R_E that lasted for 3.5 hours. The swept-back configuration of the average neutral line could therefore reflect the the spatial profile of the frequency of occurrence of reconnection events, and not the profile of steady-state reconnection at a single neutral line. In short, the average picture is not a good guide to understanding any given single encounter with the plasma sheet. We must ask what is being averaged to produce the simple picture.

5.11 Stratification of the Plasma Sheet Boundary Layer

A schematic picture of the vertical structure of the plasma sheet has been synthesized from the general experience of crossings of active plasma sheet boundary layers (Onsager et al., 1991). A north–south cut perpendicular to the plane of the plasma sheet divides it into the so-called *central plasma sheet*—a region enclosing its magnetic field reversal layer—and northern and southern *plasma sheet boundary layers*, which abut the tail lobes and are characterized by the presence of field-aligned beams of energetic ions and electrons (DeCoster and Frank, 1979; Sarris and Axford, 1979; Williams, 1981; Andrews et al., 1981; Forbes et al., 1981; Eastman et al., 1984, 1985b, 1986; Whelan and Goertz, 1987; Takahashi and Hones, 1988; Angelopoulos et al., 1989; Onsager et al., 1991).

On passing from the tail lobe into one of the boundary layers, a spacecraft first encounters high-speed electrons streaming earthward. The electron velocity distributions parallel to the magnetic field have a low-velocity cutoff. Next, both earthward- and tailward-streaming electron beams appear simultaneously; the tailward beam typically having the higher speed. The electron beams' speeds decrease with increasing depth into the boundary layer. Then ion beams begin to be observed; first earthward and then both earthward and tailward. The ion beams also have sharp low parallel velocity cutoffs; the tailward beam again is typically faster than the earthward beam. The speeds of both beams decrease with increasing depth into the boundary layer, and the pitch angle distributions evolve from field-aligned beams to "kidney bean" shapes to isotropic shells. The layering described takes place down to electron energies of the order of 0.5–1 keV (Parks et al., 1992). Below this crossover range of energies, the structure of the plasma sheet boundary layer is strikingly different. As the ISEE 1 spacecraft passed from the plasma sheet into the tail lobes, the phase–space density of electrons in the 50–200 eV range would first increase as that at higher energy was dropping out, and then return to background. Thus, a low-energy electron layer (LEL) was the last structure the spacecraft encountered as it entered the tail lobes and the first one it met upon reentry into the plasma sheet. In one event, the phase–space density increased all the way up to the crossover energy of 1 keV in the LEL. The electrons in the LEL form tailward-streaming beams, which represent a significant fraction of the total density in the plasma sheet boundary layer region (Parks et al., 1984); low-energy ions counterstream earthward over the electron streams (Parks et al., 1992).

The structure of the plasma sheet boundary layer can be rationalized in terms of the steady reconnection model. Field-aligned beams are the result of particle acceleration by a dawn–dusk electric field in the weak magnetic field regions of the current sheet (Speiser, 1965, 1967). Let us assume the acceleration region is tailward of the spacecraft. Energized ions and electrons escaping from the dusk and dawn edges of the weak-field region, respectively, stream earthward along the magnetic field to form the boundary layer. The fastest particles arrive first at the spacecraft. Since the field lines are themselves convecting toward the center of the plasma sheet, the fastest particles will be found in the outermost portions of the boundary layer. For the same energy, electrons will be found farther from the

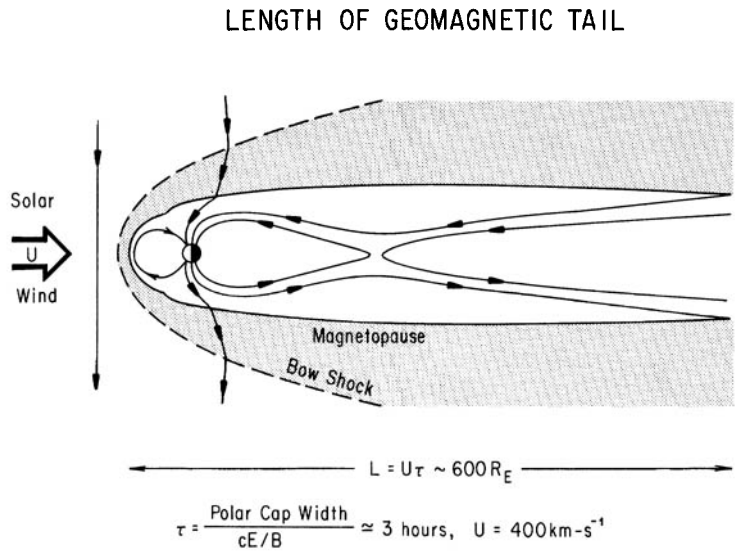

Figure 5.4. The Length of the Geomagnetic Tail. This figure shows how Dungey (1965) estimated the length of the geomagnetic tail. Measurements of the speeds of polar cap irregularities and the size of the auroral oval indicate that the foot of an open field line takes several hours to cross the polar cap. In the reconnection model, this has to be the time elapsed from magnetopause to tail reconnection for a given field line. During that time, its solar wind end has propagated downstream at the solar wind speed. Multiplying the polar cap crossing time by the solar wind speed thus indicates how far downstream the solar wind end of the field line is at the moment of tail reconnection. Original drawing.

center than ions. Tailward beams result from mirroring of the earthward beams near the earth. The reflected ions are also convected towards the center of the plasma sheet and they will be found closer to its center; they too gain energy by drifting in the direction of the electric field.

The simplicity and plausibility of this picture encourages the working assumption that the great time variability of the observed beams may be related to the burstiness of the reconnection process. If so, we expect that the burstiness of plasma sheet boundary layer ions will also be related to that in ions of even higher energy on the one hand, and with the rapid convective flow of lower energy ions on the other. It is important to remember that layering is most clearly revealed when the layers are passing rapidly over the spacecraft, in other words, when the plasma sheet is in a nonsteady state. Conversely, the fact that ion beams are not encountered on every crossing of the plasma sheet boundary indicates that reconnection does not always take place on field lines that pass near the spacecraft as it enters into or exits from the tail lobes.

5.12 The Length of the Earth's Magnetic Tail

The ensemble of ISEE 3 results indicates that the tail lobes are well-formed structures out to 220 R_E distance. The closed teardrop magnetosphere should not be that long (Dessler, 1964; Dungey, 1965). In an open magnetosphere, the solar wind will drag lobe field lines downstream at the solar wind speed until they are finally cut loose by reconnection in the tail. All one needs to know to calculate the length of this kind of tail is the solar wind speed and how long a field line is open. In Dungey's model, the open field lines map to the polar cap ionosphere. By observing the speeds of ionospheric irregularities in the polar cap, estimating the time it takes them to cross the polar cap, and multiplying this time by the solar wind speed, one finds that the tail lobes would be about 1000 earth radii long.

The prediction of a very long tail passed the test of observation (Ness et al., 1967) shortly after the discovery of the tail itself (Ness, 1965). During a 6-day interval in September, 1966, the heliocentric orbiting spacecraft Pioneer 7 was in a position to observe the tail between 900 and 1050 R_E, while Explorers 28 and 33 were monitoring the solar wind and the magnetosheath. Fairfield (1968) found 10 time intervals ranging in duration from a few minutes to several hours during which Pioneer 7 observed solar- or antisolar-directed fields whose magnitudes were several nanotesla larger than in the adjoining magnetosheath. Occasional reversals in the field direction suggested that a tail neutral sheet was still present near 1000 R_E distance. Later, Intriligator et al. (1979) presented evidence for a tail encounter 3100 R_E downstream.

5.13 Interaction of the Two Convection Systems in the Ionosphere

Stresses from both the LLBL and the plasma mantle are communicated to the ionosphere by field-aligned currents of the region 1 sense. The viscous and reconnection convection systems therefore are forced to interact in the ionosphere where they combine to drive the same currents. How do they come to terms with one another, since they must comply with a common set of electrical boundary conditions in the ionosphere? It appears the ionosphere may not only tolerate but regulate them both. Siscoe et al. (1991) pictured the flow of mantle plasma as generating most of the voltage and the vorticity in the denser LLBL creating most of the current in the convection electric circuit that closes through the ionosphere. Since the differential equation governing the steady-state convection electric field in the ionosphere is of fourthorder, its general solution has enough free parameters to allow the two systems to adjust to one another. The solutions indicate the self-consistent voltage across the low-latitude boundary layer is always smaller than that across the open polar cap. That is to say, the viscous component of convection will circulate much less magnetic flux than the reconnection component, even if the number and energy transport rates are "in the same ballpark." The statistical studies reviewed in the next chapter support this view.

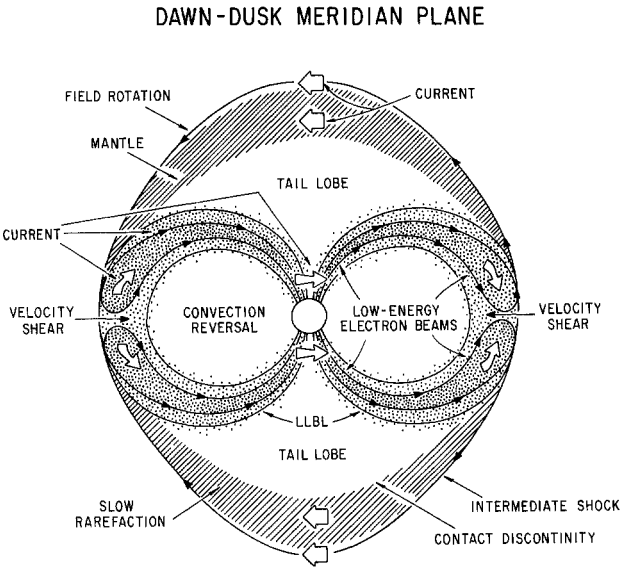

Figure 5.5. Viscosity–Reconnection-Driven Convection. Though for pedagogical and historical reasons, we tend to consider viscous and reconnection-driven convection separately, the two systems coexist in the real magnetosphere. They must come to terms with one another in the ionosphere, where the region 1 current systems they drive have to satisfy a common set of boundary conditions. This figure, which has been adapted from Siscoe, Lotko, and Sonnerup (1991), shows a slice through the magnetosphere-ionosphere system through the 0600–1800 MLT meridian plane viewed from the sun. The currents at the mantle boundary driven by reconnection combine with those generated in the low latitude boundary layer to flow into the morning side ionosphere and out of the evening side ionosphere. These currents drive two-cell convection in the high latitude ionosphere. The steady-state solution obtained by Siscoe, Lotko, and Sonnerup (1991) suggests that viscosity is responsible for most of the field aligned current, and reconnection is responsible for most of the electromagnetic force (emf) across the polar cap. By implication, the energies of the precipitating electrons, the depths to which they penetrate the ionosphere, the horizontal components of ionospheric conductivity, and ultimately the horizontal ionospheric currents will be more sensitive to reconnection than to viscosity. In short, geomagnetic activity should respond primarily to variations in the reconnection rate. Original drawing.

The relative importance of viscous convection may have been underestimated. The field-aligned potentials developed by the two convection systems scale roughly as their total dawn–dusk voltage, as the relative energies of the field-aligned electron streams associated with the LLBL and with the aurora attest. For this reason, the reconnection-related electron precipitation will create more auroral light and produce higher ionospheric conductivity, because higher-

energy electrons penetrate deeper into the atmosphere before they come to rest. Thus, geomagnetic and auroral activity is driven primarily by reconnection. However, this does not mean that the viscosity is unimportant for the dynamics and structure of the magnetosphere. Certainly the rough estimates of net transport that we are about to make will do nothing to dispel the idea that we must continue to deal with two competitive modes of magnetospheric convection.

5.14 Comparison of Viscosity- and Reconnection-Driven Transport

Now that we have introduced the basic properties of the convection components driven by viscosity and reconnection, we can return to the debate we began at the conclusion of the previous chapter. It is natural, after all, to ask which is the more important driver in the real magnetosphere. Generally speaking, the answer to this question clearly depends upon which phenomenon one is discussing. However, comparing how much plasma and how much energy circulate in the convection pattern from each source provides an objective figure of merit. Ironically, this comparison does not help us "decide" between the two mechanisms. The rates of input of both energy and of particles due to reconnection and to viscosity appear to be competitive within the rough accuracy with which it is possible to make such global estimates. On the other hand, the two mechanisms differ in their rates of magnetic flux transport.

In 1978, Perreault and Akasofu (1978) modeled the dependence upon solar wind parameters of the energy input due to dayside reconnection (Akasofu, 1979, 1981; Kan and Lee, 1979; Maezawa, 1979; Murayama, 1982; Vasyliunas et al., 1982). What has come to be called the Perreault–Akasofu energy input rate, ε, is the product of terms that scale the magnitude of the energy input and one term that declares the dependence of that rate on the orientation of the interplanetary field

$$\varepsilon = vB^2L^2 \sin^4(\theta/2)$$

The energy input scaling factor is the standard combination of solar wind speed v, the square of the magnetic field strength B, and the square of the effective length $L$of the reconnection "line" on the dayside magnetopause. This length is taken to be 7 R_E in most calculations; assuming it to be constant implies that the rate of reconnection depends upon solar wind parameters alone, and not upon the state of the magnetosphere or the magnetosphere's response to the reconnection process. The all-important angular factor is $\sin^4(\theta/2)$, where $\theta = \tan^{-1}(B_y/B_z)$ is the "clock angle" of the interplanetary field in GSM coordinates. In the next chapter, we will show that the Perreault–Akasofu function gives an excellent statistical accounting of the dependence of geomagnetic activity upon the direction of the interplanetary magnetic field. Here we are interested in the order of magnitude of the energy input rate. Over the range of typical solar wind speeds and field magnitudes, the Perreault–Akasofu function indicates that reconnection can provide 100–1000 GW of power to the magnetosphere in southward field conditions, the larger estimate

being characteristic of magnetic storms. This should be compared with a 100 GW energy injection rate across the dayside magnetopause at disturbed times due to the Kelvin–Helmholtz instability (Pu and Kivelson, 1983).

The most direct estimate of the power provided by dayside reconnection comes from measurement of the local energy dissipation rate at the magnetopause. Near the stagnation region on the dayside, the total magnetopause current I is 50–100 A/km, and the magnetopause thickness is 500–1000 km (Russell and Elphic, 1978). However, to calculate the dissipation rate, we also need to know the electric field in the frame of reference of the magnetopause, which is constantly in motion. On a couple of fortuitous occasions, the magnetic field did not vary rapidly between ISEE 1 and 2, and it was possible to transform the measured electric field into the magnetopause frame of reference and calculate $\mathbf{E}\cdot\mathbf{I}$ and multiply by the magnetopause thickness (Fahleson et al., 1979; Formisano et al., 1982; Pedersen et al., 1984). The resulting dissipation rates were in the range 50–150 W/km^2. These rates are consistent with the Perreault–Akasofu function: 50–150 W/km^2 corresponds to 2–6 GW/R_E^2, so that for a 7 R_E × 7 R_E effective area over which dissipation occurs, the total power input is 100–300 GW.

Now we compare the rates of particle input in the plasma mantle and in the low-latitude boundary layer (Lee and Akasofu, 1989). Magnetosheath particles have been observed to cross the magnetopause and enter the mantle at all distances down the magnetotail (Sibeck et al., 1985). The measured tailward particle flux increases from 1.7 D (0–60 R_E), to 6.5 D (60–120 R_E), to 21 D (120–180 R_E), to 20–200 D beyond 180 R_E (Sibeck et al., 1985). At this point, the mantles have joined at the center of the tail. Much further downstream, at 1000 R_E, the tailward flux, 570 D, is approximately equal to the unperturbed solar wind flux across a 1000 R_E^2 tail cross-section (Walker et al., 1975). Lee and Akasofu (1989) estimated theoretically how much solar wind plasma ought to enter the tail within 200 R_E via the mantle, if it all enters as a result of magnetopause reconnection. Assuming the fast flows in the reconnecting magnetopause obey the Walen momentum balance relation, they calculated a total reconnection entry flux within 200 R_E of about 70 D for a moderate southward interplanetary field component. Thus, the observed number fluxes in the mantle are consistent with a reconnection source. If a viscous boundary layer extends downtail to the distance of ISEE 3, viscous transport of particles and momentum will be an important factor in the dynamics of the plasma sheet all along its length.

Let us compare the reconnection particle source with its competitors. The ionosphere is an important source of ions in the near-earth region within 20 R_E (Shelley et al., 1972; Sharp et al., 1982; Cladis, 1986; Chappell et al., 1987). Chappell et al. (1987) estimated that the ionosphere injects 3–5 D into the magnetosphere, so that reconnection provides far more particles than the ionosphere. However, if the viscous boundary layer extends to 200 R_E downstream, the particle injection rate from viscous transport across the magnetopause, 70 D, is comparable to that from reconnection at the same distance downtail.

5.15 Discussion

A paradigm stands or falls on a balance of evidence. It is difficult to point to a moment in time when one is "proved" to everyone's satisfaction. Nonetheless, we find compelling the contemporary balance of evidence supporting the reconnection model of the magnetosphere. Certainly, no other hypothesis suggests the existence of so many different structural features of the magnetosphere; no other model accounts as simply for the access of solar particles to the polar caps or polar cap ionospheric plasma to the earth's magnetic tail, or of magnetosheath plasma to the polar cusp and mantle. No other model contains such a clean way to account for the distinction between the polar cap and auroral oval. In all this and more, the idea of reconnection has successfully organized numerous and diverse observations, even though the plasma physical process called reconnection is poorly understood. The idea of reconnection has proved its success as a paradigm.

Having said all that, we must add that the present frontier is not at the level of the existence of reconnection. Other questions now stand at the frontier. How do the viscous and reconnection components of convection manage to function together, given that they respond to different properties of the solar wind? Do they interact? Is it an accident that the two systems compete in terms of net energy and particle transport? Are there specific signatures of viscosity-and reconnection-driven convection inside the magnetosphere? The research frontier can be also glimpsed in the exceptions to the by-and-large successful studies that tested the steady reconnection model: The magnetopause was almost always in motion; not all magnetopauses were open or had fast flows; a position of the tail neutral line emerged only after extensive averaging; not all entries into the plasma sheet had fast ion beams in the boundary layer; the layering of the plasma sheet boundary is best observed when it is in motion. Such a list can be continued. Thus, not only in our data analyses, but also in the very conceptual framework we use, must we come to grips with the spatial and temporal variability that is in every observation we make.

6

CORRELATION OF GEOMAGNETIC ACTIVITY WITH THE SOLAR WIND

6.1 Introductory Remarks

Even if a steady convection state could exist in principle, the magnetosphere will be rarely in it, since the interplanetary magnetic field is hardly ever stationary over the 2–4 hour convection cycle (Rostoker et al., 1988). Indeed, the hourly average north–south component of the interplanetary field retained the same sign for two consecutive hours only 12.2% of the time during solar cycles 20 and 21 (Hapgood et al., 1991). If only for this reason, we cannot avoid dealing with time-dependent convection. In this section, we take up one method of coping with the issue. Correlation studies take advantage of solar wind variability without ever needing to consider the precise nature of the time-dependent response of the magnetosphere. Though laborious, they are a procedurally straightforward way to test the viscous and reconnection models of convection.

Geomagnetic activity, the response of geomagnetic field to currents flowing in the ionosphere and in space, has been monitored in an increasingly systematic way since the beginning of the eighteenth century. Today, a world–wide network of ground stations provides continuous records of the magnetic field at many different locations on the earth's surface. Before computational data displays enabled large quantities of data to be summarized at a glance, the complex multi–station records were combined into single parameters called *geomagnetic indices*, which were designed to characterize one aspect or another of geomagnetic activity on a global scale. We will refer frequently to the auroral electrojet (AE) index, which was designed by Davis and Sugiura (1966) as a measure of electrojet activity in the auroral zone. The index is derived from the horizontal, northern component of the geomagnetic perturbation field measured at a number of observatories in the northern hemisphere. The number of observing stations contributing to the index is occasionally indicated in parentheses as AE(12) or AE(32), and so on. The maximum and minimum perturbations recorded at any given time at the stations in the AE network are called the *AU* and *AL indices*, respectively, for "upper" and "lower." These provide a measure of the westward and eastward electrojet strengths. The difference between AU and AL is the AE index.

Studies of how various geomagnetic indices, and especially AE, correlate with the direction of the interplanetary field provided some of the earliest support for the reconnection model, and they continue to do so to this day. However, a new level of precision has been reached. Modern studies employing large data sets can now specify the precise mathematical energy-coupling function that characterizes the rate at which reconnection couples solar wind energy into the magnetosphere as well as show there is a second driver of geomagnetic activity that does not depend upon the direction of the interplanetary field (Section 6.2).

The most direct statistical test of the reconnection model is to correlate the convection electric field with the direction of the interplanetary magnetic field. Numerous studies now agree that the rate of convection in both the magnetosphere and polar caps increases with increasing southward component of the interplanetary field (Section 6.3). Furthermore, a strong sensitivity to the details of the reconnection process has been revealed by studies of how the pattern of convection in the polar cap depends upon the east–west component of the interplanetary field (Section 6.4). Reconnection changes the structure of the magnetosphere; the whole system of field-aligned currents driving convection intensifies and moves equatorward with increasing southward component of interplanetary field (Section 6.5). Other structural changes associated with southward interplanetary field will be discussed in the next chapter. Generally speaking, today's interest in statistical studies is directed more at how quickly the magnetosphere responds to short-term changes in the direction of the interplanetary field than whether it does so (Section 6.6). Several studies have clearly established the existence of not one but two response time scales. The first, 10–20 minutes, is the time for polar cap convection to adjust to a change in the rate of dayside reconnection. The second, 50–60 minutes, is the time for the tail to respond. Finally, there is a component of convection and geomagnetic activity that is not due to reconnection; statistical evidence that it is related to viscosity is outlined in Section 6.7.

6.2 Correlation of Geomagnetic Activity with the Interplanetary Magnetic Field

A semiannual variation was one of the earliest recurrent patterns of geomagnetic acitivity to be recognized (Cortie, 1912; Chapman and Bartels, 1940). It appears as spring and fall maxima in long-term averages of various measures of geomagnetic activity. For example, twice as many magnetic storms above a given magnitude occur on average during the equinoctial months as during the solstitial months. The great magnetic storms, the once-per-decade storms, seem to be accounted for by this effect. In 1973, Russell and McPherron (1973b) proposed that the semiannual variation is caused by the periodicity in the effective southward component of the magnetic field that arises because the interplanetary field is ordered in a solar-equatorial coordinate system, whereas reconnection at the dayside magnetopause is controlled by a magnetospheric system. The angle between the magnetospheric magnetic field and the interplanetary field varies as the

earth moves around the sun, keeping its rotation axis fixed in inertial space. Magnetic fields pointing outward from the sun along the Parker (1957) spiral (and therefore opposite to planetary motion) will be more southward than northward during 6 months of the year and vice versa the other six months, centered on the equinoxes. Since outward and inward interplanetary field sectors occur with equal regularity, the effect would cancel but for the fact that dayside reconnection is strongly keyed to southward field. A simple model that assumed that northward interplanetary fields are noninteracting, and that the reconnecting southward fields are ordered in geocentric solar magnetospheric (GSM) coordinates clearly predicted the phase and the amplitude of the semiannual variation. Later, Russell (1989) showed that a diurnal variation in the geomagnetic activity index, Am, could also be explained by the Russell–McPherron (1973) effect.

Since the advent of space observations, many studies have related short-term geomagnetic activity to variability in the interplanetary medium. Early in the space era, it was shown that geomagnetic activity correlates with the solar wind velocity (Snyder et al., 1963), as was expected for viscosity-driven convection. However, activity soon proved to correlate with southward interplanetary field as well (Fairfield and Cahill, 1966). It correlated with the east–west component of the $\mathbf{V} \times \mathbf{B}$ electric field (Rostoker and Falthammar, 1967) even more strongly; so it appeared that at least some of the velocity correlation was related to reconnection. Arnoldy (1971) found that the auroral electrojet index correlated with the product of the solar wind speed and the southward component of the interplanetary field better than with the individual parameters, and correlated best when AE was delayed by 1 hour. This was the first indication of the delayed response of the magnetosphere to changes in the direction of the interplanetary field.

Today's issue is not whether geomagnetic activity correlates with reconnection-related solar wind parameters, but whether statistical analyses will reveal the precise coupling function. A satisfactory answer to this question is a prerequisite to searching for any residual component of geomagnetic activity driven by viscosity. The state of the art has been advanced by our growing ability to deal with extremely large data sets. For example, Scurry and Russell (1991) applied a multiple linear regression analysis to 25 years of solar wind data in the OMNI data base at the National Space Science Data Center (NSSDC) and the Am geomagnetic index (Mayaud, 1980; Menvielle and Berthelier, 1991). Strictly speaking, this study tested the steady reconnection model, since it used 3-hour running averages of 1-hour solar wind data, which smoothed the data over a complete convection cycle. Scurry and Russell (1990) had previously found that solar wind dynamic pressure variations were primarily responsible for activity in the Am index for northward field conditions when no reconnection occurs. Their 1991 study showed that the dependence of Am upon dynamic pressure was independent of the "clock angle" of the interplanetary field; so this residual component of activity is unrelated to reconnection, and is consistent with viscous driving. When the dependence on dynamic pressure was removed, the angular dependence of the Perreault–Akasofu energy-coupling function was confirmed to high accuracy. Thus, two important conclusions were reached simultaneously; the reconnection coupling function was

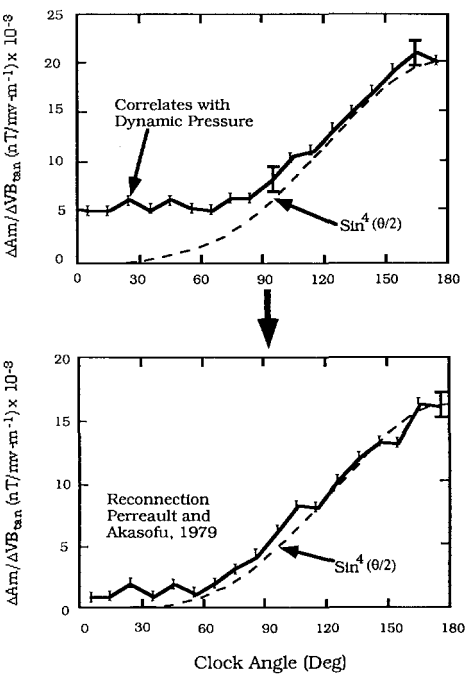

Figure 6.1. Bimodal Geomagnetic Activity. This figure, adapted from Scurry and Russell (1991), may be thought of as summarizing a generation of research on the statistical relationship between geomagnetic activity and the state of the solar wind. Indeed, it employed a generation's worth of data. Scurry and Russell (1991) applied a multiple linear regression analysis to 25 years of solar wind data in the OMNI data base at the U.S. National Space Science Data Center and the Am geomagnetic index (Mayaud, 1980; Menvielle and Berthelier, 1991). They then constructed a function of the Am index that mimics the expected response of the magnetosphere to reconnection, and plotted this as a function of the "clock angle" of the interplanetary field [the angle in the Y-Z plane in geocentric-solar-magnetospheric (GSM) coordinates, with zero degrees representing northward field, and 180 degrees, southward field]. The top panel shows the overall result: there is residual geomagnetic activity in northward field conditions; activity increases as soon as the field develops a southward component; and when the interplanetary field is due south, this measure of activity is about four times stronger than it is during northward field conditions. Scurry and Russell (1990) had previously found that solar wind dynamic pressure variations were primarily responsible for the activity in the Am index for northward field conditions. The top panel suggests that the residual activity is independent of the "clock angle" of the interplanetary field, and so is unrelated to reconnection, consistent with viscous driving. When the dependence on dynamic pressure was removed, the angular dependence of the Perreault-Akasofu (1979) energycoupling function due to reconnection was confirmed to high accuracy (bottom panel). Thus, two important conclusions were reached simultaneously; the reconnection coupling function was determined, and the relative importance of a coexisting, presumably viscously driven, component of geomagnetic activity was established. L. Scurry and C.T. Russell, *J. Geophys. Res., 96*, 9545 (1991) copyright by the American Geophysical Union.

determined, and the relative importance of a coexisting, presumably viscously driven, component of geomagnetic activity was established.

As much as 10,000 TJ may be stored in the ring current during a major magnetic storm. The energy in the ring current is proportional to the depression in geomagnetic field magnitude, which is easily measured by ground magnetometers (Dessler and Parker, 1959; Sckopke, 1966; Parker, 1968), and the energy input rate is expressed in units of nT/h. When the main phase of the storm develops, the power delivered to the ring current is a factor of 3–10 higher than than that dissipated in particle precipitation and auroral currents (Perreault and Akasofu, 1978). Fairfield and Cahill (1966) and Hirshberg and Colburn (1969) were the first to show that the direction of the interplanetary field is an important factor in the buildup of the ring current. Later, Burton et al. (1975a,b) found that the rate of energy input into the ring current is essentially zero when the interplanetary magnetic field is northward and scales approximately linearly with the east–west component of the interplanetary electric field when the interplanetary magnetic field has a southward component. The power delivered to the ring current proved to scale as the Perreault–Akasofu energy input function (Perreault and Akasofu, 1978), a more elegant way to express the same conclusion. These results made it clear that southward interplanetary field controls the development of the main phase of the magnetic storm. By implication, the substorm is a more fundamental dynamical phenomenon than the more spectacular magnetic storm (Russell, 1986).

6.3 Dependence of the Convection Rate upon the Interplanetary Field

The existence of a two-cell pattern of ionospheric convection does not uniquely confirm the reconnection model, but the dependence of the strength of that convection on the direction of the interplanetary field certainly does. The so-called DP-2 ionospheric current system associated with polar cap convection was found very early on to strengthen with increasing southward interplanetary field (Iijima and Nagata, 1972). Soon thereafter, measurements made on balloons flown out of Resolute Bay, Canada, and Thule, Greenland found the polar cap electric field to wax and wane with the north–south component of the interplanetary field (Mozer and Gonzales, 1973). One single balloon flight could not provide the global information needed to estimate the dependence of the overall convection potential on the interplanetary field, but an average two-cell pattern was fabricated from 227 hours of data taken on three flights from three polar cap sites (Mozer et al., 1974). The cross-polar cap potential in this pattern was 55 kV. The cross-polar cap potential was subsequently measured with better time resolution in three different ways. The most direct is to integrate the electric field measured by polar orbiting spacecraft along their orbits (Reiff et al., 1981; Wygant et al., 1983; Doyle and Burke, 1983; Weimer et al., 1990). Incoherent scatter radar provides the ionospheric convection pattern over much of the polar region, making it possible to estimate the polar cap potential (Oliver et al., 1983; Alcayde et al., 1986; Senior et al., 1990; de la Beaujardiere et al., 1991a,b). Finally, the so-called KRM

magnetogram inversion method (Kamide et al., 1981; Richmond and Kamide, 1988) calculates the ionospheric current distribution and from that the electric potential distribution, assuming that the electrical conductance profile is known. All three methods have roughly 1-hour time resolution. There appears to be growing agreement between them, though none is perfect (Ahn et al., 1992). All observers now agree that the north–south component of the interplanetary magnetic field is the key parameter determining both the size of the polar cap and the total electric potential difference across it (Holzworth and Meng, 1975a,b; Cowley, 1984; Holzer et al., 1986).

It is of interest to compare the measured polar cap potential with that calculated from combinations of solar wind parameters according to reconnection theories (Gonzales and Mozer, 1974; Hill, 1975; Kan and Lee, 1979; Crooker et al., 1982; Reiff and Luhmann, 1986). Generally speaking, the polar cap potential correlates much better with parameters that include the solar wind velocity as well as the north–south component of the interplanetary field than with the north–south component alone (Baker et al., 1983; Doyle and Burke, 1983; Maezawa and Murayama,1986; Reiff and Luhmann, 1986; Rossberg, 1989). By assembling numerous AE-C, AE-D, and S3-3 measurements of the polar cap electric field, Reiff et al. (1981) showed that the dawn–dusk potential difference scales as the square root of the Perreault–Akasofu rate. Using the KRM method, Ahn et al. (1992) showed that the polar cap potential is proportional to the theoretical reconnection potential function calculated by Reiff and Luhmann (1986). The best correlation was found when solar wind parameters were delayed by 40 minutes.

The range over which the polar cap potential varies with changing interplanetary field conditions is now well established. Reiff et al. (1981) found that the potential rose from a threshold of 30 kV at low values of the Perreault–Akasofu function to 150 kV at high values. The potential calculated from DE 2 measurements varied from 20 kV in the least active intervals (as defined by the geomagnetic activity index Kp) to 110 kV at the most disturbed times (Heppner and Maynard, 1987). Double probe electric field measurements made on 55 dawn–dusk orbits of the S3-3 spacecraft yielded a 15–160 kV range (Wygant et al., 1983). When the dawn–dusk component of the hourly-averaged interplanetary electric field was less than 0.5 mV/m, the polar cap potential was consistent with reconnection of all the interplanetary magnetic flux incident on a 30 R_E wide front-side magnetopause. In other words, the reconnection efficiency was near 100%. When the dawn–dusk interplanetary electric field was larger, the reconnection efficiency diminished. The polar cap potential appeared to saturate at about 100–150 kV (Wygant et al., 1983). In general, all these studies found residual potentials at low activity that suggested that some tailward transport of high-latitude flux remains even when the interplanetary field is northward.

The auroral electrojet index is linearly related to the polar cap potential Φ. A number of studies have fitted a relationship between AE and Φ of the form

$$\Phi \text{ (in kV)} = A + B \text{ (AE)},$$

where AE is expressed in nT, and A and B are coefficients to be determined empirically. In the first such study, Reiff et al. (1981) found the values $A = 41$, $B + 0.11$; later, Weimer et al. (1990) found $A = 19.2$ and $B = 0.116$ from DE-2 summer hemisphere data. Ahn et al. (1992) combined ground magnetometer data from 88 northern hemisphere stations with DMSP auroral X-ray data to compute simultaneous profiles of ionospheric electric fields, currents, and conductance using the KRM method. The data were acquired a during a convection bay, a continuously active period of convection without substorms (Sergeev, 1977; Pytte et al., 1978), during which the interplanetary field had a southward component averaging 10 nT. A two-cell convection pattern was found throughout the event. The coefficients, $A = 36$ and $B = 0.082$, were almost identical to the ones found earlier for a different event, $A = 36$, $B = 0.089$. (Ahn et al., 1984).

The ultimate question for the reconnection model of convection has to be whether the electric field inside the magnetosphere proper correlates with the north–south component of the interplanetary magnetic field. Baumjohann and Haerendel (1985) compared the electric field inferred from multiplying the solar wind speed by the north–south component of the interplanetary magnetic field with the electric field measured at geostationary orbit by the GEOS 2 electron gun experiment. The dayside electric field at geostationary orbit (averaged in 3-hour LT bins) correlated not perfectly, but well enough with the interplanetary electric field (the correlation coefficient was 0.5–0.6). The magnetospheric electric field was about about 0.1–0.2 of the solar wind electric field, so that the empirical reconnection "efficiency" was roughly that predicted by the Petschek model of reconnection (Petschek, 1964; Levy et al., 1964).

Baumjohann and Haerendel (1985) could not find a correlation of the dayside electric field with solar wind momentum flux, which would have stood out had viscosity been the dominant driver of convection.

6.4 Dependence of the Polar Cap Convection Pattern upon the Interplanetary Field

The dependence of the locations and sizes of the two convection cells on the east–west component of the interplanetary field (B_y) illustrates how subtly dayside reconnection controls polar cap convection (Russell and Atkinson, 1973). Since the polar cap electric field responds on time scales of minutes to even short-lived changes in B_y, one must average large quantities of data from passes entering and exiting the polar cap in all magnetic time zones to ascertain the B_y, dependence of the global polar cap electric field pattern. When the interplanetary field has a southward component, the electric field in the northern hemisphere is larger near the dawn or dusk convection reversal depending upon whether B_y, is positive or negative, respectively (Heppner, 1972b). Thus, the convection pattern for non zero B_y, is not symmetric with respect to the (aberrated) noon–midnight meridian, as in a purely viscous model (Heppner, 1977; Heelis and Hanson, 1980; Heppner and Maynard, 1987). In the northern hemisphere, the whole pattern shifts to dawn or

dusk in the direction opposite to B_y,, the shift reversing sense in the southern hemisphere (Heppner, 1972b; Mozer et al., 1974; Zi et al., 1987; Hairston and Heelis, 1990). The associated shift in the boundary between open and closed field lines has been confirmed by auroral observations (Holzworth and Meng, 1975b). Measurements using ground-based magnetometers (Friis-Christensen et al., 1972; Friis-Christensen and Wilhelm, 1975; Friis-Christensen et al., 1985) and ionospheric radars (Foster, 1984) confirm the B_y, dependence of polar cap convection found by spacecraft in polar orbit.

Cowley et al. (1992) argued that three effects that depend on solar wind B_y, can be explained by a "simple dipole plus uniform field" picture derived from the reconnection model (Dungey, 1963; Cowley, 1975b; Stern, 1973; Lyons, 1985). The northern boundary between open and closed field lines displaces toward dawn for positive B_y, and toward dusk for negative B_y. Where the separatrix dividing the two convection cells crosses the open–closed magnetic field separatrix on the dayside also shifts towards dusk for B_y, positive and toward dawn for B_y, negative. Finally, the plasma poleward of the open–closed boundary near local noon will flow westward for B_y, positive (eastward for B_y, negative) before it turns poleward to cross the polar cap.

6.5 Dependence of Field-Aligned Currents upon the Interplanetary Field

The power communicated to the ionosphere via field-aligned currents increases, and the entire system of field-aligned currents moves equatorward as the southward component of the interplanetary magnetic field increases. In one study, vector magnetometer data acquired onboard the sun-synchronous MAGSAT spacecraft were sorted according to hourly averages of the north–south component of the interplanetary magnetic field (Bythrow et al., 1983). The strengths of the region 1 and region 2 currents increased as B_z decreased, and both systems migrated equatorward. The poleward edge of the region 1 system on the dayside shifted on average from 77 to about 70 degrees, and the equatorward edge migrated from about 67 to 60 degrees, as the hourly average B_z decreased from 0 to --10 nT. When the interplanetary magnetic field had a northward component, the region 1 and 2 currents continued to flow with greatly reduced amplitudes, 0.2–3 mA/m^2, in the presence of considerable small-scale structure.

6.6 Time-Dependent Response to the Changing Interplanetary Field

Siscoe and Huang (1985) suggested that the dayside and nightside reconnection each has its own system of currents and ionospheric electric fields with its own response time to changes in the interplanetary magnetic field. Although the time scales could vary from event to event, the existence of two basic time scales corresponding to the two basic events in the reconnection model of magnetospheric convection ought to turn up in statistical studies of the time-delayed response.

Some of the evidence that the magnetosphere's response to the IMF has two time scales is venerable. High-latitude geomagnetic disturbances can be separated into two types, the so-called DP-1 and DP-2 current patterns, where DP-2 responds to dayside reconnection, and DP-1 is related to substorms and presumably involves the geomagnetic tail. Nishida (1968a,b) found that the DP-2 system is enhanced within about 2 minutes of the arrival of changes in B_Z at the magnetopause. This estimate was confirmed by later case studies (Pellinen et al., 1982; Nishida and Kamide, 1983; McPherron and Manka, 1985; Clauer and Kamide, 1985). On the other hand, a 1967 study of the auroral electrojet index, which characterizes nightside current systems, yielded a much longer response time (Schatten and Wilcox, 1967), and subsequent research systematically confirmed a 30–60 minute scale time (Arnoldy, 1971; Rostoker and Bostrom, 1976; Baker et al., 1981a, 1983).

Transient aurora at local midnight have two time scales (Krukonis and Whalen, 1980). Twelve flights of the Air Force Geophysics Laboratory airborne ionospheric observatory were routed to keep station near local magnetic midnight at magnetic latitudes of 69 ± 4 degrees. This made possible relatively long-duration (9–10 hour) studies of the lifetimes of discrete auroral forms. Ninety-three hours of all-sky photographs were taken at 1-minute intervals; discrete aurora were detectable 5/6 of the time, and a total of 186 distinguishable events were recorded. The occurrence frequency of the lifetimes of individual forms maximized between 10 and 20 minutes, with a second, lesser group of forms lasting between 90 and 150 minutes. In due course, we will see that sun-aligned aurora appear in the polar cap about an hour after a northward turning of the interplanetary magnetic field and disappear about 20 minutes after a southward turning.

Two time scales emerge from studies of the response of geomagnetic indices to the interplanetary magnetic field using the linear prediction filter technique (Iyemori et al., 1979; Clauer et al., 1981; Bargatze et al., 1985; McPherron et al., 1988). Bargatze et al. (1985) applied this method to 34 intervals of high-time resolution IMP 8 solar wind data and the AL index, which is an indicator of the peak current density in the westward electrojet There was a 20 and a 60 minute peak in the time-lagged linear filter response of AL to variations in (essentially) the east–west component of the interplanetary electric field. The authors suggested that the 20 minute response represented AL activity that was directly driven by solar wind coupling, and that the 60 minute response reflected the release of energy previously stored in the geomagnetic tail.

Studies with the EISCAT radar revealed that the nightside ionospheric flow and plasma parameters respond with 15–20 minute and 1-hour delays to southward shifts of the interplanetary magnetic field (Williams et al., 1989). The nightside flow often varied in a quasiperiodic way with the 1-hour period, and in two cases for which concurrent interplanetary field data were available, a similar periodicity was present in the north–south component of the interplanetary field, suggesting that the 1-hour oscillations were resonantly driven.

The auroral electrojets respond only on the 20 min time scale when the level of activity is already high (Baker et al., 1983, 1986a; Bargatze et al., 1985).

Several authors have suggested that the 60 min response disappears due to a transition to chaos at high levels of activity (Baker et al., 1990b, 1991; Roberts et al., 1991; Klimas et al., 1992). This amplitude dependence indicates that the magnetosphere's response to the solar wind is not linear, contrary to the basic assumption underlying the use of the linear prediction filter technique.

6.7 The Viscous Component of Geomagnetic Activity

The studies that relate AE to Φ agree on the two basic points. First, increased AE corresponds directly to the increased tailward transport of magnetic flux in the the polar cap, as reflected by the polar cap potential. Second, there is net tailward flux transport at very low AE. Some of the residual transport could be accomplished by small-scale structures that do not induce the relatively large-scale current systems needed to register in the AE index. In addition, at times of very low activity, the ionospheric currents move to high geomagnetic latitudes where there are no ground stations that contribute to the AE index. These factors certainly affect quantitative details. However, a similar residual appears in studies that correlate the polar cap potential with the interplanetary field direction. Thus, the "resting" polar cap potential reflects a real, second component of convection.

The fact that the residual potential is comparable to the potential across the low-latitude boundary layer suggests it has its origin in viscosity. Sergeev and Kuznetsov (1981) inverted the geomagnetic variations in the near polar cap region to obtain the regression relation

$$\Phi(\mathrm{kV}) = 6V^2 + 9\,B_Z,\ B_Z > 1\ \mathrm{nT}$$

where V is the solar wind speed in units of 300 km/s, and B_Z is the north–south component of the interplanetary field in nanotesla. The velocity scaling of the B_Z-independent component indicates it is due to viscosity. When the many-hour delayed response of Φ to changes in B_Z found by Wygant et al. (1983) is taken into account, the viscous potential diminishes by perhaps 20%, to 6.5 kV for a 400 km/s solar wind speed (Mishin, 1990). Using worldwide magnetometer data, Mishin (1990) monitored the field-aligned current boundaries of the polar cap, and estimated the variations of the magnetic flux contained therein. Multiple regression analysis showed that the high-latitude flux could be divided into a reconnection component that depends upon B_Z and a viscous component that does not (Mishin, 1990). The viscous and reconnection flux components had comparable magnitudes, consistent with the observations of a large closed-field-line viscous layer in the deep tail (Slavin et al., 1985; Heikkila, 1988). The viscous component never disappeared.

6.8 Summary

One often hears it said that "statistics lie," or, from those more sophisticated scientifically, that "correlation does not equal causation." There are good reasons for such cautionary admonitions. Yet as our understanding of the magnetosphere's chain of causation becomes more articulated, our appreciation for the accomplishments of statistical studies grows. They have provided an answer to the question "what causes geomagnetic activity?" They have taught us there are two components of geomagnetic activity. The stronger is due to reconnection and is driven primarily by the southward component of the interplanetary field. The other, weaker, one is independent of the interplanetary field direction, responds to the momentum flux density of the solar wind (the dynamic pressure), and is in all likelihood due to viscosity. Statistical studies have taught us that the reconnection component of geomagnetic activity responds with two delay times to a change in the direction of the interplanetary magnetic field. Statistical studies have related geomagnetic activity directly to convection. Indeed, they have found two components of convection. Numerous studies agree that the polar cap potential correlates with the north–south component of the interplanetary field, that the potential covers a 20–150 kV range as conditions vary in the solar wind, and that the viscous component of convection circulates magnetic flux at 10–20% the rate of the reconnection component. As we proceed further, the complexity inherent in both the reconnection and viscous components of convection will gradually emerge. With this realization will grow an appreciation of the future promise of statistical studies. With adequate coverage, statistics need not lie, and truthful statistics will one day provide essential conceptual tools for understanding unsteady convection.

7

THE RECONNECTION SUBSTORM

7.1 Introductory Remarks

The reconnection model of magnetospheric substorms was designed 20 years ago to rationalize the time-dependent changes in the magnetospheric structure associated with auroral substorms. By 1970, it was becoming apparent that there was a characteristic sequence of events prior to auroral onset: The dayside magnetopause moved earthward, the inner edge of the cross-tail current sheet approached the earth, the field strength in the tail lobes increased, and the magnetic flux in the polar caps and tail lobes increased, all while the evening side aurora were migrating equatorward prior to onset. The increase in lobe magnetic field clearly suggested that the growth phase commenced with an increase in the dayside reconnection rate. By the early 1980s, studies quantitatively correlating the ionospheric electric field with southward interplanetary field had confirmed that the changes in structure accompanied enhanced convection as had been suspected all along. Both were related somehow to substorms. There was no other choice in the reconnection model but to spotlight its two reconnection events, at the dayside magnetopause and in the plasma sheet on the nightside, as the "main events" in the magnetospheric substorm. Dayside reconnection clearly initiated the growth phase, and tail reconnection had to follow with some delay. It seemed natural to associate tail reconnection with the onset of the auroral substorm.

Sections 7.2 through 7.6 are devoted to growth-phase phenomenology. Section 7.2 deals with the changes in magnetopause position that follow a single isolated southward shift of the interplanetary field, and Section 7.3 deals with the changes in the geomagnetic tail that occur as a result. These changes take place as the rate of convection builds up in the ionosphere (Section 7.4) and the dayside magnetosphere (Section 7.5). A growth phase that begins with enhanced dayside reconnection has to lead to enhanced tail reconnection—the second key event in the reconnection model of substorms. In an MHD model, the time and place where the new reconnection event takes place is determined by the propagation of waves along the characteristics connecting the dayside reconnection region to the tail lobes (Section 7.6).

The phenomena described next are the elements of the "nearer-earth neutral line model" of the substorm (Section 7.7), in which the new tail reconnection event takes place at a new neutral line earthward of the old one. The

types of evidence that nearer-earth tail reconnection actually takes place in association with substorms are sampled in in Section 7.8. Tailward-moving plasmoids are clear evidence that a nearer-earth reconnection region does form (Section 7.9). A spacecraft in the tail lobes observes a compressional magnetic field pulse that is a remote signature of a plasmoid passing by in the plasma sheet; timing these traveling compression regions (TCRs) might also help pin down when and where the plasmoid was formed (Section 7.10). Timing plasmoids or TCRs with respect to substorm onset might shed light on when and where they are produced, assuming onset has something to do with plasmoid ejection (Section 7.11). These bright hopes have not been realized. In the aggregate, timing studies do not specify a clearcut relation between plasmoid formation and the auroral substorm onset, and there may not be a one-to-one relationship between plasmoid occurrence and substorms.

7.2 Changes in Magnetopause Position during Substorm Growth Phase

The very first geostationary spacecraft occasionally encountered the magnetopause so close to earth that even the grossly enhanced solar wind dynamic pressure during magnetic storm intervals did not explain their position (Russell et al., 1968; Cummings and Coleman, 1968; Lezniak and Winckler, 1968; Skillman and Sugiura, 1971). The record for closest approach, 5.2 R_E, seems to have been set by an Explorer 45 magnetopause encounter during an interval of unusually high solar wind velocity and magnetic field strength (Cahill and Skillman, 1977; Kauffmann and Cahill, 1977). Soon it was found that the magnetopause migrates inward following southward shifts of the interplanetary magnetic field (Aubry et al., 1970, 1971; Fairfield, 1971; Russell et al., 1974; Holzer and Slavin, 1978). This provided the key insight that led to the reconnection model of substorm growth phase (McPherron, 1970, 1972; Coroniti and Kennel, 1972a,b,c, 1973; Russell and McPherron, 1973a; Cowley, 1982).

The first detailed evidence that dayside reconnection displaces the magnetopause inward was found on an inbound pass of OGO 5 near 0900LT on March 27, 1968 (Aubry et al., 1970). OGO 5 entered the magnetosphere when the interplanetary field measured onboard Explorer 35 was northward. Twenty minutes after this magnetopause crossing, the interplanetary field at Explorer 35 turned southward, and 10 minutes later, the magnetopause moved inward over OGO 5. For the next 1 hour and 45 minutes, OGO 5 and the magnetopause moved inward together. At least 10 partial magnetopause crossings were observed, roughly one every 10 minutes. Thus, as the magnetopause was moving inward, it oscillated back and forth over the spacecraft. Had these oscillations not existed, the observers would have been unaware of the magnetopause's proximity. As it was, they could monitor the changes in both magnetosheath and magnetospheric properties. During the 1 hour and 45 minutes, the magnetosphere magnetic field magnitude increased by 20%, and the magnetosheath field direction varied around a dominantly southward orientation. When OGO 5 finally left the region of the magnetopause,

the magnetosheath field was turning northward and it remained northward for 20 minutes thereafter. The estimated distance to the subsolar magnetopause decreased by 1.85 R_E, yet there had been no significant change in the dynamic pressure of the solar wind throughout the entire period. All this took place before there was significant activity at auroral latitudes or any midlatitude ground signature of a substorm expansion (Russell et al., 1974).

This example graphically illustrates what has proved to be true in general in statistical studies. For example, after correcting for variations in solar wind dynamic pressure, Sibeck et al. (1991) found that the subsolar magnetopause moves inward about 0.7 R_E when the interplanetary field is northward and diminishes from 5 to 1 nT, but it moves twice as far inward when the interplanetary field turns southward and varies from 0 to -5 nT. The multiplicity of magnetopause crossings observed by Aubry et al. (1971) has also proved to be typical. Song et al. (1988) surveyed more than 1000 magnetopause crossings in ISEE 1 and 2 data collected from the beginning of the mission in October 1977 until the reentry of the satellites in September 1987. Of these, more than half were multiple. The duration of a set of multiple magnetopause crossings was typically 30 minutes or less, and it took about 2 minutes of data to make a definitive magnetopause identification, so that their survey was sensitive to magnetopause oscillations in the 2–30 minute period range. Two-thirds of the magnetopause passes had multiple crossings for southward interplanetary field, whereas only one-quarter of the passes for northward field had multiple crossings. The time from first to last crossing on a pass was 31 minutes for southward field, and 9.3 minutes for northward field, consistent with the fact that the average number of crossings per pass, and the amplitude, were about three times as large for southward field as northward. The amplitude increased with distance away from the subsolar point for southward field, while it was relatively constant for northward field. Analysis of the spectrum of solar wind dynamic pressure variations in the 10-minute to 1-hour period range indicated that that pressure variations could account for the northward field boundary motions but not for those associated with southward field conditions.

7.3 Changes in the Geomagnetic Tail during Substorm Growth Phase

The inward migration of the magnetopause had to mean that the rate of flux removal by dayside reconnection was not being balanced by the earthward transport of flux from the geomagnetic tail. In the Aubry et al. (1970) event, the total flux "eroded" from the front side of the magnetosphere was 10^{16} maxwells, roughly 15% of the flux in the tail lobes. When flux is eroded from the dayside magnetopause, the polar cusp ought to move equatorward as the polar cap gets bigger. Just after the inward migration of the magnetopause was discovered, the same team reported an OGO-5 encounter with the cusp at an unusually low latitudes at a time when the interplanetary field was southward (Russell et al., 1971b). Later in the event, the interplanetary field turned northward, and the cusp moved poleward; when the interplanetary field turned southward again, the cusp

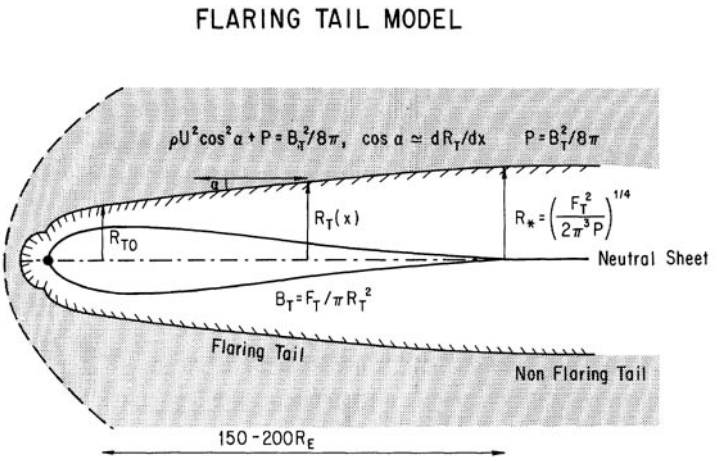

Figure 7.1. Flaring Tail Model. Suppose the tail lobes consisted of a cylindrical bundle of magnetic flux in steady state with no reconnection. The magnetic pressure in the tail lobes must balance the component of flow stress normal to the flared magnetopause boundary. This flow stress is the sum of the dynamic and static pressures of the flow. The dynamic pressure in the Newtonian approximation is proportional to the square of the cosine of the "angle of attack" between the direction of the asymptotic solar wind velocity vector and the magnetopause normal. This angle of attack, in turn, is related to the rate of change of the tail lobe radius with distance downstream. Together with the relation expressing conservation of magnetic flux in the tail lobe, these relations lead to an equation for the position of the tail magnetopause boundary (Tverskoy, 1968; Spreiter and Alksne, 1969). The tail flaring ceases at that point where the lobe magnetic pressure equals the thermal pressure of the solar wind. For typical parameters, this occurs 150–200 R_E downstream. By varying the parameters of this model, one arrives at reasonably accurate predictions for the changes in tail lobe radius and field strength that occur during the substorm growth phase. This model has no plasma sheet and no tail reconnection in it. If one adds a plasma sheet, an inactive Y-type neutral line will be found at the distance where flaring ceases (Birn et al, 1992). Original drawing.

moved equatorward over the spacecraft. These results confirmed in a most timely way the idea that the magnetopause migrates back and forth in responses to changes in the direction of the interplanetary magnetic field. Burch (1972b, 1973) studied this process statistically and found that the polar cusp moved equatorwards about one degree for every 10 minutes the interplanetary field was southward.

The erosion of the dayside magnetosphere was clearly due to a delay between the stimulation of reconnection on the dayside and in the tail. If the dayside reconnection rate exceeds the tail reconnection rate, the magnetic flux in the tail lobes, the areas of the distant tail lobes, and the areas of the polar caps will

increase with time (Coroniti and Kennel, 1972a). The emf across the transpolar magnetopause will exceed that across the polar cap ionosphere, the difference measuring the net rate of change of magnetic flux through the dawn–dusk meridian plane (Sanchez et al., 1991). Since the radius of the magnetopause decreases near the earth and increases far downstream, the tail magnetopause becomes more highly "flared," thereby intercepting more solar wind dynamic pressure and compressing the lobe magnetic field. The idea that dayside reconnection induces tail flaring has been supported in a series of statistical studies. In one recent example, a multivariate study of 1821 magnetopause crossings found that, after the dependence on solar wind dynamic pressure was accounted for, the cylindrical radius of the tail lobes at 20 R_E downstream increased from 20 R_E when B_Z was 6 nT northward to 23 R_E when B_Z was 6 nT southward (Sibeck et al., 1991).

Behannon (1968, 1970) and Mihalov and Sonett (1968) were the first to show that the magnetic field strength in the tail lobes correlates with increasing geomagnetic activity, as measured by various indices. Russell and McPherron (1973a), Caan et al.,(1973, 1975, 1977), Fairfield et al. (1981), and others proved that the field strength increases following a southward shift of the interplanetary magnetic field. Maezawa (1975) found that the radii of the tail lobes were larger, the larger the southward component; since the field strength also increases, this implied that the total magnetic flux in the lobes was larger for larger southward field. Makita and Meng (1983) found that the equatorward boundary of the region of polar rain moved to lower latitudes with increasing southward interplanetary field, also indicating that the lobe magnetic flux increases.

A simple model of the tail lobes (Tverskoy, 1968; Spreiter and Alksne, 1969a) rationalized the dayside magnetopause migration, the tail flux increase, the increase in lobe magnetic field, the increased tail flaring, and the increase in radius of the distant tail, as a function of distance downtail (Coroniti and Kennel, 1972a). It ordered the observations of the changes in field strength (Russell and McPherron, 1973; Maezawa, 1975) and tail lobe area (Baker et al., 1984b, 1986; Slavin et al., 1985) that take place during substorm growth phase. The same chain of reasoning predicted that the inner edge of the cross-tail current sheet approaches the earth on the nightside. As the tail flares, the magnetopause current increases, and so must the cross-tail current in the plasma sheet. Simple stress balance arguments (Siscoe and Cummings, 1969) indicated that the current sheet should move earthward as the cross-tail current increases (Coroniti and Kennel, 1972a). Later magnetic field and energetic particle observations from geosynchronous orbit confirmed that the cross-tail current system intensifies (Coleman and McPherron, 1976) and moves earthward (Kauffmann, 1987) during substorm growth phase. These and related observations will be discussed in more detail later.

The simple tail lobe model (Tverskoy, 1968; Spreiter and Alksne, 1969a; Coroniti and Kennel, 1972a) cannot be entirely accurate, for the model assumes a cylindrical cross section, and a multiple regression analysis of the dependence of the ISEE 1 lobe field strength upon the solar wind's static pressure, dynamic pressure, and magnetic field showed that the tail lobes expand in a pronounced way near the dawn and dusk flanks and hardly at all over the tail axis as the AE index

increases (Nakai et al., 1991). Nonetheless, the simple model probably gives a reasonable idea of the increase of magnetic energy stored in the tail during the growth phase of the CDAW 6 substorm of 1054 UT on March 22, 1979. The CDAW 6 data base was used to compare solar wind and magnetospheric pressures (Fairfield, 1985). The flaring angle, estimated by assuming that the component of solar wind pressure normal to the magnetopause equals the total pressure within the tail, increased from 18 to 32 degrees during the growth phase and decreased to 25 degrees after onset. The release of the stored magnetic energy, which exceeded 5000 TJ, was more than enough to account for the energy dissipated by ionospheric currents in the auroral substorm (Baker et al., 1985a, 1986a). Baker et al. (1981a) had reached a similar conclusion for the growth phase of another substorm, on December 29, 1976, in which the tail was monitored by IMP 8 at 35 R_E distance.

7.4 Development of Ionospheric Convection during Growth Phase

The system of field-aligned and ionospheric currents needed to increase the convection rate in the ionosphere cannot be established instantaneously after the rate of dayside reconnection increases. There will be a brief delay for MHD waves to communicate the change in magnetopause boundary conditions to the ionosphere. Only after this could polar cap convection begin to respond. However, the large-scale convection electric field in the polar caps will gradually build up over a 10–20 time scale set by the finite Pedersen conductivity of the polar cap and auroral ionosphere (Coroniti and Kennel, 1973; Holzer and Reid, 1975; Reid and Holzer, 1975; Sanchez et al., 1991).

Horwitz and Akasofu (1977) tested these ideas by studying the response of the dayside aurora to rapid changes in the north–south component of the interplanetary field. They found that discrete aurora brightened within minutes after steplike southward shifts in the interplanetary field reached the magnetopause, and that the dayside auroral oval moved 1–3 degrees equatorward 10–15 minutes thereafter. Discrete short-lived auroral features moved poleward at about 800 m/s while the oval was displacing southward, consistent with the idea that the convection electric field builds up while the magnetopause migrates inward. The 10–20 minute line-tying time scale should also apply when the interplanetary field turns northward and magnetospheric convection relaxes and/or changes its pattern. Horwitz and Akasofu (1977) found that the sequence of events described for southward shifts essentially reversed for northward shifts. In three of their cases, the auroral motions could be approximated by exponential relaxations between the initial and final latitudes; the time constants came out to be 14, 17, and 21 minutes.

Ahn et al. (1987) found that the large-scale ionospheric convection pattern inferred from ground-based magnetometer measurements responded in about 20 minutes to variations of either sign in the north–south component of the interplanetary magnetic field. An incoherent scatter radar study found that convection in the dayside ionosphere responded within minutes to a northward turning of the IMF, but that it took about 20 minutes for the ionospheric currents

and flow pattern to achieve its final configuration (Clauer and Friis-Christensen, 1988). Later, we will see that studies with the EISCAT incoherent scatter radar have found it generally takes about 10-15 minutes for a change in the rate of ionospheric convection to be established over the polar cap (Etemadi et al., 1988; Todd et al., 1988). All the results are consistent to factor of 2 accuracy with theoretical estimates of the line-tying time scale, and with statistical studies of the delayed response of geomagnetic activity to changes in the direction of the interplanetary magnetic field.

7.5 Development of Dayside Magnetospheric Convection During Growth Phase

A sudden increase in the rate of dayside reconnection creates a demand for an increased return of flux to the magnetopause from inside the magnetosphere. A fast rarefaction wave will propagate antisunward from the magnetopause to stimulate sunward convection on closed field lines prior to substorm onset (Coroniti and Kennel, 1973). In the language familiar to those working on geomagnetic pulsations, this rarefaction wave might be called a *transient global mode*. Its coupling to local Alfven resonances communicates field-aligned currents to the ionosphere, which in turn stimulate the horizontal currents that act to decelerate the flow. This view of the line-tying process was developed in part by Kan et al. (1982).

The notion that dayside and polar cap convection develops before onset was confirmed by observations of two substorms on March 22, 1979 assembled by the CDAW 6 data analysis workshop. Knott et al. (1985) found that sunward flow commenced at GEOS 2 in the dayside magnetosphere minutes after the magnetosheath field at the magnetopause turned southward, and continued through the ensuing auroral onsets and into the recovery phases of both substorms. The measured electric field strength was of order 2 mV/m. Ground magnetometer measurements showed that a two-cell convection pattern was fully established in the polar cap ionosphere 10–20 minutes after the southward turnings (McPherron and Manka, 1985; Friis-Christenson et al., 1985). It is extremely important to note that no significant electric field was detected in the tail lobes at the distance of ISEE 1 until after onset in either substorm (Pedersen et al., 1985), even though sunward convection had already been established on the dayside.

7.6 Stimulation of Convection in the Tail Lobes

Information about a sudden increase in the dayside magnetopause reconnection rate will be sent tailward along MHD characteristics over the poles and into the tail lobes (Coroniti and Kennel, 1973; Coroniti, 1985). Waves propagating along the various characteristic fields will act to increase the rate of injection of plasma into the mantle, to enhance the rate of cross-lobe convection, to adjust the direction of

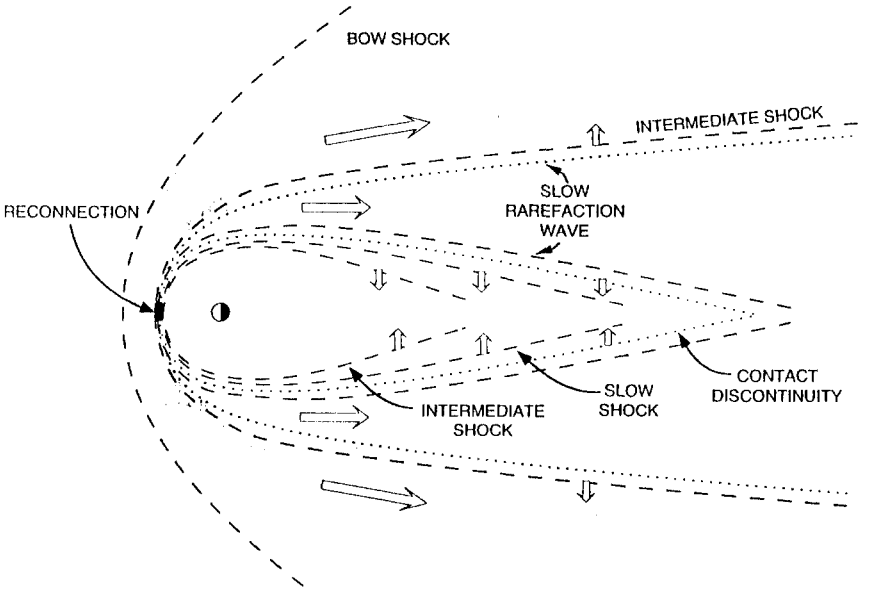

Figure 7.2. Standing MHD Waves in the Earth's Magnetic Tail. Imagine that the magnetic field directly upstream of the subsolar magnetopause suddenly switches from northward to southward. Fast, intermediate, and slow waves will be radiated forward and tailward to adjust the magnetosheath, the teardrop magnetosphere, and the ionosphere to the change in boundary conditions. The figure illustrates the standing waves that survive in the long-time limit, in which a steady reconnection-driven flow is set up in the magnetosphere. The most general Petschek reconnection configuration on the dayside involves an outward-facing intermediate shock, a slow rarefaction, a contact discontinuity that separates solar wind plasma from plasma that has been inside the magnetosphere, and inward-facing slow and intermediate shocks. When the density in the tail lobes is nonzero everywhere, we expect the tail magnetopause to consist of the same waves in the same order. We have not drawn the tail reconnection region, the plasma sheet, or the interactions between the tail-lobe waves and the plasma sheet. Original drawing (article for Geophys. Res. Lett., not yet submitted).

the lobe magnetic field to the change in direction of the interplanetary field, and to adjust the magnitude of the lobe magnetic field to the change in position of the magnetopause. Observing such changes in the tail lobes might forecast an impending tail reconnection event. Unfortunately, the missing link in magnetospheric research is measurements of waves in the tail lobes. Perhaps people have found subtle variations in the magnetic and electric fields in a quiet, very low-density region much less interesting than encounters with a constantly agitated plasma sheet. Whatever the reason, measurements of MHD waves in the low-density tail lobes are few and far between. In what follows, we array what

little we have been able to glean from the literature about this topic, in some cases from papers that were written for other purposes.

The electric field corresponding to the 15 km/s median cross-lobe convection speed (McCoy et al., 1975) is below the 0.5 mV/m threshold of the ISEE 1 electric field instrument; so it was usually too small for ISEE 1 to measure (Pedersen et al., 1984). However, enhancements to a few mV/m, often lasting several hours, were not uncommon. (Dusk-to-dawn electric fields were even encountered on rare occasions.) For typical magnetic field strengths of 10–20 nT, the dawn–dusk electric fields in the enhancements corresponded to $\mathbf{E} \times \mathbf{B}$ drifts of order 100 km/s toward the plasma sheet. While little else has been reported about these convection enhancements, their presence in the tail lobes at the distance of ISEE 1 ($< 23\ R_E$) does suggest that waves converge on the plasma sheet well earthward of the closure point of the slow rarefaction fan.

The ISEE 1 spacecraft was in the low-density tail lobes most of the time (Pedersen et al., 1984), whereas some of the Apollo 15 and 16 electric field measurements (McCoy et al., 1975) were undoubtedly made in the mantle, which often is almost completely closed near-lunar orbit. There were a number of occasions in which the dawn–dusk electric field component would have exceeded the 0.5 mV/m threshold of the ISEE 1 electric field instrument. Substantial changes were observed on time scales as short as a few minutes. In addition, there were numerous instances in which a north–south component of order 0.1–0.3 mV/m had to be present, northward and southward components occurring about equally. The north–south fields could have been due to an east–west "wagging" of the tail, but to sustain fields of 0.2 mV/m over the magnetotail for 2–3 hours would have displaced the tail by more than 20 RE. North–south components exceeding 0.3 mV/m that persisted four 4 hours were observed on occasion; had they extended uniformly across the tail, they too would have resulted in an inordinately large displacement, and it is likely they reflected the more complex action of waves, eddies, or inhomogeneities.

The first modern survey of ultralow frequency (ULF) magnetic fluctuations in the tail lobes was published in 1991 (Chen and Kivelson, 1991). Earlier studies (Mihalov et al., 1970; Hruska and Hruskova, 1969, 1970; Russell et al., 1971a; Russell, 1972a; McPherron et al., 1972) had not used particle data to distinguish the lobes in the data. Chen and Kivelson (1991) developed criteria based on plasma energy density to pick out lobe regions in the January–June, 1978, ISEE 2 data between 10 and 23 R_E downtail. They computed the magnetic field amplitude in 16–64 and 3–16 minute period bands, the second being the Pc 4–5 band of ground-based magnetometry. In general, the combined 3–64 minute amplitude was a few tenths of a nanoTesla, and only in 10% of the cases did it exceed 1 nT. The Pc 4–5 transverse component was below 0.8 nT 90% of the time, and the compressional component was below 0.6 nT. The 16–64 minute amplitude was somewhat larger. The correlations of the various amplitudes with the auroral electrojet index derived from 223 events were weak but positive.

Chen and Kivelson (1991) also reported case studies of three substorms. In two of the three (March 13 and April 1), ISEE 2 was in the lobes during both the

growth and expansion phases as characterized by AE. In the third and largest (April 10), a plasma sheet dropout put the spacecraft in the lobes of the tail only after the expansion began, so the growth phase could not be observed. We concentrate on the results for the Pc 4–5 band. For the April 1 substorm, the Pc 4–5 power increased in the growth phase, did not respond dramatically to the increase in AE to over 500 nT at onset, and maximized (0.5 nT) during the late recovery phase. On March 13, the transverse power was relatively large (0.3 nT) in the low-AE interval preceding the substorm, and diminished during a 5-hour period of elevated AE following onset. When ISEE 2 entered the lobe following the expansion of the AE > 1500 nT April 10 substorm, it encountered the largest ULF amplitudes (2 nT) in the entire data set.

So far, we cannot discern a clear pattern, but the amplitude figures that have been reported are significant. Number densities in the tail lobes typically range between 10^{-3} and 10^{-1} cm^{-3} with 10–100 eV ion temperatures (Eastman, et al., 1985b). The Alfven speed for a lobe magnetic field of 20 nT and a proton density of 2 x 10^{-2} cm^{-3} is about 3000 km/s; so a 0.5 nT amplitude corresponds to an Alfven wave power flux of 0.01 GW/R_E^2 if the waves are propagating in the same direction. The total power integrated over the area of tail lobes of 20 R_E radius would be of order 10 GW. More study is needed.

7.7 The "Nearer-Earth Neutral Line" Scenario

Dungey's (1961a) reconnection model has only two main events, the dayside reconnection and the nightside reconnection. Can we fabricate a substorm from just these two elements? The attempt to answer this question has led to what we will call the "nearer-earth" neutral line scenario. We present our version of this scenario here.

The plasma sheet should ultimately respond to the arrival of the waves from the dayside reconnection event by reconnecting. Thus, the delay until new tail reconnection occurs will depend upon the time for MHD waves to propagate from the dayside reconnection region to the plasma sheet. The new tail reconnection event will not occur where the old one did, because the places where the tail lobe waves close will have to adjust to the change in convection rate. The nearer-earth neutral line model simply assumes that a new reconnection event is triggered within the previously existing neutral line sometime during the substorm sequence. The nearer-earth scenario is less demanding than the near-earth neutral line model in the literature, which in its strictest form assumes that reconnection takes place within an Alfven wave propagation time of onset on field lines that connect to the auroral onset region. Much of the debate about substorms is a debate about the relative merits of these two models.

The new and the old reconnection regions will create between them a region of closed or semiclosed magnetic flux containing heated plasma—a plasmoid (Schindler, 1974; Hones, 1976, 1979). The reconnection at the new neutral line has to start on closed field lines within the plasma sheet. While the

reconnection event may accelerate energetic particles, the magnetic tension of the closed plasma sheet field lines surrounding the plasmoid will tend to move the plasmoid along with the general flow, and there need not be any large-scale change of configuration in this phase. Nishida et al. (1986) interpreted some of the slow flows associated with southward B_Z observed on ISEE 3 between 60 and 100 R_E as being due to the "stagnant plasmoid" that might be created during this first phase. After an unspecified delay, reconnection at the new neutral line consumes all the closed flux and reaches the open field lines of the tail lobes. At this moment, the earthward side of the nearer-earth reconnection region will be connected magnetically to the pre-existing poleward boundary of the auroral oval, and the plasma earthward of the reconnection region will be accelerated earthward. The plasmoid tailward of the reconnection region will suddenly be connected magnetically to the solar wind and will begin to accelerate tailward. This violent event ought to be accompanied by the appearance of recently accelerated energetic particles on previously open field lines, so that the plasma sheet will appear to expand. There is no guarantee that conjugate field lines will reconnect, so that sudden deviations from conjugacy at the poleward edge of the auroral oval may be an ionospheric signature of the lobe field reconnection and, by inference, the plasmoid ejection.

In the following sections, we attempt to answer two questions in a preliminary way. First, to what extent is there evidence of tail reconnection and plasmoid formation during the substorm sequence? Second, what is the relationship between these events and the onset of the substorm in the auroral ionosphere? We will return to these questions again and again.

7.8 Observational Basis of the Nearer-Earth Neutral Line Model

Here we provide a flavor of the types of evidence supporting the nearer-earth and near-earth neutral line scenarios.

Fast tailward flows in the plasma sheet are often considered to be a "smoking gun" for reconnection earthward of the spacecraft: A sudden reversal from stagnant or earthward to tailward flow naturally suggests that a new neutral region earthward of the spacecraft has become active, and there have been numerous reports of tailward plasma sheet flows in association with substorms. For example, strong tailward plasma flow was found in four of a sequence of five substorms during which IMP 7 was inside or near the plasma sheet near 30 R_E downtail (Coroniti et al., 1980). In two of the substorms, the tailward flow commenced within minutes of the onsets recorded by ground magnetometers and persisted for 30–40 minutes afterwards. Large southward magnetic field components accompanied the flows, suggesting that reconnection earthward of the spacecraft was the source. If the flows were due to an $\mathbf{E} \times \mathbf{B}$ drift, the dawn–dusk electric field component at the spacecraft was 50–75 kV/R_E corresponding to an emf of 1.5–2.25 MV across the tail, a factor 10 larger than the largest potentials observed across the polar cap. This suggested that the fast flows did not extend

uniformly across the entire width of the tail. The tailward flows following the two other onsets could only be followed for 2–4 minutes before the plasma sheet "dropped out" and spacecraft entered the tail lobes.

Tailward flow, by itself, does not prove that reconnection has reached open field lines, formed plasmoids, and has acted to reduce the open flux in the tail lobes. The multispacecraft multicase study, CDAW 8, was specifically designed to seek this evidence. In CDAW 8 event B, the 9 hours following a storm sudden commencement on March 25, 1983 were monitored by six spacecraft near geosynchronous orbit, one over the pole and three in the magnetotail. The compressions associated with the sudden commencement were first seen near the earth and then further downtail with a delay that was consistent with the passage of an interplanetary shock over the magnetosphere and tail. Ground magnetograms and synchronous orbit data were used to identify seven substorm intensifications, of which six were clearly associated with decreases in the magnetic field strength at 18 R_E distance. The four strongest were followed by increases of the northward magnetic field component at 20 and 30 R_E during the tens of minutes following auroral substorm onset.

The principal evidence that tail reconnection was important to these substorms was the following. The four principal ground onsets that were associated with major tail reconfigurations at 20 and 30 R_E were also associated with four events, lasting between 10 and 18 minutes, in which ISEE 3 at 110 R_E downtail detected weak magnetic field regions containing hot plasma flowing tailward, signalling entry into a plasma sheet containing a reconnection region earthward of the spacecraft. In the two of the four substorms in which DE 1 imaged the polar cap, the area of the polar cap decreased by 30 and 36% in the hour after onset. Although the poleward boundary of detectable auroral emission at best roughly tracks the separatrix between open and closed field lines, these results certainly suggest that closure of previously open lobe magnetic flux occurred during the expansion and/or recovery phases of the two substorms.

Strictly speaking, the examples cited support the nearer-earth, but not necessarily the near-earth, neutral line scenario. The first CDAW 6 substorm is often cited as good evidence for the near-earth neutral line model of substorms (McPherron and Manka, 1985; Baker and Kamide, 1985; Baker et al., 1985a; Barfield et al., 1985; Clauer and Kamide, 1985; Eastman and Frank, 1984; Fairfield, 1985; Friis-Christensen et al., 1985; Fritz et al., 1984; Hughes and Singer, 1985; Ipavich et al., 1985; Kamide and Baumjohann, 1985; Knott et al., 1985; Kroehl and Kamide, 1985; Lennartsson et al., 1985; Lennartsson and Shelley, 1986; N. Lin et al., 1991b; Mazaudier, 1985; Mishin et al., 1992a; Paschmann et al., 1985; Pedersen et al., 1985; Reiff et al., 1985; Stokholm et al., 1985; Tsurutani et al., 1985). The substorms on March 22, 1979 occurred at a time of equinoctial symmetry typical of isolated substorms following intervals of magnetic calm. A large increase in solar wind speed and an enhancement of the northward interplanetary magnetic field initiated a storm sudden commencement at 0826 UT on that day. This shock compressed the subsolar magnetopause to about 7 R_E. The interplanetary field remained generally northward until 1010 UT, when a solar

wind current sheet passed over the earth, and the interplanetary field turned southward and remained southward for more than an hour. At the same time, an accompanying decrease in solar wind density allowed the magnetopause to migrate outwards.

These events initiated the growth phase. The convection electric field at geosynchronous orbit on the dayside increased within minutes of the southward turning, and the 57 station AE index began to increase about 10 minutes later. Twenty minutes later, at 1030 UT, energetic protons at synchronous orbit began to drop out, and after another 10 minutes had passed, geostationary spacecraft near midnight passed through a tailward-directed current sheet into the lobe. The magnetic field at ISEEs 1 and 2 in the tail lobe approximately 15 R_E downtail remained near 15 nT until 1035 UT, at which time it began a systematic increase that reached 60 nT at the time of onset. Coincident with the changes in the near-tail region, the currents in the polar cap developed into the twin-vortex system characteristic of convection in southward interplanetary field conditions.

Ground magnetometer measurements and increases of energetic electrons at geosynchronous orbit fixed the time of substorm onset at 1054 UT; so the growth phase lasted 44 minutes. The onset may have been triggered by a northward turning of the interplanetary field at 1052 UT. The central meridian of the substorm was unusually far into the morning side, near 0300 LT. The cross-polar cap potential estimated from inversion of ground magnetometer measurements rose to 100–120 kV following the onset. During the expansion phase, AE rose to a peak of more than 1000 nT at 1140 UT, and then decreased until 1300 UT, when a second substorm onset interrupted the recovery of the first. An extremely detailed chronology of these events is contained in McPherron and Manka (1985). Probably, if we had CDAWs for every substorm, we would find equally complex scenarios.

We now focus on high-time-resolution measurements of the magnetic field and medium-energy particles made onboard ISEEs 1 and 2 in and near the plasma sheet (N. Lin et al., 1991b). The magnetic signature of the 1054 UT onset was the commencement of magnetic variability at 1058 UT. The plasma sheet must have become unusually thin, since the two ISEE spacecraft were in opposite tail lobes between 1057 and 1107 UT. At 1058 UT, there was an abrupt increase of the ion intensities in all five energy channels ($24 < E < 210$ keV) without detectable dispersion on a 36 s time scale, which suggested the ions had been accelerated relatively nearby. The ion fluxes, which had been relatively isotropic during the growth phase, exhibited strong tailward streaming in all channels beginning at 1058 UT and lasting until 1118 UT; 30–130 keV/e He^{2+} ions also streamed tailward during this interval (Ipavich et al., 1985). Medium energy electrons in the 22.5–39 keV energy channel began to increase in intensity at 1053 UT, but remained isotropic and only started to stream tailward at 1059 UT (N. Lin et al., 1991b). Like the medium energy ions, they too continued to stream tailward until 1118 UT. The sudden onset of the tailward streaming coincided with a bipolar N/S signature in B_Z, possibly due to a loop-like structure moving past the spacecraft. This signature was also seen at ISEE 2 on the opposite side of the neutral sheet. The

center of the bipolar signature at ISEE 1 lagged behind that of ISEE 2 by about 15 s; since ISEE 2 was 8800 km earthward of ISEE 1, the tailward velocity of the loop structure was about 580 km/s. The bipolar B_Z structure at ISEE 1 coincided with a bipolar electric field structure (Pedersen et al., 1985) in which northward B_Z and dawnward E_Y preceded southward B_Z and duskward E_y, so that the $\mathbf{E} \times \mathbf{B}$ drift was tailward throughout the interval. The measured E/B speed was consistent with the timing velocity of the loops between ISEE 1 and ISEE 2. At 1101–1102 UT a bipolar magnetic and electric field structure with the opposite magnetic polarity (S/N) convected tailward over ISEE 1 but was not registered at ISEE 2.

These phenomena are consistent with the formation of a neutral line between the ISEE spacecraft and geosynchronous orbit. It is important to note that ISEE 1 did not observe a large-scale plasmoid, but it did find persistent tailward jetting and convecting magnetic loop structures, consistent with impulsive and localized reconnection on closed field lines earthward of the spacecraft. The ion and electron streaming turned earthward at 1118 UT, consistent with the tailward retreat of a neutral line past the spacecraft, or the activation of a new reconnection region tailward of the spacecraft. At this time, the ground stations at the equatorward edge of the auroral oval began to recover and the high latitude stations recorded sudden intensifications. At 1124 UT, there was a sudden decrease in the density of H^+ and He^{2+} ions and an increase of O^+ density at ISEE 1, and shortly thereafter the magnetic field decreased at both ISEEs, suggesting that the plasma sheet had expanded over them. At 1134 UT a beam of aurorally accelerated oxygen ions streamed along field lines over the spacecraft, while the medium-energy ions of plasma sheet origin continued to flow earthward until AE began to recover around 1140 UT.

7.9 Plasmoids

Plasmoids moving tailward can be recognized from a bipolar excursion of the magnetic field direction, first northward and then southward, together with tailward flows in the central plasma sheet and predominantly tailward ion beams in the plasma sheet boundary layer. Within the bipolar structure, the electron heat flux parallel to the magnetic field should be small, if the plasmoid contains magnetic field loops that are effectively closed. These are the primary signatures that have been used to identify plasmoids in the plasma sheet. Strictly speaking, when the reconnection region is localized and there is an east–west component of magnetic field, the magnetic field does not form closed loops, though it is often pictured that way. For the purposes of our discussion, plasmoids need only be complex propagating magnetic field structures that restrict the escape of electron heat.

Many analyses of ISEE 3 data from the distant tail have indicated that plasmoids are ejected tailward in association with auroral substorms (Hones et al., 1984a,b; Baker et al., 1984b, 1987a; Scholer et al., 1984a,b,c,d, 1985b, 1986; Richardson and Cowley, 1985; Richardson et al., 1987a,b, Fairfield et al., 1989; Slavin et al., 1989; Richardson et al., 1989; Baker et al., 1990). The particularly

detailed study of Baker et al. (1990) of a weak, temporally isolated substorm on January 28, 1983, CDAW 8 event A, communicates the flavor of this research. Integration of the Perreault–Akasofu energy coupling rate indicated that two million GJ were added to the magnetosphere during a 60 minute growth phase that followed a southward shift of the interplanetary field; the original paper (Baker et al. 1990a) underestimated the solar wind energy input by a factor of ten (Baker et al. 1992). Various diagnostics timed the ensuing auroral onset with 2 minute accuracy. The following sequence of events was then observed at ISEE 3 at 220 R_E in the deep tail. Thirty-one minutes after onset, the spacecraft began to detect tailward-streaming energetic particles, an electron heat flux, and magnetic field perturbations consistent with an entry from the southern tail lobe into the distant plasma sheet boundary layer. Sixteen minutes after this boundary layer was first detected, there commenced a 21 minute interval containing 350 km/s tailward-flowing plasma and multiple shifts of the sign of B_Z, which was interpreted as the passage of the plasmoid itself. The plasmoid arrived 47 minutes after onset; it would have taken 67 minutes to cover 220 R_E if the speed had been a uniform 350 km/s. After this, there followed 12 more minutes in which behavior characteristic of the postplasmoid plasma sheet was observed. The plasmoid's duration and flow speed indicated it was about 70 R_E long when it passed over ISEE-3. Assuming its width was half that of the tail at 220 R_E, 25 R_E, the plasmoid's total energy content was about 10% of the energy added to the magnetosphere during the growth phase of the substorm.

Earthward-streaming ions at ISEE 1 at 7 R_E were observed six minutes after Pi 2 micropulsations marked a substorm onset on March 22, 1983 (Richardson et al., 1987). Three minutes later velocity-dispersed tailward-streaming ions were observed in the plasma sheet boundary layer by ISEE 3 at 130 R_E. These results were consistent with the creation of a new neutral line somewhere between 7 and 130 R_E distance within 9 minutes of onset. A plasmoid with a two-loop magnetic field structure was observed, and the authors suggested that the second loop was produced by a second neutral line that formed near the time of an intensification of the substorm. Three hours after all this, the plasma and the energetic ion streaming shifted from tailward to earthward, suggesting either the neutral line retreated tailward of ISEE 3, or that a new reconnection region was created downstream of 130 R_E.

Nishida et al. (1988) reported numerous signatures in ISEE 3 magnetic field, energetic proton, and plasma electron data at 80 R_E that were consistent with the production of tailward-moving plasmoids during substorms. They presented two examples of events in which substorm onset occurred when ISEE 3 was already in the plasma sheet. Before the onsets, the 30–36 keV proton anisotropy was directed sunward, indicating earthward flow across the plasma sheet. The anisotropy reversed to tailward shortly after the onsets (as identified by the AL index), and a few minutes after that the magnetic field at the spacecraft turned southward. Such events were taken as clear evidence of a new active reconnection region earthward of the spacecraft. In the majority of cases, an identifiable plasmoid was produced.

In the course of time the new reconnection region may retreat tailward to its average position near 80–100 R_E. ISEE 3 detected a magnetic signature consistent with a retreating neutral line between 80 and 140 R_E downtail on seven occasions between March 20 and 28, 1983, a frequency of about once a day (Baker et al., 1984b). The magnetic field in the plasma sheet was observed to shift strongly southward and then strongly northward, the order opposite to that expected for a plasmoid, in a period of about 15 minutes. The bulk flow velocity was typically 400 km/s tailward when the field was southward and stagnant when the field was northward, after the neutral line had passed over the spacecraft. The fast tailward flows arrived 5–10 minutes after there had been injections of energetic particles at geostationary orbit, a signature of substorm expansion. The retreating neutral line interpretation is not unique: The spacecraft could have passed in and out of an east–west-localized tailward flow from a reconnection region earthward of ISEE 3.

7.10 Traveling Compression Regions

A spacecraft need not be in the plasma sheet to detect plasmoids, since the lobe magnetic field is compressed by the passage of a plasmoid. Although the plasmoid itself might be localized and difficult to find, the compression of the tail lobe field is a nonlocal response to its passage, and detecting so-called traveling compression regions (TCRs) may be a better way to estimate plasmoid occurrence frequency. TCRs were first noted in Explorer 33 magnetic field observations (Maezawa, 1975), but were not studied in detail until later.

ISEE-3 encountered compressional magnetic field pulses in the lobes of the distant tail at a rate of several per day (Slavin et al., 1984). In each pulse, the magnetic field direction tilted first northward and then southward, with the inflection near the time of peak field amplitude. The durations of these traveling compression regions ranged from 5 to 20 minutes, and they were observed at distances ranging from 60 to 236 R_E. The durations appeared to be independent of distance, but the relative amplitudes decreased from 10% to 30% at 60–80 R_E to less than 10% beyond 200 R_E. The traveling compression regions passed over ISEE 3 10–30 minutes after increases of auroral kilometric radiation (AKR) suggested substorm onset (Slavin et al., 1984). Later, Bahnsen et al. (1989) found that the AKR emissions detected by *Viking* were associated with plasma sheet boundary layer precipitation at the poleward edge of the auroral oval. Thus, AKR intensifications may signify activations of the most poleward arc system and not of auroral onset.

The structure of plasmoids/TCRs appears not to change much as they move downtail. For one thing, their statistically derived characteristics do not change with distance (Moldwin and Hughes, 1992a,b). Plasmoids close to the earth have the same average size, velocity, amplitude of bipolar magnetic field signature, and core magnetic field strength as those in the deep tail. A case study supports this conclusion. An examination of IMP 8 and ISEE 3 magnetotail data yielded one

definite and two possible plasmoids that were detected by both spacecraft (Moldwin and Hughes, 1992a). In the clearest case, a TCR observed by IMP 8 at 35 R_E could be identified with a plasmoid observed 65 minutes later by ISEE 3 at 168 R_E. The TCR and plasmoid had similar magnetic field signatures and their durations were consistent, given that the TCR signature should last about 10–20% longer than the plasmoid's because of lobe magnetic field draping around the plasmoid. The measured plasma flow speed, 214 km/s, agreed extraordinarily well with the speed calculated from the delay between the arrival of the TCR at IMP 8 and the plasmoid at ISEE 3, which was 207 km/s. This, by the way, is perhaps the clearest evidence that TCRs are the lobe signatures of plasmoids.

7.11 Plasmoid and TCR Timing

If plasmoid ejection takes place at the time of the auroral substorm onset, the onset time, together with the plasmoid's time of arrival at the spacecraft and the measured flow velocity, would indicate where the near-earth neutral line had formed; the plasmoid's duration and flow speed would indicate how far apart the two neutral lines had been. This picture has motivated numerous studies that time plasmoid and TCR observations with respect to various substorm signatures. We sample a few of them here.

Superposed epoch analyses can highlight what is typical of many events. The following scenario emerged from a case-by-case examination and superposed epoch analysis of 15 plasmoid events observed over a 2-week period in 1983 when ISEE 3 was about 220 R_E downtail (Baker et. al., 1987a). There is a 40–60 minute growth phase, during which the tail goes through a characteristic sequence of changes (described earlier). About 20 minutes into the growth phase, ISEE 3 (on average) would enter the tail lobe. Between 16 and 40 minutes (25 minutes on average) after substorm expansion, a plasmoid would envelop the spacecraft. (It takes 23 minutes to cover 220 R_E at 1000 km/s.) Looking at the individual events, one finds a general tendency for plasmoids with higher flow speeds to arrive sooner after onset, but overall the small data set does not convey an impression of internal consistency. Eight of the 15 plasmoids arrived with almost the same delay after onset, 21–26 minutes, yet their flow speeds varied by almost a factor 2, between 575 and 1000 km/s. Of three events with flow speeds between 900 and 1000 km/s, one arrived 16, one 21, and one 25 minutes after onset.

One gets a similar impression from CDAW 8 plasma sheet observations made by ISEE 3 at 110 R_E downtail on March 25, 1983 (Fairfield et al., 1989). Four fast tailward flows began between 10 and 23 minutes after substorm onset. Only one of the four had a clear plasmoid magnetic signature. The plasma speeds had no discernible relationship to the delays after onset. For example, of the two events with the lowest speeds, both about the same, one had a 10-minute delay, 10 minutes, and one had an 18-minute delay, almost a factor two difference.

One probably cannot invoke variations in plasmoid speed to explain away the difficulties of substorm timing (Moldwin and Hughes, 1992a). For example,

one TCR/plasmoid detected both at IMP 8 and ISEE 3 simply did not accelerate between the two spacecraft; the measured flow speed was the same, 207–214 km/s, at 35 R_E and 168 R_E. If this plasmoid had formed at the time of the first preceding substorm onset observed on the ground, its speed based on the delay between 10 and 35 R_E would have been 120 km/s. Once again, the measured speed and the substorm timing speed were inconsistent.

Despite the numerous associations of fast tailward flows and plasmoids with substorms, not all plasmoids or tailward flows at 80 R_E could be associated with substorms (Nishida et al., 1988). An appreciable number of plasmoids passed over ISEE 3, and there were no indications of substorm expansion, either in auroral observations or at geosynchronous orbit. In one event, the proton anisotropy switched from earthward to tailward and the proton intensity increased, yet the AL index did not budge. (We will see shortly that fast ion flows in the plasma sheet often occur without an easily detectable ground signature.) On another occasion, an extended period of auroral activity, the proton anisotropy and the flow of thermal electrons were strongly earthward, and the magnetic field showed a number of north–south reversals, suggesting that an active and variable neutral line was tailward of 80 R_E throughout an entire convection bay. This behavior, too, is not uncommon.

There can be more TCR/plasmoids than substorm expansions. ISEE 3 was 129 R_E downstream of earth during CDAW 8 event G, the continuously disturbed day of March 22, 1983. It was in the tail lobes for 2 hours during which time three substorm expansions were identified at 0212 UT, 0226 UT, and 0303 UT in all or some of the AE index, substorm signatures at geostationary orbit, and DE images (Slavin et al., 1989). Beginning about 0236 UT, ISEE 3 detected five TCRs in the northern tail lobe, the last of which arrived at 0305 UT. The spacecraft entered the plasma sheet and began to detect more plasmoid signatures at 0310 UT, 7 minutes after the principal substorm intensification at 0303 UT. Thus, three expansions led to more than five TCR/plasmoids.

There are various ways to estimate the time of substorm onset, from the auroral brightening, from the AE index, from bursts of AKR, or from injections of energetic particles at geosynchronous orbit. A recent study indicates that not all energetic particle injections at geostationary orbit correspond to a TCR detectable by a spacecraft only 30 R_E away. An examination of 300 hours of data collected while IMP 8 was in the tail lobes at 31–37 R_E produced 16 examples of traveling compression regions (Slavin et al., 1990). Two events were studied in detail. In the first, on August 22, 1983, the IMP 8 magnetic field increased steadily during a 30 minute growth phase that terminated at the time of the first of four energetic particle injections observed at geostationary orbit near local midnight. The second injection, but not the first, was followed after 4 minutes by a TCR of relative amplitude 12.4% and duration 190 seconds. The third injection was followed after 19 minutes by an atypical TCR (the lobe field lacked a well-defined northward shift before turning southward). Thus one injection could not be associated with a TCR, and the delays between two others and the TCR differed by a factor of five. In the second event, on August 24, 1983, a well-defined TCR followed a first

geostationary injection by 3–4 minutes, and an atypical TCR followed a second injection by 5–6 minutes. A third injection did not correspond to a TCR at IMP 8. In this case, the delays between injection and TCR were consistent, but one of the injections again could not be identified with a TCR.

Perhaps most significant of all, the rate of detection of TCRs at IMP 8, one per 19 hours, was three times smaller than at ISEE 3 farther down the tail (Slavin et al., 1990). This has the natural implication that 2/3 of the TCRs observed by ISEE 3 are generated beyond 30 R_E downtail.

7.12 Discussion

The reconnection model of substorms has a venerable place in the history of magnetospheric research. In the form articulated here, it is a conscious effort in paradigm extension. By applying rules of causality embodied in the theory of MHD characteristics to Dungey's steady-state model, it outlines a sequence of events that might be expected to follow a sudden southward turning of the magnetosheath magnetic field. The first models along this line created expectations that stimulated many experimental investigations, and proved to pattern many of their results. They successfully accounted for the interlocking changes in magnetospheric structure that occur during substorm growth phase, and for the time scale on which these changes unfold. They contributed critically to the realization that the substorm had a growth phase in the first place. They led directly to the notion that a plasmoid would form at a new nearer-earth neutral line as a delayed consequence of an increase in the rate of reconnection at the dayside magnetopause, and numerous plasmoids were observed.

The problem comes when we try to tie the events in the reconnection model of substorms closely to the other events associated with substorms in the auroral ionosphere or geosynchronous orbit. There are only two big events in Dungey's model, dayside reconnection and nightside reconnection. Dayside reconnection already having been used up for the growth phase, it is the most natural thing in the world to assume there will be only one nightside reconnection event and to associate that event with the most important event in Akasofu's (1964) substorm, the auroral onset. Yet, when we try to pattern the times and places that we observe plasmoids and TCRs by assuming that they are created around the time of the auroral onset, the outcome is not persuasive. We can find individual events that seem to fit the pattern, yet when we look at our whole experience, the perspective is unsatisfying. There are just too many exceptions.

The current state of the art in plasmoid and TCR timing seems to be this: Plasmoids are frequently observed sometime after the auroral substorm onset, and most studies have implicitly assumed that onset is, or is closely related to, plasmoid ejection. There are a few cases where near-earth reconnection appears to occur close to the time of onset. Nonetheless, a clear pattern does not emerge when we look at plasmoid/TCR timing studies in general. The timing data cannot be uniquely interpreted, and do not fix the time and location of plasmoid creation

accurately enough to make the case. It is certainly risky to synthesize an overall picture by arraying the incommensurate sample of results discussed here, weighting them equally, overlooking their error bars, and interpreting them literally. If we accept the risk, the following picture emerges. One or more plasmoidlike structures often form during the same interval of time that auroral and geostationary substorm diagnostics indicate is the substorm expansion phase. But not all plasmoids are made in substorms. The nearer-earth reconnection regions responsible for ejecting the plasmoids are nearly always earthward of 220 R_E. Often, they are earthward of 80 RE, but sometimes they are tailward of 80 R_E. On occasion, they form within 35 R_E and retreat tailward within minutes. On other occasions they form and remain within 35 R_E and even within 20 R_E for 10 minutes or more. Traveling compressional regions, the tail lobe response to the passage of plasmoids, are detected three times more frequently beyond 100 R_E than near 30 R_E, suggesting that two-thirds of the reconnection events take place between 30 and 100 R_E. The data ensemble seems to be saying that plasmoid ejection occurs at different places at different times relative to onset in different substorms.

The initiation of tail reconnection has to be a natural result of the processes taking place during the growth phase of the substorm. The question is, to what auroral event does tail reconnection correspond? One problem in answering this question has been that we have yet to find and adopt an unambiguous ground signature of tail reconnection and plasmoid formation. Another problem has been our conceptual framework itself. We need to associate the auroral substorm onset, a unitary event, with a single event in space. We have unconsciously presumed that, following a single sharp southward turning of the magnetosheath field, there will be a single reconnection event on the dayside and a single reconnection event on the nightside. In the conceptual framework provided by the MHD characteristics, we have presumed that the nearer-earth tail reconnection event is triggered by the same characteristic field in each substorm; so its location and timing ought to be consistent from event to event. We have also presumed that that one reconnection event occurs at a neutral "line" that extends across much of the tail. It is not clear how such an event explains a localized onset. In the next two chapters, we will argue that the presumption that dayside and nightside reconnection are single unstructured events can no longer be sustained by the evidence.

8

BURSTY MAGNETOPAUSE RECONNECTION AND ITS CONSEQUENCES

8.1 Introductory Remarks

There is at least one way in which the reconnection model of substorms is unrealistic. Rarely if ever will the interplanetary field rotate southward, stay southward, and remain constant. Even on those infrequent occasions when it does do so, steady reconnection may not be established on the dayside: We will see that dayside reconnection proceeds in bursts even then. How likely is it then that steady convection will be established on the nightside?

In the next two chapters, we will fit together observations of bursty convection at the magnetopause, in the polar cap and auroral ionosphere, at various distances downtail in the plasma sheet, and beyond the average position of the neutral line in the deep tail. In this chapter, we deal with unsteady magnetopause reconnection. We start with one simple observation: The magnetopause is a source of escaping particles with energies higher than can be generated by the average convection potential across the ionosphere (Section 8.2). This, together with the fact that high-speed magnetopause flows can turn on and off between successive magnetopause crossings only minutes apart, suggests that the rate of reconnection is high for short periods of time and low for longer intervals. When the reconnection events are shorter than or comparable to MHD wave propagation times to the ionosphere, we call the reconnection "bursty."

We then let observation define the properties of bursty magnetopause reconnection. First, we discuss "flux transfer events" (FTEs), the traveling magnetic perturbations near the magnetopause (Section 8.3) that are signatures of bursty reconnection elsewhere on the magnetopause (Section 8.4). The magnitudes of the fluxes reconnected in FTEs are estimated in Section 8.5. Next, we discuss some of the ionospheric signatures of flux transfer events that might be expected on general theoretical grounds (Section 8.6). Variable dayside reconnection could be responsible for ULF magnetic activity in the polar cusp region (Section 8.7). We expect sudden magnetopause reconnection events to send Alfven waves (Section 8.8) and velocity-dispersed ions along field lines towards the polar cusp ionosphere (Section 8.9). The idea of bursty magnetopause reconnection ties together the soft electron precipitation, the transient aurora, the transient magnetic impulses, and the bursty plasma motions observed near the dayside polar cusp ionosphere (sections

8.10 and 8.11). Near the cusp, the convection flow responds to southward shifts of the magnetosheath magnetic field with a delay of 2–4 minutes, and the overall pattern of convection in the polar cap adjusts after a delay of 10–15 minutes. So-called "drifting F-region enhanced density patches" may be created in the polar cusp by the electron precipitation enhancements due to bursty magnetopause reconnection (Section 8.12). The ionospheric irregularities that cause amplitude and phase scintillation are primarily confined to the horizontal density gradients associated with F-region patches, which thus were ultimately responsible for the motions of irregularities that stimulated Axford and Hines (1961) to propose their convection model. Because the rate of diffusion is slow at F-region altitudes, the patches do not lose their identity, and they are tracers of convection. Some have been followed from the cusp into the the polar cap and others from the polar cap into the nightside auroral oval. Thus, the recent history of dayside reconnection may be imprinted on the high-latitude F-region ionosphere.

8.2 Bursts of Energetic Electrons and Ions Near the Magnetopause

Bursts of energetic electrons are observed on nearly every encounter with the dayside and high-latitude magnetopause. "Spikes" of energetic electrons near the magnetopause were studied in the early days of the space program (Frank and Van Allen, 1964; Anderson et al., 1965; Haskell, 1969; Singer and Bame, 1970; Brown and Stone, 1972), and soon Meng and Anderson (1970, 1975) were able to conclude that there was a more or less permanent layer of > 40 keV electrons almost everywhere near the magnetopause at low latitudes. The high-latitude magnetopause boundary was scarcely explored until the launch of HEOS 2, at which point bursts of energetic electrons were again found on nearly every magnetopause crossing (Hedgecock et al., 1973; Page et al., 1973; Domingo et al., 1974, 1977). Energetic electron spikes were typically observed over 1–2 hour intervals surrounding magnetopause encounters and were most frequently observed outside but near the magnetopause, presumably having escaped into the magnetosheath. Their differential energy spectrum, if fitted by a power–law, had a spectral index ranging between 3 and 4.5, and extended to relativistic energies (> 2 MeV). The average power lost to energetic electrons was estimated to be 10 GW. Although some or all of the energetic electrons found at the magnetopause at low latitudes could conceivably have originated in the trapped radiation belts, it was less likely that they did so at high latitudes. The high-latitude observations also provided some evidence for a reconnection source, since the occurrence of the spikes was correlated appropriately with the sign of the $x$component of the interplanetary magnetic field next to the high-latitude magnetopause boundary.

The dayside magnetopause is also a source of energetic ions. In perhaps the most graphic illustration of this fact, *Voyager 1,* which escaped the earth's magnetosphere at very high speed almost precisely along the low-latitude dawn terminator, encountered a strong tailward flow of > 30 keV ions immediately upon entering the magnetosheath (Lanzerotti et al., 1979). Given a thickness of the

annular magnetosheath layer of 5 RE, the net tailward energy flux was 20–70 GW. This result showed that a source existed in the dayside magnetopause and, together with other observations at proton energies exceeding 80 keV on the dusk side (Richter et al., 1979), the dayside flow results of Williams et al. (1979) and the magnetotail results of Williams (1979b), indicate that an antisunward flow of energetic ions is a common feature of the magnetosheath region next to the magnetopause.

In short, the magnetopause is a source of particles with energies that exceed the average convection potential across the ionosphere and approach the solar wind emf across the width of the magnetosphere. (The solar wind electric field is about 12 kV/R_E for V = 400 km/s, B = 5 nT, and the equatorial circumferential distance between terminators is about 40 R_E, leading to an emf of order 500 kV.) The fact that the 20–150 kV ionospheric convection potential is a small fraction of the solar wind emf across the dayside magnetopause requires in steady-state models that a small part of the magnetic flux approaching the magnetopause is reconnected and the rest flows around the magnetosphere in the magnetosheath (Levy et al., 1964). Alternatively, one might say that reconnection occurs in bursts whose instantaneous rates of reconnection approach, perhaps exceed, the solar wind emf, but with a correspondingly reduced duty cycle. The observations of frequent bursts of highly energetic particles near the magnetopause encourage us to take this second alternative seriously.

8.3 Flux Transfer Events

Small-scale transient magnetic structures are often encountered as the spacecraft approaches and passes through the magnetopause (Russell and Elphic, 1978, 1979; Haerendel et al., 1978; Elphic and Russell, 1979). When the vector magnetic field is transformed to "boundary normal coordinates," the component in the boundary normal direction has a distinct bipolar signature. In the northern dawn quadrant of the magnetopause, the normal component rotates first outward and then inward, and the tangential component is rotated toward a direction that is neither along the magnetosheath nor the magnetospheric field orientations. In the southern dusk quadrant, the normal component first rotates inwards, then outwards (Berchem and Russell, 1984). This magnetic signature is the defining property of "flux transfer events" (FTEs). Single events are rare; when FTEs occur, they occur almost continuously in the magnetosheath, inside the magnetosphere, and at the magnetopause (Berchem and Russell, 1984).

Flux transfer events got their name because they are signs of transient and/or localized reconnection.[1] Daly et al. (1981, 1984) showed that FTEs in the magnetosheath were accompanied by magnetospheric energetic particles flowing outward along the magnetic field, indicating that magnetospheric and magnetosheath field lines had become interconnected. Similarly, Williams and Frank (1980) detected open field lines inside the magnetopause. The ion distributions were found to be a mixture of magnetosheath and magnetosphere

plasma wherever they occurred (Paschmann et al., 1982; Daly and Keppler, 1982). A magnetopause surrounded by FTEs at the time of its crossing frequently contains a high-speed flow (Berchem and Russell, 1984), presumably signifying the action of reconnection elsewhere on the magnetopause (Papamastorakis et al., 1989). Taken together, the correlation of FTE occurrence with southward interplanetary field, the fast ion bulk flows, the mixing of magnetosheath and magnetosphere plasma, and the escape of magnetospheric energetic particles all argue that FTE field lines become connected to the magnetosphere by reconnection.

In addition, FTE occurrence correlates with southward magnetic field in the adjoining magnetosheath. Rijnbeek et al. (1984) reported that the magnetosheath field was southward on 35 of 43 passes in which magnetospheric FTE were observed. In the same vein, examination of simultaneous IMP 8 and ISEE 3 data in the solar wind indicated that the FTEs occurred almost exclusively in a southward interplanetary field, and hardly any occurred when there was even a small northward component (Berchem and Russell, 1984). They occurred about 45% of the time when the interplanetary field had a southward component, with the highest rate of occurrence for due southward field; the east–west component of the interplanetary field did not affect the FTE occurrence rate. Other authors have also reported similar positive correlations of FTE occurrence with southward field (Southwood et al., 1986; Smith and Curran, 1990).

FTEs have a multilayer structure (Rijnbeek et al., 1988). For example, each of the seven FTEs exhibited systematic layering as they passed back and forth over AMPTE/UKS (Farrugia et al., 1988). These events were distributed in local time from early dawn to midafternoon. High-time-resolution measurements of the magnetic field, ions, electrons, and plasma waves indicated that these FTEs all had the same four distinct layers. In the innermost layer, the field lines and flow generally varied smoothly and the particle populations were magnetospheric in character. The plasma pressure increased on the approach to the second layer, which was characterized by enhanced fluxes of 0.1–1 keV electrons, a major magnetic field rotation, and a fairly large ion bulk speed (150 km/s). The few hundred eV electrons exhibited pronounced bidirectional streaming along field lines, but no significant overall heat flux, unlike the otherwise similar events detected in the magnetosheath by Scudder et al. (1984); evidently, the electrons had reflected from mirror points near the ionosphere to create the bidirectional distribution. Thus the field lines were closed in the second region. The field lines were definitely open in the third layer, and the particle populations were magnetosheathlike, albeit with lower densities. The magnetic field could either be larger or smaller than in the previous region. In the fourth and final layer, the particle populations were indistinguishable from those in the magnetosheath. Although the detailed magnetic field and plasma profiles varied from event to event, in all the events the plasma pressure varied in anticorrelation with the magnetic pressure, and the total pressure exceeded that in the surrounding regions.

8.4 Locations of Reconnection Events Generating FTEs

The FTE magnetic signature was initially interpreted in terms of the unsteady and patchy reconnection of an isolated circular flux tube draped over the dayside magnetopause (Russell and Elphic, 1978, 1979). Later models ranged from the original one (Paschmann et al., 1982; Saunders et al., 1984; Southwood et al., 1986; Farrugia et al., 1988),to those where reconnected flux tubes are formed at multiple reconnection lines (Podgorny et al., 1980; Fu and Lee, 1985), by repeated merging (Sato et al., 1986), by stochastic percolation (Galeev et al., 1986), or by antiparallel merging (Ogino et al., 1989). Saunders (1983), Lee and Fu (1985), Biernat et al. (1987), Scholer (1988, 1989), Southwood et al. (1988), and Lockwood and Smith (1990) all suggested that the observations of FTEs and ionospheric convection bursts are consistent with unsteady reconnection at a more or less fixed neutral "line" on the subsolar magnetopause.

One case study presented particularly persuasive evidence in favor of the time-modulated reconnection picture. A minimum variance analysis (Sonnerup and Cahill, 1967) of AMPTE/IRM magnetic and convection electric field (i.e., $-\mathbf{V} \times \mathbf{B}$) data was applied to three adjacent FTEs and their nearby magnetopause crossings (Papamastorakis et al., 1989). The magnetopause crossings contained high-speed flows signifying the reconnection process at work. A de Hoffman–Teller (HT) frame of reference could be found for each FTE; the local plasma velocities were 70–80% of the measured local Alfven speed and were antiparallel to **B**. The best-fit velocities of motion of the three FTE frames, and the two subsequent magnetopause crossings, were so close to one another that a single HT frame ordered the data with impressive accuracy over a full hour. These results suggested that all three FTEs reflected a modulation of the same reconnection region, which was on the magnetopause north of the spacecraft and was active for at least 1 hour. The FTEs would then be due to "repeated ejections of bulges on the magnetopause from the reconnection site."

Flux transfer events may be due to a wave generated by reconnection elsewhere on the magnetopause. Its bipolar magnetic signature is more commonly observed at mid-to-high latitudes than near the magnetic equator (Southwood et al., 1986), suggesting that the FTE perturbation originates near the equator. Analysis of ISEE 2 medium-energy particle fluxes clearly showed one FTE propagating away from the equator (Daly and Keppler, 1983). The ion intensity depended only on pitch angle and the distance of the gyrocenter from a moving planar surface separating particle-rich and particle-sparse regions. The ion distribution changed sharply within a gyroradius when the gyrocenter crossed the boundary, which was the same for all pitch angles. The boundary velocity was 10–50 km/s; the FTE swept outward over ISEE 2 from the magnetopause side, and then returned inward, with a rotation to maintain a net northward motion. The northward speed of 50–100 km/s together with the event duration of 3 minutes led to an event size of a few earth radii.

Ultimately, such a signal will reach the ionosphere, where it might be observable as a magnetic or electric field transient. Indeed, Maynard (1985)

suggested that large–amplitude electric field spikes commonly found near the equatorward boundary of the polar cusp may be projections of the normal electric field components observed near the magnetopause during reconnection events.

8.5 The FTE Contribution to the Overall Convection Potential

The integrated convection potential depends on the duty cycle of the bursty reconnection events as well as the individual amplitudes of each event. We estimate the magnitudes of the individual flux transfers here. Unfortunately, our estimate is model dependent. If it is a single flux tube of circular cross section that reconnects, the width of the region perpendicular to the magnetopause in which FTEs are found suggests that the flux tube has a radius of 1 R_E. In this case, each event will develop a reconnection potential of 10–20 kV (Russell and Elphic, 1978; 1979); assuming a 2 minute duration, the net flux transfer corresponds to the flux in the projected ionospheric area of the flux tube, 0.25–0.5 x 10^7 W, which is roughly one percent of the total open flux in the polar cap. In the unsteady fixed neutral line models, the flux transfers and transfer rates scale with the poorly known and presumably variable effective length of the reconnection "line" along the magnetopause surface.[2] If the length is, say, 10 R_E, the instantaneous reconnection voltages increase to 100–200 kV and the flux transfers increase to 10% of the tail lobe flux (Lockwood et al., 1990c).[3]

Clearly, the key parameter underlying any estimate of flux transfer is the area of the region of newly opened magnetic flux in the polar cusp ionosphere. Menietti and Burch (1988) noted that the one degree width of the cusp maps magnetically into the 1 R_E radial scale of the FTE region, suggesting that the cusp precipitation pattern may be related to bursty magnetopause reconnection. Smith et al. (1992) argued that the local time distribution of cusp occurrence probabilities established from low-altitude spacecraft measurements can be explained if the cusp varies between a steady-state form and a series of discrete FTE signatures. In such a case, the instantaneous area of the cusp's footprint in the ionosphere may vary considerably. The full width at half-maximum of the ion precipitation profile of the statistical cusp is 1 hour of local time for Kp = 0, and 3 hours (800 km) for Kp = 3, 3^+ (Hardy et al., 1989; Crooker et al., 1991). Crooker et al. (1991) pointed out that impulsive reconnection ought to broaden the east–west extent of the cusp even more for short periods of time. If so, since the reconnection rate is small between bursts, the cusp will most often be too small to account for the polar cap potential, and occasionally it will be very broad. The width of the statistical cusp ought to be intermediate between these two extremes.

8.6 Ionospheric Signatures of Impulsive Magnetopause Reconnection

What do we expect to propagate away from a single impulsive magnetopause reconnection event? Imagine for illustration's sake a "square-wave" impulse of

reconnection at a neutral line of finite length centered upon the subsolar point of the equatorial magnetopause. We assume the duration of the reconnection event is less than or comparable to the times for MHD waves to communicate their existence to the magnetosphere and ionosphere. In what follows, we focus on what happens when the rate of reconnection suddenly increases; we expect that an appropriately reversed sequence events will occur when the reconnection event ends.

A magnetopause reconnection event will enhance the rate of sunward convection on closed field lines by radiating a rarefaction wave in the fast mode into the dayside magnetosphere. As the event continues, the instantaneously reconnecting field line will move earthward, and its footpoint in the ionosphere equatorward, because the rarefaction wave cannot establish a return flow of magnetic flux instantaneously. To the (unknown) extent that the rarefaction wave couples to standing Alfven wave resonances, resonant oscillations will be induced in an expanding region centered on the polar cusp. These might be registered on the ground as geomagnetic micropulsations at latitudes below that of the polar cusp. In principle, the spatio-temporal pattern of such excitations might reveal how the rarefaction wave spreads out.

Now let us imagine how an impulsive magnetopause reconnection event interacts with the ionosphere. Each time the reconnection rate changes, intermediate Alfven waves propagate to the ionosphere to adjust the field-aligned currents needed to drive convection in the ionosphere. Although the pattern of field-aligned currents associated with localized, active reconnection regions probably varies from event to event, the waves have to carry additional inward current to the eastward extremity and outward current to the westward extremity of the mapped reconnection "line" in order to enhance the rate of poleward convection. When the magnetosheath field has an east–west component, east–west flow in the ionosphere will also be stimulated, and the field-aligned currents needed to stimulate the flow will adjust accordingly. Since the footprint of an active reconnection region moves equatorward, the region of enhanced ionospheric convection will extend equatorward of the pre-existing equatorward boundary of the cusp.

Alfven waves signalling that the rate of reconnection is either or decreasing will form the equatorward boundary of the enhanced convection region.. Some Alfven wave energy will be reflected back into space in order to notify the plasma there of the line-tying boundary conditions in the ionosphere. Thus, the ionospheric footprint of a reconnection region that was active one Alfven travel time ago ought to contain traces of both downgoing and upgoing Alfven waves. When the reconnection event ends, Alfven waves will notify the ionosphere of that fact as well. At this point, there will be a bundle of newly reconnected flux tubes and enhanced ionospheric flow. Southwood (1985, 1987) has discussed how this bundle might finally merge with the large-scale pattern of convection in the polar cap. Since ionospheric flow is incompressible, a secondary pattern of convection will be established in the region surrounding the newly reconnected flux bundle.

Particles as well as waves will be sent along field lines to the ionosphere by an bursty reconnection event. Soft, few hundred eV magnetosheath electrons

suddenly let into the magnetosphere will propagate along field lines to the F region of the ionosphere, where they will come to rest by ionization and other processes. Free-streaming magnetosheath electrons will reach the F region in roughly 10 seconds; to the extent that the sudden density enhancement organizes itself into a slow shock (Pudovkin and Semenov, 1985), the increase in density will propagate to the top of the ionosphere essentially at the ion acoustic speed, an order of magnitude more slowly. When the electron heat arrives, it will create an aurora rich in red 630.0 nm emission. Electrons accelerated to keV energies in the reconnection event that precipitate into the ionosphere will also stimulate 557.7 nm auroral emissions. To the extent that the F-region density is increased by the arrival of the magnetosheath electrons, a localized patch of enhanced plasma density will be created. This patch will be entrained in the convective flow.

During the time the magnetosheath electrons propagate to the ionosphere, the foot of their field line convects poleward. If, for example, a poleward convection speed of 1 km/s is established, the first free-streaming magnetosheath electrons will hit the ionosphere about 10 km poleward of the footpoint of the magnetopause field line at the time the electrons crossed it. This time-of-flight dispersion will be much more pronounced for ions than for electrons. The ions will be accelerated to roughly the Alfven speed parallel to the magnetopause in starting their journey over the poles to the plasma mantle. However, ions will also free stream along field lines to the ionosphere. Cowley (1982) has discussed how the acceleration due to the contraction of the newly opened field lines moving along the magnetopause produces a characteristic D-shaped distribution function of free-streaming ions. Time-of-flight effects are highlighted when we focus on ions with exactly zero pitch angle. Clearly, the fastest ions hit the ionosphere first, and closest to the footprint of the actively reconnecting field line. On any other field line, the ions with the lowest parallel speed at any one instant will have been injected at the magnetopause at the time and place that reconnection of that field line occurred. As the observing spacecraft moves poleward, this minimum parallel speed decreases. Thus, one expects to observe patches of newly accelerated ions with a characteristic parallel speed–latitude signature poleward of the equatorward-moving equatorward border of the cusp (Lockwood and Smith, 1992).

This scenario was fabricated from elements we have already encountered in our discussion of convection and is meant only to guide our presentation of an elaborate phenomenology. Not all the elements will be present in every activated polar cusp, and surely our enumeration is incomplete, but the scenario does provide a list of things for which to look. It also overlooks important events that affect every observation. Some are related to the east–west component of the interplanetary field, such as east–west acceleration of flows in the magnetosheath and ionosphere or the tilting of the reconnection line relative to the geomagnetic equatorial plane. There will be important asymmetries due to seasonal and universal time effects. Finally, we have to ask about the signatures of a sequence of impulsive reconnection events, how the ionosphere fabricates a generally enhanced convective flow out of a sequence of individual events, and what effect all this activity has on the tail lobes and plasma sheet.

8.7 Cusp-Region ULF Waves

The more or less continuous presence of ULF magnetic field activity in and near the cusp was established more than 20 years ago by near-earth spacecraft observations (Frank, 1971; Heikkila and Winningham, 1971; Russell et al., 1971b). In the same year, Samson et al. (1971) found that the amplitudes of 1–30 mHz Pc 3-5 pulsations on the ground increased up to the highest latitudes sampled (77 degrees), and attributed this to a possible cusp source. Sometime later, Troitskaya (1984) and Bol'shakova and Troitskaya (1984) reported that the amplitude of Pc 3 (16–30 mHz) micropulsations does maximize in the cusp. Olson (1986) reported that the power in the 1–10 and 30–50 mHz bands measured at Cape Parry and Sachs Harbor, Canada, was enhanced near local noon on almost every day. He identified the 1–10 mHz band with the ionospheric currents associated with the cusp boundary and its motions, and the 30–50 mHz power to direct penetration of hydromagnetic radiation from the cusp. Kato et al. (1985) and Engebretsen et al. (1986a) also reported low-frequency cusp-region magnetic variations.

Holzer and Reid (1975) pointed out that the coupling of sustained dayside reconnection to the ionosphere could lead to 10-minute oscillations of the magnetopause, and, by implication, of geomagnetic pulsations. These would be akin to driven global modes. Bursty reconnection should also stimulate propagating magnetic field stuctures on a smaller scale than those associated with the breathing of the entire front-side magnetosphere. Russell and Elphic (1978, 1979) recognized that flux transfer events might generate transient pulsation events. Somewhat later, transient pulses lasting a few minutes were indeed found (Goertz et al., 1985; Sandholt et al., 1986; Lanzerotti et al., 1986, 1987; McHenry and Clauer, 1987), and were ascribed to the local field-aligned currents associated with flux transfer events (Lanzerotti et al., 1986; Lanzerotti and Maclennan, 1988). The durations of the transients were comparable to the period of a fundamental Alfven wave on a closed field line close to the magnetopause. Fukunishi and Lanzerotti (1987) clearly found that such Pc 5 transients also coincided with the transient dayside aurora.

Pc 5 transients are often accompanied by more continuous ULF magnetic oscillations; in a case study employing data from ISEE 1 and 2 near the dayside magnetopause, from the geosynchronous spacecraft GOES 2 and 3, and from a number of ground-based stations, Glassmeier et al. (1984) concluded that FTEs were likely stimuli for some but not all of the Pc 5 oscillations they observed, the others being due presumably to such things as pressure pulses and/or Kelvin–Helmholtz instability.

8.8 Alfven Waves at the Equatorward Boundary of the Active Cusp

The magnetic storm of September 5–6, 1982 provided a "once in a mission" opportunity for the experimental teams associated with DE 1 and DE 2 to study a reconnecting magnetopause and its effect on an intensely active and unusually large

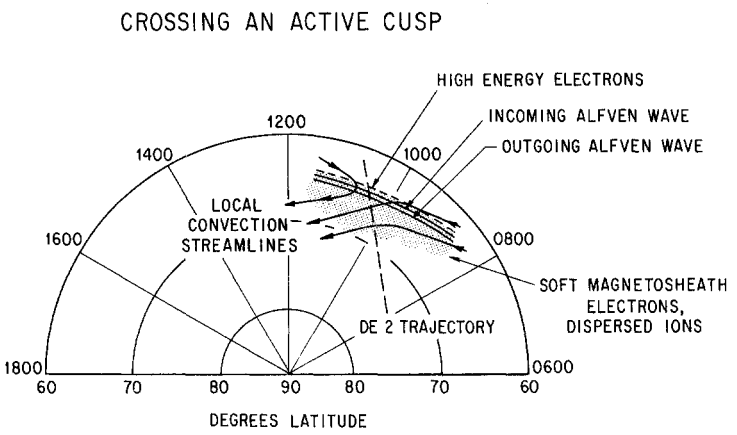

Figure 8.1. Crossing an Active Cusp. This sketch, which summarizes observations obtained by Maynard et al, (1991), also illustrates the geometrical considerations that enter into the interpretation of data obtained from any spacecraft crossing of the polar cusp region. Meynard et al. noted that the electric field equatorward of the cusp had an equatorward component and was relatively quiet. A 4 km-wide spikelike feature in which the electric field briefly swung poleward and then strongly equatorward defined the equatorward edge of the cusp. High resolution data showed that this feature had a wavelike structure. Within the cusp, the electric field returned to the equatorward direction but had many small-scale structures. The cusp field-aligned currents had a down-up-down configuration. The current was highly structured but generally downward poleward of the cusp; it reversed to upward 8 seconds before and about 40 km poleward of the electric field spike; it became smooth and downward again equatorward of the spike. There was a high correlation between the variations in the electric and magnetic fields in the two regions on either side of the electric field spike, consistent with passage through a sequence of field-aligned current sheets. During the one-second traversal of the electric field spike, however, the impedance switched rapidly between large positive and negative values that were consistent with up- and down-going Alfven waves. The Poynting flux was into the ionosphere on the equatorward side and out on the poleward side of the spike. Particle diagnostics located the Alfven waves almost precisely at the equatorward boundary of the cusp. The fluxes of > 35 keV electrons changed from trapped to isotropic within 1 s of the electric field spike, and < 1 keV precipitating magnetosheath electrons dropped by a factor 30 in 4 s across a region of ~ 20 km thickness surrounding the Alfven wave structure. The count rate was high poleward of the electric field spike, dropped most rapidly at the time of the spike, and fell below the photoelectron background 0.7 s after the spike. The soft electron precipitation region also contained few keV ions of magnetosheath composition that displayed energy-latitude dispersion due to poleward convection. Original drawing

polar cusp ionosphere (Maynard et al., 1991). We will discuss the DE 1 observations of the magnetopause first, and then turn to the corresponding DE 2 observations in the polar cusp region.

DE 1 crossed the magnetopause at midlatitudes at about 11 hours MLT, 1 hour from the subsolar point. As expected, the flow was dawnward in both the magnetosheath and boundary layer. The outbound passage through the magnetopause was characterized by a decrease in the low-energy component of ionospheric composition followed by an increase in hotter plasma of magnetosheath composition indicating entry into the LLBL. Strong field-aligned flows were observed in both components. Variance and de Hoffman–Teller analyses of electric and magnetic field data showed that the magnetopause was consistent with a rotational discontinuity with a 25 nT magnetic field component normal to the magnetopause surface. The dawn-to-dusk tangential field component was 3–4 mV/m. A 25 mV/m earthward electric field concentrated in the boundary layer corresponded to flow away from noon toward the dawn meridian. During this time, the east–west component of the interplanetary field was positive; when it changed sign, so also did the direction of the flow in the boundary layer and the sign of the radial electric field component.

The DE 2 cusp crossing provided the first direct evidence of an Alfven wave stimulated by a magnetopause reconnection event. DE 2 passed through the southern hemisphere cusp at the unusually low invariant latitude of 62° some 22 minutes before the DE 1 magnetopause crossing described previously. Due to the offsets between the earth's magnetic and geographical axes, the magnetic local time of the DE 2 cusp crossing was about 1 hour earlier than that of the DE 1 magnetopause crossing, even though both spacecraft were in the same geographical meridian plane. The electric field equatorward of the cusp had an equatorward component and was relatively quiet. A 4 km wide spikelike feature in which the electric field briefly swung poleward and then strongly equatorward defined the equatorward edge of the cusp. High-resolution data showed that this feature had a wavelike structure. Within the cusp itself, the electric field returned to the equatorward direction but had many small-scale structures, as is commonly found there (Maynard, 1985).

Calculations of the difference between the measured magnetic field and a reference field yielded estimates of the intensities and directions of the field-aligned currents threading the cusp. Three distinct regions were found. The field-aligned current was highly structured but generally downward poleward of the cusp; it reversed to upward 8 seconds before and about 40 km poleward of the electric field spike; it became smooth and downward again equatorward of the spike. There was a high correlation between the variations in the electric and magnetic fields in the two regions on either side of the electric field spike, consistent with passage through a sequence of field-aligned current sheets. The impedances estimated from the ratio of the electric and magnetic fields for the most part were consistent with the crossing of quasistatic field-aligned current structures that close in the lower ionosphere via Pedersen currents. During the approximately 1-second traversal of the electric field spike, however, the impedance switched rapidly between large positive and negative values that were quantitatively consistent with up- and down-going Alfven waves. The Poynting flux was into the ionosphere on the equatorward side and out on the poleward side of the spike.

Particle diagnostics located the Alfven wave structure almost precisely at the equatorward boundary of the cusp. The fluxes of > 35 keV electrons measured by Geiger–Mueller tubes changed from trapped to isotropic within 1 s of the electric field spike, indicating just how close the spike had been to the instantaneous last closed field line. The count rate of < 1 keV precipitating magnetosheath electrons dropped by a factor of 30 in 4 s across a region of about 20 km thickness surrounding the Alfven wave structure. The count rate was high poleward of the electric field spike, dropped the most rapidly at the time of the spike, and fell below the photoelectron background 0.7 s after the spike. Measured electron distribution functions indicated that most of the soft electron energy would be deposited at altitudes above 150 km, where it would produce primarily 630.0 nm auroral luminosity and enhance the Pedersen, but not the Hall, conductivity. The average electron energy integrated over the range 32 eV–30 keV was 115 eV, was at all times less than 160 eV, and the energy flux density exceeded 0.1 ergs cm^{-3} - s^{-1} - sr^{-1}. All of these values identified this as cusp electron precipitation, according to the statistical criteria of Newell and Meng (1988). The equatorward border of the soft electron precipitation region also contained few keV ions of magnetosheath composition that displayed energy–latitude dispersion due to poleward convection, another signature of the cusp.

A pair of triple field-aligned current structures like that described was observed on an Aureol 3 crossing of the polar cusp region at about 1300 MLT (Bosqued et al., 1991). An electric field spike marked the equatorward boundary of each structure. The up–down–up polarities at Aureol 3 in the postnoon sector were the reverse of the down–up–down on DE 2 in the prenoon sector. The upward currents at Aureol 3 were associated with a precipitation energy flux of 1–2 ergs -cm^{-3} -s^{-1} -sr^{-1} in 2–4 keV electrons. Such a flux would create 1–2 kR of 557.7 nm green auroral emission. These features were superposed on a more extended cusp that showed clear traces of ion energy–latitude dispersion. The measured separation of 12–150 km between the pair of current systems implied a 4–5 minute delay between magnetopause reconnection events, assuming a poleward convection speed of 0.5 km/s.

8.9 Ion Energy–Latitude Dispersion on Polar Cusp Field Lines

Hill and Reiff (1977) found two AE-C passes through the polar cusp in which the ion fluxes exhibited "unusually clearcut energy–latitude profiles." If the magnetosheath source distribution is a convecting Maxwellian, the distribution in the low-altitude cusp is also a Maxwellian with a bulk velocity equal to the parallel component of the bulk speed in space. Upon fitting the measured ion fluxes, Hill and Reiff (1977) found that the convection speeds, 460 and 520 km/s, were similar to those observed in accelerated flows near the magnetopause. However, many cusp passages do not show smooth energy–latitude dispersion. More often, there appear to be discrete patches without clear dispersive signatures separated by distinct jumps in properties at the boundaries. Newell and Meng (1991) detailed

three DMSP F7 examples in which an equatorward region of higher bulk flow velocity was separated by a sharp boundary from a region of lower velocity in the main cusp precipitation region. While the bulk speed in the main cusp region was 200–300 km/s, the ions in the discrete patches near the equatorward boundary of the cusp had 460–640 km/s speeds. Electrons also appeared to be accelerated in the patches, but to speeds smaller than their thermal speed, so that the electron distribution remained quasi-isotropic. In all three examples, the interplanetary field was southward. Ten additional cases in which similar patches of accelerated ions were observed probably also corresponded to southward field conditions.

The jumps in polar cusp ion spectrograms may be due to sudden changes in the rate of magnetopause reconnection. In the DMSP F7 event for which the interplanetary field was the most strongly and consistently southward, the ion spectrogram showed two very clear jumps in the lower cutoff ion energy (Newell and Meng, 1991).[4] Lockwood and Smith (1992) interpreted the two jumps as the signature of three impulsive reconnection events. Assuming an east–west "merging gap" length of 1500 km, they estimated the average reconnection voltage to be 60 kV, consistent with statistical studies of the cross-polar-cap potential. However, 90% of this was contributed by three 1 minute bursts with peak voltages of about 400 kV. The dawn–dusk magnetopause electric field would have been about 8 mV/m during these bursts, comparable with values reported by Aggson et al. (1983). The peak emf in these bursts approached but did not exceed the total solar wind emf across the magnetosphere. About $2–3 \times 10^7$ W of magnetic flux were opened in each of the events, which were spaced in time by roughly 10 minutes. The durations of the events, the intervals between them, the estimated peak voltages, and the flux transfers were all consistent with those deduced for flux transfer events using the time-dependent subsolar reconnection model.

8.10 Bursty Ionospheric Flow Events

The first detection of bursty ionospheric flow near the polar cusp region was made by van Eyken et al. (1984), who reported EISCAT observations of a 10 minute burst of 300 m/s poleward flow with an east–west scale exceeding 400 km. Subsequently, the STARE coherent scatter radar detected bursts of plasma flow from the dayside auroral oval into the polar cap during magnetically active periods (Goertz et al., 1985). The most prominent ones lasted about 2 minutes at any one location, had a spatial scale of about 200 km, and a peak speed of about 2 km/s. Shortly thereafter, bursty ionospheric flows were found to be accompanied by isolated magnetic field transients, like the transient aurora in the cusp (Lanzerotti et al., 1986, 1987). This in part prompted Todd et al. (1986) and Lanzerotti et al. (1986, 1987) to relate ionospheric flow bursts to flux transfer events. Todd et al. (1986) reported EISCAT observations of two highly structured flow bursts during a period of moderate magnetic activity when the north–south component of the interplanetary field was close to zero. The main burst had a 2 km/s peak speed, a 300 km spatial scale, and lasted about 2 minutes, figures that imply a net flux

transfer of 3×10^6 W and a 30 kV voltage for a circular cross section. On the other hand, ionospheric flow bursts appear to start in a "flow channel" whose north–south dimension is about 300 km, and whose (much less well-determined) east–west dimension could be a factor of 5–10 larger. In this case, the emf and flux transfers become 50–250 kV and $1–5 \times 10^7$ W, respectively.

Sibeck et al. (1989a) argued that some occurrences of the magnetic signatures associated with FTEs could actually be due to dynamic pressure changes in the solar wind. Some events are certainly best explained in this way. For example, Glassmeier and Heppner (1992) found a traveling twin vortex system of ionospheric currents whose polarity was opposite to that expected from magnetopause reconnection for southward magnetosheath field. The whole issue was examined in some detail by Lockwood et al. (1990c), who concluded, however, that the majority of events is best interpreted in terms of the FTE model.

Some ionospheric flow bursts are clearly a direct consequence of a change in the direction of the magnetosheath field; in one very graphic case, an isolated flow burst accompanied isolated southward turnings one for one over a 1.5 hour period in which the interplanetary field was predominantly northward (Lockwood et al., 1989b). When the magnetosheath field near the subsolar point changes direction, the flow in the polar cusp ionosphere responds almost as fast as it can. Cross-correlation of EISCAT data with AMPTE/UKS magnetic field data acquired directly upstream of the subsolar magnetopause indicated that the flow in the early afternoon sector lags changes in the north–south component by 3.9 ± 2.2 minutes (Etemadi et al., 1988). A case study of the response to sharp changes in B_Z found the delay to be 5.5 ± 3.2 minutes in the same local time sector (Todd et al. 1988). Etemadi et al. (1988) and Todd et al. (1988) found that the entire field of view of the EISCAT radar changed coherently within a few tens of seconds at the beginning of a bursty ionospheric flow event. The flows appeared all at once in a fairly large region, rather than expanding spatially from some pre-existing locus.

Taking into account the roughly 2 minute Alfven wave communication time from the equatorial magnetopause to the ionosphere, we conclude that dayside reconnection is fully active within 2 minutes after a southward turning arrives at the magnetopause, and begins to stimulate ionospheric flow about one wave propagation time after that (Lockwood et al., 1990a). The ionospheric delay time lengthens with increasing local time separation from the early afternoon fast response region. The delay time reaches 10–15 minutes at local dawn and evening, at which point much of the polar cap ionosphere has adjusted to the reconnection event (Etemadi et al., 1988; Todd et al., 1988).

The 2–4 and 10–15 minute response times also apply to reductions in the dayside reconnection rate. The flow speeds decayed first with a 2–3 minute time scale and ultimately with the longer 10–15 minute time scale following a northward shift of the interplanetary field (Etemadi et al., 1988; Todd et al., 1988). The reduction in flow speed began after a delay that depended on local time. The ionospheric responses to sharp southward and northward turnings of the interplanetary field were different: A southward turning usually produced a sudden change (few tens of seconds) to a new flow state, while northward turnings led to

smaller sudden changes that were followed by a slower monotonic variation (Todd et al., 1988).

Lockwood et al. (1986, 1990a) argued that a burst of magnetopause reconnection forms a patch of newly opened flux immediately equatorward of a pre-existing area of "old" open flux created during earlier reconnection events. The patch then expands for about 10 minutes at a rate determined by the reconnection voltage (the rate of change of open flux), which is several km/s for voltages of order 100 kV. After one or two wave travel times between the ionosphere and the magnetopause, the field-aligned currents bounding the newly opened flux tubes will have established the new twin-vortex pattern characteristic of localized convection. The observed increase in the response time of convection with distance from its point of first stimulation indicates that the area containing high-speed flow expands and merges with the entire polar cap convection pattern on a 10–15 minute time scale. The newly reconnected flux tubes move only about 600 km—five degrees in latitude—during these 10–15 minutes; so the newly opened flux itself cannot reconnect in the tail until much later (it takes 2–4 hours for a flux tube to traverse the polar cap from the dayside cusp to the nightside auroral oval). Thus, the overall pattern of polar cap convection has to be a cumulative response to numerous bursty magnetopause reconnection events, and as we will see shortly, to numerous bursty reconnection events in the magnetotail.

8.11 Transient Dayside Aurora

Transient arcs drift poleward into the polar cap when the dayside auroral oval is shifting equatorward (Vorobjev et al., 1975). Horwitz and Akasofu (1977) also noted the one-to-one correspondence between poleward moving auroral forms and equatorward displacement of the oval, and suggested that the same process was responsible for both. Reconnection was the obvious candidate, because it would cause the oval to migrate equatorward, while structured aurora would move poleward on newly reconnected, more rapidly convecting field lines. Transient cusp aurora have proved to be extremely common for southward interplanetary field (Sandholt et al., 1985, 1989a,b, 1990a), and they probably are associated with flux transfer events (Sandholt, 1988); certainly, their temporal behavior is reminiscent of FTEs: Transient cusp aurora have 2–10 minute lifetimes and 5–15 minute recurrence times.

The spatial and temporal structure of the dayside aurora is now studied by multispectral auroral photometers (Sandholt et al., 1985, 1989a,b, 1990a; Sandholt, 1988) and all-sky TV cameras (Oguti et al., 1988c) as well as all-sky photography. Multispectral photometry indicates that the midday aurora can be separated into different latitudinal zones with differing spectral properties that correspond to the cusp proper, the LLBL, and the mantle (Sandholt, 1988).[5] It is important to view the transient auroral events on the dayside against the pre-existing background of dayside aurora, so as to make a more reliable assignment to one or another of the precipitation regions (Jacobsen et al., 1991). When this is done, it apears that the

transient aurora in the cusp and in the LLBL differ. The cusp transient aurora has a large ratio of 630.0 to 557.7 nm emission, indicating that it is produced by relatively soft electron precipitation, whereas this intensity ratio is of order unity for LLBL transient aurora. The cusp transient aurora initially brightens at 630.0 nm followed by an intensification at 557.7 nm and subsequent poleward motion (Smith and Lockwood, 1990; Lockwood, 1991b). The cusp aurora fades as it moves into the polar cap (Sandholt et al., 1986; Smith and Lockwood, 1990; Lockwood, 1991b; Lui and Sibeck, 1991). The discrete transient structures in the LLBL form in the background LLBL region, remain well equatorward of the cusp aurora, never expand to cross or join the cusp aurora, and occur over a wider range of local times than the cusp aurora.

The cusp auroral transients separate from the background cusp aurora after fast poleward (<1 km/s) and east–west (2–4 km/s) motions. The magnitude and sense of the east–west motions are controlled by the y component of the interplanetary magnetic field (Jacobsen et al., 1991). In the study of Fasel et al. (1991, 1992) of a series of brightenings of the cusp aurora, the typical event began with an equatorward shift of the oval, then the dayside oval brightened, and finally the transient form moved poleward. At this point, intermittent localized brightenings were followed by eastward or westward spreading along the arc or rayed band. An arc in the oval brightened at about the same time as the intermittent brightenings. As these reached their extreme poleward position they brightened and then faded from view.

Coordinated EISCAT and meridian-scanning photometer observations proved that the transient dayside aurora is associated with bursts of ionospheric flow. Lockwood et al. (1989) studied a quasiperiodic sequence of nine early afternoon events that were separated by 5–15 minutes. Each flow burst began with a 2–3 km/s westward flow that evolved to about 1 km/s poleward. This event occurred during a period when the interplanetary field was strongly southward with a large positive B_y component, and the initial westward direction was consistent with the positive B_y. The 557.7 and 630.0 nm aurora brightened at the pre-existing equatorward edge of emission, and reached intensities exceeding 3 kR. These "arcs" contained forms that initially moved westward at 2–3 km/s and then faded as they turned poleward. The auroral emission marked the regions of upward field-aligned current in the system of currents driving the enhanced flow.

Transient aurora have been followed into the polar cap. Carlson et al. (1988) detected multiple discrete arcs with an all-sky imaging photometer located at Thule, Greenland, near 85 degrees north geomagnetic latitude. The arcs extended into the polar cap from the postnoon cleft or cusp region, which was visible on the geographic southwest horizon as a bright diffuse emission. The arcs were characterized by 630.0 nm intensities as bright as 1 kR and 427.8 nm intensities of 100–200 R, implying that they were created by precipitating electrons of about 600 eV energy (Rees and Luckey, 1974). A sequence of images taken every 10 minutes revealed that the arcs faded and brightened as if they emanated from the bright diffuse region at lower latitude on the dayside. The whole event took place during southward interplanetary field conditions.

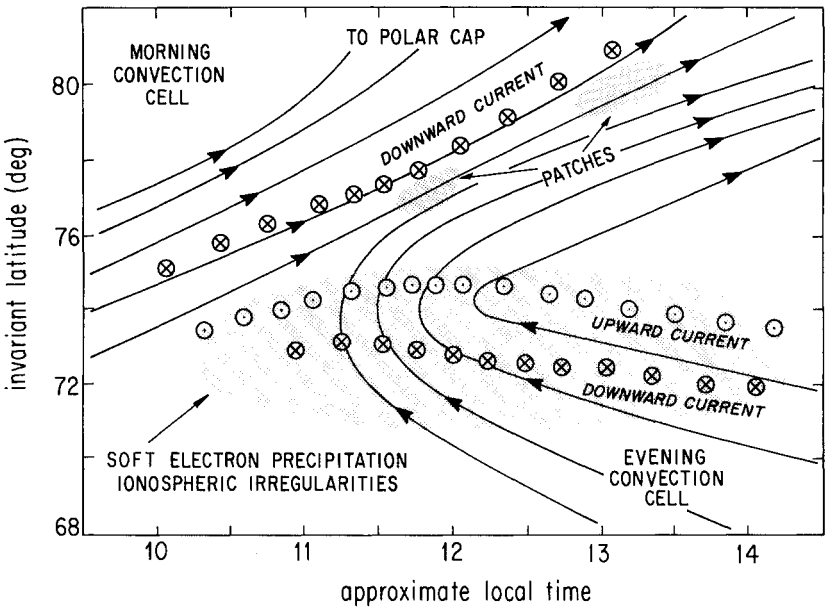

Figure 8.2. Relationship of F-Region Density Patches to the Active Polar Cusp. This figure summarizes the observations of K.B. Baker et al, (1986). As HILAT crossed the polar cusp near the noon meridian during a period of generally southward interplanetary field, a ground radar interrogated a volume east of the spacecraft track in which beacon measurements between HILAT and Sondrestromfjiord were being made. An upward current sheet bounded to the north and south by weaker downward current sheets was observed as HILAT passed through the cusp. The current sheets were in a region of low energy cusp electron precipitation. Radar data revealed a region of small-scale ionospheric irregularities aligned east-west on the magnetic meridian of the current sheets and electron precipitation; the beacon experiment had the strongest scintillations within the same region. The flows from the dawn and dusk convection cells converged and turned poleward within the experimental volume. Several additional patches of irregularities were found poleward of the main scattering region. These patches, which had linear dimensions of order 100 km, were convecting poleward with a speed that in one case was estimated to be 1.6 km/s. K.B. Baker et al., *J. Geophys. Res., 91*, 3142, (1986), copyright by the American Geophysical Union.

8.12 F-Region Density Patches

On November 28, 1983, the HILAT spacecraft crossed the dayside polar cusp near the noon meridian plane during a period of generally southward interplanetary field (K. B. Baker et al., 1986). At the same time, radar measurements were made of a

volume slightly east of the spacecraft track where beacon measurements between between HILAT and the Sondrestromfjiord ground station were being conducted. An upward current sheet bounded to the north and south by weaker downward current sheets was observed as HILAT passed through the cusp, a down–up–down triple of the type discussed earlier. The current sheets, particularly the upward one, were in a region of fairly intense low–energy electron precipitation like that commonly observed in the cusp. The radar data revealed an extended region of small-scale ionospheric irregularities aligned east–west on the magnetic meridian of the current sheets and electron precipitation. The beacon experiment showed the strongest scintillations within the same region. The flows from the dawn and dusk convection cells appeared to be converging and turning poleward within the experimental volume. These features seem typical of the active polar cusp, which makes the next point all the more interesting. Several additional patches of irregularities were found poleward of the main scattering region. These patches, which had linear dimensions of order 100 km, were convecting poleward with a speed that in one case was estimated to be 1.6 km/s. This section is devoted to observations of such convecting patches of irregularities and enhanced density.

Spatial structure in the high-latitude F-region ionosphere has been found on scales ranging from centimeters to hundreds of kilometers by ionosonde (Sato and Rourke, 1964), scintillation measurements (Aarons et al., 1969; Rino and Matthews, 1979), incoherent scatter radar (Banks et al., 1974; Vickrey et al., 1980; Kelley et al., 1982; Robinson et al., 1985; Tsunoda et al., 1985), rocket (Kelley et al., 1982), spacecraft (Dyson et al., 1974; Clark and Raitt, 1976; Phelps and Sagalyn, 1976; Rodriguez and Szusczewicz, 1984; Basu et al., 1988), and by various methods in combination (Kelley et al., 1980; Weber et al., 1985; Basinska et al., 1987). Generally speaking, the smaller-scale density structures result from plasma instabilities, some generated by the inhomogeneity of the larger–scale structures whose creation is dominated by classical production and loss processes coupled with convection.

Convecting patches of enhanced F-region plasma density were first reported by Banks et al. (1974), and have been studied by many groups. The patches' horizontal dimensions, 100–1000 km, are similar to those of the regions of newly opened magnetic flux in the polar cusp ionosphere. They have a weak but detectable airglow signature, and combined optical and radio wave diagnostics indicate that the electron density is a factor of 5–10 above background and can be as large as 10^6 cm^{-3} at F–region altitudes; the total electron content of a flux tube is enhanced by about a factor of 3 (Buchau et al., 1983; Weber et al., 1984). The patches drift in the general convection pattern with speeds of 0.1–1 km/s. As Kelley et al. (1982) pointed out, the diffusion lifetimes of such large structures are so long that that once formed they convect across the polar cap without losing their identity. Some have been followed for 3000 km, from the center of the polar cap to the poleward edge of the nightside auroral oval (Weber et al., 1986). Others have been followed from the polar cap into the auroral oval. In one case, the Sondrestromfjiord radar documented a polar cap flow whose direction remained antisunward for 8.5 hours (even though the interplanetary field changed from

northward to southward several times); the F-region patches observed during this period had almost identical altitude profiles and varied only slightly in maximum electron density. The series of patches drifted equatorward across a red arc at the poleward boundary of auroral light near 2330 hours MLT (Weber et al., 1991). This arc remained motionless for 52 minutes while the patches convected through it at speeds of 500 m/s. Still other patches have been observed to drift westward in the general convection pattern equatorward of the cutoff of the diffuse aurora on the night side (Weber et al., 1985). As these patches were being tracked by radar, the AFGL Airborne Ionospheric Observatory flew multiple north–south legs along the magnetic meridian between 65 and 69 degrees CGL. All-sky imaging photometer measurements revealed little relationship between the 630 nm red auroral emission, which measures soft electron precipitation into the F region, and the F-region patches. There was also no apparent relationship between the diffuse auroral precipitation measured by the DMSP F2 spacecraft and the patches.

How F-region patches are generated is a matter of some controversy. Sato and Rourke (1964) and, later, Weber et al. (1984, 1986) and de la Beaujardiere et al. (1985) argued that the enhanced ionization is created by solar EUV at lower latitudes and convects through the polar cusp and into the polar cap. The production of patches is more frequent in the summer polar cap, which may reflect a connection with solar EUV. It has also been suggested that the plasma is created by impact ionization in the cusp, where soft precipitating electrons ionize at F-region altitudes (Fejer and Kelley, 1980; Sojka and Schunk, 1986; Schunk and Sojka,1987; Valladares et al., 1989). To create the observed density enhancements, a flux tube must be exposed to precipitation for 5–10 minutes as it drifts through the cusp (Crooker and Burke, 1991). Smaller enhancements require shorter exposure times. In one case, a rocket launched into the morning auroral oval from Sondrestromfjiord detected a number of minipatches: 30–70% density enhancements at 300–500 km altitudes with 10–20 km scales (Labelle et al., 1989). Each minipatch was accompanied by increase in the precipitation flux of few hundred eV electrons; modeling indicated that the minipatches could be produced in 20–350 seconds.

8.13 Summary

The flux transfer event is a transient perturbation of the shape and position of the magnetopause that travels away from a region of bursty reconnection. Within minutes of a southward shift of the magnetosheath magnetic field at the magnetopause, a high-speed ionospheric flow is stimulated at the equatorward edge of the pre-existing polar cusp by the arrival of an Alfven wave. The start of the high–speed flow is often accompanied by a magnetic transient that may be a ground signature of the flux transfer event. The ionospheric flow typically first moves east–west at a relatively high speed, the sense determined by the y component of the magnetosheath field. Later, the flow slows down, turns poleward, and enters the polar cap. Like ionospheric flow bursts, transient features

in the cusp aurora first move east–west at a relatively high speed, the sense determined by the y component of the magnetosheath magnetic field, after which they too slow down and enter the polar cap. Case studies have linked the ionospheric flow bursts, transient cusp aurora, and magnetic transients together. Thus, while some of these signatures are undoubtedly produced by other effects such as pressure variations in the magnetosheath, only transient reconnection seems to account so naturally for all the interlocking signatures.

The word *patch* has been applied to three phenomena in the polar ionosphere that may be related consequences of bursty magnetopause reconnection. "Patches" of accelerated ions are found just equatorward of the main polar cusp precipitation for southward interplanetary field (Newell and Meng, 1991). A southward shift of the magnetosheath magnetic field results in the sudden formation of a "patch" of newly opened flux and fast ionospheric flow just equatorward of the pre-existing polar cusp. Finally, patches of enhanced F-region plasma density have been observed to convect across the polar cap from a dayside source probably in the cusp, move right through a poleward arc into the nightside auroral oval, and convect westward with the general flow at the equatorward edge of the diffuse auroral oval. (Although it has not been feasible to follow the same patch the entire way from the dayside cusp to the equatorward edge of the nightside auroral oval, an individual patch can follow convection for a considerable part of a complete circuit across and around the polar cap since it is not easily dispersed by cross-field diffusion.) The horizontal scales of the patches of newly opened flux and of enhanced F-layer density are both hundreds of kilometers. If the F-region patches are indeed footprints of bursty reconnection events, monitoring the ionospheric density along the convection streamlines leaving the cusp might reveal the history of the magnetopause reconnection. The number and areas of patches in the polar cap could indicate how much dayside reconnection there had been, and their order and spacing might forecast how much reconnection is about to take place in the plasma sheet.

It takes about 10–15 minutes for convection in the polar cap as a whole to adjust to a change in the direction of the magnetosheath magnetic field. This is the so-called "line-tying" time scale defined by much more primitive reasoning 20 years ago. It is probably no accident that the time interval between FTEs is comparable to this basic time scale. There is evidence the magnetopause–ionosphere system can be unsteady even if the magnetosheath field is steady. Berchem and Russell (1984) and Rijnbeek et al. (1984) found flux transfer events lasting 2 minutes and repeating every 8 minutes when the interplanetary field remained southward the whole time. The EISCAT radar, meridian-scanning photometers, and all-sky TV cameras monitored a sequence of ionospheric flow bursts and auroral transients that repeated every 8.3 ± 0.6 min for 45 minutes, during which time the interplanetary field at IMP 8 was consistently and strongly southward (Lockwood et al., 1989b). The pattern of magnetopause boundary motions determined by energetic particle "sounding" was consistent with oscillations in position with an 8–10 minute period on which boundary distortions with 1.5–2.5 minute periods were superposed (Williams et al., 1979); in retrospect,

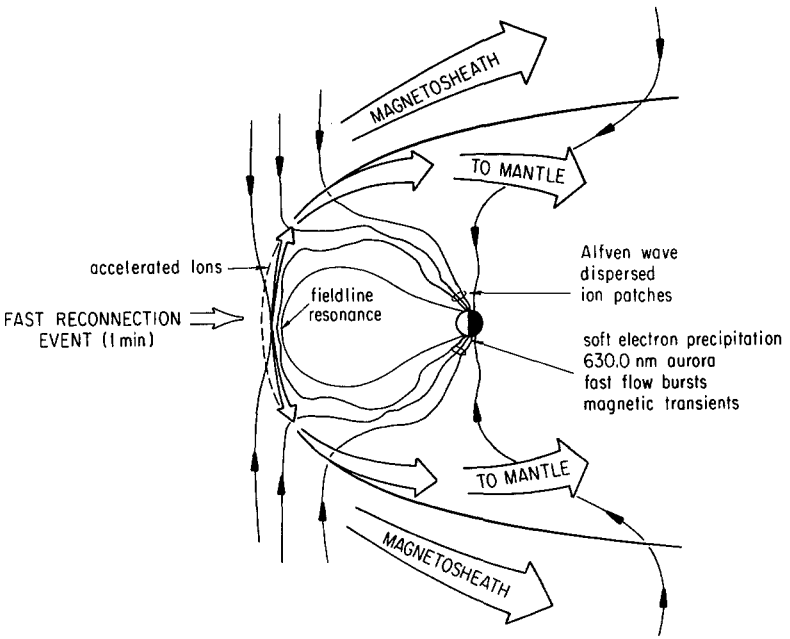

Figure 8.3. Coupling of Bursty Dayside Reconnection to the Active Cusp. A magnetopause reconnection event will radiate a fast rarefaction wave into the dayside magnetosphere that couples to resonant oscillations. The reconnecting field line moves earthward because the rarefaction wave cannot establish a return of magnetic flux instantaneously. Alfven waves carry inward current to the eastward end and outward current to the westward end of the mapped reconnection "line" to enhance the rate of poleward convection in a localized region. When the magnetosheath field has an east-west component, Alfven waves will also stimulate an east-west flow in this region. Some wave energy will reflect back into space. A few hundred eV magnetosheath electrons will propagate to the F-region where they come to rest, possibly to create a localized patch of enhanced plasma density that is caught up in the convective flow. When the electron heat arrives, it creates an aurora rich in red 6300 nm emission. Electrons accelerated to keV energies will also stimulate 5577-nm auroral emissions. As particles propagate to the ionosphere, the foot of their field line convects poleward. Ions will be accelerated to roughly the Alfven speed in starting their journey over the poles in the plasma mantle. However, some will also free-stream along field lines to the ionosphere. On any field line, the ions with the lowest parallel speed will have been accelerated at the time that reconnection of that field line occurred. This minimum parallel speed decreases with increasing latitude, so that there are patches of newly accelerated ions with a characteristic parallel speed-latitude signature poleward of the equatorward-moving equatorward border of the cusp. We have not attempted to draw the complex field of waves that is launched over the poles to notify the night side that a burst of reconnection occurred on the day side. Original drawing.

these are FTE time scales. Observations such as these are the clearest indication that magnetopause reconnection can be fundamentally unsteady, and encourage us to think of the magnetopause–ionosphere system as a relaxation oscillator whose output can range from the continuous smooth variation to a quasiperiodic series of bursts.

In summary, observations made at the magnetopause, in polar orbit, and in the polar cusp ionosphere consistently indicate that dayside reconnection often takes place in 1–2 minute bursts that repeat every 8–10 minutes, that the reconnection bursts develop several hundred kilovolt peak voltages, and that the bursts average over time to the polar cap potential typically observed for southward interplanetary field conditions. If the ionospheric crosssection of the actively reconnecting polar cusp is elongated in the east–west direction, the reconnection voltages inferred from ionospheric fast flows and from measurements of ion energy–latitude dispersion are consistent with the voltages estimated assuming bursty reconnection at a single neutral line on the magnetopause (Lockwood et al., 1989a; Lockwood and Smith, 1992). Energetic electrons and ions stream tailward out of the dayside magnetopause; the fact that their energies exceed the average polar cap potential suggests that they, too, are generated in bursty magnetopause reconnection events. We can no longer say that "dayside reconnection occurs" when the interplanetary field turns southward; we must say that "bursts of dayside reconnection become larger and/or more frequent." The cumulative effect of the bursts will still be to stimulate large-scale convection in the dayside ionosphere and in the polar cap, to cause the magnetopause to migrate inward, to increase the open flux in the tail lobes, and to increase the transport of plasma tailward in the plasma mantle–in short, to do all the things that occur in the growth phase of the substorm, but in a much more finely structured way than had been imagined 2 decades ago.

Our next task, then, is to understand how bursty reconnection at the magnetopause communicates with the rest of the magnetosphere and tail. Even if dayside reconnection is sporadic and localized, it rearranges the global magnetic topology, reorders the balance of stresses, and organizes a flow on the larger MHD space and time scale. This flow can be understood using the principles first enunciated in Petschek's reconnection model (Semenov et al., 1992), and the theory of MHD characteristics still provides guidance. The reconnecting magnetopause moves inward in an oscillatory, possibly stepwise, fashion, as the very first observations showed (Aubry et al., 1970). Fast waves couple these magnetopause motions within minutes to the inner magnetosphere and then to the inner edge of the current sheet, stimulating localized Alfven resonances on the way. Bursty magnetopause reconnection also radiates a complex pattern of waves along MHD characteristics into the plasma mantle and tail lobes, which after some delay will converge onto the plasma sheet on the nightside. What happens then is the subject of the next chapter.

NOTES

1. But see Sibeck (1992) for an alternate view, proposing that they are due to pressure pulses in the solar wind. Also, Papamastorakis et al. (1989) emphasized that the term *FTE* is used for the magnetic signature, and that magnetosheath connection with the polar cusp ionosphere has not been demonstrated in all cases.

2. If a significant fraction of FTEs are actually due to solar wind pressure pulses, as Sibeck (1992) has argued, the estimate of the average convection emf generated by overall FTE activity might be affected.

3. Crooker and Siscoe (1990) pointed out that a circular FTE crosssection in space will map into an elongated structure in the ionosphere in any case; so caution is necessary in using the crosssections of ionospheric fast flow events to estimate the overall reconnection potential.

4. The signature might not be so clear when the interplanetary field has a strong east-west component, for then the magnetic tension might shift the new reconnection patch to a different local time sector than the old one, possible to blur the jump in ion energy–latitude dispersion signature (Lockwood and Smith, 1992).

5. However, because of the electron beam component that is a characteristic feature of the LLBL in space and over the ionosphere, the overall electron precipitation energy flux in the LLBL is similar to that in the cusp (Newell et al., 1991b), which may explain why it is sometimes difficult to distinguish between the cusp and the LLBL in optical measurements (Sandholt, 1990).

9

BIMODAL PLASMA SHEET FLOW

9.1 Introductory Remarks

How does the plasma sheet respond to the complex pattern of waves coming over the poles from bursty magnetopause reconnection events, or to the vortices and other irregular perturbations coming around the flanks of the magnetosphere in the low-latitude boundary layer? It is probably too much to expect that the complex input from the dayside will sort itself out into a steady flow on the nightside, but there has been a seductive hope that, on a statistical basis, the observations of the plasma sheet could be rationalized using steady convection thinking. This hope depends on the belief that the average magnetic field configuration in the plasma sheet actually is compatible with steady convection. The first doubts on this score were raised by Erickson and Wolf (1980), and were subsequently elaborated by Tsyganenko (1982), Birn and Schindler (1983), and Liu and Hill (1985); the "plasma sheet pressure paradox" they posed is the subject of Section 9.2. Theoretical arguments are one thing, measurements are another; the truly important issue is whether the real plasma sheet manifests steady flow. Several groups have searched large data sets to see whether the statistically averaged flow in the central plasma sheet resembles the flow predicted by the steady convection model. This effort has led to a growing but still incomplete comprehension of the statistical properties of plasma sheet transport. Results obtained using ensembles of data acquired by ISEE 1 and AMPTE/IRM will be reviewed in Section 9.3. The unusual distribution of bulk flow velocities suggests that the plasma sheet flow is bimodal, alternating between a predominant irregular low-speed state and an infrequently occurring state of high-speed earthward flow.

In search of steady plasma sheet flow, one could also look into substorm-free periods of stable solar wind properties. One of the best such studies, in which great care was taken to find periods of exceptionally stable solar wind and geomagnetic conditions, is reviewed in Section 9.4. Even this study found highly irregular and bursty flow. People have been aware of the burstiness of the plasma sheet flow since the mid-1970s, and the issue has been to determine the occurrence rates, spatial scales, and multiplicity of the bursty bulk flow events in order to estimate their overall contribution to plasma sheet transport. This issue is the focus of the next five sections. More than half of all the earthward plasma and energy transport past AMPTE/IRM in 1985, and almost all the magnetic flux transport near

the midnight meridian, took place in infrequent bursts of high-speed flow of 5–10 minutes duration (Section 9.5). This striking fact renews our interest in older observations of bursty plasma sheet flows. Several studies dating back to the mid-1970s contrasted the state of slow, irregular flow on closed field lines with the high-speed flow state, and related the bursts of high-speed flow to reconnection, since the earthward flows carried magnetic flux earthward and the tailward flows carried flux tailward (Section 9.6). Bursts of flow with impressive transport rates were found in the plasma sheet when there was very little auroral activity (Section 9.7). Occasionally, high-speed flow bursts were associated with magnetic field structures resembling the "flux ropes" in Venus' ionosphere (Section 9.8). Section 9.9 moves on to mid-1980s observations of bursts of fast tailward flow beyond the distant tail neutral line. After their discovery on ISEE 3, these high speed flow events attracted considerable attention because they had the semiclosed magnetic configurations of plasmoids. Reconnection creates a continuum of structures from flux ropes to plasmoids depending upon the y component of the magnetic field in the plasma sheet. All bursty bulk flow events involve such plasmoidlike reconfigurations of the plasma sheet magnetic field, and plasmoids, which are defined observationally by their magnetic field signatures, all involve high-speed bursty bulk flows. In Section 9.10, we survey the literature to get some idea where earthward fast flows are preferentially observed and where tailward flows are more likely to be found. This survey suggests that bursty bulk flows are generated in sporadic localized reconnection events that occur with the greatest frequency between, say, 30 and 70 R_E downtail.

In addition to bursts of high-speed flow, the plasma sheet contains bursts of energetic ions (Section 9.11). The ions propagate earthward or tailward to the spacecraft while drifting westward from spatially localized regions of the temporally unsteady acceleration. Many bursts exhibit inverse velocity dispersion that places their acceleration regions where BBFs/plasmoids are frequently generated. This suggests that the ion bursts are nonlocal signatures of the reconnection events that generate bursty bulk flows and plasmoids (Section 9.12). By implication, the bursts of energetic ions of somewhat lower energy that are interpreted as activations or expansions of the plasma sheet boundary layer may also be signatures of bursty reconnection events. There is evidence that boundary layer activations and energetic ion bursts are localized in the east–west direction (Section 9.13). Few-minute bursts of the earthward-flowing ions have also been observed in the lobes of the tail (Section 9.14). These form localized filaments of plasma sheet origin that protrude into the tail lobes, bounded to the east and west by oppositely directed field-aligned currents. How these bursts are related to those in the plasma sheet is not very clear, but there may be unusually strong activations of the plasma sheet boundary layer that reach far into the tail lobes. The field-aligned currents bounding the filaments will drive localized equatorward flows in the ionosphere. Measurements made by the EISCAT incoherent scatter radar have established that the flow transport in the high-latitude nightside ionosphere is dominated by bursts of 5–10 minute duration, whose repetition rate and amplitude increase with the rate of solar wind energy input to the magnetosphere via

reconnection (Section 9.15). These may be the ionospheric counterparts of bursty bulk flow events in the plasma sheet.

The flux densities of mass, energy, and particularly magnetic field in the bursty bulk flow events are so large that it is hard to imagine they are not spatially localized. In the absence of multispacecraft measurements of the cross sections of the bursty flows, the best way to estimate their size is to find their auroral footprints. The difficulties in associating bursty plasma sheet flows with auroral and geomagnetic activity and bursty ionospheric flows suggest that the small footprints are usually missed because of inadequate space–time resolution and/or high-latitude coverage. In Section 9.16, we describe one study that succeeded in identifying the auroral footprints of bursty bulk flow events. "Local auroral flares" that occurred within minutes of bursty bulk flow events in the plasma sheet were detected at only one or two of a network of observing stations. The upper limit scale set by the spatial resolution of the observing network gives some idea of how much mass, energy, and magnetic flux is transported earthward in bursty bulk flow events. It is interesting, perhaps significant, that the flux transfers due to bursty magnetopause reconnection events, bursty ionospheric convection events on the dayside, and bursty plasma sheet bulk flow events are comparable within admittedly very wide error bars (Section 9.17).

9.2 The Plasma Sheet Pressure Paradox

The plasma sheet pressure paradox, reduced to its essence, is straightforward. Since the minimum lifetime (Kennel, 1969) for ion precipitation is extremely long in the geomagnetic tail, earthward convection proceeds without important particle losses to the ionosphere. The total number of particles contained within a flux tube will then remain constant as that flux tube convects toward the earth. If the flux tube volume changes, so also will the plasma density. Suppose the convecting plasma obeys an adiabatic equation of state; a statistical study of AMPTE/IRM plasma data collected in the quiet central plasma sheet found that the pressure and density do obey a polytropic law, with an index ranging between 4/3 at quiet times, for AE < 100 nT, and 5/3 at more disturbed times, AE > 300 nT (Goertz and Baumjohann, 1991). In this case, an increase in density as the flux tube volume shrinks implies an increase in plasma pressure. No spacecraft can measure the flux tube volume, or the pressure and density, following an element of flow. However, using any of the existing empirical magnetic field models, the flux tube volume following a hypothetical earthward streamline decreases so much that the plasma pressure eventually exceeds the magnetic pressure in the tail lobes, which clearly violates a basic condition for equilibrium.

Opinions vary as to whether this argument is fatal to steady plasma sheet convection (Tsyganenko, 1990), but no one can avoid grappling with the question. At the most primitive level, the argument states that empirical magnetic field models are inconsistent with steady convection due to a uniform dawn–dusk electric field. However, the empirical models are inconsistent with any earthward

transport over large distances, steady or unsteady, that preserves the number of particles in a flux tube defined by the ensemble average magnetic field. Of course, losses of plasma and energy by particle drifts could conceivably prevent the pressure buildup. Eventually, the energy would have to leave the magnetosphere, but no one has reported plasma sheet thermal ions entering the magnetosheath with the required energy flux, which on occasion would have to be comparable to the rate of energy dissipation in substorms.

9.3 Statistical Properties of Plasma Sheet Transport

Because the position and thickness of the plasma sheet vary, one cannot simply assign a given measurement to the plasma sheet according to the location of the spacecraft. This difficulty has motivated a search for criteria within the data that can distinguish the plasma sheet from the tail lobes, low-latitude boundary layer, and mantle. It is also important to distinguish the plasma sheet boundary layer from the plasma sheet proper. Before detailed ion velocity distribution measurements became available, no distinction was made between the plasma sheet boundary layer and the central plasma sheet. The presence of essentially field-aligned energetic ion beams whose energies span the keV to the MeV range now defines the plasma sheet boundary layer (Lui et al., 1977a,b; DeCoster and Frank, 1979; Frank and Ackerson, 1979; Eastman et al., 1984). The ion beams can flow earthward, tailward, or both simultaneously, and are highly variable in time. The beams usually have enough perpendicular pressure to reduce the magnetic field noticeably below that in the adjoining tail lobe, which makes it difficult to distinguish the boundary layer from the plasma sheet proper in magnetic field measurements. The moments of the plasma sheet ion distribution—the ion density, velocity, and pressure—are obtained by averaging over velocity space. Large bulk flow speeds, up to several thousand kilometers per second, result when the boundary layer ion beams do not balance. The distributions in the central plasma sheet more nearly resemble that of a normal fluid; the 20 eV/e–40 keV/e ion distribution functions measured by AMPTE/IRM in the central plasma sheet generally consisted of one single streaming component (Nakamura et al., 1991).

At one time it appeared that high–speed bulk flows might not occur at all in the central plasma sheet. Huang and Frank (1986) surveyed all the LEPEDEA 1 eV to 45 keV ion data acquired within the central plasma sheet on ISEE1 during 1978. They defined the central plasma sheet using criteria based upon ion bulk flow speed. They did not include data in their plasma sheet ensemble if (1) the bulk flow speed exceeded 150 km/s and the spacecraft was more than 1.5 R_E from the expected position of the neutral sheet, to exclude the plasma sheet boundary layer; (2) the bulk flow speed exceeded 150 km/s tailward, and the density exceeded 1/cm^3, to exclude the low-latitude boundary layer; and (3) the density was less than 10^{-2}/cm^3, and the bulk velocity was tailward, to exclude mantle plasma. These criteria assigned almost 3000 individual measurements of the density, temperature, and ion velocity to the central plasma sheet. The data were sorted according to the

auroral electrojet (AE) index and averaged. The ensemble average density was 0.3 cm^{-3}, independent of distance up to 1.5 R_E above the expected neutral sheet, and independent of AE. The average ion temperature peaked at the center of the plasma sheet, and increased smoothly from 4 keV at AE = 100 nT to 11 keV at AE = 1000 nT. The increase in ion temperature with AE seemed to be the one clear characteristic of substorms in the data.

Huang and Frank's (1986) results showed that the ensemble average plasma sheet pressure was roughly consistent with the pressure in the tail lobes but that the average flow was still inconsistent with the steady convection model. The average flow velocity, though earthward over the entire range of AE, was less than 20 km/s and closer to 10 km/s for most values of AE. Speeds this small are comparable with the gradient and curvature drift speeds of a 5 keV thermal ion in the few R_E magnetic field scale length of the plasma sheet, and are not necessarily due to $\mathbf{E} \times \mathbf{B}$ convection. At 10 km/s, it would take 15 hours for the flow to traverse the 100 R_E distance from the average position of the tail neutral line (Slavin et al., 1985), which does not agree with the 2–4 hours for an element of ionospheric flow to cross the polar cap, or for field lines to cross the tail lobes at the speed deduced from lunar shadowing measurements. About 0.2 GW/R_E^2 would be transported earthward during even the times of largest AE index; for a 3 R_E x 30 R_E plasma sheet crosssection, the total power would be 20 GW, a factor of 10 smaller than the power expended in a substorm. Central plasma sheet convection appeared not to transport the energy dissipated during disturbed times, leaving only the plasma sheet boundary layer to power substorms. However, three features discriminated against counting earthward plasma transport in the central plasma sheet in this survey (Cattell and Elphic, 1987). First, the survey discriminated against plasma sheets with half-thicknesses exceeding 1.5 RE. More important, the selection criteria discriminated against flows with speeds in excess of 150 km/s. Most important of all, the long cycle time of the LEPEDEA instrument, 128 or 512 s, militated against finding short bursts of high-speed flow. We will see that Huang and Frank described the "slow-flow" state of the central plasma sheet, but they could not find the bursty high-speed flow state.

In light of these considerations, Baumjohann et al. (1989) developed criteria that did not depend on flow speed to distinguish the central plasma sheet from the boundary layer. To discriminate against tail lobe data they required that the plasma density be high enough that spacecraft photoelectric charging is negligible. They avoided low-latitude boundary-layer flows by staying away from the boundary layer, selecting data with $|Y_{GSM}| < 15\ R_E$. Finally, the AMPTE/IRM plasma instrument provided moments from a full three-dimensional distribution function every 4.5 s, and was less likely to miss short bursts of flow. All in all, Baumjohann et al. (1989) analyzed some 78,000 moments of the ion distribution acquired within the central plasma sheet over 4 months in 1986. They sorted these according to the "horizontal" component of the magnetic field, $B_{xy} = (B_x^2 + B_y^2)^{1/2}$; $B_{xy} < 7.5$ nT defining an "inner central plasma sheet," and $7.5 < B_{xy} < 15$ nT, an "outer central plasma sheet." The ensemble-average ion density they found

was 0.3 cm^{-3} beyond 14 R_E downtail, independent of distance from the neutral sheet, in agreement with Huang and Frank (1986). Once again, the average density in the inner and outer central plasma sheet varied little with AE, ranging between 0.2 and 0.4 cm^{-3}. The average ion temperature in the inner central plasma sheet, 5 keV, was independent of AE, whereas it rose monotonically with increasing AE in the outer central plasma sheet. The temperatures in the two regions only became equal at the largest values of AE. The ratio of ion to electron temperature, 7, was remarkably invariant and compared favorably with the ratio of 5.5 found on ISEE-3 beyond 60 R_E (Slavin et al., 1985). Because the survey included high-speed flows, the average ion velocity in the inner central plasma sheet was larger than Huang and Frank's (1986). Moreover, it had a systematic dependence on AE, rising from 25 to 87 km/s as AE increased from 100 to 1000 nT.

The most striking AMPTE/IRM result concerned the *distribution* of ion velocities (Baumjohann et al., 1989). Flow samples with low speeds dominated the ensemble for all AE. These were obviously responsible for the low average speed in both the inner and outer central plasma sheet. On the other hand, high-speed flows were also found in the central plasma sheet for all AE. Speeds exceeding 300 km/s comprised 0.5% of the samples with AE < 500 nT and 2–3% of those with AE > 500 nT. Thus the frequency of occurrence of high-speed flows correlated with AE. The high–speed flows appeared to be highly time variable, since fewer than 30% of the $V > 300$ km/s samples were clustered in sequences lasting longer than 20 s. The dependence of the distribution of the flow directions upon speed was even more striking. Low-speed, $V < 100$ km/s, flows were distributed in a variety of directions in both the X–Y and X–Z planes, with a general though not pronounced preference for the earthward direction. In sharp contrast, the high-speed flows were directed almost precisely earthward. This, more than anything else, suggests that the plasma sheet flow state is bimodal.

Later, Baumjohann et al. (1990) culled the high-speed flow samples from some 270,000 measurements acquired over 8 months of AMPTE/IRM operation during the tail crossing seasons of 1985 and 1986. Contrary to received wisdom, ion bulk velocities exceeding 400 km/s occurred only slightly less frequently in the inner central plasma sheet than they did in the plasma sheet boundary layer, although the ion distribution functions usually differed dramatically. About 40% of all measurements of speed exceeding 400 km/s consisted of one isolated data point; only about 5% of the flow events lasted more than 30 s. The largest occurrence rates of high-speed flows were found near the center of the tail and near the 19 R_E apogee of the spacecraft. The occurrence frequency in the plasma sheet boundary layer increased only a little with AE, whereas it rose in the inner central plasma sheet from 1.5% to above 6% as AE increased from 300 to 750 nT. For AE > 600 nT, high-speed flows were actually more likely in the inner central plasma sheet than they were in the plasma sheet boundary layer. The earthward fast flows in the inner central plasma sheet were directed almost precisely earthward, and correlated with northward magnetic field, indicating that they were transporting a lot of magnetic flux toward the earth. Their Alfven Mach numbers were remarkably

close to unity, ranging from 0.7 at V= 400 km/s to about 1.5 at V = 1200 km/s. This is consistent with the generation of the fast flows by reconnection.

9.4 Bursts of Plasma Sheet Flow during Steady Solar Wind Conditions

It is possible to have persistent magnetospheric flow without clear-cut auroral substorms. Such events have been given the name, *convection bays*. Because intervals of steady solar wind plasma and magnetic field are rare, and within these there are few periods free of substorms, finding convection bays is more difficult than it might seem. According to Sergeev and Lennartsson (1988), the first 3 years of ISEE 1 data contained only two events in which the solar wind was steady, there were ground-based signatures of a steady flow lasting more than 4 hours, and ISEE 1 was in a position to diagnose that flow, near apogee and more or less continuously in the plasma sheet. Prolonged, 10-hour, plasma sheet flows were encountered about 20 R_E downtail, one just on the evening side of the midnight meridian (April 24, 1980), and one 10 R_E east of the midnight meridian (February 19–20, 1978). The interplanetary field had a stable southward component that ranged between 1.1 and 2.8 nT during the April, 1980, event, and incomplete data suggested that it also had a southward component throughout the February event. The solar wind dynamic pressure was stable to 10% for the April, 1980, event and to 25% for the February, 1978, event. In both events, the auroral oval was more or less continuously active in an unstructured way (the AL index was typically 200 nT), but there were none of the familiar ground-based signatures of substorms: midlatitude bays, bursts of Pi 1 and Pi 2 micropulsations, riometer bays, auroral onsets. Moreover, no remarkable thinnings or expansions of the plasma sheet were observed during the long periods of time the spacecraft spent within it. The plasma sheet was several earth radii thick, the normal component of its magnetic field was large (5 nT), and the 15-minute average ion velocity in the central plasma sheet was about 100 km/s earthward.

Despite the absence of substorms, Sergeev and Lennartson (1988) did not find steady MHD convection. They found sustained but time-variable and nonuniform plasma sheet flow. Two arguments led to this conclusion. The first revolved around the rate of flux transport in the high-speed flow. The dawn–dusk component of the $\mathbf{V} \times \mathbf{B}$ convection electric field was 2.5 times larger in the plasma sheet than in the solar wind for the April, 1980, event. If this $\mathbf{V} \times \mathbf{B}$ field had extended across the whole plasma sheet, more magnetic flux would have been transported toward the earth than could possibly reconnect on the dayside. The magnetotail would have had to evolve in time, which it did not do. Thus, the plasma sheet flow was probably nonuniform. More to the point was the time series of the flow speed itself. Even 15-minute averages of the ion bulk velocity had significant variability. While the flow was generally earthward, one-fifth of all the 15 minute averages showed a weak tailward flow. Intervals with speeds exceeding 200 km/s occurred more often toward the plasma sheet boundary layer, but even in the central plasma sheet they occurred about 20% percent of the time in the

February, 1978, event. Low- and high-speed flows occurred equally frequently in the April, 1980, event, even though the solar wind electric field was relatively constant.

Sergeev et al. (1990) later studied one of the two events at higher time resolution. Although direct flow velocity measurements with better than 15 minute time resolution were not available, the plasma bulk speed could be inferred from the anisotropy of the energetic ion distribution with higher time resolution. Numerous flow bursts were observed in these data, all of which were directed earthward and were accompanied by dipolarizations of the magnetic field. Three of the largest ones could be associated with flow bursts in the nightside ionosphere detected by the STARE radar. The bursts of fast equatorward flow intruded into the auroral oval from the polar cap about every 20–30 minutes, lasted about 3–5 minutes, moved equatorward at about 1 km/s, and came to rest near the latitude of maximum diffuse auroral intensity. They did not appear to be associated with discrete aurora.

9.5 Bursty Bulk Flow Events

Angelopoulos et al. (1992a,b) showed that the high-speed plasma sheet flows were organized into distinctive "bursty bulk flow events" (BBFs) of about 5–10 minutes duration. A BBF was defined to have at least one maximum in speed exceeding 400 km/s; the data were then followed backward and forward in time until the flow speed fell below 100 km/s, this defining the duration of the BBF. The speed could have multiple peaks within each event, and, indeed, substructure on the 1-minute time scale was common. As the earlier statistical studies already indicated, the flow velocities in the BBFs were directed almost precisely earthward, and one could see the magnetic field turning northward as the flow speed increased (Angelopoulos et al., 1992a,b). The Alfven Mach numbers of the flows were of order unity. The total pressure changed very little as BBFs passed over the spacecraft, suggesting that they find a way to avoid the plasma sheet pressure paradox. BBFs were found even when AE was very low, though they were encountered more frequently at times of high AE. Even within individual substorms, their occurrence bore no clear relationship to substorm phase. AE would be elevated both before and after the spacecraft encountered a brief burst of high-speed flow (Angelopoulos et al., 1992a); a lot of energy was being dissipated in the nightside ionosphere, and yet the spacecraft was encountering a quiet plasma sheet most of the time. In a similar paradoxical vein, Eastman et al. (1985b) had found earlier that of 50 periods when ISEE 1 was in the central plasma sheet near substorm onset, more than half showed no significant change in plasma flow near the time of onset.

BBF-like events had been found before, and the issue was whether they were a curiosity or whether they were an important factor in plasma sheet transport despite their infrequency. The criteria defining BBFs produced an ensemble of some 50 events in the 1985 AMPTE/IRM data set that were distributed more or less

uniformly over the plasma sheet between 10 and 19 R_E. The ensemble average number and energy flux densities of the BBFs were 0.1 D/R_E^2 and 20 GW/R_E^2, respectively. The average total transport per BBF event was 60 D/R_E^2 and 2000 GJ/R_E^2. There were spreads of somewhat more than a factor of 10 in the distributions of these quantities. The BBFs were particularly efficient transporters of magnetic flux. One indication was the fact that the dawn–dusk electric field inferred from the measured $\mathbf{V} \times \mathbf{B}$ was very large, tens of kV/R_E. Direct measurements made with the ISEE 1 electric field detector in the plasma sheet boundary region support this estimate. Pedersen et al. (1985) reported bursts of dawn–dusk field whose 5–15 minute durations and 30–60 kV/R_E amplitudes are consistent with the AMPTE/IRM BBFs. The typical AMPTE/IRM BBF transported about 4 x 10^6 W/R_E earthward, integrated over its few-minute duration.

The crossection of the region of high-speed flow need only be 10 R_E^2 for BBFs to cause transport at typical substorm rates, suggesting that a significant fraction of all earthward plasma sheet transport takes place in bursty bulk flow events. The crosssections are not known at the present time; however, one can ask what fraction of all the transport past the spacecraft occurred in bursty bulk flow events. The results of this simple compilation were striking: although BBFs composed only 7% of the data ensemble, they accounted for about half the total earthward number and energy transport, and well over half the magnetic flux transport past AMPTE/IRM when it was in the inner central plasma sheet in 1985. A different choice of BBF definition would alter these figures slightly, but their overall import would be the same. It appears that the low-speed flow state and BBFs divide the honors for overall energy and number transport, while BBFs could well be responsible for the lion's share of the magnetic flux transport.

9.6 Bimodal Plasma Sheet Flow

Frank et al. (1976) were the first to distinguish the two states of plasma sheet flow. They based their conclusion on 8.2 minute averaged LEPEDEA plasma measurements and local magnetic field measurements made on IMP 8 between 23 and 46 R_E radial distance during the 1974 tail-crossing season (March to October). They found the plasma sheet to be most often in continual but irregular motion. This irregular flow took place on closed field lines that always had a northward magnetic field component regardless of flow direction. The speed in this state was relatively low, 50–500 km/s. No unique signature of the proton bulk flow could be identified with crossings of the magnetic neutral sheet. Occasionally, IMP 8 encountered what the authors called "fireballs," localized regions of bursty plasma flow with speed above 1000 km/s. The fireball magnetic fields were disordered but generally southward for tailward jetting and northward for earthward jetting. Electron anisotropy observations showed that the earthward fireball flows were threaded with closed geomagnetic field lines, while the tailward flows were on open field lines. These features are consistent with the generation of fireballs by reconnection. The authors estimated that the fast flow regions had a 1–5 R_E

transverse spatial scale, based upon the frequency with which they were encountered in the magnetotail.

Lui et al. (1977a) noted that the high-speed plasma sheet flow at both IMP 6 and at Vela 5 and 6, at approximately 18 R_E, was organized in bursts of approximately 12 minutes duration. They picked these bursts out because they occurred during plasma sheet expansions. The flow was generally earthward and approximately parallel to the equatorial plane; the speed was 500–1000 km/s in the midnight sector, and typically less than 500 km/s in the dawn and dusk sectors, features generally consistent with BBFs. A complementary analysis of 74 IMP 6 events during plasma sheet thinnings (Lui et al., 1977b) found no preferred flow direction, but in retrospect, the highest speed events tended to be earthward within 20 R_E, and some were tailward near 30 R_E, a trend that conforms to what is found in other studies. Two statistical studies of the IMP 6 data acquired between 20 and 33 R_E downtail drew a clear distinction between the low-speed and high-speed plasma sheet flow states (Nishida et al., 1981; Hayakawa et al., 1982). Tailward flows with speeds exceeding 300 km/s were associated with southward B_Z; tailward flows with speeds less than 300 km/s could not be specifically associated with southward B_Z, and did not differ from the slow earthward flows (Hayakawa et al., 1982). In other words, the slow flows were sloshing back and forth on closed field lines with northward B_Z. These results are consistent with those of Frank et al. (1976).

9.7 High-Speed Flows at Quiet Times

It was curious at the time that not all IMP 6 flow bursts occurred at times of substorm activity. On November 17, 1971, for example, IMP 6 detected a 12 minute, 500 km/s, earthward BBF at 11 R_E in the midnight sector following 4 days of extreme geomagnetic quiet. Three minutes after the BBF started, all-sky images recorded an auroral arc that brightened to the south of Inuvik (MLAT 70.4 degrees, MLT 2200) and spread poleward. Although IMP 6 detected the increase of B_Z characteristic of earthward BBFs, the ATS spacecraft in geostationary orbit at 0130 MLT never detected a substorm dipolarization or injection of energetic particles, nor was there a positive bay in the H component of the geomagnetic field (Akasofu et al., 1971, 1973; Snyder and Akasofu, 1972; Lui et al., 1975b, 1976). In retrospect, this attenuated high-latitude auroral expansion resembles other activations of the poleward arc system that are independent of auroral expansions at lower latitudes. This event may have been one of the first, but certainly not the last, time that a highly energetic plasma sheet flow was found during a time of little or no substorm activity.

An even more spectacular example was found by Coroniti et al. (1978), who found a 5-hour quiet interval containing nine distinct pulsations in plasma sheet flow, in which the proton bulk speed varied from 0 to as much as 1500 km/s. The sequence was found in LEPEDEA measurements made on IMP 7 about 35 R_E downtail on November 9, 1972. The first four pulsations were about 30 minutes

long and separated by 30 minutes, and the last five were 15–20 minutes long and separated by 15–20 minutes. Assuming a cross-sectional area of 10 R_E^2, about 10^{22} ergs was directed earthward in these bursts, yet geomagnetic data indicated activity only near the poleward edge of the auroral oval. Coroniti et al. (1980) returned to the issue of high-speed flows at times of low auroral activity in a second IMP 7 paper. A single strong (>1000 km/s) 8–10 minute burst of tailward flow was found during the recovery phase of one substorm, and later on the same day, several 10–20 minute bursts of 500–1000 km/s eastward flow were found in the central plasma sheet and boundary layer following the recovery of another substorm. None had any noticeable relation to ground activity. In another case, a number of 10–15 minute fast flows were found during a 4-hour period of magnetic quiescence, some tailward, some earthward; their magnetic field could be either northward or southward. The flow speeds, though only moderately elevated, 300–700 km/s, were still comparable with the local sound and Alfven speeds.

9.8 High-Speed Flows and Flux Ropes

On two occasions, IMP 7 was immersed in a dawnward 300–600 km/s flow, and the magnetic field was bent out of the noon–midnight meridian toward dawn; the magnetic field had a northward component in one event and southward in the other (Coroniti et al., 1980). At times during these events, B_X was nearly zero so that the total 10–20 nT field was dawnward. The ion energy fluxes were 0.3–3 GW/R_E^2, typical of other bursty bulk flow events. Such events later came to be called *flux ropes* based on their magnetic topology, and later still were grouped into a continuum of structures ranging between the pure plasmoid limit and the pure flux rope limit.

Two structures resembling the flux ropes found in the Venus ionosphere were found near the neutral sheet at about 20 R_E downtail (Elphic et al., 1985). ISEE 1 and 2 electric field, magnetic field, and plasma data, together with the delay in the passage of the structures over the two spacecraft, indicated that their speeds were the order of 300–600 km/s earthward. The brief, 30 s, duration of each event was more like the substructure of BBFs and very different from the overall 5–10 minute durations of the AMPTE/IRM bursty bulk flow events at roughly the same distance. The magnetic axes of the flux ropes were in the $-Y$ (GSM) direction, and the magnetic field was as strong in the center of the flux ropes as it was in the lobes of the tail. Assuming a scale size of 3–5 R_E, the total field-aligned currents within them approached a million amperes. Such events appear not to be common at the ISEE 1 and 2 orbits; a survey of the data in March and April 1979 revealed few other potential flux rope candidates.

Bieber et al. (1984) found five IMP 8 events in which a pulse of heated electrons appeared near the end of an interval of fast tailward flow. A roughly 5-minute initial phase started with a 500 km/s tailward flow that was accompanied by highly variable magnetic field, with an overall average southward component, and in some cases a strong east–west component. There followed a roughly 2-minute

interval in which the electron temperature increased by a factor of 2–4, and the density decreased so as to maintain overall pressure balance. The strongest southward fields were observed while this was going on. Throughout both phases, the very energetic, > 200 keV, electrons had trapped or isotropic angular distributions; the expected transition to open field line distributions occurred only at the end of the electron heating phase.

9.9 High-Speed Flows, Plasmoids, Flux Ropes, and TCRs in the Distant Tail

The frequent occurrence of 10-minute bursts of tailward ion bulk flow was inferred from the anisotropy of suprathermal (6–150 keV/amu) ions in the very first ISEE 3 studies of the distant tail beyond 100 R_E (Gloeckler et al., 1984a; Cowley et al., 1984). Because of the relatively low time resolution of the energetic particle instrument, these first results emphasized events with longer durations (Moldwin and Hughes, 1992b). The strongest argument for the convective flow interpretation was the fact that H^+ and He^{2++} ions had a common velocity, which averaged 580 km/s in 20 events occurring between January and March 1983 (Scholer et al., 1984a; Gloeckler, et al., 1984a). The rest frame distribution functions of the suprathermal H^+ and He^{2++} ions had an exponential dependence on speed (not energy) with the same *e*-folding speed. The He-to-H ratio indicated that the solar wind was the predominant source of the particles in the fast flows (Gloeckler et al., 1984a,b). Although only a few events had been selected for detailed analysis, the general burstiness of the energetic ion fluxes gave the definite impression that bursts of high-speed flow were relatively common in the deep tail.

Energetic electrons and ions exhibited direct velocity dispersion during the initial phases of many of the ISEE 3 fast tailward flow events. Beamlike 75–115 keV electrons appeared first, followed 2–6 minutes later by dispersed ions with energies up to 300 keV, the higher-energy ions appearing earlier. Except for the absence of measurements of the low-energy electron layer, this sequence is the tailward-directed version of what is observed on crossing active plasma sheet boundary layers earthward of the tail reconnection region. From the timing of the first appearances of 120 and 32 keV protons, Scholer et al. (1984a) concluded that the acceleration source for one event was located 115 R_E downstream of earth and 105 R_E earthward of ISEE 3. The electrons' time of arrival was consistent with their having left this source 2 minutes earlier than the ions. The ion and electron beams were followed by the tailward fast-flow events themselves. The isotropy of the electrons indicated that the high-speed flow was contained in the closed field region of a plasmoid (Scholer et al., 1984a). No energetic particle dispersion was observed as the fast flows subsided.

Owen and Slavin (1992) reported on the relationship between energetic ion enhancements and traveling compression regions at ISEE 3 in the deep tail. Their data sample consisted of 116 TCR events, of which 37 were classified as isolated, 36 as paired, and 42 as multiple. An isolated TCR was separated by at least 30 minutes from any other; two observed within 30 minutes constituted a pair;

the TCRs in multiple events were separated by less than 30 minutes; there were 11 multiple events in all. Of the 78 events for which there was energetic ion coverage, 46% could be associated with an ion enhancement, indicating that the plasma sheet boundary layer expanded over the spacecraft as the plasmoid passed nearby. Almost all the enhancement-associated TCRs tailward of 100 R_E showed strong tailward streaming, whereas most of the events earthward of 80 R_E showed earthward streaming, or no definable anisotropy. The TCRs with ion enhancements were roughly a factor two stronger than those without, but there was no clear difference in event duration. The durations were typically in the 1–4 minute range.

Sibeck et al. (1984) found three high-speed tailward flows with flux rope magnetic structure in ISEE 3 data at 90–110 R_E distance. These events had rather long durations, tens of minutes. The flow velocity was about 1000 km/s, and the energy flux was roughly 4 GW/R_E^2 in the most intense of the three (Kennel et al., 1986). Scholer et al. (1985b) estimated that this particular rope had a spatial scale of 3 R_E, so that overall it transported 30–40 GW of power tailward. Hughes and Sibeck (1987) examined what would happen to the magnetic field configuration when a cross-tail component of plasma sheet magnetic field is present at the time of plasmoid formation. They found that a twisted helical structure formed, rather than a pure closed loop or magnetic island. Therefore, a continuum of complex magnetic structures ranging from flux ropes to plasmoids will be created in different reconnection events and will accompany fast flows in the plasma sheet.

Moldwin and Hughes (1992b) used a generalized magnetic field signature, a bipolar variation in *either* the y or z component of the magnetic field, to select structures in the continuum from plasmoid to flux rope. A total of 366 events were found in the data acquired during the 1983 ISEE 3 Geotail mission; all were called plasmoids. Forty-five percent of the plasmoids had their bipolar signature in the z component, 34% in the y component, and 21% in both components. There was no significant difference in the general characteristics of the y-bipolar and z-bipolar events. Most (82%) had a distinct magnetic core or field strength maximum at the inflection point of the bipolar signature. The maximum field strength could approach the strength of the exterior lobe field. The high-speed flow in the deep tail was due primarily due to such plasmoids (Moldwin and Hughes, 1992b). The very highest-speed flows corresponded one-for-one to plasmoids; every time the flow speed exceeded 1000 km/s and ISEE 3 was in the plasma sheet coincided with the passage of a plasmoid. Removing the plasmoids from the data ensemble reduced the average velocity in the plasma sheet by 50%.

9.10 Dependence of BBF/Plasmoid Properties upon Distance Downtail

What picture emerges from our survey of the literature on high-speed flows in the plasma sheet? In retrospect, the fast flows at IMP 7 near 30 R_E differed in two important ways from the AMPTE/IRM BBFs within 19 R_E. While their durations, speeds, and transport rates were similar, the IMP 7 fast flows could be earthward,

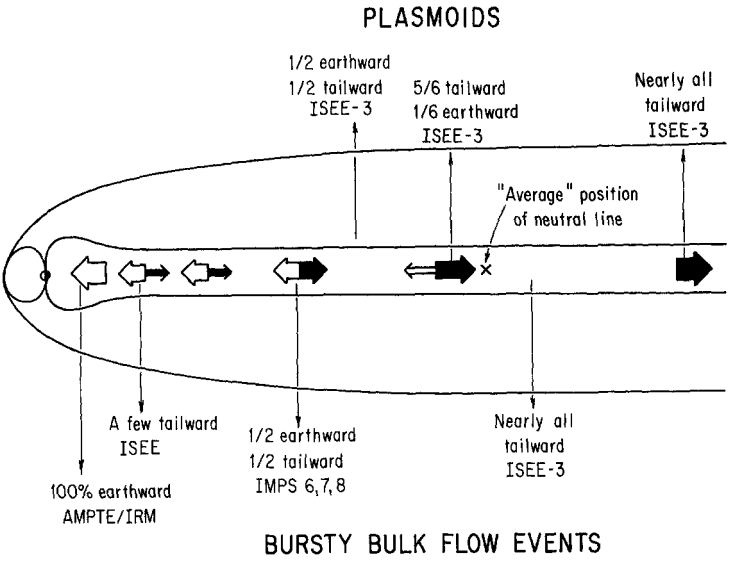

Figure 9.1. Plasmoids and Bursty Bulk Flow Events in the Earth's Magnetic Tail. This figure compares the properties of plasmoids and BBFs that emerge from a survey of the literature. The top part summarizes the results of studies that key on the plasmoid magnetic field structure, whereas the bottom part shows the results of studies that key on the existence of fast plasma sheet flows. Almost all bursty bulk flow events were earthward at AMPTE/IRM ($< 19\ R_E$), some were tailward at ISEE 1 and 2 ($< 23\ R_E$), about half were earthward and half were tailward at IMPs 6, 7, and 8 ($30–40\ R_E$), and a majority were tailward at ISEE 3 ($80\ R_E$). The distribution of plasmoids is qualitatively similar, half earthward and half tailward at $50\ R_E$, nearly all tailward beyond $100\ R_E$ downtail. This suggests that while reconnection can occur at a variety of distances downtail, it occurs most frequently in the $30–70\ R_E$ range. Studies of Traveling Compression Regions (TCRs) support this conclusion; TCRs are encountered three times more frequently at $100\ R_E$ than at $30\ R_E$. Original drawing.

dawnward, or tailward, while the AMPTE flows were almost always earthward. Both the AMPTE and IMP bursty bulk flows reconfigured the plasma sheet magnetic field, but the nature of the reconfigurations could differ. Earthward BBFs always had a northward component of magnetic field, and tailward BBFs, a southward component, but beginning about $30\ R_E$ downtail, high-speed flows flowing across the tail accompanied by enhanced B_y could be found. At ISEE 3 distances, the fast flows were primarily tailward. Although they are very similar, we gave these three types of fast flows three different names; the predominantly earthward flows at AMPTE/IRM, we called *bursty bulk flow events*; the cross-tail flow events, *flux ropes*; and the tailward flow events, *plasmoids*.

Moldwin and Hughes' (1992b) survey of ISEE 3 plasmoids complemented and extended the study of bursty bulk flow events. Moldwin and Hughes (1992b) selected their events first for bipolar magnetic field structure, and then examined

the velocity signature, whereas the studies cited previously keyed first on the high-speed flow. Most ISEE 3 encounters with the plasma sheet did not yield a plasmoid; however, when plasmoids were found, they were found all along the spacecraft orbit between 50 and 220 R_E downtail, and all across the tail right up to the magnetopause. Their normalized occurrence rate was about 4.6 per day, a lower limit since the survey did not include TCRs. Most (72%) of the associated flow velocities were within 45 degrees of the $\pm x$ directions. Half of the plasmoids between 50 and 100 R_E moved tailward and half moved earthward; the tailward-moving fraction grew to 86% between 100 and 200 R_E, and reached 96% beyond 200 R_E. Thus 5/6 of all plasmoids were moving tailward at the roughly 100 R_E position of the "average" neutral line (Tsurutani et al., 1985). This could well be the modern meaning of the word *neutral* line.

The mean speed obtained by averaging the flow velocity over the duration of the plasmoid was 490 ± 230 km/s tailward; the average maximum speed in each plasmoid was 890 ± 420 km/s (Moldwin and Hughes, 1992b). The average mean speed of tailward-moving plasmoids exceeded that of earthward plasmoids, 218 km/s. Five earthward events whose mean speeds exceeded 400 km/s certainly satisfied the speed criterion used to select AMPTE/IRM BBFs (Angelopoulos et al., 1992a), and others probably had maximum speeds exceeding 400 km/s and so would also be called BBFs. The sizes of the plasmoids estimated by multiplying the mean speed by the duration ranged from a few to about 40 R_E, with the broad distribution peaking between 10 and 20 R_E. The average size was 16.7 R_E with a standard deviation of 13.0 R_E. The average size and speed implies an average duration of about 3.5 minutes, somewhat shorter than, but in the same range as, BBFs. Plasmoids larger than 20 R_E were not found between 50 and 100 R_E downtail; thus, while small plasmoids were observed at all distances, large plasmoids were found only downstream of 100 R_E.

The features surveyed seem consistent with the generation of BBFs and plasmoids at a variety of locations distributed over a wide range of distances downtail. They appear to be most frequently generated between 30 and 70 R_E.

9.11 Energetic Particle Bursts in the Midtail

Anderson (1965) discovered high-energy electrons in the magnetotail, and shortly thereafter, Konradi (1966) and Armstrong and Krimigis (1968) reported the first observations of energetic ions in the plasma sheet. In the mid-1970s, when the IMP 7, 8, 9 spacecraft were operating in the 30–40 R_E midtail region, these impulsive bursts of energetic particles became the subject of intense investigation, which continues to the present day; later, the work was pursued somewhat closer to earth with data from ISEE 1 and 2 (Krimigis et al., 1975; Baker and Stone, 1976, 1977; Keath et al., 1976; Sarris et al., 1976a,b, 1978; West and Buck, 1976; Roelof et al., 1976; Kirsch et al., 1977, 1981; Carbary and Krimigis, 1979; Krimigis and Sarris, 1979; Lui and Meng, 1979; Sarris and Axford, 1979; Lui and Krimigis, 1981; Spieldvik and Fritz, 1981; Williams, 1981; Bieber et al., 1982; Lui et al., 1982;

Mobius et al., 1983; Baker and Fritz, 1984; Lui et al., 1984; Pavlos et al., 1985; Sarafopoulos and Sarris, 1987, 1988; Pavlos et al., 1989).

Bursts of > 0.22 MeV protons proved to be a semipermanent feature of the near-earth environment, having been found, on occasion simultaneously, upstream of the bow shock, in the magnetosheath, and plasma sheet (Sarris et al., 1976b, 1978; Krimigis et al., 1978). Their frequency of occurrence was at least 23% in the plasma sheet between 20–40 R_E downtail (Lui and Krimigis, 1981), and they were up to a factor of 10 more intense there than outside the magnetosphere (Krimigis et al., 1978). Anisotropy measurements indicated that they were streaming away from the earth in the solar wind and magnetosheath, and their energy spectra were harder, suggesting that their escape from the magnetosphere was rigidity dependent. Within the plasma sheet, the ions were generally the most intense, though not necessarily the most frequently occurring, on the dusk side, and the electrons tended to be more intense on the dawn side. The bursts were not found in the tail lobes, even when they were known to be present in the plasma sheet (Sarris et al., 1978; Krimigis and Sarris, 1979). This indicated they were generated in the plasma sheet.

The ion bursts in the plasma sheet are frequently observed to manifest inverse dispersion, wherein lower-energy (300 keV) ions are detected 10 or 20 s earlier than those of higher energy (1–2 MeV). The inverse dispersion enables one to infer that the path length from the particle source to the spacecraft is some tens of R_E (Sarafopoulos and Sarris, 1988), generally placing the source in the roughly same region that BBFs/plasmoids are generated. On one particularly spectacular day, 20 of 21 ion bursts detected exhibited inverse dispersion (Sarafopoulos and Sarris, 1988). Inverse dispersion was found in the central plasma sheet and in the boundary layer, for earthward and tailward ion streaming, during the expansion and recovery phases of substorms, and when the plasma sheet was thinning or thickening. This suggests that the ion bursts originated in roughly the same region of the midtail throughout an entire day while a sequence of substorms unfolded. The fine structure of the energetic ion bursts tells us much about their sources. The ions in the bursts typically reach very high intensities within about 10 s, while the bursts themselves decay more slowly over tens of seconds to minutes. The ions are initially highly field aligned, with anisotropies that can approach 10^5 to 1. Longer ion bursts are composed of more highly anisotropic shorter bursts which lasted a few tens of seconds and exhibit inverse velocity dispersion (Sarafopoulos and Sarris, 1988). A 300 keV proton will have a path length of about 15 R_E in 10 s, which possibly defines an upper-limit scale size of the acceleration region.

Occasionally, two spacecraft have been near the region where the particles are accelerated. In one case, IMP 6 and IMP 7, which were almost exactly lined up along the midnight meridian, observed the same five bursts of $E > 0.2$ MeV protons (Sarris et al., 1976a). Earthward fluxes were observed in the first, second, and fifth bursts, indicating the source was tailward of 33 R_E; low-energy plasma measurements on IMP 6 showed that the BBFs were in progress during these events. During the other two bursts, the anisotropies switched from earthward to tailward, and there was a 4-minute interval in which the earthward fluxes were

observed at the spacecraft closer to the earth, and tailward fluxes were observed only one earth radius further downtail, indicating that the source was less than 1 R_E in scale. In another case, four separate increases were observed at IMP 6, and only one appeared in the equivalent energy channel at IMP 7, even though the two spacecraft were only separated by 1.5 R_E in the east–west direction (Krimigis and Sarris, 1979).

The energetic ion bursts observed by IMP 8 on November 26, 1973, were among the most intense encountered during 9 years of operation of IMP 7 and 8 (Kirsch et al., 1977, 1981). The spacecraft was in an excellent position to detect westward-drifting ions, about 26 R_E downtail, and 18 R_E west of the midnight meridian. The bursts lasted 8–12 minutes in one set of events, and 30–45 minutes in another, with prominent 10–20 s substructure. All were associated with rapid reconfigurations of the magnetic field, including numerous north–south shifts that suggested proximity to an active reconnection region. Tailward-streaming electrons were found for both northward and southward magnetic field configurations. The onset of the most intense burst was marked by a 28 nT change in the north–south component in 4 s. The ions exhibited inverse velocity dispersion in this event; during this and other bursts, the electron and proton anisotropies parallel to the tail axis were oppositely directed for the order of a minute. The simultaneous presence of > 2.4 MeV alpha particles and the absence of > 2 MeV protons was consistent with an electric field capable of accelerating ions to energies of one MeV/charge. In some of the bursts, the electrons and protons both reached one MeV energies, but the electron intensities were a factor of 10–100 smaller. Despite the striking intensity of the bursts, November 26, 1973, was only moderately disturbed geomagnetically; however, each burst did occur during a brief intensification of the electrojet over a high-latitude ground station in the same local time sector as IMP 8 (Cape Chelyuskin, 71 degrees invariant latitude). This continues the pattern found earlier: Striking activity in the midtail is accompanied by activity at the poleward border of the auroral oval but not at lower latitudes.

9.12 Ion Bursts, High-Speed Flows, Boundary Layer Activations, and Bursty Reconnection

We have already encountered one occasion when a high-speed flow accompanied a burst of energetic ions. In another case, an electric field enhancement to 30–50 mV/m, signifying a high-speed plasma flow, followed the onset of a > 0.2 MeV proton burst at IMP 6 by 150 s. Assuming the electric field pulse propagated to the spacecraft at a speed of 500 km/s, the particle source was 18–20 R_E downstream of earth (Krimigis and Sarris, 1979). IMP 8 encountered an extremely interesting event on March 3, 1976 (Pavlos et al., 1989). The magnetic field, plasma density, temperature, and flow velocity had been steady for the 30 minutes before an energetic ion burst completely disrupted the quiet state of the plasma sheet. The burst onset and peak intensity point displayed inverse dispersion in a number of energy channels. A burst of relativistic electrons with normal dispersion preceded

the ion burst; the electrons streamed tailward along the field lines for 1 minute, and the ions streamed tailward for 10 minutes. The ion inverse dispersion and relative timing of electrons and ions placed the source 12 R_E earthward of the spacecraft, and 24 R_E downstream of earth. About 90 s after the electrons and ions were inferred to have reached peak acceleration at the source, a 1000 km/s tailward ion bulk flow commenced at IMP 8. The speed and delay of the flow were consistent with a source 12 R_E earthward of the spacecraft.

Williams (1981) showed that a complicated set of energetic ion bursts observed in a series of ISEE 1 encounters with the dusk-sector plasma sheet on May 3, 1978 could all be explained by the action of a single variable acceleration source tailward of the spacecraft, coupled with adiabatic bounce motion. The source was active on the ISEE flux tube for times ranging from less than one scan, < 36 s, to a few minutes. Moreover, the energetic streaming ions were always found no more than two Larmor radii (2000 km) of the plasma sheet boundary. This ties the physics of their acceleration to that of the lower-energy ion beams in the plasma sheet boundary layer, and suggests that energetic ion bursts are generated in the same events that activate the plasma sheet boundary layer.

Putting this all together, energetic ion bursts are in all likelihood generated by time-dependent reconnection in the same localized regions that create BBFs/plasmoids and activate the plasma sheet boundary layer (Sarris and Axford, 1979). The energetic particles are accelerated by an electric field with a field-aligned component, or one in a region of small magnetic field (Sarris et al., 1976a,b; Heikkila and Pellinen, 1977; Pellinen and Heikkila, 1978; Galeev, 1979; Zelenyi et al., 1984). The highest ion energies achieved in the bursts suggest that the instantaneous emf in the reconnection region reaches up to 1 or 2 MeV. Pavlos et al. (1989) estimated from ion dispersion measurements that the emf accelerating the particles in the March 3, 1976 event grew at the rate of 20 kV/s. Since the ions and electrons reach MeV energies, the reconnection events themselves last about a minute. The longer BBF and plasmoid time scale reflects how long it takes for the thermal ions and magnetic field to organize themselves into coherent flow structures on the MHD scale after a sudden reconnection event.

9.13 East–West Localization of BBF/Plasmoid/Particle Burst Generation Region

Suppose that an energetic ion burst, an activations of the plasma sheet boundary layer, a BBF, and a plasmoid are generated in the same discrete, spatially localized time-dependent reconnection event. The accelerated ions will escape the reconnection region moving both tailward and earthward along field lines. Those that escape towards the earth will reflect and return. Both tailward and earthward moving ions will drift to the west, and spread out to become nonlocal signatures of the reconnection event that generated them. The highest-energy ions spread out the fastest. The same event will activate the plasma sheet boundary layer in lower-energy, but still energetic, ions, and liberate a fast earthward flow in the central

plasma sheet. If the reconnection reaches open tail-lobe field lines, resulting in the tailward acceleration of a plasmoid, the plasma sheet boundary layer will appear to expand into the tail lobes. The boundary layer ion beams will drift westward faster than the ions in the BBF flow. If the spacecraft is west of a localized BBF, it will observe a burst of energetic ions, and possibly an expansion of the plasma sheet boundary layer, but it will encounter the low-speed flow state in the central plasma sheet. If the spacecraft is aligned with the BBF, it will encounter all three, and if it is east of the BBF, it will observe only electron signatures of the bursty reconnection event. If there is no active reconnection region nearby, the spacecraft will find the central plasma sheet in the low-speed flow state and will not find boundary layer ion beams or energetic ion bursts.

The scenario outlined may account for some highly structured events that have been observed in the plasma sheet. For example, there is the striking structuring of the plasma sheet bulk flow observed on day 110 of 1980 by Eastman et al. (1985b). On that day, ISEE 1 was close to the tail midplane near local midnight and IMP 8 was about 1.5 hours eastward in local time and 15 R_E further downtail. Although ISEE registered 3–15 keV earthward fast ion flows on four occasions, IMP 8 detected only low-speed earthward ion flows, no high-speed flow, and no boundary layer ion beams during any of the times that ISEE was seeing fast ion flows. If a localized acceleration region had been east of ISEE and west of IMP 8, only ISEE would have seen westward-drifting ions. Similar results emerged from a study of energetic ($E > 0.3$ MeV and $E > 0.2$ MeV) proton bursts observed by IMP 7 and 8 when they were roughly the same distance downtail but separated by a 10–20 R_E east–west distance from one another (Carbary and Krimigis, 1979). The two spacecraft did not always observe corresponding enhancements, and when they did, the spacecraft observing the higher fluxes detected the events first. The authors explicitly suggested that the bursts were due to "several localized sources confined to small regions of the magnetotail." Krimigis and Sarris (1979), in eloquent words, concluded that "the entire magnetotail harbors many localized acceleration regions which are prodigious producers of energetic particles observed almost everywhere within the magnetotail–magnetosheath region."

9.14 Tail Lobe Filaments

Filaments of earthward-streaming energetic plasma have been observed in the magnetotail lobes by ISEE 1 and 2 within 23 R_E distance and by IMP 7 near 30 R_E downtail (Huang et al., 1987). Approximately 60 examples were identified in the ISEE tail data from the first half of 1978. All but one were embedded in low-density tail lobe plasma at distances between 3 and 12 R_E above the expected position of the neutral sheet. The characteristic signatures of the lobe filaments were a sudden burst of ions, an increase in electron flux, and magnetic field variations indicative of field-aligned currents. The energetic electron intensities were ordinarily insufficient to determine whether all the filaments were on open or closed field lines, but some of the filaments were definitely on the closed field

lines. Simultaneous interplanetary field data, available for 16 of the events, indicated that the lobe filaments occurred during periods of both northward and southward interplanetary field. The ion bursts were observed up to energies of tens of keV, suggesting some relation to the plasma sheet boundary layer. The ion density increased in the bursts, and the overall bulk flow speed was typically several hundred km/s earthward. There was often a significant z component of velocity toward or away from the plasma sheet as well. The densest structures reached peak densities of 0.05 cm^{-3}, but many had densities below 0.001 cm^{-3}. In the 18 cases in which the O^+ density was above the threshold for detection, the densities and velocity distributions were similar to those previously reported for the plasma sheet (Peterson et al., 1981; Sharp et al., 1981), suggesting the oxygen source was the plasma sheet, and not the ionosphere, plasma mantle, or low-latitude boundary layer.

Case studies of the time evolution of the ion pitch angle distribution proved to be illuminating. In one instance, energetic ions with similar spectra were detected first at IMP 7 and then closer to earth at ISEE 1 and 2. At IMP 7, they were observed first to stream earthward, then both earthward and tailward, and finally to form an isotropic distribution, a sequence often associated with activations of the plasma sheet boundary layer. In several instances, the ions observed in the lobe had a sufficiently dense high-energy tail that the technique of "gradient sounding" (Williams, 1979a) could be used. In one case, the measured gradient was clearly parallel to the plane of the neutral sheet, with the major component along the $\pm$ Y direction; the density was first observed to decrease toward the $+Y$ direction, then no gradient was observed, and finally the density decreased along the $-Y$ direction, suggested the structure was aligned in the vertical ($X-Z$) plane and localized in the cross-tail direction.

It is possible that an ionospheric footprint of the lobe filaments may have been found. Hoffman and Evans (1968) were the first to observe bursts of low-energy electrons poleward of the peak visual auroral intensity. More recently, 29 isolated and slightly elongated patches of > 4 keV X-ray emission were found at 65–83 degree invariant latitudes by a bremsstrahlung X-ray imager on the polar-orbiting spacecraft S 81-1 (Imhof et al., 1985). The patches[1] had typical widths of 200 km. Most occurred on the nightside, but a few were found in the early afternoon hours. Their occurrence frequency averaged over all MLT for satellite paths crossing 72 degrees latitude was 2.9%. The X-ray energy spectra had 1–6 keV e-folding energies and the electron precipitation fluxes responsible for them were the order of 1 erg/cm^2 s, suggesting a plasma sheet electron source. Small isolated patches ("spikes") of > 40 keV (McDiarmid and Burrows, 1965) and > 425 keV (Brown and Stone, 1972) energetic electron precipitation at high invariant latitudes may also be signatures of localized particle acceleration regions associated with filaments.

A sheet-current model of the magnetic field data suggested that each lobe filament was bounded by a pair of field-aligned currents directed earthward and tailward whose strengths ranged between 2.1 x 10^{-10} and 4.5 x 10^{-8} A/m^2, and averaged 6.3 $\times$ 10^{-9} A/m^2 (Huang et al., 1987). The effective current sheet

thickness averaged 0.8 R_E, and ranged from 0.03 to 2.4 R_E. The average current would map into a characteristic dimension of 125 km at the ionosphere, a density of about 10^{-5} A/m^2, and a total current (in or out) of order 150 kA, though there is obviously a very wide variation. A three-dimensional, resistive, compressible MHD simulation produced in–out field-aligned currents bounding a localized reconnection region (Scholer and Otto, 1991). Cowley et al. (1992) argued that an in–out pair of field-aligned currents connects to the poleward border of the nightside auroral oval and drives the localized flow bursts in the high-latitude ionosphere that are discussed next.

9.15 Flow Bursts in the Nightside Auroral Ionosphere

EISCAT incoherent scatter radar measurements have found that the flow in the nightside auroral zone ionosphere is dominated by large bursts lasting typically 5–10 minutes (Williams et al., 1989, 1990; Cowley et al., 1992; Lewis et al., 1992). Transient distortions in flow pattern presumably associated with flow bursts have also been observed with coherent radar systems such as SABRE and STARE. STARE found one such flow perturbation to extend over 2 degrees in latitude and 5 degrees in longitude at the same time that EISCAT recorded a strong 5-minute flow burst from the same region. The few hundred kilometer scale size inferred from these measurements is consistent with the footprint areas of the field-aligned current systems in the tail lobe filaments. The ratio of maximum to minimum electric field strength in the EISCAT bursts typically exceeded three and occasionally was very much larger; typical modulation amplitudes were therefore several tens of millivolts per meter. The bursts usually enhanced the prevailing electrojet velocity, were associated with sharp peaks in Joule heating, and represented the major source of energy input into the nightside auroral atmosphere.

The ionospheric flow bursts are related to enhanced reconnection-driven convection (Lewis et al., 1992). Because the interplanetary field switches between northward and southward every few tens of minutes, and the high-latitude ionosphere responds globally to changes in the dayside reconnnection on a similar time scale, it is difficult to decide whether a given flow burst is related to a specific dayside reconnection event or to a tail reconnection event. In an attempt to avoid this ambiguity, Lewis et al. (1992) chose to compare the frequency and amplitude of the flow bursts with the Perreault–Akasofu energy coupling function for four intervals when the interplanetary field was persistently southward for at least 8 hours. In all four events, the first flow burst following the southward turning of the interplanetary field was delayed by an hour, indicating that the bursts were related to events in the tail. Either by comparing events with different average energy coupling rates, or by following the variations in that rate within a given event, it was possible to conclude that the time interval between bursts increased and decreased with the energy coupling rate. Even when the energy coupling rate was steady, the ionospheric flow was bursty. In some cases, it was possible to associate

flow bursts with Pi 2 micropulsations, but in many other cases, no association was found.

9.16 The Ionospheric Footprints of Bursty Bulk Flow Events

The large transport rates associated with bursty bulk flow events suggest they have a relatively small cross section. In the absence of multiple-spacecraft measurements, the only way to estimate the cross sections of the bursty flows is from their ionospheric footprints. However, these probably have finer spatial scales than can be resolved by the relatively sparse mesh of auroral magnetic observatories that contributes to the auroral electrojet (AE) index. The BBFs may also map to latitudes above those where the AE index provides coverage. This may be one reason why the ionospheric counterparts of bursty plasma sheet flows have usually not been found.

Sergeev et al. (1986a) found an association between minute time-scale bursts of micropulsations on the ground and high-energy particle bursts detected when IMP-J was within 2 R_E of the magnetic field reversal layer in the plasma sheet at 37 R_E distance. However, some activations observed on the ground had no counterpart in energetic particle bursts in space, suggesting that the region of high-energy particle acceleration was localized to a few earth radii across the tail. Sergeev et al. (1987) found coincidence between two structured bursts in the dawn–dusk electric field near 20 R_E downtail and micropulsation bursts, as well as an electric field burst in the plasma sheet that had no counterpart in ground micropulsation measurements. These results indicated that micropulsation bursts can be associated related to localized bursty bulk flows.

In two particular instances, transient fast flows, energetic particle bursts, and electric and magnetic field variations in the plasma sheet could be associated with "local auroral flares" in the local midnight sector (Sergeev et al., 1986c). The auroral and geomagnetic data acquired from two meridional chains of ground stations were combined with ISEE 1 and IMP 8 measurements made during two 5-hour periods of geomagnetic quiet between substorms on March 3, 1976, and March 23, 1979. Zenith photometers recorded many 3–5 minute intensifications of auroral light during the March 3 event. All-sky camera pictures showed that most of them corresponded to activations of individual discrete auroral arcs, sometimes followed by folding and/or small-scale surges. Accompanying the auroral flares were numerous intensifications of Pi 2 micropulsations recorded by at least one fluxmeter, 3/4 of which corresponded to auroral activations. Even the strongest Pi 2 bursts were barely detectable at midlatitudes; so most people would not have related the activations to substorms. IMP 8, which was within the plasma sheet during almost all 5 hours of magnetic quiet, found about 5–10 transient flow events per hour. Although most Pi 2 activations occurred within 2–4 minutes of flow bursts, the correspondence between them was neither simple nor exact nor should one have expected it to be, because the communication time between the ionosphere and plasma sheet was 2–4 minutes. What can be said is that the two

strongest plasma sheet flow bursts corresponded to the two strongest auroral activations. Similar results were obtained for the March 23, 1979 event. Eight bursts of tailward or earthward plasma sheet flow were detected on ISEE 1 during the 2.5 hour period of greatest magnetic quiet; all eight coincided with bursts of 0.3–3 Hz Pi 1 irregular micropulsation activity, and six of them had auroral intensifications recorded within 2–4 minutes at the Stertegovo ground station. The two chains of ground stations extended between 67 and 72 degrees magnetic latitude and were separated by about 40 degrees in longitude. The auroral intensifications were largely found between 67 and 70 degrees CGlat, and could often be detected at only one or two stations on a chain. The separation of the two chains defines an upper limit longitudinal scale of 40 degrees, which maps to a 5–10 R_E transverse scale in the plasma sheet.

9.17 Comparison of FTE and BBF Flux Transfers

It is illuminating to compare typical magnetic flux transfers for bursty magnetopause reconnection events, fast flows in the dayside high-latitude ionosphere, and bursty bulk flow events in the plasma sheet. The length of the "x line" on which bursty magnetopause reconnection takes place is a matter of contention; if it is 10 R_E, the peak reconnection emf is about 200 kV, and the flux transfer is of order 5×10^7 W, about 5–10% of the polar cap flux. The flux transfers based on measurements of fast ionospheric flows depend upon the correspondingly poorly resolved east–west extent of the area of newly opened flux. The estimates based on individual case studies, which fall in the range $5–10 \times 10^6$ W for circular cross sections, rise to 5×10^7 W for 5- or 10-to-1 elongations. If a bursty magnetopause reconnection event occurs once every 10 minutes, about 12–24 flux transfers will occur during the 2–4 hours it takes to convect across the polar cap; if each event transferred 5×10^7 W, bursty magnetopause reconnection could replace the open flux in the polar cap in a convection time. Is this flux consumed in bursty reconnection events in the tail?

The major unknown in evaluating BBF transport is clearly the cross section of the region of high-speed earthward flow. The fact that BBF flux densities are so large suggests they are localized. For example, while BBFs increase in frequency of occurrence with increasing AE, the BBFs found during very quiet intervals do not differ significantly from those found at more disturbed times. The fact that quiet time BBFs do not affect the already low AE index suggests that either they affect a small region in the ionosphere, or one that is not sampled efficiently by the chain of magnetometers contributing to the AE index, or both. Whether the BBF cross section changes from event to event, or with the level of geomagnetic disturbance, is even harder to ascertain at the present time. If we assume the local auroral intensifications accompanying BBFs map to the regions of high-speed plasma sheet flow, the BBFs have a transverse scale of 5–10 R_E. The estimated $\mathbf{V} \times \mathbf{B}$ in BBFs then leads to emfs of several hundred kilovolts, and a total flux transfer of $2–4 \times 10^7$ W, in each event. The dayside and nightside flux

transfers are then intriguingly close to one another. This should motivate an effort to reduce the very wide error bars associated with each estimate.

9.18 Synthesis

Brushing aside all subtle intellectual shadings for the sake of simplicity, we can distinguish two quite different flow states in the central plasma sheet. The most frequently occurring, most probable state is one of low-velocity, disorderly flow. This state is probably due to viscous driving. The second state of plasma sheet flow consists of localized high-speed flow bursts of 5–10 minutes duration, occasionally longer. They are responsible for most of the earthward magnetic flux transport in the midnight-region plasma sheet even though any one spacecraft will detect them only a few percent of the time. The state of irregular, low-speed flow appears to be responsible for circulation of plasma and energy on closed field lines, possibly half the earthward transport of plasma and energy, but a small fraction of the net earthward transport of magnetic flux. Statistical studies of the "resting state" of the cross-polar cap electric field suggest that the low-velocity plasma sheet flow state might develop a 10–20 kV emf on average, larger than is generated across the low-latitude boundary layer, which defined by the presence of magnetosheath plasma. (There are other indications that viscous transport extends inwards of the LLBL.) All in all, the process responsible for the remnant magnetic flux transport in the irregular flow state might more nearly resemble percolation than steady–state flow.

The irregular flow state can be connected with viscous convection by the following argument. The well-organized vortices occasionally observed in the plasma sheet are part of the low-velocity irregular flow ensemble. They have been found all across the plasma sheet, and they reverse polarity sharply at the midnight meridian, suggesting an origin in viscous driving at the magnetopause. The vortices have a wide range of scale sizes, making one wonder if the smaller ones are not created from the larger ones by successive bifurcations. If the system of vortices should have such a transition to chaos, the infrequent occurrence of well-organized vortices suggests that the plasma sheet is in a chaotic flow state most of the time. This argument suggests the irregular flow state is in general associated with viscous driving.

Because BBFs (and plasmoids) are relatively infrequent, the magnetic field reconfigurations associated with them are poorly reflected in empirical field models, which fit the majority of magnetic field measurements in a given volume of space, and correspond to the most probable state of the magnetic field data ensemble. The empirical models probably refer to the low-velocity, disorderly flow state even at elevated levels of geomagnetic activity. The low-speed flow state does not exhibit the "pressure balance inconsistency"; the pressure in the ensemble average low-speed flow state is roughly consistent with that in the tail lobes. Neither the ensemble average low-speed flow nor the average magnetic field represents an instantaneous flow state, and so their spatial profiles need not be

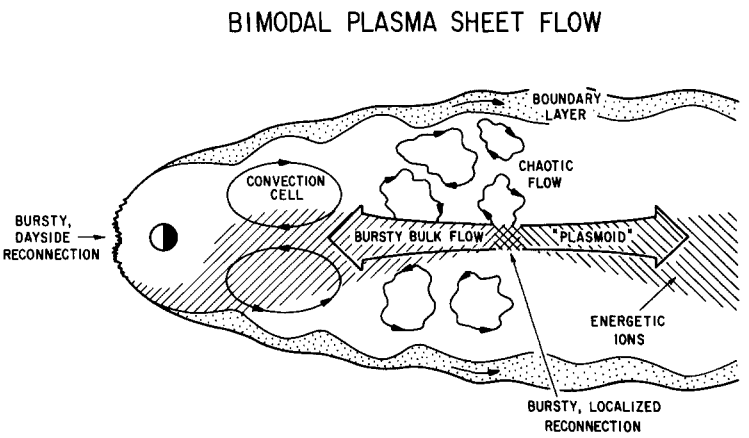

Figure 9.2. Bimodal Plasma Sheet Flow. The most frequently occurring, most probable state of plasma sheet flow is one of low-velocity, disorderly flow on closed field lines, which can be connected with viscous convection by the following speculative argument. Well-organized vortices have been found all across the plasma sheet; they reverse polarity sharply at the midnight meridian, suggesting an origin in viscous driving at the magnetopause. The vortices have a wide range of scalesizes, suggesting that the smaller ones are created from the larger ones by successive bifurcations. The infrequent occurrence of well organized vortices suggests that the plasma sheet is in the chaotic flow state most of the time (which is what we observe.) The second state of plasma sheet flow consists of infrequent localized high-speed flow bursts of 5–10 minutes duration, which are responsible for most of the earthward magnetic flux transport in the midnight-region plasma sheet. In general, fast earthward (tailward) bulk flows are associated with a northward (southward) magnetic field, and the speeds approach the Alfven speed, consistent with a reconnection source. Bursty bulk flows, plasmoids, activations of the plasma sheet boundary layer, and energetic particle bursts seem to be responses to localized events that occur most frequently in the 30–70 R_E range. The fast flows and plasmoids may be the aftermath of reconnection events that are of even shorter duration. The temporal variability of the energetic particle bursts, and the existence within bursty bulk flow events of short bursts of very high speed flow on the same time scale suggest that the reconnection events themselves last some tens of seconds to a minute. The accelerated ions stream earthward, tailward, and westward away from the reconnection region. The bursty bulk flows and plasmoids are then organized on the longer MHD time scale to transport away the magnetic flux reconfigured in one or more contiguous reconnection events. Original drawing.

those of a steady uniform flow. The high-speed flows also seem not to manifest the pressure balance inconsistency, since they are isobaric as they pass over the spacecraft. Time dependence may again be the essential ingredient, for a flux tube defined by a given cross-sectional area in the ionosphere can adjust its volume in the weak-field region of the plasma sheet so as to ensure pressure balance with the tail lobes as it moves about.

Bursty bulk flow events, plasmoids, activations of the plasma sheet boundary layer, and energetic particle bursts can be associated with one another. The durations of plasmoids are comparable with those of bursty bulk flow events.

BBFs and plasmoids both reconfigure the plasma sheet magnetic field so that B_Z and/or B_y becomes comparable to B_X. BBFs and plasmoids have similar dependences on distance downtail. Bursty bulk flows were almost entirely earthward at the AMPTE/IRM orbit within 19 R_E, a minority were tailward at ISEE 1 and 2 at 23 R_E apogee, they were mixed earthward-tailward near the IMP 6-7-8 orbits at 30–40 R_E, and predominantly tailward in the deep tail at ISEE 3. In the deep tail, the highest speed tailward fast flows were associated one for one with plasmoids. The plasmoids found on ISEE 3 were mixed earthward-tailward between 50-100 R_E, and predominantly tailward beyond 100 R_E. Both BBFs and plasmoids are often preceded by, or accompanied by, bursts of energetic ions. The energetic ion bursts are observed within a Larmor radius of the plasma sheet boundary layer, associating them with the processes that activate the lower-energy ions in the plasma sheet boundary layer. In general, fast earthward bulk flows in the central plasma sheet are associated with a northward component of magnetic field, and fast tailward flows with a southward component, and the speeds approach the Alfven speed; these features are consistent with a reconnection source. Indeed, all the arguments presented point to the conclusion that BBFs, plasmoids, activations of the plasma sheet boundary layer, and energetic particle bursts are responses to localized events which can occur at a variety of distances downtail but are the most frequent in the 30–70 R_E range. The BBFs and plasmoids appear to be the aftermath of reconnection events that are of even smaller scale. The temporal variability of the energetic particle bursts, and the existence within BBFs of short bursts of very high-speed flow on the same time scale, suggest that the reconnection events themselves last some tens of seconds to a minute. The BBF/plasmoids are then organized on the longer MHD time scale to transport away the magnetic flux reconfigured in one or more contiguous reconnection events.

In sum, magnetospheric convection appears to be almost always unsteady. The cumulative response to a series of bursty reconnection events both at the magnetopause and in the tail is superposed on an ever-present but irregular flow that one naturally associates with viscosity. To the extent that bursty bulk flow events and plasmoids are responsible for most plasma sheet magnetic flux transport, they *are* the flows visualized in the reconnection model of the magnetosphere, and they could even be the *only* flows that correspond to Dungey's model. If so, we have to reinterpret the empirical term *average position of the neutral line*. In the case of fast flows, the term means the location where it is equally probable to encounter plasmoids as BBFs. On the other hand, fossil neutral regions, spent remnants of recent reconnection events, could be carried about in the irregular viscous flow for some time after they become inactive. Thus, simple detection of a southward field in the magnetic neutral region may not signify that reconnection is active. The complex mixture of viscous and reconnection flow maps to a deceptively smooth region near the poleward border of the nightside auroral oval. The ionospheric activity stimulated there by the flow of currents along and across field lines is smoothed by the inertia of the magnetosphere–ionosphere–atmosphere coupling system; nonetheless, the occasional high-speed ionospheric flow burst and local auroral flare reveals the presence of an active

reconnection region somewhere in the tail. Indeed, localized high-speed flow bursts of 5–10 minutes duration are responsible for most of the Joule heating of the nightside ionosphere at high auroral latitudes.

NOTES

1. Other X-ray emission regions, whose shapes more nearly resembled arcs, were not included in the study.

10

CONVECTION FOR NORTHWARD INTERPLANETARY FIELD

10.1 Introductory Remarks

Besides common sense, a number of results suggest that we can learn more about the slow "viscous" flow state by studying the magnetosphere during northward interplanetary field conditions. In particular, statistical studies have consistently identified a "residual" state of magnetospheric and ionospheric convection in northward field conditions. The integrated potential across the high latitude-ionosphere does not drop below a certain resting value of about 20 kV even when the interplanetary field has been due north for several hours. There appears to be a similar residual component of geomagnetic activity that is independent of the direction of the interplanetary field (Scurry and Russell, 1991). Its correlation with the dynamic pressure of the solar wind strengthens our suspicion that it is related to viscosity. Will we be able to prove the convection in this residual state is driven by viscosity? Does the flow in northward field conditions resemble the underlying irregular flow state of the plasma sheet found at other times? Does the magnetosphere approach the teardrop configuration during prolonged intervals of northward interplanetary field? These are but a few of the questions that whet our interest in convection during northward field conditions.

One does not arrive at the state of pure viscous convection immediately after the interplanetary field swings northward. Dungey (1963) was the first of many to argue that a northward magnetosheath field line will reconnect with an open tail lobe field line to create one that is connected to the ionosphere at one end and draped over the dayside magnetopause at the other. The sudden reconfiguration of stress will lead to sunward convection on the newly reconnected field lines. In the ionosphere, this superposes a "reverse" two-cell convection pattern in the central polar cap upon the two "direct" convection cells. If and when the draped reconnected field line finds a partner in the opposite tail lobe with which to reconnect, a newly closed field line will form. Dungey had imagined that the same magnetosheath field line would reconnect simultaneously with both tail lobes, in which case the rate at which open magnetic flux is closed depends upon the rate of tail-lobe reconnection. However, it is unlikely that tail-lobe reconnection will occur simultaneously and conjugately in opposite hemispheres (Russell, 1972b).

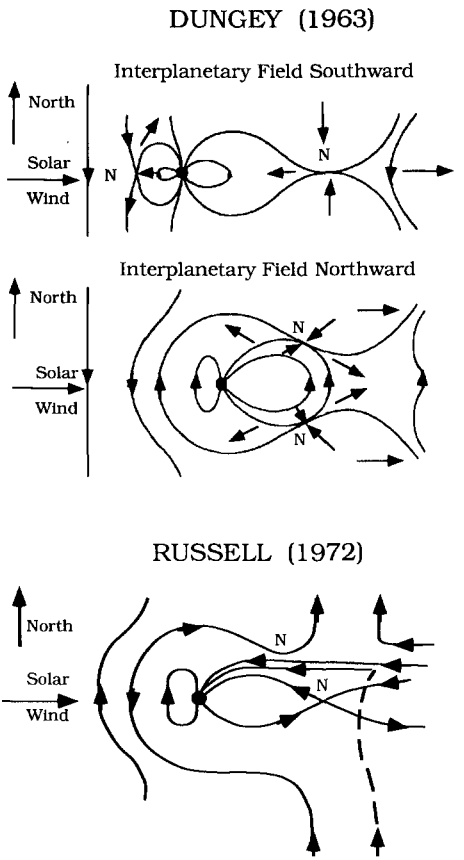

Figure 10.1. Symmetric and Asymmetric Tail-Lobe Reconnection. Dungey (1963) contrasted the reconnection model of the magnetosphere for southward and northward interplanetary field conditions (top and middle panels, respectively). For southward field, reconnection occurs at the dayside magnetopause and in the plasma sheet in the tail. In the northward field case, reconnection will occur with both tail lobes simultaneously. Later, Russell (1972b) pointed out that the conditions for symmetric northward field reconnection will rarely be met, and that reconnection is liable to occur preferentially in one tail lobe at a time (bottom panel).

Field lines without partners will circulate for at least some time within the open region of the ionosphere to which they are connected. To the extent that this occurs and tail-lobe reconnection continues, there will still be reverse convection on the open field lines of at least one polar cap, but the amount of open flux will not decrease. The duration of this reverse convection state will depend at least in part

on the rate of plasma sheet reconnection. Since it is not as persistently stimulated as it is in southward field conditions, plasma sheet reconnection will be sporadic and attenuated and may depend on such contingent factors as the variability of the solar wind in the northward field state (in truth, the situation may be even more complicated; the open field lines that manage to find partners might find the wrong partner, necessitating some "fancy footwork" before the magnetic field topology sorts itself out). At the present time, the question of how long the tail-lobe flux lasts is best approached empirically.

After the interplanetary field turns northward, the convection pattern and field-aligned currents that prevailed during the previous southward field interval decay on the 10–20 minute time scale that characterizes the convection system's response to any change in the rate of reconnection at the dayside magnetopause (Section 10.2). The polar cusp aurora migrate poleward on the same time scale, reflecting the outward expansion of the magnetopause expected in the absence of sustained southward field reconnection. However, reconnection of solar wind and terrestrial field lines does not cease; the place where it occurs simply changes. There is direct evidence for the occurrence of reconnection at the tail-lobe magnetopause (Section 10.3) as well as clear indirect signs of it at the poleward border of the polar cusp (Section 10.4). As expected, tail-lobe reconnection induces reverse, sunward convection in the center of the polar cap (Section 10.5), and a new system of field-aligned currents appears poleward of the decaying region 1 and region 2 systems to drive the sunward convection (Section 10.6). Tail-lobe reconnection turns out to occur primarily in the summer polar cap, which introduces an asymmetry between the two high-latitude ionospheres that is not present in southward field conditions (Section 10.7).

If the pattern of convection changes so dramatically when the interplanetary field swings northward, so also must the nature and distribution of the aurora. Akasofu (1985b) has given an interesting historical account of the research on polar cap arcs dating back to Mawson (1925). The location, orientation, and pattern of the high-latitude aurora differ dramatically in southward and northward interplanetary field conditions (Lassen and Danielson, 1978). When the interplanetary field is large and southward, the auroral oval is large and the polar cap is free of arcs. At the opposite extreme, when the field is large and northward, there is no clear indication of arcs in the oval, and the region that was the open polar cap during southward field intervals contains arcs that are more or less sun-aligned. These have been called "polar cap" arcs, even though much of this region maps to closed field lines during northward field intervals (Elphinstone et al., 1991). Observations that separated pairs of transpolar arcs gradually merge into one near the center of the polar cap suggest that the open flux gradually disappears if the interplanetary field remains persistently northward (Section 10.8). Evidence from several independent sources indicates that many polar cap arcs are on closed field lines, despite the unusually high latitudes at which they occur (Section 10.9). On occasion, the global convection pattern has been inferred from observations of sun-aligned aurora (Section 10.10). Measurements of the size of the region of the polar rain and of the tail magnetopause radius indicate that the tail

lobes shrink during northward interplanetary field intervals (Section 10.11). What happens as the magnetosphere becomes more nearly closed? A case study that followed the evolution of the polar cap aurora during a prolonged interval of northward field is described in Section 10.12. A statistical study isolating conditions of the most extreme geomagnetic quiet may have come close to identifying the state of pure viscous convection in the high-latitude ionosphere (Section 10.13).

10.2 Response of Pre-Existing Polar Cap Convection to Northward Field Shifts

The pattern of convection associated with southward field conditions decays after a northward shift of the interplanetary field in about the same length of time as it took to establish it in the first place. Polar cap magnetometer measurements have shown that the DP-2 system of horizontal currents associated with southward interplanetary field disappears after the field switches northward (Friis-Christensen and Wilhelm, 1975; Friis-Christensen et al., 1985). The region 1 and 2 currents that prevail during southward interplanetary field conditions may continue to flow for a time, but they will have greatly reduced amplitudes, 0.2–3 mA/m^2, and considerable small-scale structure. Ahn et al. (1987) found that the large-scale ionospheric convection pattern detected in ground-based magnetometer data responded in about 20 minutes to variations of *either* sign in the north–south component of the interplanetary magnetic field. An incoherent scatter radar study found that convection in the dayside ionosphere started to respond within minutes of a northward turning of the IMF, but that it took about 20 minutes for the ionospheric currents and flow pattern to achieve its new configuration (Clauer and Friis-Christensen 1988). Etemadi et al. (1988) and Todd et al. (1988) found that the 2–4 and 10–15 minute delay times they found for southward shifts of the magnetosheath field also applied to *reductions* in the dayside reconnection rate. In these cases, the flow speeds in the polar cusp ionosphere decayed first with a 2–3 minute time scale and ultimately with the longer 10–15 minute time scale following a northward shift of the interplanetary field. However, the responses to sharp southward and northward turnings of the interplanetary field differ in detail: A southward turning usually produced a sudden change (few tens of seconds) to a new flow state, while northward turnings led to smaller sudden changes that were followed by a slower monotonic variation (Todd et al., 1988).

Horwitz and Akasofu (1977) found that the entire polar cusp displaces poleward following a sudden northward shift of the interplanetary field. Discrete aurora brightened within minutes after steplike northward shifts in the interplanetary field reached the magnetopause, and the dayside auroral oval moved several degrees poleward 15–20 minutes thereafter. The poleward displacement of the aurora and the decay of the convection electric field both have the same time scale.

10.3 Reconnection of Interplanetary and Tail-Lobe Field Lines

There is little evidence for reconnection on the subsolar magnetopause during intervals of northward interplanetary field. Flux transfer events occur almost exclusively during southward interplanetary field conditions, and hardly any are found when there is even a small northward component (Berchem and Russell, 1984). The plasma mantle sharply decreases in thickness when the interplanetary field turns northward, possibly to disappear altogether (Sckopcke et al., 1976). In contrast, the thickness of the LLBL increases in northward interplanetary magnetic field conditions (Haerendel et al., 1978; Mitchell et al., 1987), so if anything the effects of viscosity might be more prominent.

Evidence for reverse convection was first found in ground magnetometer observations by Maezawa (1976) and in spacecraft measurements by Burke et al. (1979). Despite this and other circumstantial evidence that reconnection with tail-lobe field lines can occur (see Crooker, 1979; Reiff and Burch, 1985; Kan and Burke, 1985; Troshichev, 1990), the first direct identification of the reconnection process at work at the tail magnetopause was not reported until 1991, almost 30 years after Dungey's prediction (Gosling et al., 1991). The ISEE 2 fast plasma experiment detected accelerated magnetosheath plasma within the high-latitude dusk magnetopause layer near the terminator plane. The fast flows were found on occasions when the magnetosheath and tail-lobe fields were nearly oppositely directed; both sunward and tailward flows were encountered, and the changes in flow speed were about twice the local Alfven speed, in agreement with the predictions of reconnection theory. On those occasions when the plasma was accelerated sunward, so that the reconnection region was tailward of the spacecraft, a secondary beam of accelerated ions that presumably had reflected from the ionosphere could occasionally be found. When the reconnection region was tailward of the spacecraft, mantle plasma that had already been present on open field lines before their reconnection was mixed in with the newly accelerated flow.

The tail-lobe reconnection events reported by Gosling et al. (1991) took place at a location where the magnetosheath flow speed was comparable with the Alfven speed, and therefore comparable with the change in speed induced by reconnection. On one occasion, the accelerated flow was observed to switch from sunward to tailward, suggesting that the reconnection site was being carried tailward with the magnetosheath flow; in such a case, the polar cap convection would have been tailward rather than sunward.

10.4 Signatures of Tail-Lobe Reconnection in Polar Orbit

Ions precipitating into the polar cusp exhibit the reverse energy–latitude dispersion consistent with sunward convection during northward interplanetary field conditions. The reverse ion dispersion signature, which often goes with a rise in energy to lower latitudes to form an inverted-V-like (Reiff et al., 1977, 1980) or "butterfly" structure (Heikkila and Winningham, 1971), was originally attributed to

diffusive particle entry and not to tail-lobe reconnection. Then Burch et al. (1980) reported AE-D measurements of reverse ion dispersion together with sunward convection near the poleward boundary of the cusp during a period of northward interplanetary field. Later, Burch et al. (1986) explicitly interpreted a similar event in terms of tail-lobe reconnection. A statistical study of AUREOL 3 cusp crossings concluded that reverse ion dispersion is preferentially observed when the interplanetary magnetic field has a northward component (Escoubet and Bosqued, 1989). Finally, a *Viking* study found that accelerated ions occur with direct dispersion at the equatorward boundary of the cusp for southward interplanetary field and with reversed dispersion at the poleward boundary for northward field (Woch and Lundin, 1992). In other words, accelerated ions with the appropriate sense of energy–latitude dispersion have been found on the field lines that connect near the reconnection regions expected in both the southward and northward interplanetary field regimes.

Tail-lobe reconnection events communicate with the ionosphere via Alfven waves. The DE-2 spacecraft found an Alfven wave signature at the poleward boundary of the cusp (Basinska et al., 1992) that was essentially identical to that found at the equatorward edge of the cusp region during southward interplanetary field conditions (Maynard et al., 1991). In this event, the convection in the polar cap had been sunward before DE-2 entered the cusp. As the spacecraft crossed the poleward border of the cusp, it encountered accelerated ions with reverse dispersion and large spikelike electric and magnetic field transients. A train of almost linearly polarized, phase-shifted electric and magnetic field variations was observed for a few seconds as the spacecraft moved equatorward.

From time to time, the *Viking* uv imager found unusual, faint auroral structures that extended parallel to but poleward of the auroral oval in the noon sector. These were observed primarily during intervals of near zero or northward interplanetary field in garden hose "away" sectors (Murphree et al., 1990). Comparison with nearly simultaneous DMSP F7 particle precipitation measurements indicated that a narrow band of fairly energetic (1 keV) electron precipitation at the poleward boundary of the mantle ion precipitation created the uv emissions (Elphinstone et al., 1992b). These authors suggested that the energetic electron precipitation region was connected magnetically to a tail-lobe reconnection region. Ion precipitation cutoff precisely in the electron precipitation region, suggesting that a sunward convective flow was generated there.

10.5 Reverse Convection in the Polar Cap

Electric field measurements on balloons gave the first intimations that the high-latitude electric field can reverse direction during northward interplanetary field conditions (Mozer and Gonzales, 1973). The first description of the pattern of northward field convection came from ground magnetometer studies carried out at extremely high magnetic latitudes (Maezawa, 1976; Kuznetsov and Troshichev, 1977). Maezawa (1976) showed that a new system of horizontal currents appeared

in the polar cap ionosphere as the northward component of the interplanetary field increased. This system comprised two vortices on the dayside, whose sense corresponded to sunward convection in the center of the polar cap. Subsequently, several regression analyses of high-latitude magnetic data (Troshichev and Tsyganenko, 1978a,b, 1982; Friis-Christenson, 1979; Levitin et al., 1982; Troshichev, 1982) identified a northward field convection system consisting of two vortices of counter-rotating flow with foci at invariant latitudes exceeding 80 degrees. All in all, the most reproducible feature in observations of electric fields, horizontal ionospheric currents, and ion drifts is this band of sunward flow in the sunlit dayside high-latitude region (Burke et al., 1979; Zanetti et al., 1984; Heelis et al., 1986; Iijima and Shibaji, 1987). Even the neutral atmosphere has been observed to flow sunward from time to time (Killeen et al., 1985), indicating that the sunward plasma flow can persist for the 2–4 hours required to set the thermosphere in motion at F-region altitudes (Rasmussen and Schunk, 1987).

Superposition of two convection systems with different spatial scales and opposite electric fields will lead to a four-cell pattern. One might imagine a pair of reverse convection cells near the center of the polar cap embedded in viscous or residual southward-field cells centered at lower latitudes near 1800 and 0600 MLT. Such a pattern was derived from ground magnetic data by Horwitz and Akasofu (1979) and inferred from S3-2 spacecraft measurements (Burke et al., 1979). The four-celled pattern would be symmetric about the noon–midnight meridian for a purely northward interplanetary field, but the east–west component of the interplanetary field complicates the situation. MAGSAT observations indicated that positive (negative) B_y increases the size of the morning (evening) cell of the reverse convection component in the northern polar region and vice versa in the southern polar cap (Potemra et al., 1984; Bythrow et al., 1985). To the extent that the two lower latitude cells are due to viscosity, they might have a morning–evening asymmetry due to coupling to the vortex aurora. What is important to the argument is that there be four cells. Troshichev (1984, 1990) has sketched how a symmetric four-cell pattern might be converted to a symmetric two-cell pattern as the interplanetary field rotates in stages from purely northward to purely southward.

Despite its appealing plausibility, the four-cell pattern has not always been found. The electric field was too irregular to identify a four-cell pattern in about half the cases studied by Burke et al. (1979). Two-cell patterns in northward field conditions have emerged in some statistical studies (Friis-Christensen et al., 1985; Heppner and Maynard, 1987; Rasmussen and Schunk, 1988), and, as we will see, even more complex patterns have been observed in individual case studies.

10.6 Field-Aligned Currents

A specific system of field-aligned currents is associated with northward interplanetary field conditions. The ISIS-2 spacecraft detected magnetic perturbations due to field-aligned currents with the reverse sense of that usually observed; these were found predominantly on the morning side at high polar cap

latitudes when the interplanetary field had a strong northerly component (McDiarmid et al. 1977). Strong northerly field conditions were a necessary but not sufficient condition for the appearance of the reverse field-aligned currents. Iijima et al. (1984) characterized the northward field current system in more detail using data collected on 146 MAGSAT orbits. This system, which they named NBZ for northward B_Z, was located poleward of the region 1 current system, and had the reverse sense of the region 1 system, upward in the morning side and downward in the evening side. On occasion, the NBZ system was observed to be stable for as long as 10 hours. It is important to note that we expect to find auroral emission where the current is upward, so the NBZ system corresponds to a morning-side sun-aligned arc.

At this point, we describe a two-spacecraft case study of an intense upward field-aligned current poleward of the poleward edge of the dawnside auroral oval (Bythrow et al., 1987b). On March 25, 1986, the *Viking* and DMSP F7 spacecraft traversed the auroral oval on nearly antiparallel trajectories within 40 minutes of each other. Magnetic field measurements on *Viking*, at 0850 MLT, and DMSP, at 0630 MLT, recorded the expected large-scale upward region 2 and downward region 1 currents. In addition, both spacecraft observed a 0.5 degree band of upward current slightly poleward of the region 1 system. The current density measured on both spacecraft and projected to 800 km altitude was the same, 2.5 mA/m^2, and comparable to that of the region 1 and 2 systems at lower latitudes.

Other patterns of field-aligned currents driving reverse convection have been proposed. One, called DP-3 (Troshichev et al., 1982) or DPZ (Clauer and Friis-Christensen, 1988), places the northward field currents just poleward of the region 1 current system. Another possibility is two longitudinally extended sheets of oppositely flowing currents centered on the noon meridian, called variously region 3 (Ijima and Potemra, 1976), cusp region, or mantle currents.

10.7 Seasonal and Day–Night Asymmetries of Polar Cap Convection

Sunward convection has been observed predominantly in the summer polar cap sunward of the dawn–dusk meridian. Rasmussen and Schunk (1987) pointed out that, of the clear cases of dusk–dawn electric fields reported by Burke et al. (1979), none was in the winter hemisphere, and relatively few occurred during equinox conditions. Although Maezawa (1976) found evidence for sunward convection in the nightside polar cap, the flow was much weaker than on the dayside. Zanetti et al. (1982) found much larger field-aligned currents in the summer polar cap than in the winter polar cap on a day when the northward component of the interplanetary field was quite large (25 nT). The NBZ currents studied by Iijima et al. (1984) occurred in the sunward part of the polar cap; in the midnight part, the field-aligned currents were highly structured even when the ionosphere was still in sunlight. The small-scale structure was found over the entire region poleward of 70 degrees magnetic latitude and obscured any identifiable region 1 and region 2 current systems. A study of the magnetic and electric fields from the S3-2 and MAGSAT

data sets concluded that the transition from a regular to an irregular pattern occurred near the magnetic dawn–dusk meridian in the summer polar cap (Bythrow et al., 1985). Since, on a seasonal basis, MAGSAT's orbit remained fixed with respect to the terminator, the conductivity distribution beneath the orbit track was essentially constant from one orbit to the next, indicating that the transition to turbulent was not associated with conductivity variations. The pattern of field-aligned currents was generally irregular everywhere in the winter polar cap and tailward of the dawn–dusk meridian in the summer polar cap. However, measurements of the ionospheric Hall currents revealed a two-celled pattern or reverse convection on horizontal scales exceeding 600 km.

In short, the reverse convection in the summer polar cap undergoes a transition to turbulence near the magnetic dawn–dusk meridian, and it is always turbulent in the winter hemisphere. Bythrow et al. (1985) suggested that this is because the flow in the plasma sheet is irregular on small scales in northward interplanetary field conditions. Despite the asymmetry in morphology between the winter and summer polar caps, the net dawn–dusk potential appears to be the roughly same across both polar cap ionospheres (Reiff et al., 1981; Wygant et al., 1983; Doyle and Burke, 1983). Reverse convection is also more likely to be found in the northern (southern) summer polar cap when the interplanetary field is in an "away" (toward) sector.

Although there will be differences in convection due to the different conductivities in the sunlit (summer) and dark (winter) polar ionospheres (Burke et al., 1979), the absence of large-scale convection in the winter polar cap and the sector structure dependence appear to be better explained by the differences in reconnection efficiency in the two tail lobes (Hoffman et al., 1988). The summer end of the geomagnetic dipole is tilted more sunward than the winter end, and consequently the summer cusp connects to a region of slower magnetosheath flow, while the winter cusp connects to a region of faster flow. Large velocity shears across the magnetopause inhibit the rate of reconnection (Biernat et al., 1989), and Gosling et al. (1991) suggested that magnetopause reconnection is restricted to regions of sub-Alfvenic flow. A super-Alfvenic magnetosheath flow sweeps the reconnection region downstream and the polar cap convection is antisunward rather than sunward. The critical issue then is whether the magnetosheath and tail-lobe fields can sustain a large magnetic field shear favorable to reconnection in a region of sub-Alfvenic magnetosheath flow. The summer lobe magnetopause, being in a slower flow, is more likely to sustain reconnection, and the magnetic shear is larger for the interplanetary field sector that drapes an antiparallel field over the tail-lobe magnetopause.

10.8 Global View of Polar Cap Aurora

To a spacecraft with a view of the whole high-latitude region, the aurora is arranged in either of two closely related configurations in northward field conditions. One has been given the highly pictorial name, *horse-collar aurora* (Hones et al., 1989).

In DE 1 images, the horse-collar is a pair of bright more or less sun-aligned arcs that mark the morning and evening borders of a dark area enclosing the noon–midnight meridian. The dark area resembles the contracted, teardrop-shaped region of open field lines expected for northward interplanetary field (Elphinstone et al., 1991). Filling out the polar cap are "webs" of diffuse and weaker emission to the east and west of the horse-collar arcs. Measurements with the NOAA 7 spacecraft indicated that the webs, which looked like diffuse emissions at the resolution of the DE 1 images, actually contained numerous quasidiscrete regions of low-energy ($\lesssim 1$ keV) electron precipitation. The electron precipitation into the webs resembled that in the low-latitude boundary layer, and the webs appear to have been on field lines that map magnetically to the low-latitude boundary layers in the tail for geomagnetically quiet conditions (Elphinstone et al., 1991).

The horse collar evolves over time towards a second configuration, in which the dark area enclosing the noon–midnight meridian disappears and a single glowing band of emission extends across the polar cap and connects to the luminosity around the oval. To its discoverers, this pattern looked like the Greek letter "theta," prompting another pictorial name, *theta aurora* (Frank et al., 1982, 1986). Horse collars were observed on DE 1 more often than thetas, and more than half the thetas evolved from previously existing horse collars (Hones et al., 1989). Horse collars probably become thetas either because the the upward field-aligned current system bounding one of its sides disappears or the distance between the arcs becomes unresolvable to the high-altitude polar orbiters as the open polar cap shrinks in size, or both.

10.9 Ground-Based View of Sun-Aligned Aurora

Now we turn to the appearance of the sun-aligned aurora to the ground observer. Spacecraft imagers normally pick up large-scale diffuse luminescence, while ground-based systems detect smaller discrete structures. By combining all-sky photometer images taken at Thule and Spitsbergen, Carlson et al. (1988) showed that one sun-aligned arc observed locally at each station actually extended more than 2000 km in the noon–midnight direction and connected to the poleward border of the auroral oval near 2300 MLT. This arc had the same general shape as a theta aurora but was not luminous enough to have been detectable by a spacecraft like DE 1. A more intense band of diffuse luminescence with distinct borders that was observed over Vostok station, Antarctica, for over 3 hours would have been a detectable theta aurora, but there was no confirming observation from above (Troshichev et al., 1988). A number of discrete forms and patches were immersed within the diffuse band defining the putative theta. According to Gusev and Troshichev (1986), discrete polar caps arcs are generally superposed on a more diffuse background that has a thetalike configuration. Two discrete arcs detected from above by DMSP F1 (Ismail and Meng, 1982) agreed in position and orientation with arcs imaged from Vostok Station, and, in one case, the network of sun-aligned arcs formed a distinct transpolar band (Gusev and Troshichev, 1990).

Recent observations with sensitive all-sky imaging photometers have shown that sun-aligned arcs occur about 50% of the time in northward interplanetary field conditions (Carlson et al., 1988; Carlson, 1990). Some subvisual arcs can be rather short, while others may extend over much of the polar cap. At visual brightness levels, single, double, or multiple arcs may extend along the noon–midnight meridian or along the morning or evening boundaries of the polar cap (Berkey et al., 1976; Ismail et al., 1977; Lassen and Danielson, 1978; Yahnin and Sergeev, 1979, 1981; Gussenhoven, 1982; Ismail and Meng, 1982; Gusev and Troshichev, 1986; Troshichev et al., 1988; Troshichev, 1990). Sometimes they stretch completely across the center of the polar cap. Their location and their number depends on the sign of the B_y component of the interplanetary field (Ismail and Meng, 1982). Sun-aligned arcs could be observed at Vostok station, Antarctica, in both the morning and sectors for either sign of B_y, but the ratio of the number in the morning sector to the number in the evening sector dropped from 1.7 to 0.3 as B_y switched from positive to negative (Troshichev et al., 1988).

It takes three times as long to establish sun-aligned arcs following a northward shift of the interplanetary field than it does to disestablish them following a southward shift. Of 89 sun-aligned arcs observed from Vostok station at times when simultaneous interplanetary field data were available, 15 appeared after a well-defined northward turning and 17 disappeared after a clear southward turning (Troshichev et al., 1988). The delay times were quite different in the two cases. The sun-aligned arcs appeared 55 minutes after a northward turning on average, and could persist thereafter for hours provided the interplanetary field remained generally northward. The sun-aligned arcs disappeared on a 20 minute time scale following southward turnings. Recall that other statistical studies of the magnetosphere's response to changes in the direction of the interplanetary field find the same two time scales.

10.10 Evidence that Some Transpolar Arcs Are on Closed Field Lines

Spacecraft images and particle distribution measurements indicate that some polar cap arcs are on closed field lines despite the very high latitudes at which they are found. Transpolar arcs have been found at plausibly conjugate locations in the two polar caps at the same time (Akasofu and Tsurutani, 1984; Gorney et al., 1986; Mizera and Evans, 1986; Mizera et al., 1987; Obara et al., 1988). In one specific case, DE 1 and *Viking* imaged sun-aligned arcs that were aligned parallel to one another on opposite sides of the magnetic pole in the two polar caps, and exhibited simultaneous motions in the opposite dawn–dusk directions (Craven and Frank, 1991). The arcs were rotated slightly counterclockwise as viewed from above the North Pole.

Several independent properties of the particle distributions above sun-aligned aurora are consistent with closed field lines (Troshichev, 1990). Polar rain electron precipitation, one of the most persuasive diagnostics of open field lines in

the polar caps, is very hard to find during northward interplanetary field conditions (Riehl and Hardy, 1986). The electron energy spectrum above the polar cap aurora is roughly the same as that in the plasma sheet, and similar to that at the poleward edge of the auroral oval (Murphree et al., 1983; Peterson and Shelley, 1984; Frank et al., 1986; Gorney et al., 1986). The pitch-angle distributions of the precipitating electrons are consistent with closed field lines (Eliasson et al., 1987). The electron differential flux distributions associated with sun-aligned arcs is similar in opposite hemispheres (Mizera et al., 1987). Finally, the 1–10 keV H^+, He^{2+}, and O^+ ion composition on field lines connecting to polar cap arcs is similar to the plasma sheet's (Hoffman et al., 1985b; Frank et al., 1986; Gorney et al., 1986). It is important to remember that without simultaneous images, it is difficult to know whether a particular measurement of precipitating particles corresponds to the bar of the theta aurora, the borders of the horse collar, or to the web aurora.

10.11 Relation between Sun-Aligned Arcs and Convection

The association between sun-aligned arcs, field-aligned currents, electron precipitation, and convection appears to be the same as it is for any other arc. Accelerated electrons, of the energies required to produce the observed auroral emissions, are generally associated with negative electric field divergence when they precipitate into the polar cap (Burch et al., 1979), and the upward field-aligned current resulting from the field divergence is typically carried by the downgoing precipitating electron fluxes (Burke et al., 1982). Thus, we expect the sun-aligned arcs to mark the regions of velocity shear and upward field-aligned current in the overall convection pattern.

Carlson et al. (1988) inferred a global pattern of convection from the pattern of the sun-aligned aurora by combining all-sky imaging photometry with DE 2 plasma drift and particle data. Their fast, wide-angle photometer could image the sky at 630.0 and 427.8 nm wavelengths every 30 seconds; its field of view at the 250 km altitude of maximum auroral light production was 1200 km. The photometer's wide dynamic range encompassed not only bright visual features produced by $E > 1$ keV precipitating electrons, but also subvisual features produced by < 500 eV electrons with energy fluxes as low as 0.01 ergs/cm^2 s. Using this system, Carlson et al. (1988) obtained simultaneous ground images for two DE 2 passes over the winter polar cap on January 21, 1982. The first pass occurred just after the interplanetary field had turned weakly southward following more than 6 hours of northward field. The all-sky images showed that structured sun-aligned aurora had been present for at least 20 minutes before DE 2 passed over the field of view of the photometer. The spacecraft recorded four increases in electron precipitation, of which two were intense enough to cause the two arcs observed from the ground at the time of DE 2's passage overhead. (To make this comparison, DE 2's position was mapped along field lines from 750 km altitude to the 250 km altitude of strongest 630.0 nm emission.) The ion drifts were quite irregular near the precipitation structures, but were sheared in such a way that the

electric field divergence was negative across all four. The negative divergence implied upward field-aligned current. The ionospheric conductance, the 630.0 nm emission intensity, and the field-aligned current magnitude computed from the electron precipitation spectrum and electric field divergence for the most intense arc were consistent with each other and observation. The component of flow velocity parallel to this arc changed by 400 m/s across its 160 km thickness. The all-sky images enabled an overall convection pattern to be inferred from the measured potential distribution along the spacecraft track with some assurance, because one could assume the flow to be relatively uniform along the arcs. What emerged was a large cell on the dawn-side containing either three elongated cells that all circulated in the same counterclockwise sense as the dawn-side viscous convection cell. (Another possibility was that the dawn-side cell contained three elongated fingers.) The arcs and associated upward field-aligned currents marked the boundaries of the cells or fingers.

Ten orbits and 14.5 hours later, the interplanetary field was very strong and northward (16 nT). At this time, the all-sky photometer imaged a pair of discrete sun-aligned arcs that were displaced 12–15 degrees west of the noon–midnight meridian. These arcs were a few hundred kilometers thick in the dawn–dusk direction, and more than a thousand kilometers long in the noon–midnight direction. Once again, the arcs imaged on the ground could be identified with discrete precipitation features measured on DE 2. The associated ion drift was highly structured, but overall corresponded to negative electric field divergence and upward field-aligned current. The arcs did not clearly separate regions of sunward and antisunward convection as they did in the previous case, but were embedded in a region of larger-scale sunward convection that was highly structured on 100 km scales perpendicular to the flow. The spacecraft encountered two brief reversals to antisunward flow near the region where the two arcs were observed on the ground.

Transpolar arcs are found embedded in a variety of larger flow configurations. Frank et al. (1986) concluded that convection is sunward over polar cap arcs and antisunward outside them. The second event of Carlson et al. (1988) occurred in a structured region of generally sunward flow. Izraelovich et al. (1988) and Mende et al. (1988) found transpolar arcs in regions of antisunward and sunward flow alike. By comparing all-sky camera photographs with magnetic variation data obtained from a meridional chain of stations in Antarctica, Gusev and Troshichev (1990) concluded that discrete arcs aligned like the transpolar bar of the theta aurora are in regions of sunward convection, whereas those in the evening or morning limbs of the theta form were in regions of antisunward convection. Carlson et al. (1984, 1988) found arcs that marked the borders between oppositely directed flows.

The common feature in the observations may be the presence of structure in the flow. As we have seen, the structure becomes so pronounced in the winter hemisphere that the recognition of a large-scale convection pattern can be rendered impossible (Heppner, 1977; Heelis and Hanson, 1980). The corresponding structure in the field-aligned currents led Bythrow et al. (1985) to suggest that plasma sheet convection may be irregular and/or turbulent in northward

interplanetary field conditions. If the uniformity of the emission along sun-aligned arcs implies uniform arc electrodynamics, the irregular flow component may consist at least in part of elongated fingerlike cells conforming to the elongated optical arcs. The stability of the optical arcs then suggests that these cells are persistent.

10.12 Shrinkage of Tail Lobes in Northward Field Conditions

A statistical study of the boundary between polar rain and auroral precipitation suggested that the open part of the polar cap shrinks to a small region above 80 degrees MLAT in northward field conditions (Makita and Meng, 1983). The open polar cap disappeared almost completely during specially chosen intervals of the most extreme geomagnetic quiet (Hoffman et al., 1988). It was difficult to find intervals even as short as one minute in which there was no structured LLBL-like electron precipitation in DE 2 data. This implied that the radius of the polar cap was less than five degrees. The structured electron precipitation extended over both polar caps independent of season, suggesting that both tail lobes had disappeared.

The measurements cited suggest that the magnetic flux and area of the tail lobes progressively diminish during prolonged northward field intervals. This seems to be the case. Using the entire ISEE 3 deep tail data set, Fairfield (1992) determined the relative frequencies of observation of the magnetosheath and magnetotail in the region of space downstream of earth where the tail would be expected. These percentages were compared with the expected frequency of occurrence of a tail-lobe of a given radius, given typical variations in the direction of the solar wind flow. On this basis, the average radius of the tail-lobe at 200 R_E distance came out to be 24 R_E. The tail lobes were seen less frequently during quiet conditions (AE <150 nT), suggesting that their radius might be smaller at such times. In addition, the solar magnetospheric B_Z component in the distant plasma sheet averaged +0.6 nT during the quiet interval, and was effectively zero for AE > 150 nT. This suggested that when the polar cap shrinks, some field lines that previously formed the tail lobes closed across the equatorial plane earthward of 200 R_E. Most striking of all, the likelihood of seeing the magnetosheath near the center of the tail was as high as 30%, suggesting that all the field lines closed within the orbit of ISEE 3 in these cases.

10.13 Evolution of Polar Cap Aurora during a Prolonged Northward Field Interval

A series of interlocking spacecraft studies provided unusually complete information about the evolution of the polar cap aurora during a 36-hour period of strong northward interplanetary field on January 10-11, 1983 (Akasofu and Tsurutani, 1984; Gorney et al., 1986; Izraelevich et al., 1988). The auroral oval imaged from DMSP F6 began to contract after the interplanetary field turned northward at ISEE

3 in the magnetosheath upstream of earth. For the first 1.5 hours after the northward turning, auroral activity was concentrated in the morning sector auroral oval, which became significantly thicker than in the evening sector. During this time, surgelike structures were observed near the midnight meridian. Later, as the interplanetary field rotated into an even more northerly direction, the oval luminosity diminished and discrete sun-aligned arcs appeared in the polar cap. At least 15 arcs could be counted at one point, 17 hours into the event. Eight hours after that, a broad, diffuse, transpolar arc resembling a theta aurora was observed. Measurements of electron and ion fluxes made onboard DMSP, NOAA6, and NOAA7 showed that the plasma above the transpolar arc was similar to that in the morning sector of the auroral oval, suggesting that they both had the same source. Accelerated 1 keV electrons were observed at both boundaries of the transpolar arc. The transpolar arc precipitation structures were detected in both polar caps. Auroral emissions and the local electric and magnetic fields were measured by the Intercosmos-Bulgaria 1300 spacecraft. The intensity of 732.0 nm singly ionized oxygen emission from the transpolar arc reached several kR. A pattern comprising six large-scale field-aligned current sheets and three convection cells remained structurally stable for over 12 hours. In addition, smaller-scale downward currents were found at the edges of the polar cap arcs, with upward currents within arcs. Arcs were situated in regions of both sunward and antisunward convection.

10.14 Polar Cap Convection in Conditions of the Most Extreme Geomagnetic Quiet

A northward component of the interplanetary magnetic field may suppress flux transfer events on the subsolar magnetopause, but it does not by itself guarantee an inactive magnetosphere or a quiescent polar cap. Just what criterion to use to define exceptionally quiet conditions has not been settled in the literature. Should one use low (Burrows et al., 1984) or exceptionally low (Meng, 1981) values of the planetary magnetic index, Kp? Should one use low values of AE ? If so, should one choose an upper limit, AE < 120 nT (Carbary and Meng, 1986), or perhaps one even lower, AE < 80 nT (Rich and Gussenhoven, 1987)? Does AE adequately reflect geomagnetic activity at high geomagnetic latitudes? Is knowledge of the northward interplanetary field component 2 hours beforehand (Heelis et al., 1986) adequate? Should not one really take into account both the north–south and east–west components of the interplanetary field (Heppner and Maynard, 1987)?

To identify exceptionally quiet periods, Hoffman et al. (1988) supplemented the traditional AE index with magnetometer measurements from very high-latitude ground stations and with images of the northern polar cap made by DE 2. In the course of the study, it became abundantly clear that AE could not be used to identify the quietest periods. A total of 82 cases were found for which no horizontal field variations exceeding 35 nT occurred at any of the larger set of ground stations in the 2 hours preceding the spacecraft pass. Images were available from 34 of these passes, of which four were eliminated because they showed slight

auroral brightenings. Of the passes without images, 46 with < 20 nT magnetic variations were retained, leaving a total of 76 to be studied, of which perhaps 10% still contained some activity, despite the most stringent precautions. Data on the interplanetary magnetic field were available for 56 of the 76 passes. The field had a northward component, and there was a strong bias towards a positive B_X (toward the sun) for this set of superquiet time intervals.

What is the picture of convection that emerges from rigorous exclusion of the traditional signatures of activity? First of all, the large-scale region 1 and region 2 current systems, which had been detected in residual form in other studies of northward interplanetary field conditions, disappeared for all practical purposes. Field-aligned currents were not absent, however, but were much more smaller scale and were distributed throughout the polar cap and auroral oval regions without any pattern being particularly obvious. Structured electron precipitation extended all across both polar cap regions, presumably corresponding to the small-scale field-aligned current structures. Finally, this study made particularly clear what had already been concluded from earlier work. Definite convection patterns were inferred in 60% of the passes, but nearly all of these were over the summer polar cap. It was difficult to find any order at all in data from the winter polar cap, where disordered small-scale structure dominated the observations.

10.15 Discussion

Reverse convection is expected if reconnection with the interplanetary field takes place with tail-lobe field lines. Signatures of tail-lobe reconnection have been found at the magnetopause and at the poleward boundary of the polar cusp. Two reverse convection cells will be superposed on the background of a larger-scale pattern of direct convection, leading to four cells in all. There is no evidence that the integrated polar cap potential in this convection state reverses sign, indicating that sunward convection does not dominate overall. The "background" direct convection can arise in several different ways. First, viscous coupling should not disappear and conceivably might intensify. Second, while direct convection driven by dayside reconnection decays after the interplanetary field shifts from southward to northward, it could still be significant at the time an observation is made. Moreover, the open polar cap region containing sunward convection shrinks as time passes after a northward shift. Finally, high-latitude convection is often highly structured with multiple small-scale convection reversals, especially in the nightside portion of the summer polar cap and in the winter polar cap during northward interplanetary field. With all this, it is not surprising that different studies have reached different conclusions, perhaps because their data ensembles differed in subtle ways. No consensus pattern of polar cap convection has emerged, other than that reverse convection is frequently observed in the center of the summer polar cap. Perhaps no simple scheme will emerge, because the flow appears to be intrinsically irregular.

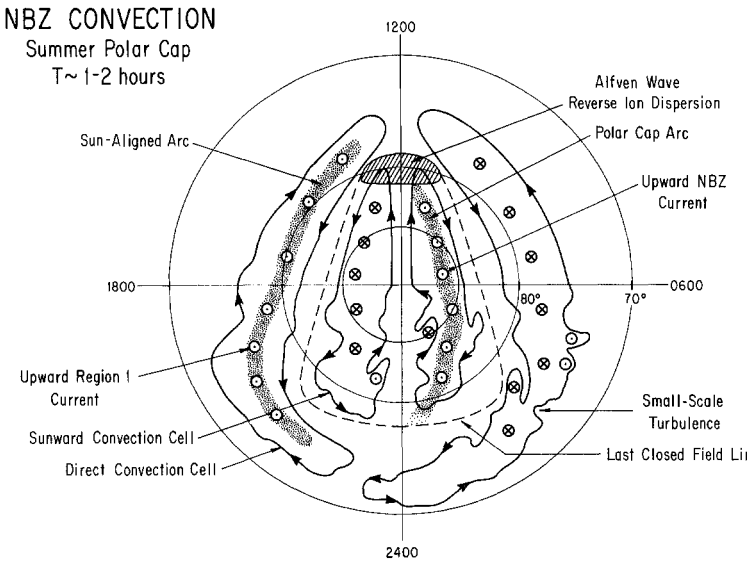

Figure 10.2. Polar Cap Convection Following a Northward Shift of the Interplanetary Magnetic Field. The pre-existing pattern of polar cap convection that prevailed for southward field conditions decays on a 10–20 minute time scale following the northward shift. After about an hour, sun-aligned arcs make their appearance, and a pattern of reverse convection associated with tail lobe reconnection develops in the summer polar cap (shown here). When tail lobe reconnection is active, ions with reversed dispersion and impulsive Alfven waves are observed from polar orbit at the poleward edge of the dayside cusp region. Two reverse convection cells on open field lines are added to direct convection cells at lower latitudes, making four cells in all; more complex patterns are also observed. The reverse cells correspond to a system of field-aligned currents of the opposite sense of the usual region 1 system. The aurora will be brightest in regions of upward field-aligned current, so that one expects two broad sun-aligned arcs when there are four convection cells. This is the "horse collar" pattern that is often observed from high-altitude polar orbiters. The flow is more irregular on the night side than on the day side, and the arc pattern could be more structured than is drawn. As time passes and the region of open flux shrinks, the reverse convection cells and associated aurora become less prominent, and the horse collar evolves into the "theta" aurora. Original drawing.

What is clear is that the open flux in the tail lobes gradually diminishes following a northward shift of the interplanetary field, due to the action of tail-lobe reconnection and a complex and unclear sequence of events that follows it. Over the course of several to many hours, the large-scale polar cap aurora coalesce into a single broad band of luminosity that extends from noon to midnight—the bar of the "theta" aurora. The theta formation time varies considerably from event to event. Several independent lines of evidence indicate that the theta aurora may be on closed field lines; the coalescence then suggests that the magnetosphere becomes

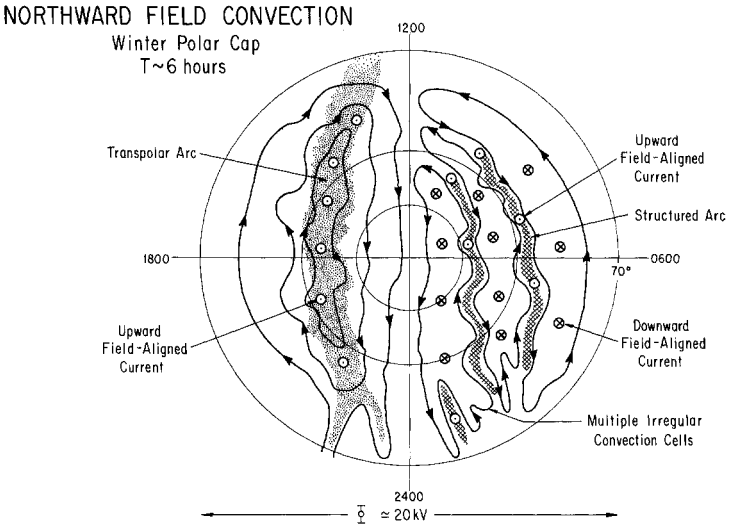

Figure 10.3. High Latitude Convection After Many Hours of Northward Interplanetary Field. After the interplanetary field has been mostly northward for six hours, or more, the integrated potential across the polar cap settles down to a "resting level" of about 20 kV. The resting potential seems to be the same in the winter and summer polar caps, and the convection flow appears to be highly spatially structured in both. This structure emerges more more clearly in studies of the winter polar cap where the reverse convection state is weak, and it is the winter polar cap we characterize here. The morning and evening sides are drawn differently to show different possibilities. On the morning side, we show a direct convection cell that trifurcated into three smaller cells (there could have been more); small-scale and structured sun-aligned aurora appear in the regions of sheared flow where the local field-aligned currents are upward. Structured arcs could also develop where a given cell develops "fingers" of strongly sheared flow. On the evening side, we show a viscous convection cell that migrated to high magnetic latitudes as the region of open magnetic flux shrank almost to zero area. As a consequence, the region 1 upward current also migrated to high latitudes, where it created a large-scale transpolar arc. This arc is the bar of the theta aurora. All traces of the second bar of the horse-collar configuration in the summer polar cap disappeared as the large-scale NBZ current system associated with tail-lobe reconnection gradually died out. We do not expect any observations to have the configuration shown in the figure, whose purpose is to illustrate some of the scenarios in the contemporary literature. Original drawing.

progressively more closed as the period of northward interplanetary field continues. The open field-line regions containing polar rain gradually shrink in both polar caps. The tail lobes are closed within 200 R_E distance about 30% of the time when AE is less than 150 nT. All this seems to be saying that the magnetosphere evolves toward the teardrop configuration.

During intervals of low geomagnetic activity, the plasma in the magnetosphere is predominantly of solar origin (Lennartsson and Shelley, 1986); so solar wind plasma finds a way to enter the teardrop. In fact, solar wind ions (H^+ and He^{2+}) are the most numerous of all during periods of extreme quiet. Their density is about a factor of 2 higher in the flanks of the plasma sheet than in the center (Lennartsson and Shelley, 1986), consistent with a particle source at the magnetopause. Not surprisingly, they are the least energetic at quiet times; the energies per nucleon of the ions of solar origin in the plasma sheet progressively approach values typical of the solar wind as AE approaches zero, indicating that they are not energized significantly upon entering the magnetosphere. A low-energy electron layer bounding the plasma sheet boundary layer similar to that found by Parks et al. (1984, 1992) has been reported in PROGNOZ-8 observations during northward interplanetary field conditions (Zwolakowska et al., 1992). The boundary layer had a high content of doubly ionized helium, indicative of a solar wind origin, and practically no ionized oxygen. These authors noted that the electron temperature and density were similar to those in the LLBL, though the observations were made in the center of the tail.

Magnetic flux still circulates as the magnetosphere approaches the teardrop state. The cross-polar cap potential declines progressively and approaches the resting level of 20 kV identified in statistical studies after about 6 hours of northward field (Wygant et al., 1983). Despite the difference in the intermediate state convection pattern between the winter and summer polar caps, there is no evidence that the resting potentials across the two polar caps differ significantly in the final residual state. This state may correspond the best to the pure viscous state originally envisioned by Axford and Hines (1961). Thus the magnetosphere approaches not the ideal teardrop, but one in which, among other things, the tail is lengthened and structured by viscosity. The circulation of plasma and magnetic field appears not to be laminar even at the quietest of times. The flow in the winter polar cap is consistently turbulent and irregular on small scales at the times of the most extreme geomagnetic quiet. The precise relation between the irregular ionospheric flow in prolonged northward field conditions and the underlying irregular flow in the plasma sheet at other times is unclear. What is clear is that the conditions in the winter polar cap during times of extreme geomagnetic quiet should be used to define the sensitivity, spatial resolution, temporal resolution, and the array of instruments that we should use to diagnose the ionosphere's response to the irregular component of convection during quiet and disturbed times alike.

11

THE NIGHTSIDE AURORAL OVAL

11.1 Introductory Remarks

The basic structure of the auroral oval was pieced together from relatively local magnetometer measurements and all-sky photographs taken on the ground. The all-sky cameras picked out relatively intense features whose intensities exceeded roughly one kilorayleigh. Their fields of view had a 500–1000 km radius at auroral altitudes, and so extended over 5–10 degrees of latitude and about 90 minutes of local time. Had the aurora been stationary and time-independent, this would have been enough, and it was enough to spot the existence of substorms. It was not enough to solve the substorm problem. As the instruments to study auroral phenomena grew in sophistication and comprehensiveness, so also did our understanding of the concept of the auroral oval. This chapter is dedicated to communicating some of this modern understanding as a prelude to the discussion of substorms in the next chapter.

Ground instruments can follow the time development of events within their fields of view but have difficulty separating changes in space and time on scales longer than an hour of universal time or local time, because the observing station rotates with the earth to a local time sector where the aurora may differ. This difficulty can be offset to some extent by airplane flights that remain at a constant local time. However, the real breakthrough came with auroral imaging from space. In the 1970s, optical wavelength imaging from low-altitude polar orbit provided snapshots of the aurora over several thousand kilometer scale portions of the oval on each polar pass of the spacecraft (Shepherd et al., 1973; Anger et al., 1973; Lui and Anger, 1973; Pike and Whalen, 1974; Snyder and Akasofu, 1974). And the spacecraft could detect the precipitating particles responsible for the auroral light emitted from the magnetic footprint of the field lines along its path. The results from the first generation of auroral imaging experiments have been summarized in excellent reviews (Akasofu, 1974, 1976; Hultquist, 1974; Burch, 1979). Ultraviolet imaging allows one to see the dayside aurora. Almost continuous imaging of the entire oval in the ultraviolet is now possible from high-altitude polar orbiters such as Dynamics Explorer 1 (Frank et al., 1982), *Viking* (May, 1990, *J. Geophys. Res.)* and EXOS-D (Ejiri et al., 1992). The *Viking* imaging systems were primarily sensitive to the light produced by the precipitation of 0.5–5 keV electrons; precipitation data from the DMSP F7 and HILAT

spacecraft in low polar orbit indicated that *Viking* images could be used to infer the instantaneous distribution of electron energy deposition over the oval with about 50% accuracy (Steele et al., 1992). Global images from high polar orbit now can document the development of a substorm around the entire auroral oval, from dayside activation to onset, expansion and recovery (Craven et al., 1983; Craven and Frank, 1985; Elphinstone et al., 1992).

As we go from ground-based to low-earth orbit to high polar orbit, spatial and temporal coverage increases while spatial resolution decreases. The basic temporal resolution of 45–50 minutes set by the half-periods of spacecraft in low earth orbit is insufficient to follow the development of substorms, a difficulty overcome in high-polar orbit at the cost of spatial resolution. Spacecraft observations give incomparably better spatial coverage, while ground-based optical measurements still provide superior spatial, spectral, and temporal resolution (Shepherd et al., 1990). At the extremes of spatial resolution, ground-based television systems can resolve auroral arc structure down to tens of meters, while resolutions of 100 km are achievable from high-polar orbit. The DE 1 spacecraft returned images that typically had been integrated for 6 minutes, so that moving auroral structures were blurred. *Viking* completed images that resolved 50–100 km structures in about a second, and returned them to ground from 3000–13,500 km altitude every 20–60 seconds. EXOS-D returned an image with tens of kilometer resolution every 8 seconds from an altitude of 2500–4800 km.

The differing views from space and the ground emphasized different phenomena and often led to different perceptions about what is important. Understanding the relationship between space and ground measurements was one of the key objectives of the *Viking* program. During the *Viking* mission in 1986 a large number of ground-based instruments monitored the high-latitude ionosphere over northern Scandinavia. A cross-shaped array of magnetometers (Luhr et al., 1984) and two bistatic coherent Doppler radars (Neilsen, 1982; Neilsen et al., 1983) recorded the two-dimensional ionospheric currents and convection flow. Riometer, all-sky camera, and photometer networks monitored auroral particle precipitation and optical emissions. The EISCAT radar, the world's only tristatic incoherent scatter radar facility, with fully steerable UHF antenna systems in Tromso, Kiruna, and Sodankyla, probed several ionospheric plasma parameters simultaneously from below 90 km to above 400 km altitude, between 64 and 76 degrees north geographical latitude, and from 5 to 35 degrees east longitude (Folkestad et al., 1983). EISCAT measured the ionospheric electron density, electron temperature, ion temperature, and, at times, neutral wind profiles for most of the *Viking* passes over Scandinavia (Opgenoorth et al., 1989; Opgenoorth and Kirkwood, 1989).

The very idea of the auroral oval stimulated a wish to "map" auroral events and structures along field lines into the magnetosphere (Section 11.2). Naively, one would have expected that the open field lines of an oval-shaped polar cap would map straightforwardly into the tail lobes, that the convection region on closed field lines would map into an enclosing auroral oval, and that the system would grow and shrink without changing its center or shape as the level of geomagnetic activity varied. This simple view, which was such a useful guide in

the early days of magnetospheric research, is misleading today. It has been replaced by a realization that the shape of the "oval" depends upon the direction of the interplanetary magnetic field (Section 11.3). A striking variation of the size and shape of the open field line region in the high latitude ionosphere is found in recent empirical magnetic field models that fit large magnetospheric data sets at various levels of geomagnetic activity. The auroral "oval" is only an oval during active periods, and closes down to a "horse-collar" shape at quiet times. Unfortunately, the magnetic field maps are inherently inaccurate just where we would wish most for good information. The mapping of the high-latitude nightside auroral oval into the plasma sheet is singular in a reconnection magnetosphere (Section 11.4).

By far most of the electron energy precipitating into the auroral oval is invested in an ever-present, usually subvisual diffuse auroral glow. The diffuse aurora is usually below the roughly 1 kR threshold of detectability in ground-based all-sky photographs, except when diffuse aurora is found equatorward of a westward-traveling surge following substorm onset. However, the diffuse aurora is the most prevalent and encompassing auroral feature when it is viewed with higher sensitivity from above from by spacecraft (Jorjio, 1959; Lui et al., 1973). Then it can be found enclosing a darker polar cap at all local times (Anger et al., 1973; Lui and Anger, 1973); so the notion of a diffuse auroral oval seems a reasonable one (Section 11.5).

While diffuse electron precipitation dominates the auroral oval's integrated light production, it does not produce the 10–100 erg/cm^2 s energy flux densities needed for the brightest auroral forms. Albert (1967) and Evans (1968) found that the large energy fluxes were carried by down-going quasimonoenergetic electron beams that are superimposed on a diffuse auroral electron background (Westerlund, 1969). Evans (1968) suggested the beam electrons were accelerated by a field-aligned potential difference. Injun 5 measurements from low-altitude polar orbit revealed that the peak electron energy characteristically rose and fell as the spacecraft moved across the auroral oval. Representing such data visually on an energy–time spectrogram produced a striking false-color image in the form of an upside down letter "V" (Frank and Ackerson, 1971). The colloquial name used to identify these structures has stuck, and although it is possible to wish for a more physically illuminating or indeed, more dignified, name, the term *Inverted-V* is in universal use in the magnetospheric research community. Inverted Vs will be the subject of Section 11.6.

Auroral arcs are thin, often folded, ribbons of light that extend more or less in the east–west direction. They are highly distinctive, and artistically and scientifically inclined ground-based observers pay special attention to them. The classic extended arcs have been studied largely but not exclusively in the local evening to midnight sector of the auroral oval, while other discrete structures that are found in the postmidnight sector have been given less attention. The distribution of discrete auroral structures provided the first empirical definition of the auroral oval, probably the one most frequently employed in casual conversation today. The motion of premidnight arcs provided the first diagnostic of an

impending substorm, and the intensification of the most equatorward one defined the substorm onset. The basic properties of arcs will be the subject of Section 11.7.

Only by the mid-1980s had the gradual accumulation of individual case studies of arc structure and electrodynamics finally forced the recognition that not all arcs are the same (Marklund, 1984). However, the differences in at least their large-scale properties can be understood in terms of their positions in the pattern of convection in the auroral oval (Timofeev et al., 1987). It is not our purpose to review the developing understanding of arc physics, but the relationship between arc properties, field-aligned currents, and convection is central to the main theme of this essay and will be the focus of Sections 11.8–11.11. The relationship between inverted Vs and the smaller-scale arcs below them is taken up in Section 11.12.

The hope that monitoring the poleward boundary of the auroral oval would indicate the waxing and waning of the the magnetic flux in the tail lobes is almost as old as the concept of the oval itself. The advent of space missions designed to make this measurement has forced us to face questions about important details. Which diagnostics best locate the separatrix between open and closed field lines, and how reliably do they do so? To what extent is the last closed field line an emitter of auroral light; if it is not, how far away is the nearest detectable arc; does this arc keep the same distance from the separatrix? Will the efforts to answer questions like these be repaid with a diagnostic of interesting events in the distant magnetotail, such as plasmoid formation and ejection? The poleward boundary of the auroral oval has now been identified in a number of different diagnostics, and the issue of distinguishing it from the more equatorward aurora has risen in importance (Section 11.13–11.15). In Section 11.13, we discuss a remarkable pair of radar observations of most poleward arc systems at local evening and midnight. In Section 11.14, we discuss some evidence that links the poleward border of the auroral oval with the plasma sheet boundary layer. The so-called *auroral kilometric radiation*, which is often used to time substorm onset, seems to be generated by poleward auroral arcs (Section 11.15).

The bottom-line question is how the structures in the nightside auroral oval map into the plasma sheet. The connections between the diffuse auroral oval, the oval of discrete aurora, the oval of inverted Vs, and the structure of the plasma sheet are matters of active inquiry revolving around several subordinate but no less important questions. Two will have been answered earlier. What is the relationship between the auroral light generated at low altitude and the inverted Vs at high altitude? How do auroral arcs map to inverted-V altitudes? Section 11.16 concentrates on the relationships between the diffuse auroral electrons, inverted Vs, and, within the plasma sheet, the boundary layer, and low-energy electron layer. Section 11.17 turns to a related set of issues. Are all auroral arcs conjugate between hemispheres, or are some related to the plasma sheet boundary layer and need not display strict conjugacy? Ultimately, we would like to know when the most poleward auroral forms display conjugacy and when they do not.

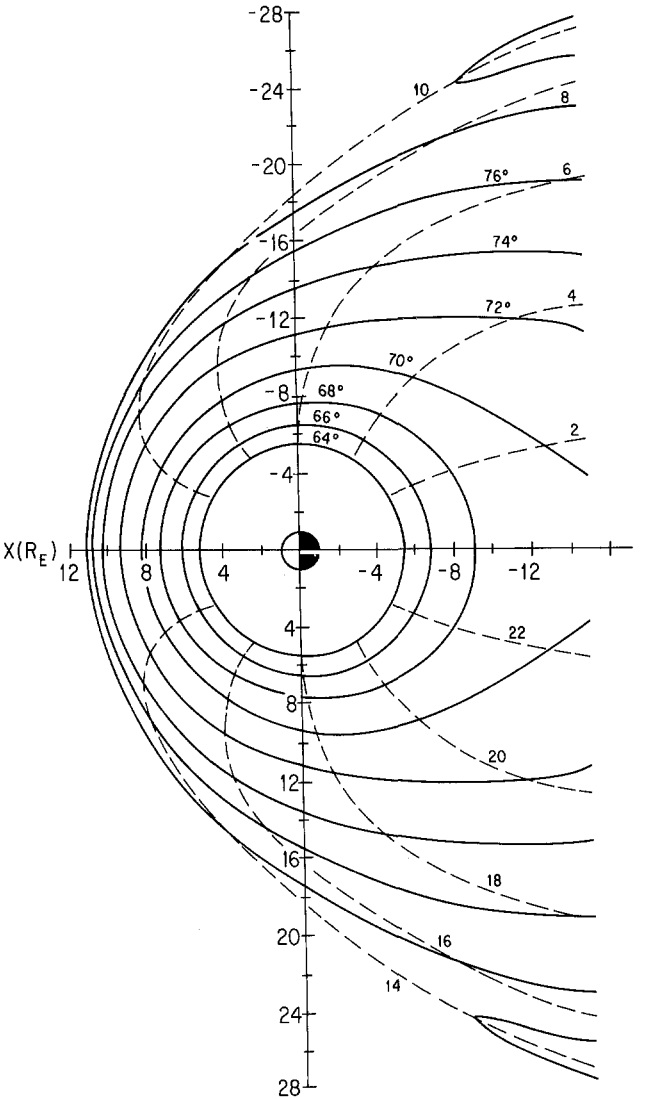
-28
-24
-20
-16
-12
-8
-4
4
8
12
16
20
24
28
X(R_E)
12
8
4
-4
-8
-12
10
8
76°
6
74°
72°
4
70°
68°
66°
64°
2
22
20
18
16
14

11.2 Magnetic Field Mapping

Two fundamental properties of magnetic fields make mapping feasible. First, the magnetic field vector is divergence free, so it is in principle possible to define where a field line threading the auroral ionosphere actually goes at all times. Thus, if all the pertinent currents were known, one could construct maps of the magnetic field itself. At present, the best we can do is determine from satellite observation roughly what the currents are on average. This approach to mapping has been recently reviewed by Tsyganenko (1990). The notion that the magnetic field orders plasma behavior is the second main conceptual tool used in practical attempts to map. Liouville's theorem assures us that the particle phase space density is conserved along particle trajectories in a collisionless plasma. This, together with the fact that magnetic fields guide the helical trajectories of single particles, suggests that measurements of particle distributions can be fingerprints of field lines. This notion leads naturally to the related idea that magnetic field lines define topological boundaries separating regions containing plasma of differing properties and dynamics. The separation of the polar regions into a polar cap and auroral oval is the oldest and most important application of this entirely natural mode of reasoning. By comparing particle distributions over the aurora with those in space, we sometimes can conclude that our measurements are made on the same field line, but more often we are only able to identify regions of space with one another. We tend therefore to associate identifiable "landmarks"—structures and boundaries—with one another. Herein lies a difficulty: Honest people can disagree about what landmarks are important and what diagnostic signatures define them.

Much progress has been made in creating quantitative magnetic field models that are constrained by large data sets acquired by many spacecraft (Russell and Brody, 1967; Mead and Fairfield, 1975; Fairfield and Mead, 1975; Tsyganenko and Usmanov, 1982; Tsyganenko, 1987, 1990). To date, the largest data set has been used in the model of Tsyganenko (1987): 36,386 magnetic field measurements

Figure 11.1 Mapping the High Latitude Ionosphere into the Magnetosphere. Shown here is part of Fairfield's (1991) map of the high-latitude ionosphere into the magnetic equatorial plane. The solid lines represent circles of constant magnetic latitude in the ionosphere, while the dashed lines are lines of constant magnetic local time. Several features are worth noting. Almost the entire dayside magnetopause maps into the 1000–1400 MLT sector of the ionosphere near 78 degrees latitude; the 0600–1000 MLT and 1400–1800 MLT regions above 76–78 degrees latitude map plausibly into the low latitude ionosphere; the geosynchronous substorm region to be discussed in Chapter 13 maps between 65 and 69 degrees latitude between about 2000 and 0400 MLT. The reader should exercise great caution in applying this, or any other map, to specific observations; we are interested here only in its qualitative properties. The map depends upon dipole tilt and therefore has a diurnal and seasonal variation, and it depends upon the level of geomagnetic activity. All maps that fit average magnetic field data are better adapted to the low speed, irregular flow state of the plasma sheet, rather than to the high speed, high transport flow state. Finally, the maps do not take into account the localized current systems in the geosynchronous region that develop in the substorm growth and expansion phases. D.H. Fairfield, *J. Geophys. Res.*, *96*, 1491 (1991), copyright by the American Geophysical Union.

acquired onboard seven IMP spacecraft throughout the magnetosphere and cislunar magnetotail, together with data acquired up to the magnetopause over the poles by the HEOS 1 and 2 spacecraft. Current systems for the tail, magnetopause, and ring current were superposed and their parameters chosen to fit these data as a function of universal time, season, and six different levels of geomagnetic activity as parametrized by the Kp index. Presumably, the small-Kp model describes intervals when the interplanetary field is statistically northward, and the large-Kp model, to periods when the interplanetary field is strong and southward.

Of course, the Tsyganenko (1987) model is not perfect. Fairfield (1991) used an independent data set consisting of 22,000 magnetic field vectors averaged over 0.5 R_E regions to evaluate the models of Tsyganenko and Usmanov (1982) and Tsyganenko (1987). Fairfield judged the 1987 model generally superior, and while the agreement was generally good, he suggested areas for future improvement, particularly for three regions critical to this review, the tail, ring current, and the polar cusps. Stern (1990) adjusted the Tsyganenko (1987) model to include a warped current sheet, which improved correspondence with the data. Fairfield (1991) voiced suspicions about whether Kp uniquely characterizes the geomagnetically active magnetosphere; clearly sorting the data according to the properties of the interplanetary field would be a significant improvement. Field-aligned currents distort the magnetic field mapping. Typical current strengths displace nightside auroral oval field lines by as much as a half-hour in local time (Kauffmann and Larson, 1989) and shift the polar cusps by 2.5 degrees in latitude (Tsyganenko, 1990). Although some effects of field currents are obviously included in the average data used to construct the magnetic field models, field-aligned currents respond sensitively and locally to changes in the convection state, and one would like to include more exact characterization of the field-aligned currents in the next generation of field models.

In closing this section, we must emphasize that data-based models essentially characterize the most probable magnetic field configuration in a data ensemble, and do not represent accurately the relatively infrequently occurring bursty reconnection/BBF/plasmoid state that may be responsible for a large fraction of the transport of magnetic flux. The empirical magnetic field models correspond primarily to the state of low-velocity irregular flow in the plasma sheet—loosely speaking, to viscous convection. Nonetheless, this criticism does not mute our admiration for the steady progress made in magnetic cartography. From now on, each stage in the development of empirical models will be mined for new qualitative insights. The next stage will be to sort the magnetic field observations according to the dynamical state of the convective flow.

11.3 Dependence of the Auroral "Oval" upon Geomagnetic Activity

The ability to map the magnetosphere into the ionosphere depends not only on knowing the magnetic field in space but also upon knowing the magnetic field near

the earth to high accuracy. By combining Tsyganenko's (1987) empirical magnetic field model (T87) with an accurate model for the internal field of the earth (Wallis et al., 1982), Elphinstone et al. (1991) calculated where ionospheric field lines at the altitude of maximum auroral light production, 120 km, map into the magnetosphere for various Kp and tilt of the earth's dipole axis. They found that the T87 auroral oval is not alway an oval. Its polar cap has the shape of a pear with its broad end on the nightside at low Kp. The shape of the open field line region for low geomagnetic activity is similar to that deduced by Lassen et al. (1988) from ground measurements of high-latitude arcs, and corresponds to *Viking* measurements. The pear shape progressively broadens to the familiar oval in the models with increasing levels of geomagnetic activity. The dayside polar cusp, which is just equatorward of the narrow end of the pear-shaped polar cap, moves about 5 degrees equatorward as Kp increases from 0 to 5, while the boundary between open and closed field lines near magnetic midnight appears not to depend on Kp, in agreement with earlier conclusions reached by Feldstein (1966). A detail important to understanding data: Variations in dipole tilt also change the shape of the oval, so that the mapping has a significant universal time and seasonal dependence.

The auroral oval defined by auroral arc and other observations maps to the nightside of the magnetosphere for nearly all local times in the T87 model (Elphinstone et al., 1991), except for the true cusp region around magnetic noon, which maps into the dayside magnetopause (Stasiewicz, 1991). Much more of the high-latitude dayside ionosphere actually connects to closed field lines on the nightside than had been suspected when the concept of the oval was first proposed. Beyond 1 hour MLT away from local noon, what had once been thought to be open field lines at higher latitudes actually mapped on closed field lines to the flanks of the tail, and therefore are related to the low-latitude boundary layer; they are LLBL component of the auroral oval. The size of the T87 LLBL region, the region that maps into the flanks of the tail, was largest for small Kp. On the basis of this result, Elphinstone et al. (1991) suggested that the "polar cap" arcs observed during periods of northward interplanetary field (corresponding to low Kp) actually connect on closed field lines to the low-latitude boundary layer in the flanks of the tail.

11.4 Inherent Uncertainty in Mapping the Poleward Aurora

Even if we knew the strength and location of all current systems, and even if we knew how they varied in time, there would still come a point where mapping from the ionosphere into the magnetosphere will be inherently inaccurate. All mappings of the ionosphere into a reconnecting magnetosphere are singular at the last closed field line. Within a degree or two equatorward of the boundary between open and closed field lines on the nightside, two points near one other in magnetic latitude will map to points far from one another in the plasma sheet. Thus measurements with finite spatial resolution prescribe increasingly uncertain mappings, the closer

they are made to the last closed field line (Akasofu et al., 1974). We could estimate the inaccuracy if we knew where the last closed field line is. Usually, we do not know its position with any great precision; so it is hard to judge how accurate the mapping of a high latitude aurora is. In effect, activity in the poleward aurora tells us that something is happening in the plasma sheet, but models cannot tell us where the plasma sheet activity is located.

The singularity in auroral mapping has subtly influenced the psychology of the magnetospheric research community. A large area near the equatorward edge of the auroral oval, where the most spectacular visual display in the auroral substorm occurs, maps to a relatively small flux tube volume connecting to the inner edge of the plasma sheet on the nightside, while the rest of the huge plasma sheet containing much of the energy of the magnetosphere maps to a thin region at the poleward edge of the oval. No wonder the "ground-based" and "space-based" magnetospheric communities sometimes have difficulty convincing each other about what is important.

11.5 The Diffuse Aurora

Discrete aurora, so eye-catching, are superimposed on the much less impressive but energetically much more important diffuse aurora. Most of the integral auroral luminosity at any given time is emitted in the diffuse background (Jorjio, 1959), and most of the plasma sheet electron energy flux is precipitated into the diffuse aurora all along the oval (Whalen, 1983). The total energy contribution from the diffuse precipitation of auroral electrons dominates the contribution of discrete aurora in all phases of a substorm (Ponomarev, 1981). Feldstein and Starkov (1971) estimated that the total power supplied by electron precipitation to the auroral oval ranged from about 10^{17} to 10^{18} ergs/s from the lowest to the highest levels of geomagnetic activity; the precipitation energy flux density ranged from 0.45 to 1.4 ergs/cm^2 s on the dayside and from 1.4 to 7 ergs/cm^2 s on the nightside. A statistical model of the distribution of precipitating electron energy fluxes in latitude and local time as a function of the AE index compiled from many thousands of orbits of the AE-C and AE-D low-altitude polar orbiting spacecraft quantitatively articulated this general picture (Spiro et al., 1982). More recent estimates based on observations made in the Defense Meteorological Satellite Program (DMSP) indicate the electron energy flux precipitated into one hemisphere increases from 8.1×10^{16} ergs/s for Kp = 1 to 7.8×10^{17} ergs/s for Kp = 6 (Hardy et al., 1985, 1989).

The electrons responsible for the diffuse auroral light are essentially isotropic in pitch angle and have energies in the range 0.1 to perhaps 10 keV, comparable with the electron thermal energies typically measured in the plasma sheet. If the pitch angle distribution is isotropic, the distribution function measured at low altitudes over the aurora will be identical to that measured simultaneously in deep space on the same field line. The equatorward portions of the diffuse auroral oval connect to quasidipolar field lines where models of the geomagnetic field are

sufficiently accurate to make it possible to guess when two spacecraft will be on essentially the same field line, and test whether the two distribution functions are indeed identical. Meng et al. (1979) and Schumaker et al. (1989) found that the measured distributions over the aurora and in space were so alike that comparing them was better than using the existing geomagnetic field models to decide when the two spacecraft were on the same field line.

The equatorward edge of the diffuse auroral luminosity near local midnight appears to map magnetically into the inner edge of the electron plasma sheet (Kennel, 1969; Vasyliunas, 1969). Newell and Meng (1987) investigated the dependences of the magnetic latitude cutoffs of auroral precipitation as a function of energy, local time, and magnetic activity. During times of moderate magnetic activity, the midnight sector equatorward precipitation edges for both electrons and ions with energies between 100 and 3000 eV were ordered by energy. The lower the energy, the further equatorward the precipitation edge. By comparing approximately simultaneous DE 1 measurements at low altitudes and DE 2 measurements at high altitudes, Horwitz et al. (1986) found that the equatorward edge of the diffuse aurora and inner boundary of the plasma sheet agreed well with each other for 100 eV, 1 keV, and 10 keV electrons in the dusk to midnight sector.

11.6 Inverted Vs

Characteristic electron precipitation structures in which the energy of maximum precipitation flux rises to a peak and then falls are frequently encountered as polar-orbiting spacecraft cross the auroral oval. The energy at the peak is in the 1–10 keV range. Because of the way these precipitation events looked on an energy–time data display, their discoverers called them *inverted Vs* (Frank and Ackerson, 1971). Inverted Vs are found predominantly in the poleward portion of the evening and early morning auroral oval; they occurred most frequently in the 2000–0200 MLT sector in a sample of 430 inverted Vs identified in 0.2–25 keV electron data acquired on Atmospheric Explorer-D (Lin and Hoffman, 1982). They are long and thin: The mean latitudinal width of the inverted Vs in the AE-D ensemble was about 0.5 degrees, or about 50 km.

Inverted Vs are associated one to one with upward field-aligned currents, and Sugiura et al. (1984) and Hoffman et al. (1985a) concluded from simultaneous magnetometer and electron precipitation measurements that the inverted-V electrons were the charge carriers of the upward currents. Experiments onboard the S3-3 spacecraft, which measured the electric field vector and the distributions of energetic electrons and ions accelerated by the field (Mozer et al., 1979; Cattell, 1982), established that 1–100 mV/m electric fields parallel to the magnetic field at altitudes exceeding several thousand kilometers above the auroral oval accelerate the inverted-V electrons downward (Mozer et al., 1980). Upward ion beams occurred together with downgoing inverted-V electrons, and both were found only in regions of upward field-aligned current (Cattell et al., 1979; Cattell, 1983). The more energetic the ion beam, the larger and more energetic was the electron flux.

The normalized probability of occurrence of upward fluxes of > 500 eV ions of ionospheric origin, most in the form of beams, had a rather sharp threshold at about 4000 km altitude, increased to a peak at 7000 km, and then fell off somewhat toward the 8000 km apogee of S3-3 (Ghielmetti et al., 1978). Typical potential drops inferred from particle measurements were in the range 1–10 kV.

A simple collisionless plasma model predicts the relationship between the upward parallel current and the parallel potential drop for a drifting Maxwellian electron distribution in a diverging mirror-type magnetic field (Knight, 1973). In this model, the field-aligned current density is approximately linearly proportional to the total potential over a wide range of parameters. The measured field-aligned conductance proved to be in the range 0.1–1 nanomho/m^2 from rocket measurements (Lyons et al., 1979) and about a factor ten larger from Dynamics Explorer 1 (DE 1) measurements at higher altitudes (Weimer et al., 1987). Coordinated DE1/DE2 measurements found that the conductance varied considerably, but its mean value was in the range 0.5–2.2 nanomho/m^2 (Lu et al., 1991). The Knight relationship is not valid for downward currents, and the measured potential drops are very small in this case (Cattell et al., 1979; Cattell, 1983). The Knight relationship is based on the highly illustrative but not always realistic assumption of a purely electrostatic field, so that the large spread in inferred conductance is not unexpected.

A *pair* of upward and downward field-aligned current sheets was associated with every intense inverted-V structure observed on AUREOL-3 (Timofeev et al., 1985, 1988; Timofeev and Galperin, 1992). The upward field-aligned current sheet left the ionosphere within the limits of the inverted-V precipitation region, while the downward return current was equatorward of the inverted V in the evening sector, and poleward of it in the morning sector. The current sheets were not necessarily symmetric. At low altitudes, the charge carriers of the downward currents are cold ionospheric electrons with a small drift parallel to the magnetic field. Above 1000 km altitude, the downward currents are carried by field-aligned beams of electrons that are accelerated to tens of eV energies. At DE 1 altitudes, such low-energy electron beams were found any time the magnetometer detected downward currents exceeding 10^{-8} A/m^2 (Burch et al., 1983; Menietti and Burch, 1987; Marshall et al., 1988).

An enhanced perpendicular electric field accompanied the inverted Vs detected by the polar-orbiting spacecraft, AE-C (Heelis et al., 1981). The meridional field rose to a peak of several tens of mV/m and then declined over a north–south distance of about 100 km. The field was directed poleward, and its peak was equatorward of the inverted V in the evening sector. The configuration was precisely opposite in the morning sector. Thus the region of enhanced electric field seems to bear the same relationship to the inverted V as the downward return current. Timofeev and Galperin (1992) emphasized that this relationship between transverse electric field, field-aligned current, and electron precipitation has also been found in ground-based optical and radar measurements of arcs in the middle and equatorward portions of the auroral oval (Timofeev et al., 1985, 1987, 1988, 1991).

11.7 Auroral Arcs

In this section, we will be concerned with the relationship of the discrete aurora to the convection and polarization electric fields in their vicinity; in the following sections, we will take up the relationship between the discrete aurora and the general patterns of convection and field-aligned currents in the auroral oval ionosphere. We must distinguish between the stable or homogeneous arcs whose lifetimes are of order 1000 s and with much more active rayed forms (Timofeev and Galperin, 1992). The discussion in this section will concentrate on homogeneous arcs.

The auroral arcs viewed by high-resolution ground-based imaging systems are much thinner than inverted Vs. Up to now, arc thicknesses have not really been well characterized, and the published values have been determined as much as anything by the spatial resolution of the measurement technique. The best measurements have been image orthicon video observations by Maggs and Davis (1968), who found transverse arc thicknesses ranging from 4 km down to the 70 m resolution of their instrument. However, the most probable thickness in their ensemble of measurements was their 70 m threshold. No other measurements of arc thickness seem to have been published until 1991, when an imaging system with 2.4 m resolution did find auroral curtains with thicknesses less than 70 m, although 100 m was typical (Borovsky et al., 1991). The thinnest arc seen without image processing was 40 m. The spatial gradients in the fluxes of precipitating electrons on the edges of the arcs had scale lengths close to the 9–22 m theoretical limit set by multiple Coulomb scattering of the electrons by the neutral molecules in the upper atmosphere.

A hierarchy of north–south spatial scales is associated with the aurora and the auroral oval (Borovsky, 1991). Among these are the 100 m thicknesses of individual arcs, the few kilometer thickness of multiple arc systems, the 10 km thickness of the region of enhanced diffuse glow surrounding arcs, the 10–100 km thicknesses of the inverted Vs above the auroral ionosphere, the 100 km separation between arc or multiple arc systems, and the 1000 km thickness of the nightside auroral oval. The perpendicular electric field in the auroral oval ionosphere has a similar hierarchy of scales (Timofeev et al., 1987; Timofeev and Galperin, 1992), ranging from the large-scale convection electric field to the part of the inverted V field (Heelis et al., 1981) that maps to low altitude, to the more local electric field associated with the arc itself (Marklund et al., 1982; Ziesolleck et al., 1983). The general convection field is a few mV/m in magnitude, while inverted V and arc-associated fields range from 10 to 100 mV/m.

Not all arcs are the same. Marklund (1984) found it useful to characterize arcs by the way the transverse component of electric field varies across their short dimension. An elementary consideration of current continuity across the discontinuities in the Hall and Pedersen conductances induced by the electron precipitation suggests there could be a continuum of arc structures. The possible electric field profiles range between extremes where the field is created dominantly by polarization effects and where the field is determined by the upward field-

aligned current flowing in the arc. Localized and intense field-aligned currents associated with structured aurora have been detected by ground-based magnetometer chains (Baumjohann et. al., 1981; Bosinger et. al., 1981) and by incoherent scatter radar (de la Beaujardiere et al., 1977; Theile and Wilhelm, 1980). A survey of rocket measurements, which have enough time resolution to measure the details of arc structure, indicated that a variety of structures do indeed occur (Marklund, 1984). The most common, in a small sample, appeared to be of the "anticorrelation" type, where either a northward or southward ambient electric field decreased in magnitude within the arc, but did not reverse sign; there was one counterexample where field magnitude actually increased. There were also cases in which the transverse electric field component reversed sign one, two, or three times in the neighborhood of the visual arc. Those arcs in which the field reverses can be confused with the Harang discontinuity, which we will discuss shortly.

If the number of observed arc structures is large, there is an even larger number of arc theories: a survey of the literature by Borovsky (1991) listed 22 different arc models. Our focus here is not on our rudimentary understanding of arc structure but on two issues related to the central themes of this essay. First, what does it mean to say that substorm onset takes place on an arc? We will discuss this question at the appropriate moment; in the meantime, we venture a few remarks concerning the second issue, the relationship between convection, field-aligned currents, and arc structure and occurrence.

11.8 Diffuse and Discrete Aurora and their Relationship to Field-Aligned Currents

Kamide and Rostoker (1977) found that during substorms the boundaries of the intense (>2 kR) auroral emissions that could be observed in DMSP pictures coincided with the boundaries of field-aligned currents defined by Triad magnetometer data taken at 800 km altitude. Triad magnetic field data were again used to define the poleward and equatorward boundaries of field-aligned currents in the premidnight sector when the entire profile of auroral luminosity along the same meridian could be scanned by another polar-orbiting spacecraft, Isis 2, whose photometer was more sensitive (Kamide et al., 1979). Six cases were found in which nearly coincident data were available; for two events in which the passes through the auroral oval were coincident within 20 minutes, the relationship between the field-aligned currents and the auroral luminosity proved to be especially clear. The latitudinal boundaries of the major portion of the field-aligned currents lined up very well with the auroral luminosity boundaries at both the poleward and equatorward edges of the oval. The boundary between upward and downward current occurred at a minimum in the auroral luminosity profiles. Poleward of the minimum, the current was upward, and the aurora was discrete in character with an intensity of 1–2 kR; in the equatorward region of downward current, the aurora was diffuse and of lower intensity, 0.5–1 kR.

11.9 Arc Occurrence and the Interplanetary Field

Since field-aligned currents are a response to changing magnetospheric conditions, arcs involve field-aligned currents, and arc electrodynamics is related to auroral oval convection, it is no surprise that arc occurrence is related statistically to the direction of the interplanetary magnetic field. In the dusk sector of the auroral oval, the focus of the discussion in this chapter, there is only diffuse aurora and there are no arcs when the interplanetary magnetic field has positive y and z components; isolated discrete forms are superposed on the diffuse aurora when B_y is negative and $B_Z$positive. The archetypical long oval-aligned arcs occur primarily when the interplanetary field is southward (Murphree et al., 1981).

11.10 The Harang Discontinuity

It has been known for almost 40 years that the nightside aurora change where convection reverses its direction in the premidnight auroral oval (Heppner, 1954). The directions of ionospheric convection and its associated Hall current flow should theoretically reverse at the midnight line of symmetry dividing the two convection cells in the auroral ionosphere. This is not what happens. The eastward and westward auroral electrojets flow *into one another* along an inclined cut across the evening-to midnight auroral oval (Harang, 1946). At the conference dedicated to Harang's seventieth birthday in 1971, Heppner (1972a) proposed that the regions into which the electrojets flow be named the *Harang discontinuity* after its discoverer. This name has lasted. To a local ground observer, the Harang discontinuity seems to extend east–west, but in fact its latitude in average data gradually decreases from near the polar cap boundary at 1800 MLT to the center of the discrete auroral oval near 2330 MLT. Homogeneous quiet arcs are typically but not always found westward (equatorward) of it, while active rayed forms, pulsating aurora, and diffuse aurora more often occur to the eastern, poleward side (Heppner, 1972). The overall auroral luminosity tends to be brightest just to the morning side of the discontinuity (Maynard, 1974).

The Harang discontinuity had been originally defined as the line across which the magnetic perturbation due to the auroral electrojets switched from northward to southward as the earth's eastward rotation carried the observer underneath it, but Davis (1962) had found that the motion of auroral forms was westward to the western and equatorward side, and eastward to the eastern and poleward side of the magnetic discontinuity, thereby indicating that the electric field also changed sign. A study of barium cloud motions supported this suggestion (Westcott et al., 1969). The position of the electric field reversal determined from OGO 6 data corresponded closely to the position of the discontinuity defined magnetically, both statistically and on a case-by-case basis (Maynard, 1974). Two-dimensional spatial maps with 15 km resolution made by the STARE coherent scatter radar showed that the electric field vector rotated in a counterclockwise manner from northward to westward to southward on passing northward through

the Harang discontinuity in the northern hemisphere (Neilsen and Greenwald, 1979). Inside the "discontinuity" the westward electric field was less than 15 mV/m, so that irregularities detectable by coherent backscatter could not be generated, whereas the field was above threshold on either side. The discontinuity, defined as the region free of irregularities, was about 100–200 km thick. The eastward ionospheric electron flow was more irregular on the poleward side of the discontinuity than was the westward flow on its equatorward side.

Direct measurements of the electric field (Cauffman and Gurnett, 1972; Banks et al., 1973; Banks and Doupnik, 1975; Wedde et al., 1977; Horwitz et al., 1978) showed that the electric field discontinuity is displaced perhaps 2 degrees poleward of the magnetic field discontinuity (Kamide and Vickrey, 1983), in part because the location of the magnetic discontinuity on the ground is influenced by the strong field-aligned current that has to flow upward out of the electric field discontinuity (Kunkel et al., 1986). The signature of the Harang discontinuity in the data acquired by the *Triad* polar orbiter was a region of upward current bordered to the north and south by downward currents (Iijima and Potemra, 1978). The Harang discontinuity has been pictured as a region where the type 1 and type 2 current systems overlap in the 2200–2400 MLT sector. In one pass of *Triad* through this system of currents, the STARE radar observed the counterstreaming electron drift pattern characteristic of the Harang discontinuity (Greenwald et al., 1980). The radar auroral irregularities occurred mainly in the regions of downward field-aligned current, and/or of larger closure Pedersen current. The maximum Joule heating occurred in the radar aurora, and model estimates indicated the peak heating rates were 2–4 mW/m^2.

11.11 The Relationship between Arcs and Ionospheric Convection

Timofeev et al. (1987) articulated a systematic relationship between the electrodynamic structure of a stable arc and its position relative to the Harang discontinuity. To understand this relationship, it is first necessary to distinguish the visual arc itself from the "radar" arc associated with it. The enhanced ionization created by the extremely large electron precipitation energy flux density in the thin visual arc often so increases the ionospheric conductivity that the electric field can be effectively reduced to zero in the arc (Marklund, 1984). Thus, a coherent scatter radar will not ordinarily find any moving irregularities in the visual arc. On the other hand, a radar arc is often found near the visual arc. The radar arc is a meridional band of enhanced Hall current caused primarily by the presence of an enhanced arc-associated electric field whose scale seems always to be about 1 degree, or 100 km, in both morning and evening sectors of the auroral oval, and for quiet and disturbed arcs. The electric field in the radar arc region exceeds the 15–30 mV/m threshold for the production of irregularities, and has essentially the same orientation as the general convection field on two sides of the Harang discontinuity, northward in the evening and southward in the morning, corresponding to eastward Hall current in the evening and westward in the morning.

Not all visual arcs have a detectable radar companion, but when they do, the radar and visual arcs have essentially the same orientation and appear, brighten, and move in harmony, and therefore should be considered part of the same electrodynamical system. The visual and radar arcs are regions of upward and downward field-aligned currents, respectively. A survey of eight stable auroral arcs in the literature indicated that the magnitude of the upward field-aligned current in the arc corresponded closely to the ionospheric (mostly) Pedersen current that enters the visual arc from the radar arc region (Timofeev and Galperin, 1992). Timofeev et al. (1987) found that the electrodynamic work done in the radar arc was positive everywhere and could exceed the energy input into the accompanying visual arc by as much as an order of magnitude. They concluded that the generator of the overall arc circuit was in the magnetosphere.

The radar and visual arcs bear opposite relationships to one another on either side of the Harang discontinuity (Timofeev et al., 1987). A study of 41 nightside auroral arcs observed over the Kola Peninsula and Scandinavia between 66 and 72 degrees north geomagnetic, using all-sky cameras, ionosondes, riometers, ground magnetometers, and a 90 MHz short-pulse radar, revealed a clear difference between the morning and evening radar and visual arc systems[1]. Morning side radar arcs were always poleward of their visual arc, and were clearly separated from it by 10–20 km. The same type of electric field meridional profile was also found in rocket measurements made across a stable, 100 km wide band of luminosity on the morning side (Bruning and Goertz, 1985). In the evening, the radar arc was always equatorward of the visual arc, and the minimum meridional distance separating the two was consistent with zero to the 5 km accuracy of the measurements (Timofeev et al., 1987). In a few cases, several homogeneous arcs were observed simultaneously on either side of the Harang discontinuity; only those in the eastward Hall current, northward electric field region developed a radar arc, and each radar arc was equatorward of its visual arc.

11.12 The Relationship between Arcs and Inverted Vs

To our knowledge, no appropriately small-scale precipitation structure has ever been detected in polar orbit, much less identified with a specific thin auroral arc below it. We need to know whether the small-scale structure so apparent at low altitudes exists above the ionosphere, or whether it is created in the ionosphere itself, perhaps by Alfven waves confined to low altitudes by waveguide effects. To resolve a 100 m arc in orbit requires measuring the distribution function over a wide dynamic range with millisecond time resolution, which will become possible only toward the end of the present decade on the *Freya, Fast, and Impact* spacecraft.

From time to time, there have been detections of intense, small-scale upward field-aligned currents in polar orbit that could plausibly be related to an auroral arc or ray. For example, a few currents with few kilometer scale sizes and current densities of order 50 mA/m^2 were found on OGO 4 (Berko et al., 1975),

and S3-2 at 1300 km altitude found two examples with 2 km scale size and 45 and 135 mA/m^2 current densities (Burke et al., 1983). The electromagnetic signature of small-scale field aligned current sheets or tubes crossed by polar-orbiting spacecraft may be the ULF electromagnetic turbulence observed by Gurnett et al. (1984), Chmyrev et al. (1985), and Berthelier et al. (1988), the frequency being the Doppler frequency due to spacecraft motion. The small-scale spatial variations of the perpendicular electric field observed in the topside ionosphere by AUREOL 3 were consistent down to 5 km scale lengths with the magnetic field perturbations induced by field aligned currents using a classical collisional conductivity model (Forget et al., 1991). This result suggested that much of the low-frequency turbulence observed by polar-orbiting spacecraft may result from encounters with small-scale field-aligned current systems. Nonetheless, such data have proves thus far insufficient to identify and classify arcs in polar orbit.

The facts that arcs and inverted Vs both contain upward field-aligned currents suggest that arcs, or arc systems, are found below inverted Vs; indeed, the similarity of the 100 km transverse scales of the visual arc–radar arc pair and inverted Vs supports this natural but unproven idea. Certainly, thin arcs and inverted Vs are found close to one another (Fennell et al., 1981). Because of the strong parallel potential drop in inverted Vs, only those perpendicular electric field structures whose scale lengths perpendicular to the magnetic field are sufficiently long will map from the inverted-V acceleration region to lower altitudes in the auroral ionosphere (Lyons, 1980, 1981; Chiu and Cornwall, 1980; Chiu et al., 1981). Comparisons of S3-3 measurements at low and high altitudes suggested that the perpendicular electric field does not map, presumably because of the intervening parallel electric potential difference (Mozer and Torbert, 1980). This result was substantiated by nearly simultaneous measurements on functionally the same field line at altitudes below 900 km and above 4500 km altitude by the two *Dynamics Explorer* spacecraft (Weimer et al., 1985). Perpendicular electric field Fourier components with wavelengths less than 160 km mapped progressively less faithfully between the two spacecraft.

11.13 Ground Observations of Arcs at the Poleward Border of the Auroral Oval

Radar and multispectral all-sky imaging photometer observations from Sondrestromfjiord, Greenland, monitored a most poleward arc in the 2000 MLT sector that remained "remarkably stable" for 30 minutes (Weber et al., 1991). This arc was well poleward of the southern limit of the field of view of the Sondrestromfjiord radar (69 degrees). It was created by soft electron precipitation, and it radiated 2 kR in 630 nm red emission, and only about 100 R at 427.8 nm. Radar scans indicated that the ionization density was enhanced below 200 km altitude, and depleted above 200 km. The electron spectrometer onboard the HILAT polar-orbiting spacecraft detected an energy flux of 0.1 ergs/cm^2 s sr in soft (100 eV) electrons precipitating into this arc. The arc was located along a velocity

and electric field shear, with an eastward (antisunward) flow at the poleward edge, zero velocity near the equatorward edge of the arc, and a 300 m/s westward flow further south. This translated to a 24 mV/m equatorward electric field poleward of the arc, reversing to 14 mV/m poleward on the other side. The measured electric fields, together with model conductivities, indicated that a 1 mA/m^2 field-aligned current flowed upward in the arc. The precipitating electron number flux could account for the field-aligned current.

A most poleward red arc was observed to brighten at 2330 MLT near Sondrestromfjiord after a period of enhanced auroral activity further equatorward, presumably an expanding substorm bulge (Weber et al., 1991). The brightening was accompanied by a negative bay in the *H* component and an increase in the *Z* component of the local geomagnetic field, implying the arc was responsible for a westward electrojet. If the most poleward arc near 2000 MLT had been aligned along the ionospheric convection, this one was more or less perpendicular to the convection flow. The plasma density in the arc was enhanced at E-layer (100–200 km) altitudes, and there were large patches of heated 3000° K plasma whose densities could exceed 8×10^5 e/cm^3 at F region altitudes. E-layer enhancement was particularly pronounced at the arc's equatorward edge. There was a 500 m/s antisunward component of flow *across* the arc, together with an east–west flow shear, east to the north and west to the south. The shear zone was just poleward of the optical arc and the associated enhancement of E-layer density, and the shear velocity went to zero almost precisely at the poleward edge of the optical arc.

A sequence of 12 all-sky images taken at 1-minute intervals showed that the arc developed a number of transient intensifications in the form of spots, rays, and double bands, localized to about one-sixth of the field of view. The radar measured a velocity averaged over a roughly 11-minute scan cycle, and so probably could not have detected any flow perturbations on this time scale. Despite these transient intensifications, the arc itself remained relatively motionless for 52 minutes. F-region patches convected directly through this arc and into the auroral oval without apparent disturbance, except for a dramatic increase in electron temperature. All the patches coming over the polar cap during this period had almost identical altitude profiles and varied only slightly in peak density.

These two arcs had two features in common. They were red, due to the precipitation of soft electrons. And they were "remarkably stable" despite the presence of activity elsewhere. This stability together with the constancy of their latitudes suggests that they had been located near the last closed field line, where everything that happens in huge volume of the plasma sheet will map to virtually the same place in the ionosphere.

11.14 The Poleward Border of the Oval and the Plasma Sheet Boundary Layer

Simultaneous DE 1 imaging of the quiet auroral oval and in situ ISEE 2 observations of the plasma sheet suggested that the poleward arc region mapped

into the plasma sheet boundary layer (Frank, 1988). The boundary layer was identified by a decrease of energetic electron intensity observed over a 10-minute period by ISEE 2, which was near 0130 MLT on the morning side about 7.4 R_E downstream of the earth and 4.8 R_E above the expected position of the neutral sheet. Global 120–155 nm ultraviolet images showed a "double oval," with a well-defined poleward arc whose latitude of peak emission varied between 72 and 75 degrees south geomagnetic latitude with local time. This poleward bright region was separated by uv-dark sky from an equatorward region of diffuse emission near 62 degrees. The intensities and latitudes of both emission regions remained stable for several tens of minutes. The ISEE 2 crossing of the plasma sheet boundary mapped magnetically into the most poleward arc according to the Tsyganenko and Usmanov (1982) magnetic field model.[2] Although the DE 1 imager could not resolve the typically 100 km distance between the most-poleward inverted V and the most-poleward structured ion beam (Zelenyi et al., 1990b), and it was not tuned to monitor the subvisual red aurora, results such as these have sustained the hope that the poleward boundary of the auroral emissions one does detect can be used at least to follow the changes in the area of the polar caps.

Cattell et al. (1982) reported ISEE 1 observations. of electric field spikes with peak amplitudes up to 80 mV/m at distances between 7 and 23 R_E. Nearly all the spikes were detected within 1 minute of an encounter with the lobe–plasma sheet boundary, as identified by energetic particle measurements, in regions of enhanced low–frequency electric field turbulence and field-aligned current flow; individual spikes were associated with local gradients in particle flux and small-scale currents. The spikes are reminiscent of the inverted-V electric fields observed in polar orbit, and probably constitute evidence that the inverted-V region maps near the plasma sheet boundary layer. A survey of plasma, magnetic field, and electric field data acquired on the polar-orbiting DE-2 spacecraft indicated that there was often a large enhancement of the electric field at the poleward boundary of particle precipitation in the midnight sector. This enhancement causes eastward particle drifts and was associated with field-aligned currents (N. Maynard and R. A. Hoffman, private communication, 1991). Similarly, a short interval of large electric fields with a complicated structure, including several field reversals, is a general feature of the poleward edge of the nightside auroral oval as observed by *Viking*. The source regions of the auroral kilometric radiation to be discussed next were usually associated with such electric field structures (Bahnsen et al., 1989).

11.15 Auroral Kilometric Radiation and the Poleward Aurora

The auroral oval is a source of intense electromagnetic radiation at kilometer wavelengths, called *auroral kilometric radiation* (AKR). Studies using data from Hawkeye (Gurnett and Green, 1978), ISIS 1 (Benson and Calvert, 1979; Calvert, 1981), and DE 1 (Shawhan and Gurnett, 1982; Mellott et al., 1984; Calvert, 1985) showed that AKR propagates predominantly in the right-hand extraordinary mode, though left-hand emissions sometimes occur, and that it is emitted nearly

perpendicular to the magnetic field near its source on auroral field lines. More recent measurements from the *Viking* V4H experiment (Bahnsen et al., 1987; de Feraudy et al., 1987) confirmed these characteristics, and provided strong evidence that AKR is generated at the local electron cyclotron frequency.

Our interest here centers on the use of AKR as a diagnostic of auroral and substorm activity; to that end, it is important to know precisely where it is emitted and by what. Dunckel et al. (1970), who first detected AKR at < 100 kHz frequencies on OGO 1, reported it was mainly a nightside phenomenon. IMP 6 and IMP 8 measurements showed that AKR was most intense between 50 and 500 kHz, occurred in sporadic bursts lasting up to several hours, and was emitted in a wide cone from a 1–3 R_E altitude region centered on 2200 MLT (Gurnett, 1974); later Hawkeye and IMP 8 measurements reduced the altitude range to 1–2 R_E (Kurth et al., 1975). Coordinated imaging from the DAPP polar-orbiting spacecraft showed that AKR was associated with discrete auroral forms (Gurnett,1974), and later Benson and Calvert (1979) and Benson et al. (1980) associated their ISIS 1 AKR measurements with inverted-V precipitation. Benson and Akasofu (1984) related the AKR measured on ISIS 1 to the aurora detected by the Alaskan network of all-sky cameras. Occultation data from the lunar-orbiting RAE 2 were used to produce two-dimensional source location maps (Kaiser and Alexander, 1976; Alexander and Kaiser, 1976) that suggested that the nightside northern hemisphere sources were located at 2–3 R_E altitude along the 70 degree invariant latitude line. This would map the AKR source near the poleward aurora.

The fact that AKR is emitted at the local electron cyclotron frequency can be used to identify AKR sources with high precision. The DE 1 plasma wave experiment determined source directions with good accuracy by measuring the relative phase of the signals from orthogonal electric dipole antennas. Assuming that AKR is generated at the electron cyclotron frequency, a candidate field line could be selected and mapped into a concurrent auroral image with a spatial resolution of about 300 km and 10% frequency resolution (Huff et al., 1988). AKR of various frequencies mapped invariably into structured aurora, and usually the most intense parts. In one case, the AKR sources at different frequencies all mapped into the same bright region near the poleward edge of the oval; in another, they mapped into the brightest of several that were detectable; and in a third case, they mapped into different parts of a longitudinally extended form. In the most interesting case, the AKR source regions tracked the time-evolution of the bright regions near the poleward edge of the oval. A so-called "double oval" formed during the recovery phase of this substorm; the AKR source was in its poleward component.

Viking actually flew through the AKR source region on 35 occasions (Bahnsen et al., 1989). The signals received by the spacecraft peaked in intensity where the frequency equalled the local cyclotron frequency. In general, AKR was generated at a geocentric distance of 2–3 R_E over a 2500 km altitude range in one or more magnetic field-aligned, east–west elongated sheets that had a north–south thickness of 100 km or less. The uv imager invariably found discrete auroral arcs at the feet of the AKR source field lines. Often the spacecraft footprint was near a

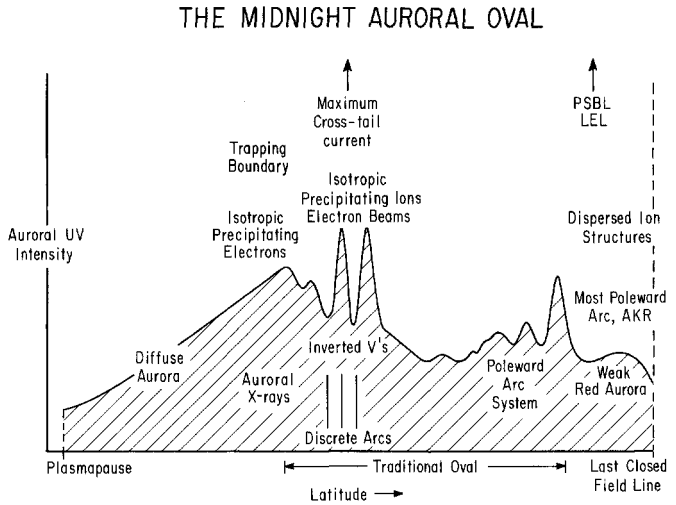

Figure 11.2. The Midnight Auroral Oval. This figure summarizes the ordering in magnetic latitude of important features of the midnight region auroral oval. The scale in latitude and the separations of the individual features vary within a considerable range from event to event. The solid shaded region is meant to convey an impression of the distribution of auroral light intensity with latitude. The lowest row of labels lists some of the structures found at auroral altitudes (The diffuse aurora, the emission region of auroral X-rays, discrete arcs, the poleward arcs and a region of weak red aurora at the poleward boundary of the oval.) The next row lists features found in polar orbit near 1000 km altitude (in order of increasing latitude, isotropic diffuse auroral electrons, the outer boundary of trapping of energetic electrons, inverted-V electron precipitation and isotropic ions, poleward arc electron precipitation and the AKR generation region, and dispersed ion structures. The labels at the top accompanied by arrows suggest that the inverted-Vs probably map to the region of strong or maximum cross-tail current, while the dispersed ion structures and the poleward red emission band likely connect to the plasma sheet boundary layer and the low energy electron layer. All in all, this configuration corresponds best to the substorm growth phase; during the expansion phase, for examply, discrete arcs may give way to rayed structures. Original drawing.

fold in an arc when an AKR source was encountered. These auroral forms persisted for tens of minutes, in agreement with the durations of AKR bursts from individual source regions. Only 6 of 35 source regions were found below 70 degrees magnetic latitude, and these were between 65 and 70 degrees. Particle data suggested that the AKR sources were located on field lines connecting to the plasma sheet boundary layer. Several keV electrons with a broad pitch angle distribution were found in a wide region around the AKR source. Upgoing ions of a few keV energy were always observed in the source regions. Magnetometer data showed that the AKR source field lines carried an upward current with no discernible fine structure.

11.16 Physical Mapping of the Nightside Oval into the Plasma Sheet

If the source of the diffuse aurora is plasma sheet thermal electrons, the poleward boundary of the nightside diffuse auroral oval should connect to the distant neutral line in the geomagnetic tail, and diffuse electron precipitation ought to go wherever convection from the tail goes, presumably extending in some attenuated form all the way to the plasmapause (Galperin and Feldstein, 1991). Certainly, diffuse auroral electrons should not be found further earthward than that. Measurements made on INJUN 3 indicated that although the diffuse auroral electron precipitation flux peaked at a higher latitude, it dropped below detector threshold near where electric field perturbations signalled a plasmapause crossing (Gurnett and Frank, 1973). We will discuss the soft electron precipitation at the poleward edge of the nightside auroral oval shortly. Thus it does seem that diffuse electron precipitation comes from all the closed convecting field lines within the magnetosphere. This is the natural definition of the diffuse auroral oval in the reconnection model.

If the natural definition is the right one, the diffuse auroral oval ought to contain all the other ovals. In particular, it should contain the oval of discrete aurora. We argued earlier that discrete arcs are found below inverted Vs; so our task here is to order inverted Vs in latitude with respect to other auroral oval structures. Newell et al. (1991c) divided the auroral electron precipitation observed from polar orbit into two broad regions, a "hard zone" characterized by relatively structureless precipitation of electrons with few keV typical energies and a "soft" zone at slightly higher latitudes with average energies typically below 600 eV. The hard zone corresponds to the equatorward diffuse aurora; bursty structures and/or inverted Vs with higher energies are embedded in the poleward soft zone. A survey of the precipitating ion and electron fluxes detected on 247 passes of the S3-3 spacecraft found no particular relationship between the locations of inverted-V and diffuse electron aurora (Lyons et al., 1988). The inverted Vs were identified with precipitating electron beams with energies exceeding 0.5 keV, and the diffuse aurora was identified with isotropic electron precipitation.

Although auroral light is created largely by electrons, the plasma sheet is dominated energetically by hot ions, and it is their kinetic properties that define the structure of the plasma sheet the most meaningfully. One cannot determine where the plasma sheet boundary layer maps into the auroral ionosphere without finding the boundary layer ion beams over the auroral oval. High-time resolution measurements from the low-altitude, polar-orbiting, Franco-Soviet spacecraft, AUREOL 3, discovered precipitating beams of 7–10 keV protons near the poleward boundary of the visual aurora (Bosqued, 1987; Kovrazhkin et al., 1987). These precipitating protons had velocity-dispersed structures similar to those in the boundary layer, motivating the identification with the plasma sheet boundary layer (Zelenyi et al., 1990b). The ion beams were of solar wind composition. The beams formed narrow 0.3–0.5 degree substructures in a band of precipitation about 1 degree MLAT thick that was always poleward of the most poleward inverted V, a decisive indication that inverted Vs are on closed field lines.

Lyons et al. (1988) found that inverted Vs invariably occurred in spatially structured regions of proton precipitation that was isotropic at all ion energies from a few keV up to above 100 keV, whenever the ion flux was above the threshold for a determination of isotropy. The absence of an ion beam component suggests that the inverted Vs were probably equatorward of the ionospheric projection of the plasma sheet boundary layer. The isotropy over a wide energy range together with the absence of an intensity threshold suggest that the inverted-V regions mapped to a region of nonadiabaticity for those ions, presumably a region of strong cross-tail current. Using the Tsyganenko (1987) empirical model, Elphinstone et al. (1991) showed that the structured aurora observed on *Viking* maps into the region of maximum cross-tail current.

A low-energy electron layer (LEL) always encloses the ion beams of the plasma sheet boundary layer and, therefore, should map into the auroral oval (slightly) poleward of the dispersed ion beams. Parks et al. (1992) suggested that the low-energy electrons observed in space were the upward component of the counterstreaming electron beams observed by Sharp et al. (1980) at 4000–8000 km altitudes, which are generally detected poleward of the poleward boundary of keV ions (Hultquist, 1975). The downgoing low-energy electrons may be responsible for the subvisual red aurora that marks the poleward boundary of the auroral oval. Almost forgotten airborne photometric observations by Eather (1969) and Eather and Mende (1971) recorded a diffuse subvisual luminescence due to soft electron precipitation that extended about 100 km poleward of the last visual arc (Feldstein and Galperin, 1985). The red arcs observed from the ground at the poleward border of the auroral oval made such a glow (Weber et al., 1991).

11.17 Conjugacy

If the diffuse aurora marks the region of closed, convecting field lines, and if the discrete aurora are all contained within the diffuse auroral oval, the discrete aurora should all be on closed field lines. If they are on closed field lines, they should display conjugacy between hemispheres. Physical conjugacy is said to exist if the details of structured auroral emissions in the northern and southern auroral ovals match. The term *displacement* refers to the displacement of physically conjugate aurora from mathematical conjugacy calculated using an internal magnetic field model. Structured aurora do display physical conjugacy and mathematical near-conjugacy during quiet and moderately disturbed times when the determination is the most feasible (DeWitt, 1962; Belon et al., 1969; Westcott, 1966; Davis et al., 1971; Akasofu, 1977). High-resolution conjugacy studies have examined the structure, intensity–time profiles, and motions of small-scale discrete auroral forms (Stenbaek-Nielsen et al., 1972, 1973; Sato et al., 1986). Variable displacements from mathematical conjugacy have been related to substorms (Bond, 1969) and may depend on latitude (Stenbaek-Neilsen et al., 1972). By comparing *Viking* uv images with South Pole keograms, Burns et al. (1990) identified three physically conjugate events in which the displacements from mathematical conjugacy ranged

up to 5 degrees in latitude and about 2 hours in local time. Sometimes, however, not even physical conjugacy can be found, at least within an instrumental field of view of about 5 degrees latitude (Belon et al., 1969; Rosenberg, 1987).

If the poleward boundary of the aurora maps to distant field lines in the plasma sheet boundary layer, time-dependent deviations from conjugacy may tell us something about plasma sheet reconnection and/or plasmoid ejection. (It is difficult to imagine that only conjugate field lines reconnect.) Global *Viking* images of the northern auroral oval were compared with simultaneous local keograms taken at South Pole Station in order to evaluate the conjugacy of the most poleward arc (Burns et al., 1991). For this purpose, a relatively quiet period that was free of westward surge activity was chosen, 0540–0620 UT on July 30, 1986. A first 0542 UT *Viking* image showed a morningside arc that had already brightened poleward of a diffuse auroral region in the northern oval. A narrow, well-defined auroral form had developed out of a diffuse glow at South Pole station by 0543 UT. At 0549 UT, the *Viking* arc suddenly changed direction to cut directly across the postmidnight oval, brightened quasiuniformly at 0551 UT, and faded at 0558 UT.[3] At the South Pole, the conjugate arc brightened between 0548 and 0553 UT, moved toward the zenith, and faded by 0605 UT. The region of best correspondence in the northern oval was displaced about 5 degrees equatorward of the point mathematically conjugate to South Pole station in the same magnetic meridian. While the intensity variations in the northern and southern hemispheres generally tracked one another within 2–3 minutes, the poleward arc activity deviated from close physical conjugacy.

11.19 Concluding Remark

Our ambitions for magnetic field mapping go much further than our achievements. We would really like to map quite localized auroral structures into the magnetosphere, in effect, to have time-dependent mappings of "single field lines." Perhaps time-dependent MHD models will one day be able to perform a useful function in the arena of detailed mapping as well as of flow visualization. In the meantime, we have no choice but to try to map the high-latitude ionosphere into the magnetosphere as though we really could separate questions of structure from questions of dynamics. This is inherently unfeasible in an unsteadily reconnecting magnetosphere. Moreover, the empirical magnetic field models on which mapping depends are ensemble models, and are therefore heavily weighted by the most probably occurring state of the magnetosphere. This implies that the mathematical mappings of the nightside auroral oval fit the underlying low-velocity flow state of the plasma sheet well, but do not reflect the bursty reconnection state, which appears to be related to the most prominent forms of geomagnetic activity. We can only hope that our present models of the "average magnetosphere" do not create misleading perceptions. At the present time, "physical" mapping probably gives the more reliable, albeit qualitative, sense of the relationship between auroral and magnetospheric structures. In the end, we have to use theory and judgment to

resolve experimental ambiguity, and we have to acknowledge that prejudices are probably unavoidably embedded in the conclusions we draw from physical mapping.

NOTES

1. Near midnight, substorms were a complicating factor.

2. Since the crossing took place relatively near the earth, the mapping was probably fairly reliable even though it involved high-latitude field lines.

3. As we will see, the formation of a sun-aligned arc can also take place during the substorm recovery phase; it is significant that it can occur when there has been relaively little substorm activity at lower latitudes. It may signify a northward turning of the interplanetary field.

12

THE AURORAL SUBSTORM

12.1 Introductory Remarks

Around the time the steady convection model was being developed, Akasofu (1964) was arranging ground-based magnetometer and all-sky camera observations of the complex time dependence of nightside auroral activity into the central phenomenological conception of time-dependent magnetospheric physics—the auroral substorm. In this chapter, we assemble a description of a substorm from modern observations. We will see that observations of electric fields, auroral X rays, cosmic noise absorption, ionospheric density, and geomagnetic micropulsations have also been successfully ordered by the substorm paradigm. At the same time, it will become clear that each individual substorm has its own irreducible individuality, and that our summary description is really a list of effects that anyone thinking about substorms ought to consider. No real substorm will look exactly like the one described here.

Spacecraft observations of auroral light, precipitation, currents, and fields from polar orbit have held out high promise for unified understanding of the development of the auroral substorm around the entire oval. Without truly global auroral observations, it would be difficult to establish decisive contact with observations of large-scale convection and the associated changes in magnetospheric configuration. Despite the high promise and the many other successes of spacecraft observations of the aurora, synthetic understanding of the time development of the auroral substorm at all local times, dayside and nightside, evening and dawn, has been slow in emerging, perhaps because a stringent combination of field of view, sensitivity, space and time resolution, and multispectral capability is required. One needs images of the whole oval with sufficient space resolution to identify important arc structures (50–100 km or better) in a temporal sequence that can articulate the evolution of activity on better than the 10-minute time scale on which polar cap convection develops. Only recently has it been possible to observe auroral activity at all local times around the auroral oval simultaneously and follow its time development from the beginning of the growth phase until well into the expansion phase. This amplification of the original paradigm is the subject of Sections 12.2 and 12.3.

Although Akasofu (1964) had in fact proposed a model of substorm behavior around the auroral oval, much of the subsequent attention was paid to the

relatively clear-cut sequence of events in the premidnight sector. For example, most of the detailed studies of arc structure were devoted to premidnight arcs until very recently. As a result, the premidnight events—equatorward drift of the arcs prior to onset, brightening of the equatorward arc, development of the westward surge afterwards—came to be viewed as the essence of the substorm. For this reason, and because so much detailed information is available, we too will devote considerable attention to the happenings in the premidnight sector. Section 12.4 discusses the properties of the growth phase there. Sections 12.5 and 12.6 take up the elusive issues of pseudoexpansions and precursors to onset; Section 12.7 describes the equatorward arc brightening that is the onset. Pi 1 and Pi 2 geomagnetic micropulsations are particularly fine diagnostics for timing onset and/or the beginning of the auroral expansion; these will be discussed in detail in the next chapter. The subsequent formation and propagation of the westward surge is the subject of Section 12.8. The westward surge is, among other things, an intense upward line current that marks the westernmost end of the auroral bulge. The properties of the auroral bulge are discussed in Section 12.9. The westward surge and auroral bulge often develop as a sequence of distinct activations separated by 5–15 minutes, each of which is accompanied by micropulsation bursts (Section 12.10). In addition, there may be more localized auroral activations and repeating micropulsation bursts on the 1–3 minute time scale (Section 12.11).

Up to this point, we will have discussed the behavior of the aurora created by electron precipitation; observations of the onset and expansion phases in the Hβ emissions due to proton precipitation are taken up in Section 12.12. We are then in a position to classify all the phases of the auroral substorm (Section 12.13). The classical substorm expansion phase begins with onset and ends when the auroral bulge has achieved its maximum poleward extent.[1] The auroral bulge typically does not reach the most poleward arcs, though on occasions it does so (Section 12.14). In Section 12.15, we will argue that activations of the most poleward auroral arc system are relatively independent of the substorm onset and expansion going on at lower latitudes, and start to become prominent around but not exactly at the beginning of the substorm recovery phase. Often a "double oval" forms, with the activity at the poleward and equatorward borders of the oval separated by a dark region. Most of the classical recovery phase phenomena in the literature take place on the equatorward portion of the double oval (Section 12.16). The recovery phase has been observed to end in at least three different ways (Section 12.17).

12.2 Growth Phase in the Polar Cap

Davis (1962) was probably the first to notice that the polar cap was usually very dark and devoid of auroras during what were soon to be named *substorms*. Starkov and Feldstein (1971) subsequently observed that both discrete and diffuse auroral forms gradually disappeared from the polar cap several tens of minutes to hours before substorm onset. Today, we would probably say that the auroral oval becomes larger and more oval shaped as the interplanetary field swings southward.

Indeed, Akasofu (1977) suggested that the polar cap auroras simply moved equatorward with the increase in magnetic activity. More recently, Pellinen et al. (1990) reported joint *Viking* and ground-based observations that showed fading of a polar cap arc at the same time that auroral oval emission was enhanced; they associated the fading of the transpolar arc with a northward-to-southward shift of the interplanetary magnetic field, and thus, by implication, with the beginning of the growth phase.

Wu et al. (1991) used zenith-pointing photometer and all-sky camera observations from South Pole Station at -74.2 degrees magnetic latitude to study the intensifications and fadings of eight polar arcs in the 1630–2400 MLT sector. In their typical cases, a pre-existing sun- or oval-aligned arc first intensified for about 10 minutes and then faded; the 630.0 nm emission would increase from 0.1 to 0.3 kR, and the 427.8 nm emission, from 0.3 to 1.5 kR. In two instances, the short-term brightening occurred 2030 minutes after a southward shift of the interplanetary field when its x component was positive and the south pole had good magnetic connection to the sun; in the one case when the fade was not preceded by arc brightening, the fade followed the southward shift by about 30 minutes, but B_X in the solar wind had the opposite sign. The brightenings were not accompanied by riometer absorption and only minor, 20–40 nT, geomagnetic perturbations. Following the brief activation, the archetypical arc would fade, sometimes to disappear below threshold, while at the same time drifting equatorward. The fade would last for 30–60 minutes and terminate with the appearance of bright aurora, presumably the activation of the poleward oval arc system, around the maximum of AE, near the beginning of the substorm recovery phase.

12.3 Growth Phase around the Auroral Oval

Now we take up observations of the development of the substorm growth phase around the auroral oval. First we will discuss the development of the electrojet current system, and then we will turn to observations of auroral emissions.

On November 11, 1976, IMP 8 was located at 36 R_E distance in the dawn magnetosheath about 6.5 R_E downstream of earth, at a position where any perturbations it detected were sure to have interacted with the whole frontside of the magnetosphere beforehand. The spacecraft was roughly the same x distance downstream of the magnetopause as the region conjugate to Scandinavia, where a two-dimensional array of 25 magnetometers, 2 all-sky cameras, 4 riometers, and 3 balloons had been assembled for a major correlation study (Pellinen et al., 1982). A worldwide set of magnetograms showed that a two-cell pattern of convection and associated currents began to develop about the time a southward shift detected on IMP 8 would have first interacted with the subsolar magnetopause. This shift followed a 1.5 hour period of northward interplanetary field and geomagnetic quiet. The current system developed in an even more pronounced fashion within a minute or so of the time the southward shift actually reached IMP 8. An eastward electrojet developed all around the afternoon sector, a westward electrojet all

around the morning sector, and sunward currents developed over the polar cap. Three minutes later, the growth of the westward electric field was observed by one of the balloons in the Scandinavian sector, which was very close to magnetic midnight. At the same time, a quiet homogeneous auroral arc formed over Norway, to the north of the observing balloon, and began its drift equatorward.

We will return to this event in due course, but here we emphasize that the electrojets developed all around the auroral oval in response to an increase in the rate of convection during substorm growth phase. Along the same line, a set of coordinated spacecraft, balloon, magnetometer, and all-sky camera measurements in the solar wind, in the magnetotail, at geostationary orbit, and on the ground indicated that the auroral electrojets intensified around the auroral oval within 5 minutes of the arrival of a sharp southward shift of the interplanetary magnetic field at the dayside magnetopause (Sauvaud et al., 1987).

Elphinstone et al. (1992) studied 15 nightside substorms with observable and well-defined dayside auroral precursors using *Viking* ultraviolet imagery. We recount here the histories of two substorms that reflect this ensemble of events. The first inkling that a substorm was to develop on September 23, 1986 was the appearance of two closely spaced bright spots in the morningside aurora near 1030 MLT. Seven minutes later, a larger auroral form appeared at the equatorward edge of the background auroral emission between 0900 and 1030 MLT, out of which a series of "fan" arc systems (Akasofu, 1981) developed over the next 5 minutes and spread westward to 0600 MLT at a speed of about 5 km/s. By this time, 12.5 minutes after the first activation, a clearly defined poleward arc had developed between 0430 and 1000 MLT, and the emission from the polar cap had faded. By the end of the growth phase, 21.5 minutes after first activation, not one but two important events had taken place in the midnight sector; an intense auroral bulge had begun to expand from the equatorward edge of the pre-existing auroral emission between 000 and 0145 MLT, and a less intense most poleward arc had appeared between 2200 and 0200 MLT, some 5–7 degrees poleward of the developing auroral bulge. This ragged poleward arc had brightenings localized to some tens of minutes MLT. After 4 more minutes had elapsed, the westward surge had intensified and propagated westward past local midnight and the bulge had expanded several degrees poleward. The bulge never reached the latitude of the most poleward arc system.

In contrast with the previous event, the first activation of a substorm on October 19, 1986 occurred on the afternoon side, between 1300 and 1500 MLT near 75 degrees MLAT. Over the next 8 minutes, the region of brightening aurora spread both eastward and westward at 1–2 km/s speeds until it filled the afternoon and part of the prenoon sector betwen 1100 and 1600 MLT. At this point activity started at even earlier local times on the morning side. This activity took the form, not of "fan" arcs, but of localized intensifications well below the poleward boundary of emission. Beginning in the 0900–1000 MLT sector, the region containing these intensifications expanded westward at a speed exceeding 5 km/s, reaching the dawn meridian about 14 minutes after the first activation. The afternoon-side aurora, which had remained bright for 12 minutes after activation,

faded briefly, and then brightened at the same time there was a general activation in the 0000–0600 MLT sector. During all this, the evening-side aurora was broken into a number of discrete forms with scale sizes < 500 km, and there was some evidence for the development of an extended poleward arc system on the morning side. Up to this time, the evening sector had actually been the least active of all. The main auroral brightenings, which started about 30 minutes after first activation, also did not involve the evening sector, at least at first. The postmidnight sector between 0230 and 0400 MLT brightened and expanded eastward and westward, and the afternoon sector aurora expanded eastward at a speed of tens of kilometers per second to fill the 1600–2000 MLT region within a few minutes. Eventually the 0000–0600 and the 1200–2000 MLT sectors were more or less uniformly bright. Only at this point, 35 minutes after first activation, was there an intensification in the premidnight sector. This soon developed into a westward surge.

Although there is not yet enough experience with global auroral observations to say that what was described previously is typical, it does graphically convey the idea that the auroral substorm has a growth phase that starts with dayside reconnection. Auroral activity had a definite beginning at a localized spot in the dayside oval, not always centered on local noon. The dayside activations were associated with southward shifts in the interplanetary field in 7 of 8 cases in which solar wind data were available. After this initial activation, the auroral brightening spread in complex fashion both eastward and westward around the oval, accompanied by the development of an eastward electrojet on the afternoon side, and a westward electrojet on the morning side (Elphinstone et al., 1992). Only after the activations had crossed into the nightside did the substorm expansion begin.

12.4 Classical Evening Sector Growth Phase

When there has been magnetic quiet for about 3 hours, the evening aurora observed from the ground settle down into several quiet and homogeneous arcs, some of which may be barely visible. Observations from polar orbit usually miss the small-scale arc structure. From the distance of polar orbit, the dominant presubstorm feature is often a smooth band of auroral emission that passes continuously through midnight to the morning sector. In one case, it was possible to know what the spacecraft was missing when it was seeing this. Coordinated all-sky camera measurements resolved a narrow well-defined arc with active ray structure located in the broader region of auroral emission that *Viking* was simultaneously observing on April 6, 1986 (Shepherd et al., 1990). This rayed arc contained folds that propagated eastward at 2 km/s.

It has been known for years that the visual arcs in the evening sector drift equatorward (Akasofu, 1964), with speeds ranging from 2.5 to 40 km/min prior to onset (Kirkwood and Eliasson, 1990). The scan of Pellinen et al. (1982) referred to was typical in this regard; it began to drift equatorward at a speed of 18 km/min (and subsequently slowed down). Global *Viking* measurements found that the

equatorward drift manifests itself at all local times around the auroral oval (Elphinstone et al., 1992). The peak of the auroral 391.4 nm emission drifted equatorward in all but one 1-hour magnetic local time interval during the growth phase of the October 19, 1986 substorm discussed. Prior to another substorm expansion on September 24, 1986, the equatorward drift speeds at 1500, 1900, and 2100 MLT were found to be 27, 16, and 14 km/min, consistent with the range of speeds derived from ground-based measurements. The equatorward drifts at all three local times commenced at the time of the first auroral activation on the dayside near 1500 MLT (Elphinstone et al., 1992).

The motions of the poleward and equatorward boundaries of the auroral light appear to be partially decoupled. While the equatorward boundary measured by *Viking* moved consistently equatorward, the poleward boundary motions proved to be much more variable (Murphree et al., 1991). Specific examples revealed cases in which the poleward boundary moved faster, slower, and at the same speed as the equatorward boundary. As one consequence, the widths of the regions of auroral emission varied from growth phase to growth phase. The poleward boundary of detectible auroral emission may not always be the open/closed field line boundary. It is not clear precisely how concordant is the motion of the poleward boundary of auroral light and the motion of the boundary between open and closed field lines. However, since they probably do correspond in a rough way, the tendency towards equatorward motion all around the oval suggests that the open flux in tail lobes begins to increase at the first auroral activation on the dayside and continues to increase throughout substorm growth phase (Murphree et al., 1991).

The EISCAT incoherent scatter radar characterized the latitude and altitude profiles and motions of the ionization created by proton and electron precipitation while *Viking* measured the precipitation directly during the growth phases of six substorms (Kirkwood and Eliasson, 1990). The times of onset of these substorms were identified by their Pi 2 micropulsation and other ground magnetometer signatures. The growth-phase evening auroral oval could be divided into three distinct latitude regions in which the ionization profiles were very different. The most poleward region contained a mixture of structured arcs and variable diffuse auroral precipitation. To EISCAT, an arc was a peak in the ionization density typically between 100 and 120 km altitude extending over some tens of kilometers in latitude. In several cases where all-sky camera observations were available, such density enhancements could be specifically identified with an auroral arc (Kirkwood et al., 1988). The more diffuse ionization component was due primarily to 1–3 keV electrons of the plasma sheet origin with a high-energy tail. In the most equatorward region, there was diffuse ionization between 100 and 130 km altitude due to the precipitation of 10–20 keV plasma sheet ions, with some some admixture 1–3 keV plasma sheet electrons that was responsible for the ionization up to 160 km. The discrete arcs drifted slowly equatorward at a speed of 2–4 km/min, while the equatorward peak in diffuse precipitation hardly migrated in latitude.

A 50–100 km thick ribbon of ionization below 100 km altitude cleanly separated the two regions (Kirkwood and Eliasson, 1990). The low-altitude density

maximum was due to the precipitation of a *distinct* population of energetic electrons. To account for the altitude minimum in density above the maximum, the electron precipitation spectrum had to have a sharp energy threshold that varied between 20 and 60 keV. In each case, just poleward of this ionization band, an arc was observed as a density enhancement between 110 and 150 km altitude that was created by the softer precipitation component. This arc and the hard-electron precipitation band were observed to comove equatorward.

The arcs poleward, hard-electron precipitation in the middle, diffuse auroral peak equatorward ordering of auroral structures at E-region altitudes is reminiscent of that found above in polar orbit: inverted-Vs poleward, outer boundary of trapping of energetic electrons in the middle, diffuse electron precipitation equatorward. Indeed, the invariant latitude of the band of hard-electron precipitation detected by EISCAT coincided with that of of the intensity peak at the outer boundary of trapping of 5–55 keV electrons observed by *Viking* in two cases where it was possible to make the comparison (Kirkwood and Eliasson, 1990). The enhanced electron fluxes at those energies were intense enough to create the observed ionization, and the latitudinal width of their intensity profile corresponded to that of the low-altitude ionization zone.

Thin bands of hard-electron precipitation like that found by EISCAT had been studied using riometer absorption and balloon X-ray measurements for many years (Hargreaves et al., 1975; Pytte et al., 1976b; Ranta et al., 1981). We will call them *auroral X-ray arcs* for short. A peak in riometer absorption due to energetic electron precipitation comoved equatorward with the arc of Pellinen, et al. (1982) remaining about 25 km southward of it at all times during a 33 minute growth phase. While the electric field measured simultaneously on the balloon yielded an equatorward drift speed that was comparable to that of the auroral arc–x-ray arc pair, the equatorward motions and the electric field variations did not correspond to one another in detail. In another study, the equatorward motion of a 50 km thick auroral X-ray arc was followed throughout the growth phase of a substorm on May 4, 1977 (Ranta and Ranta, 1983). Observations from magnetometer and riometer arrays, four balloons, and the GEOS 2 geostationary spacecraft were combined to study yet another substorm on June 23, 1979 (Tanskanen et al., 1987). We will discuss the GEOS 2 observations in Chapter 11; here, we discuss the ground measurements. The X-ray arc was tracked by different balloons and riometers from $L = 9.2$ to 5 over a 100 minute growth phase, during which time the interplanetary field was southward. The e-folding energies of the X rays evolved from 25–50 keV at $L = 8.5$ to 80–100 keV at $L = 5$. The band was tilted northwest (one degree north per 15 degrees west) and propagated equatorward at a speed of 7.2 km/min. The $\mathbf{E} \times \mathbf{B}$ speeds computed using the 15–25 mV/m ($L = 9$) and 5 mV/m ($L = 6$) dawn–dusk component of the electric field measured on two balloons were comparable to this rate of drift.

The Harang discontinuity also migrates equatorward during substorm growth phase. A sharp north-to-south shift of the meridional component of the electric field was interpreted as the equatorward passage of the Harang discontinuity over a balloon at $L = 9$ during the growth phase of the June 23, 1979

substorm studied by Tanskanen et al. (1987). This field reversal occurred 33 minutes after the auroral X-ray arc had presumably passed overhead. If both structures had been moving equatorward, the X-ray arc was equatorward of the field reversal at that point. About 20 minutes later, a smoother north-to-south reversal passed over an $L = 6$ balloon 500 km to the south. As it did so, the X-ray count rate began to increase and reached a maximum about 15 minutes later. Thus, at this point, the X-ray arc was poleward of the field reversal. One possibility is that there was only one field reversal, which overtook and passed the auroral X-ray arc. Another possibility is that the $L = 9$ balloon detected an electric field reversal associated with a poleward arc, and the $L = 6$ balloon detected the Harang discontinuity itself.

STARE measurements showed that the Harang discontinuity has low equatorward velocities (2.4 km/min) at quiet times and are much higher, 9–36 km/min, during more disturbed intervals (Neilsen and Greenwald, 1979). The rapid equatorward migrations were often terminated by the brightening and subsequent poleward expansion of an arc near or in the discontinuity. The overall range of speeds for the Harang discontinuity, 2.4–36 km/min, was essentially the same as for auroral arcs, 2.5–40 km/min. Corotation of the observer under a fixed structure that is 8 degrees higher latitude at 1800 MLT than at 2400 MLT would produce the slow, "geometrical" rate of apparent migration characteristic of quiet times. Thus, the Harang discontinuity maps to a fixed structure in space during quiet times, and to a region that is moving earthward during growth phase.

In sum, an ordered network of activity gradually moves equatorward and intensifies as the growth phase of the auroral substorm unfolds. Auroral arcs, the auroral X-ray arc, and the Harang discontinuity all migrate equatorward faster than the "geometrical" rate due to corotation.

12.5 Pseudoexpansions

On April 6, 1975, the sharp onset of an isolated substorm followed a clear southward turning of the magnetic field at IMP J, which was in the solar wind in the dawn meridian plane at the time. Untiedt et al. (1978) studied the 66-minute growth phase of this substorm using observations from meridian chains of magnetometers, short–period pulsation magnetometers, all-sky cameras, and riometers in the 2300 MLT sector. The overall pattern of magnetic disturbance was consistent with the development of a twin-vortex pattern of enhanced ionospheric convection during the growth phase. Untiedt et al. (1978) concentrated upon the local midnight region, where they observed the equatorward drift of the ordered network of activity described previously with particular clarity. The westward electrojet generally increased in intensity as the growth phase unfolded; its modeled current sheet density reached 200 A/km well before onset, and its effective width varied between 200 and 400 km in a nonmonotonic fashion. An auroral arc was located in the poleward half of the electrojet; occasionally, other arcs could be observed further poleward. The coupled electrojet–arc system moved equatorward

with an average speed of 120 m/s, or 7.2 km/min. Riometer measurements indicated that an ionospheric absorption band above the same region also moved equatorward at a speed of 100–200 m/s. Thirty-four minutes after the southward turning, the equatorward motion of electrojet and arc effectively ceased. Five minutes after that, the arc began develop localized intermittent activity. At first this activity took the form of hook-shaped folds that traveled to the east at speeds of 1–2 km/s; later, the activity developed into mature spirals (Davis and Hallinan, 1976). Activity in irregular Pi B micropulsations at auroral ground stations accompanied each distortion of the equatorward arc. Arc fadings were interspersed in between spiral intensifications. The first spirals appeared when the upward field-aligned current density estimated from electrojet parameters reached 1 A/km^2 (see also Westcott et al., 1975; Hallinan, 1976). The last spiral, which occurred 6 minutes before the onset, was accompanied by a burst of Pi 2 micropulsations, as well as by the Pi B activity noted earlier. The intermittent development of localized regions of upward field-aligned currents suggests that these events were "pseudoexpansions." Pseudoexpansions will be discussed again after we have learned more about the geosynchronous substorm.

12.6 Precursors to Onset

All-sky camera data and ground photometry indicate that the intensity of auroral light regularly fades and fluctuates on 1–5 minute time scales prior to onset (Pellinen and Heikkila, 1978; Baumjohann et al., 1981; Morse and Romick, 1982). Very often, the diffuse band of radar backscatter located near the arcs becomes weaker as the arcs fade (Uspensky et al., 1992). The X-ray arc also fades just before onset (Pytte and Trefall, 1972; Pytte et al., 1976d). For example, during the 3 minutes before the local onset of the April 6, 1975 substorm passed overhead, the northern sky became especially dark, the radar backscatter intensity totally faded, and the ionospheric riometer absorption decreased, indicating that the auroral X-ray arc was also fading (Untiedt et al., 1978). In another substorm we are following, the X-ray intensity measured by balloon faded 5 minutes before onset on November 11, 1976, just as the auroral arc and X-ray arc ceased their equatorward motion (Pellinen et al. 1982).

Viking observations suggest that visual arc fading occurs over a large spatial scale (Shepherd et al., 1990). An arc fading monitored on the ground on April 6, 1986 corresponded in space to fading from evening to morning of the diffuse band of emission that was the spacecraft's view of the arc. At one point in time, the spacecraft arc faded along its entire length, recovered to its normal value, faded away completely 5 minutes later, and then recovered again. On the ground, more than one arc can be visible. In this case, other arcs may brighten, but the one that is fluctuating is the one that fades. It is often a poleward arc that fades just prior to the abrupt brightening of the most equatorward arc that signals that onset has begun.

12.7 Onset

The substorm onset is a rapid brightening of a small region of the most equatorward auroral arc typically just before local midnight (Akasofu, 1964). *Viking* found the initial onset to occur in a region as small as 300 km^2 (Cogger and Elphinstone, 1992); EXOS-D (AKEBONO)^2 placed the initial brightening in a region less than 0.2 hours MLT or about 100 km in east–west extent (Ejiri et al., 1992). The brightening of the onset arc has been characterized as an "explosive intensification" (J. R. Kan, private communication). The integrated rate of brightening of one onset arc was obtained by a fortuitous spacecraft observation. The 391.4 nm emission integrated over the field of view of the ISIS 2 auroral scanning photometer brightened by at least a factor of 3–4 to about 3 kR in about a minute (Lui and Burrows, 1978). Because of the differing resolutions of ground and space measurements, the ISIS 2 emission region could conceivably have corresponded to one or more thin arcs.

The onset brightening spreads westward (Akasofu, 1977; Opgenoorth et al., 1983) and eastward (Opgenoorth et al., 1980) along the onset arc with typical speeds of 5–10 km/sec and occasionally more. After 1 minute, a typical brightened arc region is several hundred to a thousand kilometers long. The westward spreading of the April 6, 1975 substorm onset was described with particular eloquence by Untiedt et al. (1978). Judging from Pi 2 records, the onset probably started to the east of the observing stations about 2 minutes before it arrived overhead. About the same time beforehand, three minutes before onset arrived, the auroral X-ray arc began to fade and an intensive hooklike structure developed to the south of Kiruna; for the next two minutes, it was the only auroral form to be seen. The hook traveled eastward with an increasing speed that reached 3 km/s, at which point it suddenly stopped. Eight seconds later, this structure had become partly wound up anticlockwise into a rayed spiral. This form dissolved rapidly into an intense north–south aligned form, accompanied by rayed aurora to the northwest. These lasted precisely 48 s. Then all these pre-existing forms suddenly intensified dramatically: Onset had arrived; 20 s later the entire sky was filled with bright aurora. Strong ionospheric currents began to be detected to the north of Kiruna about 30 s before onset arrived and were fully developed 40 s later; this magnetic onset was accompanied by an intense 0.1–1 Hz Pi B irregular pulsation event (Bosinger et al., 1981) at auroral stations and a clear Pi 2 burst at the midlatitude stations in the same local time sector. The riometer absorption, which had been fading, intensified dramatically at Finnish ground stations to the east of Kiruna within a minute of local onset, indicating a sharp increase of > 40 keV electron precipitation there.

Triangulation showed that one onset arc had the same ionospheric lower border before and after brightening, about 115 km altitude, indicating that the precipitating electron flux responsible for the onset arc had about the same energy distribution but increased in intensity after the brightening passed (Opgenoorth et al., 1983), a result confirmed by Kirkwood and Eliasson (1990). This clearly indicates that onset differs from the westward surge, in which the precipitating

particles are energized by as much as a factor ten. It also indicates that the local field-aligned currents do not intensify much until the westward surge arrives.

12.8 Relation of Onset Arc to Other Auroral Oval Structures

In general, the onset occurs at latitudes distinctly below that of the poleward boundary of detectable auroral light (Murphree et al., 1991). In one case, the initial brightening occurred on the most equatorward arc of a system of multiple arcs that had been successfully resolved by the *Viking* imager (Shepherd and Murphree, 1991). EISCAT also found the onset arc to be the most equatorward one, which in turn was just poleward of the auroral X-ray arc (Kirkwood and Eliasson, 1990). A study of several substorm intensifications on January 23, 1979 led Kozelova (1992) to conclude that weak substorms start on the arc just poleward of the auroral X-ray band, whereas strong substorms start on an arc within that band.

The auroral X-ray arc is presumably related to the thin region of isotropic precipitation of energetic electrons found on polar-orbiting spacecraft to be just poleward of the outer boundary of stable trapping. As we mentioned already, ISIS 2 caught one onset arc as it was brightening; this arc was embedded in a region of diffuse auroral light at the poleward edge of the outer boundary of trapping for 40 keV electrons (Lui and Burrows, 1978). On August 28, 1979, the TIROS spacecraft happened to cross the auroral zone about 2 minutes after an auroral arc activation was recorded by ground all-sky cameras. The intense low-energy electron fluxes associated with this arc were located just poleward of the isotropy boundary/outer boundary of trapping of the tens of keV electrons. (Sergeev, 1992).

The arc brightening at onset occurs near the Harang discontinuity (Neilsen and Greenwald, 1979; Baumjohann et al., 1981; Lyons, et al., 1990); the ionospheric electric field itself intensifies at the time of auroral brightening (Baumjohann et al., 1981). In one particularly clearcut case, the STARE radar followed a 13 km/min equatorward motion of the Harang discontinuity over four degrees of latitude during a half-hour growth phase. At onset, a visual arc at the poleward edge of the electric field-reversal region suddenly activated; it subsequently surged poleward (Neilsen and Greenwald, 1979). The Harang discontinuity appeared not to move much after onset. In another instance, Lyons et al. (1990) found that the Harang discontinuity showed no consistent motion during four successive activations of the poleward arc system on September 24, 1986 that they studied using data from the Greenland magnetometer chain, the Sondrestromfjiord radar, and *Viking* images.

These results suggest that the auroral onset occurs deep within the closed field line region. In that case, the onset ought to be magnetically conjugate between magnetic hemispheres. Indeed, the onset may be more nearly magnetically conjugate than the subsequent evolution of the substorm. Using simultaneous all-sky TV camera, all-sky scanning photometer, and fixed photometer observations at the Syowa Hausfell conjugate pair of stations ($L = 6.1$), Sato and Saemundsson (1987) found that auroral onsets occurred almost

simultaneously in the northern and southern hemispheres, although the subsequent rates of poleward expansion, brightness, and fine structure of the aurora differed between north and south.

12.9 The Westward Surge

The westward-traveling surge, one of the most repeatable features of the premidnight sector substorm, was first recognized in all-sky camera and ground magnetometer data by Akasofu et al. (1965, 1966a,b). A westward electrojet intensifies (or begins) poleward of the pre-existing eastward electrojet, surges poleward and westward at speeds of 2–3 km/s (Opgenoorth et al., 1983), and intense aurora soon invade the premidnight regions that had been relatively quiet prior to onset. As viewed by spacecraft from above, the westward-traveling surge often has a characteristic "S" or spiral shape–in other words, a prominent fold at its leading edge. Occasionally, several folds may be seen simultaneously, each one presumably associated with its own substorm intensification (Shepherd and Murphree, 1991). The westward-traveling surge does not always travel; sometimes it can remain motionless for minutes at a time (Murphree et al., 1989).

It must be emphasized that the formation of the westward-traveling surge is an event distinct from the auroral onset. Simultaneous, accurately timed magnetometer and all-sky camera data were obtained for two substorms in which the onset and the subsequent formation of the westward surge occurred overhead of the observing station (Kawasaki and Rostoker, 1979). A significant westward current was observed to flow parallel to the onset arc for perhaps 2–3 minutes prior to the formation of the westward surge, at which point the westward electrojet intensified dramatically. In one case, the onset arc advanced poleward and trifurcated 2–3 minutes after first brightening, and only four minutes after that was the westward surge was definitively identifiable at the ground station.

The westward surge often if not always evolves in steplike fashion. A westward-traveling surge passing overhead creates a negative perturbation in the H and Z components, and a sudden positive variation in the D component of the geomagnetic field at ground level (Samson and Rostoker, 1983). In studying the phenomenology of "geomagnetic bays" (i.e., substorms on ground magnetometers), Rostoker (1968) noted that a single substorm can be composed of several bursts of activity, each accompanied by Pi 2 micropulsations. From this observation came the suggestion that a westward surge could could be fabricated from many intensifications, each localized to a different region of space (Vorobjev and Rezhanov, 1973; Kisabeth and Rostoker, 1974; Rostoker, 1974; Sergeev, 1974a,b; Wiens and Rostoker, 1975; Pytte et al., 1976a; Kidd and Rostoker, 1991). In other words the surge may not be a continuous displacement of a single auroral form, and its apparent traveling motion may result from the successive appearances of new regions of intense precipitation poleward and westward of earlier ones that die out. A study of ground-based all-sky camera and riometer data led Sergeev and Yahnin (1979) to conclude that localized westward surges propagate as a continuous

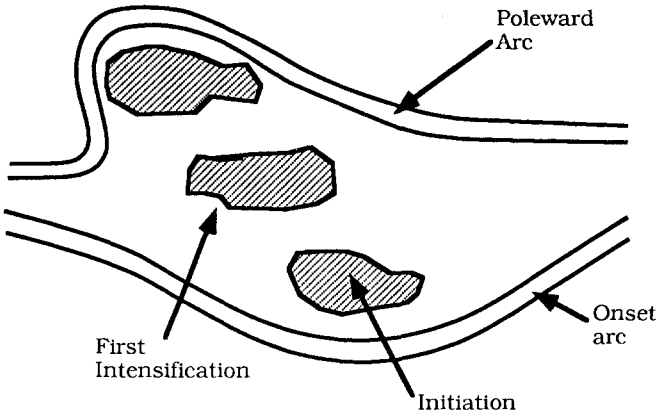

Figure 12. 1. Multiple Intensification of Westward Traveling Surge. The surge may not be a continuous displacement of a single auroral form, and its apparent traveling motion may result from the successive appearances of new regions of intense precipitation poleward and westward of earlier ones that die out. This picture sketches a westward traveling surge that started at a slightly higher latitude than the onset arc, and then faded. When the surge re-intensified several minutes later, it was displaced poleward and westward of the original surge intensification. This process can repeat several times. We have chosen to show the relatively infrequent case where the surge reaches and interacts with the poleward arc system; in many cases, the surge does not affect the poleward arc system. Original drawing.

deformation, while large ones consist of a propagating sequence of quasiperiodic intensifications.

A strong upward field-aligned current coincides with the intense folded aurora at the leading edge of the westward surge. The upward current is concentrated into a cylinder 50–100 km in radius. The compensating field-aligned current flowing downward into the ionosphere feeds the electrojet primarily on the eastern side of the substorm current wedge (McPherron et al., 1973; Kozelova and Lyatskiy, 1984) in a much more distributed fashion (Baumjohann et al., 1980). Model current systems derived from Scandinavian magnetometer chain data consistently indicated that the total current flowing out of the head of the westward surge is about $2–5 \times 10^4$ A (Baumjohann et al., 1981; Bosinger et al., 1981; Inhester et al., 1981). Baumjohann et al. (1981) found a current density of about $8 mA/m^2$ over an area comparable to their computation's 50 km × 50 km grid size. Baumjohann et al. (1981), Inhester et al. (1981), and Opgenoorth et al. (1983) used electric field data derived from STARE radar data as input for model calculations of the ionospheric currents and conductivities associated with the westward surge. Intense particle precipitation anywhere increases the ionospheric conductance, but in the westward surge, the ratio of Hall and Pedersen conductances also increases

(Baumjohann et al., 1981) due to the precipitation of relatively hard, > 10 keV, electrons (Kremser et al., 1982). These effects can suppress the ionospheric electric field below the 15 mV/m threshold for the excitation of plasma waves, whose Doppler shifts are needed to estimate the plasma drift velocity. As a result, coherent scatter radars such as STARE may not be able to measure the electric field in the surge itself. After supplementing missing STARE measurements with in situ rocket measurements, Opgenoorth et al. (1983) concluded that the electric field decreased to 10 mV/m and the Hall and Pedersen conductivities increased to 25 and 20 S, respectively, in the head of the westward surge. Incoherent scatter radars can measure much smaller electric fields than can those that depend on coherent scatter. On the basis of EISCAT, all-sky camera, and *Viking* measurements made during different phases of seven substorms, Kirkwood et al. (1988) and Opgenoorth and Kirkwood (1989) concluded that previous studies had underestimated the conductances and overestimated the electric field in intense aurora by about a factor of 3–4. The height–integrated Hall conductances reached 80 S in all cases, and even well above 100 S in one case. The ratio of the Hall to Pedersen conductances rose from about unity to 2–4 in the westward surges. The authors noted that the spatial profiles of ionospheric conductivity were highly structured.

Occasionally, the upward westward surge current has been detected in polar orbit. The sun-synchronous DMSP F7 spacecraft encountered strong magnetic field perturbations and intense electron precipitation as it passed over a strong westward surge at 830 km altitude on December 31, 1983 (Bythrow and Potemra, 1987). Flowing out of the surge was a 46 kA upward field-aligned current, and flowing into it was a beam of electrons, whose energies rose from 2 keV at the borders of the surge to a 200-km-thick 12 keV plateau at its center. The 2.5 keV temperature of the electron beam was the same as that of the isotropic electrons precipitating into the diffuse aurora ten degrees equatorward of the westward surge. The downward energy flux was about 10 erg/cm^2 s sr, corresponding to a energy deposition rate in the surge head of 0.25 GW. This westward surge was one that definitely interacted with the most poleward arc, and it will be discussed again in due course. On another occasion, April 25, 1985, DMSP F7 flew through three distinct field-aligned current systems enclosing a westward surge (Lopez et al., 1991). The most equatorward of the currents was downward and associated with diffuse auroral electron precipitation. Next came the upward current of a westward surge that apparently was traversed somewhat behind its leading edge. About 1 erg/cm^2 s sr in 12 keV electrons was precipitating into the surge at that point. The spatial profile of the precipitating energy flux was smooth and roughly constant over four degrees of latitude as the spacecraft passed over the surge region. Poleward of the surge, a weaker out–in pair of field-aligned currents was connected to a highly structured poleward arc system. All these structures were several degrees equatorward of the most poleward detectable precipitation, which may have marked the last closed field line. Thus, the same spacecraft has encountered a case in which the westward surge did interact with the poleward arc system, and a case in which it did not.

12.10 The Expanding Auroral Bulge

The surge marks the westward extremity of the so-called auroral bulge, the region of intense auroral activity which typically expands poleward, westward, and eastward following onset. Irregular micropulsations of the so-called Pi B type are characteristic of the MLT sector containing the auroral bulge (Yahnin et al., 1983). Equatorward of the bulge, the diffuse auroral light typically intensifies above the approximately one kilorayleigh threshold of all-sky cameras (Lui et al., 1973). *Viking* images suggest that the eastward expansion of the bulge often stalls very near magnetic midnight, while the westward and poleward expansion continues (Elphinstone and Hearn, 1992). On occasion, the rate of equatorward expansion of the bulge can exceed its rate of poleward expansion. Discrete auroral forms move equatorward in the bright central region of the poleward-expanding bulge (Snyder and Akasofu, 1972) at speeds of ten to hundreds of meters per second (Akasofu et al., 1966c; Craven and Frank, 1987). The discrete forms within the bulge are often north–south aligned. Measurements of balloon electric fields in the northern auroral oval showed that the northward expansion of the bulge is not associated with northward $\mathbf{E} \times \mathbf{B}$ drifts, while the slower southward drifts before onset do correspond to the measured $\mathbf{E} \times \mathbf{B}$ drift (Kelley et al., 1971). Indeed, the fact that auroral forms move equatorward suggests that the convection is equatorward during the poleward expansion of the bulge.

Timofeev et al. (1987) found that the relationship between a visual arc and its accompanying radar arc in the midnight sector depended upon the location of the arc system relative to the auroral bulge. In their data, the morning-type arc system, with the radar arc poleward of the visual arc, occurred at the poleward edge of the auroral bulge, and was associated with roughly 200 nT negative perturbations in the H component of the geomagnetic field, while the evening-type arc system, with the radar arc equatorward of the visual arc, occurred at the equatorward edge of the bulge in association with recoveries of the H component to its undisturbed level. These results imply that the auroral bulge is bounded by an up–down pair of field-aligned current systems at both its poleward and equatorward sides.

Measurements of auroral X-rays indicate that the precipitation of electrons with tens of keV energies occurs in a thin arc at the *poleward* border of the expanding auroral bulge, whereas it occurs equatorward of the structured arcs during the growth phase (Pytte et al., 1976b). Such electron precipitation creates enhanced ionization near 90 km altitude that is responsible for very intense riometer absorption "spikes" of 1–2 minute duration at the observing site. The spikes are 10–50 km thick ribbons of absorption that comove with the expanding poleward boundary of the radar aurora (Neilsen and Axford, 1977; Neilsen and Greenwald, 1978; Hargreaves et al., 1979; Neilsen, 1980). The 0.3–3 km/s poleward speeds of the absorption ribbons cannot be explained by the < 15 mV/m electric field within them[3] (Neilsen, 1980). The meridional component of the electric field is generally directed equatorward in the E-region radar aurora equatorward of the ribbons.

Simultaneous observations in the northern and southern auroral ovals showed that the auroral bulges behaved similarly in each hemisphere, though displacements from conjugacy were pronounced (Burns et al., 1990). A brightening followed 14 minutes later by a poleward expansion of the evening-side aurora (2100–2200 MLT) were observed in the northern oval by the Viking uv imager and by all-sky camera at South pole station. Both the brightening and the initiation of poleward expansion were simultaneous to within a minute at the points of best correspondence. The northern best correspondence point was displaced 5 degrees equatorward and 0.8 hour MLT later than the South Pole magnetic conjugate point. The auroral expansions each covered about 5 degrees in latitude but reached very different stopping points, about 70 degrees north latitude and 78 degrees south latitude.

12.11 Fine Structure of the Substorm Expansion

As we have argued, the propagation of the westward surge and the expansion of the auroral bulge often proceed in a stepwise fashion. *Multiple expansion substorm* is the name we have given to expansions that intensify quasiperiodically on the 5–15 minute time scale (Vorobjev and Rezhanov, 1973; Sergeev, 1974a,b; Pytte et al., 1976a; Rostoker et al., 1980). Each discrete expansion is associated with its own surge form in the ionosphere and has its own bursts of Pi 2 micropulsations (Rostoker et al., 1980).

Each expansion, multiple or not, can also have substructure on the Pi 2 time scale (40–150 s) itself. Sergeev et al. (1986b) found at least a dozen activations in Pi 1 and Pi 2 magnetic pulsations, other magnetic signatures, and cosmic noise absorption during the first 25 minutes of one substorm. Although the activations differed in intensity and spatial extent, an impulsive counterclockwise equivalent current vortex was superimposed on the continuously growing westward electrojet in all but one of the twelve elementary activations. Energetic particle precipitation maximized in the vortex regions, which were about 400 km in diameter. Such activations are often seen in midlatitude Pi 2 pulsation measurements not only as intensifications, but also as sudden changes in polarization or period (Sergeev, 1992). All this motivated Sergeev et al. (1986b) to call microstructure with the time scale of 1–3 minutes "a fine structure of the substorm intensification."

12.12 Proton Aurora Substorm

Following Vegard's (1939) discovery of hydrogen Balmer lines in the aurora, and Meinel's (1950) demonstration that they must be due to precipitating protons because they are Doppler shifted, it was realized that there should be a proton aurora substorm as well as one in electron aurora proposed by Akasofu (1964). Our understanding of the proton substorm has developed more slowly, in part because

the hydrogen Balmer lines are weak and difficult to measure against a strong and active background, and because charge exchange with atmospheric neutrals causes any structure in precipitating protons to spread out into diffuse forms, rendering it difficult to recognize and follow the evolution of characteristic features (Davidson, 1965). Below 300 km altitude, spatial structure with scale sizes < 50 km is smeared out. Nonetheless, there has been progress. The evolution of the Hβ aurora during growth phase and its subsequent expansion, and their relationships to the better understood electron aurora, are the issues of interest in this section.

Our present knowledge of the proton substorm comes primarily from Hβ measurements using meridian spectrographs and scanning photometers. Montbriand (1971) was the first to characterize individual proton aurora substorms, using meridian spectrograph observations. Fukunishi (1975) studied a large number of substorms at Syowa station using the faster meridian scanning photometer technique. He concluded that the westward surge occurs entirely in electron aurora in the premidnight region with proton aurora absent at its leading edge. In the postmidnight region, the region of proton aurora intensifies and expands rapidly poleward, essentially without discrete electron aurora. At the equatorward edges of the oval, diffuse proton emissions were observed in the premidnight region, and electron emissions predominated postmidnight.

Vallance-Jones et al. (1982) compared the electron and proton precipitation patterns in 14 substorms using data acquired by a chain of meridian scanning photometers and all-sky cameras. The scanning photometers measured the meridian profile of Hβ with 30 s time resolution and sensitivity of a few Rayleighs, and other spectral lines due to electron precipitation. In the early evening sector (1930–2130 MLT), the proton aurora extended equatorward of the discrete electron aurora during the growth phase. The proton aurora expanded poleward during the expansion phase, as determined by ground diagnostics, but the strongest proton aurora still remained well equatorward of the electron aurora. In meridian observations made in the region closer to local midnight (2130–2400 MLT), the Hβ auroral intensity peaked strongly equatorward of the electron aurora at the time of onset. After onset, the proton aurora also spread poleward with the westward surge, but the equatorward emission peak remained. There were strong intensifications of the equatorward Hβ after onset in two of five substorms studied in this local time sector. The proton aurora intensified and drifted equatorward during the growth phase of one substorm studied in the postmidnight 000–0300 MLT sector, until the proton aurora was coincident with the electron aurora at the time of onset. After onset, the Hβ emission peak moved poleward and ended up centered poleward of the center of the electron aurora. Thus, the proton and electron aurora exhibited a "cross-over" as the auroral bulge expanded eastward and poleward after midnight.

The proton aurora crossed over the electron aurora in another substorm observed in the postmidnight sector (Vallance-Jones et al., 1982); here, however, discrete electron aurora appeared at the poleward edge of the proton precipitation region 30 minutes after onset and then expanded poleward of the proton aurora. This "expansion" of the electron aurora may actually have been an independent activation of the most poleward arc, as we will see.

12.13 The Phases of the Auroral Substorm

The growth phase is that period of time preceding onset during which the region of auroral emission migrates equatorward. There can be a 5-minute preonset phase, in which the arcs flicker and fade but do not migrate. The 1 or 2 minute period in which the equatorward arc brightens is the onset. The westward-traveling surge is launched several minutes thereafter. The surge develops into the westward extremity of the expanding auroral bulge. Up to now, the behavior of the auroral bulge has defined the subsequent phases of the auroral substorm. Onset is followed by an "expansion," which can last 10–30 minutes and terminates when the bulge has achieved its maximum poleward extent (Akasofu, 1964). Precisely where the auroral expansion ends in relationship to the separatrix between open and closed field lines is a matter of considerable interest, which we will take up in detail. The expansion phase is followed by a typically longer recovery phase. During the recovery phase, the area of the auroral bulge decreases, the brightness of the aurora in it diminishes, and the relatively orderly arclike auroral forms that prevails during the growth phase gives way to more complex discrete forms, such as the "omega bands" that are superposed on intensified diffuse emissions in the postmidnight sector. The recovery phase lasts a variable length of time, until quiet auroral arcs reform and start again to migrate equatorward. The sequence of events starting with onset in which the pattern of aurora loses the order that characterized the growth phase was the original definition of the term *auroral breakup*; today the word *breakup* is often carelessly used to signify the onset itself. In fact, while the aurora may intensify at onset, their pattern does not "break up" until the expansion develops.

Weimer et al. (1992) characterized the behavior of the polar cap potential during the various phases of the auroral substorm. They made 148 double-probe electric field measurements on the DE 2 spacecraft between 300 and 1000 km altitude at times before, during, and after 64 isolated substorms. A superposed epoch analysis referred to the beginning of the expansion phase was used to synthesize a picture of the time dependence of the polar cap potential. Since the spacecraft sampled a polar cap once every 20–30 minutes, this technique should be thought of as binning the potential at roughly half-hour intervals. On average, the polar cap potential started to increase 1.5 hours before the expansion phase began, reached 70 kV in the half-hour before onset, and started to decline 1.5 hours after onset. The polar cap potential at onset always exceeded 40 kV at onset. This result may support the suggestion that onset occurs when a certain threshold polar-cap potential is exceeded (Kan et al., 1988). On a case-by-case basis, there were important deviations from the average pattern: A 120 kV potential was found one hour before onset, and potentials as low as 40 kV were found during some expansion phases. The size of the polar cap at the time of onset ranged between 23 and 38 degrees invariant latitude and averaged 31 degrees. The ratio of the auroral electrojet index to the polar cap potential before and after substorm expansion was fairly constant at 5 nT/kV; it increased somewhat during expansion, presumably due to the increase in ionospheric conductivity at that time.

12.14 The Relationship between the Auroral Bulge and the Poleward Aurora

The behavior of the the most poleward arc system during substorms was not spelled out in Akasofu's (1964) model, and until recently was not specifically set aside for systematic detailed study. The AE index, so often used as a stand in for the expansion of the auroral bulge, is composed of measurements made at geomagnetic observatories distributed around the earth at the between the magnetic latitudes of 62 and 70 degrees and so it too misses much of the electrojet activity associated with the arcs at the poleward border of the auroral electrojet. This most important *lacuna* in our picture of substorms has only recently been filled in by global measurements made on the *Viking* spacecraft.

We introduce our subject by recounting a particularly graphic, early account of two intensifications of the most poleward arc during substorm recovery phase that still communicates as much as any other single experiment how the most poleward arc behaves. The central questions are of course whether, when, and how, the poleward aurora is related to the auroral bulge equatorward of it. So, we first must ask whether the bulge ever overlaps spatially with the poleward boundary of optical emission; we will find that though it can, it generally does not. Next, we ask whether activity on the poleward arc system can be independent of activity in the auroral bulge. We will even find that the most poleward auroral activity can expand equatorward, in sharp contrast to the invariably poleward expansion of the poleward border of the auroral bulge. Honesty compels us to mention next some extraordinarily fine observations of an important counterexample to the general picture we are trying to paint, where the westward surge did reach and actually bifurcated the two arcs of a binary poleward arc system. Then we discuss joint space and ground observations of both the poleward arc system and the aurora at lower latitudes during a multiple expansion substorm with multiple electrojets.

It now appears that activity of the poleward arc system is characteristic of the substorm recovery phase, as defined by the fading of the auroral bulge, although it need not start at the precise moment the bulge begins to fade. As the bulge fades and retreats, the nightside auroral oval often appears to bifurcate, with bright equatorward and poleward regions, each with distinct forms of activity. After this "double oval" forms, at least three different sequences of events have been observed during the late recovery phases of different auroral substorms. Thus, there is no unique recovery phase to the auroral substorm.

One of the first and clearest accounts of the phenomena to be described in this section were made on an airplane flight from Goose Bay, Labrador, to Fairbanks, Alaska, on February 27, 1973 (Wolcott et al., 1976). The optical measurements of the high-latitude aurora taken on the flight were coordinated with *Vela 5A* measurements made as the spacecraft passed through the plasma sheet at a downtail distance of 18 R_E. The airplane, which remained at nearly constant magnetic local time (2100 MLT) near the nominal *Vela* conjugate point, carried all-sky cameras and a magnetic meridian-scanning photometer at 557.7 and 630.0 nm wavelengths. Two substorms occurred during the flight. In both, the photometric aurora initially brightened on the southern horizon (62–65 degrees

north MLAT), and spread poleward over the next 10 or so minutes. In the first substorm, there followed a 1-hour period of relative stability on the 2100 MLT meridian in which there was a "double auroral oval" (Cogger and Elphinstone, 1992). In other words, there was an equatorward emission peak at 62–65 degrees and a separate poleward region of more variable and structured emission near 70 degrees. The double oval interval was followed by a few-minute fading over the entire 12.5 degrees of magnetic latitude scanned by the photometer. Then, in less than 5 minutes, the poleward aurora intensified dramatically from 70 degrees up to and beyond the airplane's 75 degree northern horizon. During this interval, the less-sensitive all-sky camera recorded the poleward passage of a bright structured form over the aircraft at 68 degrees and the independent brightening of an auroral form at about 73 degrees. A magnetometer at Baker Lake at 74 degrees recorded a negative bay at this time. The strong intensification of the poleward aurora subsided after about 5 minutes, but the region above 70 degrees continued to have weak but detectable emission for another 30–40 minutes. The behavior of the second substorm was qualitatively similar, except that the poleward arc system brightened 30 rather than 90 minutes after the westward surge arrived at 2100 MLT. The energy density of the plasma at *Vela 5A* diminished dramatically when the southern aurora initially brightened in each substorm, and returned roughly to its presubstorm value in coincidence with the activation of the poleward aurora. Thus, the plasma sheet at 18 R_E "dropped out" around onset and "recovered" with the activation of the poleward aurora.

Observations such as the previous one forced people to ask whether, when, and how the westward surge, auroral bulge, and the poleward aurora interact. *Viking* images of several different substorms found that the auroral bulge progressed no further poleward than the most poleward pre-existing arc (Shepherd and Murphree, 1991). A study using the all-sky camera and riometer data from a dense net of ground stations found that the poleward expansion of the auroral bulge stopped when it approached a well-defined and motionless poleward arc (Sergeev and Yahnin, 1979). Triangulation measurements indicated that these poleward arcs had lower borders near 140 km altitude, suggesting that they were created by the precipitation of the relatively soft electrons from the plasma sheet or from its boundary layer. Neilsen and Greenwald (1979) presented examples in STARE radar data where a poleward electric field-reversal region remained essentially undisturbed despite repeated poleward surges of active arcs to the south. This behavior of the poleward field reversal region appears now to be consistent with that of the most poleward arc.

On occasion, the poleward arc and the auroral bulge interact. A DMSP F7 image taken from 830 km altitude showed that the westward surge interacted with the most poleward arc during the strong ($\Delta B = -1000$ nT) substorm on December 31, 1983 discussed earlier (Bythrow and Potemra, 1987). The images caught the development of elaborate structure in the midevening sector. A pair of narrow, 20 km, most poleward discrete arcs ran parallel to one another along a line of constant magnetic latitude over several tens of degrees in longitude before 2130 MLT. The arc pair bounded a dark polar cap and was separated by some tens of kilometers

from a broad equatorward region of diffuse aurora. At 2130 MLT, the arcs appeared to have been forced apart by the intrusion of a westward-traveling surge whose bright head spanned 3 degrees of MLAT. The most poleward of the arc pair had been forced to fold and intensify west (ahead) of the surge, and was displaced to 77.5 degrees MLAT, but it always enclosed the surge. Its lower-latitude companion remained near 72.5 degrees MLAT, and enclosed the surge at its equatorward edge. Though the two arcs had been forced apart by the surge, neither one ever lost its continuity, nor did one come into contact with the surge. The head of the surge enclosed by the arc pair spanned about 1 hour of local time. Separating the surge from its enclosing arcs was a downward field-aligned current flowing into a dark region; the discrete arcs contained upward field-aligned currents. The average energy of the precipitating electrons was less than 1 keV except in a 10 km central band, where it rose to 1.5 kev in the poleward arc, and 4 keV in its equatorward companion. The poleward enclosing arc was embedded in a structured band of few hundred eV electron precipitation, which presumably corresponds to the low-energy electron layer enclosing the plasma sheet boundary layer. Thus, the westward surge was on closed field lines, but it displaced and deformed a discrete arc at the poleward border of the auroral oval.

12.15 Activity in the Poleward Arc System

Next, we argue that the most poleward arc has activity of its own that is at best loosely related to the auroral expansion. One 5 minute sequence of *Viking* images taken just after an auroral expansion achieved its maximum poleward extent followed an extended most poleward arc that faded, then brightened, and developed one and then finally five local intensifications spread out over hours in local time. These intensifications all disappeared and reappeared from one minute to the next. Despite all this, the most poleward arc did not move in latitude, and the aurora at lower latitudes appeared to be unaffected (Shepherd and Murphree, 1991). On another occasion, the most poleward arc brightened after the formation of the westward surge but before the auroral bulge reached its maximum poleward extent. The brightening of the most poleward arc spread rapidly and quasiuniformly across local midnight into the dawn sector. The visible and ultraviolet television imagers onboard EXOS-D (AKEBONO) also recorded activations of the poleward arc region that were independent of the behavior of the discrete and diffuse aurora at lower latitudes during substorms (Ejiri et al., 1992).

The activity on the poleward arc sometimes expands equatorward, in contrast to the invariably poleward expansion of the auroral bulge. During the development of what was called a substorm on October 11, 1986, the *Viking* spacecraft detected a number of localized auroral intensifications that were spread out over 4 hours of local time (1900–2300 MLT). None of these intensifications extended very far in latitude, nor did they propagate, but their multiplicity and spatial separation in latitude and longitude were striking (Shepherd and Murphree, 1991). Just prior to a major activation, this activity faded over a region much larger

in scale than can be observed with an all-sky camera. The activation that followed differed so much from a canonical onset that we are tempted to call the event an "antisubstorm." There was a "violent explosion" of aurora that occurred within 1 minute over 4 hours of local time near the pre-existing *poleward* edge of detectable auroral luminosity. One minute later, the intensification had spread *equatorward* but not in longitude. Indeed, the auroral activity did not spread beyond the bounds of the prior transient intensifications. But for its intensity, this "violent explosion" seems to resemble other brightenings of the most poleward arc detected during substorm recovery phase by the *Viking* uv imager.

Now let us turn to coordinated ground and space observations of a series of activations of the poleward arc system during an interval of predominantly northward interplanetary field following a substorm onset on September 24, 1986 (Lyons et al., 1990). A very complex sequence of events took place before *Viking* was even in a position to observe the poleward arc system. The interplanetary field measured at ISEE 1 had had a southward component for 55 minutes during which time Greenland magnetometer chain measurements showed that a single eastward electrojet was migrating equatorward. The substorm occurred, and 3 minutes later, the interplanetary field turned northward and remained northward for more than 2.5 hours. The northward turning initiated a period during which the auroral oval was contracting, so that more and more activity moved poleward and into the range of the Sondrestromfjiord radar. There were five Pi 2 pulsation bursts before *Viking* sighted the poleward aurora. The first occurred 3 minutes before the northward turning, coincident with the development of a negative bay at the southernmost station of the Greenland magnetometer chain (67.5 degrees). The H component measured at this station had a classical substorm time profile over the next 90 minutes. The second Pi 2 burst came after the interplanetary field had been northward for 23 minutes, and the last three came during brief southward excursions in which B_Z switched to roughly zero but had been otherwise positive. Each Pi 2 burst was related to a change in the behavior of the electrojets. A strong westward electrojet was created between 66 and 70 degrees invariant latitude and began to surge poleward at the time of the first Pi 2 burst; its rate of poleward migration increased around the time of the second; an eastward electrojet formed near 74 degrees latitude and expanded *equatorward* at the third, and a new westward electrojet formed at the fourth. Thus, by the time *Viking* imagery became available, multiple electrojets had developed; *Viking* found that the more or less east–west aligned poleward border of the aurora had developed three local bright spots about 0.5 hours MLT apart. (The spots were not really very bright, 3–6 kR in 391.4 nm emission.) The easternmost was in the field of view of the radar, which showed that a pair of arcs separated by about 150 km corresponded to the *Viking* image. The arcs' peak ionization density enhancements were at 140 km and just below 120 km altitude, suggesting they were created by soft-electron precipitation. The *Viking* poleward auroral boundary remained relatively motionless for about 10 minutes, enough time for the radar to establish that an electrojet shear layer coincided with the optical boundary. The electric field was equatorward at the poleward edge and poleward at the equatorward edge of the

shear layer, the same signature found by Weber et al. (1991). After this period of stability, a small portion of the poleward auroral boundary to the east of the Sondrestromfjiord radar beam developed an equatorward-facing bulge which expanded equatorward for the next 3 minutes at an average speed of 84 km/min; the radar was not positioned to determine whether the electrojet also expanded equatorward—as it also had earlier, during the period before the *Viking* observations started. It is noteworthy that this activation occurred when the interplanetary field was northward, and had been predominantly northward for over an hour. A second electric field shear layer, presumably the original Harang discontinuity, was in continuous view of the radar four degrees equatorward of the most poleward arc throughout the period described, and the most poleward arc and this Harang discontinuity had the same electric field signature. In other words, the auroral oval electric field, observed from sufficiently high latitude over a large enough range, developed a double structure.

Cogger and Elphinstone (1992) described localized brightenings of the poleward arc system as a quasiperiodically spaced "vortex street" of counterclockwise auroral forms that forms by rapid (> 5 km/s) eastward motions near the end of the substorm expansion phase. During the 5 minute interval in which these spirals formed on the poleward arc in one event, the auroral bulge further equatorward faded while the arc structures and north–south forms within it continued to move equatorward. Thus, the motions of features within the auroral bulge were independent of those in the poleward arc. The appearance of the chain of spirals was the first indication of the formation of a "double oval," bright at its poleward and equatorward edges, with a dark space between. Sudden brightenings of the poleward part of such a double oval could certainly evoke the name "poleward leap" from ground observers predisposed to believe that the auroral bulge and poleward arc systems cannot behave independently of one another.

12.16 Equatorward Auroral Activity during the Recovery Phase

Many of the phenomena in the literature that have been identified with the recovery phase of the auroral substorm should probably be associated with the equatorward portion of the double oval. For example, it is during the double phase that the optical features known as "omega bands," because of their characteristic curvature, develop at the poleward edge of the equatorward bright region in the morning sector (Pulkkinen et al., 1991; Cogger and Elphinstone, 1992). In one case, magnetic field mapping indicated that the source of omega bands is near geostationary orbit (Pulkkinen et al., 1991). Pellinen et al. (1992) presented a clear example of *Viking* imagery in which morning-side omega bands that evidently were part of the the recovery phase of one substorm were activated at the same time as an evening-side auroral activation that marked the onset of the next substorm. While isolated substorms can and do develop omega bands, omega bands will definitely appear if a new intensification starts. Conventional AE indices cannot resolve such complex developments.

Coordinated ground and space imagery showed that optical pulsations appeared on the equatorward component of the double oval phase during a substorm recovery on April 5, 1986 (Shepherd et al., 1990). *Viking* ultraviolet images revealed two clearly defined regions of bright aurora on the nightside, one associated with the poleward arcs at 70°N MLAT, and another in more diffuse emission at 64 degrees. To the spacecraft, it was the poleward arc region that appeared variable on an 8 minute time scale, while the equatorward region seemed steady. However, Fourier analysis of ground photometric data showed that the equatorward diffuse auroral region that had seemed smoothly varying to the broad *Viking* field of view actually pulsated with well-defined periods of 59, 75, 104, and 189 seconds. The all-sky camera showed that it was only the equatorward edge of this feature that was pulsating.

Pulsating auroras, quasiperiodic fluctuations in auroral brightness with a period between 2 and 20 seconds (Johnstone, 1978, 1983),[4] spread poleward and eastward following onset, but remain near the equatorward edge of the (double?) oval (Oguti et al., 1981). Those that spread westward seem to be weaker than those in the morning sector. The shapes of the pulsating auroral forms—which include thin arc segments aligned east–west, featureless irregular patches, patches with intricate detail—is persistent and changes only over several minutes. Neighboring patches pulsate independently of one another in period and phase. The forms have a 50–100 km scale. All the forms in a display drift across the sky at nearly the same velocity, 0.1–1 km/s, which is eastward after local midnight. Pulsating aurora tend to occur at the same time as and to have similar dynamic frequency spectra as Pi C irregular geomagnetic micropulsations. Oguti (1986) argued that Pi C are caused by temporal and spatial fluctuations of the electric currents induced in enhancements of the ionospheric electrical conductivity produced by a variable rate of electron precipitation. The pulsations persist throughout the recovery phase until a new quiet arc system forms.

Detailed studies of the pulsating auroral light and the electron precipitation associated with it give a clue as to where it is generated. The spacing between maxima in a single train of auroral pulsations is not even but varies from one pulsation to the next. The light intensity does not vary sinusoidally even in a single pulse, but alternates between between low and high as if it were switching on and off. The pulsating aurora is weak compared to both quiet arcs and westward surges. While the 427.8 nm intensity of bright auroral forms can reach 100 kR, it is always less than 10 kR in the pulsating aurora, and it is often close to the 1 kR visual threshold of the eye, which enhances the perception of flickering. Rocket measurements show that the precipitating electrons responsible for the pulsating aurora have a Maxwellian energy distribution whose 1.8–12 keV temperature pulsates with a 5–20% amplitude. Triangulation measurements show that the altitude of the lower border of the pulsating auroral emission is below 100 km, lower than for most auroral forms. The ionization at low altitude is probably created by the high-energy tail of the Maxwellian electron energy spectra. There is no sign of acceleration by a parallel electric field. This and other evidence suggests that the pulsating aurora is created by modulated electron pitch angle diffusion

induced by modulations of the ELF whistler wave amplitude at the geomagnetic equator (Johnstone, 1983). This places the source of the pulsating aurora on closed quasidipolar field lines relatively near the earth.

12.17 The End of the Recovery Phase

Up to this point in the substorm sequence, there seems to be general agreement about the nature and rough order of the events in the substorm sequence. Now, for the first time, we arrive at a bifurcation, indeed a trifurcation.

All-sky camera and magnetometer data collected along the Alaska meridional chain provided clear evidence that the expansive phase of one substorm and the recovery phase of its predecessor can coexist in the same local time sector (Kamide et al., 1977). The characteristics of the auroral electrojets and of the midlatitude perturbations for the two substorms were essentially the same as those for ordinary isolated substorms. The two substorms occurred on January 12, 1973 during a 2-hour period of strong (6 nT) southward interplanetary magnetic field that began a half-hour before the first of the pair. A rapid equatorward motion of the poleward arcs commenced 10 minutes after the southward turning and continued for the next 30. Sixteen minutes after the poleward arcs started their equatorward migration, the arcs above College, Alaska, folded and began to move poleward at a speed of 0.58 km/s, marking the expansion of the first of the substorm pair. The auroral electrojet was confined to a narrow latitudinal band around College. A small positive increase in the H component of the geomagnetic field was observed at midlatitude observatories. Thirty-one minutes after the first expansion, a new sudden brightening and auroral expansion occurred at College, and there was a sharp increase in the midlatitude H component. The second auroral bulge developed within the bulge of its predecessor. Its aurora advanced poleward up to 80 degrees north geomagnetic at an unusually high speed (up to 1.5 km/s). It is important to note that during the expansive phase of the first substorm, the auroral arcs in the poleward half of the oval continued to move equatorward with undiminished speed, suggesting that open magnetic flux was accumulating at an undiminished rate in the lobes of the tail. These observations are another example of the relative independence of the poleward and equatorward arc systems.

Cogger and Elphinstone (1992) have recently reported that substorm recoveries observed by *Viking* have gone down three paths following the intensification of the most poleward arc described. The poleward arc in some cases has been reactivated by another spiral or surge form. Sometimes, a new onset and expansion has occurred on the equatorward arc system, initiating a new substorm before the old one completely recovered (as previously). In other cases, the poleward arc system has faded and or moved equatorward, while the equatorward system has moved poleward. Thus there is no unique end to the recovery phase to the auroral substorm.

12.18 Synthesis

Let us recapitulate the modernized version of Akasofu's (1964) auroral substorm paradigm that has emerged in this section. The growth phase of the auroral substorm starts with the activation of high-latitude arcs on the dayside, followed by an increase in the cross-polar cap electric field, stimulation of two-cell ionospheric convection, and equatorward arc motion around the auroral oval. The X-ray arc and the Harang discontinuity comove equatorward with the auroral arcs in local evening sector. As this evolution proceeds, the arcs can fade and recover over much of their length. Those on the nightside can also brighten locally in a miniature version of the westward surge to come. These pseudoexpansions need not be on the onset arc. About 5 minutes before onset, the evening sector equatorward motion can stop, and the auroral and X-ray arcs will fade. The substorm onset is the brightening of a small region of the most equatorward arc. The pre-existing pattern of auroral light simply intensifies. The brightening spreads eastward and westward until after a minute or so the onset arc will have brightened over several thousand kilometers of its length. The onset arc is on closed field lines. Following onset, a westward-traveling surge with important subintensifications on the 1–2 minute timescale develops on or slightly poleward of the onset arc. The region of bright aurora—the so-called auroral bulge—expands poleward, westward, and eastward for the next few tens of minutes. The westward extremity of the expanding auroral bulge continues to be marked by the westward-traveling surge, a localized region of intense aurora and upward field-aligned current. The bulge of auroral light often stops expanding at its eastward edge near local midnight. The substorm expansion phase ends when the auroral bulge achieves its maximum poleward extent. Very often, the arc marking the poleward border of auroral light in the midnight sector, sometimes called the *poleward traversing arc*, brightens across several hours of local time about the time the auroral bulge begins to subside, occasionally even before. The auroral bulge usually does not approach the poleward traversing arc, but sometimes it does. During the substorm recovery phase, as the area of the auroral bulge decreases and the brightness of the aurora in it diminishes, the auroral oval observed from above may appear to have a double structure: A bright poleward arc system with multiple localized spiral-like activations is separated by a dark lane from the declining auroral bulge. Some of the activations may be accompanied by Pi 2 pulsation bursts. After this, there seems to be no unique way in which the substorm ends.

NOTES

1. Classification of auroral expansions by their area, or perhaps by their area–intensity product as a function of time, would be more objective and quantitative way to compare the expansion phases of different substorms.

2. EXOS-D (AKEBONO) was launched on Feb. 21, 1989 and carried a visible and ultraviolet TV imager with a 30 × 40 degree field of view, a resolution of 244 × 188 pixels, a

normal exposure time of 0.4 s, and an image frequency of once every 8 s. Typical auroral exposures were taken from altitudes of 2500–4800 km.

3. The region of depressed electroc field inside the absorption spike is unable to generate ionospheric irregularities detectable by radar backscatter. It would have a signature similar to that used by Neilsen and Greenwald (1979) to identify the Harang discontinuity and other electric field reversal regions.

4. Much of our discussion is based on two reviews by Johnstone (1978, 1983).

13

THE GEOSYNCHRONOUS SUBSTORM

The reconnection model of substorms deals with the large-scale changes in the structure of the magnetosphere and tail as convection intensifies following a sudden increase in the dayside reconnection rate. The model has difficulty making statements relevant to the small scales that characterize auroral onset. However, there has been considerable progress in assembling high-resolution observations of the events in space that now appear to be tightly coupled to the dramatic auroral events that first defined the term *substorm.* We will call this clear and consistent ensemble the *geosynchronous model of substorms*, since most of it was first conceived from observations made on geostationary spacecraft. We will also include in this ensemble the recent observations made using the quasigeostationary spacecraft, AMPTE/CCE, and so, by the geosynchronous substorm, we really mean the substorm as it appears on the earth's nightside typically between 6 and, say, 10 R_E downtail.

The earth's magnetic field at geosynchronous orbit is about 100 nT, some three times larger than in the tail lobes. Study of quiet field intervals singles out the dependence of the geosynchronous field on solar wind dynamic pressure, since the modulation due to changes in the direction of the interplanetary field is presumably negligible during quiet conditions. The periodic variations in the quiet field depend on local time, season, and orientation of the earth's dipole axis relative to spacecraft location (McPherron and Barfield, 1980; Rufenach et al., 1992). Superposed on the quiet field are perturbations up to about 50 nT due to several magnetospheric current systems, including the magnetopause current, the ring current, and the cross-tail current; the most striking are due to changes in the cross-tail current system. Observations from geosynchronous orbit were the first to indicate that the nightside magnetic field becomes more "tail-like" during substorm growth phase, and more dipolar during the expansion phase. This simple observation is the foundation on which today's elaborate geosynchronous substorm model rests.

13.1 Development of a Tail-Like Field during the Growth Phase

The geosynchronous field becomes progressively more "tail-like" as the cross-tail current system intensifies and/or moves earthward during the substorm growth phase (McPherron et al., 1975; Coleman and McPherron, 1976; McPherron, 1979;

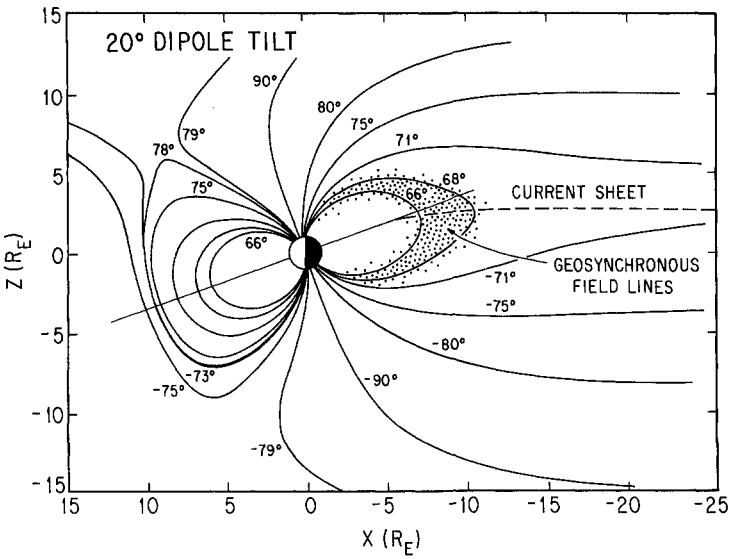

Figure 13.1. The "Geosynchronous Region." The magnetic field lines in the (magnetic) noon–midnight meridian plane are labeled according to the (magnetic) latitudes of their footpoints for a dipole tilt of 20 degrees (Fairfield, 1991). We have shaded the region, near the geosynchronous orbit, where the phenomena discussed in this chapter occur. The inner boundary of the geosynchronous region is well defined; dipolarizations and related phenomena occur very infrequently within $L = 6.4$. The outer boundary is less clear, but functionally is at a distance of the order of ten earth radii from the earth. D. H. Fairfield, *J. Geophys. Res.*, *96*, 1484 (1991), copyright by the American Geophysical Union.

Kauffmann, 1987). A geostationary spacecraft can be as far as 11 degrees from the geomagnetic equator, depending upon its local time; the nongeostationary spacecraft, AMPTE/CCE, sampled magnetic latitudes up to 16 degrees. While such spacecraft observe the development of the tail-like field away from the equator, near the nominal equator they find the magnetic field retains its dipole direction but diminishes in magnitude. The low-latitude subset of APMTE/CCE observations indicated that as much as 5/6 of the earth's dipole field can be outright cancelled by the fringing fields of the cross-tail current system just before onset (Lui et al., 1991). Among other things, this illustrates how problematical auroral oval mappings based on average empirical geomagnetic field models become once the substorm growth phase has started to unfold in earnest.

The development of the tail-like field is a delayed consequence of dayside reconnection. In the substorm of January 28, 1983, the magnetic field at GEOS-2 started to become tail-like 15 minutes after an abrupt southward shift in the

interplanetary magnetic field arrived at the magnetopause (Baker et al., 1990a). The tail-like field developed somewhat more rapidly in the substorm of March 4, 1979. Measurements on ISEE 3 and IMP 8 in the solar wind, on GEOS 2 at synchronous orbit on the nightside, and on ISEE 1 and 2 in the near-earth plasma sheet were coordinated with multipoint balloon-borne and ground-based magnetometry and photometry in an unusually integrated study of the auroral and magnetospheric response to a sharp southward turning of the interplanetary magnetic field (Savaud et al., 1987). The eastward and westward electrojets began to increase within 5 minutes of the southward turning at the magnetopause, and the magnetic field at geostationary orbit started to become tail-like within 10 minutes. The fact that the tail-like field develops on the time scale associated with the development of convection, the inward migration of the magnetopause, and enhanced tail flaring had been anticipated theoretically. As flaring increases, the tailward stress exerted on the tail lobes by the solar wind increases, and the the cross-tail current sheet will have to approach the earth to maintain stress balance with the earth's dipole field (Siscoe and Cummings, 1969; Coroniti and Kennel, 1972a). As a result, the magnetic field on the earth's nightside should become more "tail-like," and the fringing field from the inner edge of the current sheet will depress the magnitude of the magnetic field near the geomagnetic equator.

The growth of the tail-like magnetic field at geosynchronous orbit is accompanied by the development of "cigar-shaped" field-aligned energetic electron anisotropies (Baker et al., 1978). At the same time, the fluxes of energetic particles drop, often to background (Walker et al., 1976; Baker et al., 1978; Sauvaud and Winckler, 1980; Baker, 1984; Lopez et al., 1988c). Measurements from low-altitude polar orbit indicate that the poleward boundary of trapping of energetic electrons moves equatorward during the growth phase, consistent with the progression earthward of a current sheet so thin that trapped energetic electrons are lost when they drift into it (Galperin and Feldstein, 1991). The > 10 keV electrons responsible for the X-ray arc and for the thin equatorward-propagating band of low-altitude ionization (Kirkwood and Eliasson, 1990) were precipitated from field lines close to this radiation belt trapping boundary. These electrons were scattered into the atmosphere as the region of tail-like magnetic field moved earthward. Substorm onset often starts on the most equatorward of the equatorward drifting auroral arcs (Pellinen and Heikkila, 1984). Since this arc is immediately poleward of the > 10 keV electron trapping boundary and > 10 keV electron precipitation band, the onset arc maps near the earthward edge of the tail-like region. Given the inapplicability of empirical magnetic field maps to the dynamically evolving substorm growth phase, observations such as these provide independent evidence that connects the onset arc to the inner cross-tail current region.

13.2 How Thin Does the Current Sheet Get?

The experimenters associated with the OGO 5 spacecraft devoted an early version of a coordinated data analysis workshop to the substorm of August 15, 1968. As

part of that effort, Buck et al. (1973) applied the "particle sounding technique" to 100–800 keV proton data to track the position of the plasma sheet boundary layer at 2 minute intervals during the substorm's 34 minute growth phase. The plasma sheet near 8 R_E downtail appeared to thin from a half-thickness exceeding 1.5 R_E before the growth phase started to a few tenths of an R_E at onset. The authors suggested that a "thinning wave" developed beyond OGO 5 about 15 minutes into the growth phase and passed over OGO 5 just before onset. This wave had an initial *e*-folding length of 0.1 R_E which dropped to 0.03 R_E at onset; its velocity perpendicular to the magnetic field varied from 4 km/s in the early growth phase to a peak of 10 km/s just before onset. The plasma sheet and magnetic field configuration then expanded rapidly outward with an initial speed of 90 ± 30 km/s.

Later ISEE 1 and 2 measurements made at 13 R_E downtail during the growth phase of an official CDAW substorm, the CDAW 6 substorm of March 22, 1979, led to the same general conclusion: The current sheet scale height thinned from 6 to 0.5 R_E (McPherron et al., 1987). Immediately after the onset of this substorm, the current sheet thinned a factor of 8 more, to 400 km. A complementary analysis using a global magnetic field model reached the same conclusion, and suggested that the field had been sufficiently stretched to scatter low-energy electrons nonadiabatically (Pulkkinnen et al., 1992). On another occasion, when ISEE 1 and 2 were 10 R_E downstream of earth, one spacecraft found itself above and the other below the current sheet: The entire sheet had to be thinner than the distance between the spacecraft, about 400–800 km (Mitchell et al., 1990). To put these measurements in context, Larmor radius of a 10 keV plasma sheet hydrogen ion was 100 km in the surrounding enhanced tail-lobe field (50 nT), clearly larger in the plasma sheet, and 5000 km in current sheet normal field (1 nT). This thin current sheet was encountered three times over a 10 minute period; on the fourth meeting, the current sheet thickened. Thus, the current sheet can thin to half-thickness of a very few ion Larmor radii and remain stable for at least 10 minutes.

How is the current carried as the plasma sheet thins? The plasma current perpendicular to the magnetic field can be expressed as a sum of a term involving the gradient of the perpendicular pressure and another containing a "firehose" pressure anisotropy term divided by the radius of curvature of the magnetic field in a collisionless, adiabatic plasma. Twenty years ago, Rich et al. (1972) and Cowley (1978) inferred that the parallel pressure has to exceed the perpendicular pressure to account for the current densities in the thin current sheets observed during growth phase, but only recently have there been direct measurements of the pressure anisotropy. An electron anisotropy developed during the growth phase of the CDAW 6 substorm and disappeared just before onset. In the Mitchell et al. (1990) event, the measured electron firehose anisotropy was able to sustain about one-third of the cross-tail current during the first two current sheet encounters, but in the encounter just prior to the dipolarization, the current was carried entirely by the serpentine motions of nonadiabatic ions described by Speiser (1965). AMPTE/CCE measurements showed that the energy density of ionospheric ions was enhanced during the early growth phase of another substorm (Daglis et al., 1990). The measured anisotropy of ions of ionospheric origin could carry a cross-

tail current that sustains a magnetic field radius of curvature of two earth radii and a 10 nT amplitude; since these were single-spacecraft measurements, there was no independent estimate of the thickness of the current sheet.

13.3 Dipolarization

Dipolarization, a return from a tail-like to a more dipolar configuration, is the most striking feature of the substorm at geostationary orbit (Cummings et al., 1968; Russell and McPherron, 1973a; Savaud and Winckler, 1980; Nagai, 1982; Baker, 1984). The AMPTE/CCE spacecraft often found itself in the region where that reconfiguration is the most abrupt, occurring within 1 or 2 minutes, and the observers associated with this spacecraft came to give dipolarization another vivid name, "current disruption." If the tail-like field develops because a cross-tail current system approaches geostationary orbit, dipolarization corresponds to the retreat of that system (Coleman and McPherron, 1976). The amplitude of a given dipolarization is roughly proportional to the degree to which the field previously became tail-like, and the magnetic field tends to return to the average quiet day configuration (Kokobun and McPherron, 1981). The ground signature of dipolarization is a "positive bay," a small increase in the H component of the geomagnetic field observed at midlatitudes (Iijima and Nagata, 1972; McPherron, 1972; Clauer and McPherron, 1974; Rostoker et al., 1980). Dipolarizations at geostationary orbit correlate well with positive bays recorded on the ground in the same local time sector (Kokobun and Mc Pherron, 1981). In one especially well-timed case, large variations of the magnetic field at AMPTE/CCE commenced less than a minute after ground measurements of a positive bay indicated the expansion of a dipolarization into the AMPTE/CCE local time sector (Lui et al., 1991).

The elliptical orbit of AMPTE/CCE permitted study of the radial as well as the azimuthal distribution of dipolarizations out to 8.8 R_E. Magnetic field and energetic particle data were used to identify 103 dipolarizations occurring between March and August, 1985, a period when AMPTE/CCE was typically a few degrees south of the magnetic dipole equator (Lopez et al., 1988b,c). No dipolarizations whose amplitude exceeded 15 degrees were observed inside 6.4 R_E; the normalized occurrence frequency increased with radial distance beyond 6.4 R_E. The occurrence frequency was four times larger for Kp > 4+ than for Kp < 3-, no surprise since Kp in part measures substorm activity; what was somewhat surprising was a shift in the central meridian with increasing activity from 2300–2400 MLT for Kp < 3- to 0100–0200 MLT for Kp > 4+.

Dipolarization is a feature of the generalized geostationary region we have defined here, and seems not extend further downstream. This point was made by Pytte et al. (1976b), who studied four multiple expansion substorms using data from OGO 5 and *Vela 4a*, which were both located near local midnight at about the same distance from the expected position of the neutral sheet but were separated by 3–10 R_E radially. OGO 5 was in the generalized geostationary region, whereas *Vela 4A*, in a circular orbit at 17–18 R_E, was in the near-tail region studied later by

ISEE 1 and 2 and AMPTE/IRM. The individual expansions in each substorm were separated by 10–15 minutes. Successive dipolarizations and ancillary phenomena were observed at OGO 5 in an almost one-to-one relationship with the ground Pi 2 bursts marking the multiple expansions, whereas *Vela 4A* observed either plasma sheet thinning or found itself in the tail lobes at these times.

13.4 Dispersionless Injections

Dipolarization is accompanied by a rapid and simultaneous increase in the intensities of both energetic ions and electrons, with little or no time-of-flight velocity dispersion up to energies of several hundred keV on the 1-minute time-scale (McIlwain, 1974). These events are called "dispersionless injections." The intensities after dipolarization often greatly exceed those measured prior to plasma sheet thinning; the 50–150 keV electron intensity, for example, typically increases by a factor of 10 or more (Lezniak and Winckler, 1970; Erikson et al., 1979; Neilsen et al., 1982). The energy densities of H^+, O^+, He^+, and He^{2+} ions increase simultaneously at the time of dipolarization (Daglis et al., 1990a,b). The particle energy of maximum contribution to the ion pressure increases from before to after injection, and the overall plasma plus magnetic pressure within 10 R_E increases (Kistler et al., 1992). Since the total pressure beyond 10 R_E either remains the same or decreases, the increase in total pressure may reflect a reduction in tailflaring following dipolarization.

Energetic electrons, which develop a field-aligned anisotropy prior to onset, change to the opposite "pancake" distribution after onset (Baker, et al., 1978). When such energetic electrons or ions are observed far from their injection region, the dispersal with energy in the particles' arrival times may be used to estimate the magnetic longitude and time of injection. Following injection, energetic electrons drift toward the morning side, and when their fluxes approach the stably trapped limit (Kennel and Petschek, 1966), their pitch angle distribution approaches isotropy, the rate of precipitation of electrons with tens of keV energy nears the strong diffusion limit (Kennel, 1969), and there are intense riometer absorption events in the morning side ionosphere following substorms in the midnight sector. (Baker et al., 1981b). In a continuation of the study of the substorm of July 3, 1979, Kremser et al. (1986) confirmed that much of the energetic electron precipitation observed by their balloon X-ray measurements resulted from the pitch angle scattering of equatorial electrons with measured whistler mode waves. However, the X-ray arcs equatorward of the visual arcs during growth phase and poleward of the auroral bulge during the early expansion phase could not be explained by wave–particle interactions.

The energy-independent equatorward boundary of the diffuse aurora created by a dispersionless injection is easily recognizable to a polar-orbiting spacecraft. Except at times of profound magnetic quiet, the equatorward cutoff latitudes of the diffuse auroral precipitation are usually ordered by energy, with electrons equatorward of the ions at all local time sectors except local evening,

where the ions are equatorward of the electrons. The signature of a dispersionless particle injection therefore stands out: an abrupt shift of the diffuse electron and ion precipitation to a common energy-independent equatorward boundary. Newell and Meng (1987) found 10 examples, in 25 days of DMSP F6 and F7 data, of isolated injections in both electrons and ions for which the equatorward precipitation boundaries shifted by a degree or more from their positions observed on the previous orbit. For each dispersionless event observed by F7 in the 1035–2235 meridian plane, an injection was observed within 20 minutes at F6 in the 0640–1840 MLT meridian plane; the two equatorward cutoffs of the diffuse auroral precipitation typically agreed within 0.1 degrees. In general, ions were dispersionless up to 30 keV, whereas electron dispersion appeared above 10 keV. In 4 of the 10 cases, injections that were dispersionless near midnight were also dispersionless at other local times, ranging from 1040 to 1740 MLT. In the remaining 6, the injections appeared either dispersed or not at all at other local times. The spacecraft typically caught the injections about 10 minutes after onset, and so some dispersion was to be expected, as the more energetic particles drifted to the spacecraft from an earlier injection at the central meridian of the substorm.

13.5 The Substorm Current Wedge

Since dipolarization implies a diminution of the cross-tail current in an azimuthally localized region, we expect to find field-aligned currents into the ionosphere on the morning side of the dipolarizing region, and outwards on the evening side. Field-aligned currents are usually too weak to be detectable at geostationary orbit except in association with substorms. Then, perturbations in the D component of the magnetic field, indicators of field-aligned current, begin to be observed at ground onset and reach peak amplitude at local dipolarization in the H and V components at the spacecraft. The rate, duration, and magnetic signature of the dipolarization depends on the azimuthal separation of the spacecraft from the central longitude of the substorm. In particular, dipolarizations observed to the west and to the east of the substorm central meridian have positive and negative D variations, implying that the field-aligned currents are into the ionosphere to the east and out of the ionosphere to the west (Kokobun and McPherron, 1981).

The D-variation pattern described is the observational foundation of the *substorm current wedge* model. According to this model, the cross-tail currents are diverted in distributed fashion down field lines into the postmidnight auroral oval ionosphere, where they flow westward to enhance the auroral electrojet following onset (McPherron et al., 1973; Baumjohann, 1983). The currents return to the plasma sheet in the premidnight sector, flowing upwards along magnetic field lines largely out of the westward surge. The observed diversion of the cross-tail current can produce the observed decrease in the magnitude of the tail-like component of the magnetic field, B_X, together with the increase in the northward (dipole) component, B_Z (Kamide et al., 1974). The decrease in B_X is closely associated with the dispersionless injections (Lopez et al., 1988a, 1989).

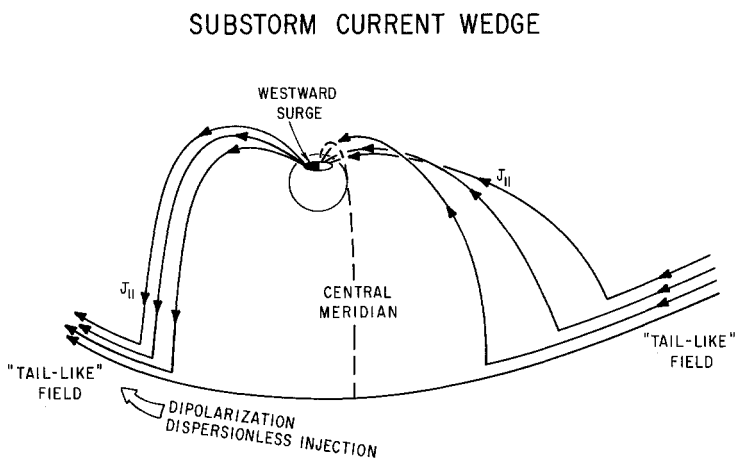

Figure 13.2. The Substorm Current Wedge. The magnetic field near the inner edge of the cross-tail current sheet becomes progressively more tail-like during the growth phase of the substorm. At onset, the tail-like field begins to dipolarize in a small azimuthal region surrounding the central meridian of the substorm. This dipolarization is accompanied by a dispersionless injection of electrons and ions with energies ranging up to hundreds of KeV. As time passes, the dipolarization propagates both westward and eastward, always accompanied by a localized dispersionless injection. The field outside the current wedge continues to become more tail-like until the dipolarization arrives. The westward dipolarization front maps to the westward surge in the ionosphere. A field-aligned current flows out of the westward surge and connects to the westward extremity of the current wedge. A more distributed field-aligned current feeds into the ionosphere from the eastward portion of the current wedge. The current wedge can thus be pictured as a diversion of part of the cross-tail current into the auroral ionosphere, where it flows across the substorm central meridian in the westward electrojet. Original drawing.

The field-aligned currents forming the eastward and westward limbs of the substorm current wedge are far from smooth and unstructured. The existence of extraordinarily fine structure in the field-aligned currents has been inferred in a roundabout way. Broad-band bursts of magnetic field noise are frequently detected in association with substorms at geostationary orbit (Robert et al., 1984). These so-called *short irregular pulsations* extend in frequency from the Pi 2 range (see the following) to above 10 Hz. They were always found at the times dipolarizations propagated over GEOS 2, but also occurred at other times during the substorm sequence. The short irregular pulsations appear to be signatures of intense, highly localized, fast-moving field-aligned current filaments. Current filaments were found in both sides of the current wedge, but the majority in the GEOS 2 data set propagated eastward and involved earthward field-aligned currents. Twenty-eight events lasted less than 2 seconds and could be analyzed unambiguously. Intense (3–25 mV/m) electric field spikes preceded the passage of the localized currents over the spacecraft by 10–20 seconds; the corresponding $\mathbf{E} \times \mathbf{B}$ speeds in the spikes

were 15–170 km/s. A simple transformation of the magnetic field data yielded a direction of propagation of the current filaments. Those associated with substorm dipolarizations propagated within 40 degrees of the negative $\mathbf{E} \times \mathbf{B}$ direction; the radii of the current tubes could be calculated by assuming they moved with the $\mathbf{E} \times \mathbf{B}$ speed. The inferred 20–900 km radii were comparable to the ion inertial length at geostationary orbit. They projected to 1–50 km in the ionosphere, while the current densities at GEOS 2, 6–300 nA/m^2, projected to 3–150 mA/m^2. These figures correspond to the most intense and localized field-aligned currents observed in low polar orbit.

The fine structure in the current wedge is more than a detail. Robert et al. (1984) noted that the current density frequently rose to, but never exceeded, the Kruskal–Shafranov MHD stability limit (Kruskal and Schwarzschild, 1953; Shafranov, 1956). In other words, the substorm current wedge drives small-scale field-aligned currents to the edge of instability, where the field line develops a 180 degree corkscrew between the ionosphere and magnetic equator, but no further. The effects of the filamentary structure of the substorm current wedge are not all clear, but it does seem that the small-scale currents radiate oscillations that are seen on the ground as micropulsations.

13.6 Pi 1 and Pi 2 Pulsations and the Timing and Location of Substorm Onset

Bursts of Pi 2 geomagnetic pulsations, damped oscillations of 40–150 s period with an irregular waveform, are associated one for one with substorm onsets and intensifications. They were recognized before substorms were invented (Holmberg, 1953) and became the subject of intensive study as their connection with substorms became clear (see Saito, 1961, 1969; Kato, 1965; Morozumi, 1965; Heacock, 1967; Akasofu, 1968; Rostoker, 1967a,b, 1968; Saito et al., 1976; Southwood and Stuart, 1979). High-latitude Pi 2 activity comes in two forms—bursts of a few minutes duration that occur predominantly near local midnight and that tend to be distributed spatially along the Harang discontinuity, and in continuous activity that is restricted to the post-midnight region (Heacock, 1982). The Pi 2 bursts were first associated with substorm onset by Rostoker (1967), and shortly thereafter it was shown that they accompany each and every expansion of multiple expansion substorms (Pytte et al., 1976a; Sakurai and Saito, 1976). Bursts of magnetic field oscillations in the Pi 2 frequency band are seen in almost every substorm at geosynchronous orbit in the midnight sector, and virtually every burst found in orbit can also be found at ground stations at the same meridian as the spacecraft (Coleman and McPherron, 1976; McPherron, 1980; Sakurai and McPherron, 1983, Sakurai et al., 1983; Singer et al., 1983). Their periods are roughly 2–10 times times longer than the Alfven wave travel time from the geosynchronous equatorial plane to the auroral ionosphere (Sergeev, 1992). The Pi 2 bursts in geosynchronous orbit have a shocklike initial deflection whose D component has the same sense as the D variations of the current wedge on either side of the substorm central meridian (McPherron, 1980). After the first deflection, the bursts have an irregular

waveform, and fade to background in 5–15 minutes. These observations make it clear that Pi 2 oscillations are the fine structure of the current wedge.

Many of the Pi 2 bursts observed in space have a strong compressional component, indicating they will stimulate a response at midlatitude ground stations, where they provide excellent diagnostics for the time and central longitude of substorm onset, the width of the initial current wedge, and its subsequent azimuthal expansion (Heacock, 1982; Hughes, 1983; Samson and Rostoker, 1983; Sakurai and McPherron, 1983; Baumjohann and Glassmeier, 1984, 1986; Vero, 1986; Yumoto, 1986). Because midlatitude Pi 2 bursts are not obscured by other activity, they are one of the most reliable ways to time and locate substorm onset, short of being present underneath the onset arc at the moment it brightens. The polarization of low-latitude Pi 2 pulsations is typically right-handed with respect to the magnetic field in the premidnight sector and left-handed in the postmidnight sector; the polarization reversal may be used to determine the central meridian of the substorm current wedge. The Pi 2 amplitude falls off with increasing distance from the substorm central meridian. Sutcliffe (1980) found that he could almost always observe a Pi 2 burst at substorm onset within 1 or 2 hours of 2300 MLT. Farther away, it was progressively less likely that a Pi 2 burst would be detected, though there remained a distinct probability of detecting Pi 2 at all local times, even on the dayside. A technique of data-adaptive filtering has recently been used to identify low-latitude dayside Pi 2 bursts concealed by other noise sources (Sutcliffe and Yumoto, 1989). Thirty-nine of 47 bursts observed on the nightside were detected simultaneously on the dayside, and the 8 events missed on the dayside corresponded to small-amplitude events on the nightside.

It is generally thought that Pi 2 are detectable on the ground within a minute or so of the initiation of dipolarization somewhere in the magnetosphere. Yumoto et al. (1989) studied the relationship between Pi 2 onset at midlatitudes and magnetic dipolarizations observed on AMPTE/CCE when it was in the local midnight sector 5–8 R_E from earth. In general, Pi 2 started on the ground several minutes before dipolarization propagated to AMPTE/CCE. However, in one event, when large fluctuations in the north–south component of the magnetic field suggested that the spacecraft was in or near the active current disruption region, the midlatitude Pi 2 oscillations observed on the ground started 60–80 s *after* dipolarization began at AMPTE/CCE.

The term *Pi 1* stands for irregular magnetic pulsations with 5–40 s period, periods comparable with the Alfven travel time to the ionosphere from the equatorial plane at geostationary orbit (Sergeev, 1992). High-latitude Pi 1 activity also comes in bursty and postmidnight continuous forms (Heacock, 1982); the Pi 1 bursts time substorm onset even more accurately than Pi 2 bursts do (Bosinger et al., 1981; Yahnin et al., 1983; Bosinger and Yahnin, 1987). If the ground detector is within several degrees of latitude and 1–2 hours MLT of the auroral activation, Pi 1 bursts time the onset with 10–20 second accuracy. Indeed, since the periods of Pi 2 micropulsations are comparable with the duration of the auroral substorm onset, it is more accurate to say that Pi 1 bursts can time onset, while Pi 2 bursts can only time the beginning of the expansion of the substorm current wedge. Since

Pi 1 bursts are reliable indicators of onset, one infers that processes that occur on or faster than the Alfven wave communication time between the ionosphere and magnetosphere play a role in the physics of onset. Indeed, as we will see, magnetic field structure on the Pi 1 time scale was found in one onset observed when AMPTE/CCE was unusually close to the onset region (Ohtani et al., 1991), and indeed is commonly observed (Ohtani et al. (1992).

13.7 Generation of Midlatitude Pi 2

Rostoker (1967b) may have been the first to suggest that standing Alfven waves are excited during substorms; soon thereafter, Saito (1969) proposed that the main components of the Pi 2 pulsations were driven by odd-order torsional eigenmodes anchored in the auroral oval. However, Fukunishi and Hirasawa (1970) emphasized that low-latitude Pi 2 oscillations are fairly sinusoidal, while those observed at auroral latitudes have complex and irregular waveforms. They suggested, together with Sutcliffe (1980), that at least low-latitude Pi 2 was caused by a single surface wave on the plasmapause that is excited at the time of substorm onset. Kuwashima and Saito (1981) found that Pi 2 pulsations with a common predominant period commenced almost simultaneously from auroral (L = 7.5) to low (L = 1.8) latitudes at substorm onset. The Pi 2 pulsations had similar waveforms at magnetically conjugate stations, consistent with torsional oscillations of resonant field lines. The Pi 2 amplitude had a primary maximum in the auroral oval and a secondary maximum near the plasmapause. In short, it seems that while high-latitude Pi 2 may be due to waves that directly propagate time dependences in the current wedge along the geomagnetic field (Southwood and Stuart, 1979; Lester et al., 1984), midlatitude Pi 2 observed must be due to resonances stimulated by a compressional mode (Allan et al., 1986a).

Although damped magnetic field oscillations in the Pi 2 frequency band had been found in space in numerous substorms, there had been no direct demonstration that the modes were standing until Takahashi et al. (1988) used AMPTE/CCE medium-energy particle data to infer the phase relation between the electric and magnetic field amplitudes. Four substorm injections observed during a 4-hour period initiated oscillations in the ion anisotropy; two of these events displayed regular waveforms. The anisotropy oscillations could be explained by the **E x B** drift due to a radial electric field oscillation of 6 mV/m amplitude peak to peak. The electric field oscillation led a 1 nT oscillation of the torsional component of the magnetic field by 90 degrees in phase, the lag expected for standing waves. The magnetic perturbations also had a significant compressional component, suggesting the possibility of significant cross-field coupling to resonances deeper inside the magnetosphere. The anisotropy oscillations at AMPTE/CCE at 8–9 R_E radial distance started virtually simultaneously with Pi 2 oscillations observed at Syowa Station (L = 6.1) in one event. A second Pi 2 event started about 3 minutes after the corresponding injection, a delay possibly explainable by the longitudinal propagation of dipolarization. The waves observed in space had different

frequencies than those observed on the ground. On the ground, the Pi 2 pulsations had periods of 100 and 90 s for the first and second events, whereas the periods measured at AMPTE/CCE were 180 and 120 s, respectively.

Observations of four Pi 2 bursts on May 22–23, 1985 during geomagnetic quiet suggested that a driven global mode stimulated the micropulsations in the inner magnetosphere (Yumoto et al., 1990). Data from ground stations that were widely distributed in local time and between L = 1.2 and 6.9 established that the dominant periods were nearly identical at all stations. Indeed, the H and D components were both nearly in phase between nightside and dayside low latitude ground stations. All four magnetic waveforms observed at the Syowa–Iceland conjugate stations (L = 5.9–6.9) indicated an odd-mode field-line oscillation. The H and D components were nearly anti–phase and in phase, respectively, between high- and low-latitude ground stations in the midnight southern hemisphere. The amplitude was largest at high-latitude stations and decreased to lower latitudes. The identical periods, the phase relations, and the polarization characteristics at the conjugate stations indicated that the four Pi 2 pulsations were forced global modes with discrete frequencies that couple to the ionosphere via toroidal resonances. Just as in Takahashi et al. (1988), the wave periods at AMPTE/CCE beyond 8 R_E distance differed from those observed below L = 6.9 on the ground, suggesting that the global modes were confined within the inner edge of the plasma sheet.

13.8 Azimuthal Propagation of Dipolarization near Geostationary Orbit

Dipolarization starts in a relatively narrow magnetic longitude sector and propagates eastward and westward (Kokobun and McPherron, 1981; Nagai, 1982; Arnoldy and Moore, 1983; Nagai et al., 1983; Lopez et al., 1988b,c). Arnoldy and Moore (1983) found that dipolarization at synchronous orbit began within about 2 hours local time of 2300 LT, though occasionally the substorm central meridian could be found much farther away. By coordinating GOES 2 and GOES 3 data with ground magnetometer data, Nagai (1982) found that the positive bay onset in ground magnetometer measurements typically occurred earlier than dipolarization onset at geosynchronous orbit, consistent with the idea that ground measurements will detect the onset of dipolarization first, wherever it may be in space. The D component of the geosynchronous magnetic field began began to vary at ground onset at every local time position of the spacecraft. The lag between the ground onset and the arrival of dipolarization at a geostationary spacecraft was usually a minimum when the spacecraft was near local midnight and increased with increasing distance east or west from midnight (Nagai, 1982), indicating that the substorm central meridian was typically near local midnight; Nagai et al. (1983) found that it was usually somewhat west of midnight.

A geosynchronous spacecraft within about an hour's local time of the central meridian of the substorm will detect dipolarization within minutes of auroral onset. Geostationary spacecraft a few hours away from the central meridian find that the field continues to become more tail-like after onset on the central meridian

during the time that the dipolarization is propagating from its point of origin. According to McPherron and Kokobun (1981), a typical dipolarization propagates in azimuth 1 hour of local time in about 7.5 minutes—a speed of 24 km/s at 6.6 R_E distance. Nagai (1982) estimated that the dipolarized region expands westward *and* eastward at a rate of 1 to 3 minutes per hour of local time, for an effective azimuthal speed of 60–180 km/s. Nagai et al. (1983) found that the westward expansion velocity was usually greater than the eastward expansion velocity.

Nagai (1991) constructed an average time sequence of the magnetic field variations at geosychronous orbit from 194 substorm events monitored by the GOES 5 and 6 spacecraft during the PROMIS study interval (March 10–June 16, 1986). The tail-like field began to develop in the superposed epoch analysis roughly 45 minutes before onset. The onset was defined to be the time where the field inclination reached its minimum at the spacecraft just before local dipolarization was encountered. Local dipolarization was found in more than 80% of the cases when the two GOES spacecraft were located in the 1800–0300 MLT time sector. Dipolarization started in a region of less than 2 hours MLT extent centered on 2330 MLT, and propagated east and west, reaching 0300 MLT in 11 minutes and 2000 MLT in 15 minutes. At local times more than 1 hour away from the initial dipolarization sector, the field continued to become more tail-like until dipolarization arrived.

GEOS 2, in geosynchronous orbit 4 degrees south of the geomagnetic equator, found a consistent electric field pattern to be associated with dipolarization (Pedersen, 1992). In the leading edge of the dipolarization, the electric field was generally azimuthal and westward, corresponding to radially inward $\mathbf{E} \times \mathbf{B}$ drift. The amplitudes were in the 2–4 mV/m range and were sometimes larger. Occasionally, this initial signature, which lasted 1 or more minutes, was followed by oscillations with Pi 2 time scales and amplitudes of several tens of mV/m. All but 3 of the more than 50 substorm electric fields recorded by GEOS 2 in the 1800–0600 MLT sector between December 1978 and April 1979 had an essentially radially inward $\mathbf{E} \times \mathbf{B}$ convection velocity of order 50–150 km/s during the expansion phase (Pedersen et al., 1984). The flows encountered prior to about 0200 MLT tended to have a slight dawnward component as well. Only three were tailward at the geostationary orbit..

Dispersionless particle injections continue to accompany dipolarizations as they move away from their points of origin after substorm onset. It appears that almost every dispersionless injection is associated with dipolarization at the spacecraft. One hundred sixty-seven AMPTE/CCE injections that were dispersionless within 72 s between 25 and 285 keV and were located within 4.5 hours of local midnight were accompanied by magnetic field dipolarization (Lopez et al., 1990). Not all of these can have been observed on the substorm central meridian, and we infer that dipolarization and dispersionless injections propagate together. McIlwain (1974) had observed that if the trajectories of the injected particles observed by ATS 5 were traced back, the electrons *and* ions of all energies seemed to coincide at a common "injection boundary" at the time of substorm onset. If this boundary were tangent to the L = 6.6 geostationary orbit, a

geosynchronous spacecraft would infer that the injection had occurred at one single local time. Thus, in the limit, injections would appear dispersionless in both energy and spatial location. However, since dispersionless injections accompany dipolarizations, the injection region will broaden in local time as dipolarization propagates and appear to form an extended boundary.

13.9 Size of Initial Dipolarization Region

How small is the region in which dipolarization starts? What does dipolarization look like when it is observed near its point of origin? Are there any special properties of the initial dipolarization when it is observed close-up that might shed light on the physics of onset? In this section, we discuss observations made on an occasion when AMPTE/CCE was sufficiently near the central meridian of a substorm to produce new insight about the answers to such questions. The violent onset phenomena that swept over AMPTE/CCE on that occasion have rarely if ever been observed before. In fact, AMPTE/CCE was fortuitously situated to study not one but two substorms 56 minutes apart. Not only that but the geosynchronous spacecraft GOES 5 and GOES 6 and AMPTE/CCE were all about one earth radius from one another in the premidnight sector when the two substorms started (Ohtani et al., 1991). In the first substorm, AMPTE/CCE was about one earth radius beyond synchronous orbit. For the second, AMPTE/CCE at 2224 MLT was extremely close its neighbors at virtually the same radial distance (6.7 R_E). The dipolarizations from both onsets appeared to propagate from origins whose radial and azimuthal scales could be localized to 1 R_E or less.

AMPTE/CCE was privy to a sequence of rapid changes in the magnetic field both before and after the dipolarization of the second substorm. A 15 nT decrease in the H component of the magnetic field, signifying increasing cross-tail current density, occurred over the 80 s *before* dipolarization. The H component decrease was modulated with a roughly 20 s period, in the Pi 1 frequency band (5–40 s). During the same 80 s interval, there was a 25–30 nT depression in the D component, suggesting the intensification of a nearby field-aligned current. No simultaneous auroral observations were reported; so one cannot say whether this "explosive growth phase" corresponds to the rapid arc brightening that precedes the initiation of the westward surge, but the time scales of the auroral onset and of these changes in the magnetic field at AMPTE/CCE are similar.

The decrease in the H component over the 80 s before dipolarization was about half of the entire decrease observed in the growth phase and comparable in magnitude to the recovery that followed at dipolarization. The dipolarization itself was extremely rapid: the H component increased by 30 nT in 5 seconds. The V component had a single 20 nT positive spike of about 5 s duration that coincided with dipolarization. The recovery of the negative D component was also simultaneous with the H component dipolarization. There followed a series of 10–20 nT amplitude D-component oscillations in the Pi 1 frequency band that decayed with a roughly 1-minute time scale. When combined with the fact that ground Pi 1

measurements are good diagnostics of substorm onset, these local observations suggest that not only this one but many dipolarization onsets involve phenomena with timescales comparable with the Alfven communication time to the ionosphere.

No phenomena quite this violent were observed at the two nearby GOES spacecraft. It was evident, however, that the dipolarization started between the two spacecraft and propagated to them. Their dipolarizations did have complex D-component signatures that probably would only simplify to the basic expanding current wedge as the dipolarizations propagated farther beyond them. At GOES 5, 0.8 hours MLT east of AMPTE/CCE, the D component decreased slightly over the 4 minutes prior to the AMPTE/CCE dipolarization, and decreased even more rapidly afterward. The negative D perturbation maximized when the dipolarization arrived at GOES 5, 2–3 minutes after it started near AMPTE/CCE. The overall negative perturbation was consistent with the eastward-propagating dipolarization. At GOES 6, 0.7 hours MLT west of AMPTE/CCE, the D component, which had decreased almost to zero during the previous 20 minutes, developed a 20 nT positive spike of about 2 minutes duration that started at AMPTE/CCE dipolarization, returned briefly to its previously depressed value, and increased again. It completed its recovery just *before* the dipolarization arrived at GOES 6, about 4 minutes after dipolarization at AMPTE/CCE. The overall D component change of +25 nT from before to after dipolarization was consistent with the westward-propagating dipolarization, but its timesignature was complex and nonstandard. In this substorm, the dipolarization had an effective speed of 48–72 km/s eastward and 32 km/s westward.

A substorm studied by Tanskanen et al. (1987) may be another example where the observing spacecraft was near the initial dipolarization region. GEOS 2 was at 2330 MLT when electric field measurements began just before the onset. At the time of onset (which was determined by Pi 2 measurements) the dawn–dusk and antisunward components of the electric field were comparable. Less than a minute later, the D component of the magnetic field and the 28–403 keV perpendicular ion intensity began to increase. About 1 minute after that, the dawn–dusk electric field component suddenly decreased (from 2.4 to 0.5 mV/m) and remained small thereafter. The auroral X-ray intensity measured by a balloon at $L = 5$ faded by 20% during the 80 s surrounding this electric field decrease; since similar fading was not observed on a nearby balloon, it was a local phenomenon. One hundred seconds after this abrupt event, the H component of the magnetic field at GEOS 2 started to drop rapidly, behavior similar to that observed by AMPTE/CCE (Ohtani et al., 1991). The H component started to dipolarize at the moment the D component maximized, about 5 minutes after ground onset. The antisunward electric field component gradually tended to zero over the next 15 minutes as the dipolarization progressed. Relatively small-amplitude Pi 2 oscillations were detected in both the electric (< 1 mV/m) and magnetic (< 5 nT) field from the time of the electric field decrease until the H component completed its dipolarization 20 minutes later. The D perturbation remained positive throughout the dipolarization, its sign and relatively simple profile suggesting that the dipolarization propagated westward.

13.10 Radial Propagation of Dipolarization

The very first timing study had dipolarization propagating radially inward since it occurred 94 s earlier at OGO-5 at $X = -8.2\ R_E$ than it did at ATS-1 at $X = -5.9\ R_E$ (Russell and McPherron 1973a). Fifteen years later, Fairfield (1988) suggested that azimuthal propagation could have compromised this determination. The substorm central meridian had been west of both spacecraft, so that the dipolarization front could have reached OGO-5 first by propagating eastward, since OGO-5 was 3/4 of a degree west of ATS-1. Moore et al. (1981) also found that dipolarization generally propagated inward between SCATHA and ATS-6. However, the azimuthal separations of these spacecraft exceeded their radial separations in all but one of the substorms studied, and again confusion between radial and azimuthal propagation was possible (Lopez et al. (1990). Fairfield and Zanetti (1989) found no persuasive evidence for inward propagation in a study of a number of substorms using GOES 5, GOES 6, and AMPTE/CCE data; they argued that the time of onset of dipolarization is uncertain because it depends on the spacecraft's unknown distance from the plane of the current sheet (Fairfield and Zanetti, 1989). Difficulties such as these have led to a rather confused situation.

One strategy to avoid confusion between radial and azimuthal propagation is to choose dipolarizations for which two spacecraft are lined up azimuthally. In a case of particularly good alignment, one degree of longitude, dipolarization did propagate inward from GOES-3 to SCATHA (Nagai et al., 1987). On the other hand, dipolarization propagated outward in the event that sets the record for good alignment, 0.2 degrees (Lopez et al., 1990). In this event, dipolarization started at geosynchronous orbit 8 minutes earlier than at AMPTE/CCE at 8.8 R_E. The current sheet continued to thin at CCE until the dipolarization arrived, propagating outward at a speed of about 29 km/s. Lopez et al. (1988b) examined seven energetic particle increases associated with dipolarizations observed on AMPTE/CCE and either of two geostationary spacecraft, when azimuthal separation between the spacecraft was less than 7.5 degrees longitude. Four events were consistent with tailward propagation, and two with earthward propagation.

Using four spacecraft led to an even more complex picture (Lopez and Lui, 1990). At substorm onset, GOES 6 was 8.9 degrees east of AMPTE/IRM at 11.6 R_E. Both were east of the substorm central meridian, which was near local midnight. Dipolarization appeared at IRM less than a minute after it did at GOES 6. The outward radial velocity based on this timing exceeded 500 km/s. The dipolarization arrived at GOES 5, 37.1 degrees east of GOES 6, 4 minutes after it did at GOES 6, for an eastward propagation speed of 85 km/s, typical of other studies (Kokobun and McPherron, 1981; Nagai, 1982). Adding another spacecraft added complexity. AMPTE/ CCE was between GOES 5 and 6 in longitude, 14.5 degrees west of GOES 5 and 22.6 degrees east of GOES 6. At 8 R_E radial distance, CCE was situated radially between geostationary orbit and AMPTE/IRM. Dipolarization arrived 5 minutes later at CCE than at GOES 6; it arrived at CCE 1

minute later than at GOES 5, which was east of CCE, and it arrived and 4 minutes later at CCE than at IRM, which was further from earth. The only clear result supported by the pairwise comparison of the timing results from all four spacecraft is that dipolarization started west of all four spacecraft and propagated eastward over them.

A different approach to determining how dipolarization propagates radially is to compare a model cross-tail current sheet with magnetic field data taken entirely in the lobes of the tail, thus avoiding the problems due to changes in the vertical structure in the plasma sheet. Jacquey et al. (1991) found that the ISEE 1 magnetic field signatures at 20 R_E downtail were consistent with a retreat of the inner edge of the current sheet that started at a distance of 6–8 R_E and propagated tailward at a speed of 300 km/s for 15 minutes. At the end of this time, the inner edge of the model current sheet would have been about 50 R_E downtail. Two successive substorm intensifications had similar signatures. How this relates to the oft-reported observation that the plasma sheet thins beyond the geostationary region is unclear.

13.11 Plasmoids Escaping from the Geostationary Region

The previous discussion concerning the radial propagation of dipolarization is a good introduction to the topic of this section, since it is natural to wonder whether dipolarization is a consequence of a nearby reconnection event, or whether, conversely, dipolarization might trigger a nearby reconnection event. If the cross-tail current flowing prior to dipolarization can cancel 5/6 of the earth's dipole field, it takes a small stretch of the imagination to see that it might reverse it altogether and induce a neutral line. The key issue is not whether reconnection in the geostationary region is conceivable; it is to find the evidence that it occurs. The CDAW 6 event discussed earlier is one example of such observations. In this section are discussed two more examples that indicate that the phenomena observed during the CDAW 6 event, while they may be relatively rarely observed, they are not unique.

On April 11, 1980, ISEE 1 was in a perfect position to receive the aftereffects of a substorm expansion (Nishida et al., 1983; Sauvaud et al., 1984; Sergeev et al., 1987). The spacecraft was 21.8 R_E downtail, about 1 R_E from the center of the magnetic neutral sheet, and mapped magnetically to the 2300–0000 MLT region of the auroral oval, roughly the central meridian of the substorm. The event occurred in an interval of strongly southward interplanetary field and relatively high speed (500 km/s) solar wind during which AE varied between 700 and 1200 nT and there was a complicated mixture of multiple substorm expansions and convection bay behavior. However, the 1 hour before the substorm was relatively quiet, and throughout this hour ISEE 1 was within the plasma sheet according to both magnetic field and keV electron data. The spacecraft detected a northward component of magnetic field and was on closed field lines. Observations of a Pi 2 pulsation burst and a positive bay at mid-latitudes and a

high-latitude Pi 1 burst on the nightside consistently timed the onset to within 2 minutes. Pronounced magnetic field variations appeared at ISEE 1 about 1 minute after the first enhancement of Pi 1 activity, which was detected at three ground stations. The northward component doubled to 12 nT within 1–2 minutes after onset and then, over the next 24 seconds, the entire field dropped to 1 nT. It appeared that the core of a plasmoid was passing over the spacecraft at this time. Over the next 4 minutes, the magnitude recovered smoothly, but the north–south component remained small and variable. No significant electric field was detected during the first 5 minutes after onset, at which time strong electric fields appeared within 15 s of a second burst of Pi 1 pulsations as a strong tailward flow got under way. Thereafter, the east–west electric field and the north–south magnetic field components had a number of impulsive variations, all phased in such a way that the $\mathbf{E} \times \mathbf{B}$ flow remained tailward. Each followed a Pi 1 burst on the ground, and was associated with a burst of high-energy particles. The next 20 minutes continued to be characterized by strong and variable magnetic and electric fields and tailward flow—signatures of an active reconnection region earthward of the spacecraft.

In another substorm on April 24, 1979, a few-hundred km/s tailward flow began at ISEE 1 and 2 about 20 R_E downtail a minute after ground magnetometers at College, Alaska, registered the sharp onset of a negative bay (Hones et al., 1982, 1986). The tailward flow continued for the next 3 minutes, during which time the plasma sheet pressure first increased slightly and then dropped out, and the magnetic field briefly developed a very large y component and the z component reversed from northward to southward. It appeared that before the plasma sheet dropout eliminated the possibility of seeing anything, the spacecraft observed the tailward passage of the core of a small plasmoid, as well as the tailward flow from the reconnection region just earthward of it. All this happened in just 4 minutes, suggesting that plasmoids escaping from the geostationary region can be easily missed. Whatever the reason, relatively few have been reported in the literature. The dropout itself is the more commonly observed aftermath of dipolarization.

13.12 Plasma Sheet Dropouts in the Post-Geosynchronous Region

Two of the more striking phenomena found between 10 and 20 R_E downtail are the plasma sheet "dropout" and "recovery." Their basic properties were outlined 20 years ago by Hones and his collaborators using *Vela* and other data. The *Vela* spacecraft gave a view of plasma sheet and tail dynamics at one radial distance from the earth, since they were in circular orbits at 17–18 R_E distance. This view was remarkably consistent, just as the phenomenology developed from observations made at the single radial distance of geostationary orbit proved to be. It was supplemented later by observations made on spacecraft that sampled the near tail at other radial distances. We discuss the dropout in this section, and the recovery in the next.

The dropout was extraordinarily simple: A spacecraft in the plasma sheet would suddenly find itself itself in the tail lobes. To the *Vela* spacecraft, which

had no magnetometers, the particle fluxes, which signify presence in the plasma sheet, would drop to background—thus, the term *plasma sheet dropout.* Dropouts occurred for all the energies measured and for both electrons and ions. Simultaneous *Vela 3A* and *Vela 4A* observations at different absolute distances from the center of the plasma sheet indicated that dropouts were more likely to occur when the spacecraft were within the plasma sheet but farther from its center, thereby suggesting that the plasma sheet was thinning (Hones et al., 1971a,b). There were even occasions when one spacecraft near the center of the plasma sheet did not observe a dropout when its companion farther away would. A statistical study of *Vela* dropouts suggested that the plasma sheet could thin to half-heights of 1 R_E or less near local midnight, but that it would not thin to less than about 4 R_E at 2100 or 0300 MLT (Lui et al., 1975b). Akasofu's (1977) book presented evidence that showed that dropouts could be found throughout a broad area of the plasma sheet out to the IMP 6 apogee, 30 R_E downtail. The same result was obtained later for ISEE 1 and 2 dropouts (Dandouras et al., 1986).

Very often, a spacecraft that had been in the plasma sheet during the growth phase of the substorm would find itself in the tail lobes within minutes of the beginning of the expansion phase. For example, Pytte et al. (1976b) studied four multiple expansion substorms using data from OGO 5 and *Vela 4a*, which were located near local midnight at about the same distance from the expected position of the neutral sheet but separated by 3–10 R_E radially. OGO 5 was effectively in the generalized geostationary region, whereas *Vela 4A*, in a circular orbit at 17–18 R_E, was in the near-tail region intensively studied later by ISEE 1 and 2 and AMPTE/CCE spacecraft among others. The expansions in each substorm were separated by 10–15 minutes. Successive dipolarizations and ancillary phenomena were observed at OGO 5 in an almost one-to-one relationship with the ground Pi 2 bursts that marked the multiple expansions, whereas *Vela 4A* observed either plasma sheet thinning or found itself in the tail lobes at these times. It is because of observations like this that the dropout has been associated with the expansion phase in many substorm models (e.g., Hones, 1979).

Sauvaud et al. (1984) studied the relationship between energetic particle injections at geostationary orbit and particle dropouts observed further downtail. The injection times were determined using the $E > 22$ keV electron and $E > 27$ keV proton fluxes measured onboard GEOS 2, and the dropout times were found using ISEE 1 and 2 $E = 2$ and 6 keV electron measurements made during the 1979 and 1980 ISEE tail-crossing seasons (February through May). Both individual case studies and a statistical survey of 100 events indicated that the geostationary injections and plasma sheet dropouts were coincident within 5 minutes.

We first review the case studies of Sauvaud et al. (1984) and then we discuss their statistical results. On February 23, 1979, the electron and ion fluxes at GEOS 2 began to increase within a minute of one another at the same time as a well-defined increase in AE was registered on the ground. Thus, the spacecraft had caught a dispersionless injection at an early stage even though it was nearly on the dawn meridian (0550 MLT). The electron flux at ISEE 2, 22 R_E downtail near 0300 MLT, began to decrease within 2 minutes of the injection at GEOS 2; the

decrease proceeded gradually over the next 10 minutes until it amounted to a factor of 100, at which point the detectors were registering at background, and ISEE 2 entered the tail lobe. On March 29, 1979, flux decreases at ISEE 1 and 2 commenced 2 minutes after a dispersionless injection at GEOS 2 and took 12 minutes to reach background. The 30 s difference between the times of exit into the tail-lobe at the two ISEEs, which were separated by 2400 km in the z direction, implied that the boundary speed had been 80 km/s toward the center of the plasma sheet. In this case GEOS 2 was again near local dawn, while ISEE 1 and 2 were about 2 hours closer to the midnight meridian. In the third example, the very disturbed day on April 11, 1979, GEOS and ISEE were both near 2300 MLT but 16 R_E apart; each of seven major injections observed at GEOS over a 2-hour period corresponded to a dropout at ISEE. These examples provided "anecdotal" evidence of a connection between dipolarizations and dropouts; the survey of 100 dropouts indicated that the vast majority of dropouts at ISEE came within ± 6 minutes of injections at GEOS, and the distribution peaked around zero delay. The authors pointed out that such time differences are comparable with the fast wave propagation time from GEOS 2 to the ISEEs. A few of the injections in the Sauvaud et al. (1984) survey led *or followed* dropout by as much as 12 minutes. Certainly, one has to expect a spread of time differences between injections and dropouts. The injected particles propagate different distances from the central meridian of the substorm to the observing geostationary spacecraft, and the dipolarization itself propagates to the spacecraft.

But this leads to the next question: Could there be a more detailed relation between when dropout occurs and the propagation of dipolarization, or, equivalently, the advance of the auroral bulge? Hones et al. (1988) addressed this issue in a case study of a substorm on May 4, 1986. *Viking* images fixed the time of the auroral onset to within 20 s; the brightening started near 2200 MLT and spread eastward and westward. The Alaska magnetometer chain, near 2400 MLT, recorded a westward electrojet enhancement 2 minutes after onset, and shortly thereafter, the geosynchronous spacecraft 1984-129 near 0130 MLT began to detect variable fluxes consistent with energetic electrons drifting eastward from a dispersionless injection near 2200 MLT. At the time of onset, ISEE 1 and 2, were 18.5 R_E downtail and mapped to the same local time sector as 1984-129 according to the Tsyganenko (1987) magnetic field model. The ISEE 27–33 keV proton fluxes did not respond to the auroral onset: There was no immediate dropout. Successive *Viking* images showed the auroral bulge advancing eastward, until it eventually passed over the ISEE footprint 22 minutes after onset. The geosynchronous spacecraft recorded a large flux increase and ISEE 1 recorded a dropout when the auroral bulge expanded over their local time sector. A similar thing occurred in an isolated substorm whose onset followed 4 hours of magnetic quiet (Hones, 1988). At the time of onset, ISEE 1 was in the morning sector 20 R_E downtail, and judging from the variability and slow decline of the 6 keV proton flux, already near the southern boundary of the plasma sheet. Within minutes, the proton flux increased and remained elevated for about 20 minutes. Once again, there was no dropout at onset; indeed there was a plasma sheet "recovery." About

20–30 minutes later, DE 1 images indicated that a dropout occurred as the auroral bulge expanded into ISEE's local time sector. After the dropout, ISEE 1 remained outside the plasma sheet despite a large poleward expansion of the auroral bulge that reached within one degree of the nominal ISEE 1 field line. The plasma sheet finally re-expanded over the spacecraft 90 minutes later.

13.13 Plasma Sheet Recoveries in the Postgeosynchronous Region

The defining signature of the plasma sheet recovery is the reverse of the dropout's: The particle flux suddenly recovers. Plasma sheet recovery has been associated with the beginning of the recovery phase of the geomagnetic substorm (Hones et al., 1984c). One hundred eighty-five recoveries were identified in *Vela 5A, 5B, and 6A* data by a rise of particle count rates to enduring high values over a few minutes. Those that occurred when the spacecraft was within 6 R_E of the neutral sheet were selected. The times of these plasma sheet recoveries defined $T = 0$ in a superposed epoch analysis of the geomagnetic AL index for the accompanying substorms. The time profile of the superposed-epoch AL index had the classical signature of the substorm negative bay. The recovery of this synthetic bay began at $T = 0$. Thus it is that the word *recovery*, so suggestive in the substorm context, has come to be applied to the sudden appearance of the plasma sheet boundary layer at a spacecraft that is in the tail lobes.

Pytte et al. (1978b) examined 28 plasma sheet thickening events observed on at least two of the OGO 5, *Vela 4A*, and *Vela 5A* spacecraft. Thickening of the plasma sheet appeared to occur in two stages. The first stage involved single or multiple expansions of the plasma sheet at multiple onsets. These events were accompanied by Pi 2 bursts. The later stage started near the time of maximum auroral zone activity; this, the true recovery, was observed over a broad region in space, and was associated with the activation of the poleward arc system (the poleward leap) in several clear instances. However, there were no ground signatures of dipolarization, such as Pi 2 bursts or midlatitude positive bays in the H component.

Despite the symmetry of their defining signatures, other physical properties of dropouts and recoveries are strikingly different. Forbes et al. (1981) compared 66 dropouts and recoveries detected at both ISEE 1 and 2. Dropouts were due to true plasma convection, whereas recoveries were not due to convection. When the plasma sheet thinned, the speed determined from the arrival times of the plasma sheet boundary at the two spacecraft (the timing velocity) and the measured bulk flow speed along the spacecraft separation vector were about the same. The typical thinning speeds, roughly 20 km/s, were in the same range as the typical cross-lobe convection speeds found using lunar shadowing techniques (McCoy et al., 1975). The boundary layer motion was of an entirely different character when the plasma sheet expanded outward over the two spacecraft: Recoveries had a much higher timing velocity, averaging 133 km/s outward, yet the measured bulk speed was essentially zero. Electric field measurements made during three CDAW-6

substorms support this conclusion; the $\mathbf{E} \times \mathbf{B}$ drift was toward the center of the plasma sheet whether the plasma sheet thinned or thickened (Pedersen et al., 1985).

A low-energy electron layer (LEL) of few hundred eV electrons always encloses the energetic ion beams of the plasma sheet boundary layer (Parks et al., 1992). The LEL probably connects the poleward boundary of the auroral oval to the tail neutral region, so that its outer boundary marks the last-closed field line. Putting all this together, we arrive at the following scenario. When the plasma sheet drops out, the plasma, any ion beams in the plasma sheet boundary layer, and the last-closed field line (the LEL) all convect together toward the center of the plasma sheet at the $\mathbf{E} \times \mathbf{B}$ speed. There is insufficient compensating reconnection of tail-lobe field lines to enable the plasma sheet boundary layer to retain its position. If the timing and bulk velocities were exactly equal, there would be no tail reconnection at all. As for recoveries, there are occasions when the boundary layer simply convects over the spacecraft; Eastman et al. (1985b) presented examples of dropouts and recoveries in which the plasma sheet ion boundary layer passed back and forth over the spacecraft with symmetric time-reversed signatures. However, on other occasions the plasma sheet reappears because reconnection causes the last-closed field line to move over the spacecraft, followed by newly activated boundary layer ion beams, while $\mathbf{E} \times \mathbf{B}$ continues to have a component toward the center of the plasma sheet. If the reconnection region is tailward of the spacecraft, an earthward plasma sheet flow would follow.

13.14 Summary

Years of research with geosynchronous spacecraft have created a remarkably consistent picture of the substorm at 6.6 R_E radial distance. The results from elliptical orbiters that pass through the same radial distance region near the geomagnetic equator, notably APMTE/CCE, have elaborated and enriched the overall picture while leaving its overall design still recognizable as the one first obtained in geosynchronous orbit. It is for this reason that we can think of a generalized geostationary region, on the nightside between 6 R_E and a less well-defined outer boundary of perhaps 10 R_E, in which the "geosynchronous substorm" occurs.

The motions and activity of the cross-tail current sheet control the events in the geosynchronous substorm. Its growth phase starts with the development of a "tail-like" magnetic field that is due to the approach and intensification of the current sheet. The tail-like field begins to develop roughly 10 minutes after a southward turning of the magnetosheath field at the subsolar magnetopause. From this, we infer that the cross-tail current responds to magnetopause reconnection on the same general time scale that a fast wave takes to reach the current sheet from the subsolar magnetopause, that the new convection rate is established in the polar cap ionosphere, and that the magnetopause oscillates back and forth. As the current sheet thins, the fluxes of energetic particles may drop out. The current sheet has been observed to become very thin during the growth phase, to the point where the

adiabaticity of the motions of trapped energetic particles may be compromised. The loss of particles from the thinnest part of the current sheet may be responsible for the precipitation of energetic electrons into the X-ray arc at the outer boundary of trapping. Evidently the mix of approach, oscillation, intensification, and thinning of the cross-tail current sheet and/or its coupling to the magnetopause and ionosphere creates some sort of threshold for substorm onset. The best evidence that the onset has to do with this mix is the fact that the onset arc lies just poleward of the outer boundary of trapping and the auroral X-ray arc, in the region connecting to the inner edge of the amplifying cross-tail current.

Dipolarization starts in a region that is less than one earth radius in radial and azimuthal extent. The events that occur in the initial dipolarization region are much more violent than those observed later as the dipolarization expands. The H component of the magnetic field decreases dramatically on the 1-minute time scale just before it increases again as dipolarization starts. In the initial dipolarization itself, the magnetic field changes substantially in a few seconds; Fourier decomposition of this activity would yield considerable power in the Pi 1 frequency band. Although there is good correspondence between Pi 1 micropulsations and substorm expansions observed on the ground, not much is known about the relationship between the details of the initial dipolarization and the auroral onset. The dipolarization is accompanied by the dispersionless injections of tens to hundreds of keV protons and electrons. These may be due to the nonadiabatic particle acceleration that takes place in the rapidly changing electromagnetic fields in the dipolarization region. The electrons and protons drift eastward and westward, respectively, and are observed as energy-dispersed injections away from their points of injection.

After about 2 minutes, the initial dipolarization organizes itself into an expanding current wedge. In its simplest form, the current wedge consists of a pair of field-aligned currents, into the ionosphere to the morning side and out into the evening side of the central meridian of the substorm. The currents move slowly eastward and westward, respectively, and so the wedge expands. The field dipolarizes over a 10-minute period after the dipolarization "front" passes over the spacecraft. "Ahead" of the expanding current wedge, the magnetic field continues to become more tail-like until the dipolarization arrives. Dispersionless injections always accompany the dipolarization front as it propagates azimuthally. The leading edges of the current wedge resemble slowly propagating shocks with an oscillatory electric and magnetic field structure, which is the source of Pi 2 pulsations that can be detected worldwide. Each oscillatory structure consists of an abrupt leading edge with the same polarity as the overall dipolarization followed by a decaying oscillatory "wave train." Miniature dispersionless injections accompany each oscillation of the magnetic field. The expansion of the current wedge corresponds closely to the expansion of the auroral bulge, so much so that on one occasion the oscillations at the westward edge of one wedge were found to be related to small westward surges at the footpoint conjugate to the spacecraft observing the dipolarization.

Dipolarization is not observed within 6 R_E radial distance; the basic scenario defined by observations in geosynchronous orbit also applies to the results obtained on AMPTE/CCE, whose apogee is 8.8 R_E; we are probably safe in assigning geosynchronouslike behavior to the 6–10 R_E region. But where does it all end downtail? How are events in the geostationary region related to those occurring downtail? Without answering these questions, we will be unable to make progress in understanding how convection and substorms are related. Of course, people have asked how dipolarization propagates radially. Unfortunately, we can draw no general conclusion from the ensemble of radial propagation studies carried out to date: There is no consensus about the sign of the radial velocity of dipolarization, much less its magnitude, and similarly conducted studies disagree even when the spacecraft alignment is a degree or better. The lack of pattern emerging from studies conducted in similar ways by respected groups and individuals may not be due to insufficient diligence or not enough spacecraft; our working conceptual structure may be at fault. We will try to explain what we mean. Azimuthal spacecraft alignment within a degree and 1-minute timing accuracy are needed to distinguish radial from azimuthal propagation. At this level of precision, one cannot ignore the fact that dipolarizing systems ring in Pi 1 and Pi 2 micropulsations in the 5–150 s period range. The currents in the wedge appear to be highly filamentary, and the temporal and spatial structure of the current wedge and current sheet may confound interpretations based on the picture of a smooth uniformly propagating dipolarization "front" on the 1 or 2 minute time scale.

Even if we cannot connect the geosynchronous substorm to what happens downstream on a minute-by-minute basis, we can say with some assurance what generally happens during substorms just downstream of the geosynchronous region. What is *not* observed all that frequently is the tailward passage of a plasmoid generated in the geosynchronous region. More of the time, the plasma sheet in the region 10–20 R_E downstream of earth thins during the substorm expansion phase, and the spacecraft finds itself in the tail lobes. The spacecraft in this region detects no clear signature of reconnection until later, when the plasma sheet boundary layer expands over it, most likely because of reconnection and plasmoid production further downstream.

14

COORDINATION OF THE GEOSYNCHRONOUS AND AURORAL SUBSTORMS

14.1 Introductory Remarks

Studies using data from the ATS-5 geosynchronous spacecraft revealed a clear relationship between midnight region injection events near the spacecraft and auroral displays near the ATS magnetic conjugate point (Hones et al., 1971a; Mende et al., 1972; Eather et al., 1976; Mende and Shelley, 1976). A comparison of ATS-5 particle and magnetic field data with all-sky photographs taken at the conjugate point, Great Whale River, indicated that an injection at geostationary orbit generally corresponded to the brightening of the onset arc when the spacecraft was in the midnight sector (Akasofu et al., 1974). Results such as this whetted the collective appetite. How closely can the initial onset and injection be related to one another in time, do the onset and injection start on the same field field line, does the westward propagation of dipolarization correspond to the westward surge, can one relate the fine structures of the auroral expansion and the dipolarization? As time passed, increasingly precise answers have been given to these and similar questions, and auroral and geosynchronous substorm phenomenology has become more tightly integrated. In this chapter, we sample some of the evidence that supports this statement.

The GEOS 2 spacecraft was stationed with its magnetic conjugate point near Kiruna, Sweden, so that the conjugate aurora could be studied with the extensive network of ground-based observatories in Scandinavia (Knott, 1975; Knott et al., 1979). In the first part of this chapter, we review some of the correlation studies carried out in the GEOS 2 project. In one particular series of four substorms, it was found that the dipolarization occurred at the same time as the aurora brightened and expanded poleward over the ground conjugate region (Section 14.2). In another case, a dispersionless injection at GEOS 2 corresponded to an intensification of the auroral X-ray band in Scandinavia (Section 14.2). Westward surges at the auroral conjugate point were associated with dipolarization at the spacecraft on a statistical basis (Section 14.3). Finally, the close relationship between both the auroral and geostationary substorm phenomena was extended to small spatio-temporal scales. In one particularly well-diagnosed substorm, a series of quasiperiodic dipolarizations and dispersionless injections on the Pi 2 time scale at GEOS 2 were related on a minute-by-minute basis to intensifications of the

westward surge over Kiruna (Section 14.4). It was also clear that the close relationship with the geosynchronous region broke down for the activity of the aurora well poleward of the GEOS 2 conjugate point. In one particularly striking case, three intensifications of the auroral electrojet near Kiruna had definite counterparts at GEOS 2, while nothing happened at GEOS 2 when the poleward auroral electrojet intensified around the very beginning of the recovery phase (Section 14.5).

In the second part of this chapter, we turn to a different kind of evidence that can be used to relate phenomena in the ionosphere and space: composition. The link between the aurora and plasma composition was forged by the S3-3 spacecraft, which carried a 0.5–16 keV/*e* mass spectrometer up to 8000 km altitude in high polar orbit. When S3-3 was on field lines connecting to the auroral acceleration region, the mass spectrometer detected upward flowing H^+, O^+, and (some) He^+ ions with energies up to the 16 keV limit (Ghielmetti et al., 1978; Sharp, et al., 1979; Collin et al., 1981). This showed that the aurora injects ions into the magnetosphere with energies corresponding to the auroral field-aligned potential drop. The spectrometer onboard DE 1, which extended the composition measurements to higher altitudes (4.6 R_E) and to lower energies, found that few hundred eV ions stream out of the polar cap as well (Shelley et al., 1982). Both ion sources respond to the short-term changes in geomagnetic activity associated with substorms. Our questions here are: How do ionospheric plasma sources, and particularly the auroral source, affect the plasma sheet, and what can the study of composition in the plasma sheet teach us about substorms?

Because we have not discussed plasma composition thus far, we digress somewhat to present a general overview of the topic before returning specifically to substorms. Singly ionized oxygen of ionospheric origin is known to be injected into the magnetosphere at times of geomagnetic disturbance, the rate of injection depending on the solar cycle through the flux of solar EUV (Section 14.6). Oxygen can be the dominant ring current component during magnetic storms. The plasma sheet contains a mixture of ions of solar wind and ionospheric origin that depends upon the AE index, and thus varies with the strength of the auroral current system (Section 14.7). In the first CDAW 6 substorm, energetic O^+ accelerated directly out of the auroral ionosphere arrived 15 R_E downtail about 20 minutes after substorm onset (Section 14.8). Nearer earth, in the geosynchronous region, the O^+ density increases somewhat during growth phase, perhaps reflecting the inward migration of the current sheet and the equatorward migration of the aurora, and all ionic species increase in density at the time of dipolarization (Section 14.9).

14.2 The Auroral Expansion and Dipolarization

During the winter of 1978–1979, a 630.0 nm zenithal photometer was operated at Kilpisjarvi, Finland (66.1 degrees invariant latitude), which was near the GEOS 2 conjugate point at the time. One striking event was observed regularly in the daily plots of 630.0 nm emission. The intensity would rise in a few minutes from a

background of 100 R to a peak intensity of about 1.5 kR and then decay over roughly the next hour (Shepherd et al., 1980b). Over 100 such events were recorded over a 4 month period. Often three or four occurred in the same night. Comparison with GEOS 2 data revealed various response patterns, but one stood out in about half the events. Four such characteristic events took place on the night of December 18, 1978, each preceded by a growth phase in which a tail-like magnetic field developed at GEOS 2. Data from a system of seven all-sky cameras showed that the intensifications of the red emissions were coincident with poleward propagating aurora, identifying the events as substorm expansions. The auroral expansions at Kilpisjarvi were essentially coincident with dipolarizations at GEOS 2. Within a minute or two of the brightenings of the 630.0 nm emission, the magnetic field at GEOS 2 dipolarized, the energetic particle intensities increased, the dawn–dusk electric field increased from 3 to 15 mV/m, and there were brief bursts of broadband 0–15 Hz magnetic noise, the "short irregular pulsations" later associated by Robert et al. (1984) with the substorm current wedge. In the second dipolarization, the most sharply defined, the rate of change of the H component was 1 nT/s, suggesting the betatron mechanism might account for the factor of 20 increase in the 30–37 keV electron flux that took place over 2 minutes.

Each intensification of the red auroral emissions coincided with a mysterious disappearance of 50–500 eV plasma sheet electrons at GEOS 2 (Shepherd et al., 1980b). Shepherd et al. (1980a) had shown empirically that electrons with energies less than 300 eV generate 630 nm emission efficiently, while those with energies greater than 1 keV do not. Thus, the electrons most able to produce the red emissions disappeared at GEOS 2 just as the emissions intensified near the footpoint of the GEOS 2 field line. The electrons had been there during the growth phase of the substorms, and they returned as the auroral emission subsided. The total release of 630 nm energy in each event was comparable with the energy in electrons with energies less than 500 eV stored in the magnetic flux tubes connecting to the aurora prior to dipolarization. The events described seemed to be typical. For example, on December 29, 1978, there were six more major 630.0 nm events exceeding 1 kR, or counting multiple intensifications within individual substorms, 10 in all. Nine of the 10 had bursts of sudden irregular pulsations. Of the six major events, five were preceded by the growth of a tailward field during growth phase, a magnetic field dipolarization, and decreases in the 50–500 eV electron fluxes.

One expects the westward electric field increase during the growth phase. This *is* what happened at geosynchronous orbit on the dayside in the CDAW 6 substorm, but this is *not* what happened on the nightside during this series of substorms. The electric field was not measured during the first of the substorms. It was measured for only a few minutes before the onset of the second. For these few minutes, it had a 2.0 mV/m sunward component and a small but nonzero westward component. In the growth phase of the third substorm, the sunward component grew from zero to 2.5 mV/m over half an hour and then remained relatively constant for the next 70 minutes until the dipolarization passed over GEOS 2 at 2245 MLT. The sudden enhancement of the electric field to 15 mV/m in the

dipolarization was comparable to the inductive electric field expected from the observed magnetic field changes in the dipolarization. After these violent perturbations subsided, the sunward component returned to roughly the strength it had before the dipolarization, which it then held for another 2.5 hours until the dipolarization associated with the fourth substorm passed over the spacecraft. By this time GEOS 2 was at 0200 MLT. Thus, throughout the third substorm and the growth phase of the fourth, the dawn–dusk electric field was small while the sunward component was about 2.5 mV/m. The $\mathbf{E} \times \mathbf{B}$ drift was eastward, not earthward, prior to local dipolarization at geosynchronous orbit.

One event revealed a close relationship between the dispersionless particle injection that accompanies dipolarization and the thin band of intense > 30 keV electron precipitation and riometer absorption that surrounds the poleward boundary of the expanding auroral bulge (Kremser et al., 1982). On July 3, 1979, a poleward moving burst of 30–100 keV auroral X rays was tracked by two balloons that were located 51 minutes MLT west of the GEOS 2 conjugate point (0012 MLT). The X-ray burst started about 2 minutes after a Pi 2 burst marked the onset and lasted about 5 minutes. A factor of 20 dispersionless injection of > 22 keV electrons and a factor of 3 dispersionless injection of > 27 keV ions at GEOS 2 began simultaneously with the precipitation into the ionosphere. The intensity of 90 degree pitch angle electrons increased before that of the parallel electrons, but at the time of peak electron intensity at GEOS 2 and peak auroral X-ray intensity, the electrons were strongly field aligned up to 113 keV, but not up to 154 keV. The large > 27 keV ion anisotropy indicated the spacecraft was in a strong gradient of ion pressure; the ion density maximum was earthward of GEOS 2 at the time the energetic electrons were the most strongly field aligned and retreated tailward over the spacecraft afterwards.

14.3 The Westward Surge and Dipolarization

Pellinen et al. (1984) found that dipolarization arrived at GEOS 2 and the westward-traveling surge crossed the GEOS 2 magnetic meridian typically within 30 s of one another. However, not all westward surges observed on the ground had counterparts in electric field measurements at the spacecraft. Weaker events that started poleward of the GEOS 2 footprint had little or no effect at GEOS 2. A similar study during the Global Auroral Dynamics Campaign (Oguti et al., 1988a,b) reached essentially the same conclusion. The Campaign employed a six-station all-sky auroral TV camera network in Canada and Alaska, together with two other stations to the east. Two stations were conjugate within several hundred kilometers to the GOES 5 and 6 spacecraft, which were separated by 33.4 degrees longitude. Five westward-traveling surges that took place in a 5.5 hour interval on January 7, 1986, were studied in detail. Four of the five occurred within minutes of a dipolarization at the conjugate geostationary spacecraft. The fifth was shifted out of conjugacy with either spacecraft. The eastward expansion of the auroral bulge also has a close counterpart at geostationary orbit. Nishitani and Oguti (1988)

showed that eastward-propagating dipolarizations in the morning sector correlated with eastward expansions of auroral activity near the spacecraft conjugate point.

The mounting evidence of a tight connection between dipolarization and the westward surge moves us to make the following remarks. Auroral observations indicate that the motion of the westward surge is not always even and steady, and so the working idea of a dipolarization front that propagates with a slowly varying speed is an oversimplification. Spacecraft observations of order unity oscillations of the D component of the magnetic field and in the electric field in the Pi 2 frequency range are a warning that the dipolarization "front" contains inherent time dependences. This point was taken up directly in the next study, in which Roux et al. (1991) documented the counterpart in space of the fine structure of westward surge intensification noted by many authors.

14.4 Multiple Surge Intensification and Oscillatory Dipolarization

The final GEOS 2 case study we will discuss documented a close relationship between multiple westward surge intensifications on the Pi 2 time scale and oscillatory dipolarizations at geostationary orbit (Roux, 1985; Roux et al., 1991). The growth phase of the isolated substorm of January 25, 1979 was characterized by a gradual 30 minute buildup of a tail-like magnetic field at GEOS 2; the energetic ion and electron fluxes gradually decreased as the tail-like field developed. The density of 100–500 eV electrons indicated that GEOS 2 remained in the plasma sheet prior to the arrival of dipolarization. At that point, fast all-sky cameras, a narrow-beam 630 nm photometer, and ground magnetometers recorded the passage of the first of four auroral intensifications propagating westward through the GEOS 2 magnetic foot-point (Roux et al., 1991). This surge had the remarkably high speed of 6.8 km/s. Its maximum was simultaneous to 1 minute with the beginning of a complex dipolarization and dispersionless injection event at GEOS 2 at 2245 MLT. The radial electric field reversed when dipolarization arrived, became very impulsive, oscillated twice between earthward and tailward near the end of the dipolarization, and settled down to a generally tailward direction afterwards. Even though the auroral forms at the conjugate point were propagating westward, the D component of the magnetic field developed an overall negative perturbation, usually associated with the eastward propagation of dipolarization. Reversals of the D component began at the onset of dipolarization and and lasted until it was completed. During this phase, the fluxes of 100–500 eV electrons disappeared while the fluxes of energetic ions (electrons) rose to values comparable with (exceeding) those before the field started to become tail-like. The low-energy electrons returned by the time dipolarization was finished, 8 minutes after it began at the spacecraft. The energetic ion spatial gradient was on average earthward, as in Kremser et al. (1982), with superposed rotations to eastward.

There were three more westward surge activations poleward of the original surge, for a total of four during the first 5 minutes after dipolarization started at GEOS 2. The quasiperiodic auroral activations had definite counterparts at

geostationary orbit. Large oscillations between a dipolelike and a tail-like configuration in all three magnetic field components at the spacecraft were coupled to an in–out–in–out sequence of field-aligned currents. The fluxes of > 20 keV electrons were in phase with the magnetic oscillations with no measurable dispersion in energy or pitch angle (Roux, 1985). Since the electron intensity was high when the field was dipolelike and low when it was tail-like, these electron oscillations were like repeated dispersionless injections on the Pi 2 time scale. This behavior was consistent with multiple crossings of an oscillating spatial boundary separating regions of high and low electron flux. A calculation of the minimum variance direction of the magnetic field suggested that these oscillations propagated azimuthally. They were the oscillatory fine structure of the expanding current wedge.

The radial component of the electric field in the GEOS 2 frame of reference increased slightly and became active as the tail-like field developed during the growth phase of the January 25, 1979 substorm (Roux, 1985; Roux et al., 1991). It increased monotonically to 2 mV/m earthward in the last 20 minutes before the dipolarization arrived. The azimuthal electric field remained near zero throughout the growth phase, so that just before dipolarization, the $\mathbf{E} \times \mathbf{B}$ drift was azimuthal and eastward at 30 km/s. While the dipolarization was in progress, the average azimuthal electric field was westward, with superposed transient electric field spikes whose amplitudes exceeded 10 mV/m. The field direction reversed from east to west and back between successive spikes about a minute apart (the Pi 2 timescale). When the dipolarization was completed, the field settled down to have a tailward radial component and a slightly larger westward component, both about 1 mV/m and variable. Thus, the convection was eastward before onset and had a significant earthward component only after dipolarization.

In all these substorms, the growth-phase electric field developed a strong earthward component. In the absence of a significant corkscrew effect due to field-aligned currents, an earthward electric field maps into an equatorward electric field in the ionosphere, suggesting that that the GEOS 2 footprint was poleward of the Harang discontinuity, where the ionospheric electron drifts are eastward (Fontaine et al., 1986). However, in one case (Tanskanen et al., 1987), the growth-phase electric field mapped equatorward of the Harang discontinuity. Since the auroral expansion starts near the Harang discontinuity, the fact that the growth-phase electric field at geostationary orbit has mapped both poleward and equatorward of the Harang discontinuity in different substorms is one more bit of circumstantial evidence linking the geosynchronous and auroral substorm expansions.

14.5 Dipolarization and Poleward Arc Brightening

The next substorm we review revealed a close relationship between dipolarizations at goesynchronous orbit and electrojet intensifications in the equatorward portion of the auroral oval, yet showed little or no geosynchronous region activity at the intensification of a poleward electrojet late in the expansion phase. Measurements

of 1–3 keV electrons indicated that the inner edge of plasma sheet moved inwards over GEOS 2 prior to the onset of a substorm on January 30, 1979 (Kozelova et al., 1992). At this time, a quiet auroral arc appeared at 64 degrees latitude, near the footprint of GEOS 2. The dipolarization appeared to unfold in stages, with a small initial dipolarization or pseudodipolarization in the magnetic field, accompanied by increases in the energetic ion ($E > 27$ keV) and low-energy electron ($E < 5$ keV) fluxes. After about 8 minutes, there was a second Pi 2 burst, and a new arc formed poleward of the GEOS 2 footprint and expanded poleward. This expansion was associated with an decrease in the ion fluxes, an increase in electron flux, and a magnetic field dipolarization at GEOS 2. A third auroral intensification that led to further expansion of the auroral bulge was accompanied mainly by oscillations in the magnetic field at GEOS 2. At this point, two relatively standard auroral expansions had taken place, accompanied by dipolarizations at geostationary orbit, and a third had an oscillatory response. The last stage was a different story altogether. The westward electrojet achieved its maximum intensity in a final intensification at a latitude of 71 degrees. The response at geostationary orbit to the intensification of this poleward arc was unlike the first three. Up to that point, the magnetic field had mainly rotated in direction as it dipolarized. Over the 18 minutes following the poleward arc intensification, the magnitude of the field increased without much change in direction, and there was very little variation in the D component, indicating that any field-aligned currents had to be flowing well away from the geostationary region.

We now turn to the issue of plasma composition.

14.6 Dependence of Plasma Composition on Solar and Geomagnetic Activity

The first ion mass spectrometer capable of measuring keV particles in space was flown on the polar-orbiting spacecraft 1971-89A at 800 km altitude. The measured abundances of H^+ and He^{2+} ions over the aurora and in the solar wind were often quite similar, indicating that the solar wind was indeed a source of energetic plasma in the magnetosphere (Sharp et al., 1974). At the same time, the large fluxes of precipitating O^+ found during the main phases of magnetic storms meant that the ionosphere was an important source of magnetospheric plasma at disturbed times (Shelley et al., 1972). There had been the possibility that low-altitude measurements over-emphasize the relative amount of O^+ (because H^+ can be depleted by charge exchange with neutral hydrogen), but the first GEOS 1 composition measurements demonstrated that (below 16 keV) O^+ is at times the dominant ion by number density at 3–8 R_E geocentric distances (Balsiger et al., 1980). Examination of 20 magnetic storms indicated that that the ionosphere and solar wind contributed comparable amounts of 1–16 keV plasma in the high-altitude magnetosphere. The overall results of the GEOS 1 and 2 ion composition experiments were reviewed by Balsiger et al. (1983).

The study of ring current composition has recently been extended to many more species and to higher energy/charge by AMPTE/CCE (Hamilton et al., 1988;

Kistler et al., 1989a,b). Gloeckler and Hamilton (1987) reported typical quiet-time number densities at the AMPTE/CCE orbit of 0.7 cm^{-3} for H^+, 0.034 cm^{-3} for O^+, 0.006 cm^{-3} for He^{2+}, and 0. 001 cm^{-3} for He^+; the fraction of O^+ ions increased with decreasing geocentric distance. The average spatial distributions of O^+, O^{2+}, O^{6+}, and C^{6+} ions have been characterized by Kremser et al. (1987).

Given the existence of a variable ionospheric source of magnetospheric plasma, it was natural to ask whether aeronomic effects related to the solar cycle influenced magnetospheric particle populations. The answer was a definite yes, from 48 months of 1-month average composition measurements taken on GEOS 1 and 2 (Young et al., 1982). The injection of terrestrial ions into the magnetosphere depended upon a complex interplay between geomagnetic processes, as represented by the Kp index, and aeronomic processes associated with solar EUV, as measured by the flux of 10.7 cm radio waves. Some increases in He^+, O^+, and O^{2+} were clearly entirely due to increased solar EUV during the rising phase of the solar cycle; Lennartsson (1989) later reported that the O^+ number density in the near-earth magnetosphere increased by one order of magnitude during the rising phase of solar cycle 21 (mid-1977 to late 1979). The O^+ density also increased with increasing geomagnetic activity (by roughly a factor of 8), but there was no corresponding increase in either He^+ or O^{2+}, and only a small increase in H^+; the He^{2+} to H^+ ratio was found to be remarkably constant at 0.01.

14.7 Dependence of Plasma Sheet Composition on Auroral Activity

The first mass spectrometer measurements in the plasma sheet were made on ISEE 1 spacecraft (Shelley et al., 1978). The plasma sheet proved to contain a highly variable mixture of H^+, He^{2+}, He^+ and O^+ ions, all with characteristic energies of a few keV (Peterson et al., 1981). Of these, He^{2+} was of solar origin, O^+ and He^+ were of ionospheric origin, and hydrogen ions were of mixed origin. The distribution functions of ions of solar wind origin differ noticeably from those of ionospheric origin; comparing the energy spectra of H^+ and He^{2+} showed that the terrestrial portion of H^+ ranged between 10% and 65% in five 1–2 hour intervals of geomagnetic quiet (Gloeckler and Hamilton, 1987). Lennartsson and Sharp (1982) found that the He^+ to H^+ and He^{2+} to H^+ ratios in the near equatorial magnetosphere beyond $L = 5$ ranged between 1–3%, during both quiet and disturbed times, while the O^+ to H^+ ratio varied over a huge range, 1–200%, and was proportional to the level of magnetic activity. Later, Gloeckler and Hamilton (1987) estimated that the overall ionospheric contribution to the plasma sheet number density increases from about 35% at quiet times to about 65% at disturbed times.

Since mass analysis requires a slow instrument cycle, often 30–60 minutes, there has been no study of plasma sheet composition on the time scales of high-speed flows and plasmoids, but a consistent pattern of plasma sheet composition changes has been associated with geomagnetic activity on slightly longer time scales. Sharp et al. (1982) related plasma sheet composition variations

to hourly AE averages, thus forging the link with geomagnetic activity. The plasma at ISEE 1 proved to be of predominantly solar origin during quiet times (AE < 100 nT), whereas the solar and ionospheric sources contributed roughly equally during active times (AE > 500 nT). The solar ions increased in energy with increasing activity, while the terrestrial ion energy did not change much. Lennartsson and Shelley (1986), who examined all available ISEE 1 plasma sheet data from the solar maximum years, 1978 and 1979, found a clear relationship between plasma sheet composition and the AE index on the time scale of several hours. The solar ions (H^+ and He^{2+}) decreased in number density but increased in energy as AE increased; their energization was more nearly proportional to ion mass than to ionic charge. As AE grew, the solar ions were partially replaced by terrestrial ions of keV energies, notably O^+; the O^+ to H^+ ratio increased roughly linearly with the AE index.

The approximate linear relationship between the O^+ to H^+ ratio and AE suggests that the O^+ injection rate is related to the strength of the currents flowing in the auroral ionosphere, as one might expect if most of the energetic O^+ in the plasma sheet were accelerated in the aurora.

14.8 Injection of O^+ into the Plasma Sheet during Substorm Expansion Phase

The statistical connection between composition and AE naturally suggested a relationship between composition and substorms. Accordingly, the two CDAW 6 events became the subject of the first case study of composition variations during substorms (Lennartsson et al., 1985; Lennartsson and Shelley, 1986). The first substorm marked the transition between a prolonged, 2-day interval of geomagnetic quiet and a persistent period of enhanced geomagnetic activity. During the preceding quiet interval, the plasma sheet H^+ density around 18 R_E downtail had hovered around its long-term average of 0.3 cm^{-3}; the O^+ density was about a factor of 30 smaller. Comparison of H^+ and He^{2+} indicated that the H^+ ions were primarily of solar wind origin. The H^+ density slowly increased to 1 cm^{-3} over the 3 hours before onset, while the 0.1–16 keV O^+ density began to increase only following the southward turning of the interplanetary field 44 minutes before onset. The onset occurred without the presence in the plasma sheet of many ionospheric ions, suggesting they were not a prerequisite for onset. (Recall that, at the time of onset, ISEE 1, moving inbound, was near 0200 LT, about 1 R_E below the magnetic equatorial plane, and about 15 R_E downtail.) The first change in composition came 20–25 minutes after onset. At this point, the 0.1–16 keV H^+ and He^{2+} densities dropped sharply, and within the next 10 minutes, the O^+ density increased by almost an order of magnitude, resulting in comparable densities of O^+ and H^+. Much of the O^+ was in a tailward-lowing beam with an energy below 1 keV but occasionally rising to 6–7 keV. The resemblance of this beam to those observed in polar orbit suggested that ISEE 1 was magnetically connected to an auroral acceleration region during the expansion phase of the substorm. The composition at ISEE 1 continued without significant change through the second CDAW 6

substorm about 2 hours later. The central meridian of the second substorm was centered very far westward of its predecessor.

14.9 Variation of O^+ in the Geosynchronous Region During Substorms

The charge–energy–mass spectrometer (CHEM) instrument onboard AMPTE/CCE used a combination of electrostatic analysis, postacceleration, and time-of-flight and energy measurement to determine the energy, mass, and mass per charge of 1 to 300 keV/*e* ions. The improved time resolution of the CHEM instrument also enabled it to track more accurately the evolution of composition with substorm phase. A study of substorm-associated flux dropout events indicated a mild increase in the O^+ to H^+ flux ratio during substorm growth phase like that observed in the CDAW 6 case study is a rather general occurrence (Daglis et al., 1988). In one particular case, there was a remarkable correlation between the development of the tail-like magnetic field and increased energy densities of H^+, O^+, and He^{2+} ions (Daglis et al., 1990). While the proton energy density was dominant, the most intense enhancement occurred for O^+ ions. The ion energy densities peaked when the field became the most tail-like, after which time they began a gradual dropout that continued until the arrival of the dipolarization. This dipolarization was accompanied by a dispersionless injection in each ion species.

Daglis et al. (1992) examined the variations in composition of the 1–300 keV/*e* ions associated with a set of 131 substorm expansions recorded on AMPTE/CCE. They monitored the mean value of each species' energy density during the first 15 minutes after local substorm onset, as identified by the initiation of dipolarization and/or dispersionless injection. The energy density of O^+ ions increased nonlinearly with the AE measured during early expansion phase, whereas there was no clear relationship between AE and the energy density of He^{2+} ions. The larger the AE, the closer to earth the injection events on average. The He^{2+} energy density tended to be largest nearer local dawn, whereas the O^+ energy density was clearly largest towards dusk in strong substorms. The behavior of the H^+ and He^+ ions was intermediate between that of O^+ and He^{2+}, consistent with the fact that H^+ and He^+ can come from either the ionosphere or the solar wind.

14.10 Discussion

The substorm is a magnetospheric convulsion of global scale. Its manifestations are widespread, and it is tempting for an observer working with data from one spacecraft to hope that the region of space it samples will prove to be the critical one for substorm dynamics. However, events at one point speedily communicate their existence over a vast region of space via MHD waves, and without numerous multispacecraft measurements resolved to 1 minute or better, it is difficult to perceive where an event really "starts." The same problem complicates attempts to relate auroral brightenings to events in space. Events taking place near

geostationary orbit communicate with the ionosphere via Alfven waves on time scales comparable with the time resolutions of many existing measurement techniques (Sergeev, 1992). Even if the measurements had the requisite resolution, more than one wave mode could be propagating back and forth on the same field line. A magneto-ionosphere uncertainty principle may therefore apply to two-point comparisons, and a full tomographic approach may be needed to interpret the relative timing of events on time scales comparable with the Alfven communication time between the ionosphere and current sheet.

How then are we to relate auroral substorm events to those in space? Clearly, simple timing measurements carry us only so far, and we have to supplement them with a more complete diagnostic panoply and physical argument. From this point of view, it is the distinctiveness of the auroral onset that may ultimately identify where the substorm starts in space. The extremely small spatial scale of the auroral onset, and the short duration of the onset phase, make it clear that spacecraft will rarely be in the onset region, and even more rarely will there be an auroral observatory at the footpoint of the onset region. Geosynchronous orbit is about the only practical one where coordinated observations can be made continuously, so there is the best chance of catching an onset. In the future, the network of auroral observatories may be sufficiently dense that the footpoints of other spacecraft will be in continuous view for significant periods of time. In the meantime, every observation is precious.

What do we know now? In Chapter 13, we discussed one set of observations made in and near geosynchronous orbit of extremely violent phenomena that took place on the onset time scale and were localized to a region less than 1 R_E in scale. Because the magnetic field changed rapidly, mapping to the ionosphere was highly unreliable during the two events. Unfortunately, there were no ground observations; so we do not know with 100% certainty that there was a simultaneous auroral onset. In the first part of this chapter, we reviewed cases where auroral observations were coordinated with GEOS 2 observations. In general, when the ground stations observed a westward surge near the nominal footpoint of the spacecraft, it was simultaneous with a dipolarization at the spacecraft within a minute or two. In one particular instance, each oscillation of the dipolarization corresponded to localized surges near the footpoint. On the other hand, auroral activity at higher latitudes did not always correspond to activity at geosynchronous orbit. In one particularly clearcut case, the activation of a poleward arc near the beginning of substorm recovery phase had little or no effect at geosynchronous orbit.

We will probably never be sure the spacecraft is in the substorm onset region until we can determine whether it connects magnetically to an auroral arc (Coroniti, 1991). This will require highly resolved distribution function and composition measurements. Composition measurements do not yet have enough time resolution to identify auroral field lines. However, it is well established from measurements in polar orbit that oxygen ions stream upward out of the auroral acceleration region, so that the detection of field-aligned streams of oxygen ions would be a signature of connection to an inverted V or the head of the westward

surge, if not to the onset arc at 100 km altitude. Such a detection was made in the CDAW 6 substorm.

In summary, there have been no simultaneous measurements of the onset in space and on the ground; in some cases, there has been an extremely close relationship between the fine details of the dipolarization and the expansion of the auroral bulge; in many cases, there has been a general relationship; and there is no reported signature at geostationary orbit of the activation of the poleward arc system. It should be emphasized that the association of the substorm expansion phase with the timing and the structure of expanding current wedge is much clearer than with the signatures of tail reconnection, such as fast flows, plasmoids, and energetic particles.

15

TRIGGERED SUBSTORMS

15.1 Introductory Remarks

Do events in the solar wind "trigger" substorms, or do substorms occur independently? Is there a difference between triggered and untriggered substorms? What kinds of events trigger onsets? Expansions? Can we learn about their physics from the things that do and do not trigger them? Does the switch from expansion to recovery phase require external prompting? Even if it is not required, can the recovery be prompted anyway? If conditions in the solar wind are steady, can we still have substorms? In this chapter, we review studies that have addressed questions like these. "Pseudoexpansions" resemble the first several minutes of development of the dipolarization and westward surge, but later fail to sustain an expanding current wedge or auroral bulge (Section 15.2). They may be triggered by minor dayside reconnection events that occur before the threshold condition for the full substorm is reached. Interplanetary shocks can trigger a substorm within minutes of their arrival at earth, provided they are sufficiently strong and a growth phase is already in progress (Section 15.3). Other compressional solar wind discontinuities also can trigger substorms, but rarefactions cannot. Northward turnings of the interplanetary field can also trigger substorms after a growth phase has already started (Section 15.4). During intervals of steady southward interplanetary field, either quasisteady convection bays or quasiperiodically recurring substorms can occur (Section 15.5).

15.2 Pseudo-Expansions

An inkling of pseudoexpansion behavior has been around since before the auroral substorm existed (Elvey, 1957), and in his original paper Akasofu (1964) not only had taken them into account but suggested that they occur on other than the most equatorward arc. Later, Davis and Hallinan (1976) and Untiedt et al. (1978) pointed out that pseudoexpansions are brief activations of local small-scale auroral spirals to the ground observer. Now it appears that pseudoexpansions are attenuated versions of complete expansions in several important respects: brightening of an auroral arc, Pi 2 pulsation bursts, and enhancements of the auroral electrojet, (McPherron, 1991). In this section, we show the auroral

pseudoexpansion has a counterpart in geostationary orbit, and present evidence that both may be responses to variations in the dayside reconnection rate.

At least two clear pseudoexpansions were found during the growth phase of a substorm on March 4, 1979 (Sauvaud et al., 1987). In this event, the electrojets around the oval intensified and began to migrate equatorwards less than 5 minutes after a sharp southward interplanetary field shift reached the dayside magnetopause. The magnetic field at GEOS 2, in geosynchronous orbit, started to become more tail-like about 15 minutes afterwards. This growth phase was terminated by a full substorm expansion that started 80 minutes after the southward turning. The pseudoexpansions were characterized by attenuated versions of phenomena associated with the full expansion—plasma sheet flux decreases at the ISEE orbits in midtail, weak dipolarization and dispersionless particle injection events at GEOS 2 ("pseudodipolarizations"), and perturbations in the ionospheric electric field and limited impulsive motions of the westward electrojet. Sauvaud et al. (1987) suggested that the pseudoexpansions were responses to small changes in the direction of the interplanetary field. The measured solar wind parameters, shifted by the solar wind propagation time between the spacecraft and the magnetopause, were used to construct the Perreault–Akasofu energy coupling function. The two pseudoexpansions occurred less than 5 minutes after small transient increases in this function.

Koskinen et al. (1992) compared a pseudoexpansion that occurred on August 31, 1986 with the full expansion that followed it using data from multiple spacecraft near geostationary orbit, ground magnetometers, and the STARE radar. The pseudoexpansion occurred 27 minutes after the interplanetary field at IMP 8 had turned southward, and the true expansion followed 22 minutes later. The Perreault–Akasofu energy-coupling rate reached 100 GW 22 minutes before the pseudoexpansion and remained at that level until 16 minutes after the full expansion. The ground magnetometers and STARE began to detect enhanced convection in the ionosphere about ten minutes after the southward turning reached the magnetopause. Two minutes before the pseudoexpansion, STARE picked up the Harang discontinuity slightly south of 70 degrees geographic latitude, moving slowly equatorward in typical growth-phase behavior. At the time of the pseudoexpansion, a small disturbance extending over four degrees of longitude appeared and penetrated to the eastward electrojet region south of the Harang discontinuity. The disturbance expanded to the west and north, and ultimately produced a slight enhancement of the westward electrojet. After 2 minutes and 40 seconds, the disturbance disappeared and the Harang discontinuity emerged again in the data. Two distinct Pi 2 bursts had been detected, one associated with the pseudoexpansion and one with the full expansion. Throughout the interval between the pseudoexpansion and expansion Pi 2 bursts, there was quasicontinuous activity in the Pi 1 band, suggesting there was continuous exchange of Alfven waves between the geostationary region and the ionosphere during this time. Similar activity in the Pi B band had been reported earlier by Untiedt et al. (1978).

Now let us compare the signatures of the pseudoexpansion and expansion in the geostationary region. Three spacecraft were near one another in favorable

observing positions at the time of the pseudoexpansion (Koskinen et al., 1992). AMPTE/CCE, 8.6 R_E downtail, observed a turbulent magnetic field dipolarization and a small injection of energetic ions that occurred about a minute after the first Pi 2 burst was observed on the ground. Roughly the same phenomena occurred at the time of the full expansion 22 minutes later, which followed the ground Pi 2 burst by about 2 minutes. Based upon data from this one spacecraft, one could not have distinguished the pseudoexpansion from the true expansion. However, nearby, at geostationary orbit, the two dipolarization events were quite different. Only one of the two geostationary spacecraft saw even a weak energetic particle signature at the time of the pseudoexpansion, while the expansion led to full substorm signatures at both. Thus, the pseudoexpansion remained localized, whereas the full expansion created an expanding substorm wedge.

Nakamura et al. (1992) compared the spatial and temporal scales of pseudoexpansions and multiple expansions in two substorms, using high-resolution energetic particle and magnetic field data at synchronous orbit and simultaneous ground magnetometer and auroral data. Ground data were available from the ionospheric footprints of both GOES 5 and GOES 6, which were separated by 33 degrees in longitude. Both pseudobreakups corresponded to the passage of vortical auroral structures and horizontal currents over the conjugate ground stations. The smaller vortex had a scale size of 200 km, and the larger, 450 km; the time scale of its rotational auroral motions was 7 minutes, and an upward field-aligned current was flowing out if it. At GOES 5, a sharp and strong positive enhancement in the D component, consistent with field-aligned current flow out of the ionosphere, commenced 1 minute after the pseudoexpansion at its footprint. An electron flux enhancement started a minute after that; its energy–time dispersion corresponded to an injection region of about 30 degrees, or 3 R_E, in longitude, which compared favorably with the 2 R_E scale size corresponding to the 450 km auroral footprint. The subsequent major substorm expansions were less localized, but they too consisted of a number of localized injections, each of which had 5–10 minute time scales.

15.3 Triggering by Interplanetary Shocks and Other Compressions

Heppner (1955) had reported even before substorms were substorms that negative bay onsets at high latitudes were often associated with magnetic storm sudden commencements (SSCs) or sudden impulses (SIs). Later research established that the SSC was the ground signature of a fast compressional mode driven into the magnetosphere by the passage of an interplanetary shock. Smaller, so-called sudden impulses are caused by tangential discontinuities and other sudden pressure variations. The SSCs are always compressional, while sudden impulses can be either compressional or rarefactive. Kawasaki et al. (1971) reported that all SSCs with magnitudes greater than 40 nT were accompanied by negative bays with amplitudes exceeding 50 nT. Along with Schieldge and Siscoe (1970), they found that the probability of triggering a substorm increased with increasing SSC

magnitude. It was also clear that the triggering probability depended on prior history: Burch (1972a) showed that triggering was more likely when the interplanetary field had been southward or horizontal with a large magnitude for the 30 minutes before the passage of the discontinuity. Similar arguments were advanced from various lines of evidence by Kokobun (1972), Iijima (1973), and Ondoh (1973).

The relationship between substorm occurrence and magnetospheric compression was examined for 125 SSCs and compressional SIs observed during 1967–1970 (Kokobun et al., 1977). Forty-two of these events had previously been identified as having been caused by interplanetary shocks (Hundhausen, 1972; Chao and Lepping, 1974). The data set for the 125 events included ground magnetograms, AE indices, and Explorer 33, 34, 35, and OGO 5 magnetic field data. Negative bays with amplitudes exceeding 150 nT at auroral latitudes followed within 15 minutes of 43% of these compressions. Such auroral electrojet intensifications were said to be triggered. In about 90% of these cases, the AE index had exceeded 100 nT in the 15 minutes before the onset; in those cases where the previous AE had been less than 100 nT, the probability of triggering was only 8%. If a substorm had already been in progress at the time of an SSC or SI, a further enhancement of the auroral electrojet immediately followed. Nine of the 10 largest SSCs with amplitudes exceeding 40 nT triggered negative bays, and the one exception occurred in a quiet magnetic condition (AE < 100 nT). The fact that 11 of the 12 triggered substorms for which interplanetary field data were available had been preceded by at least 30 minutes of southward field clearly indicated that a substorm growth phase had to be in progress before compressions could trigger substorm expansions.

Kokobun et al. (1977) made a number of individual events the subjects of case studies. On September 30, 1968, an interplanetary shock that passed over Explorer 33 following a 5-hour period of southward interplanetary field subsequently created an SSC with a 21 nT average amplitude on the ground. At the time of the ground SSC, OGO 5 was in the evening sector magnetosphere at 9 R_E distance downtail; the OGO 5 magnetic field strength, which had been increasing slowly, began to increase more rapidly. Three minutes after the SSC, sharp negative bays began at ground magnetometer stations near local midnight; the field magnitude at OGO 5 began a strong decrease, accompanied by strong Pi 2 time-scale variations in B_y and abrupt increases in the fluxes of energetic electrons and protons. Thus it appeared that a conventional substorm expansion was triggered within 3 minutes of the arrival of the shock compression front at the earth's surface. On November 20, 1968, a shock also encountered during a southward field interval triggered a substorm expansion within minutes of its SSC. On the other hand, on October 29, 1968, an interplanetary shock encountered during a prolonged interval of northward field led to a ground SSC 4 minutes later but did not enhance the auroral electrojet. The November 20 and October 19 SSCs had roughly the same magnitude. On February 15, 1967, a strong shock that propagated over earth following a 1-hour interval of northward field created a 50 nT SSC but did not trigger a substorm expansion.

The case studies of Kokobun, et al. (1977) and statistical results suggested that the probability of triggering is significantly enhanced if the shock arrives at the earth following a period of southward interplanetary field. There were, however, two exceptions to this pattern. An interplanetary shock on February 10, 1968 created structureless but intense activity at high and auroral latitudes. This shock propagated over earth during a southward field interval that began about 30 minutes before the ground SSC was recorded and continued southward for several hours thereafter; Pi 2 micropulsations and low-latitude positive bays started not at the time of the SSC but 40 minutes afterwards. The second exceptional case, a shock on July 13, 1968, triggered an enhancement in the auroral electrojet after a *northward* field interval. However, in this case, the interplanetary field turned southward immediately after the passage of the shock, and the authors argued that it was the southward shift that stimulated all the (nonsubstorm) electrojet activity, which was much stronger at polar than at auroral latitudes.

Iyemori and Tsunomura (1983) investigated the statistical relationships between the recent history of the interplanetary field, the magnitude of the storm sudden commencements, and Pi 2 pulsation bursts. A clear peak of Pi 2 burst occurrence appeared around 10 minutes after compressional SSCs, and no Pi 2 bursts followed negative sudden impulses. This clearly indicates that only compressions of the magnetosphere trigger Pi 2 bursts and by implication, substorms. Iyemori and Tsunomujra (1983) also found that, although pre-existing southward field conditions were important for SSCs to lead to a large response in the auroral electrojet currents, triggered Pi 2 bursts seemed not to require a prior history of southward field.

A substorm expansion was observed within 2 minutes of the arrival of a fast mode compression at geostationary orbit on the nightside (Ullaland et al., 1992; Kremser et al., 1992). A 90 minute growth phase had been in progress at the time the substorm was triggered. GEOS 2, which was in geostationary orbit at about 2100 LT, observed four clearly distinct phases of this event. Phase I, which began 16 minutes before the SSC, was marked by increases in the ion phase-space density at all values of the magnetic moment. The magnetic field energy decrease was equal to the ion energy increase, the ion pressure exceeded the electron pressure, and the plasma beta rose to about unity. These features were typical of the substorm growth phase at geostationary orbit. Phase II began when the fast mode compression arrived at GEOS 2 about 2 minutes after the SSC was received on the ground. The magnetic field strength increased, the ion phase-space density increased at all values of the magnetic moment, and the parallel and perpendicular ion pressures increased from 8 to 20 keV cm^{-3}, while remaining equal to one another; the plasma beta rose above 2. A variety of diagnostics placed the substorm onset to be approximately 2 minutes after the arrival of the fast wave at the spacecraft. Assuming its speed in the tail was 1500 km/s, it was 30 R_E tailward of GEOS 2 when the first signs of the substorm were registered at the spacecraft. This began phase III at GEOS 2. An increase in ion phase-space density started first at the highest measured values of the magnetic moment and spread to lower values. The magnetic moment–time dispersion indicated that a dispersionless ion injection

was occurring east of the spacecraft. The ion energy density was enhanced, and the cross-tail current remained strong throughout phase III. Phase IV began 9 minutes after onset, when the magnetic field dipolarization and accompanying electron injection passed over the spacecraft.

This study conveys one important point: The shock compression only hastened an expansion that would have come in anycase. It enhanced the ion energy density and, by implication, the cross-tail current in the same way that the more gradual compression of the dayside of the magnetosphere had been doing all along during the growth phase. Presumably, the compression of the magnetosphere induced by the interplanetary shock simply put the system over a threshold that it was bound to reach on its own.

15.4 Triggering by Northward Shifts of the Interplanetary Field

Northward shifts of the interplanetary field may enhance the auroral electrojet following a period of enhanced southward field and/or electrojet activity (Foster et al., 1971; Caan et al., 1977; Caan, 1979; Pellinen et al., 1982; Rostoker et al., 1982, 1983; Rostoker, 1983). The first reported evidence seems to have been a superposed-epoch study of 54 large, isolated substorms in which the AE index intensified dramatically at the moment that the interplanetary field reached its maximum southward value and began to turn northward (Foster et al., 1971). This result was subsequently criticized by Hirshberg and Holzer (1975). Caan et al. (1977) discussed several events in which either a sudden lessening of a southward interplanetary field or a true northward turning was associated with a substorm onset. Whenever such events were observed, they had been preceded by an interval of southward interplanetary field.

The 1054 UT CDAW 6 substorm may have been triggered by a northward turning of the interplanetary field (McPherron and Manka, 1985). The very first Coordinated Data Analysis Workshop, CDAW 1, was devoted to substorm triggering by northward shifts of the interplanetary magnetic field (Rostoker et al., 1983). The study interval was an 8-hour period on December 12, 1977, when IMP 8 was in the solar wind about 26 R_E upstream of earth, and ISEEs 1 and 2 were inside the magnetosphere for the first 2 hours and 45 minutes and in the magnetosheath for the rest of the interval. The interplanetary field at IMP 8 was dominantly southward for the first 5 hours and completely northward for the last 3 hours of the 8-hour period. When ISEE 1 entered the magnetosheath, it detected a southward field component and an overall magnitude about three times larger than that measured at IMP 8, consistent with the field compression expected across the bow shock. The responses to four isolated northward turnings of the interplanetary field that occurred during the prolonged interval of generally southward field, as well as to the final northward turning, were studied using data from a chain of ground magnetometers. The first northward turning came 30 minutes into the study interval, the second an hour later, the third, less pronounced, 50 minutes later, and the fourth 30 minutes after that. The first three were separated by the 50–60 minute

response time that characterizes the development of substorms following southward turnings and of reverse convection and transpolar arcs following northward turnings; the last was separated from its predecessor by about half this characteristic time. All four transient northward turnings corresponded to definite H-component bays at at least one of two high-latitude ground stations, Leirvogur, Iceland (70.2° MLAT), or Nassarsuaq, Greenland (71.0° MLAT). The first two turnings also led to similar changes at four Scandinavian stations at auroral latitudes (65.0–67.6° MLAT). The first turning coincided within minutes with a small, 50 nT, perturbation in the north–south field at the Scandinavian stations and in the H component at Leirvogur. The second corresponded to a much larger, 500 nT, decrease in the H component at Leirvogur and Nassarsuaq, and a 200-400 nT decrease in the north–south component at the Scandinavian stations. At subauroral latitudes, the H component decreased by roughly 20 nT over a 106° range of magnetic longitude, which the authors attributed to the enhancement of the asymmetric ring current. The third northward turning intensified the strong electrojet that had already been activated at Nassarsuaq, but not at Leirvogur, only 24 degrees to the east. The fourth turning activated the electrojet at Leirvogur, yet initiated a long recovery at Nassarsuaq. The four transient northward turnings discussed were followed by 90 minutes of continuously southward field prior to a final and permanent northward turning; the interplanetary field strength remained steady at about 10 nT during the last hour of this period. During this quiet period, an small, untriggered substorm activation took place, characterized by a 40–80 nT decrease in the north–south component at the Scandinavian stations, a slightly larger H-component decrease at Nassarsuaq, and noticeable decreases at four subauroral stations. Then came the final, permanent northward turning of the interplanetary field at IMP 8. At that time, the H component at Leirvogur suddenly began a recovery of about 750 nT that took an hour to complete before it ended in quiescence. (At Nassarsuaq, this recovery had begun 2 hours earlier.)

Let us now summarize the CDAW 1 study. The primary response to three of four isolated northward turnings occurring during generally southward field conditions was at highlatitudes and localized, while one transient northward turning triggered a substorm at auroral latitudes. The final, sustained northward turning dramatically *reduced* activity at Leirvogur at high latitudes. But what was truly remarkable was the simultaneous development of a substorm current wedge at subauroral stations. In other words, this northward turning immediately started to diminish activity on the poleward arc system but did not affect ongoing substorm activity at lower latitudes.

15.5 Quasiperiodic Substorm Recurrence

Sergeev and Lennartsson (1988) documented two cases in which the solar wind dynamic pressure and magnetic field were stable for a time longer the convection circulation time, there was persistent and variable convection in the plasma sheet, but there were no substorms. There are other examples of such convection bays

during times of intense quasisteady solar wind energy input. However, the convection bay is not the only response to steady solar wind conditions. Several authors have reported stable solar wind periods in which substorms recur quasiperiodically.

In studies of two magnetic storms, Akasofu (1985a) and Lee et al. (1985) found that the (southward) interplanetary field and the energy-coupling function (Akasofu, 1981a) were basically constant for the order of a day, yet the AE index showed impulsive increases, and all-sky cameras recorded several westward surges. The recurrence time of these substorms was 2–4 hours. These studies found quasiperiodic substorm recurrence using ground-based data. Giant quasiperiodic 2-4 hour global variations in the fluxes of high-energy particles are not uncommon at geostationary orbit (Belian et al., 1992). Global flux oscillations were found at all local times during the magnetic storm of February 8, 1986, in which the interplanetary field was steadily southward and the solar wind speed exceeded 800 km/s for the better part of a day. Quasiperiodic substorm behavior has also been found in the tail. The ISEE 1 spacecraft recorded a series of four recurring tail-current disruptions during a 12-hour period of constant solar wind conditions on April 3–4, 1978 (Jacquey and Sauvaud, 1992). The southward component of the interplanetary field was about 10 nT, the Perreault–Akasofu energy-coupling rate was about 80 GW, and the AE index exceeded 600 nT throughout most of this period. ISEE 1 was in the northern tail-lobe and able to monitor the lobe magnetic field and the cross-tail current throughout the interval. The lobe field strength increased more or less monotonically in two of the three intervals between disruptions. The four disruptions had similar trends. The lobe field strength decreased by 10–30% of its previous maximal value and dipolarized: Its northward component increased from about 6 nT to roughly 12 nT. These changes took 12–30 minutes. In each case, the northward component first decreased before it increased, suggesting that the disruption first took place earthward of the spacecraft, which was 18–22 R_E downtail, and then moved tailward. During the growth phases, when the tail field strength was increasing, the highly prominent variations in the AE index appeared to be decoupled from the minor oscillations of the lobe field, but each disruption corresponded to a larger increase in AE than usual. The last tail disruption, which began as the interplanetary magnetic field was turning northward, was accompanied by the most intense burst of auroral electrojet activity recorded during the whole study period.

Horwitz (1985) singled out substorms and sequences of substorms that occurred during intervals of prolonged calm in the interplanetary magnetic field. The peak auroral electrojet had to exceed 250 nT to qualify as a substorm in this study. The average expansion phase of these presumably "pure" and untriggered substorms lasted 13 minutes, about the ionospheric line-tying time and significantly less than the classical 30 minutes (Akasofu, 1964); the average recovery phase was 41 minutes long.

15.6 Summary and Discussion

Sometimes pseudoexpansions are stimulated by southward shifts of the interplanetary field, sometimes expansions are set off by an interplanetary shock, sometimes substorms intensify following a northward shift of the interplanetary field, sometimes substorms recur quasiperiodically when the field is steady, and sometimes substorms disappear altogether into a blurred high-dissipation state, but when substorms occur, it is because there has been a growth phase during which the interplanetary field was predominantly southward beforehand. The growth phase phenomena leading up to expansions and pseudoexpansions are similar, and expansions and pseudoexpansions are similar except for spatial scale. The principal difference between them seems to be that the pseudoexpansion does not develop a current wedge and auroral bulge that can expand through successive intensifications. There seem to have been no reports of triggered onset phenomena, so we have chosen to call them "pseudoexpansions" and not "pseudo-onsets."

The compressions of the magnetosphere by interplanetary shocks and other sudden pressure increases in the solar wind clearly induce an auroral and geostationary substorm by accelerating the processes that occur in the cross-tail current region during the growth phase. There is some evidence that pseudoexpansions and pseudodipolarizations may be triggered by sudden small increases in the dayside reconnection rate during growth phase. Since the pseudoexpansions occur within 5 minutes of the variations in the dayside reconnection rate, they cannot involve reconnection far downtail. The common denominator with compressional triggering may be the fast modes that propagate tailward as the magnetopause oscillates in response to a variable reconnection rate. Certainly, the delays between southward turnings at the magnetopause and the pseudoexpansions found by Sauvaud et al. (1987) were roughly equal to the time that fast waves travel from the nose of the magnetosphere to the geostationary region on the nightside.

Assuming that substorm onset occurs when the cross-tail current reaches a certain threshold leads to following speculative scenario for triggered substorms. A general southward turning of the interplanetary field causes the cross-tail current system to oscillate, intensify, and approach the earth. Sudden solar wind pressure increases also cause the dayside magnetopause to move inwards and couple to fast waves that intensify the cross-tail current in the geosynchronous region. As the current sheet approaches some overall stability limit, the oscillations in the cross-tail current induced by modulations in the dayside reconnection rate, or by the natural periodicities associated with flux transfer events and magnetopause motions, might trigger pseudoexpansions that will be extinguished after a half-cycle. Finally the threshold is reached permanently. At that point, the onset occurs, followed by a sustained rather than transient expansion of the current wedge. Should current sheet oscillations continue to be driven after the threshold is reached, a number of further intensifications with similar auroral and geostationary signatures might take place. This suggests that the recurrence periods of pseudoexpansions prior to onset and the multiple expansions following breakup

might be related to one another and to the periodicities of the magnetopause and cross-tail current system.

Sometimes structureless convection bays are observed during steady southward field conditions and sometimes quasiperiodically recurring substorms have been reported. The 2–4 hour recurrence time is approximately the full convection cycle time, that is to say, the time for an element of ionospheric flow to cross the polar cap, or for the solar wind to traverse the length of the tail. Quasiperiodic substorm recurrence has been found in the auroral oval, at geostationary orbit, and in the geomagnetic tail during prolonged intervals of southward interplanetary field associated with magnetic storms. Perhaps a transition to chaos (Baker et al., 1990a,b, 1991; Roberts et al., 1991; Klimas et al., 1992) explains this behavior, but we do not know what the relevant control parameter(s) may be.

16

ON THE RELATION BETWEEN CONVECTION AND SUBSTORMS

16.1 Introductory Remarks

Why after 30 years of research have we not settled the relationship between substorms and convection? Why after 30 years are there still substantially different, competing models of substorm onset? Why has the progression from phenomenological to fully quantitative understanding not occurred? Answers to such questions will probably only become clear in retrospect, after the transition to quantitative understanding has taken place; in the meantime, we can only express our individual views.

In our view, there have been three central difficulties. Contradictory pictures of plasma sheet transport have been able to flourish side–by–side because this fundamentally unsteady and highly spatially structured system was and is undersampled. As a result, people can still argue about when and where tail reconnection occurs in the substorm sequence, and other issues equally fundamental. Moreover, it is still not possible to connect the substorm onset in the auroral ionosphere to an event in space. For one thing, there is the timing problem: Waves communicate events' existence across the magnetosphere and to the auroral ionosphere within a minute or two. We are only beginning to study the magneto-ionosphere system globally with the required time resolution, and until we do so, there will be a "chicken and egg" problem. Finally, two key measurements are missing. No plasma sheet signatures of auroral arcs have been identified, so we do not know when a spacecraft is connected to a potential auroral onset region. We do not yet have an accepted ionospheric diagnostic of plasma sheet reconnection and the plasmoid formation; there is no *auroral* data display that illustrates at a glance the relationship of plasma sheet events to the onset and expansion of the substorm.

Despite all this, there is real cause for optimism. The sheer magnitude of the observational effort and the volume and diversity of the results produced over the years have finally enabled us to perceive how complex the behavior of the magnetosphere really is. As our perceptions have evolved, we have designed multi-instrument, multi-spacecraft studies of ever-increasing comprehensiveness, articulation, and resolution, which further clarified our perceptions. All this effort is beginning to pay off. A new condensation of understanding, if not a fully

quantitative theory, seems at hand. Our essay closes with our best guess as to how this might come about.

The old reconnection model of substorms needs to be updated to reflect the fact that magnetopause reconnection is bursty and localized. Generalized versions of the Petschek reconnection model still can describe the MHD aspects of reconnection-induced flows in an average sense, and we would still expect bursty reconnection to activate the MHD characteristic fields. Some of the waves launched by dayside reconnection events induce convection in the dayside of the magnetosphere and polar cap ionosphere (Section 16.2) and others stimulate convection in the tail lobes and ultimately reconnection in the plasma sheet (Section 16.3). The number of different characteristics that can be excited suggests that the magnetosphere may, depending upon subtle details, respond to dayside reconnection differently from event to event, and the burstiness of magnetopause reconnection implies that the response will be spatially and temporally complex. Despite the additional complexity, the substorm growth phase still appears to be a consequence of a persistent increase in the average magnetopause reconnection rate. Now, however, the ensuing tail reconnection is triggered at various places and times by a complex field of waves from the dayside reconnection region (Section 16.4). The complexity makes the hitherto ambiguous outcome of plasmoid timing studies more understandable (Section 16.6).

The complexity also leads us away from the idea that tail reconnection is responsible for the single event that is the onset of the auroral substorm. Somehow, the substorm growth phase leads naturally to the onset, but we need to find a second path from growth phase to onset besides the evolution of the tail towards a massive reconnection event. An alternative has been there all along: The growth of the magnetopause and cross-tail current system, together with field-aligned currents and the polar cap convection electric field, might lead to some kind of catastrophe. The first model of this type, now outmoded, had the field-aligned currents that feed the preonset auroral electrojets rising above the threshold of anomalous resistance instabilities, increasing the field-aligned electric potential, polarizing the midnight-region ionosphere, and enhancing the westward electrojet to launch the westward surge (Coroniti and Kennel, 1972c). Today, we understand that the catastrophe probably occurs somewhere in the system of cross-tail currents and field-aligned currents connecting to the onset region in the ionosphere. A number of modern candidates have been suggested: reconnection at a near-earth x line, "disruption" of the cross-tail current, a failure to sustain large field-aligned currents, the "ballooning mode" instability, destruction of the line-tying stress and current balance by the increased conductivity due to auroral ionization, or a sudden loss of equilibrium.

The substorm growth and expansion phases in the geosynchronous region and in the auroral ionosphere are so closely linked (Section 16.5) that the onset probably involves the physics of the geosynchronous region. We have seen there is a loose relationship between onset/dipolarization and plasmoid ejection. If, then, onset/dipolarization and plasmoid ejection are independent events that each activate the aurora, substorms ought to exhibit two distinct active phases, as recent analyses

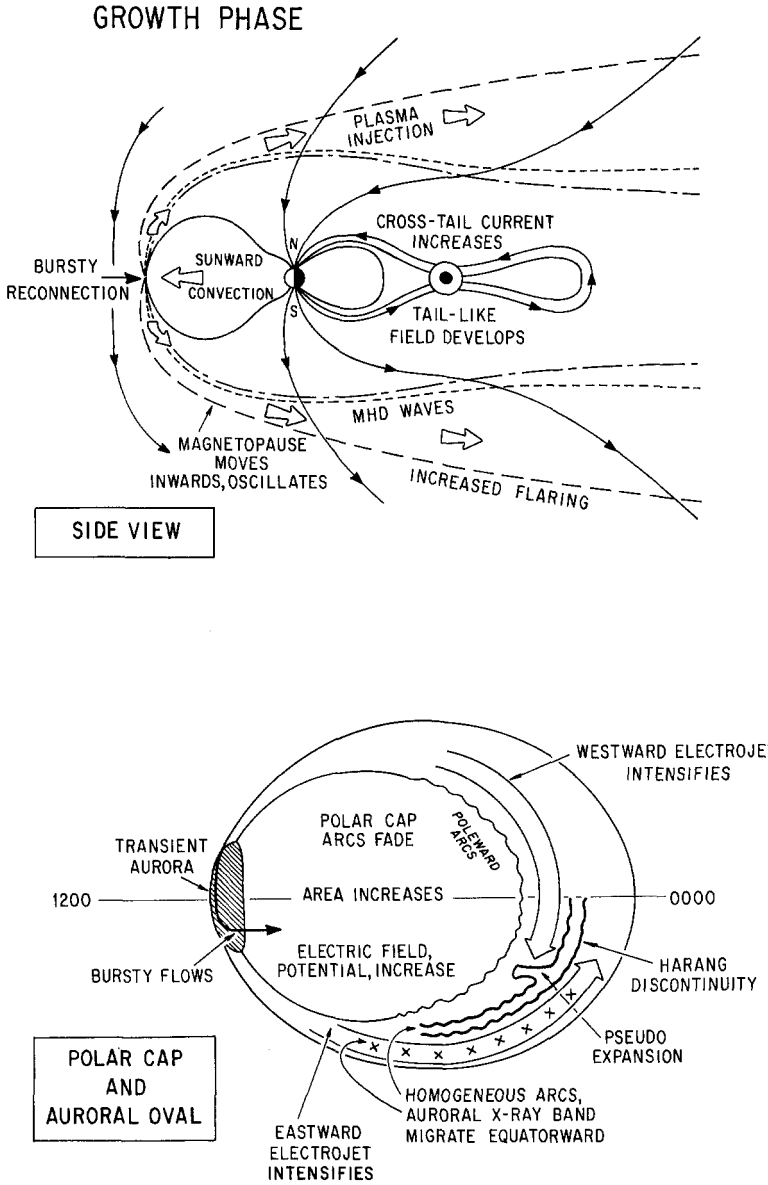

Figure 16.1. The Substorm Growth Phase. The growth phase of the auroral substorm starts with the activation of high-latitude arcs on the dayside, followed by an increase in the cross-polar cap electric field, stimulation of two-cell ionospheric convection, activation of the eastward and westward electrojets, and equatorward arc motion around the auroral oval. The X-ray arc and the Harang discontinuity comove equatorward with the auroral

of ground magnetometer data with good high-latitude coverage suggest (Section 16.7). In a few instances, however, the reconnection has been found to occur near the geostationary region around the time of onset, but these cannot account for all of the substorms (Section 16.8). In most substorms, the magnetic field in the geosynchronous region appears to dipolarize without reconnecting locally, and it is the plasma sheet recovery that likely marks the production of one or more of the plasmoids in the reconnection events that are further downtail. These events activate the poleward arc system in the second active phase of the auroral substorm (Section 16.9).

All in all, the relationship between convection and substorms has been obscured by our failure to distinguish between tantalizingly similar phenomenologies at the poleward and equatorward edges of the nightside auroral oval. Yet the two regions respond to very different physical influences. High-latitude arcs connect to the drivers of convection, to magnetopause reconnection, viscous transport, and tail reconnection, while the auroral expansion connects to the nightside geostationary region, where there is no clear evidence that classical convection occurs. Certainly much of what did and did not happen since 1964 depended upon what was and was not in Akasofu's great paper. The difficulty could be that the first formulation of the substorm paradigm missed one key element, the poleward arc system, because of incomplete geographical coverage at the dawn of the space age.

16.2 Magnetopause Reconnection and the Stimulation of Dayside Convection

The issue of how convection is stimulated is simple in conception but rich in important detail. In general, three systems of waves are needed to adjust the magnetosphere and ionosphere to an increase in the dayside reconnection rate. A fast rarefaction wave will propagate tailward while coupling to localized Alfven resonances on closed field lines in the dayside magnetosphere. Its function is to increase the rate of sunward convection. Intermediate waves will propagate along field lines from the reconnection region to the polar cusp ionosphere to increase

---

arcs in local evening sector. As this evolution proceeds, the arcs can fade and recover over much of their length. Those on the nightside can also brighten locally in a miniature version of the westward surge to come. The growth phase of the geosynchronous substorm starts with the development of a "tail-like" magnetic field that is due to the approach and intensification of the current sheet. As the current sheet thins, the fluxes of energetic particles may drop out. The current sheet has been observed to become very thin during the growth phase, to the point where the adiabaticity of the motions of ions and energetic electrons may be compromised. The dayside magnetopause migrates inward in an oscillatory fashion. The tail magnetopause becomes more highly flared, and the flux and magnetic field strength in the tail lobes increases with time. Waves launched by bursty reconnection on the dayside magnetopause propagate over the poles and into the tail lobes. riginal drawing.

the convection rate there. Finally, fast, and in general, intermediate and slow compressional waves will be sent over the poles on open field lines to adjust the tail lobes, and ultimately, the plasma sheet to the change in magnetopause reconnection rate. How much each characteristic field is stimulated will depend upon the details of the magnetopause reconnection events. Let us now discuss each of these systems in more detail.

An increase in the dayside reconnection rate launches a wave that propagates across field lines into the magnetospheric cavity and initiates an enhanced flux return in its wake (Coroniti and Kennel, 1973). Since the flow speed behind exceeds that ahead, it is a rarefaction wave. Any time-dependent reconnection rate could be resolved into a series of steplike changes, so the time development of convection could also be so resolved—each step increase in reconnection rate launching its own rarefaction wave. The waves resemble a fast global mode that, by decreasing both the plasma and the magnetic pressure establishes a stress gradient that accelerates plasma and field lines toward the dayside magnetopause. Since the wave reduces the total pressure behind it, the pressure balance condition at the magnetopause has to be satisfied by inward motion of the magnetopause and strengthening of the inward-facing compression waves that connect to the reconnection region. Whereas for times short in comparison with an Alfven travel time along the lines of force, the rarefaction wave accelerates the plasma and field lines in space without affecting the ionosphere, for longer times the convection in space must be consistent with the convection in the ionosphere. As the fast rarefaction spreads out from the reconnection region, it induces distributed field-aligned currents type by coupling to intermediate waves in roughly the same way that localized toroidal magnetic pulsations are stimulated by fast compressions and rarefactions. The finite conductivity of the ionosphere opposes the development of convection by allowing a perpendicular current to short part of the electric field established inductively by the intermediate waves. This process is called "line tying."

An increase in the dayside reconnection rate also causes intermediate and slow waves to propagate along field lines from the magnetopause to the polar cusp to stimulate ionospheric convection and increase the density of magnetosheath plasma above the ionosphere. If the conductivity of the ionosphere were infinite, the field-aligned current carried by an incoming intermediate wave would be precisely cancelled by that of the reflected wave, and the flow in the ionosphere would be perfectly line tied. However, when the ionospheric conductivity is finite, some of the incoming intermediate wave energy is absorbed, the field-aligned current adjusts to ensure closure of the system of perpendicular currents associated with ionospheric convection, and the ionospheric convection electric field is modified. The function of the reflected waves is clearly to notify the flow in space that it is partially line tied; multiple reflections between space and the ionosphere will take place until all the Alfven wave energy is damped away, and the flows in space and the ionosphere have adjusted to one another.

The global pattern of convection responds in both the ionosphere and the magnetosphere on a time scale determined by the ionospheric dissipation and the

fast-mode propagation time. The empirical time scales for polar cap convection to adjust globally to a flux-transfer event, for the fast mode to cross back and forth between the inner edge of the plasma sheet and the dayside magnetopause, and the repetition interval between flux-transfer events are all the order of 10 minutes—probably no accident. The entire coupled magnetopause–dayside flow system oscillates on the 10-minute time scale (Holzer and Reid, 1975; Reid and Holzer, 1975).

16.3 The Stimulation of Convection in the Tail

The sudden acceleration of the flow by a magnetopause reconnection event will send compression waves over the poles on open field lines. Depending upon circumstances, all three types, fast, intermediate, and slow, could be sent tailward. In addition to enhancing the rate of convection across the tail lobes, the fast wave adjusts the lobe magnetic pressure, the position and strength of the cross-tail current system, and the thickness of the plasma sheet to the changes in current strength and position of the dayside magnetopause (Coroniti, 1985). It also raises the flaring angle of the tail magnetopause so that more solar wind momentum flux is intercepted by the tail (Coroniti and Kennel, 1972a). The sudden injection of new plasma into the old mantle might introduce a slow compression, and an appropriate rotation of the magnetic field during dayside reconnection could introduce an intermediate shock as well (Yu Lin and L. C. Lee, private communication, 1992). Each will converge onto the plasma sheet at a different distance downstream at a different time. The convergences will be arrayed in a specific order in the ideal case that the waves are all activated by the same sudden reconnection event on the dayside. In order of increasing distance and delay, there will be the closures of the fast, intermediate, and slow compressions, followed by the slow rarefaction fan.

We can only guess at closure distances and times. Slow rarefaction, or mantle, closure times are in the 2–4 hour range, the time scale of a complete convection cycle, and closure distances scale accordingly. Studies of SSCs and SIs indicate that a fast compressional wave crosses the inner magnetosphere on closed field lines and enters the tail in 5–10 minutes; the more difficult question is when and where the fast compression waves sent over the poles by a sudden magnetopause reconnection event converge on the plasma sheet. When they do, they will cause it to thin and induce a tailward flow inside it (Coroniti, 1985). Numerical solution of the three-dimensional MHD equations indicated that this occurred 14 R_E downtail in one case (Walker et al., 1992). The slow shock propagates slowly across field lines, and its closure distance and characteristic delay ought to be slightly smaller than for the steady–state mantle. The closure point of the intermediate wave or shock should be between that of the fast and slow waves.

16.4 Multiple Tail Reconnection Events

The logic of the theory of characteristics is strict: The plasma sheet ultimately has to respond to the arrival of the waves from the dayside reconnection event by reconnecting somewhere. The precise timing and the location(s) of the new reconnection event(s) will be determined by the pattern of plasma sheet illumination by the tail-lobe waves. Let us assume that explosive reconnection is triggered by wave-induced compressions or other appropriate perturbations. The waves in the low-density tail-lobe are highly dispersive (the ion inertial length is the order of one earth radius); so the wave field illuminating the plasma sheet is liable to be highly complex spatially, suggesting that tail reconnection should actually be a multiple spatially structured event. In the presumed irregular convection state that prevails much of the time, a "fossil" neutral region or regions will be located fairly far downstream. If the stimulus from the dayside simply activated the old neutral region(s), the convection would adjust quasiadiabatically to the change in dayside boundary conditions. No plasmoid would be produced. The general association of plasmoids and substorms indicates that the new reconnection event is triggered by a wave field that closes nearer the earth than the pre-existing neutral region(s). Such a structurally unstable perturbation is needed to organize plasmoids in the first place.

Let us now put our arguments together. When the interplanetary field turns southward, reconnection does not turn on and stay on; bursts of magnetopause reconnection become larger and more frequent. The magnetopause currents, the ionospheric currents, and the cross-tail currents in the near-earth plasma sheet all adjust to this forcing in a mutually interdependent way. They often oscillate in a quasiperiodic fashion with a 10-minute time scale. The bursts of dayside reconnection often repeat on the same time scale. Modulated bursty magnetopause reconnection creates a spatially complex, bursty field of waves that propagates into the tail. Each type of wave does a different thing. Fast waves propagate across field lines and quickly adjust the inner edge of the current sheet on the nightside to the change in magnetopause position. Others, in the slow and intermediate modes, propagate in more leisurely fashion over the poles and into the tail. Ultimately, as the waves converge onto the plasma sheet they stimulate localized reconnection bursts at a number of different times and places. These explosive events generate bursts of energetic particles that spread out from the reconnection sites. Some reconnection events reach open field lines to form plasmoids and fast earthward flows, in so doing expanding the plasma sheet boundary layer. As these become more frequent and more closely spaced, their aftermaths viewed from afar blend into a convection state that resembles ever more closely the one envisioned in the original steady reconnection model. If many reconnection events respond nearly at once to a single large-scale stimulus, they could reproduce the single event visualized in the original reconnection model of substorms.

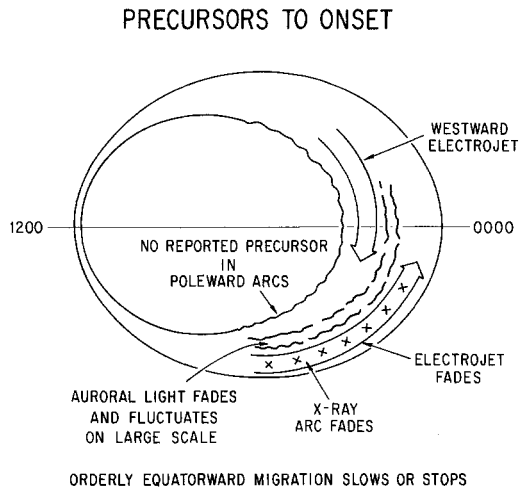

Figure 16.2. Precursors to Substorm Onset. The intensity of auroral light often fades and fluctuates on 1–5 minute time scales prior to onset, More than one arc can be visible; while other arcs may brighten. The one that is fluctuating is the one that fades. It is often a more poleward arc that fades just prior to the abrupt brightening of the onset arc. The diffuse band of radar backscatter located near the arcs has been observed to weaken as the arcs fade. The X-ray arc also fades just before onset. In one substorm, the X-ray intensity faded five minutes before onset, just as the auroral arc and X-ray arc ceased their equatorward motion. Similar oscillations in intensity can occur earlier in the growth phase. *Viking* observations suggest that visual arc fading occurs over a large spatial scale; in one case, a fading monitored on the ground corresponded in space to fading from evening to morning of the diffuse band of emission, which was the spacecraft's view of the arc. The spacecraft arc faded along its entire length, recovered, faded away completely five minutes later, and then recovered again. Original drawing.

16.5 Relation between Auroral and Geosynchronous Substorms

The growth and expansion phases of the auroral substorm have clear counterparts in the geosynchronous region. It has been suggested that the bright auroral arcs on the nightside map to the region of maximum cross-tail current. If so, the equatorward march of the ordered network of auroral arcs, the Harang discontinuity, and the X-ray arc reflects the progressive displacements earthward of the dayside magnetopause and nightside current sheet as the growth phase evolves. The cross-tail current sheet may also vary its strength and thickness in response to the oscillations of the magnetopause. Localized pseudoexpansions in the aurora have counterparts in small magnetic field dipolarizations and small dispersionless injections of energetic particles near geosynchronous orbit—"pseudo-dipolarizations" and "pseudoinjections." These events indicate that the auroral ionosphere is tightly coupled to the geosynchronous region during the growth phase. There is no accepted geostationary signature of the brightening of

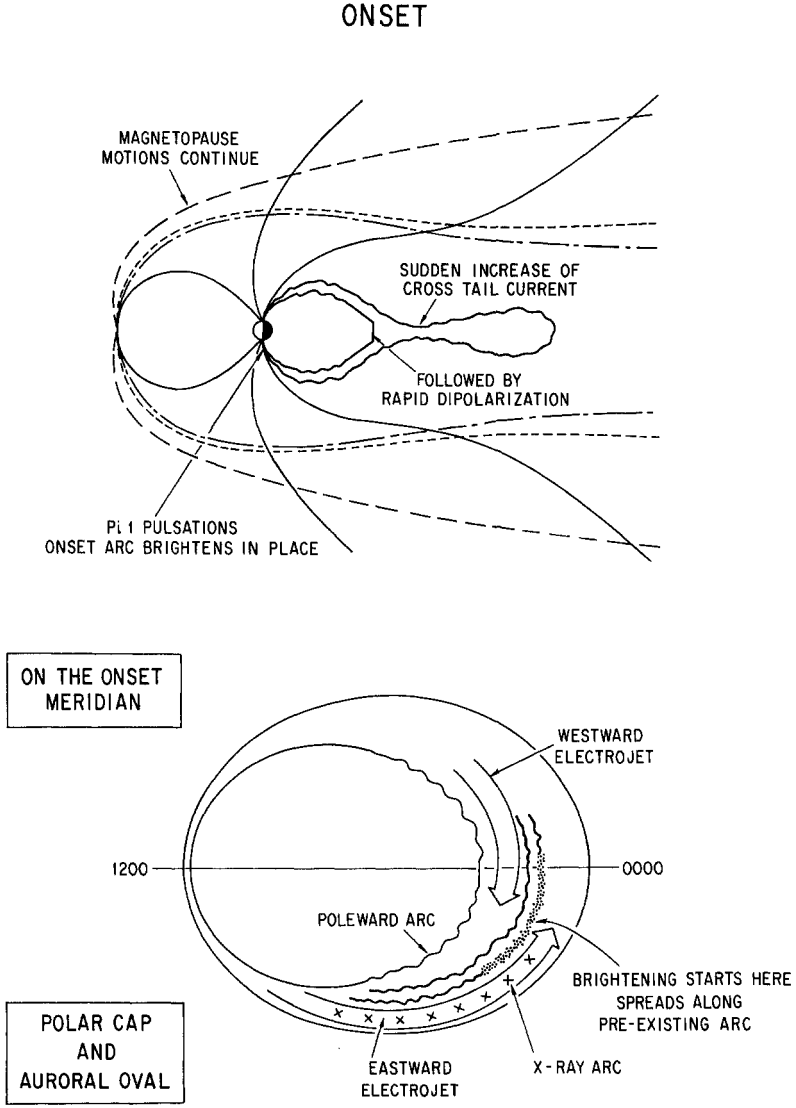

Figure 16.3. Substorm Onset. The substorm onset is the brightening of a small region of the most equatorward arc near the Harang discontinuity. The preexisting pattern of auroral light simply intensifies. The brightening spreads eastward and westward—until after a minute or so—the onset arc will have brightened over several thousand kilometers of its length. The onset arc is on closed field lines at lower latitudes than the poleward arc system.. At about the same time, dipolarization is initiated in the geosynchronous region. The events in the initial dipolarization region are much more violent than those observed later as the dipolarization expands. The H-component of the magnetic field decreases on the one-minute

the onset arc, but there is excellent correspondence on a minute-by-minute basis between the formation of the westward-traveling surge, the development of structure on the time scale of the Pi 2 geomagnetic micropulsations, and dipolarizations and dispersionless injections near geosynchronous orbit. These in turn develop into the substorm current wedge, which expands azimuthally and feeds the expanding auroral bulge with field-aligned current. These close correspondences suggest that substorm onset is closely linked to the physics of the geosynchronous region (Kennel, 1992).

In contrast, there is no clear signature in the geosynchronous region of the beginning of the substorm recovery phase.

16.6 Ambiguity of Plasmoid Timing

The fact that tail reconnection is no longer a single event at a single neutral line following a single onset of dayside reconnection makes it difficult to relate tail reconnection to the unitary event that is the onset of the auroral substorm. Earlier we deliberately arrayed the results of plasmoid timing studies, each of which reached a definite conclusion, but which taken together did not lead to a consistent view. Our purpose was not to adjudicate experimental technique, but to suggest that substorm onset and plasmoid formation are not uniquely related. If this were true, we would get precisely the situation we have in the literature. Not all reconnection events could be placed close enough to earth to be associated with onset; we would not be faced with explaining how events in the tiny onset and initial dipolarization region close to earth are related to those in the huge plasmoid ejection region in the midtail; the delays between onset and events like plasmoid passage or plasma sheet thickening would vary from event to event in a confusing way. Near-earth reconnection has to be induced as part of the evolution of the near-earth cross-tail current sheet, which is influenced by fast-mode compressions and rarefactions radiated from the reconnecting and oscillating magnetopause. Reconnection occurring farther downtail may have more to do with the closure of other characteristic fields. Thus, there may different types of plasmoids; while we need to find and probably do find at least one plasmoid per substorm far downtail, they do not all have to be generated near the earth at the time of onset.

---

the magnetic field decreases on the one-minute time scale just before it increases again as dipolarization starts. In the initial dipolarization, the magnetic field changes substantially in a few seconds; Fourier decomposition would yield considerable power in the Pi 1 frequency band. Although there is good correspondence between Pi 1 micropulsations and substorm expansions observed on the ground, not much is known about the relationship between the details of the initial dipolarization and the auroral onset. The dipolarization is accompanied by the dispersionless injections of tens-to-hundreds of keV protons and electrons. The electrons and protons drift eastward and westward, respectively, and are observed as energy-dispersed injections away from their points of injection. Original drawing.

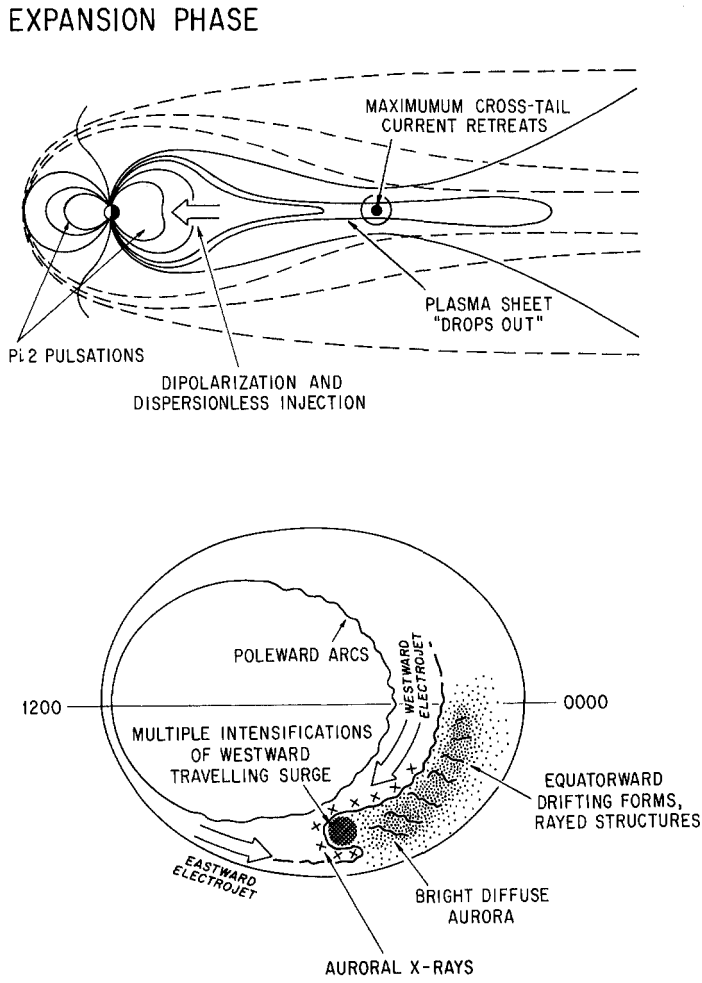

Figure 16.4. Substorm Expansion Phase. Following onset, a westward traveling surge with important subintensifications on the 1–2 minute time-scale develops on or slightly poleward of the onset arc. The region of bright aurora—the so-called auroral bulge—expands poleward, westward, and eastward for the next few tens of minutes. The bulge of auroral light often stops expanding at its eastward edge near local midnight. The X-ray arc has been found poleward of the auroral bulge. The westward extremity of the expanding auroral bulge is marked by the westward-traveling surge, a localized region of intense aurora and upward field-aligned current. From time to time the surge has been observed to stall, in other words, to halt its westward advance temporarily.

After onset, the initial dipolarization organizes itself into an expanding current wedge consisting of field-aligned currents into the ionosphere to the morning side and out into the evening side of the central meridian of the substorm. The currents move slowly eastward and westward, respectively. The field dipolarizes over a ten-minute period after the dipolarization "front" passes over the spacecraft. "Ahead" of the front, the magnetic field continues to become more tail-like until the dipolarization

There are a few incontrovertible observations of plasmoids and/or fast flows escaping from a source in or near the geostationary region shortly after substorm onset. These have been cited as candidates for the near-earth reconnection model. The examples we discussed and others like them (see McPherron, 1991) are of great interest because they are rare. Surveys of high-speed flows and of plasmoids indicate that both tailward-propagating flows and plasmoids are relatively infrequent within 30 R_E, while substorms are an everyday occurrence; Hughes and Kivelson (1989), for example, estimated there are six substorms per day on average (see Moldwin and Hughes, 1992b). The absence of a one to one relationship between substorms and observations of near-earth reconnection leads us to ask what the special circumstances are when near- earth reconnection is observed. Does the plasma sheet thin to undetectability in all but a few substorms while still reconnecting and accelerating particles, or is near-earth reconnection not associated with every substorm?

16.7 Substorms with Two Active Phases

The tradition division of the substorm into growth phase, expansion phase, and recovery phase implies there might be two distinct phases in which magnetospheric energy is dissipated in the ionosphere. Research has shown that the auroral onset initiates the expansion phase, and a "recovery" of the plasma sheet initiates the recovery phase. We associate these with dipolarization and tail reconnection, respectively. Cowley (1992) and Kozelova (1992) noted that substorm dissipation may be a two-stage process since dipolarization and tail reconnection ordinarily take place at different distances downtail.

Global inversion of data from a worldwide network of 77 ground magnetometer stations indicates that the substorm has two active phases (Mishin et al., 1992a,b; Opgenoorth et al., 1992; Saifudinova et al., 1992). Twenty-four stations of the network were above 70 degrees geomagnetic latitude, so that the equatorward and poleward electrojets could be monitored simultaneously. This is a crucial factor, since many other studies could not follow the full evolution of the poleward electrojet with adequate spatial coverage. Mishin et al. (1992a,b) associated the first active phase with the expansion of the current wedge and major injections of energetic particles into the ring current. A study of 15 substorms revealed that energy continued to be fed into the tail from the solar wind during the

arrives. Dispersionless injections always accompany the front as it propagates azimuthally. The leading edges of the current wedge resemble slowly propagating shocks with a trailing oscillatory electric and magnetic field structure—the source of Pi 2 pulsations detected world-wide. Miniature dispersionless injections accompany each oscillation of the magnetic field. On one occasion the oscillations could be related to small westward surges at the footpoint of the field line. The plasma sheet downstream of the geosynchronous region often thins during the substorm expansion phase, and the spacecraft finds itself in the tail lobes. Original drawing.

first active phase. The second phase, in which the electrojet was activated over a wide range of local times, was when the energy accumulated in the geomagnetic tail was dissipated, presumably via production of one or more plasmoids. In applying their magnetogram inversion technique to the March 22, 1979 CDAW 6 substorm (McPherron and Manka, 1985), Mishin et al. (1992a) concluded that the 1054–1118 UT interval after onset, when ISEE 1 and 2 observed tailward flow, corresponded to the first active phase, whereas the interval after 1118 UT, which was initiated by a plasma sheet recovery and enhanced the activity at the poleward border of the nightside oval, corresponded to the second active phase.

The two active phases could be triggered in different ways by different solar wind perturbations. The first active phase, dipolarization, is the one triggered by compressions of the magnetopause due to interplanetary shocks. The oscillations of the cross-tail and magnetopause current system might induce pseudoexpansions of the first kind before onset and multiple substorm intensifications of the first kind after onset. Mishin et al. (1992a) suggested that an active phase of the second kind is triggered by northward shifts of the interplanetary field. Sudden rarefactions of the solar wind pressure are observed not to trigger expansions of the first kind, probably because they reduce the magnetopause cross-tail current; similarly, since a northward shift induces the dayside magnetopause to migrate outward, it tends to relax the cross-tail current system, so that a dipolarization might not be so easily triggered. On the other hand, northward shifts lead to the decrease of energy stored in the tail lobes, which is what defines the second active phase in the magnetogram inversions.

16.8 Plasma Sheet Recovery, Plasmoid Formation, and Activation of the Poleward Arcs

The plasma sheet just beyond the geosynchronous region often "drops out" around the time of substorm onset. Hones (1976, 1979) proposed that the dropout is a signature of Y-type asymmetric reconnection earthward of the spacecraft. In this picture, a plasmoid is formed in a reconnection event at substorm onset and soon escapes downtail; the plasma sheet remains thin after the plasmoid has passed, so that the spacecraft is unable to detect the energy dissipated in any ongoing reconnection taking place nearer the earth; eventually, the near-earth neutral line retreats past the spacecraft, the plasma sheet recovers, and the substorm recovers. However, plasmoids are found escaping from the substorm initiation site only rarely. To account for plasma sheet recovery, symmetric reconnection need only start downtail of the observing spacecraft after substorm onset, in the second active phase of the substorm. If the reconnection process reaches open field lines, the energetic beams of an activated plasma sheet boundary layer expand over the spacecraft as open flux is consumed. Just as the boundary layer expands over ISEE 3 preceding the tailward passage of plasmoids, so could it pass over ISEE 1 and 2 preceding an earthward fast flow. In this case, the plasma sheet recovery is the signature of symmetric reconnection downtail.

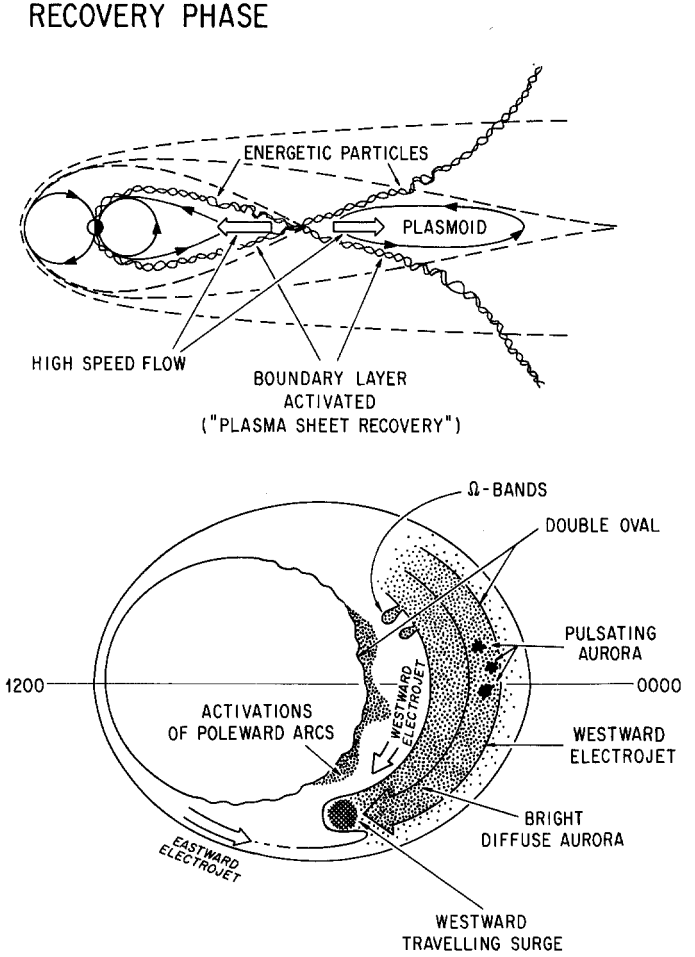

Figure 16.5. Substorm Recovery Phase. The substorm expansion phase ends when the auroral bulge achieves its maximum poleward extent. Very often, the arc marking the poleward border of auroral light in the midnight sector, sometimes called the poleward traversing arc, brightens across several hours of local time about the time the auroral bulge begins to subside, occasionally even before. The auroral bulge usually does not approach the poleward traversing arc, but it does sometimes. During the substorm recovery phase, as the area of the auroral bulge decreases and the brightness of the aurora in it diminishes, the auroral oval observed from above may appear to have a double structure: a bright poleward arc system with multiple localized spiral-like activations is separated by a dark lane from the declining auroral bulge. Some of the activations may be accompanied by Pi 2 pulsation bursts. After this, there seems to be no unique way in which the substorm ends. Poleward and equatorward auroral activity may both fade away, a new onset may occur while the poleward arc is still bright, a polar cap arc may grow out of the poleward traversing arc (presumably signifying a northward shift of the interplanetary field), and there are probably other possibilities.

From the fact that plasma sheet recoveries occur around the beginning of the recovery phase of the auroral substorm, we infer that plasmoid ejection typically occurs after onset. Since plasmoid ejection is due to reconnection of previously open field lines, it should stimulate activity at the poleward border of the auroral oval. Indeed, plasma sheet recoveries have been related to the brightening of the poleward arc. This arc's rapid, simultaneous to 1-minute localized intensifications and fadings extending over hours of local time seem like imprints of complex reconnection events in the deep tail. (They certainly contrast dramatically with the localized onset and contiguous growth of the auroral bulge.) When a double oval forms, it is evidence that tail reconnection is occurring tailward of the region that maps into the auroral bulge. What, then, of those substorms where near-earth reconnection does occur? Could these be the events in which the auroral bulge reaches and interacts with the poleward arc system?

There is no striking signature of the recovery phase in the geosynchronous region. Spacecraft in the postgeosynchronous region often detect no clear signature of reconnection until the recovery phase, when the plasma sheet boundary layer re-expands, most likely because of reconnection and plasmoid production further downstream. The expansion of the plasma sheet boundary layer has on occasion been associated with the brightening of poleward aurora. Original drawing.

17

EPILOGUE

The reader who has endured to the end, and even the one who skips to the end to see why he should read what is in the middle, deserves an answer to certain questions. Why, for example, did we employ a writing style so at odds with prevailing standards of scientific exposition? Of what use is it to read so much "anecdotal science"? Why, most of all, why did we place such a light emphasis upon theory, or for that matter, quantitative experimental results? The reader need only look as far as the comparison between the rates of transport due to viscosity and reconnection for an answer. These estimates were made with "back-of-the-envelope accuracy" in the 1960s, they are still made the same way on the eve of the twenty-first century, and we still do not know how the two systems of convection interact when they are time dependent. Magnetospheric physics, despite thirty-five years of the most intense, world wide activity, is still in the stage of paradigm clarification. It is, contrary to what one hears in many quarters, not a mature subject at all.

There had been such optimism when the space age opened. A few rocket flights, a few spacecraft, and we thought we would know, really know, what the earth's space environment was like. And in a sense, we learned, we really did learn. Standing out there in the solar wind was a bow shock and a magnetosphere of convecting plasma connecting to highly time-variable auroral displays. These first broad brush strokes of the picture were created by a confident, mid-twentieth-century command technology, and it seemed that only a few more strokes would fill the canvas. Yet as time passed, the pattern seemed no clearer than it had at the beginning. It turned out that we were painting our picture as a pointillist would, each spacecraft, each ground experiment a single dot. Seurat, as he painted, had a clear idea of the picture he wanted to create, but we had to wait for our picture to emerge, one dot a time, dots of one color at a time.

What emerged? Certainly not a single, splashy pattern, but one of delicate yet controlling complexity—a problem for twenty-firxt-century physics to solve. The complexity did not manifestly violate the convection and substorm paradigms, yet our paradigms were not sufficiently articulated to comprehend the experimentalists' full experience, leaving them somewhat at sea, even about fundamentals. Theory seemed to be of little help; the conceptual content of modern plasma physics is still too attenuated to deal with the complexity of plasma behavior except by the most laborious and "brute-force" means. (Anyone who

doubts this, please note the similar histories of fusion and space plasma physics.) And numerical simulations and modeling are not yet really helping; they still cannot deal globally with the small space and time scales that seem increasingly to be central to our observational experience. There are rumblings from the direction of the renewed discipline of nonlinear science that new guiding concepts may be on the way, but the outriders only now are beginning to arrive. Already has nonlinear science by its example taught us not to be afraid of complexity, that simplicity lies therein, that the essence of the matter may be found by dealing with it headon.

The author, who has endured thus far, has earned the opportunity to ask a few questions of his readers. Are we, are you, properly organized to meet the challenge of twenty-first-century magnetospheric physics? Problems in nonlinear science are information-hungry; can we, will you collect enough? How much is enough, anyway? Must we continue to paint in the pointillist style?

REFERENCES

Aarons, J., J. P. Mullen, and H. E. Whitney, The scintillation boundary, *J. Geophys. Res., 74,* 884, 1969.

Aggson, T. L., P. J. Gambardella, and N. C. Maynard, Electric field measurements at the magnetopause, 1, Observation of large convective velocities at rotational magnetopause discontinuities, *J. Geophys. Res., 88,* 10000, 1983.

Ahn, B.-H, S.-I. Akasofu, Y. Kamide, and J. H. King, Cross-polar cap potential drop and the energy coupling function, *J. Geophys. Res., 89,* 11028, 1984.

Ahn, G.-H., Y. Kamide, S.-I. Akasofu, and C.-I. Meng, Convection patterns in the polar ionosphere for northward IMF inferred from ground-based magnetometer data, *J. Geomagn. Geoelectr., 39,* 313, 1987.

Ahn, B.-H., Y. Kamide, H. W. Kroehl, and D. J. Gorney, Cross-polar cap potential difference, auroral electrojet indices, and solar wind parameters, *J. Geophys. Res., 97,* 1345, 1992.

Akasofu, S.-I., The development of the auroral substorm, *Planet. Space Sci., 12,* 273, 1964.

Akasofu, S.-I., *Polar and Magnetospheric Substorms,* D. Reidel, Dordrecht, Holland, 1968.

Akasofu, S.-I., A study of auroral displays photographed from the DMSP-2 satellite and from the Alaska meridian chain of stations, *Space Sci. Rev., 16,* 617, 1974.

Akasofu, S.-I., Recent progress in studies of DMSP auroral photographs, *Space Sci. Rev., 19,* 169, 1976.

Akasofu, S.-I., *Physics of Magnetospheric Substorms*, D. Reidel, Hingham, MA, 1977.

Akasofu, S.-I., What is a magnetospheric substorm? p. 447 in *Dynamics of the Magnetosphere,* edited by S.-I. Akasofu, D. Reidel, Dordrecht-Holland, 1979.

Akasofu, S.-I., Energy coupling between the solar wind and the magnetosphere, *Space Sci. Revs., 28,* 121, 1981a.

Akasofu, S.-I., Auroral arcs and potential auroral structure, in *Physics of Auroral Arc Formation,* Geophysical Monograph 26, edited by S.-I. Akasofu and J. R. Kan, p. 1, American Geophysical Union, Washington, DC, 1981b.

Akasofu, S.-I., A magnetospheric storm with a nearly constant input rate for about 24 hours, *Planet. Space Sci., 33,* 81, 1985a.

Akasofu, S.-I., The polar caps, *Memoirs of the National Institute of Polar Research, # 38, Energetics and Dynamics of the Middle and Upper Atmosphere at High Southern Latitudes,* 1985b.

Akasofu, S.-I., D. S. Kimball, and C.-I Meng, Dynamics of the aurora, II, Westward travelling surges, *J. Atmos. Terr. Phys., 27,* 173, 1965.

Akasofu, S.-I., D. S. Kimball, and C.-I Meng, Dynamics of the aurora, IV, *J. Atmos, Terr. Phys., 28,* 489, 1966a.

Akasofu, S.-I., D. S. Kimball, and C.-I Meng, Dynamics of the aurora, V, Poleward motions, *J. Atmos, Terr. Phys., 28,* 497, 1966b.

Akasofu, S.-I., D. S. Kimball, and C.-I Meng, Dynamics of the aurora, VII, Equatorward motion and the multiplicity or auroral arcs, *J. Atmos. Terr. Phys., 28,* 627, 1966c.

Akasofu, S.-I., C. R. Wilson, A. L. Snyder, and P. D. Perrault, Results from a meridian chain of observations in the Alaska sector, 1, *Planet Space. Sci., 19,* 497, 1971.

Akasofu, S.-I., and S. Chapman, *Solar-Terrestrial Physics,* Clarendon Press, Oxford, England, 1972.

Akasofu, S.-I, P. D. Perrault, F. Yasuhara, and C.-I. Meng, Auroral substorms and the interplanetary magnetic field, *J. Geophys. Res., 78,* 7490, 1973a.

Akasofu, S.-I., E. W. Hones, Jr., S. J. Bame, J. R. Asbridge, and A. T. Y. Lui, Magnetotail and boundary layer plasma at geocentric distance of 18 RE: Vela 5 and 6 observations, *J. Geophys. Res., 78,* 7257, 1973b.

Akasofu, S.-I., S. deForest, and C. McIlwain, Auroral displays near the "foot" of the field line of the ATS-5 satellite, *Planet. Space Sci., 22,* 25, 1974.

Akasofu. S.-I, and B. T. Tsurutani, Unusual auroral features observed on January 10–11, 1983 and their possible relationships to the interplanetary magnetic field, *Geophys. Res. Letts., 11,* 1086, 1984.

Akasofu, S.-I., T. Iijima, B.-H. Ahn, D. Weimer, and Y. Kamide, Excellent agreements between ground-based and satellite-based observations, *Planet. Space. Sci., 38,* 1533, 1990.

Albert, R. D., Energy and flux variations of nearly monoenergetic auroral electrons, *J. Geophys. Res., 72,* 5811, 1967.

Alcayde, D., G. Caudal, and J. Fontanari, Convection electric fields and electrostatic potential over $61° < \Lambda < 72°$ invariant latitude observed with the European incoherent scatter facility, 1, Initial results, *J. Geophys. Res., 91,* 233, 1986.

Alexander, J. K., and M. L. Kaiser, Terrestrial kilomtric radiation, 1, Spatial structure studies, *J. Geophys. Res., 81,* 5948, 1976.

Alfven, H., *Cosmical Electrodynamics,* Oxford University Press, Oxford, 1950.

Alksne, A. Y., The steady-state magnetic field in the transition region between the magnetosphere and the bow wave, *Planet. Space Sci., 15,* 239, 1967.

Alksne, A. Y., and D. L. Webster, Magnetic and electric fields in the magnetosheath, *Planet. Space Sci., 18,* 1203, 1970.

Allan, W., E. M. Poulter, and E. Nielsen, Pc5 pulsations associated with ring current proton drifts: STARE radar observations, *Planet. Space Sci., 31,* 1279, 1983.

Allan, W., E. M. Poulter, K.-H. Glassmeier, and H. Junginger, Spatial and temporal structure of a highlatitude ULF pulsation, *Planet. Space Sci., 33,* 159, 1985.

Allan, W., S. P. White, and E. M. Poulter, Impulse-excited hydromagnetic cavity and field-line resonances in the magnetosphere, *Planet. Space Sci., 34,* 371, 1986a.

Allan, W., E. M. Poulter, and S. P. White, Hydromagnetic wave coupling in the magnetosphere–plasmapause effects on impulse-excited resonances, *Planet. Space Sci., 34,* 1189, 1986b.

Anderson, B. J., M. J. Engebretson, and L. J. Zanetti, Distortion effects in spacecraft observations of MHD toriodal standing waves: Theory and observation, *J. Geophys. Res., 94,* 13425, 1989.

Anderson, B. J., M. J. Engebretsen, S. P. Rounds, L. J. Zanetti, and T. A. Potemra, A statistical study of Pc 3–5 pulsations observed by the AMPTE/CCE magnetic fields experiment, 1, Occurrence distributions, *J. Geophys. Res., 95,* 10495, 1990.

Anderson, B. J., T. A. Potemra, L. J. Zanetti, and M. J. Engebretson, Statistical correlation between Pc 3–5 pulsations and solar wind/IMF parameters and geomagnetic indices, in *Physics of Space Plasmas, SPI Conf. Proc. Reprint Ser.,* Vol. 10, p. 419, edited by T. Chang, G. B. Crew, and J. R. Jasperse, Scientific, Cambridge, MA, 1991.

Anderson, K. A., Energetic electron fluxes in the tail of the geomagnetic field, *J. Geophys. Res., 70,* 4741, 1965.

Anderson, K. A., Method to determine send and magnitude of electric field from lunar particle shadows, *J. Geophys. Res., 75,* 2591, 1970.

Anderson, K. A., H. K. Harris, and R. P. Paoli, Energetic electron fluxes in and beyond the earth's outer magnetosphere, *J. Geophys. Res., 70,* 1039, 1965.

Anderson, K. A., and R. P. Lin, Observations of interplanetary field lines in the magnetotail, *J. Geophys. Res., 74,* 3953, 1969.

Andrews, M. K., P. W. Daly, and E. Keppler, Ion jetting at the plasma sheet boundary: simultaneous observations of incident and reflected particles, *Geophys. Res. Lett., 8,* 987, 1981.

Angelopoulos, V., R. C. Elphic, S. P. Gary, and C. Y. Huang, Electromagnetic instabilities in the plasma sheet boundary layer, *J. Geophys. Res., 94,* 15373, 1989.

Angelopoulos, V., W. Baumjohann, C. F. Kennel, F. V. Coroniti, M. G. Kivelson, R. Pellat, R. J. Walker, H. Luhr, and G. Paschmann, Bursty bulk flows in the inner central plasma sheet, *J. Geophys. Res., 97,* 4027, 1992a.

Angelopoulos, V., W. Baumjohann, C. F. Kennel, F. V. Coroniti, M. G. Kivelson, R. Pellat, R. J. Walker, H. Luhr, and G. Paschmann, Bursty bulk flows in the inner central plasma sheet: an efficient means of plasma sheet

transport, *Proceedings First International Conference on Substorms,* edited by B. Hultquist, March 23–28, 1992b, Kiruna, Sweden.

Anger, C. D., A. T. Y. Lui, and S.-I. Akasofu, Observations of the auroral oval and westward traveling surge from ISIS 2 and Alaska meridian all-sky cameras, *J. Geophys. Res., 78,* 3020, 1973.

Annexstad, J. O., and C. R. Wilson, Characteristics of Pg micropulsations at conjugate points, *J. Geophys. Res., 73,* 1805, 1968.

Armstrong, T. P., and S. M. Krimigis, Observations of protons in the magnetopshere and magnetotail with Explorer 33, *J. Geophys. Res., 73,* 143, 1968.

Arnoldy, R. L., Signature in the interplanetary medium for substorms, *J. Geophys. Res., 76,* 5189, 1971.

Arnoldy, R. L., K. Dragoon, L. J. Cahill, Jr., S. B. Mende, and T. J. Rosenberg, Detailed correlations of magnetic field and riometer absorption at l = 4, *J. Geophys. Res., 87,* 10449, 1982.

Arnoldy, R. L., and T. E. Moore, The longitudinal structure of substorm injections at synchronous orbit, *J. Geophys. Res., 88,* 6213, 1983.

Arnoldy, R. L., L. J. Cahill, Jr., M. J. Engebretsen, L. J. Lanzerotti, and A. Wolfe, Review of hydromagnetic wave studies in the Antarctic, *Revs. Geophys. 28,* 181, 1988a.

Arnoldy, R. L., M. J. Engebretsen, and L. J. Cahill, Jr., Bursts of Pc 1–2 near the ionospheric footprint of the cusp and their relation to flux transfer events, *J. Geophys. Res., 93,* 1007, 1988b.

Ashour-Abdalla, M., J. Berchem, J. Buchner, and L. Zelenyi, Chaotic acceleration of ions in the earth's magnetotail: mode, *Geophys. Res. Lett., 17,* 2317, 1990.

Ashour-Abdalla, M., J. Buchner, and L. Zelenyi, The quasiadiabatic ion distribution in the central plasma sheet and its boundary layer, submitted, *J. Geophys. Res., 96,* 1601, 1991.

Atkinson, G., and T. Watanabe, Surface waves on the magnetospheric boundary as a possible orogin of long period geomagnetic micropulsations, *Earth Planet. Sci. Letts., 1,* 89, 1966.

Aubry, M. P., C. T. Russell, and M. G. Kivelson, On inward motion of the magnetopause before a substorm, *J. Geophys. Res., 75,* 7018, 1970.

Aubry, M. P., M. G. Kivelson, and C. T. Russell, Motion and structure of the magnetopause, *J. Geophys. Res., 76,* 1673, 1971.

Aubry, M. P., M. G. Kivelson, R. L. McPherron, and C. T. Russell, Outer magnetosphere near midnight at quiet and disturbed times, *J. Geophys. Res., 77,* 5487, 1972.

Axford, W. I., The interaction between the solar wind and the earth's magnetosphere, *J. Geophys. Res., 67,* 3791, 1962.

Axford, W. I., Viscous interaction between the solar wind and the earth's magnetosphere, *Planet. Space. Sci., 12,* 45, 1964.

Axford, W. I., The polar wind and the terrestrial helium budget, *J. Geophys. Res., 73,* 6855, 1968.

Axford, W. I., Magnetospheric convection, *Revs. Geophys., 7,* 421, 1969.

Axford, W. I., and C. O. Hines, A unifying theory of high-latitude geophysical phenomena and geomagnetic storms, *Can. J. Phys., 39,* 1433, 1961.

Axford, W. I., H. E. Petschek, and G. L. Siscoe, Tail of the magnetosphere, *J. Geophys. Res., 70,* 1231, 1965.

Bahnsen, A., J. Mogns, E. Ungstrup, and I. B. Iverson, Auroral hiss and kilometric radiation measured from the Viking satellite, *Geophys. Res. Lett., 14,* 471, 1987.

Bahnsen, A., B. M. Pedersen, M. Jespersen, E. Ungstrup, L. Eliasson, J. S. Murphree, R. D. Elphinstone, L. Blomberg, G. Holmgren, and L. J. Zanetti, Viking observations at the source region of auroral kilometric radiation, *J. Geophys. Res., 94,* 6643, 1989.

Baker, D. N., Particle and field signatures of substorms in the near magnetotail, in *Magnetic Reconnection in Space and Laboratory Plasmas,* edited by E. W. Hones, Jr., p. 193, AGU, Washington, DC, 1984.

Baker, D. N., and E. C. Stone, Energetic electron anisotropies in the magnetotail: identification of open and closed field lines, *Geophys. Res. Lett., 3,* 557, 1976.

Baker, D. N., and E. C. Stone, Observations of energetic electrons (> 200 keV) in the earth's magnetotail: Plasma sheet and fireball observations, *J. Geophys. Res., 82,* 1532, 1977.

Baker, D. N., P. R. Higbie, E. W. Hones, Jr., and R. D. Belian, High-resolution energetic particle measurements at 6.6 Re 3. Low-energy electron anisotropies and short-term substorm predictions, *J. Geophys. Res., 83,* 4863, 1978.

Baker, D. N., P. R. Higbie, and R. D. Belian, Multispacecraft observations of energetic electron flux pulsations at 6.6 Re, *J. Geophys. Res., 85,* 6709, 1980.

Baker, D. N., E. W. Hones, Jr., P. R. Higbie, R. D. Belian, and P. Stauning, Global properties of the magnetosphere during a substorm growth phase: a case study, *J. Geophys. Res., 86,* 8941, 1981a.

Baker, D. N., P. Stauning, E. W. Hones, Jr., P. R. Higbie, and R. D. Belian, Near-equatorial, high-resolution measurements of electron precipitation at L = 6.6, *J. Geophys. Res., 86,* 2295, 1981b.

Baker, D. N., T. A. Fritz, D. T. Young, and J. Birn, The possible role of ionospheric oxygen in the initiation and development of plasma sheet instabilities, *Geophys. Res. Lett., 9,* 1337, 1982.

Baker, D. N., R. D. Zwickl, S. J. Bame, E. W. Hones, Jr., B. T. Tsurutani, E. J. Smith, and S.-I. Akasofu, An ISEE 3 high time resolution study of interplanetary parameter correlations with magnetospheric activity, *J. Geophys. Res., 88,* 6230, 1983.

Baker, D. N., and Fritz, T. A., Hot plasma and energetic particles within the earth's magnetosphere: new understanding during the IMS, *Proc. Conf. Achievements IMS,* ESA, SP-217, 85, 1984.

Baker, D. N., S. J. Bame, J. Birn, W. C. Feldman, J. T. Gosling, E. W. Hones, Jr., R. D. Zwickl, J. A. Slavin, E. J. Smith, B. T. Tsurutani, and D. G. Sibeck, Direct observations of passages of the distant neutral line (80–140 Re) following substorm onsets: ISEE-3, *Geophys. Res. Lett., 11,* 1042, 1984a.

Baker, D. N., S. J. Bame, R. D. Belian, W. C. Feldman, J. T. Gosling, P. R. Higbie, E. W. Hones, Jr., D. J. McComas, and R. D. Zwickl, Correlated dynamical changes in the near-earth and distant magnetotail regions: ISEE 3, *J. Geophys. Res., 89,* 3855, 1984b.

Baker, D. N., T. A. Fritz, R. L. McPherron, D. H. Fairfield, Y. Kamide, and W. Baumjohann, Magnetotail energy storage and release during the CDAW-6 substorm analysis intervals, *J. Geophys. Res., 90,* 1205, 1985a.

Baker, D. N., T. A. Fritz, W. Lennartsson, B. Wilken, and H. W. Kroehl, The role of heavy ionospheric ions in the localization of substorm disturbances on March 22, 1979: CDAW 6, *J. Geophys. Res., 90,* 1273, 1985b.

Baker, D. N., L. F. Bargatze, and R. D. Zwickl, Magnetospheric response to the IMF: substorms, *J. Geomag. Geoelectr., 38,* 1047, 1986a.

Baker, D. N., S. J. Bame, W. C. Feldman, J. T. Gosling, R. D. Zwickl, J. A. Slavin, and E. J. Smith, Strong electron bidirectional anisotropies in the distant tail: ISEE 3 observations of polar rain, *J. Geophys. Res., 91,* 5637, 1986b.

Baker, D. N., R. C. Anderson, R. D. Zwickl, and J. A. Slavin, Average plasma and magnetic field variations in the distant magnetotail associated with near-earth substorm effects, *J. Geophys. Res., 92,* 71, 1987a.

Baker, D. N., S. J. Bames, J. T. Gosling, and M. S. Gussenhoven, Observations of polar rain at low and high altitudes, *J. Geophys. Res., 92,* 13547, 1987b.

Baker, D. N., S. J. Bame, W. C. Feldman, J. T. Gosling, R. D. Zwickl, J. A. Slavin, and E. J. Smith, Bidirectional anisotropies in the distant tail: ISEE 3 observations of polar rain, p. 47, in *Magnetotail Physics,* edited by A. T. Y. Lui, Johns Hopkins University Press, Baltimore, 1987c.

Baker, D. N., S. J. Bames, J. T. Gosling, and M. S. Gussenhoven, Plasma electrons as tracers of distant magnetotail structure: ISEE 3, *Adv. Space. Res., 8,* 179, 1988.

Baker, D. N., D. H. Fairfield, J. A. Slavin, I. G. Richardson, J. D. Craven, L. A. Frank, R. C. Elphic, H. J. Singer, C. J. Owen, and R. D. Zwickl, The substorm event of 28 January, 1983: a detailed global study, *Planet Space Sci., 38,* 1495, 1990a.

Baker, D. N., A. J. Klimas, R. L. McPherron, and J. Buchner, The evolution from weak to strong geomagnetic activity: an interpretation in terms of deterministic chaos, *Geophys. Res. Letts., 17,* 41, 1990b.

Baker, D. N., A. J. Klimas, and D. A. Roberts, Examination of time-variable effects in a nonlinear analogue magnetospheric model, *J. Geophys. Res., 18,* 1631, 1991.

Baker, D. N., D. H. Fairfield, J. A. Slavin, I. G. Richardson, C. J. Owen, J. D. Craven, L. A. Frank, R. C. Elphic, H. J. Singer, and R. D. Zwickl, Correction to "The substorm event of 28 January, 1983: A detailed global study", by D. N. Baker, et al., *Planet. Space Sci., 40,* 589, 1992.

Baker, K. B., and Y. Kamide, A comparison of ionospheric electric fields inferred from Scandinavian twin auroral radar experiment drift data and from global international magnetospheric study magnetometer data, *J. Geophys. Res., 90,* 1339, 1985.

Baker, K. B., R. A. Greenwald, A. D. M. Walker, P. F. Bythrow, L. J. Zanetti, T. A. Potemra, D. A. Hardy, F. J. Rich, and C. L. Rino, A case study of plasma processes in the dayside cleft, *J. Geophys. Res., 91,* 3130, 1986.

Balsiger, H., P. Eberhart, J. Geiss, and D. T. Young, Magnetic storm injection of 0. 9- and 16-keV/e solar and terrestrial ions into the high-altitude magnetosphere, *J. Geophys. Res., 85,* 1645, 1980.

Balsiger, H., J. Geiss, and D. T. Young, The composition of thermal and hot ions observed by the GEOS-1 and -2 spacecraft, p. 195 in *Energetic Ion Composition in the Earth's Magnetosphere,* edited by R. G. Johnson, Terra Scientific Publishing Co. (TERRAPUB), Tokyo, 1983.

Bame, S., R. C. Anderson, J. R. Asbridge, D. N. Baker, W. C. Feldman, J. T. Gosling, E. W. Hones, Jr., D. J. McComas, and R. D. Zwickl, Plasma regions in the deep magnetotail: ISEE-3, *Geophys. Res. Letts., 10,* 912, 1983.

Banks, P. M., and T. E. Holzer, The polar wind, *J. Geophys. Res., 73,* 6486, 1968.

Banks, P. M., and T. E. Holzer, Features of plasma transport in the upper atmosphere, *J. Geophys. Res., 74,* 6304, 1969a.

Banks, P. M., and T. E. Holzer, High latitude plasma transport: the polar wind, *J. Geophys. Res., 74,* 6319, 1969b.

Banks, P. M., J. R. Doupnik, and S.-I. Akasofu, Electric field observations by incoherent scatter radar in the auroral zone, *J. Geophys. Res., 78,* 6607, 1973.

Banks, P. M., C. R. Chappell, and A. F. Nagy, A new model for the interaction of auroral electrons with the atmosphere: spectral degradation, backscatter, optical, *J. Geophys. Res., 79,* 1459, 1974.

Banks, P. M., and J. R. Doupnik, A review of auroral zone electrodynamics deduced from incoherent scatter radar observations, *J. Atmos. Terr. Phys., 37,* 951, 1975.

Banks, P. M., and T. E. Holzer, The polar wind, *J. Geophys. Res., 73,* 6846, 1986.

Barcus, J. R., and T. J. Rosenberg, Observations on the spatial structure of pulsating electron precipitation accompanying low frequency hydromagnetic disturbances in the auroral zone, *J. Geophys. Res., 70,* 1707, 1965.

Barfield, J. N., and R. L. McPherron, Statistical characteristics of storm-time associated Pc 5 micropulsations observed at the synchronous equatorial orbit, *J. Geophys. Res., 77,* 4720, 1972.

Barfield, J. N., and R. L. McPherron, Stormtime Pc 5 magnetic pulsations observed at synchronous orbit and the correlation with the partial ring current, *J. Geophys. Res., 83,* 739, 1978.

Barfield, J. N., R. L. McPherron, P. J. Coleman, Jr., and D. J. Southwood, Storm-associated Pc 5 micropulsation events observed at the synchronous equatorial orbit, *J. Geophys. Res., 77,* 143, 1972.

Barfield, J. N., C. S. Lin, and R. L. McPherron, Observations of magnetic field perturbations at GOES 2 and GOES 3 during the March 22, 1979 substorms: CDAW 6 analysis, *J. Geophys. Res., 90,* 1289, 1985.

Bargatze, L. F., D. N. Baker, R. L. McPherron, and E. W. Hones, Jr., Magnetospheric impulse response for many levels of geomagnetic activity, *J. Geophys. Res., 90,* 6387, 1985.

Basinska, E. M., W. J. Burke, S. Basu, F. J. Rich, and P. F. Fougere, Low-frequency modulation of plasmas and soft electron precipitation near the dayside cusp, *J. Geophys. Res., 92,* 3304, 1987.

Basinska, E. M., W. J. Burke, N. C. Maynard, W. J. Hughes, J. D. Winningham, and W. B. Hanson, Small-scale electrodynamics of the cusp with northward interplanetary magnetic field, *J. Geophys. Res., 97,* 6369, 1992.

Basu, Su., Basu, S., E. MacKenzie, P. F. Fougere, W. R. Coley, N. C. Maynard, J. D. Winningham, M. Sugiura, W. B. Hanson, and W. R. Hoegy, Simultaneous density and electric field fluctuation spectra associated with velocity shears in the auroral oval, *J. Geophys. Res., 93,* 115, 1988.

Baumjohann, W., Ionospheric and field-aligned current systems in the auroral zone: a concise review, *Adv. Space Res., 2,* 55, 1983.

Baumjohann, W., Some recent progress in substorm studies, *J. Geomag. Geoelectr., 38,* 633, 1986.

Baumjohann, W., J. Untiedt, and R. A. Greenwald, Joint two-dimensional observations of ground magnetic and ionospheric electric fields associated with auroral zone currents, 1, Three-dimensional current flows associated with a substorm-intensified eastward electrojet, *J. Geophys. Res., 85,* 1963, 1980.

Baumjohann, W., J. Pellinen, H. J. Opgenoorth, and E. Nielsen, Joint two-dimensional observations of ground magnetic and ionospheric electric fields associated with auroral zone currents: current systems associated with local auroral breakups, *Planet. Space Sci., 29,* 431, 1981.

Baumjohann, W., O. H. Bauer, G. Haerendel, H. Junginger, and E. Amata, Magnetospheric plasma drifts during a sudden impulse, *J. Geophys. Res., 88,* 9287, 1983.

Baumjohann, W., H. Junginger, G. Haerendel, and O. H. Bauer, Resonant Alfven waves excited by a sudden impulse, *J. Geophys. Res., 89,* 2765, 1984a.

Baumjohann, W., and K.-H. Glassmeier, The transient response mechanism and Pi2 pulsations at substorm onset-Review and outlook, *Planet. Space Sci., 32,* 1361, 1984b.

Baumjohann, W., and G. Haerendel, Magnetospheric convection observed between 0600 and 2100 LT: solar wind and IMF dependence, *J. Geophys. Res., 90,* 6370, 1985.

Baumjohann, W., and K.-H. Glassmeier, The transient response mechanism and Pi 2 pulsations at substorm onset–review and outlook, *Planet. Space Sci., 34,* 1189, 1986.

Baumjohann, W. G., Paschmann, N. Sckopke, C. A. Cattell, and C. W. Carlson, Average ion moments in the plasma sheet boundary layer, *J. Geophys. Res., 93,* 11507, 1988.

Baumjohann, W., G. Paschmann, and C. A. Cattell, Average plasma properties in the central plasma sheet, *J. Geophys. Res., 94,* 6597, 1989.

Baumjohann, W., G. Paschmann, and H. Luhr, Characteristics of high-speed ion flows in the plasma sheet, *J. Geophys. Res., 95,* 3801, 1990.

Beard, D. B., The interaction of the terrestrial magnetic field with the solar corpuscular radiation, *J. Geophys. Res., 65,* 3559, 1960.

Beard, D. B., The interaction of the terrestrial magnetic field with the solar corpuscular radiation, II, Second order approximation, *J. Geophys. Res., 67,* 4771, 1962.

Behannon, K. W., Mapping of the earth's bow shock and magnetic tail by Explorer 33, *J. Geophys. Res., 73,* 907, 1968.

Behannon, K. W., Geometry of geomagnetic tail, *J. Geophys. Res., 75,* 743, 1970.

Belian, R. D., T. E. Cayton, and G. D. Reeves, Quasi-periodic, global flux variations observed at geosynchronous orbit, p. 165 in *Substorms 1: Proc. Int'l. Conf. Substorms (ICS-1), ESA SP-335,* European Space Agency, Paris, 1992.

Belon, A. E., J. E. Maggs, T. N. Davis, K. B. Mather, N. W. Glass, and G. F. Hughes, Conjugacy of visual aurora during magnetically quiet periods, *J. Geophys. Res., 74,* 1, 1969.

Benson, R. F., and W. Calvert, ISIS 1 observations at the source of the auroral kilometric radiation, *Geophys. Res. Lett., 6,* 479, 1979.

Benson, R. F., and S.-I Akasofu, Auroral kilometric radiation/aurora correlation, *Radio Sci., 19,* 527, 1984.

Benson, R. F., W. Calvert, and D. M. Klumpar, Simultaneous wave and particle observations in the auroral kilometric radiation source rgion, *Geophys. Res. Lett., 7,* 959, 1980.

Berchem, J., and C. T. Russell, The thickness of the magnetopause current layer: ISEE 1 and 2 observations, *J. Geophys. Res., 87,* 2108, 1982.

Berchem, J., and C. T. Russell, Flux transfer events at the magnetopause: spatial distribution and controlling factors, *J. Geophys. Res., 89,* 6689, 1984.

Berkey, F. T., L. L. Cogger, S. Ismail, and Y. Kamide, Evidence for a correlation between sun-aligned arcs and the interplanetary magnetic field direction, *Geophys. Res. Lett., 3,* 145, 1976.

Berko, F. W., R. A. Hoffmann, R. K. Burton, and R. E. Holzer, Simultaneous particle and field observations of field-aligned currents, *J. Geophys. Res., 80,* 3746, 1975.

Berthelier, J.-J., C. Machard, J.-C. Cerisier, A. Berthelier, and J.-M. Bosqued, ULF electromagnetic turbulence in the high latitude ionosphere, *J. Geophys. Res., 93,* 5701, 1988.

Bieber, J. W., E. C. Stone, E. W. Hones, D. N. Baker, and S. J. Bame, Plasma behavior during energetic electron streaming events: Further evidence for substorm-associated magnetic reconnection, *Geophys. Res. Lett., 9,* 664, 1982.

Bieber, J. W., E. C. Stone, E. W. Hones, Jr., D. N. Baker, S. J. Bame, and R. P. Lepping, Microstructure of magnetic reconnection in the earth's magnetotail, *J. Geophys. Res., 89,* 6705, 1984.

Biermann, L., Kometenschweife and solare korpuscular-strahlung, *Z. Astrophys., 29,* 274, 1951.

Biermann, L., Physical processes in comet tails and their relation to solar activity, *Mon. Not. Roy. Soc. Liege,* Quatr. Ser., *13,* 291, 1953.

Biermann, L., Solar corpuscular radiation and the interplanetary gas, *Observatory, 77,* 109, 1957.

Biernat, H. K., M. F. Heyn, and V. S. Semenov, Unsteady Petschek reconnection, *J. Geophys. Res., 92,* 3392, 1987.

Biernat, H. K., M. F. Heyn, R. P. Rijnbeek, V. S. Semenov, and C. J. Farrugia, The structure of reconnection layers: applications to the earth's magnetopause, *J. Geophys. Res., 94,* 287, 1989.

Birkeland, K., Sur les rayons cathodiques sous l'action de forces magnetiques intenses, *Arch. Sci. Phys. Naturelles, 1,* 497, 1896.

Birkeland, K., Expedition Norvegienne de 1899–1900 pour l'etude des aurores boreales, resultants des recherches magnetiques, *Skr. Nor. Vidensk. Akad. Kl. 1, Mat. Naturvidensk Kl., 1,* 7, 1901.

Birkeland, K., On the cause of magnetic storms and the origin of terrestrial magnetism, *Norwegian Aurora Polaris Expedition, 1902–3,* Vol. 1, 1st and 2nd sections, H. Aschehoug and Co., Christiania, 1908.

Birn, J., Computer studies of the dynamic evolution of the geomagnetic tail, *J. Geophys. Res., 85,* 1214, 1980.

Birn, J., and E. W. Hones, Jr., Three-dimensional computer modeling of dynamic reconnection in the geomagnetic tail, *J. Geophys. Res., 86,* 6802, 1981.

Birn, J., and K. Schindler, Self-consistent theory of three-dimensional convection in the geomagnetic tail, *J. Geophys. Res., 88,* 6969, 1983.

Birn, J., T. G. Forbes, E. W. Hones, Jr., and S. J. Bame, On the velocity distribution of ion jets during substorm recovery, *J. Geophys. Res., 86,* 9001, 1981.

Birn, J., G. Yur, H. U. Rahman, and S. Minami, On the termination of the closed field line region of the magnetotail, *J. Geophys. Res., 97,* 14833, 1992.

Bol'shakova, O. V., and V. A. Troitskaya, The relation of the high-latitude maximum of Pc 3 intensity to the dayside cusp, *Geomag. Aeron., 24,* 633, 1984.

Bond, F. R., Auroral morphological similarities at two magnetically conjugate stations, *Aust. J. Physics., 22,* 421, 1969.

Borovsky, J. E., D. M. Suszcynsky, M. I. Buchwald, and H. V. DeHaven, Measuring the thicknesses of auroral curtains, *Arctic, 44,* 231, 1991.

Borovsky, J. E., Auroral arc thicknesses as predicted by various theories, *J. Geophys. Res., 98,* 6101, 1993.

Bosinger, T., K. Alanko, J. Kangas, H. Opgenoorth, and W. Baumjohann, Correlations between PiB type magnetic micropulsations, auroras, and equivalent current structures during two isolated substorms, *J. Atm. Terr. Phys., 43,* 933, 1981.

Bosinger, T., and A. G. Yahnin, Pi1B type magnetic pulsations as a high time resolution monitor of substorm development, *Ann. Geophys., 5A,* 231, 1987.

Bosqued, J. M., AUREOL-3 results on ion precipitation, *Phys. Scr., 18,* 158, 1987.

Bosqued, J. M., A. Berthelier, J. J. Berthelier, and C. P. Escoubet, A case study of the cusp electrodynamics by the Aureol-3 satellite: Evidence for FTE signatures, *Geophys. Res. Lett., 18,* 1833, 1991.

Bostrom, R., Ionosphere–magnetosphere coupling, p. 45, in *Magnetospheric Physics,* edited by B. M. McCormac, D. Reidel, Dordrecht, Holland, 1974.

Brecht, S. H., J. G. Lyon, J. A. Fedder, and K. Hain, A time-dependent three-dimensional simulation of the earth's magnetosphere:Reconnection events, *J. Geophys. Res., 87,* 6098, 1982.

Brice, N. M., Bulk motion, *J. Geophys. Res., 72,* 5192, 1967.

Bridge, H., A. Egidi, A. Lazarus, E. Lyon, and L. Jacobsen, Preliminary results of plasma measurements on IMP A, *Space Res., 5,* 969, 1965.

Broun, J. A., On certain results of magnetical observations, *Philos. Magazine, 16,* 81, 1858.

Brown, J. W., and E. C. Stone, High-energy electron spikes at high latitudes, *J. Geophys. Res., 77,* 3384, 1972.

Bruning, K., and C. K. Goertz, Influence of the electron source distribution on field-aligned currents, *Geophys. Res. Lett., 12,* 53, 1985.

Bryant, D. A., and S. Riggs, At the edge of the earth's magnetosphere: a survey by APMTE-UKS, *Phils. Trans. Roy. Soc. London A, Ser. 328,* 43, 1989.

Buchau, J., B. W. Reinisch, E. J. Weber, and J. G. Moore, Structure and dynamics of the winter polar cap F region, *Radio Sci., 18,* 995, 1983.

Buchner, J., and L. M. Zelenyi, Deterministic chaos in the dynamics of charged particles near a magnetic field reversal, *Phys. Lett. A., 118,* 395, 1986.

Buchner, J., and L. M. Zelenyi, Chaotization of electron motion as the cause of internal magnetotail instability and substorm onset, *J. Geophys. Res., 92,* 13456, 1987.

Buchner, J., and L. M. Zelenyi, Regular and chaotic charged particle motion in magnetotaillike field reversals. 1. Basic theory of trapped motion, *J. Geophys. Res., 94,* 11821, 1989.

Buck, R. M., H. I. West, Jr., and R. G. D'Arcy, Satellite studies of magnetospheric substorms on August 15, 1968, 7: Ogo 5 energetic proton observations–spatial boundaries, *J. Geophys. Res., 78,* 3103, 1973.

Burch, J. L., Low-energy elctron fluxes at latitudes above the auroral zone, *J. Geophys. Res., 73,* 3585, 1968.

Burch, J. L., Preconditions for the triggering of polar magnetic substorms by storm sudden commencements, *J. Geophys. Res., 77,* 5629, 1972a.

Burch, J. L., Precipitation of low-energy electrons at high latitudes: effects of interplanetary magnetic field and dipole tilt angle, *J. Geophys. Res., 77,* 6696, 1972b.

Burch, J. L., Rate of erosion of dayside magnetic flux based on a quantitative study of the dependence of polar cusp latitude on the interplanetary magnetic field, *Radio Sci., 8,* 955, 1973.

Burch, J. L., Effects of the interplanetary magnetic field on the auroral oval and plasmapause, *Space Sci. Rev., 23,* 449, 1979.

Burch, J. L., Dynamics explorer observations of auroral particle acceleration phenomena, in *Auroral Physics,* edited by C.-I. Meng, M. J. Rycroft, and L. A. Frank, Cambridge University Press, Cambridge UK, 1991.

Burch, J. L., S. A. Fields, and R. A. Heelis, Polar cap electron acceleration regions, *J. Geophys. Res., 84,* 5863, 1979.

Burch, J. L., P. H. Reiff, R. A. Heelis, R. W. Spiro, and S. A. Fields, Cusp region particle precipitation and ion convection for northward interplanetary field, *Geophys. Res. Lett., 7,* 393, 1980.

Burch, J. L., P. H. Reiff, and M. Sugiura, Upward electron beams measured by DE-1: a primary source of dayside region 1 Birkeland currents, *Geophys. Res. Lett., 10,* 753, 1983.

Burch, J. L., J. D. Menietti, and J. N. Barfield, DE-1 observations of solar wind–magnetosphere coupling processes in the polar cusp, in *Solar Wind–Magnetosphere Coupling,* edited by Y. Kamide and J. A. Slavin, p. 441, Terra Scientific, Tokyo, 1986.

Burke, W. J., Electric fields, Birkeland currents, and electron precipitation in the vicinity of discrete auroral arcs, in *Physics of the Auroral Arc Formation, Geophysical Monograph Ser.,* Vol. 25, edited by S.-I. Akasofu and J. R. Kan, pp. 164–172, 1981.

Burke, W. J., M. C. Kelley, R. C. Sagalyn, M. Smiddy, and S. T. Lai, Polar cap electric field structures with northward interplanetary magnetic field, *Geophys. Res. Lett., 6,* 21, 1979.

Burke, W. J., M. S. Gussenhoven, M. C. Kelley, D. A. Hardy, and F. J. Rich, Electric and magnetic field characteristics of discrete arcs in the polar cap, *J. Geophys. Res., 87,* 2431, 1982.

Burke, W. J., M. Silevitch, and D. A. Hardy, Observation of small-scale auroral vortices by the S3-2 satellite, *J. Geophys. Res., 88,* 3127, 1983.

Burlaga, L. F., and K. W. Ogilvie, Causes of sudden commencements and sudden impulses, *J. Geophys. Res., 74,* 2815, 1969.

Burns, G. B., D. J. McEwen, R. A. Eather, F. T. Berkey, and J. S. Murphree, Optical auroral conjugacy, Viking uv imager–south pole station ground data, *J. Geophys. Res., 95,* 5781, 1990.

Burrows, J. R., T. J. Hughes, and M. D. Wilson, A study of high latitude current systems during quiet geomagnetic conditions using Magsat data, ip. 104, in *Magnetospheric Currents,* edited by T. A. Potemra, *Geophysical Monograph Ser. 28,* American Geophysical Union, Washington, DC, 1984.

Burton, R. K., R. L. McPherron, and C. T. Russell, The terrestrial magnetosphere: a half-wave rectifier of the interplanetary electric field, *Science, 189,* 717, 1975a.

Burton, R. K., R. L. McPherron, and C. T. Russell, An empirical relationship between interplanetary conditions and Dst, *J. Geophys. Res., 80,* 4204, 1975b.

Bythrow, P. F., and T. A Potemra, Birkeland currents and energetic particles associated with optical auroral signatures at westward traveling surge, *J. Geophys. Res., 92,* 8691, 1987.

Bythrow, P. F., R. A. Heelis, W. B. Hanson, and R. A. Power, Simultaneous observations of field-aligned currents and plasm a drift velocities by Atmospheric Explorer C, *J. Geophys. Res., 85,* 151, 1980.

Bythrow, P. F., R. A. Heelis, W. B. Hanson, R. A. Power, and R. A. Hoffman, Observational evidence for a boundary layer source of dayside region 1 field aligned currents, *J. Geophys. Res., 86,* 5577, 1981.

Bythrow, P. F., T. A. Potemra, and L. J. Zanetti, Variat ion of the auroral Birkeland current pattern associated with the north–south component of the IMF, in *Magnetospheric Currents, Geophys. Monographs, 28,* p. 131, American Geophysical Union, Washington, DC, 1983.

Bythrow, P. F., W. J. Burke, T. A. Potemra, L. J. Zanetti, and A. T. Y. Lui, Ionospheric evidence for irregular reconnection and turbulent plasma flows in the magnetotail during periods of northward interplanetary magnetic field, *J. Geophys. Res., 90,* 5319, 1985.

Bythrow, P. F., T. A. Potemra, L. J. Zanetti, R. A. Erlandson, D. A. Hardy, F. J. Rich, and M. H. Acuna, High latitude currents in the 0600 to 0900 MLT sector: observations from Viking and DMPS F7, *Geophys. Res. Lett., 14,* 423, 1987.

Caan, M. N., Interplanetary magnetic field changes and the magnetotail, p. 63, in *Dynamics of the Magnetosphere,* edited by S.-I. Akasofu, D. Reidel, Hingham, MA, 1979.

Caan, M. N., R. L. McPherron, and C. T. Russell, Solar wind and substorm-related changes in the lobes of the magnetotail, *J. Geophys. Res., 78,* 8087, 1973.

Caan, M. N., R. L. McPherron, and C. T. Russell, Substorm and interplanetary magnetic field effects on the tail lobes, *J. Geophys. Res., 80,* 191, 1975.

Caan, M. N., R. L. McPherron, and C. T. Russell, Characteristics of the association between the interplanetary magnetic field and the substorm, *J. Geophys. Res., 82,* 4837, 1977.

Cahill, L. J., Jr., and P. G. Amazeen, The boundary of the geomagnetic field, *J. Geophys. Res., 68,* 1835, 1963.

Cahill, L. J., Jr., and V. L. Patel, The boundary of the geomagnetic field, August to November, 1961, *Planet. Space Sci., 15,* 997, 1967.

Cahill, L. J., Jr., and T. L. Skillman, The magnetopause at 5.2 RE on August 4, 1972; magnetopause motion, *J. Geophys. Res., 82,* 1566, 1977.

Cahill, L. J., Jr., and J. R. Winckler, Periodic magnetopause oscillations observed with the GOES satellites on March 24, 1991, *J. Geophys. Res., 97,* 8239, 1992.

Calvert, W., The signature of auroral kilometric radiation on ISIS 1, *J. Geophys. Res., 86,* 76, 1981.

Calvert, W., DE 1 measurements of AKR wave directions, *Geophys. Res. Lett., 12,* 381, 1985.

Carbary, J. F., and S. M. Krimigis, Energetic particle activity at 5-min and 10-s time resolution in the magnetotail and its relation to auroral activity, *J. Geophys. Res., 84,* 7123, 1979.

Carbary, J. F., and C.-I. Meng, Relations between the interplanetary magnetic field Bz, AE index, and cusp latitude, *J. Geophys. Res., 91,* 1549, 1986.

Carlson, H. C., Dynamics of the quiet polar cap, *J. Geomagn. Geoelect., 42,* 697, 1990.

Carlson, H. C., V. B. Wickwar, E. J. Weber, J. Buchau, J. G. Moore, and W. Whiting, Plasma characteristics of polar cap F-layer arcs, *Geophys. Res. Lett., 11,* 895, 1984.

Carlson, H. C., R. A. Heelis, E. J. Weber, and J. R. Sharber, Coherent mesoscale convection patterns during northward interplanetary field, *J. Geophys. Res., 93,* 14501, 1988.

Carpenter, D. L., Whistler studies of the plasma-pause in the magnetosphere, 1., Temporal variations in the position of the knee and some evidence of plasma motions near the knee, *J. Geophys. Res., 71,* 693, 1966.

Carrington, R., Description of a singular appearance seen in the sun of September 1, 1859, *Mon. Not. Roy. Astron. Soc., 20,* 13, 1860.

Casserly, R. T., Jr., and P. A. Cloutier, Rocket-based magnetic observations of auroral Birkeland currents in association with a structured auroral arc, *J. Geophys. Res., 80,* 2165, 1975.

Cattell, C. A., S3-3 satellite instrumentation and data, *The IMS Source Book,* p. 91, American Geophysical Union, Washington, DC, 1982.

Cattell, C. A., Association of field-aligned currents with small scale auroral phenomena, in, *Magnetospheric Currents,* edited by T. A. Potemra, American Geophysical Union, Washington, DC, 1983.

Cattell, C. A., and R. C. Elphic, Comment, *Geophys. Res. Lett., 14,* 773, 1987.

Cattell, C. A., R. L. Lysak, R. B. Torbert, and F. S. Mozer, Observations of differences between regions of current flowing into and out of the ionosphere, *Geophys. Res. Lett., 6,* 621, 1979.

Cattell, C. A., M. Kim, R. P. Lin, and F. S. Mozer, Observations of large electric fields near the plasma sheet boundary by ISEE 1, *Geophys. Res. Lett., 9,* 539, 1982.

Cauffman D. P., and D. A. Gurnett, Satellite measurements of high latitude convection electric fields, *Space Sci. Rev., 13,* 369, 1972.

Celsius, A., Bemerkungen uber der magnetnadel stundliche veranderungen in ihrer abweichung, *Svensk Vet. Acad. Handl.,* 296, 1740.

Chandler, M. O., J. H. Waite, Jr., and T. E. Moore, Observations of polar ion outflows, *J. Geophys. Res., 96,* 1421, 1991.

Chao, J. K., and R. P. Lepping, A correlative study of ssc's, interplanetary shocks, and solar activity, *J. Geophys. Res., 79,* 1799, 1974.

Chapman, S., The energy of magnetic storms, *Monthly Not. Roy. Astron. Soc., 79,* 70, 1918.

Chapman, S., An outline of a theory of magnetic storms, *Proc. Roy. Soc. London, A95,* 61, 1919.

Chapman, S., The motion of a neutral ionised stream in the earth's magnetic field, *Proc. Camb. Phil. Soc., 21,* 577, 1923.

Chapman, S., Foreword, p. xv, in *The Solar Wind,* edited by R. J. Mackin, Jr., and M. Neugebauer, Pergamon Press, Oxford, 1966.

Chapman, S., History of aurora and airglow, p. 15 in *Aurora and Airglow,* edited by B. M. MacCormac, Reinhold Publishing Co., 1967

Chapman, S., and V. C. A. Ferraro, A new theory of magnetic storms, *Nature, 126,* 129, 1930.

Chapman, S., and V. C. A. Ferraro, A new theory of magnetic storms, *Terr. Magn. and Atmos. Electr., 36,* 171, 1931a.

Chapman, S., and V. C. A. Ferraro, A new theory of magnetic storms, *J. Geophys. Res., 36,* 77, 1931b.

Chapman, S., and V. C. A. Ferraro, A new theory of magnetic storms, *J. Geophys. Res., 36,* 171, 1931c.

Chapman. S., and V. C. A. Ferraro, A new theory of magnetic storms, *Terr. Magn. and Atmos. Electr., 38,* 79, 1933.

Chapman, S., and J. Bartels, *Geomagnetism,* Oxford University Press, N. Y., 1940.

Chapman, S., and P. C. Kendall, Liquid instability and energy transformation near a magnetic neutral line: a soluble nonlinear hydromagnetic problem, *Proc. Roy. Soc. A, 271,* 435, 1963.

Chappell, C. R., T. E. Moore, and J. H. Waite, Jr., The ionosphere as a fully adequate source of plasma for the earth's magnetosphere, *J. Geophys. Res., 92,* 5896, 1987.

Chen, L., and A. Hasegawa, A theory of long-period magnetic pulsations, 1, Steady state excitation of field line resonance, *J. Geophys. Res., 79,* 1024, 1974a.

Chen, L., and A. Hasegawa, A theory of long-period magnetic pulsations, 2, Impulse excitation of surface eigenmode, *J. Geophys. Res., 79,* 1033, 1974b.

Chen, J., and P. J. Palmadesso, Chaos and nonlinear dynamics of single-particle orbits in magnetotail-like magnetic field, *J. Geophys. Res., 91,* 1499, 1986.

Chen, S.-H., and M. G. Kivelson, On ultralow frequency waves in the lobes of the earth's magnetotail, *J. Geophys. Res., 96,* 15711, 1991.

Chiu, Y. T., and J. M. Cornwall, Electrostatic model of a quiet auroral arc, *J. Geophys. Res., 85,* 543, 1980.

Chiu, Y. T., A. L. Newman, and J. M. Cornwall, On the structure and mapping of auroral electrostatic potentials, *J. Geophys. Res., 86,* 10029, 1981.

Chmyrev, V. M., V. N. Oraevsky, S. V. Bilichenko, N. V. Isaev, G. A. Stanev, D. K. Teodosiev, and S. I. Shkolnikova, The fine structure of intensive small-scale electric and magnetic fields in the high-latitude ionosphere as observed by Intercosmos-Bulgaria 1300 satellite, *Planet. Space Sci., 33,* 1383, 1985.

Choe, J. Y., D. B. Beard, and E. C. Sullivan, Precise calculation of the magnetosphere surface for a tilted dipole, *Planet. Space Sci., 21,* 485, 1973.

Christon, S. P., D. G. Mitchell, D. J. Williams, L. A. Frank, C. Y. Huang, and T. E. Eastman, Energy spectra of plasma sheet ions and electrons from 50 eV/e to 1 MeV during plasma temperature transitions, *J. Geophys. Res., 93,* 2562, 1988.

Chu, C. K., and Y. M. Lynn, Steady magnetohydrodynamic flow past a non-conducting wedge, *AIAA Journal, 1,* 1062, 1962.

Cladis, J. B., Parallel acceleration and transport of ions from polar ionosphere to plasma sheet, *Geophys. Res. Lett., 13,* 893, 1986.

Clark, D. H., and W. J. Raitt, The global morphology of irregularities in the topside ionosphere as measured by the total ion current probe on ESRO-4, *Planet. Space Sci., 24,* 873, 1976.

Clauer, C. R., and R. L. McPherron, Mapping the local-universal time development of magnetospheric substorms using mid-latitude magnetic observatories, *J. Geophys. Res., 79,* 2811, 1974.

Clauer, C. R., R. L. McPherron, C. Searls, and M. G. Kivelson, Solar wind control of auroral zone geomagnetic activity, *Geophys. Res. Lett., 8,* 915, 1981.

Clauer, C. R., and Y. Kamide, DP 1 and DP 2 current systems for the March 22, 1979 substorms, *J. Geophys. Res., 90,* 1343, 1985.

Clauer, C. R., and E. Friis-Christensen, High-latitude dayside electric fields and currents during strong northward interplanetary magnetic field: observations and model simulations, *J. Geophys. Res., 93,* 2749, 1988.

Cogger, L. L., and R. D. Elphinstone, The *Viking* auroral substorm, submitted, *Proc. First Int'l. Conf. Substorm,* edited by B. Hultquist, R. Lundin, and J. Woch, ESA, 1992.

Cogger, L. L., J. S. Murphree, S. Ismail, and C. D. Anger, Characterstics of dayside 5577 A and 3914 A aurora, *Geophys. Res. Lett., 4,* 413, 1977.

Cole, K. D., R. J. Morris, E. T. Matveeva, V. A. Troitskaya, and O. A. Pokhetelov, The relationship of the boundary layer of the magnetosphere to IPRP events, *Planet. Space Sci., 30,* 129, 1982.

Coleman, P. J., Jr., and R. L. McPherron, Substorm observations of magnetic perturbations and ULF waves at synchronous orbit by ATS-1 and ATS-6, p. 345, in *The Scientific Satellite Programme during the International Magnetospheric Study,* edited by K. Knott and B. Battrick, D. Reidel, Hingham, Mass., 1976.

Coley, W. R., R. A. Heelis, W. B. Hansen, P. H. Reiff, J. R. Sharber, and J. D. Winningham, Ionospheric convection signatures and magnetic field topology, *J. Geophys. Res., 92,* 12352, 1987.

Collin, H. L., R. D. Sharp, E. G. Shelley, and R. G. Johnson, Some general characteristics of upflowing ion beams over the auroral zone and their relation to auroral electrons, *J. Geophys. Res., 86,* 6820, 1981.

Coppi, B., G. Laval, and R. Pellat, A model for the influence of the earth magnetic tail on geomagnetic phenomena, *Phys. Rev. Lett., 16,* 1207, 1966.

Coroniti, F. V., On the tearing mode in quasi-neutral sheets, *J. Geophys. Res., 85,* 6719, 1980.

Coroniti, F. V., Space plasma turbulent dissipation:myth or reality? *Space Sci. Rev., 42,* 399, 1985a.

Coroniti, F. V., Explosive tail reconnection: the growth and expansion phases of magnetospheric substorms, *J. Geophys. Res., 90,* 7427, 1985b.

Coroniti, F. V., Introductory remarks made to the Alaska Workshop on Substorms, Fairbanks, AK, Sept. 18–21, 1991.

Coroniti, F. V., and C. F. Kennel, Changes in magnetospheric configuration during substorm growth phase, *J. Geophys. Res., 77,* 3361, 1972a.

Coroniti, F. V., and C. F. Kennel, Magnetospheric substorms, in *Cosmic Plasma Physics,* edited by K. Schindler, p. 15, Plenum, New York, 1972b.

Coroniti, F. V., and C. F. Kennel, Polarization of the auroral electrojet, *J. Geophys. Res., 77,* 2835, 1972c.

Coroniti, F. V., and C. F. Kennel, Can the ionosphere regulate magnetospheric convection?, *J. Geophys. Res., 78,* 2837, 1973.

Coroniti, F. V., and A. Eviatar, Magnetic field reconnection in a collisionless plasma, *Astrophys. J. Suppl. Ser., 33,* 189, 1977.

Coroniti, F. V., L. A. Frank, R. P. Lepping, F. L. Scarf, and K. L. Ackerson, Plasma flow pulsations in earth's magnetic tail, *J. Geophys. Res., 83,* 2162, 1978.

Coroniti, F. V., and C. F. Kennel, Magnetospheric reconnection, substorms, and energetic particle acceleration, p. 169 in *Particle Acceleration in Planetary Magnetospheres,* edited by J. Arons, C. Max, and C. McKee, American Institute of Physics, New York, 1979.

Coroniti, F. V., L. A. Frank, D. J. Williams, R. P. Lepping, F. L. Scarf, S. M. Krimigis, and G. Gloeckler, Variability of plasma sheet dynamics, *J. Geophys. Res., 85,* 2957, 1980.

Cortie, A. L., Sunspots and terrestrial magnetic phenomena, 1898–1911, *Mon. Not. Roy. Astron. Soc., 73,* 52, 1912.

Cowley, S. W. H., A qualitative study of the reconnection between the earth's magnetic field and an interplanetary magnetic field of arbitrary orientation, *Radio Sci., 8,* 903, 1973.

Cowley, S. W. H., The effect of pressure anisotropy on the equilibrium structure of magnetic neutral sheets, *Planet. Space Sci., 26,* 1037, 1978.

Cowley, S. W. H., Plasma populations in a simple open model magnetosphere, *Space Sci. Rev., 26,* 217, 1980.

Cowley, S. W. H., The causes of convection in the earth's magnetosphere: a review of the developments during the IMS, *Rev. Geophys., 20,* 531, 1982.

Cowley, S. W. H., Solar wind control of magnetospheric convection, in *Achievements of the IMS, ESA SP-217,* p. 483, ESTEC, Nooordwijk, The Netherlands, 1984.

Cowley, S. W. H., The role and location of magnetic reconnection in the geomagnetic tail during substorms, p. 401 in in *Substorms 1: Proc. Int'l Conf. Substorms (ICS-1), ESA SP-335,* European Space Agency, Paris, 1992.

Cowley, S. W. H., and D. J. Southwood, Some properties of a steady state geomagnetic tail, *Geophys. Res. Lett., 7,* 833, 1980.

Cowley, S. W. H., R. J. Hynds, I. G. Richardson, P. W. Daly, T. R. Sanderson, K.-P Wenzel, J. A. Slavin, and B. T. Tsurutani, Energetic ion regimes in the deep geomagnetic tail: ISEE 3, *Geophys. Res. Lett., 11,* 275, 1984.

Cowley, S. W. H., J. P. Morelli, M. P. Freeman, M. Lockwood, and M. F. Smith, Excitation and decay of flows in the magnetosphere–ionosphere system due to magnetic reconnection at the dayside magnetopause and in the geomagnetic tail, p. 117 in *Substorms 1: Proc. Int'l Conf. Substorms (ICS-1), ESA SP-335,* European Space Agency, Paris, 1992.

Craven, J. D., and L. A. Frank, The temporal evolution of a small auroral substorm as viewed from high altitudes with Dynamics Explorer 1, *Geophys. Res. Lett., 12,* 465, 1985.

Craven, J. D., and L. A. Frank, Latitudinal motions of the aurora during substorms, *J. Geophys. Res., 92,* 4565, 1987.

Craven, J. D., and L. A. Frank, Diagnosis of auroral dynamics using global auroral imaging with emphasis on large-scale evolution, p. 273 in *Auroral Physics,* edited by C.-I Meng, M. J. Rycroft, and L. A. Frank, Cambridge University Press, Cambridge, UK, 1991.

Craven, J. D., Y. Kamide, L. A. Frank, S.-I Akasofu, and M. Sugiura, Distribution of aurora and ionospheric currents observed simultaneously on a global scale, in *Magnetospheric Currents, Geophysical Monograph 28,* p. 137, American Geophysical Union, Washington, DC, 1983.

Crooker, N. U., Explorer 33 entry layer observations, *J. Geophys. Res., 82,* 515, 1977.

Crooker, N. U., Dayside merging and cusp geometry, *J. Geophys. Res., 84,* 1979.

Crooker, N. U., and G. L. Siscoe, Birkeland currents as the cause of the low-latitude asymmetric disturbance field, *J. Geophys. Res., 86,* 11201, 1981.

Crooker, N. U., and G. L. Siscoe, On mapping flux transfer events to the ionosphere, *J. Geophys. Res., 95,* 3795, 1990.

Crooker, N. U., and W. J. Burke, The cusp/cleft, *Revs. Geophysics (suppl.), U. S. National Report to the International Union of Geodesy and Geophysics, 1987–90,* p. 1017, 1991.

Crooker, N. U., G. L. Siscoe, and R. B. Geller, Persistent pressure anisotropy in the subsonic magnetosheath region, *Geophys. Res. Lett., 3,* 65, 1976.

Crooker, N. U., and G. L. Siscoe, A mechanism for pressure anisotropy and mirror instability in the dayside magnetosheath, *J. Geophys. Res., 82,* 185, 1977.

Crooker, N. U., T. E. Eastman, and G. S. Stiles, Observations of plasma depletion in the magnetosheath at the magnetopause, *J. Geophys. Res., 84,* 869, 1979.

Crooker, N. U., G. L. Siscoe, P. R. Mullen, C. T. Russell, and E. J. Smith, Magnetic field compression on the dayside magnetosphere, *J. Geophys. Res., 87,* 10407, 1982.

Crooker, N. U., F. R. Toffoletto, and M. S. Gussenhoven, Opening the cusp, *J. Geophys. Res., 96,* 3497, 1991.

Crowley, G., W. J. Hughes, and T. B. Jones, Observational evidence of cavity modes in the earth's magnetosphere, *J. Geophys. Res., 92,* 12233, 1987.

Cummings, W. D., and P. J. Coleman, Jr., Magnetic fields in the magnetopause and vicinity at synchronous altitude, *J. Geophys. Res., 73,* 5699, 1968.

Cummings, W. D., J. N. Barfield, and P. J. Coleman, Jr., Magnetospheric substorms observed at the synchronous orbit, *J. Geophys. Res., 73,* 6687, 1968.

Cummings, W. D., R. J. O'Sullivan, and P. J. Coleman, Jr., Standing Alfven waves in the magnetosphere, *J. Geophys. Res., 74,* 778, 1969.

Cummings, W. D., C. Countee, D. Lyons, and W. Wiley III, The dominant mode of standing Alfven waves at the synchronous orbit, *J. Geophys. Res., 80,* 3705, 1975.

Cummings, W. D., R. L. O'Sullivan, and P. J. Coleman, Jr., Measurements of the Poynting vector of standing hydromagnetic waves at synchronous orbit, *J. Geophys. Res., 83,* 697, 1978.

Daglis, I. A., G. Kremser, W. Studemann, B. Wilken, G. Gloeckler, D. C. Hamilton, and F. M. Ipavich, Observations of the ion distribution in the nightside magnetosphere during substorm-associated dropout events, *Adv. Space Res., 8,* 87, 1988.

Daglis, I. A., E. T. Sarris, and G. Kremser, Indications for ionospheric participation in the substorm processs from AMPTE/CCE observations, *Geophys. Res. Lett., 17,* 57, 1990.

Daglis, I. A., E. T. Sarris, and G. Kremser, Ionospheric contribution to the cross-tail current enhancement during the substorm growth phase, *J. Atm. Terr. Phys. (7th SCOSTEP Symposium Special Issue), 53,* 1091, 1991.

Daglis, I. A., E. T. Sarris, W. I. Axford, G. Kremser, B. Wilken, and G. Gloeckler, Statistical features of the substorm expansion-phase as observed by the AMPTE/CCE spacecraft, in *Magnetospheric Substorms,* Proc. Hakone Conf. Japan, AGU Monograph, edited by T. A. Potemra, J. R. Kan, S. Kokobun, and T. Iijima, 1992.

Daly, P. W., and E. Keppler, Observations of a flux transfer event on the earthward side of the magnetopause, *Planet. Space. Sci., 30,* 331, 1982.

Daly, P. W., and E. Keppler, Remote sensing of a flux transfer event with energetic particles, *J. Geophys. Res., 88,* 3971, 1983.

Daly, P. W., D. J. Williams, C. T. Russell, and E. Keppler, Particle signatures of magnetic flux transfer events at the magnetopause, *J. Geophys. Res., 86,* 1628, 1981.

Daly, P. W., M. A. Suunders, R. P. Rijnbeek, N. Sckopke, and C. T. Russell, The distribution of reconnection geometry in flux transfer events using energetic ion, plasma, and magnetic data, *J. Geophys. Res., 89,* 3843, 1984.

Dandouras, J., H. Reme, A. Saint-Marc, J. A. Sauvaud, G. K. Parks, K. A. Anderson, and R. P. Lin, A statistical study of plasma sheet dynamics using ISEE 1 and 2 energetic particle flux data, *J. Geophys. Res., 91,* 6861, 1986.

Davidson, G. T., Expected spatial distribution of low-energy protons precipitated in the auroral zones, *J. Geophys. Res., 70,* 1061, 1965.

Davis, T. N., The morphology of the auroral displays of 1957–58, 2. Detail analysis of Alaska data and analysis of high-latitude data, *J. Geophys. Res., 67,* 75, 1962.

Davis, T. N., and M. Sugiura, Auroral electrojet activity index AE and its universal times variations, *J. Geophys. Res., 71,* 785, 1966.

Davis, T. N., and T. J. Hallinan, Auroral spirals, 1, Observations, *J. Geophys. Res., 81,* 3953, 1976.

Davis, T. N., T. J. Hallinan, and H. C. Stenbaek-Nielson, Auroral conjugacy and time-dependent geometry of auroras, in *Radiating Atmosphere,* edited by B. M. McCormac, D. Reidel, Dordrecht, Holland, p. 160, 1971.

DeCoster, R. J., and L. A. Frank, Observations pertaining to the dynamics of the plasma sheet, *J. Geophys. Res., 84,* 5099, 1979.

de Feraudy, H., B. M. Pedersen, A. Bahnsen, and M. Jespersen, Viking observations of auroral kilometric radiation from the plasmasphere to night auroral oval source regions, *Geophys. Res. Lett., 14,* 511, 1987.

De Hoffman, F., and E. Teller, Magnetohydrodynamic shocks, *Phys. Rev., 80,* 692, 1950.

de la Beaujardiere, O., R. Vondrak, and M. Baron, Radar observations of electric fields and currents associated with auroral arcs, *J. Geophys. Res., 82,* 5051, 1977.

de la Beaujardiere, O., V. B. Wickwar, G. Caudal, J. M. Holt, J. D. Craven, L. A. Frank, L. H. Brace, D. S. Evans, J. D. Winningham, and R. A. Heelis, Universal time dependence of nighttime F region densities at high latitudes, *J. Geophys. Res., 90,* 4319, 1985.

de la Beaujardiere, O. D. Alcayde, J. Fontanari, and C. Leger, Seasonal dependence of the high-latitude electric fields, *J. Geophys. Res., 96,* 5723, 1991a.

de la Beaujardiere, O., L. R. Lyons, and E. Friis-Christensen, Sondrestrom radar measurements of the reconnection electric field, *J. Geophys. Res., 96,* 13907, 1991b.

de Mairan, J. J. d'O, *Traite physique and historique de l'aurore boreale,* Suite des mem. Acad. Roy. Sci., Editions 1 and 2, Paris, 1733, 1754.

Dessler, A. J., Solar wind interactions and the magnetosphere, p. 65, in *Physics of the Magnetosphere,* edited by R. L. Carovillano, D. Reidel Publishing Company, Dordrecht, Holland, 1968.

Dessler, A. J., Length of magnetospheric tail, *J. Geophys. Res., 69,* 3913, 1964.

Dessler, A. J., and E. N. Parker, Hydromagnetic theory of geomagnetic storms, *J. Geophys. Res., 64,* 2239, 1959.

Dessler, A. J., and F. C. Michel, Plasma in the geomagnetic tail, *J. Geophys. Res., 71,* 1421, 1966.

DeWitt, R. N., The occurrence of aurora in geomagnetically conjugate areas, *J. Geophys. Res., 67,* 1347, 1962.

Domingo, V. E., D. E. Page, and K.-P. Wenzel, Energetic electrons at the magnetopause, p. 159 in *Correlated Interplanetary and Magnetospheric Observations,* edited by D. E. Page, D. Reidel, Dordrecht, Holland, 1974.

Domingo, V. E., D. E. Page, and K.-P. Wenzel, Energetic and relativistic electrons near the polar magnetopause, *J. Geophys. Res., 82,* 2327, 1977.

Doyle, M. A., and W. J. Burke, S3-2 measurements of the polar cap potential, *J. Geophys. Res., 88,* 9125, 1983.

Dryer, M., and R. Faye-Peterson, Magnetogasdynamic boundary conditions for a self-consistent solution to the closed magnetopause, *AIAA J, 4,* 246, 1966.

Dryer, M., and G. R. Heckman, On the hypersonic analogue as applied to planetary interaction with the solar plasma, *Planet. Space Sci., 15,* 515, 1967.

Duncan, R. A., Some studies of geomagnetic micropulsations, *J. Geophys. Res., 66,* 2087, 1961.

Dunckel, N., B. Ficklin, L. Rorden, and R. A. Helliwell, Low-frequency noise observed in the distant magnetosphere with OGO 1, *J. Geophys. Res., 75,* 1854, 1970.

Dungey, J. W., Conditions for the occurrence of electrical discharges in astrophysical systems, *Phil. Mag., 44,* 725, 1953.

Dungey, J. W., Electrodynamics of the outer atmosphere, *Sci. Rep. 69,* Ionos. Res. Lab., Pennsylvania State University, University Park, Pa., 1954.

Dungey, J. W., Electrodynamics of the outer atmosphere, p. 229 in *The Physics of the Ionosphere,* 1954 Cambridge Conference, Physical Society, London, England, 1955.

Dungey, J. W., *Cosmic Electrodynamics,* p. 98, Cambridge University Press, New York, 1958.

Dungey, J. W., Interplanetary magnetic field and the auroral zones, *Phys. Rev. Lett., 6,* 47, 1961a.

Dungey, J. W., The steady state of the Chapman–Ferraro problem in two dimensions, *J. Geophys. Res., 66,* 1043, 1961b.

Dungey, J. W., The structure of the exosphere or adventures in velocity space, in *Geophysics, The Earth's Environment,* edited by C. DeWitt, J. Hieblot, and L. LeBeau, p. 503, Gordon and Breach, New York, 1963.

Dungey, J. W., The length of the magnetospheric tail, *J. Geophys. Res., 70,* 1753, 1965.

Dungey, J. W., Hydromagnetic waves, p. 913 in *Physics of Geomagnetic Phenomena,* edited by S. Matsushita and W. H. Campbell, Academic Press, San Diego, California, 1967.

Dyson, P. L., J. P. McClure, and W. B. Hanson, *In situ* measurements of the spectral characteristics of F region ionospheric irregularities, *J. Geophys. Res., 79,* 1497, 1974.

Eastman, T. E., The plasma boundary layer and magnetopause layer of the earth's magnetosphere, Ph.D. dissertation, *Rep. LA-7842,* Los Alamos National Laboratory, Los Alamos, NM, 1979.

Eastman, T. E., and E. W. Hones, Jr., Characteristics of the magnetospheric boundary layer and magnetopause layer as observed by IMP 6, *J. Geophys. Res., 84,* 2019, 1979.

Eastman, T. E., and L. A. Frank, Boundary layers of the Earth's outer magnetosphere, p. 249 in *Magnetic Reconnection in Space and Laboratory Plasmas, Geophys. Monogr. Ser. 30,* edited by E. W. Hones, Jr., American Geophysical Union, Washington, DC, 1984.

Eastman, T. E., E. W. Hones, Jr., S. J. Bame, and J. R. Asbridge, The magnetospheric boundary layer: site of plasma, momentum, and energy transfer from the magnetosheath into the magnetosphere, *Geophys. Res. Lett., 3,* 685, 1976.

Eastman, T. E., L. A. Frank, W. K. Peterson, and W. Lennartson, The plasma sheet boundary layer, *J. Geophys. Res., 89,* 1553, 1984.

Eastman, T. E., B. Popielawska, and L. A. Frank, Three-dimensional plasma observations near the outer magnetospheric boundary, *J. Geophys. Res., 90,* 9519, 1985a.

Eastman, T. E., L. A. Frank, and C. Y. Huang, The boundary layers as the primary transport regions of the earth's magnetotail, *J. Geophys. Res., 90,* 9541, 1985b.

Eastman, T. E., R. J. DeCoster, and L. A. Frank, Velocity distributions of ion beams in the plasma sheet boundary layer, in *Ion Acceleration in the Magnetosphere and Ionosphere, Geophys. Monographs, 38,* edited by T. S. Chang, p. 117, AGU, Washington, DC, 1986.

Eather, R. H., Latitudinal distributions of auroral and airglow emissions: the soft auroral zone, *J. Geophys. Res., 74,* 153, 1969.

Eather, R. H., and S. B. Mende, Airborne observations of of auroral precipitation patterns, *J. Geophys. Res., 76,* 1746, 1971.

Eather, R. H., S. B. Mende, and R. J. R. Judge, Plasma injection at synchronous orbit and spatial and temporal auroral morphology, *J. Geophys. Res., 81,* 2805, 1976.

Egidi, A., V. Formisano, F. Palmiotto, P. Saraceno, and G. Moreno, Solar wind and location of shock front and magnetopause at the 1969 solar maximum, *J. Geophys. Res., 75,* 6999, 1970.

Ejiri, M., A. Kadokura, and T. Oguti, Small-scale auroral dynamics associated with a substorm development observed by the ATV-VIS imager onboard EXOS-D (AKEBONO), p. 457 in *Proc. First Int. Conf. Substorms,* edited by B. Hultquist, R. Lundin, and J. Woch, European Space Agency *SP-335,* 1992.

Eliasson, L., R. Lundin, and J. S. Murphree, Polar cap arcs observed by the *Viking* satellite, *Geophys. Res. Lett., 14,* 451, 1987.

Ellis, P., and D. J. Southwood, Reflection of Alfven waves by non-uniform ionosphere, *Planet. Space Sci., 31,* 107, 1983.

Elphic, R. C., and C. T. Russell, ISEE 1 and 2 magnetometer observations of the magnetopause, p. 43 in *Magnetospheric Boundary Layers,* edited by B. Battrick, Rep. *ESA Sp-148* European Space Agency, Paris, 1979.

Elphic, R. C., C. A. Cattell, K. Takahashi, S. J. Bame, and C. T. Russell, ISEE-1 and 2 observations of magnetic flux ropes in the magnetotail: FTE's in the plasma sheet?, *Geophys. Res. Lett., 13,* 648, 1985.

Elphinstone, R. D., and D. J. Hearn, Mapping of the auroral distribution during quiet times and substorm recovery phase, p. 13 in *Substorms 1, Proc. International Conf. on Substorms (ICS-1),* ESA SP-335, European Space Agency, Paris, 1992.

Elphinstone, R. D., D. Hearn, J. S. Murphree, and L. L. Cogger, Mapping using the Tsyganenko long magnetospheric model and its relationship to *Viking* auroral images, *J. Geophys. Res., 96,* 1467, 1991.

Elphinstone, R. D., J. S. Murphree, L. L. Cogger, D. Hearn, and M. G. Henderson, Observations of changes to the auroral distribution prior to substorm onset, in *Magnetospheric Substorms,* Proc. Hakone Conf. Japan, AGU Monograph, edited by T. A. Potemra, J. R. Kan, S. Kokobun, and T. Iijima, 1992a.

Elphinstone, R. D., J. S. Murphree, D. J. Hearn, L. I. Cogger, P. T. Newell, and H. Vo, Viking observations of the uv dayside aurora and their relationship to DMSP particle boundary definitions, *Ann. Geophysicae, 10,* 815, 1992b.

Elvey, C. T., Problems of auroral morphology, *Proc. Nat. Acad. Sci. of the U. S., 43,* 63, 1957.

Engebretsen, M. J., C.-I. Meng, R. L. Arnoldy, and L. J. Cahill, Jr., Pc 3 pulsations observed near the south polar cusp, *J. Geophys. Res., 91,* 9809, 1986a.

Engebretsen, M. J., L. J. Zanetti, T. A. Potemra, and M. H. Acuna, Harmonically structured ULF pulsations observed by the AMPTE CCE magnetic field experiment, *Geophys. Res. Lett., 13,* 905, 1986b.

Engebretsen, M. J., L. J. Zanetti, T. A. Potemra, W. Baumjohann, H. Luehr, and M. H. Acuna, Simultaneous observations of Pc 3–4 pulsations in the solar wind and in the earth's magnetosphere, *J. Geophys. Res., 92,* 10053, 1987.

Engebretsen, M. J., N. Lin, W. Baumjohann, H. Luehr, B. J. Anderson, L. J. Zanetti, T. A. Potemra, R. L. McPherron, and M. G. Kivelson, A comparison of ULF fluctuations in the solar wind, magnetosheath, and dayside magnetosphere, 1, Magnetosheath morphology, *J. Geoophys. Res., 96,* 3441, 1991.

Engebretsen, M. J., D. L. Murr, K. N. Erickson, R. J. Strangeway, D. M. Klumpar, S. A. Fuselier, L. J. Zanetti, and T. A. Potemra, The spatial extent of radial magnetic pulsation events observed in the dayside near synchronous orbit, *J. Gophys. Res., 97,* 13741, 1992.

Erickson, G. M., and R. A. Wolf, Is steady convection possible in the earth's geomagnetic tail?, *Geophys. Res. Lett., 7,* 897, 1980.

Erickson, K. N., R. L. Swanson, R. J. Walker, and J. R. Winckler, A study of magnetospheric dynamics during auroral electrojet events by observation of electron intensity changes at synchronous orbit, *J. Geophys. Res., 84,* 931, 1979.

Escoubet, C. P., and J. M. Bosqued, The influence of IMF-Bz and/or AE on the polar cusp: an overview of observations from the Aureol-3 satellite, *Planet. Space Sci., 37,* 609, 1989.

Etemadi, A., S. W. H. Cowley, M. Lockwood, B. J. I. Bromage, D. M. Willis, and H. Luhr, The dependence of high-latitude ionospheric flows on the north–south component of the IMF: A high time resolution correlation analysis using EISCAT POLAR and AMPTE UKS and IRM data, *Planet. Space Sci., 36,* 471, 1988.

Evans, D. S., The observations of a nearly monoenergetic flux of auroral electrons, *J. Geophys. Res., 73,* 2316, 1968.

Evans, D. S., The characteristics of a persistent auroral arc at high latitude in the 1400 MLT sector, in *The Polar Cusp,* edited by J. Holtet and A. Egeland, p. 99, D. Reidel, Boston, Mass., 1985.

Evans, D. S., and T. E. Moore, Precipitating electrons associated with the diffuse aurora; evidence for electrons of atmospheric origin in the plasma sheet, *J. Geophys. Res., 84,* 6451, 1979.

Fahleson, U., C. G. Falthammar, P.-A. Lindquist, F. S. Mozer, B. Torbert, A. Gonfalone, and A. Pedersen, Quasistatic electric fields observed during a number of magnetopause crossings by ISEE 1, in *Magnetospheric Boundary Layers, ESA SP-148,* p. 51, European Space Agency, Paris, 1979.

Fairfield, D. H., Simultaneous measurements on three satellites and the observation of the geomagnetic tail at 1000 RE, *J. Geophys. Res., 73,* 6179, 1968.

Fairfield, D. H., Average and unusual locations of the earth's magnetopause and bow shock, *J. Geophys. Res., 76,* 6700, 1971.

Fairfield, D. H., Magnetic field signatures of substorms on high-latitude field lines in the night-time magnetosphere, *J. Geophys. Res., 78,* 1553, 1973.

Fairfield, D. H., Structure of the magnetopause: observations and implications for reconnection, *Space Sci. Rev., 23,* 427, 1979.

Fairfield, D. H., Solar wind control of magnetospheric pressure, *J. Geophys. Res., 90,* 1201, 1985.

Fairfield, D. H., Multipoint measurements of magnetotail dynamics, *Adv. Space Res., 8,* 97, 1988.

Fairfield, D. H., Solar wind control of the size and shape of the magnetosphere, *J. Geomag. Geoelectr., 43, suppl.,* 117, 1991a.

Fairfield, D. H., An evaluation of the Tsyganenko Magnetic Field Model, *J. Geophys. Res., 96,* 1481, 1991b.

Fairfield, D. H., On the structure of the distant magnetotail: ISEE 3, *J. Geophys. Res., 97,* 1403, 1992.

Fairfield, D. H., and L. J. Cahill, Jr., Transition region magnetic field and polar magnetic disturbances, *J. Geophys. Res., 71,* 155, 1966.

Fairfield, D. H., and N. F. Ness, Magnetic field measurements with the IMP-2 satellite, *J. Geophys. Res., 72,* 2379, 1967.

Fairfield, D. H., and G. D. Mead, Magnetospheric mapping with a quantitative geomagnetic field model, *J. Geophys. Res., 80,* 535, 1975.

Fairfield, D. H., and J. D. Scudder, Polar rain: solar coronal electrons in the earth's magnetosphere, *J. Geophys. Res., 90,* 4055, 1985.

Fairfield, D. H., and L. J. Zanetti, Three-point magnetic field observations of substorms in the inner magnetotail, *J. Geophys. Res., 94,* 3565, 1989.

Fairfield, D. H., R. P. Lepping, E. W. Hones, Jr., S. J. Bame, and J. R. Asbridge, Simultaneous measurements of magnetotail dynamics by IMP spacecraft, *J. Geophys. Res., 86,* 1396, 1981.

Fairfield, D. H., D. N. Baker, J. D. Craven, R. C. Elphic, J. F. Fennell, L. A. Frank, I. G. Richardson, H. J. Singer, J. A. Slavin, B. T. Tsurutani, and R. D. Zwickl, Substorms, plasmoids, flux ropes, and magnetotail flux loss on March 25, 1983: CDAW 8, *J. Geophys. Res., 94,* 15, 135, 1989.

Farrugia, C. J., R. P. Rijnbeek, M. A. Saunders, D. J. Southwood, D. J. Rodgers, M. F. Smith, C. P. Chaloner, D. S. Hall, P. J. Christiansen, and L. J. C. Wooliscroft, A multi-instrument study of flux transfer event structure, *J. Geophys. Res., 93,* 14465, 1988.

Fasel, G. J., J. Minow, R. W. Smith, C. S. Deehr, and J. V. Olson, Accelerated rate of transient auroral arc formation during rapid polar cap expansion, *EOS, Trans., 72,* no. 44, 370, 1991.

Fasel, G. J., J. I. Minow, R. W. Smith, C. S. Deehr, and L. C. Lee, Multiple brightenings of transient dayside auroral forms during oval expansions, *Geophys. Res. Lett., 19,* 2429, 1992.

Fejer, B. G., and M. C. Kelley, Ionospheric irregularities, *Revs. Geophys., 18,* 401, 1980.

Feldstein, Y. I., Geographical distribution of aurorae and azimuth of auroral arcs, in *Investigations of the Aurorae, No. 4,* edited by B. A. Bargajatsky, p. 61, Acad. Sci. USSR, Moscow, 1960.

Feldstein, Y. I., On morphology of aurorae and magnetic disturbances in high latitudes (in Russian), *Geomagn. Aeron., 3,* 227, 1963a.

Feldstein, Y. I., The morphology of aurorae and geomagnetism, in *Aurorae and Airglow, No. 10,* edited by B. A. Bargajatsky and V. I. Krassovsky, p. 121, Acad. Sci. USSR, Moscow, 1963b.

Feldstein, Y. I., Peculiarities in aurora and magnetic disturbances distribution in high latitudes caused by the asymmetrical form of the magnetosphere, *Planet. Space Sci., 14,* 121, 1966.

Feldstein, Y. I., The auroral oval, *J. Geophys. Res., 78,* 1210, 1973.

Feldstein, Y. I., and E. K. Solomatina, Aurorae in the southern hemisphere (in Russian), *Geomag. and Aeron., 1,* 534, 1961.

Feldstein, Y. I., and G. V. Starkov, The auroral oval and the boundary of closed field lines of geomagnetic field, *Planet. Space Sci., 18,* 501, 1970.

Feldstein, Y. I., and G. V. Starkov, Auroral oval planetary energetics, *J. Atmos. Terr. Phys., 33,* 197, 1971.

Feldstein, Y. I., and. Yu. I. Galperin, The auroral luminosity structure in high-latitude upper atmosphere: its dynamics and relationship to the large-scale structure of the earth's magnetosphere, *Revs. Geophys., 23,* 217, 1985.

Fennell, J. F., Access of solar protons to the earth's polar caps, *J. Geophys. Res., 78,* 1036, 1973.

Fennell, J. F., P. F. Mizera, and D. R. Croley, Jr., Low energy polar cap electrons during quiet times, *Proc. Intl. Conf. Cosmic Rays 14th,* 1267, 1975.

Fennell, J. F., D. J. Gorney, and P. F. Mizera, Auroral particle distribution functions and their relationship to inverted-V's and auroral arcs, in *Physics of Auroral Arc Formation,* edited by S.-I. Akasofu and J. R. Kan, American Geophysical Union, Washington, DC, 1981.

Ferraro, V. C. A., On the theory of the first phase of a geomagnetic storm: a new illustrative calculation based on an idealised (plane not cylindrical) model field distribution, *J. Geophys. Res., 57,* 15, 1952.

Ferraro, V. C. A., An approximate method of estimating the size and shape of the stationary hollow carved out in a neutral ionozed stream of corpuscles impinging on the geomagnetic field, *J. Geophys. Res., 65,* 3805, 1960.

Fitzgerald, G. F., Sunspots and magnetic storms, *The Electrician, 30,* 48, 1892 (see also Editorial, p. 25).

Fitzgerald, G. F., Sunspots, magnetic storms, comet tails, atmospheric electricity, and aurorae, *The Electrician, 46,* 287, 1900.

Folkestad, K., T. Hagfors, and S. Westerlund, EISCAT: an updated description of technical characteristics and operational capabilities, *Radio Science, 18,* 867, 1983.

Fontaine, D., S. Perrault, D. Alcayde, G. Caudal, and B. Higel, Large scale structures of the convection inferred form coordinated measurements by EISCAT and GEOS 2, *J. Atmos. Terr. Phys., 48,* 973, 1986.

Forbes, T. G., E. W. Hones, Jr., S. J. Bame, J. R. Asbridge, G. Paschmann, N, Sckopke, and C. T. Russell, Substorm-related plasma sheet motions as determined from differential timing of plasma changes at the Isee satellites, *J. Geophys. Res., 86,* 3459, 1981.

Forget, B., J.-C. Cerisier, A. Berthelier, and J.-J. Berthelier, Closure of small-scale Birkeland Currents, *J. Geophys. Res., 96,* 1883, 1991.

Formisano, V., Orientation and shape of the bow shock in three dimensions, *Planet. Space Sci., 27,* 1979.

Formisano, V., Heos 2 observations of the boundary layer from the magnetopause to the ionosphere, *Planet. Space Sci., 28,* 245, 1980.

Formisano, V., V. Domingo, and K.-P. Wenzel, The three-dimensional shape of the magnetopause, *Planet. Space Sci., 27,* 1137, 1979.

Formisano, V., A. Pedersen, and P.-A. Lindquist, The fine structure of the front side magnetopause during two successive crossings, *J. Geophys. Res., 87,* 2115, 1982.

Foster, J. C., Ionospheric signatures of magnetospheric convection, *J. Geophys. Res., 89,* 855, 1984.

Foster, J. C., D. H. Fairfield, K. W. Ogilvie, and T. J. Rosenberg, Relationship of interplanetary parameters and occurrences of magnetospheric substorms, *J. Geophys. Res., 76,* 6971, 1971.

Frank, L. A., Plasma in the earth's polar magnetosphere, *J. Geophys. Res., 76,* 5202, 1971.

Frank, L. A., Dynamics of the near-earth magnetotail, p. 261 in *AGU Monograph #zz, American Geophysical Union,* Washington, DC, 1988.

Frank, L. A., and J. A. Van Allen, Measurements of energetic electrons in the vicinity of the sunward magnetospheric boundary with Explorer 14, *J. Geophys. Res., 69,* 4923, 1964.

Frank, L. A., and K. A. Ackerson, Observations of charged particle precipitation into the auroral zone, *J. Geophys. Res., 76,* 3612, 1971.

Frank, L. A., and K. L. Ackerson, Several recent findings concerning the dynamics of the earth's magnetotail, *Space Sci. Rev., 23,* 375, 1979.

Frank, L. A., K. L. Ackerson, and R. P. Lepping, On hot tenuous plasma, fireballs, and boundary layers in the earth's magnetotail, *J. Geophys. Res., 81,* 5859, 1976.

Frank, L. A., R. L. McPherron, R. J. DeCoster, B. G. Burek, K. L. Ackerson, and C. T. Russell, Field-aligned currents in the earth's magnetotail, *J. Geophys. Res., 86,* 687, 1981.

Frank, L. A., J. D. Craven, J. L. Burch, and J. D. Winningham, Polar views of the earth's aurora with Dynamics Explorer, *Geophys. Res. Lett., 9,* 1001, 1982.

Frank, L. A., J. D. Craven, D. A. Gurnett, S. D. Shawhan, D. R. Weimer, J. L. Burch, J. D. Winningham, C. R. Chappell, J. H. Waite, R. A. Heelis, N. C. Maynard, M. Sugiura, W. K. Peterson, and E. G. Shelley, The theta aurora, *J. Geophys. Res., 91,* 3177, 1986.

Franklin, B., p. 504 in *Political, Miscellaneous, and Philosophical Pieces,* edited by Vaughn, Johnson, London (1779).

Fraser-Smith, A. C., ULF/lower ELF electromagnetic field measurements in the polar caps, *Revs. Geophys. 20,* 497, 1982.

Friis-Christensen, E., The effect of the IMF on convection patterns and equivalent currents in the polar cap and cusp, paper presented at the International Workshop on Selected Topics of Magnetospheric Physics, Jpn. Int. Magnetospheric Study Comm., Tokyo, 1979.

Friis-Christensen, E., and J. Wilhelm, Polar cap currents for different directions of the interplanetary magnetic field in the Y-Z plane, *J. Geophys. Res., 80,* 1248, 1975.

Friis-Christensen, E., K. Lassen, J. Wilhelm, J. M. Wilcox, W. Gonzales, and D. S. Cotburn, Critical component of the interplanetary magnetic field responsible for large geomagnetic effects in the polar cap, *J. Geophys. Res., 77,* 3371, 1972.

Friis-Christensen, E., Y. Kamide, A. D. Richmond, and S. Matsushita, Interplanetary magnetic field control of high-latitude electric fields and

currents determined from Greenland magnetometer data, *J. Geophys. Res., 90,* 1325, 1985.

Friis-Christensen, E., M. A. McHenry, C. R. Clauer, and S. Vennerstrom, Ionospheric traveling convection vortices observed near the the polar cleft: a triggered response to sudden changes in the solar wind, *Geophys. Res. Lett., 15,* 253, 1988.

Fritz, T. A., D. N. Baker, R. L. McPherron, and W. Lennartsson, Implications of the 1100 UT March 22, 1979 CDAW 6 substorm event for the role of magnetic reconnection in the geomagnetic tail, p. 203 in *Magnetic Reconnection in Space and Laboratory Plasmas, Geophys. Monogr. Ser., 30,* edited by E. W. Hones, Jr., American Geophysical Union, Washington, DC, 1984.

Fu, Z. F., and L. C. Lee, Simulation of multiple X-line reconnection at the dayside magnetopause, *Geophys. Res. Lett., 12,* 291, 1985.

Fukunishi, H., Dynamic relationship between proton and electron auroral substorm, *J. Geophys. Res., 80,* 553, 1975.

Fukunishi, H., Latitude dependence of power spectra of magnetic pulsations near L = 4 excited by sscs and sis, *J. Geophys. Res., 84,* 7191, 1979.

Fukunishi, H., and T. Hirasawa, Progressive changes in Pi 2 power spectra with the development of magnetospheric substorm, *Rep. Ionos. Space Res. Jpn., 24,* 45, 1970.

Fukunishi, H., and L. J. Lanzerotti, ULF pulsation evidence of the plasmapause, 2, Polarization studies of Pc 3 and Pc 4 pulsations near L = 4 and at a latitude network in the conjugate region, *J. Geophys. Res., 79,* 4632, 1974.

Fukunishi, H., and L. J. Lanzerotti, Magnetic pulsations in the dayside cusp region and ground signatures of flux transfer events, in *Plasma Waves and Instabilities in Magnetospheres and at Comets,* AGU Chapman Conf., Sendai, Japan, 1987.

Galeev, A. A., Reconnection in the magnetotail, *Space Sci. Revs., 23,* 411, 1979.

Galeev, A. A., and L. M. Zelenyi, Tearing instability in plasma configuration, *Sov. Phys. JETP, Engl. Trans., 43,* 1113, 1976.

Galeev, A. A., F. V. Coroniti, and M. Ashour-Abdalla, Explosive tearing mode reconnection in the magnetospheric tail, *Geophys. Res. Lett., 5,* 707, 1978.

Galeev, A. A., M. M. Kuznetsova, and L. M. Zelenyi, *Space Sci. Rev., 44,* 1, 1986.

Galperin, Yu. I., and Ya. I. Feldstein, Auroral luminosity and its relationship to magnetospheric plasma domains, p. 207, in *Auroral Physics,* edited by C.-I. Meng, M. J. Rycroft, and L. A. Frank, Cambridge University Press, Cambridge, UK, 1991.

Galperin, Yu. I., V. N. Ponomarev, and A. G. Zosimova, Plasma convection in polar ionosphere, *Ann. de Geophysique, 30,* 1, 1974.

Gary, S. P., and T. E. Eastman, The lower hybrid drift instability at the magnetopause, *J. Geophys. Res., 84,* 7378, 1979.

Gary, S. P., and A. G. Sgro, The lower hybrid drift instability at the magnetopause, *Geophys. Res. Lett., 17,* 909, 1990.

Gassendi, P., *Opera Omnia,* Lugduni (Lyons, France), 1658.

Ghielmetti, A. G., R. G. Johnson, R. D. Sharp, and E. G. Shelley, The latitudinal, diurnal, and altitudinal distributions of upflowing energetic ions of ionospheric origin, *Geophys. Res. Lett., 5,* 59, 1978.

Gilbert, W., *De Magnete-Magneticisque Corporibus, et de Magno magnete Tellure: Physiologia Nova* (English trans. by P. F. Mottelay, 368 pp., John Wiley and Sons, New York, 1893; also, Dover Publications reprint, New York, 1958).

Giovanelli, R. G., Magnetic and electric phenomena in the sun's atmosphere associated with sunspots, *Mon. Not. Roy. Astron. Soc., 107,* 338, 1947.

Glassmeier, K.-H., and C. Heppner, Traveling magnetospheric convection twin vortices: another case study, global characteristics, and a model, *J. Geophys. Res., 97,* 3977, 1992.

Glassmeier, K.-H., M. Lester, W. A. C. Mier-jedrzejowicz, C. A. Green, G. Rostoker, D. Orr., J. Wedeken, H. Junginger, and E. Amata, Pc5 pulsations and their possible source mechanisms: a case study, *J. Geophys., 55,* 108, 1984.

Glassmeier, K.-H., M. Honisch, and J. Untiedt, Ground-based and satellite observations of travelling magnetospheric convection twin vortices, *J. Geophys. Res., 94,* 2520, 1989.

Gloeckler, G., and D. C. Hamilton, AMPTE ion composition results, *Physica Scripta, T18,* 73, 1987.

Gloeckler, G., M. Scholer, F. M. Ipavich, D. Hovestadt, B. Klecker, and A. B. Galvin, Abundances and spectra of suprathermal H^+, He^{++}, and heavy ions in a fast moving plasma structure (plasmoid) in the distant geotail, *Geophys. Res. Lett., 11,* 603, 1984a.

Gloeckler, G. M., F. M. Ipavich, D. Hovestadt, M. Scholer, A. B. Galvin, and B. Klecker, Characteristics of suprathermal H^+ and He^{++} in plasmoids in the distant magnetotail, *Geophys. Res. Lett., 11,* 1030, 1984b.

Goertz, C. K., and R. A. Smith, The thermal catastrophe model of substorms, *J. Geophys. Res., 94,* 6581, 1989.

Goertz, C. K., and W. Baumjohann, On the thermodynamics of the plasma sheet, *J. Geophys. Res., 96,* 20991, 1991.

Goertz, C. K., E. Nielsen, A. Korth, K.-H. Glassmeier, C. Haldoupis, P. Hoeg, and D. Hayward, Observations of a possible ground signature of flux transfer events, *J. Geophys. Res., 90,* 4069, 1985.

Gold, T., Contribution to discussion, p. 103 in *Gas Dynamics of Cosmic Clouds,* North-Holland, Amsterdam, 1955.

Gold, T., Motions in the magnetosphere of the earth, *J. Geophys. Res., 64,* 1219, 1959a.

Gold, T., Origin of the radiation near the earth discovered by means of satellites, *Nature (London), 183,* 355, 1959b.

Gonzales, W. D., and F. S. Mozer, A quantitative model for the potential resulting from reconnection with an arbitrary interplanetary magnetic field, *J. Geophys. Res., 79,* 4186, 1974.

Gorney, D. J., D. S. Evans, M. S. Gussenhoven, and P. F. Mizera, A multiple-satellite observation of the high-latitude auroral activity on January 11, 1983, *J. Geophys. Res., 91,* 339, 1986.

Gosling, J. T., J. R. Asbridge, S. J. Bame, A. J. Hundhausen, and I. B. Strong, Measurements of the interplanetary solar wind during the large geomagnetic storm of April 17–18, 1965, *J. Geophys. Res., 72,* 1813, 1967a.

Gosling, J. T., J. R. Asbridge, S. J. Bame, A. J. Hundhausen, and I. B. Strong, Discontinuities in the solar wind associated sudden geomagnetic impulses and storm commencements, *J. Geophys. Res., 72,* 3357, 1967b.

Gosling, J. T., J. R. Asbridge, S. J. Bame, and I. Strong, Vela 2 measurements of the magnetopause and bow shock positions, *J. Geophys. Res., 72,* 101, 1967c.

Gosling, J. T., D. N. Baker, S. J. Bame, E. W. Hones, Jr., D. J. McComas, R. D. Zwickl, J. A. Slavin, E. J. Smith, and B. T. Tsurutani, Plasma entry into the distant tail lobes: ISEE 3, *Geophys. Res. Letts., 11,* 1078, 1984.

Gosling, J. T., M. F. Thomsen, S. J. Bame, and C. T. Russell, Accelerated plasma flows at the near-tail magnetopause, *J. Geophys. Res., 91,* 3029, 1986.

Gosling, J. T., M. F. Thomsen, S. J. Bame, and R. C. Elphic, Plasma flow reversals at the dayside magnetopause and the origin of asymmetric polar cap convection, *J. Geophys. Res., 95,* 8073, 1990.

Gosling, J. T., M. F. Thomsen, S. J. Bame, R. C. Elphic, and C. T. Russell, Observations of reconnection of interplanetary and lobe field lines at the high-latitude magnetopause, *J. Geophys. Res., 96,* 14097, 1991.

Graham, G., *Phil. Trans., London, 383,* 96, 1724.

Greene, J. M., Geometrical properties of three-dimensional reconnecting magnetic fields with nulls, *J. Geophys. Res., 93,* 8583, 1988.

Greenspan, M. E., C.-I. Meng, and D. H. Fairfield, Simultaneous polar cap and magnetotail observations of intense polar rain, *J. Geophys. Res., 91,* 1123, 1986.

Greenwald, R. A., and A. D. M. Walker, Energetics of long-period resonant hydromagnetic waves, *Geophys. Res. Letts., 7,* 745, 1980.

Greenwald, R. A., T. A. Potemra, and N. A. Saflekos, Stare and triad observations of field-aligned current closure and Joule heating in the vicinity of the Harang Discontinuity, *J. Geophys. Res., 85,* 563, 1980.

Gringauz, K. I., V. V. Bezrukhikh, V. D. Ozerov, and R. Ye. Rypchinski, A study of interplanetary ionized gas, energetic electrons, and corpuscular solar emission, using three electrode charged-particle traps set up on the second Soviet cosmic rocket Luna II, *Dokl. Akad. Nauk. USSR, 131,* 1301, 1960 (English transl. *Sov. Phys. Dokl., 5,* 361, 1960).

Gurnett, D. A., The earth as a radio source: terrestrial kilometric radiation, *J. Geophys. Res., 79,* 4227, 1974.

Gurnett, D. A., and L. A. Frank, Observed relationships between electric fields and auroral particle precipitation, *J. Geophys. Res., 78,* 145, 1973.

Gurnett, D. A., and J. L. Green, On the polarization and origin of auroral kilometric radiation, *J. Geophys. Res., 83,* 689, 1978.

Gurnett, D. A., R. L. Huff, J. D. Menietti, J. L. Burch, J. D. Winningham, and S. D. Shawhan, Correlated low frequency electric and magnetic noise along the auroral field lines, *J. Geophys. Res., 89,* 8971, 1984.

Gusev, M. G., and O. A. Troshichev, Hook-shaped arcs in dayside polar cap and their relation to the IMF, *Planet. Space Sci., 34,* 489, 1986.

Gusev, M. G., and O. A. Troshichev, Relation of sun-aligned arcs to polar cap convection and magnetic disturbances, *Planet. Space Sci., 38,* 1, 1990.

Gussenhoven, M. S., Extremely high-latitude auroras, *J. Geophys. Res., 87,* 2401, 1982.

Haerendel, G., G. Paschmann, N. Sckopke, H. Rosenbauer, and P. C. Hedgecock, The frontside boundary layer of the magnetosphere and the problem of reconnection, *J. Geophys. Res., 83,* 3195, 1978.

Hairston, M. R., and R. A. Heelis, Model of the high-latitude ionospheric convection pattern during southward interplanetary magnetic field using DE 2 data, *J. Geophys. Res., 95,* 2333, 1990.

Halley, E., An account of the late surprising appearance of the light seen in the air on the sixth of March last; with an attempt to explain the principal phenomena, *Phil Trans. Roy. Soc.,* 55, 406, 1716.

Hallinan, T. J., Auroral spirals, 2, Theory, *J. Geophys. Res., 81,* 3059, 1976.

Hamilton, D. C., G. Gloeckler, and F. M. Ipavich, Ring current development during the great geomagnetic storm of February 1986, *J. Geophys. Res., 93,* 14343, 1988.

Hansen, H. J., B. J. Fraser, F. W. Menk, Y.-D. Hu, P. T. Newell, C.-I. Meng, and R. J. Morris, High-latitude Pc 1 bursts arising in the dayside boundary layer region, *J. Geophys. Res., 97,* 3993, 1992.

Hapgood, M. A., M. Lockwood, G. A. Bowe, D. M. Willis, and Y. K. Tulunay, Variability of the interplanetary medium at 1 a.u. over 24 years: 1963–1986, *Planet. Space Sci., 39,* 411, 1991.

Harang, L., The mean field of disturbance of polar geomagnetic storms, *Terr. Magn. Atmos. Elec., 51,* 353, 1946.

Hardy, D. A., Intense fluxes of low energy electrons at geomagnetic latitudes above 85°, *J. Geophys. Res., 89,* 3883, 1984.

Hardy, D. A., H. K. Hills, and J. W. Freeman, A new plasma regime in the distant magnetotail, *Geophys. Res. Lett., 2,* 169, 1975.

Hardy, D. A., W. J. Burke, and M. S. Gussenhoven, DMSP optical and electron measurements in the vicinity of polar cap arcs, *J. Geophys. Res., 87,* 2413, 1982.

Hardy, D. A., M. S. Gussenhoven, and E. Holeman, A statistical model of auroral electron precipitation, *J. Geophys. Res., 90,* 4229, 1985.

Hardy, D. A., M. S. Gussenhoven, and D. Brautigam, A statistical model of auroral ion precipitation, *J. Geophys. Res., 94,* 370, 1989.

Harel, M, R. A. Wolf, P. H. Reiff, R. W. Spiro, W. J. Burke, F. J. Rich, and M. Smiddy, Quantitative simulation of a magnetospheric substorm, 1. Model logic and overview, *J. Geophys. Res., 86,* 2217, 1981.

Hargreaves, J. K., H. J. A. Chivers, and W. I. Axford, The development of the substorm in auroral radio absorption, *Planet. Space Sci., 23,* 905, 1975.

Hargreaves, J. K., H. J. A. Chivers, and E. Neilsen, Properties of spike events in auroral radio absorption, *J. Geophys. Res., 84,* 4245, 1979.

Hasegawa, A., K. H. Tsui, and A. S. Assis, A theory of long period magnetic oscillations, 3, Local field line oscillation, *Geophys. Res. Lett., 10,* 765, 1983.

Haskell, G. P., Anisotropy fluxes of energetic particles in the outer magnetosphere, *J. Geophys. Res., 74,* 1740, 1969.

Hayakawa, H., A. Nishida, E. W. Hones, Jr., and S. J. Bame, Statistical characteristics of plasma flow in the magnetotail, *J. Geophys. Res., 87,* 277, 1982.

Heacock, R. R., Two subtypes of type Pi micropulsations, *J. Geophys. Res., 72,* 3905, 1967.

Heacock, R. R., Midday Pc 1–2 pulsations observed at a subcleft location, *J. Geophys. Res., 79,* 4239, 1974.

Heacock, R. R., Morphology of spatial patterns in Pi 1–2 magnetic field pulsation activity, *J. Geomag. Geoelectr., 34,* 195, 1982.

Hedgecock, P. C., P. Cerulli, A. Coletti, A. Egidi, R. Marconero, V. Domingo, D. Kohn, D. E. Page, D. E. Taylor, and K.-P. Wenzel, Magnetosheath observations at high northern latitudes by Heos 2, *J. Geophys. Res., 78,* 1715, 1973.

Heelis, R. A., and W. B. Hanson, High-latitude ion convection in the night-time F region, *J. Geophys. Res., 85,* 1995, 1980.

Heelis, R. A., Hanson, W. B., and Burch, J. L., AE-C observations of electric fields around auroral arcs, in *Physics of Auroral Arc Formation,* edited by S.-I. Akasofu and J. R. Kan, American Geophysical Union, Washington, D. C., 1981.

Heelis, R. A., P. H. Reiff, J. D. Winningham, and W. B. Hanson, Ionospheric convection signatures observed by DE 2 during northward interplanetary field, *J. Geophys. Res., 91,* 5817, 1986.

Heikkila, W., Impulsive plasma transport through the magnetopause, *Geophys. Res. Lett., 9,* 159, 1982.

Heikkila, W., Current sheet crossings in the distant magnetotail, *Geophys. Res. Lett., 15,* 299, 1988.

Heikkila, W. J., and J. D. Winningham, Penetration of magnetosheath plasma to low altitudes through the dayside magnetospheric cusps, *J. Geophys. Res., 76,* 883, 1971.

Heikkila, W. J., and R. J. Pellinen, Localized induced electric field within the magnetotail, *J. Geophys. Res., 82,* 1610, 1977.

Heppner, J. P., *A study of relationships between the aurora borealis and the geomagnetic disturbances caused by electric currents in the ionosphere,* unpublished Ph.D. dissertation, California Institute of Technology, 1954.

Heppner, J. P., Note on the occurrence of world-wide ssc's during the onset of negative bays at College, Alaska, *J. Geophys. Res., 60,* 29, 1955.

Heppner, J. P., The Harang discontinuity in auroral belt ionospheric currents, *Geophys. Norv., 29,* 105, 1972a.

Heppner, J. P., Polar cap electric field distribution related to the interplanetary magnetic field direction, *J. Geophys. Res., 77,* 4877, 1972b.

Heppner, J. P., p. 107 in *Critical Problems of Magnetospheric Physics, Proc. Joint Cospar/IAGA/URSI Symposium,* Madrid, Spain, 11–13 May, 1972c.

Heppner, J. P., Empirical models of high-latitude electric fields, *J. Geophys. Res., 82,* 11115, 1977.

Heppner, J. P., and N. C. Maynard, Empirical high-latitude electric field models, *J. Geophys. Res., 92,* 4467, 1987.

Heppner, J. P., M. Sugiura, T. L. Skillman, B. G. Ledley, and H. M. Campbell, OGO A magnetic field observations, *J. Geophys. Res., 72,* 5417, 1967.

Hesse, M., and K. Schindler, A theoretical foundation of general magnetic reconnection, *J. Geophys. Res., 93,* 5559, 1990.

Heyn, M. F., H. K. Biernat, R. P. Rijnbeek, and V. S. Semenov, The structure of reconnection layers, *J. Plasma Phys., 40,* 235, 1988.

Hill, T. W., Magnetic merging in a collisionless plasma, *J. Geophys. Res., 80,* 4689, 1975.

Hill, T. W., and P. H. Reiff, Evidence of magnetospheric cusp proton acceleration by magnetic merging at the dayside magnetopause, *J. Geophys. Res., 82,* 3623, 1977.

Hines, C. O., The magnetopause: a new frontier, *Science, 141,* 130, 1963.

Hiorter, O. P., Von der magnetnadel verschiedenen bewegungen, *Svensk Vet. Acad. Handl.,* 273, 1747.

Hirasawa, T., and T. Nagata, Spectral analysis of geomagnetic pulsations from 0.5 to 100 sec in period for the quiet sun condition, *Pure Appl. Geophys., 65,* 102, 1966.

Hirshberg, J., and D. S. Colburn, Interplanetary field and geomagnetic variations: A unified view, *Planet. Space Sci., 17,* 1183, 1969.

Hirshberg, J., and T. E. Holzer, Relationship between the interplanetary magnetic field and "isolated substorms," *J. Geophys. Res., 80,* 3553, 1975.

Hoffman, J. H., Studies of the composition of the ionosphere with a magnetic deflection mass spectrometer, *Int. J. Mass Spectrom. Ion Physics, 4,* 315, 1970.

Hoffman, J. H., W. H. Dodson, C. R. Lippincott, and H. D. Hammack, Initial ion composition results from the Isis 2 satellite, *J. Geophys. Res., 79,* 4246, 1974.

Hoffman, J. H., and W. H. Dodson, Light ion concentrations and fluxes in the polar regions during magnetically quiet times, *J. Geophys. Res., 85,* 626, 1980.

Hoffman, R. A., M. Sugiura, N. C. Maynard, R. M. Candey, J. D. Craven, and L. A. Frank, Electrodynamic patterns in the polar regions during periods of extreme magnetic quiescence, *J. Geophys. Res., 93,* 14515, 1988.

Hoffman, R. A., and D. S. Evans, Field-aligned electron bursts at high latitudes observed by OGO 4, *J. Geophys. Res., 73,* 6201, 1968.

Hoffman, R. A., M. Sugiura, and N. C. Maynard, Current carriers for the field-aligned current system, magnetospheric and ionospheric plasmas, *Adv. Space Res., 5,* 109, 1985a.

Hoffman, R. A., R. A. Heelis, and J. S. Prasad, A sun-aligned arc observed by DMSP and AE-C, *J. Geophys. Res., 90,* 9627, 1985b.

Holmberg, E. R., Rapid periodic fluctuations of the geomagnetic field, I, *Mon. Not. Roy. Astron. Soc., Geophys. Suppl. 6,* 476, 1953.

Holzer, R. E., and J. A. Slavin, Magnetic flux transfer associated with expansions and contractions of the dayside magnetosphere, *J. Geophys. Res., 83,* 3831, 1978.

Holzer, R. E., M. G. McLeod, and E. J. Smith, Preliminary results from the OGO 1 search coil magnetometer: boundary positions and magnetic noise spectra, *J. Geophys. Res., 71,* 1481, 1966.

Holzer, R. E., R. L. McPherron, and D. A. Hardy, A quantitative empirical model of the magnetospheric flux transfer process, *J. Geophys. Res., 91,* 3287, 1986.

Holzer, T. E., and G. C. Reid, The response of the dayside magneto-ionosphere system to time-varying field line reconnection at the magnetopause, 1, Theoretical model, *J. Geophys. Res., 80,* 2041, 1975.

Holzworth, R. H., and C.-I. Meng, Mathematical representation of the auroral oval, *Geophys. Res. Lett., 2,* 377, 1975a.

Holzworth, R. H., and C.-I. Meng, Auroral boundary variations and the interplanetary magnetic field, *Planet. Space Sci., 32,* 377, 1975b.

Hones, E. W., Jr., The magnetotail: its generation and dissipation, in *Physics of Solar–Planetary Environments,* Vol. II, edited by D. J. Williams, p. 558, 1976.

Hones, E. W., Jr., Transient phenomena in the magnetotail and their relation to substorms, *Space Sci. Rev., 23,* 393, 1979.

Hones, E. W., Jr., Plasma flow in the plasma sheet and its relation to substorms, *Radio Sci., 8,* 879, 1983.

Hones, E. W., Jr., The poleward leap of the auroral electrojet as seen in auroral images, *J. Geophys. Res., 90,* 5333, 1985.

Hones, E. W., Jr., Association of plasma sheet variations with auroral changes during substorms, *Adv. Space. Res., 8,* 129, 1988.

Hones, E. W., Jr., J. R. Asbridge, and S. J. Bame, Poleward expansion of the auroral oval and associated phenomena in the magnetotail during auroral substorms, *J. Geophys. Res., 75,* 8241, 1971a.

Hones, E. W., Jr., R. H. Karas, L. J. Lanzerotti, and S.-I. Akasofu, Magnetospheric substorms on 14 September 1968, *J. Geophys. Res., 76,* 6765, 1971b.

Hones, E. W., Jr., J. R. Asbridge, S. J. Bame, M. D. Montgomery, S. Singer, and S.-I. Akasofu, Measurements of magnetotail plasma flow made with *VELA 4B, J. Geophys. Res., 77,* 5503, 1972.

Hones, E. W., Jr., G. Paschmann, S. J. Bame, J. R. Asbridge, N. Sckopke, and K. Schindler, Vortices in magnetospheric plasma flow, *Geophys. Res. Letts., 5,* 2069, 1978.

Hones, E. W., Jr., J. Birn, S. J. Bame, J. R. Asbridge, G. Paschmann, N. Sckopke, and G. Haerendel, Further determination of the characteristics of magnetospheric plasma vortices with ISEE 1 and 2, *J. Geophys. Res., 86,* 814, 1981.

Hones, E. W., Jr., J. Birn, S. J. Bame, G. Paschmann, and C. T. Russell, On the three-dimensional magnetic structure of the plasmoid created at substorm onset, *Geophys. Res. Lett., 9,* 203, 1982.

Hones, E. W., Jr., J. Birn, S. J. Bame, and C. T. Russell, New observations of plasma vortices and insights into their interpretation, *Geophys. Res. Lett., 10,* 674, 1983.

Hones, E. W., Jr., D. N. Baker, S. J. Bame, W. C. Feldman, J. T. Gosling, D. J. McComas, R. D. Zwickl, J. A. Slavin, E. J. Smith, and B. T. Tsurutani, Structure of the magnetotail at 220 R_E and its response to geomagnetic activity, *Geophys. Res. Lett., 11,* 5, 1984a.

Hones, E. W., Jr., J. Birn, D. N. Baker, S. J. Bame, W. C. Feldman, D. J. McComas, and R. D. Zwickl, Detailed examination of a plasmoid in the distant magnetotail with ISEE 3, *Geophys. Res. Lett., 11,* 1046, 1984b.

Hones, E. W., Jr., T. Pytte, and H. I. West, Jr., Associations of geomagnetic activity with plasma sheet thinning and expansion: a statistical study, *J. Geophys. Res., 89,* 5471, 1984c.

Hones, E. W., Jr., T. A. Fritz, J. Birn, J. Cooney, and S. J. Bame, Detailed observations of the plasma sheet during a substorm on April 24, 1979, *J. Geophys. Res., 91,* 6845, 1986.

Hones, E. W., Jr., R. D. Elphinstone, A. B. Galvin, F. R. Higbie, and J. S. Murphree, Study of a substorm on May 4, 1986, *Adv. Space. Res., 8,* 119, 1988.

Hones, E. W., Jr., J. D. Craven, L. A. Frank, D. S. Evans, and P. T. Newell, The horse-collar aurora: a frequent pattern of the aurora in quiet times, *Geophys. Res. Lett., 16,* 37, 1989.

Horwitz, J. L., The substorm as an internal magnetospheric instability: substorms and their characteristic times scales during intervals of steady interplanetary magnetic field, *J. Geophys. Res., 90,* 4164, 1985.

Horwitz, J. L., and S.-I. Akasofu, The response of the dayside aurora to sharp northward and southward transitions of the interplanetary magnetic field and to magnetospheric substorms, *J. Geophy. Res., 82,* 2723, 1977.

Horwitz, J. L., J. R. Doupnik, and P. M. Banks, Chatanika radar observations of the latitudinal distributions or auroral zone electric fields, conductivities, and currents, *J. Geophys. Res., 83,* 1463, 1978.

Horwitz, J . L., and S. –I. Akasofu, On the relationship of the polar cap current system to the north–south component of the interplanetary magnetic field, *J. Geophys. Res., 84,* 2567, 1979.

Horwitz, J. L., S. Menteer, J. Turnley, J. L. Burch, J. D. Winningham, C. R. Chappell, J. D. Craven, L. A. Frank, and D. W. Slater, Plasma boundaries in the inner magnetosphere, *J. Geophys. Res., 91,* 8861, 1986.

Horwitz, J. L., J. R. Doupnik, and P. M. Banks, Chatanika radar observations of the latitudinal distributions of auroral zone electric fields, conductivities, and currents, *J. Geophys. Res., 83,* 1463, 1988.

Hoshino, M., and A. Nishida, Numerical simulation of the dayside reconnection, *J. Geophys. Res., 88,* 6926, 1983.

Howe, H. C., and G. L. Siscoe, Magnetopause motions at lunar distance determined from the Explorer 35 plasma experiment, *J. Geophys. Res., 77,* 6071, 1972.

Hoyle, F., *Some Recent Researches in Solar Physics,* Cambridge Univ. Press, Cambridge, 1949.

Hruska, A., and J. Hruskova, Long time-scale magnetohydrodynamic noise in the geomagnetic tail, *Planet. Space Sci., 17,* 1497, 1969.

Hruska, A., and J. Hruskova, Transverse structure of the earth's magnetotail and fluctuation of the tail magnetic field, *J. Geophys. Res., 75,* 2449, 1970.

Huang, C. Y., and L. A. Frank, A statistical study of the central plasma sheet: implications for substorm models, *Geophys. Res. Lett., 13,* 652, 1986.

Huang, C. Y., L. A. Frank, W. K. Peterson, D. J. Williams, W. Lennartsson, D. G. Mitchell, R. C. Elphic, and C. T. Russell, Filamentary structures in magnetotail lobes, *J. Geophys. Res., 92,* 2349, 1987.

Huba, J. D., N. T. Gladd, and K. Papadopoulos, The lower-hybrid drift instability as a source of anomalous resistivity for magnetic field reconnection, *Geophys. Res. Lett., 4,* 125, 1977.

Huba, J. D., N. T. Gladd, and K. Papadopoulos, Lower hybrid drift turbulence in the distant magnetotail, *J. Geophys. Res., 83,* 5217, 1978.

Huba, J. D., J. F. Drake, and N. T. Gladd, Lower-hybrid-drift instability in field-reversed plasmas, *Phys. Fluids, 23,* 552, 1980.

Huba, J. D., N. T. Gladd, and J. F. Drake, The lower hybrid drift instability in nonantiparallel reversed field plasmas, *J. Geophys. Res., 87,* 1697, 1982.

Huff, R. L., W. Calvert, J. D. Craven, L. A. Frank, and D. A. Gurnett, Mapping of auroral kilometric radiation sources to the aurora, *J. Geophys. Res., 93,* 11445, 1988.

Hughes, W. J., The effect of the atmosphere and ionosphere on long period magnetic micropulsations, *Planet. Space Sci., 22,* 1157, 1974.

Hughes, W. J., Hydromagnetic waves in the magnetosphere, *Revs. Geophys., 21,* 508, 1983.

Hughes, W. J., and D. J. Southwood, Effect of atmosphere and ionosphere on magnetospheric micropulsation signals, *Nature, 248,* 493, 1974.

Hughes, W. J., and D. J. Southwood, The screening of micropulsation signals by the atmosphere and ionosphere, *J. Geophys. Res., 81,* 3234, 1976.

Hughes, W. J., and H. J. Singer, Mid-latitude Pi 2 pulsations, geosynchronous substorm onset signatures and auroral zone currents on March 22, 1979: CDAW 6, *J. Geophys. Res., 85,* 1297, 1985.

Hughes, W. J., and D. G. Sibeck, On the 3-dimensional structure of plasmoids, *Geophys. Res. Letts., 14,* 636, 1987.

Hughes, W. J., and M. G. Kivelson, A test of the bent tail hypothesis of substorm triggering using the AL index, Paper presented at IAGA 6th scientific assembly, Int. Assoc. of Geomag. and Aeronomy, Exeter, UK, August, 1989.

Hughes, W. J., R. L. McPherron, and C. T. Russell, Multiple satellite observations of pulsation resonance structure in the magnetosphere, *J. Geophys. Res., 82,* 651, 1977.

Hughes, W. J., D. J. Southwood, B. Mauk, R. L. McPherron, and J. N. Barfield, Alfven waves generated by an inverted plasma energy distribution, *Nature, 275,* 43, 1978a.

Hughes, W. J., R. L. McPherron, and J. N. Barfield, Geomagnetic pulsations observed simultaneously on three geostationary satellites, *J. Geophys. Res., 83,* 1109, 1978b.

Hultquist, B., Rocket and satellite observations of energetic particle precipitation in relation to optical aurora, *Ann. Geophys., 30,* 223, 1974.

Hultquist, B., The aurora, in *The Magnetospheres of Earth and Jupiter,* edited by V. Formisano, D. Reidel Publishing Co., Dordrecht, Holland, 1975.

Hultquist, B., Welcoming address, p. 3, in *Substorms 1, Proc. Int'l. Conf. Substorms (ICS-1), ESA SP-335,* European Space Agency, Paris, 1992.

Hundhausen, A. J., *Coronal Expansion and Solar Wind,* Springer-Verlag, New York, 1972.

Hurley, J., Interaction of a streaming plasma with the magnetic field of a line current, *Phys. Fluids, 4,* 109, 1961a.

Hurley, J., Interaction of a streaming plasma with the magnetic field of a two-dimensional dipole, *Phys. Fluids, 4,* 854, 1961b.

Iijima, T., Interplanetary and ground magnetic signatures preceding ssc-triggered substorms, *Rep. Ionos. Space Res. Jap., 27,* 205, 1973.

Iijima, T., Signatures af field-aligned currents at geostationary satellite ATS-1 and a refined three-dimensional substorm current system, *Rep. Ionos. Space Res. Japan, 28,* 173, 1974.

Iijima, T., and T. Nagata, Signatures for substorm development of the growth phase and expansion area, *Planet. Space Sci., 20,* 1095, 1972.

Iijima, T., and T. A. Potemra, The amplitude distribution of field-aligned currents at northern high latitudes, *J. Geophys. Res., 81,* 2165, 1976.

Iijima, T., and T. A. Potemra, Large–scale characteristics of field–aligned currents associated with substorms, *J. Geophys. Res., 83,* 599, 1978.

Iijima, T., and T. A. Potemra, Large-scale characteristics of field-aligned currents associated with substorms, *J. Geophys. Res., 83,* 599, 1978.

Iijima, T., and T. Shibaji, Global characteristicsa of northward IMF-associated (NBZ) field-aligned currents, *J. Geophys. Res., 92,* 2408, 1987.

Iijima, T., T. A. Potemra, L. J. Zanetti, and P. F. Bythrow, Large scale Birkeland currents in the dayside polar region during strongly northward IMF: A new Birkeland current system, *J. Geophys. Res., 89,* 7441, 1984.

Imhof, W. L., H. D. Voss, D. W. Datlowe, and J. Mobilia, Bremsstrahlung X ray images of isolated electron patches at high latitudes, *J. Geophys. Res., 90,* 6515, 1985.

Inhester, B., Numerical modeling of hydromagnetic wave coupling in the magnetosphere, *J. Geophys. Res., 92,* 4751, 1987.

Inhester, B., W. Baumjohann, R. A. Greenwald, and E. Nielsen, Joint two dimensional observations of ground magnetic and ionospheric electric fields associated with auroral zone currents, *J. Geophys., 49,* 155, 1981.

Inoue, Y., Wave polarizations of geomagnetic pulsations observed in high latitudes on the earth's surface, *J. Geophys. Res., 78,* 2959, 1973.

Intriligator, D. S., and J. H. Wolfe, Evidence of a diffuse magnetopause boundary, *J. Geophys. Res., 77,* 5480, 1972.

Intriligator, D. S., H. R. Collard, J. D. Mihalov, O. L. Vaisberg, and J. H. Wolfe, Evidence for earth magnetospheric tail associated phenomena at 3100 RE, *Geophys. Res. Lett. 6,* 585, 1979.

Ipavich, F. M., A. B. Galvin, M. Scholer, G. Gloeckler, D. Hovestadt, and B. Klecker, Suprathermal O^+ and H^+ ion behavior during the March 22, 1979 (CDAW 6) substorm, *J. Geophys. Res., 90,* 1263, 1985.

Ismail, S., and C.-I. Meng, A classification of polar cap auroral arcs, *Planet. Space Sci., 30,* 319, 1982.

Ismail, S., D. D. Wallis, and L. L. Cogger, Characteristics of polar cap sun-aligned arcs, *J. Geophys. Res., 82,* 4741, 1977.

Iyemori, T., and S. Tsunomura, Characteristics of the association betyween an SC and a substorm onset, *Mem. Natl. Inst. Polar Res., Spec. Issue, 26,* 139, 1983.

Iyemori, T., H. Maeda, and T. Kamei, Impulse repsonses of geomagnetic indices to interplanetary magnetic field, *J. Geomagn. Geoelectr., 6,* 577, 1979.

Izraelovich, P. L., I. M. Podgorny, A. K. Kuzmin, N. S. Nikolaeva, and E. M. Dubinin, Convection and field-aligned currents related to transpolar arcs during strongly northward IMF, *Planet. Space Sci., 36,* 1317, 1988.

Jacobs, J. A., Y. Kato, S. Matsushita, and V. A. Troitskaya, Classification of geomagnetic micropulsations, *J. Geophys. Res., 69,* 180, 1964.

Jacobsen, B., P. E. Sandholt, B. Lybekk, and A. Egeland, Transient auroral events near midday: relationship with solar wind/magnetosheath plasma and magnetic field conditions, *J. Geophys. Res., 96,* 1327, 1991.

Jacquey, C., and J. A. Sauvaud, Dynamics of the cross-tail current during a long period of enhanced energy input from the solar wind to the magnetosphere, p. 155, in *Substorms 1, Proc. Int'l. Conf. on Substorms (ICS-1),* ESA SP-335, European Space Agency, Paris, 1992.

Jacquey, C., J. A. Sauvaud, and J. Dandouras, Location and propagation of the magnetotail current disruption during substorm expansion: analysis and

simulation of an ISEE multi-onset event, *Geophys. Res. Lett., 18,* 389, 1991.

Jain, A. R., and K. G. Srinavasacharya, A study of magnetic pulsations in the Indian equatorial region, *J. Atmos. Terr. Phys., 37,* 1977, 1975.

Johnson, F. S., The gross character of the geomagnetic field in the solar wind, *J. Geophys. Res., 65,* 3049, 1960.

Johnson, R. G., R. D. Sharp, M. F. Shea, and G. B. Shook, Satellite observations of two distinct zones of dayside auroral precipitation (abstract), *EOS, Trans. AGU, 47,* 64, 1966.

Johnstone, A. D., Pulsating aurora, *Nature, 274,* 119, 1978.

Johnstone, A. D., The mechanism of pulsating aurora, *Annales Geophysicae, 1,* 397, 1983.

Jorjio, N. V., Electrophotometrical measurements in the auroral zone, in *Spectral, Electrophotometrical, and Radar Research of Aurora and Airglow,* edited by V. I. Krassovsky, no. 1, p. 30. Acad. Sci. USSR, Moscow, 1959.

Judge, D. L., and P. J. Coleman, Jr., Observations of low-frequency hydromagnetic waves in the distant geomagnetic field: Explorer 6, *J. Geophys. Res., 67,* 5071, 1962.

Junginger, H., O. H. Bauer, G. Haerendel, F. Meltzner, B. Higel, and E. Amata, Plasma drift measurements with the electron beam experiment on GEOS-2 during long period pulsations on April 7, 1979, *Geophys. Res. Lett., 10,* 667, 1983.

Kaiser, M. L., and J. K. Alexander, Source location measurement of terrestrial kilometric radiation obtained from lunar orbit, *Geophys. Res. Lett., 3,* 37, 1976.

Kamide, Y., and G. Rostoker, The spatial relationship of field–aligned currents and auroral electrojets to the distribution of nightsode auroras, *J. Geophys. Res., 82,* 5589, 1977.

Kamide, Y., and A. D. Richmond, Ionospheric conductivity dependence of electric fields and currents detimated from ground magnetic observations, *J. Geophys. Res., 87,* 8331, 1982.

Kamide, Y., and J. F. Vickrey, Variability of the Harang discontinuity as observed by the Chatanika radar and the IMS Alaska magnetometer chain, *Geophys. Res. Lett., 10,* 159, 1983.

Kamide, Y., and W. Baumjohann, Estimation of electric fields and currents from international magnetospheric study magnetometer data for the CDAW 6 intervals: implications for substorm dynamics, *J. Geophys. Res., 90,* 1305, 1985.

Kamide, Y., F. Yasuhara, and S.-I. Akasofu, On the cause of northward magnetic field along the negative X axis during magnetospheric substorms, *Planet. Spcae Sci., 22,* 1219, 1974.

Kamide, Y., S.-I. Akasofu, and E. P. Rieger, Coexistence of two substorms in the midnight sector, *J. Geophys. Res., 82,* 1620, 1977.

Kamide, Y., J. S. Murphree, C. D. Anger, F. T. Berkey, and T. A. Potemra, Nearly simultaneous observations of field-aligned currents and visible auroras at the Triad and Isis 2 satellites, *J. Geophys. Res., 84,* 4425, 1979.

Kamide, Y., A. D. Richmond, and S. Matsushita, Estimation of ionospheric electric fields and currents estimated from ground magnetic observations, *J. Geophys. Res., 86,* 801, 1981.

Kan, J. R., and L. C. Lee, Energy coupling function and the solar wind magnetospheric dynamo, *Geophys. Res. Lett., 6,* 577, 1979.

Kan, J. R., and J. Burke, A theoretical model of polar cap auroral arcs, *J. Geophys. Res., 90,* 4171, 1985.

Kan, J. R., L. C. Lee, Y. T. Chiu, and D. U. Longenecker, Generation of Alfven waves by deceleration of magnetospheric convection and broadband PI pulsations, *J. Geophys. Res., 87,* 3511, 1982.

Kan, J. R., L. Zhu, and S.-I. Akasofu, A theory of substorms: onset and subsidence, *J. Geophys. Res., 93,* 5624, 1988.

Kantrowitz, A. R., and H. E. Petschek, MHD characteristics and shock waves, p. 148, in *Plasma Physics in Theory and Applications,* edited by W. B. Kunkel, McGraw–Hill, New York, 1966.

Kato, Y., Geomagnetic micropulsations associated with sudden changes in the magnetic field in the interplanetary space and the geomagnetic tail, *Proc. Jpn. Acad., 41,* 711, 1965.

Kato, Y., and T. Saito, Morphological study of geomagnetic pulsations, *J. Phys. Soc. Japan,* 17, 34, 1962.

Kato, Y., and T. Utsumi, Polarization of the long period geomagnetic pulsation Pc 5, *Rep. Ionos. Space Res. Jap., 18,* 214, 1964.

Kato, Y., Y. Tonegawa, and K. Tomomura, Dynamics spectral study of Pc 3–5 magnetic pulsations observed in the north polar cusp region, *Mem. Natl. Inst. Polar Res. Spec. Issue, Jpn., 36,* 58, 1985.

Kauffmann, R. L., Substorm currents: growth phase and onset, *J. Geophys. Res., 92,* 7471, 1987.

Kauffmann, R. L., and A. Konradi, Explorer 12 magnetopause observations: large-scale non-uniform motion, *J. Geophys. Res., 74,* 3609, 1969.

Kauffmann, R. L., and A. Konradi, Speed and thickness of the magnetopause, *J. Geophys. Res., 78,* 6549, 1973.

Kauffmann, R. L., and D. N. Walker, Hydromagnetic waves excited during an ssc, *J. Geophys. Res., 79,* 5187, 1974.

Kauffmann, R. L., and L. J. Cahill, Jr., The magnetopause at 5.2 RE on August 4, 1972: Magnetopause shape and structure, *J. Geophys. Res., 82,* 1572, 1977.

Kauffmann, R. L., and D. J. Larson, Electric field mapping and auroral Birkeland currents, *J. Geophys. Res., 94,* 15307, 1989.

Kawasaki, K., and G. Rostoker, Auroral motions and magnetic variations associated with the onsets of auroral substorms, *J. Geophys. Res., 84,* 7113, 1979.

Kawasaki, K., S.-I. Akasofu, F. Yasuhara, and C.-I. Meng, Storm sudden commencements and polar magnetic substorms, *J. Geophys. Res., 76,* 6781, 1971.

Keath, E. P., E. C. Roelof, C. O. Bostrom, and D. J. Williams, Fluxes of ≥ 50-keV protons and ≥ 30-keV electrons at 35 Re, 2, Morphology of flow patterns in the magnetotail, *J. Geophys. Res., 81,* 2315, 1976.

Kelley, M. C., J. A. Starr, and F. S. Mozer, Relationship between magnetospheric electric fields and the motion of auroral forms, *J. Geophys. Res., 76,* 5269, 1971.

Kelley, M. C., K. D. Baker, J. C. Ulwick, C. L. Rino, and M. J. Baron, Simultaneous rocket probe, scintillation, and incoherent scatter observations of irregularities in the auroral zone ionosphere, *Radio Science, 15,* 481, 1980.

Kelley, M. C., J. F. Vickrey, C. W. Carlson, and R. Torbert, On the origin and spatial extent of high-latitude F region irregularities, *J. Geophys. Res., 87,* 4469, 1982.

Kellogg, P. J., Flow of plasma around the earth, *J. Geophys. Res., 67,* 3805, 1962.

Kelvin, W. T., Address to the Royal Society at their anniversary meeting, Nov. 30, 1892, *Proc. Roy. Soc. London A52,* 300, 1892.

Kennel, C. F., Consequences of a Magnetospheric Plasma, *Revs. Geophys., 7,* 379, 1969.

Kennel, C. F., The Kiruna conjecture: the strong version, p. 599 in *Substorms 1: Proc. Int'l. Conf. Substorms (ICS-1), ESA SP-335,* European Space Agency, Paris, 1992.

Kennel, C. F., and H. E. Petschek, Limit on stably trapped particle fluxes, *J. Geophys. Res., 71,* 1, 1966.

Kennel, C. F., and H. E. Petschek, Van Allen belt plasma physics, p. 95 in *Proc. Second Orsay Summer Institute on Plasma Physics,* edited by G. Kalman and M. Feix, Gordon and Breach, NY, 1969.

Kennel, C. F., and M. H. Rees, Dayside auroral oval plasma density and conductivity enhancements due to magnetosheath electron precipitation, *J. Geophys. Res., 77,* 2294, 1972.

Kennel, C. F., F. V. Coroniti, and F. L. Scarf, Plasma waves in magnetotail flux ropes, *J. Geophys. Res., 91,* 1424, 1986.

Kennel, C. F., R. D. Blandsford, and P. Coppi, MHD intermediate shock discontinuities, part 1, Rankine–Hugoniot conditions, *J. Plasma Phys., 42,* 299, 1989.

Kern, J. W., Analysis of polar magnetic storms, *J. Geomagn. Geoelectr., 18,* 125, 1966.

Kettmann, G., and P. W. Daly, Detailed determination of the motion and orientation of the plasma sheet boundary layer using energetic protons on ISEE 1 and 2: waves, curves, and flapping, *J. Geophys. Res., 93,* 7376, 1988.

Kettmann, G., T. A. Fritz, and E. W. Hones, Jr., CDAW 7 revisited: further evidence for the creation of a near-earth neutral line, *J. Geophys. Res., 95,* 12045, 1990.

Khorosheva, O. V., On the space–time distribution of aurorae in the Arctic during the winter 1957–58, in *Aurorae and Airglow, No. 7,* edited by B. A. Bagarjatsky, p. 14, Acad. Sci. USSR, Moscow, 1961a.

Khorosheva, O. V., About the connection of high-latitude geomagnetic disturbances with aurorae (in Russian), *Geomagn. Aeron., 1,* 695, 1961b.

Khorosheva, O. V., Diurnal drift of the auroral closed ring (in Russian), *Geomagn. Aeron., 2,* 839, 1962.

Khorosheva, O. V., On the isochasms of aurorae, in *Aurorae and Airglow, No. 10,* edited by B. A. Bagarjatsky and V. I. Krassovsky, p. 126, Acad. Sci. USSR, Moscow, 1963.

Kidd, S. R., and G. Rostoker, Distribution of auroral surges in the evening sector, *J. Geophys. Res., 96,* 5697, 1991.

Killeen, T. L., R. A. Heelis, P. B. Hays, N. W. Spencer, and W. B. Hanson, Neutral motions in the polar thermosphere for northward interplanetary magnetic field, *Geophys. Res. Lett., 12,* 159, 1985.

Kirkwood, S., and L. Eliasson, Energetic particle precipitation in the substorm growth phase measured by EISCAT and Viking, *J. Geophys. Res., 95,* 6025, 1990.

Kirkwood, S., H. J. Opgenoorth, and J. S. Murphree, Ionospheric conductivities, electric fields, and currents associated with auroral substorms measured by the EISCAT radar, *Planet. Space Sci., 36,* 1359, 1988.

Kirsch, E., S. M. Krimigis, E. T. Sarris, R. P. Lepping, and T. P. Armstrong, Possible evidence for large, transient electric fields in the magnetotail from oppositely directed anisotropies of energetic electrons and protons, *Geophys. Res. Lett., 4,* 137, 1977.

Kirsch, E., S. M. Krimigis, E. T. Sarris, and R. P. Lepping, Detailed study on acceleration and propagation of energetic protons and electrons in the magnetotail during substorm activity, *J. Geophys. Res., 86,* 6727, 1981.

Kisabeth, J. L., and G. Rostoker, The expansive phase of magnetospheric substorms, 1, Development of the auroral electrojets and auroral arc configurations during a substorm, *J. Geophys. Res., 79,* 972, 1974.

Kistler, L. M., F. M. Ipavich, D. C. Hamilton, G. Gloeckler, B. Wilken, G. Kremser, and W. Studemann, Energy spectra of the major ion species in the ring current during geomagnetic storms, *J. Geophys. Res., 94,* 3579, 1989a.

Kistler, L. M., F. M. Ipavich, D. C. Hamilton, and G. Gloeckler, The ion energy spectra in the ring current during the geomagnetic storm of February 1986, *Adv. Space Res., 9,* 183, 1989b.

Kistler, L. M., E. Mobius, W. Baumjohann, G. Paschmann, and D. C. Hamilton, Pressure changes in the plasma sheet during substorm injections, *J. Geophys. Res., 97,* 2973, 1992.

Kitamura, T., Geomagnetic pulsations and the exosphere, Part 1, Statistical results, *Rep. Ionos. Space Res. Jpn., 17,* 67, 1963.

Kivelson, M. G., and D. J. Southwood, Resonant ULF waves: a new interpretation, *Geophys. Res. Lett., 12,* 49, 1985.

Kivelson, M. G., and D. J. Southwood, Coupling of global magnetospheric MHD eigenmodes to field line resonances, *J. Geophys. Res., 91,* 4345, 1986.

Kivelson, M. G., and D. J. Southwood, Hydromagnetic waves and the ionosphere, *Geophys. Res. Letts., 15,* 1271, 1988.

Kivelson, M. G., J. Etcheto, and J. G. Trotignon, Global compressional oscillations of the terrestrial magnetosphere: the evidence and a model, *J. Geophys. Res., 89,* 9851, 1984.

Klimas, A. J., D. N. Baker, D. A. Roberts, D. H. Fairfield, and J. Buchner, A nonlinear dynamic analogue model of substorms, *J. Geophys. Res., 97,* 12253, 1992.

Knight, L., Parallel electric fields, *Planet. Space Sci., 21,* 741, 1973.

Knott, K., Payload of the Geos scientific geostationary satellite, *ESA/ASE Sci. Tech. Rev., 1,* 173, 1975.

Knott, K., A. Durney, and K. Ogilvie, *Advances in Magnetospheric Physics with Geos-1 and Isee,* D. Reidel Publishing Co., Hingham, Mass., 1979.

Knott, K., A. Pedersen, and U. Wedeken, GEOS 2 electric field observations during a sudden commencement and subsequent substorms, *J. Geophys. Res., 90,* 1283, 1985.

Kokobun, S., Relationship of interplanetary magnetic field structure with development of substorm and storm main phase, *Planet. Space Sci., 10,* 1033, 1972.

Kokobun, S., Statistical characteristics of pc 5 waves in the magnetosphere: satellite–ground correlation, *J. Geomagn. Geoelectr., 32, suppl. II,* SII 7, 1980.

Kokobun, S., Statistical characteristics of Pc 5 waves at geostationary orbit, *J. Geomag. Geoelectr., 37,* 759, 1985.

Kokobun, S., and T. Nagata, Geomagnetic pulsation PC-5 in and near the auroral zones, *Rep. Ionos. Space Res. Japan, 19,* 158, 1965.

Kokobun, S., and R. L. McPherron, Substorm signatures at synchronous altitude, *J. Geophys. Res., 86,* 11, 265, 1981.

Kokobun, S., R. L. McPherron, and C. T. Russell, OGO 5 observations of Pc 5 waves: ground–magnetosphere correlation, *J. Geophys. Res., 81,* 5141, 1976.

Kokobun, S., M. G. Kivelson, R. L. McPherron, C. T. Russell, and H. I. West, Jr., OGO 5 observations of Pc 5 waves: particle flux modulation, *J. Geophys. Res., 82,* 2774, 1977.

Kokobun, S., K. N. Erickson, T. A. Fritz, and R. L. McPherron, Local time asymmetry of Pc 4–5 pulsations and associated particle modulations at synchronous orbit, *J. Geophys. Res., 94,* 6607, 1989.

Konradi, A., Electron and proton fluxes in the tail of the magnetosphere, *J. Geophys. Res., 71,* 2317, 1966.

Koskinen, H. E. J., T. I. Pulkinen, R. J. Pellinen, T. Bosinger, D. N. Baker, and R. E. Lopez, Characteristics of pseudobreakups, p. 111, in *Substorms 1, Proc. Int'l. Conf. on Substorms (ICS-1),* ESA SP-335, European Space Agency, Paris, 1992.

Kovrazhkin, R. A., J. M. Bosqued, L. M. Zelenyi, and N. V. Jorjio, Observation of evidence of reconnection and plasma acceleration at a distance of about 5 x 10E5 km in the tail of the earth's magnetosphere, *JETP Lett.,* Engl. translation, *45,* 479, 1987.

Kozelova, T. V., Peculiarities of the development of various intensity substorms from ground-based and satellite data, p. 343 in *Substorms 1: Proc. Int'l. Conf. Substorms (ICS-1), ESA SP-335,* European Space Agency, Paris, 1992.

Kozelova, T., and V. B. Lyatskiy, A longitudinal current in front of a westward traveling surge, *Geomagn. Aeron.,* Engl. Transl., *24,* 191, 1984.

Kozelova, T. V., M. I. Pudovkin, and J.-P. Treilhou, Development of the auroral bulge and dipolization at 6.6 Re, p. 347 in *Substorms 1: Proc. Int'l. Conf. Substorms (ICS-1), ESA SP-335,* European Space Agency, Paris, 1992.

Krauss-Verban, D., and V. L. Patel, Numerical analysis of the coupled hydromagnetic wave equations in the magnetosphere, *J. Geophys. Res., 93,* 9721, 1988.

Kremser, G., and R. Lundin, Average spatial distributions of energetic particles in the midlatitude cusp/cleft region observed by *Viking, J. Geophys. Res., 95,* 5753, 1990.

Kremser, G., J. Bjordal, L. P. Block, K. Broenstad, M. Havag, I. B. Iversen, J. Kangas, A. Korth, M. M. Madsen, J. Niskanen, W. Riedler, J. Stadsnes, P. Tanskanen, K. M. Torkar, and S. L. Ullaland, Coordinated balloon–satellite observations of energetic particles at the onset of a magnetospheric substorm, *J. Geophys. Res., 87,* 4445, 1982.

Kremser, G., A. Korth, S. Ullaland, J. Stadsnes, W. Baumjohann, L. Block, K. M. Torkar, W. Riedler, B. Aparicio, P. Tanskanen, I. B. Iversen, N. Cornilleau-Wehrlin, J. Solomon, and E. Amata, Energetic electron precipitation during a magnetospheric substorm and its relationship to wave–particle interaction, *J. Geophys. Res., 91,* 5711, 1986.

Kremser, G., W. Studemann, B. Wilken, G. Gloeckler, D. C. Hamilton, and F. M. Ipavich, Average spatial distributions of energetic O^+, O^{2+}, O^{6+}, and C^{6+} ions in the magnetosphere observed by AMPTE CCE, *J. Geophys. Res., 92,* 4459, 1987.

Kremser, G., P. Tanskanen, S. Ullaland, S. Perraut, A. Roux, and A. Korth, Influence of storm sudden commencements on magnetospheric substorms, p. 291, in *Substorms 1, Proc. Int'l. Conf. on Substorms (ICS-1), ESA SP-335,* European Space Agency, Paris, 1992.

Krimigis, S. M., and E. T. Sarris, Energetic particle bursts in the earth's magnetotail, p. 599, in *Dynamics of the Magnetosphere,* edited by S.-I. Akasofu, D. Reidel, Hingham, Mass., 1979.

Krimigis, S. M., J. W. Kohl, and T. P. Armstrong, The magnetospheric contribution to the quit-time low energy nucleon spectrum in the vicinity of earth, *Geophys. Res. Lett., 3,* 457, 1975.

Krimigis, S. M., D. Venkatesan, J. C. Barichello, and E. T. Sarris, Simultaneous measurements of energetic protons and electrons in the distant magnetosheath, magnetotail, and upstream in the solar wind, *Geophys. Res. Lett., 5,* 961, 1978.

Kroehl, H. W., and Y. Kamide, High-latitude indices of electric and magnetic variability during the CDAW 6 intervals, *J. Geophys. Res., 90,* 1367, 1985.

Krukonis, A. P., and J. A. Whalen, Occurrence and lifetimes of discrete auroras near midnight, *J. Geophys. Res., 85,* 119, 1980.

Kruskal, M., and M. Schwarzschild, Some instabilities of a completely ionized plasma, *Proc. Roy. Soc. London, A233,* 348, 1953.

Kunkel, W., B. J. Baumjohann, T. Untiedt, and R. W. Greenwald, Electric fields and currents at the Harang discontinuity: A case study, *J. Geophys., 59,* 73, 1986.

Kuppers, F., J. Untiedt, W. Baumjohann, K. Lange, and A. G. Jones, A two-dimensional magnetometer array for ground-based observations of auroral zone electric currents during the International Magnetospheric Study (IMS), *J. Geophys., 46,* 429, 1979.

Kurth, W. S., M. M. Baumback, and D. A. Gurnett, Direction–finding measurements of auroral kilometric radiation, *J. Geophys. Res., 80,* 2764, 1975.

Kuwashima, M., and T. Saito, Spectral characteristics of magnetic Pi 2 pulsations in the auroral region and lower latitudes, *J. Geophys. Res., 86,* 4686, 1981.

Kuznetsov, B. M., and O. A. Troshichev, On the nature of polar cap magnetic activity during undisturbed periods, *Planet. Space Sci., 25,* 15, 1977.

Labelle, J., R. J. Sica, C. Kletzing, G. D. Earle, M. C. Kelley, D. Lummerzheim, R. B. Torbert, K. D. Baker, and G. Berg, Ionization from soft electron precipitation in the auroral F region, *J. Geophys. Res., 94,* 3791, 1989.

La Belle-Hamer, A. L., Z. F. Fu, and L. C. Lee, A mechanism for patchy reconnection at the dayside magnetopause, *Geophys. Res. Lett., 15,* 152, 1988.

Lanzerotti, L., and C. G. Maclennan, Hydromagnetic waves associated with possible flux transfer events, *Astrophys. Space Sci., 144,* 279, 1988.

Lanzerotti, L. J., H. Fukunishi, and L. Chen, ULF pulsation evidence of the plasmapause, 3, Interpretation of polarization and spectral amplitude studies of Pc 3 and Pc 4 pulsations near L = 4, *J. Geophys. Res., 79,* 4648, 1974.

Lanzerotti, L. J., S. M. Krimigis, C. O. Bostrom, W. I. Axford, R. P. Lepping, and N. F. Ness, Measurements of plasma flow at the dawn magnetopause by Voyager 1, *J. Geophys. Res., 84,* 6483, 1979.

Lanzerotti, L. J., L. C. Lee, C. G. Maclennan, A. Wolfe, and L. V. Medford, Possible evidence of flux transfer events in the polar ionosphere, *Geophys. Res. Lett., 13,* 1089, 1986.

Lanzerotti, L. J., R. D. Hunsucker, D. Rice, L.-C. Lee, A. Wolfe, C. G. MacLennan, and L. V. Medford, Ionosphere and ground-based response to field-aligned currents near the magnetospheric cusp region, *J. Geophys. Res., 92,* 7739, 1987.

Lassen, K., and C. Danielson, Quiet time pattern of auroral arcs for different directions of the interplanetary magnetic field in the Y-Z plane, *J. Geophys. Res., 83,* 5277, 1978.

Lassen, K., C. Danielson, and C.-I. Meng, Average configuration of the quiet auroral oval, *Planet. Space Sci., 36,* 791, 1988.

Laval, G., R. Pellat, and M. Vuillemin, Instabilites electromagnetiques des plasmas sans collisions, *Plasma Phys. Controlled Nucl. Fusion Res., Proc. Intl. Conf. 2nd, 2,* 259, 1966.

LeBoeuf, J. N., T. Tajima, C. F. Kennel, and J. M. Dawson, Global simulations of the time-dependent magnetosphere, *Geophys. Res. Lett., 5,* 609, 1978.

LeBoeuf, J. N., T. Tajima, C. F. Kennel, and J. M. Dawson, Global simulations of the three-dimensional magnetosphere, *Geophys. Res. Lett., 8,* 257, 1981.

LeBoeuf, J. N., T. Tajima, and J. M. Dawson, Dynamic magnetic X-points, *Phys. Fluids, 25,* 784, 1982.

Lee, D.-H., and R. L. Lysak, Magnetospheric ULF wave coupling in the dipole model: initial results, *J. Geophys. Res., 94,* 17097, 1989.

Lee, D.-H., and R. L. Lysak, Impulsive excitation of ULF waves in the three-dimensional; dipole model: the initial results, *J. Geophys. Res., 96,* 3479, 1991.

Lee, L. C., Ion two-stream and modified two-stream instabilitties in the magnetic neutral sheet, *Geophys. Res. Lett., 9,* 1159, 1982.

Lee, L. C., Time-dependent magnetic reconnection: two- and three-dimensional MHD simulations, *Comput. Phys. Commun., 59,* 163, 1990.

Lee, L. C., and Z. F. Fu, A theory of magnetic flux transfer at earth's magnetopause, *Geophys. Res. Lett., 12,* 105, 1985.

Lee, L. C., and S.-I. Akasofu, Entry of solar wind particles into earth's magnetosphere, *J. Geophys. Res., 94,* 12015, 1989.

Lee, L. C., R. K. Albano, and J. R. Kan, Kelvin–Helmholtz instability in the magnetopause boundary layer region, *J. Geophys. Res., 86,* 54, 1981.

Lee, L. C., Z. F. Fu, and S.-I. Akasofu, A simulation study of forced reconnection processes and magnetospheric storms and substorms, *J. Geophys. Res., 90,* 10896, 1985.

Lee, L. C., M. Yan, and J. G. Hawkins, A study of slow mode structures in the dayside magnetosheath, *Geophys. Res. Lett., 18,* 381, 1991.

Lees, L., Interaction between the solar plasma wind and the geomagnetic cavity, *AIAA J., 2,* 1576, 1964.

Lemaire, J., Impulsive penetration of filamentary plasma element into the magnetosphere of earth and Jupiter, *Planet. Space Sci., 25,* 887, 1977.

Lemaire, J., and M. Roth, Penetration of solar wind plasma elements into the magnetosphere, *J. Atmos. Terr. Phys., 40,* 331, 1978.

Lembege, B., and R. Pellat, Stability of a thick two-dimensional quasi-neutral sheet, *Phys. Fluids, 25,* 1995, 1982.

Lennartsson, W., Energetic (0.1–16 keV/e) magnetospheric ion composition at different levels of solar F10. 7, *J. Geophys. Res., 94,* 3600, 1989.

Lennartsson, W., and R. D. Sharp, A comparison of the 0.1–17 keV/e ion compoisition in the near equatorial magnetosphere between quiet and disturbed conditions, *J. Geophys. Res., 87,* 6109, 1982.

Lennartsson, W., and E. G. Shelley, Survey of 0.1–16 keV/e plasma sheet ion composition, *J. Geophys. Res., 91,* 3061, 1986.

Lennartsson, W., R. D. Sharp, and R. D. Zwickl, Substorm effects on the plasma sheet ion composition on March 22, 1979 (CDAW 6), *J. Geophys. Res., 90,* 1243, 1985.

Lester, M., W. J. Hughes, and H. J. Singer, Longitudinal structure in Pi 2 pulsations and the substorm current wedge, *J. Geophys. Res., 89,* 5489, 1984.

Levitin, A. E., R. G. Afonina, B. A. Belov, and Y. I. Feldstein, Geomagnetic variation and field–aligned currents at northern high latitudes, and their relations to solar wind parameters, *Philosoph. Trans. R. Soc. London Ser. A, 304,* 253, 1982.

Levy, R. H., H. E. Petschek, and G. L. Siscoe, Aerodynamic aspects of the magnetospheric flow, *J. AIAA, 2,* 2066, 1964.

Lewis, R. V., P. J. S. Williams, T. S. Virdi, T. K. Yeoman, and M. Lester, EISCAT measurements of of bursts in plasma velocity during substorm activity, p. 125 in *Substorms 1, Proc. First Int'l. Conf. on Substorms, ESA SP-335,* Paris, 1992.

Lezniak, T. W., and J. R. Winckler, Styructure of the magnetopause at 6.6 RE in terms of 50- to 150-keV electrons, *J. Geophys. Res., 73,* 5733, 1968.

Lezniak, T. W., and J. R. Winckler, Experimental study of magnetospheric motions and the acceleration of energetic electrons during substorms, *J. Geophys. Res., 75,* 7075, 1970.

Lin, C. P., and L. J. Cahill, Jr., Pi 2 micropulsations in the magnetosphere, *Planet. Space Sci., 23,* 693, 1975.

Lin, C. S., and R. A. Hoffman, Observations of inverted-V electron precipitation, *Space Sci. Rev., 33,* 415, 1982.

Lin, N., M. J. Engebretson, R. L. McPherron, M. G. Kivelson, W. Baumjohann, H. Luehr, T. A. Potemra, B. J. Anderson, and L. J. Zanetti, A comparison of ULF fluctuations in the solar wind, magnetosheath, and dayside magnetosphere, 2, Field and plasma conditions in the magnetosheath, *J. Geophys. Res., 96,* 3455, 1991a.

Lin, N., R. L. McPherron, M. G. Kivelson, and R. J. Walker, Multipoint reconnection in the near-earth magnetotail: CDAW 6 observations of energetic particles and magnetic field, *J. Geophys. Res., 96,* 19427, 1991b.

Lin, R. P., Observations of lunar shadowing of energetic particles, *J. Geophys. Res., 73,* 3066, 1968.

Lin, R. P., and K. A. Anderson, Evidence for connection of geomagnetic tail lines to the interplanetary magnetic field, *J. Geophys. Res., 71,* 4213, 1966.

Lin, R. P., K. A. Anderson, and T. L. Cline, Detection of interplanetary electrons from 18 keV to 1. 8 MeV during solar quiet times, *Phys. Rev. Lett., 29,* 1035, 1972.

Lin, R. P., K. A. Anderson, J. E. McKoy, and C. T. Russell, Observations of magnetic merging and the formation of the plasma sheet in the earth's magnetotail, *J. Geophys. Res., 82,* 2761, 1977.

Lin, Y., L. C. Lee, and C. F. Kennel, The role of intermediate shocks in magnetic reconnection, *Geophys. Res. Lett., 19,* 229, 1992.

Lindemann, F. A., Note on the theory of magnetic storms, *Phil. Mag., 38,* 669, 1919.

Link, F., On the history of the aurora borealis, p. 297 in *Vistas in Astronomy, Vol. 9,* edited by A. Beer, Pergamon Press, Oxford, 1957.

Liu, W. W., and T. W. Hill, Velocity filter effects and dynamics of distant magnetotail, *Planet. Space Sci., 34,* 197, 1985.

Lockwood, M., On flow-reversal boundaries and transpolar voltage in average models of high-latitude convection, *Planet. Space Sci., 39,* 397, 1991a.

Lockwood, M., The excitation of ionospheric convection, *J. Atm. Terr. Phys., 53,* 177, 1991b.

Lockwood, M., and M. F. Smith, Reply to Newell, *Geophys. Res. Lett., 17,* 305, 1990.

Lockwood, M., and M. F. Smith, The variation of the reconnection rate at the dayside magnetopause and cusp ion precipitation, *J. Geophys. Res., 97,* 14841, 1992.

Lockwood, M., A. P. van Eyken, B. J. I. Bromage, D. M. Willis, and S. W. H. Cowley, Eastward propagation of a plasma convection enhancement following a southward turning of the interplanetary magnetic field, *Geophys. Res. Lett., 13,* 72, 1986.

Lockwood, M., S. W. H. Cowley, H. Todd, D. M. Willis, and C. R. Clauer, Ion flows and heating at a contracting polar cap boundary, *Planet Space Sci., 36,* 1229, 1988.

Lockwood, M., P. E. Sandholt, and S. W. H. Cowley, Dayside auroral activity and magnetic flux transfer from the solar wind, *Geophys. Res. Lett., 16,* 33, 1989a.

Lockwood, M., P. E. Sandholt, S. W. H. Cowley, and T. Oguti, Interplanetary magnetic field control of dayside auroral activity and the transfer of momentum across the dayside magnetopause, *Planet. Space Sci., 37,* 1347, 1989b.

Lockwood, M., S. W. H. Cowley, and M. P. Freeman, The excitation of plasma convection in the high-latitude ionosphere, *J. Geophys. Res., 95,* 7961, 1990a.

Lockwood, M., P. E. Sandholt, A. D. Farmer, S. W. H. Cowley, B. Lybekk, and V. N. Davda, Auroral and plasma flow transients at magnetic noon, *Planet.. Space Sci., 38,* 973, 1990b.

Lockwood, M., S. W. H. Cowley, P. E. Sandholt, and R. P. Lepping, The ionospheric signatures of flux transfer events and solar wind dynamic pressure changes, *J. Geophys. Res., 95,* 17113, 1990c.

Lodge, O., Sunspots, magnetic storms, comet tails, atmospheric electricity and aurorae, *The Electrician, 46,* 249, 1900.

Loomis, E., The great auroral exhibition, August 28th to September 4th, 1859, *Amer. J. Sci. Art., 30,* 49, 1860.

Lopez, R. E., and A. T. Y. Lui, A multisatellite case study of the expansion of a substorm current wedge in the near-earth magnetotail, *J. Geophys. Res., 95,* 8009, 1990.

Lopez, R. E., D. G. Sibeck, A. T. Y. Lui, K. Takahashi, R. W. McEntire, T. A. Potemra, and D. Klumpar, Substorm variations in the magnitude of the magnetic field: AMPTE/CCE observations, *J. Geophys. Res., 93,* 14444, 1988a.

Lopez, R. E., A. T. Y. Lui, D. G. Sibeck, R. W. McEntire, L. J. Zanetti, T. A. Potemra, and S. M. Krimigis, The longitudinal and radial distribution of magnetic reconfigurations in the near-earth magnetotail as observed by AMPTE/CCE, *J. Geophys. Res., 93,* 997, 1988b.

Lopez, R. E., D. N. Baker, A. T. Y. Lui, D. G. Sibeck, R. D. Belian, R. W. McEntire, T. A. Potemra, and S. M. Krimigis, The radial and longitudinal propagation characteristics of substorm injections, *Adv. Space Res., 8,* 91, 1988c.

Lopez, R. E., A. T. Y. Lui, D. G. Sibeck, K. Takahashi, R. W. McEntire, L. J. Zanetti, and S. M. Krimigis, On the relationship between the energetic particle flux morphology and the change in the magnetic field magnitude during substorms, *J. Geophys. Res., 94,* 17105, 1989.

Lopez, R. E., R. W. McEntire, T. A. Potemra, D. N. Baker, and R. D. Belian, A possible case of radially antisunward propagating substorm onset in the near-earth magnetotail, *Planet. Space Sci., 38,* 771, 1990a.

Lopez, R. E., A. T. Y. Lui, R. W. McEntire, T. A. Potemra, and S. M. Krimigis, A statistical study of magnetic field magnitude changes during substorms in the near-earth tail, *Adv. Space Res., 10,* 37, 1990b.

Lopez, R. E., H. E. Spence, and C.-I. Meng, DMSP F7 observations of a substorm field-aligned current, *J. Geophys. Res., 96,* 19409, 1991.

Lu, G., P. H. Reiff, J. L. Burch, and J. D. Winningham, On the auroral current–voltage relationship, *J. Geophys. Res., 96,* 3523, 1991.

Luhr, H., S. Thurey, and N. Klocker, The EISCAT–magnetometer cross, *Geophys. Surv., 6,* 305, 1984.

Lui, A. T. Y., Estimates of current changes in the geomagnetotail associated with a substorm, *Geophys. Res. Lett., 5,* 853, 1978.

Lui, A. T. Y., and C. D. Anger, A uniform belt of diffuse auroral emission seen by the ISIS 2 scanning photometer, *Planet. Space Sci., 21,* 799, 1973.

Lui, A. T. Y., and J. R. Burrows, On the location of auroral arcs near substorm onsets, *J. Geophys. Res., 83,* 3342, 1978.

Lui, A. T. Y., and C.-I. Meng, Relevance of southward magnetic fields in the neutral sheet to anisotropic distribution of energetic electrons and substorm activity, *J. Geophys. Res., 84,* 5817, 1979.

Lui, A. T. Y., and S. M. Krimigis, Earthward transport of energetic protons in the earth's plasma sheet, *Geophys. Res. Lett., 8,* 527, 1981.

Lui, A. T. Y., and. G. Sibeck, Dayside auroral activities and their implications for impulsive entry processes in the dayside magnetopshere, *J. Atm. Terr. Phys., 53,* 219, 1991.

Lui, A. T. Y., P. Perreault, S.-I. Akasofu, and C. D. Anger, The diffuse aurora, *Planet. Space Sci., 21,* 857, 1973.

Lui, A. T. Y., C. D. Anger, and S.-I Akasofu, The equatorward boundary of the diffuse aurora and auroral substorms as seen by the ISIS 2 auroral scanning photometer, *J. Geophys. Res., 80,* 3603, 1975a.

Lui, A. T. Y., E. W. Hones, Jr., D. Venkatesan, S.-I. Akasofu, and S. J. Bame, Distribution of plasma sheet thinning and recovery events in the magnetotail survey by the IMP 6 satellite, *J. Geophys. Res., 80,* 1975b.

Lui, A. T. Y., S.-I. Akasofu, E. W. Hones, Jr., S. J. Bame, and C. E. McIlwain, Observation of the plasma sheet during a contracted oval substorm in a prolonged quiet period, *J. Geophys. Res., 81,* 1415, 1976.

Lui, A. T. Y., E. W. Hones, Jr., F. Yasuhara, S.-I. Akasofu, and S. J. Bame, Magnetotail plasma flow during plasma sheet expansions: VELA 5 and 6 and IMP 6 observations, *J. Geophys. Res., 82,* 1235, 1977a.

Lui, A. T. Y., L. A. Frank, K. L. Ackerson, C.-I. Meng, and S.-I. Akasofu, Systematic study of plasma flow during plasma sheet thinning, *J. Geophys. Res., 82,* 4815, 1977b.

Lui, A. T. Y., S. M. Krimigis, and T. P. Armstrong, Association between magnetic field fluctuations and energetic particle bursts in the earth's magnetotail, *J. Geophys. Res., 87,* 8315, 1982.

Lui, A. T., D. J. Williams, T. E. Eastman, L. A. Frank, and S.-I. Akasofu, Streaming reversal of energetic particles in the magnetotail during a substorm, *J. Geophys. Res., 89,* 1540, 1984.

Lui, A. T. Y., D. Venkatesan, G. Rostoker, J. S. Murphree, C. D. Anger, L. L. Cogger, and T. A. Potemra, Dayside auroral intensifications during an auroral substorm, *Geophys. Res. Lett., 14,* 425, 1987.

Lui, A. T. Y., D. Venkatesan, and J. S. Murphree, Auroral bright spots on the dayside oval, *J. Geophys. Res., 94,* 5515, 1989.

Lui, A. T. Y., R. E. Lopez, B. J. Anderson, K. Takahashi, L. J. Zanetti, R. W. McEntire, T. A. Potemra, D. M. Klumpar, E. M. Greene, R. Strangeway, Current disruptions in the near-earth neutral sheet region, submitted, *J. Geophys. Res., 96,* 1991.

Lundin, R., Acceleration/heating of plasma on auroral field lines; preliminary results from the *Viking* satellite, *Ann. Geophys., 6,* 143, 1988.

Lundin, R., and E. Dubinin, Solar wind energy transfer regions inside the dayside magnetopause, 1, Evidence for magnetosheath plasma penetration, *Planet. Space Sci., 32,* 745, 1984.

Lundin, R., and E. Dubinin, Solar wind energy transfer regions inside the dayside magnetopause, accelerated heavy ions as traces for MHD-like processes in the dayside boundary layer, *Planet. Space Sci., 33,* 891, 1985.

Lundin, R., K. Stasiewiecz, and B. Hultquist, On the interpretation of different flow vectors of different ion species in the magnetospheric boundary layer, *J. Geophys. Res., 92,* 3214, 1987.

Lyon, J. G., S. H. Brecht, J. D. Huba, J. A. Fedder, and P. J. Palmadesso, Computer simulation of a geomagnetic substorm, *Phys. Rev. Lett., 46,* 1038, 1981.

Lyons, L. R., Generation of large-scale regions of auroral currents, electric potentials, and precipitation by divergence at the convection electric fields, *J. Geophys. Res., 85,* 17, 1980.

Lyons, L. R., Discrete aurora as the direct result of an inferred high-altitude generating potential distribution, *J. Geophys. Res., 86,* 1, 1981.

Lyons, L. R., A simple model for polar cap convection and generation of auroras, *J. Geophys. Res., 90,* 1561, 1985.

Lyons, L. R., and T. W. Speiser, Evidence for current sheet acceleration in the geomagnetic tail, *J. Geophys. Res., 87,* 2276, 1982.

Lyons, L. R., D. S. Evans, and R. Lundin, An observed relation between magnetic field-aligned electric field and downward electron energy fluxes in the vicinity of auroral forms, *J. Geophys. Res., 84,* 457, 1979.

Lyons, L. R., J. F. Fennell, and A. L. Vampola, A general association between discrete auroras and ion precipitation from the tail, *J. Geophys. Res., 93,* 12932, 1988.

Lyons, L. R., O. de la Beaujardiere, G. Rostoker, J. S. Murphree, and E. Friis-Christensen, Analysis of substorm expansion and surge development, *J. Geophys. Res., 95,* 10575, 1990.

Maezawa, K., Magnetotail boundary motion associated with geomagnetic substorms, *J. Geophys. Res., 80,* 3543, 1975.

Maezawa, K., Magnetospheric convection induced by positive and negative z components of the interplanetary magnetic field: quantitative analysis using polar cap magnetic records, *J. Geophys. Res., 81,* 2289, 1976.

Maezawa, K., Statistical study of the dependence of geomagnetic activity on solar wind parameters, in *Quantitative Modeling of Magnetospheric Processes, Geophys. Monogr., Ser., Vol. 21,* edited by W. P. Olson, p. 436, AGU, Washington, DC, 1979.

Maezawa, K., and T. Murayama, Solar wind velocity effects on the auroral zone magnetospheric disturbances, in *Solar Wind–Magnetosphere Coupling,* edited by Y. Kamide and J. A. Slavin, p. 59, D. Reidel, Hingham, Mass., 1986.

Maggs, J. E., and T. N. Davis, Measurements of the thicknesses of auroral structures, *Planet. Space Sci., 16,* 205, 1968.

Makita, K., and C.-I. Meng, The shift of the auroral electron precipitation boundaries in the dawn–dusk sector in association with geomagnetic activity and interplanetary magnetic field, *J. Geophys. Res., 88,* 7967, 1983.

Marklund, G., Auroral arc classification scheme based on the observed arc-associated electric field, *Planet. Space Sci., 32,* 193, 1984.

Marklund, G., I. Sandahl, and H. Opgenoorth, A study of the dynamics of a discrete auroral arc, *Planet. Space Sci., 30,* 179, 1982.

Marshall, J. A., J. L. Burch, J. R. Kan, and J. A. Slavin, DE 1 observations of return current regions in the nightside auroral oval, *J. Geophys. Res., 93,* 14542, 1988.

Martyn, D. F., The theory of magnetic storms and auroras, *Nature, 167,* 92, 1951.

Maunder, E. W., *Mon. Not. Roy. Astron. Soc., 50,* 251, 1890.

Mawson, D., Records of the *Aurora Polaris, Australas. Antarct. Exped. 1911–1914, Sci. Rep., Ser. D.,* Vol. 2, Pt. 1, p. 11, 1925.

Mayaud, P. N., *Derivation, Meaning, and Use of Geomagnetic Indices, Geophysical Monogr. Ser.,* Vol. 22, 154 pp., AGU, Washington, DC, 1980.

Maynard, N. C., Electric field measurements across the Harang discontinuity, *J. Geophys. Res., 79,* 4620, 1974.

Maynard, N. C., Structure in the dc and ac electric fields associated with the dayside cusp region, p. 305 in *The Polar Cusp,* edited by J. A. Holtet and A. Egeland, D. Reidel, Hingham, Mass., 1985.

Maynard, N. C., T. L. Aggson, E. M. Basinska, W. J. Burke, P. Craven, W. K. Peterson, M. Sugiura, and D. R. Weimer, Magnetospheric boundary dynamics: DE 1 and DE 2 observations near the magnetopause and cusp, *J. Geophys. Res., 96,* 3503, 1991.

Mazaudier, C., Electric currents above Saint-Santin, 3, A preliminary study of disturbances: June 6, 1978, March 22, 1979; March 23, 1979, *J. Geophys. Res., 90,* 1355, 1985.

McCoy, J. E., R. P. Lin, R. E. McGuire, L. M. Chase, and K. A. Anderson, Magnetotail electric fields observed from lunar orbit, *J. Geophys. Res., 80,* 3217, 1975.

McDiarmid, I. B., and J. R. Burrows, Electron fluxes at 1000 kilometers associated with the tail of the magnetosphere, *J. Geophys. Res., 70,* 3031, 1965.

McDiarmid, I. B., E. E. Budzinski, M. D. Wilson, and J. R. Burrows, Reverse polarity field-aligned currents at high latitudes, *J. Geophys. Res., 82,* 1513, 1977.

McHenry, M. A., and C. R. Clauer, Modeled ground magnetic signatures of flux transfer events, *J. Geophys. Res., 92,* 11231, 1987.

McHenry, M. A., C. R. Clauer, E. Friis-Christensen, P. T. Newell, and J. D. Kelly, Ground observations of magnetospheric boundary layer phenomena, *J. Geophys. Res., 95,* 14995, 1990.

McIlwain, C. E., Coordinates for mapping the distribution of magnetically trapped particles, *J. Geophys. Res., 66,* 3681, 1961.

McIlwain, C. E., Substorm injection boundaries, in *Magnetospheric Physics,* edited by B. M. McCormac, p. 143, D. Reidel, Hingham, Mass., 1974.

McPherron, R. L., Growth phase of magnetospheric substorms, *J. Geophys. Res., 75,* 5592, 1970.

McPherron, R. L., Substorm-related changes in the geomagnetic tail: the growth phase, *Planet. Space Sci., 20,* 1521, 1972.

McPherron, R. L., Magnetospheric substorms, *Revs. Geophys., 17,* 657, 1979.

McPherron, R. L., Substorm-associated micropulsations at synchronous orbit, *J. Geomag. Geoelectr., 32,* Suppl. II, SII 57, 1980.

McPherron, R. L., Physical processes producing magnetospheric substorms and magnetic storms, p. 593, in *Geomagnetism,* Vol. 4, edited by J. A. Jacobs, Academic Press, London, 1991.

McPherron, R. L., and J. N. Barfield, A seasonal change in the effects of field-aligned currents at synchronous orbit, *J. Geophys. Res., 85,* 6746, 1980.

McPherron, R. L., and R. H. Manka, Dynamics of the 1054 UT March 22, 1979, substorm event: CDAW 6, *J. Geophys. Res., 90,* 1175, 1985.

McPherron, R. L., C. T. Russell, and P. J. Coleman, Jr., Fluctuating magnetic fields in the magnetosphere, *Space Sci. Revs., 13,* 411, 1972.

McPherron, R. L., C. T. Russell, and M. P. Aubry, Satellite studies of the magnetospheric substorms on August 16, 1968, 9, Phenomenological model for substorms, *J. Geophys. Res., 78,* 3131, 1973.

McPherron, R. L., P. J. Coleman, Jr., and R. C. Snare, ATS 6 UCLA fluxgate magnetometer, *IEEE Trans. Aerosp. Electron. Syst., AES-11,* 1110, 1975.

McPherron, R. L., A. Nishida, and C. T. Russell, Is near-earth current sheet thinning the cause of auroral substorm onset?, Paper presented at the conference on Quantitative Modeling of Magnetosphere–Ionosphere Coupling Processes, Kyoto Sangyo University, Kyoto, Japan, March 9–13, 1987.

McPherron, R. L., D. N. Baker, L. F. Bargatze, C. R. Clauer, and R. E. Holzer, IMF control of geomagnetic activity, *Adv. Space Res., 8,* 71, 1988.

Mead, G. D., Deformation of the geomagnetic field by the solar wind, *J. Geophys. Res., 69,* 1181, 1964.

Mead, G. D., and D. B. Beard, Shape of the geomagnetic field solar wind boundary, *J. Geophys. Res., 69,* 1169, 1964.

Mead, G. D., and D. H. Fairfield, A quantitative magnetospheric model derived from spacecraft magnetometer data, *J. Geophys. Res., 80,* 523, 1975.

Meadows, A. J., *Early Solar Physics,* p. 47, Pergamon Press, Oxford, 1966.

Meinel, A. B., Hydrogen lines in aurora, *Astrophys. J., 111,* 555, 1950.

Mellott, M. M., W. Calvert, R. L. Huff, D. A. Gurnett, and S. D. Shawhan, DE-1 observations of auroral kilometric radiation in the ordinary and extraordinary wave modes, *Geophys. Res. Lett., 11,* 1188, 1984.

Mende, S. B., and E. G. Shelley, Coordinated ATS-5 electron flux and simultaneous auroral observations, *J. Geophys. Res., 81,* 97, 1976.

Mende, S. B., R. D. Sharp, E. G. Shelley, G. Haerendel, and E. W. Hones, Jr., Coordinated observations of the magnetosphere: The development of a substorm, *J. Geophys. Res., 77,* 4682, 1972.

Mende, S. B., J. H. Doolittle, R. M. Robinson, R. P. Vondrak, and F. J. Rich, Plasma drifts associated with a system of sun-aligned arcs in the polar cap, *J. Geophys. Res., 93,* 256, 1988.

Meng, C.-I., The auroral electron precipitation during extremely quiet geomagnetic conditions, *J. Geophys. Res., 86,* 4607, 1981.

Meng, C.-I., and K. A. Anderson, A layer of energetic electrons (> 40 keV) near the magnetopause, *J. Geophys. Res., 75,* 1827, 1970.

Meng, C.-I., and K. A. Anderson, Charatcteristics of the magnetopause energetic electron layer, *J. Geophys. Res., 80,* 4237, 1975.

Meng, C.-I., and H. W. Kroehl, Intense uniform precipitation of low energy electrons over the polar cap, *J. Geophys. Res., 82,* 2305, 1977.

Meng, C.-I., B. Mauk, and C. E. McIlwain, Electron precipitation of evening diffuse aurora and its conjugate electron fluxes near the magnetosphere equator, *J. Geophys. Res., 84,* 2545, 1979.

Meng, C.-I., and B. H. Mauk, Global auroral morphology: quadrennial report to the I.U.G.G. on U.S. contributions, in *U.S. National Report to International Union of Geodesy and Geophysics, 1987–98, Reviews of Geophysics Supplement,* p. 1028, 1991.

Menietti, J. D., and J. L. Burch, DE 1 observations of the theta aurora plasma source regions and Birkeland current charge carriers, *J. Geophys. Res., 92,* 7503, 1987.

Menietti, J. D., and J. L. Burch, Spatial extent of the plasma injection region in the cusp–magnetosheath interface, *J. Geophys. Res., 93,* 105, 1988.

Menvielle, M., and A. Berthelier, The K-derived planetary indices: description and availability, *Rev. Geophys., 29,* 415, 1991.

Midgley, J. E., and L. Davis, Jr., Calculation by a moment technique of the perturbation of the geomagnetic field by the solar wind, *J. Geophys. Res., 68,* 5111, 1963.

Mihalov, J. D., and C. P. Sonett, The cislunar geomagnetic tail gradient in 1967, *J. Geophys. Res., 73,* 6837, 1968.

Mihalov, J. D., C. P. Sonett, and D. S. Colburn, Reconnection and noise in the geomagnetic tail, *Cosmic Electrodyn., 1,* 178, 1970.

Mishin, V. M., The magnetogram inversion technique and some applications, *Space Sci. Rev., 53,* 83, 1990.

Mishin, V. M., T. I. Saifudinova, A. D. Barzhapov, D. Sh. Shirapov, and S. B. Lunyushkin, The magneospheric substorm scenario with two active phases, p. 297, in *Substorms 1: Proc. Int'l. Conf. Substorms (ICS-1), ESA SP-335,* European Space Agency, Paris, 1992a.

Mishin, V., J. Woch, L. Eliasson, T. Saifudinova, A Bazharzapov, D. Shirapov, and S. Lunyushkin, Substorm scenario with two active phases: a study of CDAW ac events, p. 383 in *Substorms 1: Proc. Int'l. Conf. Substorms (ICS-1), ESA SP-335,* European Space Agency, Paris, 1992b.

Mitchell, D. G., F. Kutchko, D. J. Williams, T. E. Eastman, L. A. Frank, and C. T. Russell, An extended boundary layer on the dawn and dusk flanks of the magnetosphere, *J. Geophys. Res., 92,* 7394, 1987.

Mitchell, D. G., D. J. Williams, C. Y. Huang, L. A. Frank, and C. T. Russell, Current carriers in the near-earth cross-tail current sheet during substorm growth phase, *Geophys. Res. Lett., 17,* 583, 1990.

Miura, A., Anomalous transport by magnetohydrodynamic Kelvin–Helmholtz instabilities in the solar-wind magnetosphere interaction, *J. Geophys. Res., 89,* 801, 1984.

Mizera, P. F., and J. F. Fennell, Satellite observations of polar, magnetotail lobe, and interplanetary electrons at low energies, *Rev. Geophys., 16,* 147, 1978.

Mizera, P. F., and D. S. Evans, Simultaneous measurements of polar cap electrons in opposite hemispheres, *J. Geophys. Res., 91,* 9007, 1986.

Mizera, P. F., D. J. Gorney, and D. S. Evans, On the conjugacy of the aurora: high and low latitudes, *Geophys. Res. Lett., 14,* 190, 1987.

Mobius, E., M. Scholer, D. Hovestadt, G. Paschmann, and G. Gloeckler, Energetic particles in the vicinity of a possible neutral line in the plasma sheet, *J. Geophys. Res., 88,* 7742, 1983.

Moldwin, M. B., and W. J. Hughes, Multi-satellite observations of plasmoid: IMP 8 and ISEE 3, *Geophys. Res. Lett., 19,* 1081, 1992a.

Moldwin, M. B., and W. J. Hughes, On the formation and evolution of plasmoids: a survey of ISEE 3 geotail data, *J. Geophys. Res., 97,* 19259, 1992b.

Montbriand, L. E., The proton aurora and auroral substorm, in *The Radiating Atmosphere,* edited by B. M. McCormac, p. 366, D. Reidel, Hingham, Mass., 1971.

Moore, T. E., R. L. Arnoldy, J. Feynman, and D. A. Hardy, Propagating substorm injection fronts, *J. Geophys. Res., 86,* 6713, 1981.

Moos, N. A. F., *Calaba Magnetic Data, 1846 to 1905; Part I: Magnetic data and instruments; Part II: the phenomenon and its discussion,* Bombay, 1910.

Morris, R. J., K. D. Cole, E. T. Matveeva, and V. A. Troitskaya, Hydromagnetic "whistles" at the dayside cusp, *Planet. Space Sci., 30,* 113, 1982.

Morse, T. H., and G. J. Romick, The fluctuation and fading of auroral arcs preceding substorm onsets, *Geophys. Res. Lett., 9,* 1065, 1982.

Morozumi, H. M., Dirunal variation of auroral zone geophysical disturbances, *Rep. Ionos. Space Res., Jpn., 19,* 286, 1965.

Mozer, F. S., Electric field evidence for viscous interaction at the magnetopause, *Geophys. Res. Lett., 11,* 135, 1984.

Mozer, F. S., and W. D. Gonzales, Response of polar cap convection to the interplanetary magnetic field, *J. Geophys. Res., 78,* 6784, 1973.

Mozer, F. S., and R. B. Torbert, An average parallel electric field deduced from the latitude and altitude variations of the perpendicular electric field below 8000 km, *Geophys. Res. Lett., 7,* 219, 1980.

Mozer, F. S., W. D. Gonzales, F. Bogott, M. C. Kelley, and S. Schutz, High-latitude electric fields and the three-dimensional interaction between the interplanetary and terrestrial magnetic fields, *J. Geophys. Res., 79,* 56, 1974.

Mozer, F. S., R. B. Torbert, U. V. Fahleson, C.-G. Falthammar, A. Gonfalone, and A. Pedersen, Electric field measurements in the solar wind, bow shock, magnetosheath, magnetopause, and magnetosphere, *Space Sci. Rev., 22,* 791, 1978.

Mozer, F. S., C. A. Cattell, M. Temerin, R. B. Torbert, S. von Glinski, M. Woldorf, and J. Wygant, The dc and ac electric field, plasma density and field-aligned current experiments on the S3-3 satellite, *J. Geophys. Res., 84,* 5875, 1979.

Mozer, F. S., C. A. Cattell, R. L. Lysak, M. K. Hudson, M. Temerin, and R. B. Torbert, Satellite measurements and theories of low altitude auroral particle acceleration mechanisms, *Space Sci. Rev., 27,* 15, 1980.

Murayama, T., Coupling function between solar wind parameters and geomagnetic indices, *Revs. Geophys., 20,* 623, 1982.

Murphree, J. S., L. L. Cogger, and C. D. Anger, Characteristics of the instantaneous auroral oval in the 1200–1800 MLT sector, *J. Geophys. Res., 86,* 7657, 1981.

Murphree, J. S., S. Ismail, L. L. Cogger, D. D. Wallis, and G. G. Shepherd, Characteristics of optical emissions and particle precipitation in polar cap arcs, *Planet. Space Sci., 31,* 161, 1983.

Murphree, J. S., L. L. Cogger, and R. D. Elphinstone, Observations of distortions of optical features in the uv auroral distribution, *IEEE Trans. Plasma Sci., 17,* 109, 1989.

Murphree, J. S., R. D. Elphinstone, D. Hearn, and L. I. Cogger, Large-scale high latitude dayside auroral emissions, *J. Geophys. Res., 95,* 2345, 1990.

Murphree, J. S., R. D. Elphinstone, L. L. Cogger, and D. Hearn, Viking optical substorm signatures, in *Magnetospheric Substorms,* Geophys. Monograph 64, Proc. Hakone Conf. Japan, p. 241, edited by T. A. Potemra, J. R. Kan, S. Kokobun, and T. Iijima, American Geophysical Union, Washington, DC, 1991.

Nagai, T., Observed magnetic substorm signatures at synchronous altitude, *J. Geophys. Res., 87,* 4405, 1982.

Nagai, T., An empirical model of substorm-related magnetic field variations at synchronous orbit, in *Magnetospheric Substorms (Proc. Chapman Conf., Hakone Japan, Sept. 3–7, 1990),* p. 91, edited by J. R. Kan, T. A. Potemra, S. Kokobun, and T. Iijima, Geophysical Monograph 64, AGU, Washington, DC, 1991.

Nagai, T., D. N. Baker, and P. R. Higbie, Development of substorm activity in multiple-onset substorms at synchronous orbit, *J. Geophys. Res., 88,* 6994, 1983.

Nagai, T., J. H. Waite, J. L. Green, C. R. Chappell, R. C. Olsen, and R. H. Comfort, First measurements of supersonic polar wind in the polar magnetosphere, *Geophys. Res. Lett., 11,* 669, 1984.

Nagai, T., H. J. Singer, B. G. Ledley, and R. C. Olsen, Field–aligned currents associated with substorms in the vicinity of substorm orbit, 1, the July 5, 1979, substorm observed by SCATHA, GOES 3, and GOES 2, *J. Geophys. Res., 92,* 2425, 1987.

Nagata, T., S. Kokobun, and T. Iijima, Geomagnetically conjugate relationships of giant pulsations at Syowa base, Antarctica, and Reykyavik, Iceland, *J. Geophys. Res., 68,* 4621, 1963.

Nakai, H., Y. Kamide, and C. T. Russell, Influences of solar wind parameters and geomagnetic activity on the tail lobe magnetic field: a statistical study, *J. Geophys. Res., 96,* 5511, 1991.

Nakamura, M., G. Paschmann, W. Baumjohann, and N. Sckopke, Ion distributions and flows near the neutral sheet, *J. Geophys. Res., 96,* 5631, 1991.

Nakamura, R., D. N. Baker, R. D. Belian, and T. Yamamoto, Spatial scale of the substorm onset region determined from multi-point satellite and ground-based observations, p. 353, in *Substorms 1: Proc. Int'l. Conf. Substorms (ICS-1), ESA SP-335,* European Space Agency, Paris, 1992.

Neilsen, E., Dynamics and spatial scale of auroral absorption events associated with the substorm expansion phase, *J. Geophys. Res., 85,* 2092, 1980.

Neilsen, E., The STARE system and some of its applications, p. 213, in *The IMS Source Book,* edited by C. T. Russell and D. J. Southwood, American Geophysical Union, Washington, DC, 1982.

Neilsen, E., and W. I. Axford, Small scale auroral absorption events associated with substorms, *Nature, 267,* 502, 1977.

Neilsen, E., and R. A. Greenwald, Variations in ionospheric currents and electric fields in association with absorption spikes during the substorm expansion phase, *J. Geophys. Res., 83,* 5645, 1978.

Neilsen, E., and R. A. Greenwald, Electron flow and visual aurora at the Harang discontinuity, *J. Geophys. Res., 84,* 4189, 1979.

Neilsen, E., A. Korth, G. Kremser, and F. Mariani, The electron pitch angle distribution at geosynchronous orbit associated with absorption spikes during the substorm expansion phase, *J. Geophys. Res., 87,* 887, 1982.

Neilsen, E., W. Guttler, E. C. Thomas, C. P. Stuart, T. P. Jones, and A. Hedberg, A new radar auroral backscatter experiment, *Nature, 304,* 712, 1983.

Ness, N. F., The earth's magnetic tail, *J. Geophys. Res., 70,* 2989, 1965.

Ness, N. F., Observations of the interaction of the solar wind with the geomagnetic field during quiet conditions, p. 57, in *Solar Terrestrial Physics,* edited by J. W. King and W. S. Newman, Academic Press, New York, 1967.

Ness, N. F., C. S. Scearce, and J. B. Seek, Initial results of the IMP 1 magnetic field experiment, *J. Geophys. Res., 69,* 3531, 1964.

Ness, N. F., C. S. Scearce, and S. C. Cantarano, Probable observations of the geomagnetic tail at 10^3 RE by Pioneer 7, *J. Geophys. Res., 72,* 3769, 1967.

Neugebauer, M., and C. Snyder, The mission of Mariner II: Preliminary observations: Solar plasma experiments, *Science, 138,* 1095, 1962.

Neugebauer, M., C. T. Russell, and E. J. Smith, Observations of the internal structure of the magnetopause, *J. Geophys. Res., 79,* 499, 1974.

Newell, P. T., and C.-I. Meng, Energy dependence of the equatorward cutoffs in auroral electron and ion precipitation, *J. Geophys. Res., 92,* 7519, 1987.

Newell, P. T., and C.-I. Meng, The cusp and the cleft/LLBL: Low altitude identification and statistical local time variation, *J. Geophys. Res., 93,* 14549, 1988.

Newell, P. T., and C.-I. Meng, On quantifying the distinctions between the cusp and the cleft/LLBL, in *Electromagnetic Coupling in the Polar Clefts and Caps,* NATO ASI Sec. C, Vol. 278, edited by P. E. Sandholt and A. Egeland, p. 87, Kluwer Academic, Dordrecht, 1989.

Newell, P. T., and C.-I. Meng, Ion acceleration at the equatorward edge of the cusp: low altitude observations of patchy merging, *Geophys. Res. Lett., 18, 1829,* 1991.

Newell, P. T., and C.-I. Meng, Mapping the dayside ionosphere to the magnetosphere using particle precipitation characteristics, *Geophys. Res. Lett., 19,* 609, 1992.

Newell, P. T., C.-I. Meng, D. G. Sibeck, and R. Lepping, Some low-altitude dependencies on the interplanetary magnetic field, *J. Geophys. Res., 94,* 8921, 1989.

Newell, P. T., W. J. Burke, C. I. Meng, E. R. Sanchez, and M. Greenspan, Identification of the plasma mantle at low altitude, *J. Geophys. Res., 96,* 35, 1991a.

Newell. P. T., W. J. Burke, E. R. Sanchez, C.-I. Meng, M. E. Greenspan, and C. R. Clauert, The low-latitude boundary layer and the boundary plasma sheet at low altitude: prenoon precipitation regions and convection reversal boundaries, *J. Geophys. Res., 96,* 21013, 1991b.

Newell, P. T., C.-I. Meng, and D. A. Hardy, Overview of electron and ion precipitation in the auroral oval, p. 85, in *Auroral Physics,* edited by C.-I. Meng, M. J. Rycroft, and L. A. Frank, Cambridge University Press, Cambridge, UK, 1991c.

Newton, R. S., D. J. Southwood, and W. J. Hughes, Damping of geomagnetic pulsations by the ionosphere, *Planet. Space Sci., 26,* 201, 1978.

Nishida, A., Ionospheric screening effect and storm sudden commencement, *J. Geophys. Res., 69,* 1861, 1964.

Nishida, A., Formation of the plasmapause, or magnetospheric knee, by the combined action of magnetospheric convection and plasma escape from the tail, *J. Geophys. Res., 71,* 5669, 1966.

Nishida, A., Geomagnetic DP 2 fluctuations and associated magnetospheric phenomena, *J. Geophys. Res., 73,* 1795, 1968a.

Nishida, A., Coherence of geomagnetic DP 2 fluctuations with interplanetary magnetic variations, *J. Geophys. Res., 73* 5549, 1968b.

Nishida, A., *Geomagnetic Diagnosis of the Magnetosphere,* Springer-Verlag, New York, 1978.

Nishida, A., and L. J. Cahill, Sudden impulses in the magnetosphere observed by Explorer 12, *J. Geophys. Res., 69,* 2243, 1964.

Nishida, A., and Y. Kamide, Magnetospheric processes preceding the onset of an isolated substorm: A case study of the march 31, 1978 substorm, *J. Geophys. Res., 88,* 7005, 1983.

Nishida, A., H. Hayakawa, and E. W. Hones, Jr., Observed signatures of reconnection in the magnetotail, *J. Geophys. Res., 86,* 1422, 1981.

Nishida, A., Y. K. Tulunay, F. S. Mozer, C. A. Cattell, E. W. Hones, Jr., and J. Birn, Electric field evidence for tailward flow at substorm onset, *J. Geophys. Res., 88,* 9109, 1983.

Nishida, A., M. Scholer, T. Teresawa, S. J. Bame, G. Gloeckler, E. J. Smith, and R. D. Zwickl, Quasi-stagnant plasmoid in the middle tail: a new pre-expansion phase phenomenon, *J. Geophys. Res., 91,* 4245, 1986.

Nishida, A., S. J. Bame, D. N. Baker, G. Gloeckler, M. Scholer, E. J. Smith, T. Teresawa, and B. Tsurutani, Assessment of the boundary layer model of substorms, *J. Geophys. Res., 93,* 5579, 1988.

Nishitani, N., and T. Oguti, Auroral activity and corresponding magnetic signatures at synchronous orbit, *J. Geomag. Geoelectr., 40,* 423, 1988.

Nopper, R. W., Jr., W. J. Hughes, C. G. Maclennan, and R. L. McPherron, Impulse-excited pulsations during the July 29, 1977, event, *J. Geophys. Res., 87,* 5911, 1982.

Obara, T., M. Kitayama, T. Mukai, N. Kaya, J. C. Murphree, and L. L. Cogger, Simultaneous observations of sun-aligned polar cap arcs in both hemiospheres by EXOS-C and Viking, *Geophys. Res. Lett., 15,* 713, 1988.

Ogilvie, K. W., L. F. Burlaga, and T. D. Wilkerson, Plasma observations on Explorer 34, *J. Geophys. Res., 73,* 6809, 1968.

Ogilvie, K. W., J. D. Scudder, and M. Sugiura, Magnetic field and electron observations near the dawn magnetopause, *J. Geophys. Res., 76,* 3534, 1971.

Ogilvie, K. W., T. von Rosenvinge, and A. C. Durney, International sun–earth explorer: a three-spacecraft program, *Science, 198,* 131, 1977.

Ogilvie, K. W., R. J. Fitzenreiter, and J. D. Scudder, Observations of electron beams in the low–latitude boundary layer, *J. Geophys., Res., 89,* 10723, 1984.

Ogino, T., A three-dimensional MHD simulation of the interaction of the solar wind with the earth's magnetosphere: the generation of field-aligned currents, *J. Geophys. Res., 91,* 6791, 1986.

Ogino, T., and R. J. Walker, A magnetohydrodynamic simulation of the bifurcation of the tail lobes during intervals with a northward interplanetary magnetic field, *Geophys. Res. Lett., 11,* 1018, 1984.

Ogino, T., R. J. Walker, M. Ashour-Abdalla, and J. M. Dawson, An MHD simulation of By dependent magnetospheric convection and field-aligned currents during northward IMF, *J. Geophys. Res., 90,* 10835, 1985.

Ogino, T., R. J. Walker, M. Ashour-Abdalla, and J. M. Dawson, An MHD simulation of the effects of the interplanetary magnetic field by component on the interaction of the solar wind with the earth's magnetosphere during southward interplanetary magnetic field, *J. Geophys. Res., 91,* 10029, 1986.

Ogino, T., R. J. Walker, and M. Ashour-Abdalla, A magnetohydrodynamic simulation of the formation of magnetic flux tubes at the earth's dayside magnetopause, *Geophys. Res. Lett., 16,* 155, 1989.

Oguti, T., Relationships between auroral and concurrent geomagnetic micropulsations, *J. Geomag. Geoelectr., 38,* 837, 1986.

Oguti, T., Relationship between auroral and magnetic activity in the polar cusp/cleft, p. 253, in *Electromagnetic Coupling in the Polar Clefts and Cusps,* edited by P. E. Sandholt and A. Egeland, D. Reidel, Norwell, Mass., 1989a.

Oguti, T., Questions on the dayside reconnection in connection with magnetospheric convection and open–close boundary, *J. Geomag. Geoelectr., 41,* 879, 1989b.

Oguti, T., S. Kokobun, K. Hayashi, K. Tsuruda, S. Machida, T. Kitamura, O. Saka, and T. Watanabe, Statistics of pulsating auroras on the basis of all-sky TV data from five stations, I, Occurrence frequency, *Can. J. Phys., 59,* 1150, 1981.

Oguti, T., T.-I. Kitamura, and T. Watanabe, Global auroral dynamics campaign, 1985–86, *J. Geomag. Geoelectr., 40,* 485, 1988a.

Oguti, T., T. Yamamoto, K. Hayashi, S. Kokobun, T. Ogawa, N. Iwagami, T. Kitamura, O. Saka, T. Araki, K. Makita, N. Sato, T. Watanabe, R. E. Horita, and J. S. Kim, Fast auroral evolution and related magnetic field changes on the ground and at conjugate satellites, *J. Geomag. Geoelectr., 40,* 505, 1988b.

Oguti, T., T. Yamamoto, K. Hayashi, S. Kokobun, A. Egeland, and T. Holtet, Dayside auroral activity and related magnetic impulses in the polar cusp region, *J. Geomag. Geoelectr., 40,* 387, 1988c.

Ohtani, S., K. Takahashi, L. J. Zanetti, T. A. Potemra, R. W. McEntire, and T. Iijima, Tail current disruption in the geosynchronous region, in *Magnetospheric Substorms,* Geophys. Monograph 64, Proc. Hakone Conf. Japan, pp. 131, edited by T. A. Potemra, J. R. Kan, S. Kokobun, and T. Iijima, American Geophysical Union, Washington, DC, 1991.

Ohtani, S., K. Takahashi, L. J. Zanetti, T. A. Potemra, R. W. McEntire, and T. Iijima, Initial signatures of magnetic field and energetic particle fluxes at tail reconfiguration: Explosive growth phase, *J. Geophys. Res, 97,* 19311, 1992.

Oliver, W. I., J. M. Holt, R. H. Wand, and J. V. Evans, Millstone Hill incoherent scatter observations of auroral convection over $60° < \Lambda < 75°$, average pattern versus Kp, *J. Geophys. Res., 88,* 5505, 1983.

Olson, J. V., ULF signatures of the polar cusp, *J. Geophys. Res., 91,* 10055, 1986.

Olson, J. V., and L. C. Lee, Pc 1 wave generation by sudden impulses, *Planet. Space Sci., 31,* 295, 1983.

Olson. J. V., and G. Rostoker, Longitudinal phase variations of PC 4–5 micropulsations, *J. Geophys. Res., 83,* 2481, 1986.

Olson, W. F., Shape of tilted magnetopause, *J. Geophys. Res., 74,* 5642, 1969.

Ondoh, T., A comparison of magnetospheric field changes at sudden impulses and substorm onsets, *Rep. Ionos. Space Res. Jap., 27,* 137, 1973.

Onsager, T. G., M. F. Thomsen, R. C. Elphic, and J. T. Gosling, Model of electron and ion distributions in the plasma sheet boundary layer, *J. Geophys. Res., 96,* 20999, 1991.

Opgenoorth, H. J., and S. Kirkwood, Ground-based observations coordinated with *Viking* satellite measurements, *Phil. Trans. Roy. Soc. Lond. A, 328,* 221, 1989.

Opgenoorth, H. J., R. J. Pellinen, H. Maurer, F. Kuppers, W. J. Heikkila, K. U. Kaila, and P. Tanskanen, Ground-based observations of an onset of localized field-aligned currents during auroral breakup around local midnight, *J. Geophys., 48,* 101, 1980.

Opgenoorth, H. J., R. J. Pellinen, W. Baumjohann, E. Nielsen, G. Marklund, and L. Eliasson, Three-dimensional current flow and particle precipitation in a westward travelling surge observed during the barium-GEOS rocket experiment, *J. Geophys. Res., 88,* 3138, 1983.

Opgenoorth, H. J., B. Bromage, D. Fontaine, C. La Hoz, A. Huuskonen, H. Kohl, U. P. Lovhaug, G. Wannberg, G. Gustavsson, J. S. Murphree, L. Eliasson, G. Marklund, T. A. Potemra, S. Kirkwood, E. Nielson, and J.–E. Wahlund, Coordinated observations with EISCAT and the Viking satellite: The decay of a westward travelling surge, *Ann. Geophys., 7,* 479, 1989.

Opgenoorth, H. J., M. A. L. Persson, V. M. Mishin, T. I. Saifudinova, A. D. Bazarzhapov, S. B. Lunyushkin, and D. Sh. Shirapov, On the distinction of various energy sources for magnetospheric substorms, p. 377 in *Substorms 1: Proc. Int'l. Conf. Substorms (ICS-1), ESA SP-335,* European Space Agency, Paris, 1992.

Otto, A., Three-dimensional magnetohydrodynamic simulations of processes at the earth's magnetopause, *Geophys. Astrophys. Fluid Dynamics, 62,* 69, 1991.

Otto, A., M. Hesse, and K. Schindler, General magnetic reconnection in 3D systems, p. 225, in *Topological Fluid Mechanics,* edited by H. K. Moffatt and A. Tsinober, Cambridge University Press, Cambridge, UK, 1990.

Owen, C. J., and J. A. Slavin, Energetic ion events associated with travelling compression regions, p. 365, in *Substorms 1: Proc. Int'l. Conf. Substorms (ICS-1), ESA SP-335,* European Space Agency, Paris, 1992.

Page, D. E., V. Domingo, D. Kohn, B. G. Taylor, K. -P. Wenzel, and P. C. Hedgecock, High Energy Electrons at the Magnetopause Above the North Pole: Preliminary Results from the HEOS 2 Satellite, p. 631 in *Space Research XIII,* Akademie-Verlag, Berlin, 1973.

Pangia, M. J., C. S. Lin, and J. N. Barfield, A correlative study of Pc 5 magnetic pulsations with substorm onsets, *J. Geophys. Res., 95,* 10699, 1990.

Papamastorakis, I., G. Paschmann, W. Baumjohann, B. U. O. Sonnerup, and H. Luhr, Orientation, motion, and other properties of flux transfer events on September 4, 1984, *J. Geophys. Res., 94,* 8852, 1989.

Parker, E. N., Interaction of the solar wind with the geomagnetic field, *Phys. Fluids, 1,* 171, 1957.

Parker, E. N., Swett's mechanism for merging magnetic fields in conducting fluids, *J. Geophys. Res., 62,* 509, 1957.

Parker, E. N., Kinematical hydrodynamic theory and its application to the low solar photosphere, *Astrophys. J., 138,* 552, 1963.

Parker, E. N., Dynamical properties of the magnetosphere, p. 3, in *Physics of the Magnetosphere,* edited by R. L. Carovillano, J. F. McClay, and H. R. Radoski, D. Reidel, Dordrecht, Holland, 1968.

Parks, G. K., M. McCarthy, R. Fitzenreiter, J. Etcheto, K. A. Anderson, R. A. Anderson, T. Eastman, L. A. Frank, D. Gurnett, C. Huang, R. P. Lin, A. T. Y. Lui, K. W. Ogilvie, A. Pedersen, H. Reme, and D. Williams, Particle and field characteristics of the high latitude plasma sheet boundary layer, *J. Geophys. Res., 89,* 8885, 1984.

Parks, G. K., R. Fitzenreiter, K. W. Ogilvie, C. Huang, K. A. Anderson, J. Dandouras, L. Frank, R. P. Lin, M. McCarthy, H. Reme, J. A. Sauvaud, and S. Werden, Low-energy particle layer outside of the plasma sheet boundary, *J. Geophys. Res., 97,* 2943, 1992.

Paschmann, G., N. Sckopke, and H. Grunwaldt, Plasma in the polar cusp and plasma mantle, p. 37, in *Magnetospheric Particles and Fields,* edited by B. M. MacCormac, D. Reidel, Hingham, Mass., 1976a.

Paschmann, G., G. Haerendel, N. Sckopke, H. Rosenbauer, and P. D. Hedgecock, Plasma and magnetic field characteristics of the distant polar cusp near local noon: the entry layer, *J. Geophys. Res., 81,* 2883, 1976b.

Paschmann, G., N. Sckopke, G. Haerendel, I. Papamastorakis, S. J. Bame, J. R. Asbridge, J. T. Gosling, E. W. Hones, Jr., and E. R. Tech, Isee plasma observations near the subsolar magnetopause, *Space Sci. Rev., 22,* 717, 1978.

Paschmann, G., B. U. O. Sonnerup, I. Papamastorakis, N. Sckopcke, G. Haerendel, S. J. Bame, J. B. Asbridge, J. T. Gosling, C. T. Russell, and R. C. Elphic, Plasma acceleration at the earth's magnetopause: evidence for reconnection, *Nature, 282,* 243, 1979.

Paschmann, G., G. Haerendel, I. Papamastorakis, N. Sckopke, S. J. Bame, J. T. Gosling, and C. T. Russell, Plasma and magnetic field characteristics of magnetic flux transfer events, *J. Geophys. Res., 87,* 2159, 1982.

Paschmann, G., N. Sckopke, and E. W. Hones, Jr., Magnetotail plasma observations during the 1054 UT substorm on March 22, 1979 (CDAW 6), *J. Geophys. Res., 90,* 1217, 1985.

Paschmann, G., I. Papamastorakis, W. Baumjohann, N. Sckopcke, C. W. Carlson, B. U. O. Sonnerup, and H. Luhr, The magnetopause for large magnetic shear: APMTE/IRM observations, *J. Geophys. Res., 91,* 11099, 1986.

Patel, V. L., Sudden impulses in the magnetotail, *J. Geophys. Res., 73,* 3407, 1968.

Patel, V. L., R. J. Greaves, S. A. Wahab, and T. A. Potemra, Dodge satellite obsertvations of Pc 3 and Pc 4 magnetic pulsations and correlated effects in the ground observations, *J. Geophys. Res., 84,* 4257, 1979.

Paulikas, G. A., Tracing of high-latitude field lines by solar particles, *Rev. Geophys. Space Phys., 12,* 117, 1974.

Pavlos, G. P., E. T. Sarris, and G. Kaliabetsos, Monitoring of energy spectra of particle bursts in the plasma sheet and magnetosheath, *Planet. Space Sci., 33,* 1109, 1985.

Pavlos, G. P., E. T. Sarris, and N. Paschalidis, The growth rate and location of the acceleration of energetic particles inside the plasma sheet, *Planet. Space Sci., 37,* 503, 1989.

Pedersen, A., Substorm electric and magnetic field signatures on GEOS-1, GEOS-2, and ISEE-1, p. 237, in *Substorms 1: Proc. Int'l. Conf. Substorms (ICS-1), ESP SP-335,* European Space Agency, Paris, 1992.

Pedersen, A., C. A. Cattell, C.-G. Falthammar, V. Formisano, P.-A. Lindquist, F. Mozer, and R. Torbert, Quasistatic electric field measurements with spherical double probes on the GEOS and ISEE satellites, *Space Sci. Rev., 37,* 269, 1984.

Pedersen, A., C. A. Cattell, C.-G. Falthammar, K. Knott, P.-A. Lindquist, R. H. Manka, and F. S. Mozer, Electric fields in the plasma sheet and plasma sheet boundary layer, *J. Geophys. Res., 90,* 1231, 1985.

Pellinen, R. J., and W. J. Heikkila, Energization of charged particles to high energies by an induced electric field within the magnetotail, *J. Geophys Res., 83,* 1544, 1978.

Pellinen, R. J., and W. J. Heikkila, Inductive electric fields and their relation to auroral and substorm phenomena, *Space Sci. Rev., 37,* 1, 1984.

Pellinen, R. J., W. Baumjohann, W. J. Heikkila, V. A. Sergeev, A. G. Yahnin, G. Marklund, and A. O. Melnikov, Event study on pre-substorm phases and their relationship to the energy coupling between the solar wind and magnetosphere, *Planet. Space Sci., 30,* 371, 1982.

Pellinen, R., A. Huuskonen, M. Vallinkoski, A. Pedersen, and R. Schmidt, GEOS 2 E-field behavior during dynamic auroral development near the satellite footprint, *Eur. Space Agency Publ., ESA SP-217,* 358, 1984.

Pellinen, R., H. E. J. Koskinen, T. I. Pulkkinen, J. S. Murphree, G. Rostoker, and H. J. Opgenoorth, Satellite and ground-based observations of a fading transpolar arc, *J. Geophys. Res., 95,* 5817, 1990.

Perreault, P., and S.-I. Akasofu, A study of geomagnetic storms, *Geophys. J. Roy. Astron. Soc., 54,* 547, 1978.

Peterson, W. K., and E. E. Shelley, Origin of the plasma in across-polar auroral feature (theta aurora), *J. Geophys. Res., 89,* 6729, 1984.

Peterson, W. K., R. D. Sharp, E. G. Shelley, R. G. Johnson, and H. Balsiger, Energetic ion composition of the plasma sheet, *J. Geophys. Res., 86,* 761, 1981.

Petschek, H. E., Magnetic field annihilation, p. 425, in *The Physics of Solar Flares, NASA Spec. Publ., SP-50,* edited by W. N. Hess, NASA, Washington, DC, 1964.

Petschek, H. E., The mechanism for reconnection of geomagnetic and interplanetary field lines, in *The Solar Wind,* edited by R. J. Mackin and M. Neugebauer, p. 257, Pergamon, New York, 1966.

Petschek, H. E., and C. F. Kennel, Tail flow, auroral precipitation, and ring currents (abstract), *Trans. AGU, 47,* 137, 1966.

Petschek, H. E., and R. M. Thorne, The existence of intermediate waves in neutral sheets, *Astrophys. J., 147,* 1157, 1967.

Phan, T. D., B. U. O. Sonnerup, and W. Lotko, Self-consistent model of the low-latitude boundary layer, *J. Geophys. Res., 94,* 1281, 1989.

Phelps, A. D., and R. Sagalyn, Plasma density irregularities in the high-latitude topside ionosphere, *J. Geophys. Res., 81,* 515, 1976.

Pike, C. P., and J. A. Whalen, Satellite observations of auroral substorms, *J. Geophys. Res., 79,* 985, 1974.

Pilipp, W. G., and G. Morfill, The formation of the plasma sheet resulting from plasma mantle dynamics, *J. Geophys. Res., 83,* 5670, 1978.

Podgorny, I. M., E. M. Dubinin, and Yu. A. Potanin, On magnetic curl in front of the magnetopause boundary, *Geophys. Res. Lett., 7,* 247, 1980.

Ponomarev, E. A., Energy relationships for the magnetosphere, *Stud. Geomagn. Aeron. Sol. Phys. Moscow, 53,* 27, 1981.

Potemra, T. A., Current systems in the earth's magnetosphere, *Rev. Geophys. Space Phys., 17,* 640, 1979.

Potemra, T. A., L. J. Zanetti, P. F. Bythrow, A. T. Y. Lui, and T. Iijima, B_y-dependent convection patterns during northward interplanetary magnetic field, *J. Geophys. Res., 89,* 9753, 1984.

Potemra, T. A., H. Luhr, L. J. Zanetti, K. Takahashi, R. E. Erlandson, G. T. Marklund, L. P. Block, L. G. Blomberg, and R. P. Lepping, Multi-satellite and ground-based observations of transient ULF waves, *J. Geophys. Res., 94,* 2543, 1989.

Potemra, T. A., H. Vo, D. Venkatesan, L. L. Cogger, R. E. Erlandson, L. J. Zanetti, P. F. Bythrow, and B. J. Anderson, Periodic auroral forms and geomagnetic oscillations in the 1400 MLT region, *J. Geophys. Res., 95,* 5835, 1990.

Poulter, E. M., and E. Nielsen, The hydromagnetic oscillation of individual shells of the geomagnetic field, *J. Geophys. Res., 87,* 10432, 1982.

Poulter, E. M., and W. Allan, Transient ULF pulsation decay rates observed by ground-based magnetometers: the contribution of spatial integration, *Planet. Space Sci., 33,* 607, 1986.

Priest, E., and T. G. Forbes, Steady magnetic reconnection in three dimensions, *Solar Phys., 119,* 211, 1989.

Pu, Z. Y., and M. G. Kivelson, Kelvin–Helmholtz instability at the magnetopause: energy flux into the magnetosphere, *J. Geophys. Res., 88,* 853, 1983.

Pudovkin, M. L., O. I. Shumilov, and S. A. Zaitseva, Dynamics of the zone of corpuscular precipitations, *Planet. Space Sci., 16,* 881, 1968.

Pudovkin, M. I., and V. S. Semenov, Magnetic field reconnection theory and the solar wind-magnetosphere interaction: a review, *Space Sci. Rev., 41,* 1, 1985.

Pulkkinen, T. I., et al., Auroral signatures of substorm recovery phase: a case study, p. 333, in *Magnetospheric Substorms (Proc. Chapman Conf., Hakone,*

Japan, Sept. 3–7, 1990), edited by J. R. Kan, T. A. Potemra, S. Kokobun, and T. Iijima, Geophysical Monograph 64, AGU, Washington, DC, 1991.

Pulkkinen, T. I., D. N. Baker, D. G. Mitchell, R. L. McPherron, C. Y. Huang, and L. A. Frank, Global and local current sheet thickness estimates during the late growth phase, *Substorm 1: Proc. Int'l. Conf. Substorms (ICS-1), ESA SP-335,* European Space Agency, Paris, 1992.

Pytte, T., and H. Trefall, Auroral-zone electron precipitation events observed before and at the onset of negative magnetic bays, *J. Atmos. Terr. Phys., 34,* 315, 1972.

Pytte, T., R. L. McPherron, and S. Kokobun, The ground signatures of the expansion phase during multiple onset substorms, *Planet. Space Sci., 24,* 1115, 1976a.

Pytte, T., H. Trefall, G. Kremser, P. Tauskanen, and W. Riedler, On the morphology of high-energy (30 keV) electron precipitation at the onset of negative magnetic bays, *J. Atmos. Terr. Phys., 38,* 757, 1976b.

Pytte, T., R. L. McPherron, M. G. Kivelson, H. I. West, Jr., and E. W. Hones, Jr., Multiple-satellite studies of magnetospheric substorms: radial dynamics of the plasma sheet, *J. Geophys. Res., 81,* 5921, 1976c.

Pytte, T., H. Trefall, G. Kremser, L. Jalonen, and W. Riedler, On the morphology of energetic (> 30 keV) electron precipitation during the growth phase of magnetospheric substorms, *J. Atmos. Terr. Phys., 38,* 739, 1976d.

Pytte, T., R. L. McPherron, E. W. Hones, Jr., and H. West, Multiple satellite studies of magnetospheric substorms: distinction between polar magnetic substorms and convection-driven negative bays, *J. Geophys. Res., 83,* 663, 1978a.

Pytte, T., R. L. McPherron, M. G. Kivelson, H. I. West, Jr., and E. W. Hones, Jr., Multiple-satellite studies of magnetospheric substorms: Plasma sheet recovery and the poleward leap of auroral zone activity, *J. Geophys. Res., 83,* 5256, 1978b.

Radoski, H. R., Magnetic toroidal resonances and vibrating field lines, *J. Geophys. Res., 71,* 1891, 1966.

Radoski, H. R., Highly asymmetric MHD resonance, the guided poloidal mode, *J. Geophys. Res., 72,* 4026, 1967.

Radoski, H. R., A note on the problem of hydromagnetic resonances in the magnetosphere, *Planet. Space Sci., 19,* 1012, 1971.

Radoski, H. R., and R. L. Carovillano, Axisymmetric plasmasphere resonances, toroidal mode, *Phys. Fluids, 9,* 285, 1966.

Raitt, W. J., and R. W. Schunk, Composition and characteristics of the polar wind, p. 99, in *Energetic Ion Composition in the Earth's Magnetosphere,* edited by R. J. Johnson, Terra Scientific, Tokyo, 1983.

Rankin, D., and R. Kurtz, Statistical study of micropulsation polarizations, *J. Geophys. Res., 75,* 5444, 1970.

Ranta, A., and H. Ranta, Satellite and ground observations of a presubstorm phase on May 4, 1977, *J. Geophys. Res., 88,* 4097, 1983.

Ranta, H., A. Ranta, P. N. Collis, and J. K. Hargreaves, Development of the auroral absorption substorm: studies of pre-onset phase and sharp onset using an extensive riometer network, *Planet. Space Sci., 29,* 1287, 1981.

Rasmussen, C. E., and R. W. Schunk, Ionospheric convection driven by NBZ currents, *J. Geophys. Res., 92,* 4491, 1987.

Rasmussen, C. E., and R. W. Schunk, Ionospheric convection inferred from interplanetary magnetic field-dependent Birkeland currents, *J. Geophys. Res., 93,* 1909, 1988.

Rees, M. H., and D. Luckey, Auroral electron energy derived from ratios of spectroscopic emissions, 1, Model comparisons, *J. Geophys. Res., 79,* 5181, 1974.

Reid, G. C., and T. E. Holzer, The response of the dayside magnetosphere–ionosphere system to time-varying field-line reconnection at the magnetopause, 2, Erosion event of March 27, 1968, *J. Geophys. Res., 80,* 2050, 1975.

Reiff, P. H., and J. L. Burch, IMF By-dependent plasma flow and Birkeland currents in the dayside magnetosphere 2. A global model for northward and southward IMF, *J. Geophys. Res., 90,* 1595, 1985.

Reiff, P. H., and J. G. Luhmann, Solar wind control of the polar-cap voltage, in *Solar Wind–Magnetosphere Coupling,* edited by Y. Kamide and J. A. Slavin, p. 453, Terra Scientifica, Tokyo, 1986.

Reiff, P. H., T. W. Hill, and J. L. Burch, Solar wind plasma injection at the dayside magnetospheric cusp, *J. Geophys. Res., 82,* 479, 1977.

Reiff, P. H., J. L. Burch, and R. W. Spiro, Cusp proton signatures and the interplanetary magnetic field, *J. Geophys. Res., 85,* 5997, 1980.

Reiff, P. H., R. W. Spiro, and T. W. Hill, Dependence of polar cap potential drop on interplanetary parameters, *J. Geophys. Res., 86,* 7639, 1981.

Reiff, P. H., R. W. Spiro, R. A. Wolf, Y. Kamide, and J. H. King, Comparison of polar cap potential drops estimated from solar wind and ground magnetometer data, CDAW-6, *J. Geophys. Res., 90,* 1318, 1985.

Rich, F. J., and M. S. Gussenhoven, The absence of region 1/region 2 field-aligned currents during prolonged quiet times, *Geophys. Res. Lett., 14,* 689, 1987.

Rich, F. J., V. M. Vasyliunas, and R. A. Wolf, On the balance of stresses in the plasma sheet, *J. Geophys. Res., 77,* 4670, 1972.

Rich, F. J., C. A. Cattell, M. C. Kelley, and W. J. Burke, Simultaneous observations of auroral zone electrodynamics by two satellites: evidence for height variations in the topside ionosphere, *J. Geophys. Res., 86,* 8929, 1981.

Richardson, I. G., and S. W. H. Cowley, Plasmoid-associated energetic ion bursts in the deep geomagnetic tail: properties of the boundary layer, *J. Geophys. Res., 90,* 12, 133, 1985.

Richardson, I. G., M. Scholer, B. T. Tsurutani, P. W. Daly, D. N. Baker, and R. C. Elphic, Simultaneous observations of the near-earth and distant geomagnetic tail during a substorm by ISEE-1, ISEE-3, and geostationary spacecraft, *Planet. Space Sci., 35,* 209, 1987a.

Richardson, I. G., S. W. H. Cowley, E. W. Hones, Jr., and S. J. Bame, Plasmoid-associated energetic ion bursts in the deep geomagnetic tail: properties of plasmoids and the post-plasmoid plasma sheet, *J. Geophys. Res., 92,* 9997, 1987b.

Richardson, I. G., C. J. Owen, S. W. H. Cowley, A. B. Galvin, T. R. Sanderson, M. Scholer, J. A. Slavin, and R. D. Zwickl, ISEE 3 observations during the CDAW 8 intervals: case studies of the distant geomagnetic tail covering a wide range of geomagnetic activity, *J. Geophys. Res., 94,* 15189, 1989.

Richmond, A. D., and Y. Kamide, Mapping electrodynamic features of the high-latitude ionosphere from localized observations: techniques, *J. Geophys. Res., 93,* 5741, 1988.

Richter, A. K., E. Keppler, W. I. Axford, and K. U. Denskat, Dynamics of low-energy electrons ($\geq$ 17 keV) and ions ($\geq$ 80 keV) in the vicinity of the low-latitude dusk-side magnetopause: Helios 1 and 2 results, *J. Geophys. Res., 84,* 1453, 1979.

Riehl, K. B., and D. A. Hardy, Average characteristics of the polar rain and their relationship to the solar wind and the interplanetary magnetic field, *J. Geophys. Res., 91,* 1557, 1986.

Rijnbeek, R. P., S. W. H. Cowley, D. J. Southwood, and C. T. Russell, A survey of dayside flux transfer events observed by the ISEE-1 and -2 magnetometers, *J. Geophys. Res., 89,* 786, 1984.

Rijnbeek, R. P., C. J. Farrugia, D. J. Southwood, C. P. Chaloner, D. S. Hall, M. F. Smith, M. W. Dunlop, and W. A. C. Mier-Jedrzejowicz, A magnetic boundary signature within flux transfer events, *Planet. Space Sci., 35,* 871, 1988.

Rino, C. L., and S. J. Matthews, On the morphology of auroral zone radiowave scintillation, *J. Geophys. Res., 85,* 4139, 1979.

Robert, P., R. Gendrin, S. Perrault, and A. Roux, GEOS 2 identification of rapidly moving current structures at the equatorial outer magnetosphere during substorms, *J. Geophys. Res., 89,* 819, 1984.

Roberts, D. A., D. N. Baker, A. J. Klimas, and L. F. Bargatze, Indications of low dimensionality in magnetopsheric dynamics, *Geophys. Res. Lett., 18,* 151, 1991.

Robinson, R. M., R. T. Tsunoda, and J. F. Vickrey, Sources of F-region ionization enhancements in the nighttime auroral zone, *J. Geophys. Res., 90,* 7533, 1985.

Robinson, R. M., R. R. Vondrak, D. Hardy, M. S. Gussenhoven, T. A. Potemra, and P. F. Bythrow, Electrodynamics of very high latitude arcs in the morning sector auroral zone, *J. Geophys. Res., 93,* 913, 1988.

Rodriguez, P., and E. P. Szuszczewicz, High-latitude irregularities in the lower F region: intensity and scale size distributions, *J. Geophys. Res., 89,* 5575, 1984.

Roelof, E. C., E. P. Keath, C. O. Bostrom, and D. J. Williams, Fluxes of $\geq$ 50-keV and $\geq$ 30 -keV electrons at 35 Re, 1: Velocity anisotropies and plasma flow in the magnetotail, *J. Geophys. Res., 81,* 2304, 1976.

Rosenbauer, H., H. Grunwald, M. D. Montgomery, G. Paschmann, and N. Sckopke, HEOS 2 plasma observations in the distant polar magnetosphere: the plasma mantle, *J. Geophys. Res., 80,* 2723, 1975.

Rosenberg, T. J., Cosmic noise absorption at south pole and Frobisher bay: initial results, *Mem. National Inst. Polar Research Jpn., 48,* 161, 1987.

Rosenberg, T. J., J. C. Siren, D. L. Matthews, K. Mathinsen, J. A. Holtet, A. Egeland, D. L. Carpenter, and R. A. Helliwell, Conjugacy of electron microbursts and VLF chorus, *J. Geophys. Res., 86,* 5819, 1981.

Rossberg, L., The effect of solar wind velocity on substorm activity, *J. Geophys. Res., 94,* 13571, 1989.

Rostoker, G., The frequency spectrum of Pi 2 micropulsation activity and its relationship to planetary magnetic activity, *J. Geophys. Res., 72,* 2032, 1967a.

Rostoker, G., The polarization characteristics of Pi 2 micropulsations and their relation to the determination of possible source mechanisms for the production of night-time impulsive micropulsation activity, *Can. J. Phys., 45,* 1319, 1967b.

Rostoker, G., Macrostructure of geomagnetic bays, *J. Geophys. Res., 73,* 4217, 1968.

Rostoker, G., Ground based magnetic signatures of the phases of magnetospheric substorms, in *Magnetospheric Physics,* edited by B. M. MacCormac, p. 325, D. Reidel, Hingham, Mass., 1974.

Rostoker, G., Triggering of expansive phase intensifications of magnetospheric substorms by northward turnings of the interplanetary magnetic field, *J. Geophys. Res., 88,* 6981, 1983.

Rostoker, G., and C.-G. Falthammar, Relationship between changes in the interplanetary field and variations in the magnetic field at the earth's surface, *J. Geophys. Res., 72,* 5853, 1967.

Rostoker, G., and F. P. Camidge, The localized character of magnetotail magnetic fluctuations during polar magnetic substorms, *J. Geophys. Res., 76,* 6944, 1971.

Rostoker, G., and J. C. Samson, Pc micropulsations with discrete latitude dependent frequencies, *J. Geophys. Res., 77,* 6249, 1972.

Rostoker, G., and R. Bostrom, A mechanism for driving the gross Birkeland current configuration in the auroral oval, *J. Geophys. Res., 81,* 235, 1976.

Rostoker, G., and T. Eastman, A boundary layer model for magnetospheric substorms, *J. Geophys. Res., 92,* 12187, 1987.

Rostoker, G., S.-I. Akasofu, J. Foster, R. A. Greenwald, Y. Kamide, K. Kawasaki, A. T. Y. Lui, R. L. McPherron, and C. T. Russell, Magnetospheric substorms–definition and signatures, *J. Geophys. Res., 85,* 1663, 1980.

Rostoker, G., M. Mareschal, and J. C. Samson, Response of dayside net downward field-aligned current to changes in the interplanetary magnetic field and substorm perturbations, *J. Geophys. Res., 87,* 3489, 1982.

Rostoker, G., W. Baumjohann, and C. T. Russell, A case study of the response of the magnetosphere to changes in the interplanetary medium, *J. Geophys., 53,* 170, 1983.

Rostoker, G., D. Savoie, and T. D. Phan, Response of magneotsphere–ionosphere current systems to changes in the interplanetary magnetic field, *J. Geophys. Res., 93,* 8633, 1988.

Rostoker, G., B. Jackel, and R. L. Arnoldy, The relationship of periodic structures in auroral luminosity in the afternoon sector of (sic) ULF pulsations, *Geophys. Res. Lett., 19,* 613, 1992.

Roux, A., Generation of field-aligned current structures at substorm onsets, *Proc. ESA Workshop on Fututre Missions in Solar, Heliospheric, and Space Plasma Physics,* Garmisch-Partenkirchen, Germany, 30 April–3 May, 1985, ESA SP-235, June 1985.

Roux, A., S. Perrault, P. Robert, A. Morane, A. Pedersen, A. Korth, G. Kremser, B. Aparicio, D. Rodgers, and R. Pellinen, Plasma sheet instability related to the westward travelling surge, *J. Geophys. Res., 96,* 17697, 1991.

Rufenach, C. L., R. F. Martin, Jr., and H. H. Sauer, A study of geosynchronous magnetopause crossings, *J. Geophys. Res., 94,* 15125, 1989.

Rufenach, C. L., R. L. McPherron, and J. Schaper, The quiet geomagnetic field at geosynchronous orbit and its dependence on solar wind dynamic pressure, *J. Geophys. Res., 97,* 25, 1992.

Russell, C. T., Noise in the geomagnetic tail, *Planet. Space Sci., 20,* 1541, 1972a.

Russell, C. T., The configuration of the magnetosphere, p. 1, in *Critical Problems of Magnetospheric Physics,* edited by E. R. Dryer, Inter-Union Commission on Solar-Terrestrial Physics, National Academy of Sciences, Washington, DC, 1972b.

Russell, C. T., On the occurrence of magnetopause crossings at 6.6 RE, *Geophys. Res. Lett., 3,* 593, 1976a.

Russell, C. T., Reconnexion, p. 526, in *Physics of Solar–Planetary Environments,* edited by D. J. Williams, American Geophysical Union, Washington, DC, 1976b.

Russell, C. T., Some comments on the topology of the geomagnetic tail, *J. Geophys. Res., 82,* 1625, 1977.

Russell, C. T., The control of the magnetopause by the interplanetary magnetic field, p. 3, in *Dynamics of the Magnetosphere,* edited by S.-I. Akasofu, D. Reidel Publishing Co., Dordrecht, Holland, 1979.

Russell, C. T., Solar wind control of magnetospheric configuration, p. 209, in *Solar-Wind Magnetospheric Coupling,* edited by Y. Kamide and J. A. Slavin, Terra Scientific Publishing Company, Tokyo, 1986.

Russell, C. T., The universal time variation of geomagnetic activity, *Geophys. Res. Lett., 16,* 555, 1989.

Russell, C. T., and K. I. Brody, Some remarks on the position and shape of the neutral sheet, *J. Geophys. Res., 72,* 6104, 1967.

Russell, C. T., and G. Atkinson, Comments on a paper by J. T. Heppner, Polar cap electric field distributions related to interplanetary magnetic field direction, *J. Geophys. Res., 78,* 4001, 1973.

Russell, C. T., and R. L. McPherron, The magnetotail and substorms, *Space Sci. Rev., 15,* 205, 1973a.

Russell, C. T., and R. L. McPherron, Semiannual variation of geomagnetic activity, *J. Geophys. Res., 78,* 92, 1973b.

Russell, C. T., J. V. Olson, R. E. Holzer, and E. J. Smith, OGO-3 search coil magnetometer data correlated with the reported crossing of the magnetopause at 6.6 RE by ATS-1, *J. Geophys. Res., 73,* 5769, 1968.

Russell, C. T., R. L. McPherron, and P. J. Coleman, Jr., Magnetic field variations in the near geomagnetic tail associated with weak substorm activity, *J. Geophys. Res., 76,* 1823, 1971a.

Russell, C. T., C. R. Chappell, M. D. Montgomery, M. Neugebauer, and F. L. Scarf, Ogo-5 observations of the polar cusp on November 1, 1968, *J. Geophys. Res., 76,* 6743, 1971b.

Russell, C. T., and R. C. Elphic, Initial ISEE magnetometer results: magnetopause observations, *Space Sci. Revs., 22,* 681, 1978.

Russell, C. T., and R. C. Elphic, ISEE observations of flux transfer events at the dayside magnetopause, *Geophys. Res. Lett., 6, 33,* 1979.

Russell, C. T., M. Neugebauer, and M. G. Kivelson, OGO-5 observations of the magnetopause, p. 139, in *Correlated Interplanetary and Magnetospheric Disturbances,* edited by D. E. Page, D. Reidel, Dordrecht, Holland, 1974.

Saifudinova, T. I., A. D. Bazarzhapov, D. Sh. Shirapov, S. B. Lunyushkin, and V. M. Mishin, Substorm scenario with two active phases, p. 391, in *Substorms 1: Proc. Int'l. Conf. Substorms (ICS-1), ESA SP-335,* European Space Agency, Paris, 1992.

Saito, T., Oscillations of geomagnetic field with the progress of Pt-type pulsations, *Sci. Rep. Tohoku Univ., Ser. 5, 13,* 53, 1961.

Saito, T., *Rep. Ionos. Space. Res., Japan, 16,* 295, 1962.

Saito, T., Geomagnetic pulsations, *Space Sci. Revs., 10,* 319, 1969.

Saito, T., and S. Matsushita, Geomagnetic pulsations associated with sudden commencements and sudden impulses, *Planet. Space Sci., 15,* 573, 1967.

Saito, T., K. Yumoto, and Y. Koyama, Magnetic pulsation Pi 2 as a sensitive indicator of magnetospheric substorm, *Planet. Space Sci., 24,* 1025, 1976.

Saito, K., K. Takahashi, and T. Sakurai, Examination of the resonance theory on Pcs by means of an analysis of magnetic fluctuations in the magnetosheath and in the magnetosphere, *Planet. Space Sci., 27,* 809, 1979.

Sakurai, T., and T. Saito, Magnetic pulsation Pi 2 and substorm onset, *Planet. Space Sci., 24,* 573, 1976.

Sakurai, T., and R. L. McPherron, Satellite observations of Pi 2 activity at synchronous orbit, *J. Geophys. Res., 88,* 7015, 1983.

Samson, J. C., and G. Rostoker, Polarization characteristics of Pi 2 pulsations and implications for their source mechanisms, 2, Influence of the westward travelling surge, *Planet. Space Sci., 31,* 435, 1983.

Samson, J. C., J. A. Jacobs, and G. Rostoker, Latitude-dependent characteristics of long-period geomagnetic micropulsations, *J. Geophys. Res., 76,* 3675, 1971.

Sanchez, E. R., G. L. Siscoe, J. T. Gosling, E. W. Hones, Jr., R. P. Lepping, Observations of rotational discontinuity—slow expansion fan structure of the magnetotail boundary, *J. Geophys. Res., 95,* 61, 1990.

Sanchez, E. R., G. L. Siscoe, and C.-I. Meng, Inductive attenuation of the transpolar voltage, *Geophys. Res. Lett., 18,* 1173, 1991.

Sandahl, I., and P. A. Lindquist, Electron populations above the night-side auroral oval during magnetic quiet times, *Planet. Space Sci., 38,* 1031, 1990.

Sanders, G. D., L. J. Maher, and J. W. Freeman, Observation of the plasma boundary layer at lunar distance: direct injection of plasma into the plasma sheet, *J. Geophys. Res., 85,* 4607, 1980.

Sandholt, P. E., IMF control of the polar cusp and cleft auroras, *Adv. Space Res., 8,* 21, 1988.

Sandholt, P. E., Dayside auroral activity and magnetospheric boundary layer phenomena, *J. Geomag. Geoelectr., 42,* 711, 1990.

Sandholt, P. E., A. Egeland, J. A. Holtet, B. Lybekk, K. Svenes, and S. Asheim, Large- and small-scale dynamics of the polar cusp, *J. Geophys. Res., 90,* 4407, 1985.

Sandholt, P. E., C. S. Deehr, A. Egeland, B. Lybekk, R. Viereck, and G. J. Romick, Signatures in the dayside aurora of plasma transfer from the magnetosheath, *J. Geophys. Res., 91,* 10063, 1986.

Sandholt, P. E., B. Lybekk, A. Egeland, B. Jacobson, P. F Bythrow, and D. A. Hardy, Electrodynamics of the polar cusp ionosphere—a case study, *J. Geophys. Res., 94,* 6713, 1989a.

Sandholt, P. E., B. Lybekk, A. Egeland, R. Nakamura, and T. Oguti, Midday auroral breakup, *J. Geomag. Geoelect., 41,* 371, 1989b.

Sandholt, P. E., M. Lockwood, T. Oguti, S. W. H. Cowley, K. S. C. Freeman, B. Lybekk, A. Egeland, and D. M. Willis, Midday auroral breakup events and related energy and momentum transfer from the magnetosheath, *J. Geophys. Res., 95,* 1039, 1990a.

Sandholt, P. E., M. Lockwood, B. Lybekk, and A. D. Farmer, Auroral bright spot sequence near 14 MLT: coordinated optical and ion drift observations, relationship with magnetopause boundary layer dynamics, *J. Geophys. Res., 95,* 21095, 1990b.

Sarafopoulos, D. V., and E. T. Sarris, Transient field-aligned electric fields inside the plasma sheet inferred from measurements of energetic particles, *Planet. Space Sci., 35,* 9991, 1987.

Sarafopoulos, D. V., and E. T. Sarris, Inverse velocity dispersion of energetic particle bursts inside the plasma sheet, *Planet. Space Sci., 36,* 1181, 1988.

Sarma, S. V. A., K. R. Ramanuchang, and P. V. S. Narayan, Diurnal and seasonal occurrence patterns of Pc and Pi pulsations at Choutoppal (Hyderabad) India, *Indian J. Radio Space Phys., 3,* 221, 1974.

Sarris, E. T., and Axford, W. I., Energetic protons near the plasma sheet boundary, *Nature, 277,* 460, 1979.

Sarris, E. T., S. M. Krimigis, T. Iijima, C. O. Bostrom, and T. P. Armstrong, Location of the source of magnetospheric energetic particle bursts by multispacecraft observations, *Geophys. Res. Lett., 3,* 437, 1976a.

Sarris, E. T., S. M. Krimigis, and T. P. Armstrong, Observations of magnetospheric bursts of high-energy protons and electrons at 35 Re with IMP-7, *J. Geophys. Res., 81,* 2341, 1976b.

Sarris, E. T., S. M. Krimigis, C. O. Bostrom, and T. P. Armstrong, Simultaneous multispacecraft observations of energetic proton bursts inside and outside the magnetosphere, *J. Geophys. Res., 83,* 4289, 1978.

Sato, N., R. Fujii, T. Ono, H. Fukunishi, T. Hirasawa, T. Araki, S. Kokobun, K. Makita, and Th. Saemundsson, Conjugacy of proton and electron aurora observed near L = 6.1, *Geophys. Res. Lett., 13,* 1368, 1986.

Sato, N., and T. Saemundsson, Conjugacy of electron auroras observed by scanning photometers and all-sky cameras, *Mem. Nat'l. Inst. Polar Rsch., 48,* 58, 1987.

Sato, T., and G. F. Rourke, F region enhancements in the antarctic, *J. Geophys. Res., 69,* 4591, 1964.

Sato, T., T. Shimada, T. Hayashi, and K. Watanabe, Formation of field-twisting flux tubes on the magnetopause and solar wind particle entry into the magnetosphere, *Geophys. Res. Lett., 13,* 1986.

Saunders, M. A., Recent ISEE observations of the magnetopause and low-latitude boundary layer: a review, *J. Geophys., 52,* 190, 1983.

Saunders, M. A., Origin of the cusp Birkeland currents, *Geophys. Res. Lett., 16,* 151, 1989.

Saunders, M. A., D. J. Southwood, E. W. Hones, Jr., and C. T. Russell, A hydromagnetic vortex seen by ISEE-1 and 2, *J. Atm. Terr. Phys., 43,* 927, 1981.

Saunders, M. A., C. T. Russell, and N. Sckopke, A dual-satellite study of spatial properties of FTEs, in *Magnetic Reconnection in Space and Laboratory Plasmas,* edited by E. W. Hones, Jr., p. 145, Geophysical Monograph 30, American Geophysical Union, Washington, DC, 1984.

Sauvaud, J. A., and J. R. Winckler, Dynamics of plasma, energetic particles, and fields near synchronous orbit in the nighttime sector during magnetospheric substorms, *J. Geophys. Res., 85,* 2043, 1980.

Sauvaud, J. A., A. Saint-Marc, J. Dandouras, H. Reme, A. Korth, G. Kremser, and G. K. Parks, A multi-satellite study of the plasma sheet dynamics at substorm onset, *Geophys. Res. Lett., 11,* 503, 1984.

Sauvaud, J. A., J. P. Treilhou, A. Saint-Marc, J. Dandouras, H. Reme, A. Korth, G. Kremser, G. K. Parks, A. N. Zaitsev, V. Petrov, L. Lazutine, and R. Pellinen, Large scale response of the magnetosphere to a southward turning of the interplanetary magnetic field, *J. Geophys. Res., 92,* 2365, 1987.

Scarf, F. L., R. W. Fredricks, C. F. Kennel, and F. V. Coroniti, Satellite studies of magnetospheric substorms on August 15, 1968, *J. Geophys. Res., 78,* 3119, 1973.

Schatten, K. H., and J. M. Wilcox, Response to the geomagnetic activity index K_p to the interplanetary magnetic field, *J. Geophys. Res., 72,* 5185, 1967.

Schieldge, J. P., and G. L. Siscoe, A correlation of the occurrence of simultaneous sudden magnetospheric compressions and geomagnetic onsets with selected geophysical indices, *J. Atmos. Terr. Phys., 32,* 1819, 1970.

Schindler, K., A theory of the substorm mechanism, *J. Geophys. Res., 79,* 2803, 1974.

Schindler, K., and J. Birn, On the generation of field-aligned plasma flow at the boundary of the plasma sheet, *J. Geophys. Res., 92,* 95, 1987.

Schindler, K., M. Hesse, and J. Birn, General magnetic reconnection: Parallel electric field and helicity, *J. Geophys. Res., 93,* 5547, 1988.

Schindler, K., D. N. Baker, J. Birn, E. W. Hones, Jr., J. A. Slavin, and A. B. Galvin, Analysis of an extended period of earthward plasma sheet flow at 220 Re: CDAW 8, *J. Geophys. Res., 94,* 15177, 1989.

Schmidt, A., Erdmagnetismus, in *Enzyklopadie der Mathematischen Wissenschaften, Band VI,* Leipzig, 1917.

Scholer, M., Energetic ions and electrons and their acceleration processes in the magnetotail, p. 216, in *Magnetic Reconnection in Space and the Laboratory, Geophysical Monograph 30,* American Geophysical Union, Washington, DC, 1984.

Scholer, M., Magnetic flux transfer at the magnetopause based on single X-line reconnection, *Geophys. Res. Lett., 15,* 291, 1988.

Scholer, M., Asymmetric time-dependent and stationary magnetic reconnection at the magnetopause, *J. Geophys. Res., 94,* 15099, 1989.

Scholer, M., and A. Otto, Magnetotail reconnection: Current diversion and field-aligned currents, *Geophys. Res. Lett., 18,* 733, 1991.

Scholer, M., G. Gloeckler, B. Klecker, F. M. Ipavich, D. Hovestadt, and E. J. Smith, Fast moving plasma structures in the distant magnetotail, *J. Geophys. Res., 89,* 6717, 1984a.

Scholer, M., G. Gloeckler, D. Hovestadt, B. Klecker, and F. M. Ipavich, Characteristics of plasmoid-like structures in the distant magnetotail, *J. Geophys. Res., 89,* 8872, 1984b.

Scholer, M., D. Hovestadt, B. Klecker, G. Gloeckler, and F. M. Ipavich, Average flow between 70 RE and 200 RE in the geomagnetic tail, *Geophys. Res. Lett., 11,* 343, 1984c.

Scholer, M., G. Gloeckler, D. Hovestadt, F. M. Ipavich, B. Klecker, D. N. Baker, W. Baumjohann, B. T. Tsurutani, and R. D. Zwickl, Simultaneous observations of the plasma sheet in the near-earth and distant magnetotail: ISEE-1 and ISEE-3, *Geophys. Res. Lett., 11,* 1034, 1984d.

Scholer, M., B. Klecker, D. Hovestadt, G. Gloeckler, F. M. Ipavich, and A. B. Galvin, Correlated observations of substorm effects in the near Earth region and in the deep magnetotail, *J. Geophys. Res., 90,* 4021, 1985a.

Scholer, M., B. Klecker, D. Hovestadt, G. Gloeckler, F. M. Ipavich, and A. B. Galvin, Energetic particle characteristics of magnetotail flux ropes, *Geophys. Res. Lett., 12,* 191, 1985b.

Scholer, M., D. N. Baker, G. Gloeckler, B. Klecker, F. M. Ipavich, T. Teresawa, B. T. Tsurutani, and A. B. Galvin, Energetic particle beams in the plasma sheet boundary layer following substorm expansion: simultaneous near-earth and distant tail observations, *J. Geophys. Res., 91,* 4277, 1986.

Schumaker, T. L., M. S. Gussenhoven, D. A. Hardy, and R. L. Carovillano, The relationship between diffuse auroral and plasma sheet electron distributions near local midnight, *J. Geophys. Res., 94,* 10061, 1989.

Schunk, R. W., and J. J. Sojka, A theoretical study of the lifetime and transport of large ionospheric density structures, *J. Geophys. Res., 92,* 12343, 1987.

Schuster, A., *Proc. Roy. Soc. Lon. A, 24,* 121, 1912.

Schutz, S., G. J. Adams, and F. S. Mozer, Electric and magnetic fields measured during a sudden impulse, *J. Geophys. Res., 79,* 2002, 1974.

Sckopke, N., A general relation between the energy of trapped particles and the disturbance field near the earth, *J. Geophys. Res., 71,* 3125, 1966.

Sckopke, N., and G. Paschmann, The plasma mantle, a survey of magnetotail boundary layer observations, *J. Atm. Terr. Phys., 40,* 261, 1978.

Sckopke, N., G. Paschmann, H. Rosenbauer, and D. H. Fairfield, Influence of the interplanetary magnetic field on the occurrence and thickness of the plasma mantle, *J. Geophys. Res., 81,* 2687, 1976.

Sckopke, N., G. Paschmann, G. Haerendel, B. U. O. Sonnerup, S. J. Bame, T. G. Forbes, E. W. Hones, Jr., and C. T. Russell, Structure of the low-latitude boundary layer, *J. Geophys. Res., 86,* 2099, 1981.

Scudder, J., D., K. W. Ogilvie, and C. T. Russell, The relation of flux transfer events to magnetic reconnection, p. 153, in *Magnetic Reconnection in Space and Laboratory Plasmas, Geophys. Monogr. Ser., 30,* American Geophysical Union, Washington, DC, 1984.

Scurry, L., *The Solar Wind Control of Reconnection at the Dayside Magnetopause,* Ph.D. dissertation, UCLA, 1992.

Scurry, L., and C. T. Russell, Geomagnetic activity for northward interplanetary magnetic field: am index response, *Geophys. Res. Lett., 17,* 1065, 1990.

Scurry, L., and C. T. Russell, Proxy studies of energy transfer to the magnetosphere, *J. Geophys. Res., 96,* 9541, 1991.

Semenov, V. S., I. V. Kubyshkin, V. V. Lebedeva, R. P. Rijnbeek, M. F. Heyn, H. K. Biernat, and C. J. Farrugia, A comparison and review of steady-state and time-varying reconnection, *Planet. Space Sci., 40,* 63, 1992.

Senior, C., R. M. Robinson, and T. A. Potemra, Relationship between field-aligned currents, diffuse auroral precipitation, and the westward electrojet in the early morning sector, *J. Geophys. Res., 87,* 10469, 1982.

Senior, C., D. Fontaine, G. Caudal, D. Alcayde, and J. Fontanari, Convection electric fields and electrostatic potential over $60^{\circ} < \Lambda < 72^{\circ}$, 2, statistical results, *Ann. Geophys., 8,* 257, 1990.

Sergeev, V. A., On the longitudinal localization of the substorm active region and its changes during the substorm, *Planet. Space Sci., 22,* 1341, 1974a.

Sergeev, V. A., The discrete activations of the magnetosphere during the substorm explosive phase, p. 22, in *Proc. STP Symposium, Sao Paulo, Brazil, 2,* edited by the Brazilian Organizing Committee, 1974b.

Sergeev, V. A., On the state of the magnetosphere during prolonged periods of southward-oriented interplanetray magnetic field, *Phys. Solariterr., Potsdam, 5,* 39, 1977 (in Russian).

Sergeev, V. A., Tail–aurora direct relationship, p. 277 in *Proceedings of the First International Conference on Substorms,* edited by B. Hultquist, March 23-28, 1992, Kiruna, Sweden, ESA SP-335, 1992.

Sergeev, V. A., and A. G. Yahnin, The features of auroral bulge expansion, *Planet Space Sci., 27,* 1429, 1979.

Sergeev, V. A., and V. M. Kuznetsov, Qualitative dependence of the polar cap electric field on the IMF B_Z-component and solar wind velocity, *Planet. Space Sci., 29,* 205, 1981.

Sergeev, V. A., and W. Lennartsson, Plasma sheet at X = - 20 Re during steady magnetospheric convection, *Planet. Space Sci., 36,* 353, 1988.

Sergeev, V. A., T. Bosinger, and A. T. Y. Lui, Impulsive processes in the magnetotail during substorm expansion, *J. Geophys., 60,* 175, 1986a.

Sergeev, V. A., R. J. Pellinen, T. Bosinger, W. Baumjohann, P. Stauning, and A. T. Y. Lui, Spatial and temporal characteristics of impulsive structure of magnetospheric substorm, *J. Geophys., 60,* 186, 1986b.

Sergeev, V. A., A. G. Yahnin, R. A. Rakhmatulin, S. I. Solovjev, F. S. Mozer, D. J. Williams, and C. T. Russell, Permanent flare activity in the magnetosphere during periods of low magnetic activity in the auroral zone, *Planet. Space Sci., 34,* 1169, 1986c.

Sergeev, V. A., V. S. Semenov, and M. V. Sidneva, Impulsive reconnection in the magnetotail during substorm expansion, *Planet. Space Sci., 35,* 1199, 1987.

Sergeev, V. A., O. A. Aulamo, R. J. Pellinen, M. K. Vallinkoski, T. Bosinger, C. A. Cattell, R. C. Elphic, and D. J. Williams, Non-substorm transient injection events in the ionosphere and magnetosphere, *Planet. Space Sci., 38,* 231, 1990.

Shafranov, V. D., The stability of a cylindrical gaseous conductor in a magnetic field, *Soviet J. At. Energy Engl. Transl., 1,* 709, 1956.

Sharp, R. D., R. G. Johnson, E. G. Shelley, and K. K. Harris, Energetic O^+ ions in the magnetosphere, *J. Geophys. Res., 79,* 1844, 1974.

Sharp, R. D., R. G. Johnson, and E. G. Shelley, Energetic particle measurements from within ionospheric structures responsible for auroral acceleration processes, *J. Geophys. Res., 84,* 480, 1979.

Sharp, R. D., E. Shelley, R. Johnson, and A. Ghielmetti, Counter streaming electron beams at altitudes of 1 RE over the auroral zone, *J. Geophys. Res., 85,* 92, 1980.

Sharp, R. D., D. L. Carr, W. K. Peterson, and E. G. Shelley, Ion streams in the magnetotail, *J. Geophys. Res., 86,* 4639, 1981.

Sharp, R. D., W. Lennartsson, W. K. Peterson, and E. G. Shelley, The origins of the plasma in the distant plasma sheet, *J. Geophys. Res., 87,* 10420, 1982.

Shawhan, S. D., and D. A. Gurnett, Polarization measurements of auroral kilometric radiation by Dynamics Explorer-1, *Geophys. Res. Lett., 9,* 913, 1982.

Shelley, E. G., R. G. Johnson, and R. D. Sharp, Satellite observations of energetic heavy ions during a geomagnetic storm, *J. Geophys. Res., 77,* 6104, 1972.

Shelley, E. G., R. D. Sharp, and R. G. Johnson, He^{++} and H^{+} flux measurements in the dayside magnetospheric cusp, *J. Geophys. Res., 81,* 2363, 1976.

Shelley, E. G., R. D. Sharp, R. G. Johnson, J. Geiss, P. Eberhart, H. Balsiger, G. Haerendel, and H. Rosenbauer, Plasma composition experiment on ISEE-A, *IEEE Trans. Geosci. Elect., GE-16,* 266, 1978.

Shelley, E. G., W. K. Peterson, A. G. Ghielmetti, and J. Geiss, The polar ionosphere as a source of energetic magnetospheric plasma, *Geophys. Res. Lett., 9,* 941, 1982.

Shepherd, G. G., and J. S. Murphree, Diagnosis of auroral dynamics using global auroral imaging with emphasis on localized and transient features, p. 289, in *Auroral Physics,* edited by C.-I. Meng, M. J. Rycroft, and L. A. Frank, Cambridge University Press, Cambridge, UK, 1991.

Shepherd, G. G., C. D. Anger, L. H. Brace, J. R. Burrows, W. J. Heikkila, J. Hoffman, E. Maier, and J. H. Whitteker, An observation of polar aurora and airglow from the ISIS 2 spacecraft, *Planet. Space Sci., 21,* 819, 1973.

Shepherd, G. G., J. D. Winningham, F. E. Bunn, and F. W. Thirkettle, An empirical determination of the production efficiency for auroral 6300-A emission by energetic electrons, *J. Geophys. Res., 85,* 715, 1980a.

Shepherd, G. G., R. Bostrom, H. Derblom, C.-G. Falthammar, R. Gendrin, K. Kaila, A. Korth, A. Pedersen, R. Pellinen, and G. Wrenn, Plasma and field signatures of poleward propagating auroral precipitation observed at the foot of the Geos 2 field line, *J. Geophys. Res., 85,* 4587, 1980b.

Shepherd, G. G., A. Steen, and J. S. Murphree, Auroral boundary dynamics observed simultaneously from the Viking spacecraft and from the ground, *J. Geophys. Res., 95,* 5845, 1990.

Shi, Y., and L. C. Lee, Structure of the reconnection layer at the dayside magnetopause, *Planet. Space Sci., 38,* 437, 1990.

Sibeck, D. G., Transient events in the outer magnetosphere: boundary waves or flux transfer events?, *J. Geophys. Res., 97,* 4009, 1992.

Sibeck, D. G., G. L. Siscoe, J. A. Slavin, E. J. Smith, S. J. Bame, and F. L. Scarf, Magnetotail flux ropes, *Geophys. Res. Lett., 11,* 1090, 1984.

Sibeck, D. G., G. L. Siscoe, J. A. Slavin, E. J. Smith, B. T. Tsurutani, and S. J. Bame, Magnetic field properties of the distant magnetotail magnetopause and boundary layers, *J. Geophys. Res., 90,* 9561, 1985.

Sibeck, D. G., W. Baumjohann, and R. E. Lopez, Solar wind dynamic variations and transient magnetospheric signatures, *Geophys. Res. Lett., 16,* 13, 1989a.

Sibeck, D. G., W. Baumjohann, R. C. Elphic, D. H. Fairfield, J. F. Fennell, W. B. Gail, L. J. Lanzerotti, R. E. Lopez, H. Luehr, A. T. Y. Lui, C. G. Maclennan, R. W. McEntire, T. A. Potemra, T. J. Rosenberg, and K. Takahashi, The magnetospheric response to 8-minute period strong-amplitude upstream pressure variations, *J. Geophys. Res., 94,* 2505, 1989b.

Sibeck, D. G., R. E. Lopez, and E. C. Roelof, Solar wind control of the magnetopause shape, location, and motion, *J. Geophys. Res., 96,* 5489, 1991.

Singer, H. J., and M. G. Kivelson, The latitudinal structure of Pc 5 waves in space: magnetic and electric field observations, *J. Geophys. Res., 84,* 7213, 1979.

Singer, H. J., C. T. Russell, M. G. Kivelson, T. A. Fritz, and W. Lennartsson, Satellite observations of the spatial extent and structure of Pc 3, 4, 5 pulsations near the magnetospheric equator, *Geophys. Res. Lett., 6,* 889, 1979.

Singer, H. J., W. J. Hughes, and C. T. Russell, Standing hydromagnetic waves observed by ISEE 1 and 2, radial extent and harmonic, *J. Geophys. Res., 87,* 3519, 1982.

Singer, H., W. J. Hughes, P. F. Fougere, and D. J. Knecht, The localization of Pi 2 pulsations: Ground–satellite observations, *J. Geophys. Res., 88,* 7029, 1983.

Singer, S., and S. J. Bame, Anisotropic distributions of energetic electrons in the earth's magnetotail and magnetosheath, p. 122, in *Particles and Fields in the Magnetosphere,* edited by B. M. MacCormac, D. Reidel, Dordrecht, Netherlands, 1970.

Siscoe, G. L., A unified treatment of magnetospheric dynamics with applications to magnetic storms, *Planet. Space Sci., 14,* 947, 1966.

Siscoe, G. L., Solar–terrestrial relations: stone age to space age, *Technology Review, 78,* 1, 1976 (Alumni Association of the Massachusetts Institute of Technology, Cambridge, Mass.).

Siscoe, G. L., and W. E. Cummings, On the cause of geomagnetic bays, *Planet. Space Sci., 17,* 1795, 1969.

Siscoe, G. L., and T. S. Huang, Polar cap inflation and deflation, *J. Geophys. Res., 90,* 543, 1985.

Siscoe, G. L., and E. R. Sanchez, An MHD model for the complete open magnetotail boundary, *J. Geophys. Res., 92,* 7405, 1987.

Siscoe, G. L., V. Formisano, and A. J. Lazarus, Relation between geomagnetic sudden impulses and solar wind pressure changes: an experimental investigation, *J. Geophys. Res., 73,* 4869, 1968.

Siscoe, G. L., W. Lotko, and B. U. O. Sonnerup, A high-latitude, low-latitude boundary layer model of the convection current system, *J. Geophys. Res., 96,* 3487, 1991.

Skillman, T. L., and M. Sugiura, Magnetopause crossing of the geostationary satellite ATS 5 at 6. 6 RE, *J. Geophys. Res., 76,* 44, 1971.

Slavin, J. A., and R. E. Holzer, Solar wind flow about the terrestrial planets, 1, Modeling bow shock position and shape, *J. Geophys. Res., 86,* 11401, 1981.

Slavin, J. A., R. E. Holzer, J. R. Spreiter, S. S. Stahara, and D. S. Chaussee, Solar wind flow about the terrestrial planets, 2, Comparison with gas dynamic theory and implications for solar–planetary interactions, *J. Geophys. Res., 88,* 19, 1983.

Slavin, J. A., E. J. Smith, B. T. Tsurutani, D. G. Sibeck, H. J. Singer, D. N. Baker, J. T. Gosling, E. W. Hones, and F. L. Scarf, Substorm associated traveling compression regions in the distant tail: Isee-3 geotail observations, *Geophys. Res. Lett., 11,* 657, 1984.

Slavin, J. A., E. J. Smith, D. G. Sibeck, D. N. Baker, R. D. Zwickl, and S.-I Akasofu, An ISEE 3 study of average and substorm conditions in the distant magnetotail, *J. Geophys. Res., 90,* 10875, 1985.

Slavin, J. A., et al., Magnetic configuration of the distant plasma sheet: ISEE-3 observations, p. 59, in *Magnetotail Physics,* edited by A. T. Y. Lui, Johns Hopkins University Press, Baltimore, 1987.

Slavin, J. A., D. N. Baker, J. D. Craven, R. C. Elphic, D. H. Fairfield, L. A. Frank, A. B. Galvin, W. J. Hughes, R. H. Manka, D. G. Mitchell, I. G. Richardson, T. R. Sanderson, D. J. Sibeck, E. J. Smith, and R. D. Zwickl, CDAW 8 observations of plasmoid signatures in the geomagnetic tail: an assessment, *J. Geophys. Res., 94,* 15153, 1989.

Slavin, J. A., R. P. Lepping, and D. N. Baker, IMP-8 observations of traveling compression regions: new evidence for near-earth plasmoids and neutral lines, *Geophys. Res. Lett., 17,* 913, 1990.

Slutz, R. J., and J. R. Winkelman, Shape of the magnetopause boundary under solar wind pressure, *J. Geophys. Res., 69,* 4933, 1964.

Smiddy, M., W. J. Burke, M. C. Kelley, N. A. Saflekos, M. S. Gussenhoven, D. A. Hardy, and F. J. Rich, Effects of high latitude conductivity on observed convection electric fields and Birkeland currents, *J. Geophys. Res., 85,* 6811, 1980.

Smith, E. J., Interplanetary magnetic fields, *Revs. Geophys. Space Phys., 17,* 610, 1979.

Smith, E. J., J. A. Slavin, R. D. Zwickl, and S. J. Bame, Shocks and storm sudden commencements, p. 345, in *Solar-Wind Magnetosphere Coupling,* edited by Y. Kamide and J. A. Slavin, Terra, Tokyo, 1986.

Smith, M. F., and D. B. Curran, On the correlation between a magnetopause penetration parameter and FTE occurrence, *Ann. Geophys., 8,* 579, 1990.

Smith, M. F., and M. Lockwood, The pulsating cusp, *Geophys. Res. Lett., 17,* 1069, 1990.

Smith, M. F., M. Lockwood, and S. W. H. Cowley, The statistical cusp: a flux transfer event model, *Planet. Space Sci., 40,* 1251, 1992.

Snyder, A. L., and S.-I. Akasofu, Observations of the auroral oval by the Alaska meridian chain of stations, *J. Geophys. Res., 77,* 3419, 1972.

Snyder, A. L., and S.-I. Akasofu, Major auroral substorm features in the dark sector observed by a USAF DMSP satellite, *Planet. Space Sci., 22,* 1511, 1974.

Snyder, C. W., M. Neugebauer, and U. R. Rao, The solar wind velocity and its correlation with cosmic-ray variations and with solar and geomagnetic activity, *J. Geophys. Res., 68,* 6381, 1963.

Sojka, J. J., and R. W. Schunk, A theoretical study of the production and decay of localized electron density enhancements in the polar ionosphere, *J. Geophys. Res., 91,* 3245, 1986.

Sonett, C. P., E. J. Smith, and A. R. Sims, Surveys of the distant magnetic field: Pioneer I and Explorer II, *Space Res., 1,* 921, 1960.

Song, P., R. C. Elphic, and C. T. Russell, ISEE 1 and 2 observations of the oscillating magnetopause, *Geophys. Res. Lett., 15,* 744, 1988.

Song, P., C. T. Russell, N. Lin, and R. J. Strangeway, p. 463, in *Physics of Space Plasmas (1989), SPI Conference and Preprint Series, No. 9,* edited by T. Chang, G. B. Crew, and J. P. Jasperse, Scientific Publishers, Inc., Cambridge, Mass.., 1990a.

Song, P., C. T. Russell, J. T. Gosling, M. F. Thomsen, and R. C. Elphic, Observations of the density profile in the magnetosheath near the stagnation streamline, *Geophys. Res. Lett., 17,* 2035, 1990b.

Song, P., C. T. Russell, and M. F. Thomsen, Slow mode transition in the frontside magnetosheath, *J. Geophys. Res., 97,* 8295, 1992a.

Song, P., C. T. Russell, and M. F. Thomsen, Waves in the inner magnetosheath: a case study, *Geophys. Res. Lett., 22,* 2191, 1992b.

Sonnerup, B. U. O., Theory of the low-latitude boundary layer, *J. Geophys. Res., 85,* 2017, 1980.

Sonnerup, B. U. O., and L. J. Cahill, Jr., Magnetopause structure and attitude from Explorer 12 observations, *J. Geophys. Res., 72,* 171, 1967.

Sonnerup, B. U. O., and E. R. Priest, Resistive MHD stagnation-point flows at a current sheet, *J. Plasma Phys., 14,* 283, 1975.

Sonnerup, B. U. O., and B. G. Ledley, OGO 5 magnetopause structure and classical reconnection, *J. Geophys. Res., 84,* 399, 1979.

Sonnerup, B. U. O., G. Paschmann, I. Papamastorakis, N. Sckopcke, G. Haerendel, S. J. Bame, J. R. Asbridge, J. T. Gosling, and C. T. Russell, Evidence for magnetic field reconnection at the earth's magnetopause, *J. Geophys. Res., 86,* 10049, 1981.

Southwood, D. J., The hydromagnetic stability of the magnetospheric boundary, *Planet. Space Sci., 11,* 587, 1968.

Southwood, D. J., Some features of field line resonancs in the magnetosphere, *Planet. Space Sci., 22,* 483, 1974.

Southwood, D. J., The role of hot plasma in magnetospheric convection, *J. Geophys. Res., 82,* 5512, 1977.

Southwood, D. J., Theoretical aspects of ionosphere–magnetosphere–solar wind coupling, in *Physics of the Ionosphere–Magnetosphere, Adv. Space Res., 5*, 4, 1985.

Southwood, D. J., The ionospheric signature of flux transfer events, *J. Geophys. Res., 92,* 3207, 1987.

Southwood, D. J., and W. F. Stuart, Pulsations at the substorm onset, p. 341, in *Dynamics of the Magnetosphere,* edited by S.-I. Akasofu, D. Reidel, Dordrecht, 1979.

Southwood, D. J., and M. G. Kivelson, The effect of parallel inhomogeneity on magnetospheric hydromagnetic wave coupling, *J. Geophys. Res., 91,* 6871, 1986.

Southwood, D. J., and M. G. Kivelson, The magnetohydrodynamic response of the magnetospheric cavity to changes in solar wind pressure, *J. Geophys. Res., 95,* 2301, 1990.

Southwood, D. J., and M. G. Kivelson, On the form of the flow in the magnetosheath, *J. Geophys. Res., 97,* 2873, 1992.

Southwood, D. J., M. A. Saunders, M. W. Dunlop, W. A. C. Mier-Jedrzejowicz, and R. P. Rijnbeek, A survey of flux transfer events recorded by UKS spacecraft magnetometer, *Planet. Space Sci., 34,* 1349, 1986.

Southwood, D. J., C. J. Farrugia, and M. A. Saunders, What are flux transfer events?, *Planet. Space Sci., 36,* 503, 1988.

Speiser, T. W., Particle trajectories in model current sheets, 1, Analytical solutions, *J. Geophys. Res., 70,* 4219, 1965.

Speiser, T. W., Particle trajectories in model current sheets, 2, Applications to auroras using a geomagnetic tail model, *J. Geophys. Res., 72,* 3919, 1967.

Spiro, R. W., P. H. Reiff, and L. J. Maher, Jr., Precipitating electron energy flux and auroral zone conductances—an empirical model, *J. Geophys. Res., 87,* 8215, 1982.

Spjeldvik, W. N., and T. A. Fritz, Energetic ion and electron observations of the geomagnetic plasma sheet boundary layer: Three-dimensional reults from ISEE 1, *J. Geophys. Res., 86,* 2480, 1981.

Spreiter, J. R., and B. R. Briggs, Theoretical determination of the form of the boundary produced of the corpuscular stream produced by interaction with the magnetic dipole field of the earth, *J. Geophys. Res., 67,* 37, 1962.

Spreiter, J. R., and B. J. Hyett, The effect of a uniform external pressure on the boundary of the geomagnetic field in a steady solar wind, *J. Geophys. Res., 68,* 1631, 1963.

Spreiter, J. R., and W. P. Jones, On the effect of a weak interplanetary field on the interaction between the solar wind and the geomagnetic field, *J. Geophys. Res., 68,* 3555, 1963.

Spreiter, J. R., and A. L. Summers, On conditions near the neutral points on the magnetosphere boundary, *Planet. Space Sci., 15,* 787, 1967.

Spreiter, J. R., and A. Y. Alksne, Effect of neutral sheet currents on the shape and mgnetic field of the magnetosphere tail, *Planet. Space Sci., 17,* 223, 1969a.

Spreiter, J. R., and A. Y. Alksne, Plasma flow around the magnetosphere, *Rev. Geophys., 7,* 11, 1969b.

Spreiter, J. R., and A. Y. Alksne, Solar-wind flow past objects in the solar system, p. 313, in *Annual Reviews of Fluid Mechanics,* edited by M. D. Van Dyke, W. G. Vincenti, and J. V. Wehausen, Annual Reviews, Inc., Palo Alto, Calif., 1970.

Spreiter, J. R., and A. W. Rizzi, Aligned magnetohydrodynamic solution for solar wind flow past the earth's magnetosphere, *Acta Astronaut., 1,* 15, 1974.

Spreiter, J. R., and S. S. Stahara, A new predictive model for determining solar wind–terrestrial planet interactions, *J. Geophys. Res., 85,* 6769, 1980.

Spreiter, J. R., and S. S. Stahara, Magnetohydrodynamic and gas dynamic theories for planetary bow waves, p. 85, in *Collisionless Shocks in the Heliosphere: Reviews of Current Research, Geophysical Monograph 35,* edited by B. T. Tsurutani and R. G. Stone, American Geophysical Union, Washington, DC, 1985.

Spreiter, J. R., A. L. Summers, and A. Y. Alksne, Hydromagnetic flow around the magnetosphere, *Planet. Space Sci., 14,* 223, 1966.

Starkov, G. V., and Y. I. Feldstein, Substorm in auroras, *Geomagn. Aeronom., 11,* 478, 1971.

Stasiewicz, K., Polar cusp topology and position as a function of interplanetary magnetic fild and magnetic activity: comparison of a model with *Viking* and other observations, *J. Geophys. Res., 96,* 15789, 1991.

Steele, D. P., D. J. McEwen, and J. S. Murphree, Possibility of auroral remote sensing with the *Viking* ultraviolet imager, *J. Geophys. Res., 97,* 2845, 1992.

Steinolfson, R. S., and A. J. Hundhausen, MHD intermediate shocks in coronal mass ejections, *J. Geophys. Res., 95,* 6389, 1990a.

Steinolfson, R. S., and A. J. Hundhausen, Concave-outward slow shocks in coronal mass ejections, *J. Geophys. Res., 95,* 15251, 1990b.

Stenbaek-Nielsen, H. C., T. N. Davis, and N. W. Glass, Relative motion of auroral conjugate points during substorms, *J. Geophys. Res., 77,* 1844, 1972.

Stenbaek-Nielsen, H. C., E. M. Westcott, T. N. Davis, and R. W. Peterson, Differences in auroral intensity at conjugate points, *J. Geophys. Res., 78,* 659, 1973.

Stern, D. P., A study of the electric field in an open magnetospheric model, *J. Geophys. Res., 78,* 7292, 1973.

Stern, D. P., A model of the magnetospheric tail with current-free lobes, *Planet. Space Sci., 38,* 255, 1990.

Stewart, B., On the great magnetic disturbance which extended from August 28 to September 7, 1859, as recorded by photography at the Kew Observatory, *Phil. Trans., Roy. Soc. London,* 423, 1861.

Stokholm, M., E. Amata, H. Balsiger, M. Candidi, S. Orsini, and A. Pedersen, Low energy (< 130 eV) oxygen ions at the geosynchronous orbit during the CDAW 6 events of March 22, 1979, *J. Geophys. Res., 90,* 1253, 1985.

Storey, L. R. O., An investigation of whistling atmospherics, *Phil. Trans. Roy. Soc., A 246,* 113, 1953.

Stormer, C., Sur les trajectoires des corpuscules electrisees dans l'espace sous l'action du magnetisme terrestre avec application aux aurores boreales, pp. 5, 113, 221, 317, in *Arch. Sci. Phys. Geneve, 24,* 1907.

Stuart, W. F., V. E. Sherwood, and S. M. NcIntosh, An analysis of micropulsation spectra (pc) obtained from U. K. observatories, *J. Atmos. Terr. Phys., 33,* 869, 1971.

Sugiura, M., A fundamental magnetosphere–ionosphere coupling mode involved field-aligned currents as deduced from DE-2 observations, *Geophys. Res. Lett., 9,* 877, 1984.

Sugiura, M., and C. R. Wilson, Oscillation of the geomagnetic field lines and associated magnetic perturbations at conjugate points, *J. Geophys. Res., 69,* 1211, 1964.

Sugiura, M., T. L. Skillman, B. G. Ledley, and J. P. Heppner, Propagation of the sudden commencement of July 8, 1966, to the magnetotail, *J. Geophys. Res., 73,* 6699, 1968.

Sugiura, M., N. C. Maynard, W. H. Farthing, J. P. Heppner, B. G. Ledley, and L. J. Cahill, Jr., Initial results on the correlation between the magnetic and electric fields observed from the DE-2 satellite in the field-aligned current regions, *Geophys. Res. Lett., 9,* 985, 1982.

Sugiura, M., T. Iyemori, R. A. Hoffman, N. C. Maynard, J. L. Burch, and J. D. Winningham, Relationships between field-aligned currents and particle precipitation as observed by Dynamics Explorer-2, p. 96, in *Magnetospheric Currents,* edited by T. A. Potemra, Geophysical Monograph 28, American Geophysical Union, 1983.

Sugiura, M., T. Iyemori, R. A. Hoffman, and N. C. Maynard, Relationships between field-aligned currents, electric fields, and particle acceleration as observed by Dynamics-Explorer-2, in *Magnetospheric Currents, Geophys. Monograph Ser., 28,* edited by T. A. Potemra, p. 96, American Geophysical Union, Washington, DC, 1984.

Sun, W., J. R. Kan, and S.-I. Akasofu, Evolution of magnetic configurations in the plasma sheet during a substorm on March 19, 1978, *J. Geophys. Res., 96,* 15831, 1991.

Sutcliffe, P. R., The longitudinal range of Pi 2 propagation at low latitudes, *Planet. Space Sci., 28,* 9, 1980.

Sutcliffe, P. R., and K. Yumoto, Pi 2 pulsations at low latitudes, *Geophys. Res., Lett., 16,* 857, 1989.

Sweet, P. A., The neutral point theory of solar flares, pp. 123–40, in *Electromagnetic Phenomena in Cosmical Physics, Proc. IAU Symposium No. 6, Stockholm, 1956,* edited by B. Lehnert, Cambridge University Press, New York, 1958.

Takahashi, K., and R. L. McPherron, Harmonic structure of Pc 3–4 pulsations, *J. Geophys. Res., 87,* 1504, 1982.

Takahashi, K., and R. L. McPherron, Standing hydromagnetic waves in the magnetosphere, *Planet. Space Sci., 32,* 1343, 1984.

Takahashi, K. and E. W. Hones, Jr., ISEE 1 and 2 observations if ion distributions at the plasma sheet–tail lobe boundary, *J. Geophys. Res., 93,* 8558, 1988.

Takahashi, K., R. L. McPherron, and W. J. Hughes, Multispacecraft observations of the harmonic structure of Pc 3–4 magnetic pulsations, *J. Geophys. Res., 89,* 6758, 1984.

Takahashi, K., C. T. Russell, and R. R. Anderson, ISEE 1 and 2 observations of the spatial structure of a compressional Pc 5 wave, *Geophys. Res. Lett., 12,* 613, 1985.

Takahashi, K., S. Kokobun, T. Sakurai, R. W. McEntire, T. A. Potemra, and R. E. Lopez, AMPTE/CCE observations of substorm-associated standing Alfven waves in the midnight sector, *Geophys. Res. Lett., 15,* 1287, 1988.

Tamao, T., Geomagnetic pulsations and the earth's exosphere, *Rep. Ionos. Space Res. Japan, 15,* 293, 1961.

Tamao, T., Transmission and coupling resonance of hydromagnetic disturbances in the non-uniform earth's magnetosphere, *Sci. Rep. Tohoku Univ., Ser. 5, 17,* 43, 1965.

Tamao, T., Hydromagnetic coupling oscillations and drift instabilities in nonuniform, collisionless plasma, *Phys. Fluids, 12,* 1, 1969.

Tanskanen, P., J. Kangas, L. Block, G. Kremser, A. Korth, J. Woch, I. B. Iversen, K. M. Torkar, W. Riedler, S. Ullaland, J. Stadnes, and K.-H. Glassmeier, Different phases of a magnetospheric substorm on June 23, 1979, *J. Geophys. Res., 92,* 7443, 1987.

Teresawa, T., Numerical study of explosive tearing mode instability in one-component plasmas, *J. Geophys. Res., 86,* 9007, 1981.

Theile, B., and K. Wilhelm, Field-aligned currents above an auroral arc, *Planet. Space Sci., 28,* 351, 1980.

Timofeev, E. E., and Yu. I. Galperin, Convection and currents in stable auroral arcs and inverted-V's, *J. Geomag. Geoelect., 44,* 1992.

Timofeev, E. E., V. M. Smyshliayev, N. V. Jorjio, Yu. I. Galperin, J. M. Bosqued, J. J. Berthelier, M. K. Vallinkoski, and R. J. Pellinen, Coordinated data on auroral electrodynamics from ground-based radar diagnostics and AUREOL-3 satellite, in *Results of the ARCAD-3 Project and of the Recent Programs in Magnetospheric and Ionospheric Physics,* edited by CNES, CEPADUES-EDITIONS, Toulouse, France, 1985.

Timofeev, E. E., M. K. Vallinkoski, T. V. Kozelova, A. G. Yahnin, and R. J. Pellinen, Systematics of arc-associated electric fields and currents as inferred from radar backscatter measurements, *J. Geophys., 61,* 122, 1987.

Timofeev, E. E., O. M. Raspopov, Yu. I. Galperin, N. V. Jorjio, J. M. Bosqued, J. J. Berthelier, M. K. Vallinkoski, and R. J. Pellinen, *Cosmic Research, 10,* 500, 1988 (in Russian).

Timofeev, E. E., O. M. Raspopov, Yu. I. Galperin, N. V. Jorjio, J. M. Bosqued, J. J. Berthelier, A. Berthelier, O. A. Aulamo, M. K. Vallinkoski, and R. J.

Pellinen, in *Auroral Physics,* edited by C.-I. Meng, M. J. Rycroft, and L. A. Frank, Cambridge University Press, Cambridge, UK, 1991.

Todd, H., B. J. I. Bromage, S. W. H. Cowley, M. Lockwood, A. P. van Eyken, and D. M. Willis, EISCAT observations of bursts of rapid flow in the high latitude dayside ionosphere, *Geophys. Res. Lett., 13,* 909, 1986.

Todd, H., S. W. H. Cowley, A. Etemadi, B. J. I. Bromage, M. Lockwood, D. M. Willis, and H. Luhr, Response-time of the high-latitude ionosphere to sudden changes in the north–south component of the IMF, *Planet. Space Sci., 36,* 1415, 1988.

Traver, D. P., D. G. Mitchell, D. J. Williams, L. A. Frank, and C. Y. Huang, Two encounters with the flank low-latitude boundary layer: further evidence for closed field topology and investigation of the internal structure, *J. Geophys. Res., 96,* 21025, 1993.

Troitskaya, V. A., Micropulsations and the state of the magnetosphere, in *Solar–Terrestrial Physics,* edited by J. W. King and W. S. Newman, Academic Press, New York, 1967.

Troitskaya, V. A., Results of ULF–wave investigations in the USSR, in *Achievements of the International Magnetospheric Study (IMS), Proc. Intl. Symp. Graz,* ESA publications, Noordwijk, Holland, 1984.

Tromholt, S., Sur les periodes de l'aurore boreale, *Proc. Inst. Met. Danois, Copenhague,* 1880.

Troshichev, O. A., Polar magnetic disturbances and field–aligned currents, *Space Sci. Rev., 32,* 275, 1982.

Troshichev, O. A., Solar wind control of electric fields and currents in the magnetosphere and ionosphere, p. 407, in *Proc. Conf. Achievements of the IMS , 26–28 June, Graz, Austria,* ESA pub., 1984.

Troshichev, O. A., Global dynamics of the magnetosphere for northward IMF conditions, *J. Atm. Terr. Phys., 52,* 1135, 1990.

Troshichev, O. A., and N. A. Tsyganenko, *Geomagn. Res., 25,* 47, 1978 (in Russian).

Troshichev, O. A., and N. A. Tsyganenko, *Magnetospheric Res., 1,* 77, 1982 (in Russian).

Troshichev, O. A., V. A. Gizler, and A. V. Shirochkov, Field–aligned currents and magnetic disturbances in the dayside polar region, *Planet. Space Sci., 30,* 1033, 1982 .

Troshichev, O. A., M. G. Gusev, S. V. Nickolashkin, and V. P. Samsonov, Features of the polar cap auroras in the southern polar cap region, *Planet. Space Sci., 36,* 429, 1988.

Tsunoda, R. T., I. Haggstrom, A. Pellinen-Wannberg, A. Steen, and G. Wannberg, Direct evidence of plasma density structuring in the auroral F region ionosphere, *Radio Sci., 20,* 762, 1985.

Tsurutani, B., and R. M. Thorne, Diffusion processes in the magnetopause boundary layer, *Geophys. Res. Lett., 9,* 1247, 1982.

Tsurutani, B. T., et al., Lion roars and nonoscillatory drift mirror waves in the magnetosheath, *J. Geophys. Res., 87,* 6060, 1982.

Tsurutani, B. T., J. A. Slavin, Y. Kamide, R. D. Zwickl, J. H. King, and C. T. Russell, Coupling between the solar wind and the magnetosphere: CDAW 6, *J. Geophys. Res., 90,* 1191, 1985.

Tsyganenko, N. A., On the convective mechanism for formation of the plasma sheet in the magnetospheric tail, *Planet. Space Sci., 30,* 1007, 1982.

Tsyganenko, N. A., Global quantitative models of the geomagnetic field in the cislunar magnetosphere for different disturbance levels, *Planet. Space Sci., 35,* 1347, 1987.

Tsyganenko, N. A., Quantitative models of the magnetospheric magnetic field: methods and results, *Space Sci. Rev., 54,* 75, 1990.

Tsyganenko, N. A., and A. V. Usmanov, Determination of the magnetospheric current system parameters and development of experimental geomagnetic field models based on the data from IMP and HEOS satellites, *Planet. Space Sci., 30,* 985, 1982.

Tverskoy, B. A., *Dynamics of the Earth's Radiation Belts,* Physical–mathematical literature, Science Publishing House, Moscow, 1968.

Ullaland, S., et al., Influence of a storm sudden commencement on the development of a magnetospheric storm: ground, balloon, and satellite observations, submitted, *J. Geophys. Res.,* 1992.

Untiedt, J., R. Pellinen, F. Kuppers, H. J. Opgenoorth, W. D. Pelster, W. Baumjohann, H. Ranta, J. Kangas, P. Czechowsky, and W. J. Heikkila, Observations of the initial development of an auroral and magnetic substorm at magnetic midnight, *J. Geophys., 45,* 41, 1978.

Uspensky, M. V., G. V. Starkov, O. Aulamo, and K. Kaila, Breakup signatures in the VHF auroral radar backscatter and optical emissions, p. 337, in *Substorms 1: Proc. Int'l. Conf. Substorms (ICS-1), ESA SP-335,* European Space Agency, Paris, 1992.

Valladares, C. E., Su. Basu, R. J. Niciejewski, and R. E. Sheehan, Simultaneous radar and satellite observations of the polar cusp/cleft at Sondre Stromfjord, in *Electromagnetic Coupling in the Polar Clefts and Caps,* edited by P. E. Sandholt and A. Egeland, p. 1, Kluwer Academic Publishers, Boston, 1989.

Vallance-Jones, A., F. Creutzberg, R. L. Gattinger, and F. R. Harris, Auroral studies with a chain of meridian-scanning photometers 1. Observations of proton and electron aurora in magnetospheric substorms, *J. Geophys. Res., 87,* 4489, 1982.

Van Allen, J. A., The geomagnetically-trapped corpuscular radiation, *J. Geophys. Res., 64,* 1683, 1959.

van Eyken, A. P., H. Rishbeth, D. M. Willis, and S. W. H. Cowley, Initial EISCAT observations of plasma convection at invariant latitudes of 70–77°, *J. Atmos. Terr. Phys., 50,* 635, 1984.

Vasyliunas, V. M., A survey of low-energy electrons in the evening sector of the magnetosphere with OGO 1 and OGO 3, *J. Geophys. Res., 73,* 2839, 1968.

Vasyliunas, V. M., unpublished independent research described in C. F. Kennel, Consequences of a magnetospheric plasma, *Rev. Geophys., 7,* 379, 1969.

Vasyliunas, V. M., Mathematical models of magnetospheric convection and its coupling to the ionosphere, p. 60, in *Particles and Fields in the Magnetosphere,* edited by B. M. McCormac, D. Reidel Publ. Co., Dordrecht, Holland, 1970.

Vasyliunas, V. M., Interaction between the magnetospheric boundary layers and the ionosphere, p. 387, Proc. Magnetospheric Boundary Layers Conference, *ESA Spec. Publ. SP-148,* ESTEC, Noordwijk, Holland, 1979.

Vasyliunas, V. M., J. R. Kan, G. L. Siscoe, and S.-I. Akasofu, Scaling relations governing magnetospheric energy transfer, *Planet. Space Sci., 30,* 359, 1982.

Vegard, L., Hydrogen lines in the auroral spectrum, *Nature, 114,* 1089, 1939.

Vernov, S. N., N. I. Grigorov, Y. I. Logachev, and A. Y. Chudakov, Artificial satellite measurements of cosmic radiation, *Dokl. Akad. Nauk SSSR, 120,* 1231, 1958.

Vero, J., Experimental aspects of low-latitude pulsations—a review, *J. Geophys., 60,* 106, 1986.

Vickrey, J. F., C. L. Rino, and T. A. Potemra, Chatanika/Triad observations of unstable ion enhancements in the auroral F region, *Geophys. Res. Lett., 7,* 789, 1980.

Villante, U., Neutral sheet observations at 1000 RE, *J. Geophys. Res., 81,* 212, 1976.

Voelker, H., On geomagnetic pulsations accompanying storm sudden commencements and sudden impulses, *Earth Planet. Sci. Letts., 1,* 383, 1966.

Vorobjev, V. G., and B. V. Rezhanov, Progressive westward displacements of the region of the auroral substorm localizations in conjunction with impulsive variations of the geomagnetic field, *Geomag. Aeron., 34,* 441, 1973.

Vorobjev, V. G., G. Gustafsson, G. V. Starkov, Y. I. Feldstein, and N. F. Shernina, Dynamics of day and night aurora during substorms, *Planet. Space Sci., 23,* 269, 1975.

Walker, A. D. M., and R. A. Greenwald, Statistics of occurrence of hydromagnetic oscillations in the Pc 5 range observed by the STARE auroral radar, *Planet. Space Sci., 29,* 293, 1981.

Walker, R. J., and T. Ogino, Field-aligned currents and magnetospheric convection: a comparison between MHD simulations and observations, p. 39, in *Modeling Magnetospheric Plasma (Geophys. Monograph, Ser. 44),* edited by T. E. Moore and J. H. Waite, Jr., American Geophysical Union, Washington, DC, 1988.

Walker, R. J., U. Villante, and A. J. Lazarus, Pioneer 7 observations of plasma flow and field reversal regions in the distant geomagnetic tail, *J. Geophys. Res., 80,* 1238, 1975.

Walker, R. J., K. N. Erickson, R. L. Swanson, and J. R. Winckler, Substorm-associated particle boundary motion at synchronous orbit, *J. Geophys. Res., 81,* 5541, 1976.

Walker, R. J., T. Ogino, M. Ashour-Abdalla, and J. Raeder, A global magnetohydrodynamic simulation of magnetospheric dynamics when the IMF is southward: mapping to the auroral zone, p. 571 in *Substorms 1: Proc. Int'l. Conf. Substorms (ICS-1), ESA SP-335,* European Space Agency, Paris, 1992.

Wallis, D. D., J. R. Burrow, T. J. Hughes, and M. D. Wilson, Eccentric dipole coordinates for Magsat data presentation and analysis of external current effects, *Geophys. Res. Lett., 9,* 353, 1982.

Weber, E. J., J. Buchau, J. G. Moore, J. R. Sharber, R. C. Livingston, J. D. Winningham, and B. W. Reinisch, F layer ionization patches in the polar cap, *J. Geophys. Res., 89,* 1683, 1984.

Weber, E. J., R. T. Tsunoda, J. Buchau, R. E. Sheehan, D. J. Strickland, W. Whiting, and J. G. Moore, Coordinated measurements of auroral zone enhancements, *J. Geophys. Res., 90,* 6497, 1985.

Weber, E. J., J. A. Klobuchar, J. Buchau, H. C. Carlson, Jr., R. C. Livingston, O. de la Beaujardiere, M. McCready, J. G. Moore, and G. J. Bishop, Polar cap F layer patches: structure and dynamics, *J. Geophys. Res., 91,* 12121, 1986.

Weber, E. J., J. F. Vickrey, H. Gallagher, L. Weiss, C. J. Heinselman, R. A. Heelis, and M. C. Kelley, Coordinated radar and optical measurements of stable auroral arcs at the polar cap boundary, *J. Geophys. Res., 96,* 17847, 1991.

Wedde, T., J. R. Doupnik, and P. M. Banks, Chatanika observations of the latitudinal structure of electric fields and particle precipitation on November 21, 1975, *J. Geophys. Res., 82,* 2743, 1975.

Wedde, T., J. R. Doupnik, and P. M. Banks, Chatanika observations of the latitudinal structure of electric fields and particle precipitation on November 21, 1975, *J. Geophys. Res., 82,* 2743, 1977.

Wei, C. Q., L. C. Lee, and A. L. La Belle-Hamer, A simulation study of the vortex structure in the low–latitude boundary layer, *J. Geophys. Res., 95,* 20793, 1990

Weimer, D. R., C. K. Goertz, D. A. Gurnett, N. C. Maynard, and J. L. Burch, Auroral zone electric fields from DE 1 and 2 at magnetic conjunctions, *J. Geophys. Res., 90,* 7479, 1985.

Weimer, D. R., D. A. Gurnett, C. K. Goertz, J. D. Menietti, J. L. Burch, and M. Sugiura, The current–voltage relationship in auroral current sheets, *J. Geophys. Res., 92,* 187, 1987.

Weimer, D. R., N. C. Maynard, W. J. Burke, and C. Liebrecht, Polar cap potentials and the auroral electrojet indices, *Planet. Space Sci., 38,* 1207, 1990.

Weimer, D. R., J. R. Kan, and S.-I. Akasofu, Variations of the polar cap potential measured during magnetosphric substorms, *J. Geophys. Res., 97,* 3945, 1992.

West, H. I., Jr., and A. L. Vampola, Simultaneous observations of solar flare electron spectra in interplanetary space and within the earth's magnetosphere, *Phys. Rev. Lett., 26,* 458, 1971.

West, H. I., Jr., and R. M. Buck, Observations of > 100 keV protons in the earth's magnetosheath, *J. Geophys. Res., 81,* 569, 1976.

Westcott, E. M., Magnetoconjugate phenomena, *Space Sci. Rev., 5,* 507, 1966.

Westcott, E. M., J. D. Stolarik, and J. P. Heppner, Electric fields in the vicinity of auroral forms from motions of barium vapor releases, *J. Geophys. Res., 74,* 3469, 1969.

Westcott, E. M., H. C. Stenbaek-Nielsen, T. N. Davis, W. B. Murcray, H. M. Peek, and P. J. Bottoms, The L = 6.6 OOsik barium injection experiment and magnetic storm of March 7, 1972, *J. Geophys. Res., 80,* 951, 1975.

Westerlund, L. H., The auroral energy spectrum extended to 45 eV, *J. Geophys. Res., 74,* 351, 1969.

Whalen, J. A., A quantitative description of the spatial distribution and dynamics of the energy flux in the continuous aurora, *J. Geophys. Res., 88,* 7155, 1983.

Whelan, T., and C. K. Goertz, A new model for the ion beams in the plasma sheet boundary layer, *Geophys. Res. Lett., 14,* 68, 1987.

Wiens, R. G., and G. Rostoker, Characteristics of the development of the westward electrojet during the expansive phase of magnetospheric substorms, *J. Geophys. Res., 80,* 2105, 1975.

Wilken, B., D. N. Baker, P. R. Higbie, T. A. Fritz, W. P. Olson, and K. A. Pfitzer, Magnetospheric configuration and energetic particle effects associated with a SSC: study of the CDAW 6 event on March 22, 1979, *J. Geophys. Res., 91,* 1459, 1986.

Williams, D. J., Magnetopause characteristics inferred from three-dimensional energetic particle distributions, *J. Geophys. Res., 84,* 101, 1979a.

Williams, D. J., Observations of significant magnetosheath anti-solar energy flow, *J. Geophys. Res., 84,* 2105, 1979b.

Williams, D. J., Magnetopause characteristics at 0840–1040 hours local time, *J. Geophys. Res., 85,* 3387, 1980.

Williams, D. J., Energetic ion beams at the edge of the plasma sheet: ISEE-1 observations plus a simple explanatory model, *J. Geophys. Res., 86,* 5507, 1981.

Williams, D. J., T. A. Fritz, B. Wilken, and E. Keppler, An energetic particle perspective of the magnetopause, *J. Geophys. Res., 84,* 6385, 1979.

Williams, D. J., D. G. Mitchell, T. E. Eastman, and L. A. Frank, Energetic particle observations in the low-latitude boundary layer, *J. Geophys. Res., 90,* 5097, 1985.

Williams, P. J. S., T. S. Virdi, and S. W. H. Cowley, Substorm processes in the geomagnetic tail and their effect on the nightside auroral zone ionosphere as observed by EISCAT, *Phil. Trans. Roy. Soc. Ser. A, 328,* 173, 1989.

Williams, P. J. S., T. S. Virdi, S. W. H. Cowley, and M. Lester, Short-lived bursts of plasma velocity in the auroral zone, 1, Observational evidence from radar measurements, *J. Atm. Terr. Phys., 52,* 421, 1990.

Wilson, C. R., and M. Sugiura, Hydromagnetic interpretation of sudden commencements of magnetic storms, *Geophys. Res., 66,* 4097, 1961.

Winningham, J. D., and W. J. Heikkila, Polar cap auroral electron fluxes observed with ISIS 1, *J. Geophys. Res., 79,* 949, 1974.

Winningham, J. D., F. Yasuhara, S.-I. Akasofu, and W. J. Heikkila, The latitudinal morphology of 10 eV–10 keV electron fluxes during magnetically quiet and disturbed times in the 2100–0300 MLT sector, *J. Geophys. Res., 80,* 3148, 1975.

Winterhalter, D., M. G. Kivelson, and C. T. Russell, ISEE-1, -2, and -3 observation of the interaction between an interplanetary shock and the earth's magnetosphere: a rapid traversal of the magnetopause, *Geophys. Res. Lett., 8,* 911, 1981.

Woch, J., and R. Lundin, Magnetosheath plasma precipitation in the polar cusp and its control by the interplanetary magnetic field, *J. Geophys. Res., 97,* 1421, 1992.

Wolcott, J. H., M. B. Pongratz, E. W. Hones, Jr., and R. W. Peterson, Correlated observations of two auroral substorms from an aircraft and from a Vela spacecraft, *J. Geophys. Res., 81,* 2709, 1976.

Wolfe, J. H., R. W. Silva, and M. A. Myers, Observations of the solar wind during the flight of IMP-1, *J. Geophys. Res., 71,* 1319, 1966.

Wolfson, R., The configuration of slow-mode shocks, *J. Geophys. Res., 92,* 9875, 1987.

Wu, B. H., L. C. Lee, M. E. Mandt, and J. K. Chao, Magnetospheric response to solar wind dynamic pressure variations: Interactions of interplanetary tangential discontinuities with the bow shock, submitted, *J. Geophys. Res.,* 1992.

Wu, C. C., Shape of the magnetosphere, *Geophys. Res. Lett., 10,* 545, 1983.

Wu, C. C., The effects of dipole tilt on the structure of the magnetosphere, *J. Geophys. Res., 89,* 11048, 1984.

Wu, C. C., The effect of northward IMF on the structure of the magnetosphere, *Geophys. Res. Lett., 12,* 839, 1985.

Wu, C. C., Kelvin–Helmholtz instability at the magnetospheric boundary, *J. Geophys. Res., 91,* 3042, 1986.

Wu, C. C., Formation, structure, and stability of MHD intermediate shocks, *J. Geophys. Res., 95,* 8149, 1990.

Wu, C. C., MHD flow past an obstacle: large-scale flow in the magnetosheath, *Geophys. Res. Lett., 19,* 87, 1992.

Wu, C. C., and C. F. Kennel, Structure and evolution of time-dependent intermediate shocks, *Phys. Rev.. Lett, 68,* 56, 1992a.

Wu, C. C., and C. F. Kennel, Structural relations of time-dependent intermediate shocks, *Geophys. Res. Lett., 19,* 2087, 1992b.

Wu, C. C., R. J. Walker, and J. M. Dawson, A three-dimensional MHD model of the earth's magnetosphere, *Geophys. Res. Lett., 8,* 523, 1981.

Wu, Q., T. J. Rosenberg, F. T. Berkey, and R. H. Eather, Intensification and fading of auroral arcs in the dusk–midnight sector of the polar cap, *J. Geophys. Res., 96,* 7709, 1991.

Wurm, K., Die natur die kometen, *Mitt. Hamb. Sternw. in Bergendorf, 8,* 57, 1943.

Wygant, J. R., R. B. Torbert, and F. S. Mozer, Comparison of S3-3 polar cap potential drops with the interplanetary magnetic field and models of magnetic field reconnection, *J. Geophys. Res., 88,* 5727, 1983.

Yahnin, A. G., and V. A. Sergeev, Frequency of the aurora occurrence in the polar cap and the IMF vector orientation, *Geomagn. and Aeronomy, 19,* 556, 1979 (in Russian).

Yahnin, A. G., and V. A. Sergeev, Polar cap aurorae and dependence on the IMF orientation and on substorms, *Aurora Airglow, 28,* 27, 1981 (in Russian).

Yahnin, A. G., V. A. Sergeev, R. J. Pellinen, W. Baumjohann, K. U. Kaila, H. Ranta, J. Kangas, and O. M. Raspopov, Substorm time sequence and microstructure on 11 November, 1976, *J. Geophys., 53,* 182, 1983.

Yang, C. K., and B. U. O. Sonnerup, Compressible magnetic field reconnection: a slow wave model, *Astrophys. J., 206,* 570, 1976.

Young, D. T., H. Balsiger, and J. Geiss, Correlations of magnetospheric ion composition with geomagnetic and solar activity, *J. Geophys. Res., 87,* 9077, 1982.

Yumoto, K., Generation and propagation mechanisms of low-latitude magnetic pulsations, *J. Geophys., 60,* 79, 1986.

Yumoto, K., K. Takahashi, T. Saito, F. W. Menk, B. J. Fraser, T. A. Potemra, and L. J. Zanetti, Some aspects of the relation between Pi 1–2 magnetic pulsations observed at L = 1.3–2. 1 on the ground and substorm-associated magnetic field variations in the near-earth magnetotail observed by AMPTE CCE, *J. Geophys. Res., 94,* 3611, 1989.

Yumoto, K., K. Takahashi, T. Sakurai, P. R. Sutcliffe, S. Kokobun, H. Luhr, T. Saito, M. Kuwashima, and N. Sato, Multiple ground-based and satellite observations of global Pi 2 magnetic pulsations, *J. Geophys. Res., 95,* 15175, 1990.

Zanetti, L. J., T. A. Potemra, J. P. Doering, J. S. Lee, J. F. Fennell, and R. A. Hoffmann, Interplanetary magnetic field control of high-latitude activity on July 29, 1977, *J. Geophys. Res., 87,* 5963, 1982.

Zanetti, L. J., T. A. Potemra, T. Iljima, W. Baumjohann, and P. F. Bythrow, Ionospheric and Birkeland current distributions for northward interplanetary field: inferred polar convection, *J. Geophys. Res., 89,* 7453, 1984.

Zelenyi, L. M., A. S. Lipatov, D. G. Lominadze, and A. L. Taktashvili, The dynamics of the energetic proton bursts in the course of the magnetic field topology reconstruction in the earth's magnetotail, *Planet. Space Sci., 32,* 313, 1984.

Zelenyi, L. M., A. A. Galeev, and C. F. Kennel, Ion precipitation from the inner plasma sheet due to stochastic diffusion, *J. Geophys. Res., 95,* 3871, 1990a.

Zelenyi, L. M., R. A. Kovrazhkin, and J. M. Bosqued, Velocity-dispersed ion beams in the night-side auroral zone: AUREOL 3 observations, *J. Geophys. Res., 95,* 12119, 1990b.

Zhigulev, V. N., and E. A. Romishevskii, Concerning the interaction of currents flowing in a conducting medium with the earth's magnetic field, *Sov. Phys. Dokl., 4,* 859, 1960.

Zhu, X., and M. G. Kivelson, Analytic formulation and quantitative solutions of the coupled ULF wave problem, *J. Geophys. Res., 93,* 8602, 1988.

Zhu, X., and M. G. Kivelson, Global mode ULF pulsations in a magnetosphere with a nonmonotonic Alfven velocity profile, *J. Geophys. Res., 94,* 1479, 1989.

Zhuang, H. C., C. T. Russell, E. J. Smith, and J. Y. Gosling, Three-dimensional interaction of interplanetary shock waves with the bow shock and magnetopause: a comparison of theory with ISEE observations, *J. Geophys. Res., 86,* 5590, 1981.

Zi, M.-Y., E. Nielsen, W. B. Hanson, and T. A. Potemra, Polar convection and Birkeland currents dirung strongly positive IMF By, *J. Geophys. Res., 92,* 3417, 1987.

Ziesolleck, C., W. Baumjohann, K. Bruning, C. W. Carlson, and R. I. Bush, Comparison of height-integrated current densities derived from ground-based magnetometer and rocket-borne observations during the Porcupine F3 and F4 flights, *J. Geophys. Res., 88,* 8063, 1983.

Zmuda, A. J., J. H. Martin, and F. T. Heuring, Transverse magnetic disturbances at 1100 km in the auroral region, *J. Geophys. Res., 71,* 5033, 1966.

Zmuda, A. J., J. C. Armstrong, and F. T. Heuring, Characteristics of transverse magnetic disturbances observed at 1100 km in the auroral oval, *J., Geophys. Res., 75,* 4757, 1970.

Zmuda, A. J., and J. C. Armstrong, The diurnal flow pattern of field-aligned currents, *J. Geophys. Res., 79,* 4611, 1974.

Zwan, B. J., and R. A. Wolf, Depletion of solar wind plasma near a planetary boundary, *J. Geophys. Res., 81,* 1636, 1976.

Zwickl, R. D., D. N. Baker, S. J. Bame, W. C. Feldman, J. T. Gosling, E. W. Hones, Jr., D. J. McComas, and E. J. Smith, Evolution of the earth's distant magnetotail: ISEE-3 electron plasma results, *J. Geophys. Res., 89,* 11007, 1984.

Zwolakowska, D., P. Koperski, and B. Popielawska, Plasma populations in the tail during northward IMF, p. 57, in *Substorms 1: Proc. Int'l. Conf. Substorms, ICS-1,* ESA SP-335, European Space Agency, Paris, 1992.

This page intentionally left blank

INDEX